



Office of the NASA Chief Engineer

NASA TECHNICAL HANDBOOK

**NASA-HDBK-5010, VOLUME 2, REVISION A
APPROVED: 2024-01-09**

Superseding NASA-HDBK-5010 Baseline w/Change 1

METRIC/SI (ENGLISH)

FRACTURE CONTROL IMPLEMENTATION HANDBOOK FOR SPACEFLIGHT HARDWARE

VOLUME 2: EXAMPLE APPLICATIONS AND ADDITIONAL GUIDELINES

Trade names and trademarks are used in this NASA Technical Handbook for identification only. Their usage does not constitute an official endorsement, either expressed or implied, by NASA.

APPROVED FOR PUBLIC RELEASE – DISTRIBUTION IS UNLIMITED

NASA-HDBK-5010, VOLUME 2, REVISION A

DOCUMENT HISTORY LOG

Status	Document Revision	Change Number	Approval Date	Description
Baseline			2005-05-24	Initial Release
Revision	A		XXXX-XX-XX	Complete rewrite to expand to all spaceflight hardware consistent with NASA-STD-5019A.

APPROVED FOR PUBLIC RELEASE – DISTRIBUTION IS UNLIMITED

NASA-HDBK-5010, VOLUME 2, REVISION A

FOREWORD

This NASA Technical Handbook is published by the National Aeronautics and Space Administration (NASA) as a guidance document to provide engineering information; lessons learned; possible options to address technical issues; classification of similar items, materials, or processes; interpretative direction and techniques; and any other type of guidance information that may help the Government or its contractors in the design, construction, selection, management, support, or operation of systems, products, processes, or services.

This Handbook accompanies NASA-HDBK-5010, Volume 1, Revision A, and it is a companion document to NASA-STD-5019A, Fracture Control Requirements for Spaceflight Hardware. This Handbook documents best practices, examples, checklists, and provides additional resources for the implementation of fracture control requirements consistent with NASA-STD-5019A.

Submit requests for information via “Email Feedback” at <https://standards.nasa.gov>. Submit requests for changes to this Handbook via Marshall Space Flight Center (MSFC) Form 4657, Change Request for a NASA Engineering Standard, or the “Suggest a Change to this Standard” link on the Standard’s Summary Page at <https://standards.nasa.gov>.

Original Signed By:

Januray 9th, 2024

Joseph W. Pellicciotti
NASA Chief Engineer

Approval Date

APPROVED FOR PUBLIC RELEASE – DISTRIBUTION IS UNLIMITED

NASA-HDBK-5010, VOLUME 2, REVISION A

TABLE OF CONTENTS

DOCUMENT HISTORY LOG	2
FOREWORD	3
TABLE OF CONTENTS	4
LIST OF APPENDICES	10
LIST OF FIGURES	11
LIST OF TABLES	18
1. SCOPE	20
1.1 Purpose	20
1.2 Applicability	22
1.3 Document Structure and Examples	22
2. REFERENCE DOCUMENTS	23
2.1 General	23
2.2 Government Documents	23
2.3 Non-Government Documents	25
2.4 Order of Precedence	33
3. ACRONYMS, ABBREVIATIONS, SYMBOLS, AND DEFINITIONS	33
3.1 Acronyms, Abbreviations, and Symbols	33
3.2 Definitions	38
4. GENERAL GUIDANCE	48
4.1 Fracture Control Plan (FCP)	48
4.1.1 Example 1: Space Launch System (SLS) Multipurpose Stage Adaptor (MSA) Fracture Control Plan (FCP)	49
4.1.2 Example 2: Cubesat for Artemis 1 Fracture Control Plan (FCP)	50
4.2 Responsibilities	50
4.2.1 Responsible Fracture Control Board	50
4.2.1.1 NASA Fracture Control Organizations	50
4.2.1.2 Establishment of a NASA Fracture Control Board (FCB): Marshall Space Flight Center	51
4.2.1.3 Example of a JPL Fracture Control Board (FCB) Charter	52
4.2.1.4 Example of a KSC Fracture Control Panel Charter	53
4.2.2 Responsible Program	56
4.2.2.1 Hardware Developer Fracture Control Board (FCB)	56
4.2.2.2 SLS Fracture Control Organizations	57

APPROVED FOR PUBLIC RELEASE – DISTRIBUTION IS UNLIMITED

NASA-HDBK-5010, VOLUME 2, REVISION A

4.2.2.3	Examples of a Hardware Developer’s FCB Organizations and Relationship with NASA FCBs.....	58
4.2.2.4	Example of FCB Residing with the Hardware Developer.....	59
4.2.2.5	Fracture Control Coordinator (FCC) Roles and Responsibilities	59
4.2.3	Fracture Control Implementation.....	60
4.3	Classification of Parts and Implementation of Requirements.....	61
4.3.1	Example Classifications.....	61
4.3.1.1	Example: Solid Propellant, Fracture Critical	61
4.3.1.2	Example: Valve Internal Spring, Nonfracture Critical	61
4.3.1.3	Example: Structural Strut, Fracture Critical	62
4.3.1.4	Example: Pressure Vessel, Fracture Critical.....	62
4.3.1.5	Example(s): Composite Cover, Exempt, or Nonfracture Critical	62
4.3.1.6	Example: Ceramic Ball Bearings, Fracture Critical.....	62
4.3.1.7	Example: Fracture Control Summary List.....	63
4.3.1.8	Example: Fracture Summary Results.....	65
4.3.2	Classification of Pressurized Hardware	65
4.3.2.1	Pressurized Hardware Definitions and Categorization	66
4.3.2.2	Calculating Stored Energy in a Vessel under Pressure	67
4.4	Other Requirements	68
5.	EXEMPT PARTS	69
5.1	Example 1: Insulation Blanket, Exempt	69
5.2	Example 2: Elastomeric O-ring Seal, Exempt	69
6.	ASSESSMENT OF NONFRACTURE CRITICAL (NFC) PARTS.....	70
6.1	Established Approaches for Specific NFC Hardware.....	70
6.1.1	NFC Metallic Fasteners, Rivets, Shear Pins, and Locking Devices.....	70
6.1.1.1	NFC Low-Released Mass Fasteners, Rivets, and Shear Pins.....	70
6.1.1.2	NFC Contained Fasteners, Rivets, and Shear Pins.....	70
6.1.1.3	NFC Fail-Safe Rivets	70
6.1.1.4	NFC Low-Risk Fasteners	70
6.1.1.5	NFC Fail-Safe Fasteners	72
6.1.1.6	NFC Locking Devices	73
6.1.2	NFC Shatterable Components and Structure	73
6.1.3	NFC Rotating Hardware.....	73
6.1.3.1	Classification of Rotating Hardware with Kinetic Energy Less Than 14,240 ft-lbs	74

APPROVED FOR PUBLIC RELEASE – DISTRIBUTION IS UNLIMITED

NASA-HDBK-5010, VOLUME 2, REVISION A

6.1.3.2	Role of Jamming and Sudden Rotor Stoppage for Fracture Critical Classification	76
6.1.3.3	Angular Momentum and Sudden-Stop Loads Calculation	76
6.1.3.4	Rotary Mechanical Assembly Example Assessments.....	77
6.1.3.5	Simplified Models of Sudden-Stop Induced Loadings	78
6.1.3.6	References	80
6.1.4	NFC Sealed Container.....	80
6.1.5	NFC Tools, Mechanisms, and Tethers	81
6.1.6	NFC Batteries	81
6.2	General Approaches for NFC Parts.....	83
6.2.1	NFC Low-Released Mass.....	83
6.2.2	NFC Contained.....	84
6.2.2.1	Containment Punch Equation Calculation	85
6.2.2.2	Discussion on Containment of Rotating Parts.....	86
6.2.2.3	Containment Example Calculation for Rotating Hardware	86
6.2.2.4	General Containment Analysis.....	87
6.2.2.5	Container Fastener Analysis.....	88
6.2.3	NFC Fail-Safe	89
6.2.4	NFC NHLBB Pressurized Component	89
6.2.5	NFC Low-Risk Parts	92
6.2.5.1	NFC Low-Risk Metallic Parts.....	92
6.2.5.2	NFC Low-Risk Composite Parts.....	95
6.2.6	NFC Documented Nonhazardous Failure Mode	97
6.3	Additional Activities for Composite or Bonded NFC.....	98
7.	ASSESSMENT OF FRACTURE CRITICAL PARTS.....	98
7.1	Fracture Critical Parts.....	98
7.2	Established Approaches for Specific Fracture Critical Hardware Types.....	98
7.2.1	Fracture Critical Metallic Pressure Vessels.....	98
7.2.1.1	Example 1.....	98
7.2.1.2	Example 2.....	100
7.2.1.3	Example 3.....	101
7.2.2	Fracture Critical Composite Overwrapped Pressure Vessels (COPVs) and Composite Overwrapped Pressurized Fluid Containers.....	102
7.2.2.1	Limitations of LEFM	102
7.2.2.2	Guidance for Liner-to-Overwrap Debonds	103
7.2.2.3	Liner Inspections	104

APPROVED FOR PUBLIC RELEASE – DISTRIBUTION IS UNLIMITED

NASA-HDBK-5010, VOLUME 2, REVISION A

7.2.2.4	Best Practices Based on the NESC COPV Life Test Assessment	106
7.2.3	Other Fracture Critical Pressure Vessels and Pressurized Fluid Containers	113
7.2.4	Fracture Critical Lines, Fittings, and Other Pressurized Components	115
7.2.4.1	Example 1	116
7.2.4.2	Example 2	116
7.2.4.3	Example 3	116
7.2.4.4	Example 4	116
7.2.4.5	Example 5	117
7.2.4.6	Bellows	122
7.2.5	Fracture Critical Habitable Modules and Volumes	124
7.2.6	Fracture Critical Pressurized Structures	124
7.2.7	Fracture Critical Rotating Hardware	126
7.2.8	Fracture Critical Fasteners	127
7.2.9	Fracture Critical Shatterable Components and Structures	128
7.2.10	Fracture Critical Tools, Mechanisms, and Tethers	133
7.2.11	Fracture Critical Batteries	133
7.3	General Approach for Fracture Critical Metallic Parts Assessment	133
7.3.1	Loading Spectra	133
7.3.2	Assessment by Analysis	134
7.3.2.1	Assessment by Closed-Form Solution	134
7.3.2.2	Assessment by Crack Growth Computer Code	136
7.3.3	Assessment by Test	136
7.4	General Approach for Fracture Critical Composite or Bonded Hardware Assessment	137
7.4.1	Damage Threat Assessment/Damage Protection Plan	141
7.4.2	Impact Damage Mitigation Plan	143
7.4.2.1	Example Impact Damage Mitigation Plan for Generic Hardware	143
7.4.2.2	Example Impact Damage Mitigation Plan for COPVs	144
7.4.3	Residual Threat Determination	157
7.4.4	Loading Spectra	159
7.4.5	Damage Tolerance Tests of Coupons	159
7.4.6	Damage Tolerance Tests of Hardware Elements	160
7.4.7	Strength and Life Assessments	161
7.4.8	Damage Tolerance Tests Full-Scale Flight-Like Hardware	162
7.4.9	Evaluate Flaws or Damage that Occurs during Building Block Approach (BBA) Testing	163

APPROVED FOR PUBLIC RELEASE – DISTRIBUTION IS UNLIMITED

NASA-HDBK-5010, VOLUME 2, REVISION A

7.5	Optional Approaches for Fracture Critical Parts	163
7.5.1	Single-Event Fracture Critical Components	163
7.5.2	High-Cycle Fatigue (HCF) Components.....	164
7.5.3	Proof Test Approach for Composite or Bonded Hardware	172
7.5.4	Fleet Leader Testing	172
7.5.5	Hazardous Fluid Containers for Payloads and Experiments	174
8.	FLAW SCREENING, TRACEABILITY, AND MATERIAL SELECTION.....	174
8.1	Flaw Screening	175
8.1.1	NDE for Metallic Parts.....	175
8.1.2	NDE for Composite or Bonded Parts	178
8.1.3	Proof Test	184
8.1.4	Process Control	184
8.1.5	Detected Flaws	184
8.2	Traceability for Fracture Control	184
8.3	Material Selection and Usage for Fracture Critical Parts.....	184
9.	FRACTURE CONTROL DOCUMENTATION AND VERIFICATION	184
9.1	Fracture Control Documentation.....	184
9.1.1	Fracture Control Plan (FCP)	185
9.1.2	Engineering Drawings.....	185
9.1.3	Fracture Control Summary Report.....	186
10.	ALTERNATIVES	186
10.1	Example 1: Impractical Full-Scale Testing	186
10.2	Example 2: Proof Test of Full-scale Composite Structures	187
10.3	Example 3: Thermal Protection System Challenges	187
10.4	Example 4: Catastrophic Composite Failure Risk Mitigation	188
10.5	Example 5: Composite Damage Tolerance – Analysis Validated by Test	188
10.6	Example 6: Delaminations in Composite Overwrapped Pressure Vessels	190
10.7	Impact Damage of Composite Structures.....	195
10.7.1	General Impact Damage Approach	195
10.7.2	Compression-After-Impact Strength Testing.....	195
10.7.3	Burst-After-Impact COPV Testing	196
10.7.4	Impact Damage of Sandwich Panels	198
11.	SPECIAL TOPICS	200
11.1	Leak Before Burst.....	200
11.1.1	Background and Introduction	200
11.1.2	Leak Before Burst Limitations and Considerations	203
11.1.3	Initial Flaw Sizes, Geometries, and Failure Modes.....	204
11.1.4	Uniform versus Nonuniform Stress Fields	206
11.1.5	Proof Testing at $1.23 \times \text{MDP}$	207
11.1.6	Leakage Detection	207

APPROVED FOR PUBLIC RELEASE – DISTRIBUTION IS UNLIMITED

NASA-HDBK-5010, VOLUME 2, REVISION A

11.1.7	Summary.....	208
11.1.8	LBB Examples.....	209
11.1.8.1	Example 1: Sharp-Notched Features	209
11.1.8.2	Example 2: LBB Issues with Secondary Bending.....	218
11.1.8.3	Example 3: LBB Issues with Stiffened Plates	222
11.1.8.4	Example 4: LBB Issues with Plate Dominated by Bending Loads	232
11.2	Proof Test Logic	234
11.2.1	Example 1	235
11.2.2	Example 2	239
11.3	Guidelines for LEFM and EPFM Assessments	242
11.3.1	Limitations of LEFM Assessments	242
11.3.2	Determination of the Appropriate Damage Tolerance Assessment	243
11.3.3	EPFM Assessment Guidelines.....	246
11.3.4	EPFM Using NASGRO®: Benchmarks and Examples	248
11.3.4.1	Validation of EPFCG Properties Derived from LEFCG Properties.....	248
11.3.4.2	EPFM Benchmark – Al 6061-T6 Elastic-Plastic Coupon Testing	257
11.3.4.3	EPFM Benchmark – Ti-6Al-4V Elastic-Plastic Coupon Testing.....	269
11.3.5	EPFM Benchmarks and Examples – Lessons Learned	277
11.4	Damage Tolerance for Additive Manufacturing Parts	278
11.4.1	Example 1: AM Component with Machined Surface	280
11.4.2	Example 2: AM Rotating Part	281
11.4.3	Additive Manufacturing (AM) Damage Tolerance Evaluation.....	284
11.5	Heatshield Damage Tolerance.....	287
11.6	Thrust Chamber Liner Damage Tolerance	288
11.7	Loading Spectra.....	290
11.7.1	Relevance to Damage Tolerance Assessments.....	290
11.7.2	Spectra Calculation Overview	290
11.7.3	Case 1: Unpressurized Secondary Hardware.....	291
11.7.4	Case 2: Pressurized Secondary Hardware	294
11.7.5	Case 3: Engine Feedlines.....	295
11.7.6	Case 4: Engine Nozzle.....	299
11.7.7	Case 5: Primary Structure.....	300
11.8	Analysis Conservatism.....	305
11.9	Composites Damage Tolerance: Delamination	308
11.9.1	Fracture Toughness Characterization	310
11.9.2	Virtual Crack Closure Technique	313
11.9.2.1	Virtual Crack Closure Technique Modeling Overview.....	314
11.9.2.2	Fracture Margin Assessment Using the Virtual Crack Closure Technique (VCCT).....	317
11.9.2.3	Example # 1: Application of VCCT to a Composite Joint	318
11.9.2.4	Example # 2: Application Using the Virtual Crack Closure Technique	322
11.9.3	Cohesion-Decohesion Elements	323
11.9.3.1	Traction-Separation Constitutive Law.....	324
11.9.3.2	Validation Cases	326
11.9.3.3	Cautions.....	331

APPROVED FOR PUBLIC RELEASE – DISTRIBUTION IS UNLIMITED

NASA-HDBK-5010, VOLUME 2, REVISION A

11.9.4	Analytical Fatigue Assessments	332
--------	--------------------------------------	-----

LIST OF APPENDICES

A	Space Launch System (SLS) Multipurpose Stage Adaptor (MSA) Fracture Control Plan (FCP) and Accompanying Form 1676.....	335
B	SPIE Multi-Purpose Crew Vehicle Stage Adapter (MSA) Fracture Control Summary Report	391
C	Fracture Control Plan for the Lunar Flashlight Propulsion System.....	426
D	Fracture Control Report – Lunar Flashlight Propulsion System.....	455
E	Fracture Control Board Example	523
F	Acknowledgements	527

APPROVED FOR PUBLIC RELEASE – DISTRIBUTION IS UNLIMITED

NASA-HDBK-5010, VOLUME 2, REVISION A

LIST OF FIGURES

1-1	NASA-STD-5019A Fracture Control Requirements Diagram.....	21
4.2-1	Membership of MSFC FCB Showing Areas of Emphasis	51
4.2-2	Memorandum Establishing MSFC FCB Membership.....	52
4.2-3	JPL FCB Charter.....	53
4.2-4	SLS Fracture Control Organization	58
4.2-5	Traditional Fracture Control Governance.....	58
4.2-6	RFCB Residing with the Hardware Developer.....	59
4.3-1	Flowchart to Determine Pressurized Hardware Type	66
6.1-1	Flowchart to Classify NFC Rotating Hardware.....	74
6.1-2	Picture of 8PU Locker with Centrifuge Inside.....	75
6.1-3	Sudden-Stop Simplified Models	78
6.2-1	NFC Contained Flowchart	85
6.2-2	Analytical Sketch for Rotating Hardware for the Example Problem.....	87
6.2-3	Critical Flaw Size Criteria for Nonhazardous Leak Before Burst for a $2c = 10t$ Flaw.....	91
6.2-4	Dimensions and Loads of the Aluminum 6061-T6 Bracket	93
6.2-5	Best-fit S/N Curves for Unnotched 6061-T6 Aluminum Alloy.....	95
7.2-1	NASGRO® Input for an Axially Aligned Flaw in a Hollow Cylinder.....	99
7.2-2	NASGRO® Input for a Circumferentially Aligned Flaw in a Hollow Cylinder.....	99
7.2-3	Section View of a Tube, with the Pipe Running Horizontally.....	117
7.2-4	Input for Axially Aligned Crack in a Hollow Cylinder	119
7.2-5	Input for Circumferentially Aligned Crack in a Hollow Cylinder.....	119
7.2-6	Load Blocks for Axially Aligned Crack (SC04).....	120
7.2-7	Load Blocks for Circumferentially Aligned Crack (SC05)	121
7.2-8	Build Schedule for Initial Flight (Block 1) and Reuse Flights (Block 2)	121
7.2-9	Depiction of Analysis Results for a Circumferential Crack with a 0.2 Crack Aspect Ratio.....	122
7.2-10	Stress Intensity Factor Calculation as a Function of Pressure and Various Flaw Sizes	125
7.2-11	Geometry Input for a Semi-elliptical Surface Crack in a Plate.....	129
7.2-12	Material Input for Fused Silica in Distilled Water.....	130
7.2-13	Load Block Definition for this Example.....	132
7.2-14	Analysis Results for this Example	133
7.4-1	Relationship of QA and NDE to BAI of COPVs.....	145

APPROVED FOR PUBLIC RELEASE – DISTRIBUTION IS UNLIMITED

NASA-HDBK-5010, VOLUME 2, REVISION A

7.4-2	Manufacturer's Impact Control Requirements	146
7.4-3	Shipping ICP Requirements	148
7.4-4	Receiving Inspection ICP Requirements	150
7.4-5	Installation and System-Level Procedures for Procedural-only ICP	151
7.4-6	Installation and System-Level Procedure for Implementation of ICP with Impact Indicators	153
7.4-7	Installation and System-Level Procedure for Implementation of ICP with Impact Protectors	155
7.4-8	Cross-Section of COPV Impact Protector	156
7.4-9	Bonded Joint under Consideration.....	157
7.4-10	Material Obstructs the Ability to Perform NDE on a Composite Joint.....	158
7.5-1	Stress Distribution and Critical Crack Orientation of the Impeller	165
7.5-2	Stress Distribution at the Critical Crack Orientation.....	166
7.5-3	Geometry Input for a Through Crack at the Edge of a Plate	167
7.5-4	Load Blocks Input.....	169
7.5-5	Output of 4 × Life Analysis of Low-Cycle Loading	169
7.5-6	NASSIF Geometry Input for Through Crack at the Edge of a Plate	170
7.5-7	Output Options for NASSIF	171
7.5-8	Results of NASSIF for the Minimum (Left) and Maximum (Right) Stress Intensity Factors.....	171
8.1-1	Minimum Detectable Crack Sizes for Fracture Analysis Based on Standard NDE Methods [NASA-STD-5009B].....	176
8.1-2	Assumed Flaw Geometries	177
8.1-3	Pulse-Echo C-Scan of a COPV Subjected to a 7.5 ft-lb Impact.....	179
8.1-4	(a) Initial Shearography Image and (b) Post-Impact Shearography Image	180
8.1-5	Thermography Indications on a COPV Subjected to Two Impact Levels	181
8.1-6	Eddy Current Image of a COPV Subjected to Various Impact Levels.....	182
8.1-7	Acoustic Emission Data: (a) Before Impact and (b) After Impact	183
8.1-8	COPV Example Comparisons of Various NDE Methods	184
9.1-1	Drawing for a Fracture Critical Part with a Note Providing the Expected Inspections and Associated Acceptable Flaw Size	185
10.5-1	Complicated Sandwich Structure is Subject to Internal Core Pressure during Ascent	189
10.6-1	A Typical COPV with Boundary Conditions	193
10.6-2	Delamination Location for this Example.....	193
10.6-3	Hypothetical Fiber Defect near Delamination.....	194
10.6-4	Direction of Delamination Growth in this Example	194

APPROVED FOR PUBLIC RELEASE – DISTRIBUTION IS UNLIMITED

NASA-HDBK-5010, VOLUME 2, REVISION A

10.6-5	Predicted Delamination Growth for Low and High Fracture Toughness Values.....	194
10.7-1	Compression-After-Impact Test Data Shows Reduction in Residual Strength due to Foreign Object Impact Damage	196
10.7-2	Sandwich Structure Impacted by a Free-Falling Mass	198
10.7-3	Ultrasonic C-Scan Image of Impacted Panel Showing Delamination Damage ...	199
10.7-4	Strain Response at Bottom Facesheet of the Sandwich Structure	200
10.7-5	Delamination Predicted by Analysis Compared Well with the Test	200
11.1-1	Illustration of Full Through-Crack of $10t$ Length (shown in blue), and Elliptical Part Through-Crack of $2c = 10t$ (shown in orange).....	204
11.1-2	Schematic Representation of (a) an LBB Response with Detectable Leakage and (b) a Non-LBB Response with Burst Failure Occurring Prior to Leakage Detection	208
11.1-3	Welded Aluminum Cylinder with Unfused Depth $a (= a_{notch})$	209
11.1-4	Through-Thickness Crack in Cylinder Representing the Fused Thickness t_{weld} ..	210
11.1-5	Material Definition: Al 2219-T87, GTA Weld (Bk is set to 0, Conservatively) .	210
11.1-6	Stress Spectrum: $S_{0weld} = 101.5\text{MPa}$ (Obtained by Manual Iteration), $R = 0$	210
11.1-7	Surface Crack in Cylinder Representing the Fused Thickness Weld	211
11.1-8	Results Plot of Crack Sizes (a and c) and Aspect Ratio (a/c) as Function of Load Cycles.....	212
11.1-9	Example Characterization of a Complex Flaw	213
11.1-10	Part-Through Crack in Cylinder Representing a Sharp Notch in the Wall Thickness t_{cyl}	214
11.1-11	Stress Spectrum: $S_{0tube} = 26.37\text{MPa}$, $R = 0$	214
11.1-12	Input Data for the NASSIF Module of NASGRO®	215
11.1-13	Surface Cracks (Symmetric) at a (Sharp) Central Notch in a Plate, Approximating a Surface Crack in the Partially Fusing Cylindrical Weld of Thickness t_{weld}	216
11.1-14	Stress Spectrum: $S_{0tube} = 26.37\text{MPa}$, $R = 0$	216
11.1-15	Results Plot of Crack Sizes (a and c) and Aspect Ratio (a/c) as Function of Load Cycles.....	217
11.1-16	Results Plot of $K(a)$ (Surface) and $K(c)$ (Depth) as Function of Load Cycles ...	218
11.1-17	Surface Crack at a (Sharp) Edge Notch in a Plate	219
11.1-18	Material Definition: Al 7075-T7351 (Bk is set to 0, Conservatively)	219
11.1-19	Stress Spectrum: $S_{0plate} = 10\text{MPa}$, $R = 0$	220
11.1-20	Results Plot of Crack Sizes (a and c) and Aspect Ratio (a/c) as Function of Load Cycles.....	221

NASA-HDBK-5010, VOLUME 2, REVISION A

11.1-21	Results Plot of K(a) (Surface) and K(c) (Depth) as Function of Load Cycles) ...	222
11.1-22	Through-Thickness Crack in Flat Wall of Thickness t_{plate} , with Stiffeners Omitted.....	223
11.1-23	Stress Spectrum: $S_{0LBB} = 125$ MPa (Obtained by Manual Iteration), $R = 0$	223
11.1-24	Through-Thickness Crack in a Plate, Allowing Local Introduction of the Stiffener Load	224
11.1-25	Plot of K as Function of Crack Length, TC11, Uniform Stiffener Stress Distribution S_1 over $t_{stiff} = 5$ mm	225
11.1-26	Stress Distribution Plot: Triangular Distribution S_1 of Stiffener Load over $2c = 10t_{plate} = 50$ mm Crack Length (Left Half not Shown).....	226
11.1-27	Stress Spectrum: Factor on Stress that Allows Crack-Growth of $2c$ up to ' $10t_{plate}$ ', $R = 0$	226
11.1-28	Plot of K as Function of Crack Length, TC11, Triangular Stiffener Stress Distribution over ' $10t_{plate}$ '	227
11.1-29	Through-Thickness Crack from a Loaded Hole in a Plate, Allowing Local Introduction of the Stiffener Load	227
11.1-30	The Plate with a Cracked Stiffener can be Addressed by the Superposition of 3 Crack Cases (Item a), where the 2 Pin Load Cases Provide Identical K (Item b).....	228
11.1-31	Stress Spectrum: Representative of $S_{opanel} = 125$ MPa, $R = 0$	229
11.1-32	Plot of K as Function of Crack Length (Add 2.5mm Offset due to Pin Radius) .	230
11.1-33	Stress Spectrum: Factor that Allows Crack-Growth from $2c = 1.1$ mm to ' $10t_{plate}$ ', $R = 0$	230
11.1-34	SIF Results Based on a Simple 2D NASBEM Model of the Stiffened Plate	231
11.1-35	Through-Thickness Crack in Flat Wall of Thickness t_{plate} , Submitted to Uniform Tension	232
11.1-36	Surface Crack in Flat Wall of Thickness t_{plate} , Submitted to Bending.....	233
11.1-37	Stress Spectrum: Factor on Stress Applied S_{0LBB} as Pure Bending (S_1). $R = 0$...	233
11.2-1	Input for the NASCCS Module to Determine the Critical Crack Size for an Axial Crack in a Hollow Cylinder (SC04).....	237
11.2-2	Output Options Input for NASCCS	238
11.2-3	Results of Critical Crack Size Analysis (NASCCS) for an Interior Axial Surface Crack in a Hollow Cylinder with Crack Aspect Ratio of 0.2	238
11.2-4	Input for the NASCCS Module to Determine the Critical Crack Size for a Semi-elliptical Surface Crack in a Plate (SC30).....	240
11.2-5	Output Options Input for NASCCS	241
11.2-6	Results of Critical Crack Size Analysis (NASCCS) for a Surface Crack in a Plate with Crack Aspect Ratio of 0.2.....	241

NASA-HDBK-5010, VOLUME 2, REVISION A

11.3-1	Comparisons of LEFM and EPFM FCG Curves for Al 2014-T6: R = -1, a = 0.025 inch, a/c = 0.2, w = 10 inches, t = 0.1 inch, Failure Represents Unstable Crack Growth or Plastic Collapse.....	243
11.3-2	Flowchart to Determine Validity of LEFM Assessments	244
11.3-3	Surface Crack Cross-Section	245
11.3-4	EPFCG Analytical Inputs Required by NASGRO®	250
11.3-5	LEFCG Curves in NASGRO® for Q3LE13AB1	251
11.3-6	Closure Corrected LEFCG Curves for Q3LE13AB1	252
11.3-7	EPFCG Material Inputs for Surface and Corner Cracks, R > 0, Constraint Alpha Evaluated at a Value of both 1 and 3	255
11.3-8	NASGRO® EPFCG Predictions vs. Test Cycles	256
11.3-9	Accessing NASGRO® EPFM Module	262
11.3-10	Relevant EPFM Crack Geometries	263
11.3-11	Material-Specific Parameters Available to Determine EPFCG Parameters when a Single da/dN Curve Exists	264
11.3-12	Load Block for Test Case FL-LT-032-11	266
11.3-13	Percent of Predictions that were Conservative Compared to Aluminum 6061- T6 Fatigue Crack Growth Test Results for Different Analysis Methods	268
11.3-14	Ramberg-Osgood Plasticity Model for Ti-6Al-4V	271
11.3-15	da/dN Test Data Available in Mill Annealed Ti-6Al-4V	272
11.3-16	EPFCG Properties used to Analyze Ti-6A-4V Surface Cracks	272
11.3-17	Dye Penetrant Inspection of Specimen 6 Back Surface at Breakthrough of Surface Crack	273
11.3-18	Cycles to a Through Crack for Specimen 2 with a Constraint Factor of 1.15 as Reported in the NASGRO® EPFM Module.....	273
11.3-19	Half-Crack Width When a Through Cracked Developed for Specimen 2 with a Constraint Factor of 1.15	275
11.3-20	Cycles to Exceedance of J_{crit} for Specimen 2	275
11.3-21	Predicted EPFM Cycles Versus Test Cycles for all Three Tests	277
11.3-22	Predicted LEFM and EPFM Cycles Versus Test Cycles for all Three Tests	278
11.4-1	Effects on Cycles to Failures for Various Conditions.....	280
11.4-2	Approach to Determine Whether As-built Surface Finishes Require Full Fatigue Characterization	282
11.4-3	Penny-Shaped Cracks in Cylindrical Samples at 10% and 30% Depth.....	283
11.4-4	Tests Demonstrated that Fatigue Life was Sensitive to Surface Finish (Circles); with Prescribed Flaws, the Fatigue Life was Similar Regardless of Surface Finish (Exes and Triangles)	283

APPROVED FOR PUBLIC RELEASE – DISTRIBUTION IS UNLIMITED

NASA-HDBK-5010, VOLUME 2, REVISION A

11.4-5	Material Parameters Selection to Define Material Properties Based on a da/dN curve	285
11.4-6	Input of Custom Material Data into NASGRO® Crack Growth Module	286
11.4-7	Example da/dN Data to be Entered in the Crack Growth Parameters Table of the NASGRO® New Data Material Input.....	287
11.7-1	Example Cases for Load Spectra Development	291
11.7-2	Combined Stress Spectrum.....	294
11.7-3	Pressure Spike Amplitude to Strain Correlation.....	296
11.7-4	Rainflow Counting Example	297
11.7-5	Binning of Pressure Spikes.....	298
11.7-6	Strain to Cycles to Failure Correlation	299
11.7-7	Example Time History.....	302
11.7-8	Example Force Spectrum.....	302
11.7-9	Water Tank Analogy for SEA	304
11.7-10	Example SEA Model	304
11.7-11	Example SEA Results.....	305
11.8-1	Analysis Crack Sizes for Detected Cracks	306
11.8-2	Analysis Crack Sizes for Detected Cracks	307
11.9-1	Three Modes of Fracture	308
11.9-2	Building Block Approach for Damage Tolerance Evaluations	310
11.9-3	VCCT Applied to a Delamination Modeled with Three-Dimensional Eight-Noded Solid Elements	316
11.9-4	Three-Dimensional Eight-Noded Solid Elements VCCT Nomenclature.....	316
11.9-5	Schematic of the Composite Joint Configuration.....	318
11.9-6	Edge Flaws were Assumed between the Facesheet and the Doublers	320
11.9-7	A Large Flaw is Assumed to be Located between the Facesheet and the Insert (Bottom) Away from the Reentrant Corners of the Joint, and Another Large Flaw is Assumed to be Located between the Facesheet and the Doubler (Top) .	320
11.9-8	Margin of Safety for an Edge Flaw between the Facesheet and the Doubler.....	321
11.9-9	Margin of Safety for a Flaw between the Facesheet and the Insert.....	322
11.9-10	Margin of Safety for a Flaw between the Facesheet and the Insert.....	323
11.9-11	Interface Element Consists of a Continuous Distribution of Breakable Springs	324
11.9-12	Traction-Displacement Constitutive Relationship of a Cohesive Element	325
11.9-13	Decohesion Elements Placed between Laminates (Gray Solid Elements).....	325
11.9-14	Predictions by Predictive Failure Analysis (PFA) of the Double Cantilever Beam Compare Well to Experimental Data and Analytical Solutions.....	327

APPROVED FOR PUBLIC RELEASE – DISTRIBUTION IS UNLIMITED

NASA-HDBK-5010, VOLUME 2, REVISION A

11.9-15	Predictions by PFA for the End Load Split Compare Well to Analytical Solutions.....	327
11.9-16	Predictions by PFA for the End Notch Flexure Compare Well to Analytical Solutions.....	328
11.9-17	Predictions by PFA for the Fixed Ratio Mixed Mode Compare Well to Analytical Solutions	328
11.9-18	CZM Predicted Load-Displacement Response for Double Cantilever Beam and End Load Split Accurately	329
11.9-19	Failure and Response of the Single Lap Joint Test Configuration.....	330
11.9-20	Failure and Response of a Double Cantilever Beam Test.....	330
11.9-21	Failure and Response of a Crack Lap Shear Test.....	331
E.1-1	Fracture Control Board Structure	523
E.2-1	Interaction of the Contractor FCB and MSFC FC Team	525

APPROVED FOR PUBLIC RELEASE – DISTRIBUTION IS UNLIMITED

NASA-HDBK-5010, VOLUME 2, REVISION A

LIST OF TABLES

4.2-1	Applicable Requirements and Handbook Documents for Different Programs....	56
4.2-2	Checklist to Aid in Ensuring Steps for Fracture Control Implementation are Complete	60
4.3-1	Fracture Control Classification Example	64
4.3-2	Fracture Summary Results	65
4.3-3	Hardware Item Classification Guide and Corresponding Section in NASA-STD-5019A	67
6.1-1	Checklist for NFC Low-Risk Fasteners	71
6.1-2	Checklist for NFC Fail-Safe Fasteners	72
6.1-3	Checklist for NFC Sealed Container.....	80
6.1-4	Checklist for NFC Batteries	82
6.2-1	Checklist for NFC NHLBB Pressurized Component	90
6.2-2	Checklist for NFC Low-Risk Metallic Parts.....	92
6.2-3	Checklist for NFC Low-Risk Composite Parts.....	96
7.2-1	MDP Cycles to Failure Prior to Life Factor of 4 for Different Dye Penetrant Crack Orientations and Aspect Ratios in a Hollow Cylinder	100
7.2-2	NASGRO® Thickness Limits for Various NDE Techniques in Hollow Cylinders	101
7.2-3	Checklist for FC Lines, Fittings, and Other Pressurized Components	115
7.2-4	Load History of the Pipe	118
7.2-5	Safe Flights for Different Crack Orientations and Aspect Ratios in the Pipe.....	122
7.2-6	Checklist for Fracture Critical Fasteners	128
7.2-7	Flaw Growth Analysis Uncertainty Factor Base on Design Life.....	132
7.3-1	Dimensions Used in the Assessment of Hardware	134
7.4-1	Criteria for FC Composite Hardware.....	137
7.4-2	General Example of a Threat Assessment and Accompanying Protection Plan..	141
7.4-3	Evaluation of Various NDE Techniques for the Bonded Joint Application in Figure 7.4-9	159
7.4-4	Load Enhancement Factor as a Function of Sample Size Based on the Following Assumptions: $\alpha_L = 1.25$, $\alpha_R = 20$, $\ell = 0.9$, $\gamma = 0.95$	161
7.5-1	Stress Distribution from the FEM and the Corresponding Normalized NASGRO® Input.....	168
7.5-2	Hazardous Fluid Containers for Payloads and Experiments Checklist.....	174
9.1-1	Load History Log for a Pressurized Component such as a Valve on an Upper Stage Engine	185
10.7-1	Comparison of Burst Strengths for Cylindrical COPV	197

APPROVED FOR PUBLIC RELEASE – DISTRIBUTION IS UNLIMITED

NASA-HDBK-5010, VOLUME 2, REVISION A

11.2-1	Critical Crack Depth for Axial Flaws in a Hollow Cylinder for Combinations of Crack Aspect Ratios and Positions in the Cylinder.....	239
11.2-2	Critical Crack Depth for Axial Flaws in a Hollow Cylinder for Combinations of Crack Aspect Ratios and Positions in the Cylinder.....	241
11.3-1	EPFM Assessment Criteria.....	246
11.3-2	Test Specimens and Conditions from McClung, et al. [11.3-4].....	249
11.3-3	LEFM Validity Checks for McClung, et al., Tests [11-3-4]	249
11.3-4	Key Equations Associated with Deriving EPFCG Properties in NASGRO®	255
11.3-5	NASGRO® EPFCG Predictions vs. Test Cycles.....	256
11.3-6	Fatigue Crack Growth Measurement Test Results for Surface Cracks in Aluminum 6061-T6 Rolled Sheet [11.3-9].....	258
11.3-7	LEFM Limit Checks for the Initial Crack and Loading Condition for the Tests Outlined in Table 11.3-6.....	260
11.3-8	LEFM Limit Checks for the Final Crack and Loading Condition for the Tests Outlined in Table 11.3-6.....	261
11.3-9	Material Properties used for the NASGRO® EPFCG Analysis for the LT and TL Orientations of Aluminum 6061-T6	266
11.3-10	Comparison of the Test Results with the NASGRO® EPFM Predictions; Crack Predictions that are not Conservative are Highlighted in Red	267
11.3-11	Test Specimens and Test Conditions for Notched Ti-6Al-4V Coupons	269
11.3-12	Test Results and Analytical Predictions for Ti-6Al-4V Specimens	274
11.3-13	Test Results and Analytical Predictions for Ti-6Al-4V Through Crack Specimens Taken to Failure	276
11.9-1	Summary Table for Fracture Test Configurations.....	313
11.9-2	Mechanical Properties for the Material Systems used in the Composite Joint ...	319

APPROVED FOR PUBLIC RELEASE – DISTRIBUTION IS UNLIMITED

**FRACTURE CONTROL IMPLEMENTATION HANDBOOK
FOR SPACEFLIGHT HARDWARE**

**VOLUME 2: EXAMPLE APPLICATIONS AND ADDITIONAL
GUIDELINES**

1. SCOPE

1.1 Purpose

It is NASA policy that fracture control be imposed on all human-rated spaceflight systems to promote safety by mitigating the risk of catastrophic failure due to the presence of flaws. The purpose of this Handbook is to provide interpretation of fracture control requirements and methodology and approaches that are acceptable to NASA for implementation of fracture control requirements for spaceflight hardware. Following the interpretations and guidelines of Volume 1 for this hardware will satisfy the intent of the applicable NASA fracture control requirements in NASA-STD-5019A. Volume 2 of NASA-HDBK-5010A provides examples of acceptable methodologies, checklists, assessment approaches, and other resources for the implementation of fracture control requirements of spaceflight hardware.

The requirement for imposing fracture control on hardware used in human spaceflight is based upon safety. Any program, human spaceflight or otherwise, may choose to impose fracture control to enhance mission success, although it is not specifically required for a nonhuman-rated program. NASA requires fracture control to advance the safety of human spaceflight hardware.

Volume 2 of this Handbook provides additional resources such as specific examples, approaches, and checklists for the implementation of fracture control requirements consistent with NASA-STD-5019A. Volume 2 also provides additional flowcharts and recommendations not addressed in Volume 1 of NASA-HDBK-5010A or NASA-STD-5019A. Some sections do not have content because Volume 1 and NASA-STD-5019A were deemed sufficient.

This revision of the Handbook expands the application beyond payloads and is organized similarly to NASA-STD-5019A requirements with each section in parallel. Volume 1 of this Handbook provides guidelines and additional explanatory text of the requirements to aid in the implementation of fracture control requirements of NASA-STD-5019A. Volume 2 contains examples and other supporting materials such as checklists and references to pertinent reference documents. The 5019A Fracture Control Diagram is repeated for convenience in Figure 1-1, NASA-STD-5019A Fracture Control Requirements Diagram.

NASA-HDBK-5010, VOLUME 2, REVISION A

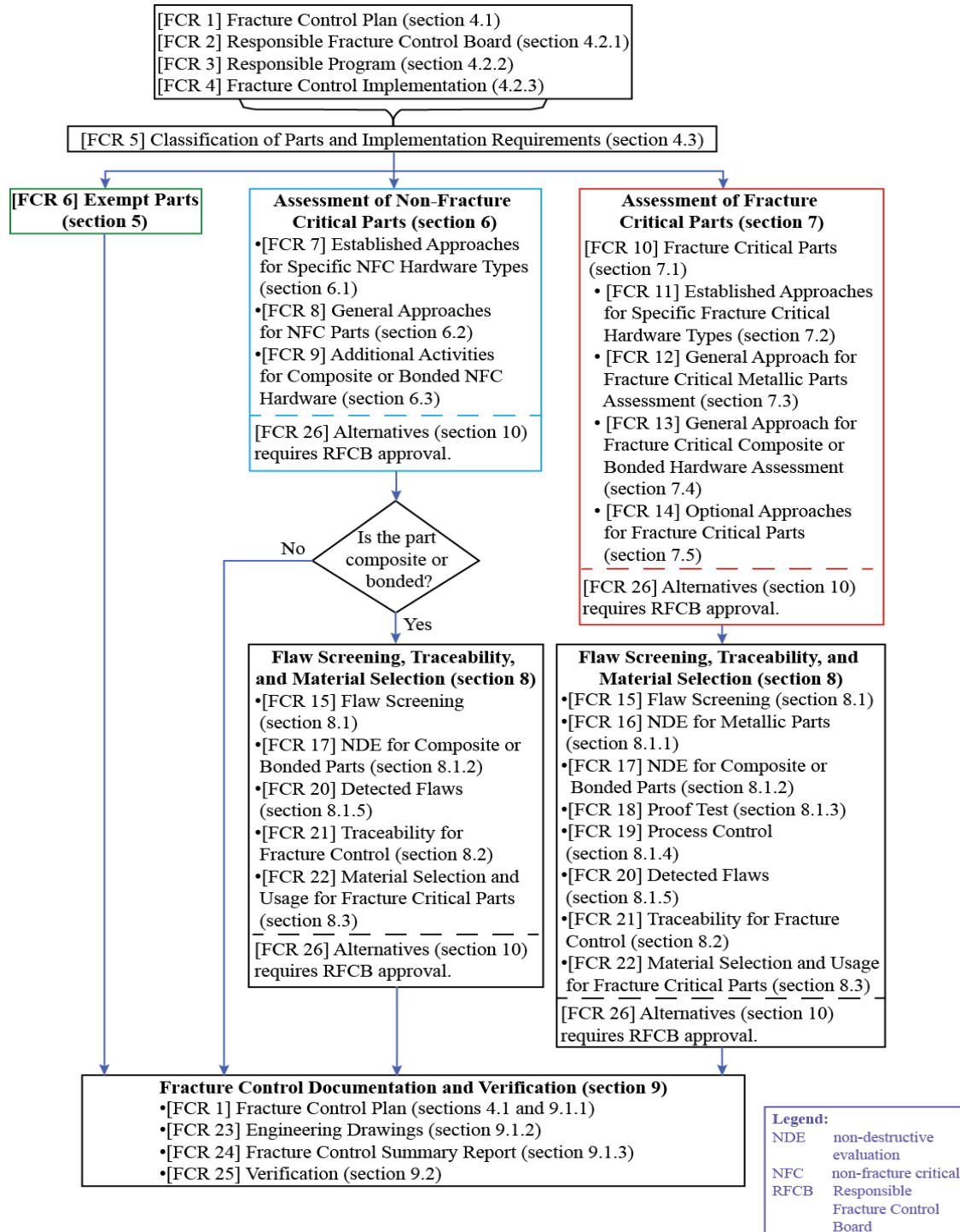


Figure 1-1—NASA-STD-5019A Fracture Control Requirements Diagram

NASA-HDBK-5010, VOLUME 2, REVISION A

1.2 Applicability

1.2.1 This Handbook is applicable to all spaceflight hardware.

1.2.2 This Handbook is approved for use by NASA Headquarters and NASA Centers and Facilities. This language applies to the Jet Propulsion Laboratory (a Federally Funded Research and Development Center), other contractors, recipients of grants, cooperative agreements, or other agreements only to the extent specified or referenced in the applicable contracts, grants, or agreements.

1.2.3 References to “this Handbook” refer to this NASA-HDBK-5010, Volume 2, Revision A; references to external documents state the specific document information.

1.2.4 This Handbook, or portions thereof, may be referenced in contract, program, and other Agency documents for guidance.

1.2.5 In this Handbook, the terms “may” or “can” denote discretionary privilege or permission, “should” denotes a good practice and is recommended but not required, “will” denotes expected outcome, and “is/are” denotes descriptive material or a statement of fact.

1.3 Document Structure and Examples

This Handbook is organized by section to mirror the corresponding requirements in NASA-STD-5019A. The documents applicable to this Handbook are listed in section 2. Acronyms and definitions are listed in section 3. Section 4 provides guidance for general requirements and responsibilities in fracture control. Sections 5, 6, and 7 address hardware classified as exempt, nonfracture critical, and fracture critical, respectively. Section 8 deals with screening, traceability, and material selection. Section 9 addresses documentation and verification, while section 10 discusses implementation of alternative approaches for fracture control. Section 11 is a new section and does not have a corresponding section in NASA-STD-5019A; it covers special topics such as additive manufacturing materials, composite analysis, leak before burst, proof test logic, and many other special topics associated with damage tolerance verification.

Examples presented in Volume 2 are based on historical experience from past programs, but the presentation of these examples does not automatically imply that the Responsible Fracture Control Board (RFCB) will accept it for future programs as the circumstances (e.g., heritage, flight experience) can vary from program to program.

Some of the examples were selected from journal papers and nonpeer-reviewed conference papers; conference publications may have gone through extensive peer review under the publishing organization. The creation of this Handbook incorporated reviews by experts within NASA and other non-NASA industry experts.

NASA-HDBK-5010, VOLUME 2, REVISION A

2. REFERENCE DOCUMENTS

2.1 General

Documents listed in this section provide references supporting the guidance in this Handbook. Latest issuances of reference documents apply unless specific versions are designated. Access reference documents at <https://standards.nasa.gov> or obtain documents directly from the Standards Developing Body, other document distributors, information provided or linked, or by contacting the office of primary responsibility designee for this Handbook.

2.2 Government Documents

Department of Defense

DOT/FAA/CT-86/39, Report No. NADC 87042-60, October 1986, Eq. 17, Certification Testing Methodology for Composite Structures, Volume II

MIL-HDBK-17F, Vol 3, Eq. 7.6.3, Certification Testing Methodology for Composite Structures, Vol II, DOT/FAA/CT-86/39, Report No. NADC-87042-60, Oct. 1986, Eq. 17

MIL-PRF-26514, Polyurethane Foam, Rigid or Flexible, for Packaging

SMC-S-016, Test Requirements for Launch, Upper-Stage, and Space Vehicles

Federal

FED-STD-101C(4) (Cancelled), Test Procedures for Packaging Materials
(The shock test procedure in cancelled FED-STD-101C(4) is clear, detailed, and preferred.)

NASA

NPR 1441.1, NASA Records Management Program Requirements

NPR 7120.5, NASA Space Flight Program and Project Management Requirements

NPR 8705.2, Human-Rating Requirements for Space Systems

NASA-STD-5001, Structural Design and Test Factors of Safety for Spaceflight Hardware

NASA-STD-5009, Nondestructive Evaluation Requirements for Fracture Critical Metallic Components

NASA-STD-5012B, Strength and Life Assessment Requirements for Liquid-Fueled Space Propulsion System Engines

APPROVED FOR PUBLIC RELEASE – DISTRIBUTION IS UNLIMITED

NASA-HDBK-5010, VOLUME 2, REVISION A

NASA-STD-5017A, Design and Development Requirements for Mechanisms

NASA-STD-5018, Strength Design and Verification Criteria for Glass, Ceramics, and Windows in Human Space Flight Applications

NASA-STD-5019A, Fracture Control Requirements for Spaceflight Hardware

NASA-STD-5020, Requirements for Threaded Fastening Systems in Spaceflight Hardware

NASA-STD-5021, Thermal Protection System Design Standard for Crewed Spacecraft

NASA-STD-6008 (Superseded by NASA-STD-8739.14), NASA Fastener Procurement, Receiving Inspection, and Storage Practices for Spaceflight Hardware

NASA-STD-6016, Standard Materials and Processes Requirements for Spacecraft

NASA-STD-6030, Additive Manufacturing Requirements for Spaceflight Systems

NASA-STD-6033, Additive Manufacturing Requirements for Equipment and Facility Control

NASA-STD-8739.14, NASA Fastener Procurement, Receiving Inspection, and Storage Practices for Spaceflight Hardware

NASA-HDBK-6007, Handbook for Recommended Material Removal Processes for Advanced Ceramic Test Specimens and Components

NASA/CR-1999-209427, Guidelines for Proof Test Analysis

NASA/CR-2012-217347, Chang, J.B., Goyal, V.K., Klug, J.C., and Rome, J.I. "Composite Structures Damage Tolerance Analysis Methodologies," March 2012

NASA SP-8052, *Liquid Rocket Engine Turbopump Inducers*, NASA Space Vehicle Design Criteria (Chemical Propulsion), 1971

NASA/TM-2003-2 12420, "Advanced Durability and Damage Tolerance Design and Analysis Methods for Composite Structures: Lessons Learned From NASA Technology Development Programs," Charles E. Harris, James H. Starnes, Jr., and Mark J. Shuart

NASA/TM-102165, Behavior of Surface and Corner Cracks Subjected to Tensile and Bending Loads in Ti-6Al-4V Alloy, 1990

NASA/TM-2002-211737, "Mixed-Mode Decohesion Finite Elements for the Simulation of Delamination in Composite Materials." Camanho, P.P., and Dávila, C.G. Hampton, VA, June 2002

APPROVED FOR PUBLIC RELEASE – DISTRIBUTION IS UNLIMITED

NASA-HDBK-5010, VOLUME 2, REVISION A

NASA/TP-2020-220584, "Evaluation of Fatigue Damage Accumulation Functions for Delamination Initiation and Propagation." Dávila, Carlos G., Cheryl A. Rose, Gretchen B. Murri, Wade C. Jackson, and William M. Johnston. Hampton, VA, April 2020

NASA/TM-2020-5006765, "Composite Overwrapped Pressure Vessel (COPV) Damage Tolerance Life Analysis Methodology and Test Best Practices," August 2020: Volumes I/II

KDP-KSC-F-2616A, KSC Councils, Boards, and Committees Charter

JSC 20793, Crewed Space Vehicle Battery Safety Requirements

JSC 25863C, Fracture Control Plan for JSC Space-Flight Hardware

JSC 66901, Damage Threat Assessment and Damage Control Plan Template for Composite Overwrapped Pressure Vessels

JSC-67035A, Best Practices and Guidelines (BP&G) for Thin Wall Pressure Boundaries (TWPB) for Human Spaceflight Applications

MSFC-RQMT-3479, Fracture Control Requirements for Composite and Bonded Vehicle and Payload Structures

MSFC-STD-3029, Guidelines for the Selection of Metallic Materials for Stress Corrosion Cracking Resistance in Sodium Chloride Environments

MWI 8071.1, Fracture Control Board

MA2-00-057, PSRP letter on Mechanical Systems Safety, September 28, 2000, in NSTS/ISS 18798b, "Interpretations of NSTS/ISS Payload Safety Requirements"

NSTS 07700, Volume X, Book 1, Revision M, NASA Space Shuttle-Flight and Ground System Specification, Requirements

NASA/TM-2020-5006765/Volume I, NESC-RP-16-01183, NASA Technical Memo (TM) entitled "Composite Overwrapped Pressure Vessel (COPV) Damage Tolerance Life Analysis Methodology and Test Best Practices"

2.3 Non-Government Documents

Ainsworth, R.A., "The Assessment of Defects in Structures of Strain Hardening Materials." Engineering Fracture Mechanics, Vol. 19, 1984, p. 633

Airoldi, Alessandro, and Dávila, C.G. "Identification of Material Parameters for Modelling Delamination in the Presence of Fibre Bridging." Composite Structures 94, No. 11 (2012): 3240–49

APPROVED FOR PUBLIC RELEASE – DISTRIBUTION IS UNLIMITED

NASA-HDBK-5010, VOLUME 2, REVISION A

Bisagni, C., Vescovini, R., and Dávila, C.G. "Single-Stringer Compression Specimen for the Assessment of Damage Tolerance of Postbuckled Structures." *Journal of Aircraft* 48, No. 2 (2011): 495–502

Blach, Harry, *Turbo Charger Impeller*, GrabCAD, 2020, <https://grabcad.com/library/turbo-charger-impeller-2>

Boyer, R.R.; Spurr, W.F. (January 1978). "Characteristics of Sustained-Load Cracking and Hydrogen Effects in Ti-6Al-4V," *Metallurgical Transactions A*. Vol. 9A, pp. 23-29

Chang, J. B., "Implementation Guidelines for ANSI/AIAA S-081: Space Systems Composite Overwrapped Pressure Vessels Test Requirements," SMC-TR-03-07

Chang, J., and Seibold, R. "Operational Guidelines for Spaceflight Pressure Vessels," ATR-2005(5128)-1, 31 March 2005

Goyal, V.K., Babuska, P., Patel, D., Chen, Z., Maghsoudy-Louyeh, S., Maqueda, I. and Gutierrez, J., 2021. "Composite Damage Tolerance Approach for Reusable Launch Vehicle Applications." In *AIAA Scitech 2021 Forum* (p. 1166). (<https://arc.aiaa.org/doi/pdfplus/10.2514/6.2021-1166>)

Cotter, K.H. Leak-Before-Burst Criteria Applied to Cryoformed Pressurant Tanks, AIAA-86-1503

Babuska, P., Goyal, V.K., Maqueda, I., Gutierrez, J. and Carpenter, T., 2020. "Damage Tolerance Approach for Composite Space Structures with Curved Bends." In *AIAA Scitech 2020 Forum* (p. 1214). (<https://arc.aiaa.org/doi/abs/10.2514/6.2020-1214>)

Dávila, C.G., Camanho, P.P., and Turon, A. "Effective Simulation of Delamination in Aeronautical Structures Using Shells and Cohesive Elements." *Journal of Aircraft* 45, No. 2 (April 2008): 663–72

Glaessgen, E.H., Riddell, W.T., Raju, I.S. (2002). Nodal constraint, shear deformation and continuity effects related to the modeling of debonding of laminates, using plate elements. *CMES*, 3, 103-116

Golinveaux, F.S., Lynch, C.S., Sagrillo, C.N., Rivera, K.B., Rome, J., McLouth, T.D., and Lohser, J.R. "Fracture Behavior of Thin-Walled Inconel® 718 Manufactured with Selective Laser Melting," AIAA 2020-1473

Goyal, V., "Analytical Modeling of the Mechanics of Nucleation and Growth of Cracks," Ph.D. dissertation. Virginia Tech, 2002

APPROVED FOR PUBLIC RELEASE – DISTRIBUTION IS UNLIMITED

NASA-HDBK-5010, VOLUME 2, REVISION A

Goyal, V.K. "Computational Techniques for the Thermostructural Analysis of Composites", AIAA SciTech Forum (AIAA 2015-0462)

Goyal, V.K., Higuera, B., and Friedman, D. "Fatigue of a Shaft with a Surface Flaw Subject to Cyclic Torsion Loads," AIAA 2018-1470, 7 Jan 2018

Goyal, V.K., Jaunky, N.R., Johnson, E.R., and Ambur, D.R. "Intralaminar and Interlaminar Progressive Failure Analysis of Composite Panels with Circular Cutouts," Composite Structures 64 (2004), pp 91-105

Goyal, V.K., Johnson, E.R., and Davila, C.G. "Irreversible constitutive law for modeling the delamination process using interfacial surface discontinuities," Composite Structures 65 (2004), pp 289-305

Goyal, V.K., Johnson, E.R., and Goyal, V.K. "Predictive Strength – Fracture Model for Composite Bonded Joints," Composite Structures 82 (2008), pp 434-446

Goyal, V.K., and Rome, J.I. "Failure Modeling and Simulation of Composites Subjected to Bypass and Bearing Loads," 47th AIAA Structures, Structural Dynamics, and Materials Conference, Newport, RI, May 2006, (AIAA 2006-2172)

Goyal, V.K., and Rome, J.I. "Analysis Methodology for Assessing Delaminations in Composite Overwrapped Pressure Vessels," 53rd AIAA/ASME/ASCE/AHS/ASC Structures, Structural Dynamics, and Materials Conference, Honolulu, HI, 23-26 April 2012, (AIAA 2012-1614)

Goyal, V.K., Rome, J.I., and Klug, J.C. "Burst Pressure Predictions of Composite Cylindrical Vessels with Wrinkled Plies," 41st AIAA/ASME/SAE/ASEE Joint Propulsion Conference and Exhibit, Tucson, Arizona, July 2005, (AIAA 2005-3612)

Goyal, V.K., Rome, J.I., and Schubel, P.M. "Structural Analysis of Solid Rocket Motor Cases," 49th AIAA Structures, Structural Dynamics, and Materials Conference, Schaumburg, IL, April 7-10, 2008, (AIAA 2008-2110)

Goyal, V., Sagrillo, C., Ni, Y. "Key Requirements and Challenges for Space Vehicle Bellows Designs," 2021 AIAA SciTech Forum (AIAA-2021-1618)

Goyal, V.K., Schubel, P.M., and Rome, J.I. "Enhancement to the Interfacial Element Formulation for the Prediction of Delamination," 48th AIAA Structures, Structural Dynamics, and Materials Conference, Honolulu, HI, April 2007 (AIAA 2007-2095)

Chen, H., Chiu, S. and Chang, J., 1999. "Impact damage effects on Gr/Ep composite overwrapped pressure vessels". In 40th Structures, Structural Dynamics, and Materials Conference and Exhibit (p. 1321)

Janssen, Zuidema & Wanhill, "Fracture Mechanics," 2nd ed, 2002

APPROVED FOR PUBLIC RELEASE – DISTRIBUTION IS UNLIMITED

NASA-HDBK-5010, VOLUME 2, REVISION A

Johnson, E.C., and Nokes, J.P. Nondestructive Evaluation (NDE) Techniques Assessment for Graphite/Epoxy (Gr/Ep) Composite Overwrapped Pressure Vessels, TR-98(8504)-3, The Aerospace Corporation, October 1998

König, M., Krüger, R., Rinderknecht, S. (2000) Finite element analysis of delamination growth in a multidirectional composite ENF specimen. *Composite Materials: Theory and Practice*, ASTM STP 1383. American Society for Testing and Materials

Krueger, R. “Virtual crack closure technique: History, approach and applications.” *Applied Mechanics Reviews*, 57, 109-143 (2004)

Krueger, Ronald. “Development of benchmark examples for quasi-static delamination propagation and fatigue growth predictions.” SIMULIA Community Conference, Providence, RI, May 14-17, 2012

Kumar, V., German, M.D., Shih, C.F., “An Engineering Approach for Elastic-Plastic Fracture Analysis”, Electric Power Research Institute – Nuclear Power Division, Palo Alto, CA, 1981

Landgraf, R.W., Morrow, JoDean, and Endo, T. “Determination of the Cyclic Stress-Strain Curve,” *Journal of Materials (JMLSA)*, Vol 4, No. 1, March 1969, pp. 176–188

Leone, F.A., Dávila, C.G., and Girolamo, D. “Progressive Damage Analysis as a Design Tool for Composite Bonded Joints.” *Composites Part B: Engineering* 77, no. 0 (2015): 474–83.
<http://dx.doi.org/10.1016/j.compositesb.2015.03.046>

Levesque, G. “Critical Flaw Size in Silicon Nitride Ball Bearings.” University of Florida

Lewis, J.C., Kenny, J.T. (July 1976). *Sustained Load Crack Growth Design Data for Ti-6Al-4V Titanium Alloy Tanks Containing Hydrazine*. Paper presented at AIAA/SAE 12th Propulsion Conference. Palo Alto, CA

Liang, Yu-Jui, Dávila, C.G., and Iarve E.V. “A Reduced-Input Cohesive Zone Model with Regularized Extended Finite Element Method for Fatigue Analysis of Laminated Composites in Abaqus.” *Composite Structures*, August 3, 2021, 114494.
<https://doi.org/10.1016/j.compstruct.2021.114494>

McClung, R.C., Chell, G.G., Lee, Y.D., Russel, D.A., Orient, G.E., “Development of a Practical Methodology for Elastic-Plastic and Fully Plastic Fatigue Crack Growth”, NASA/CR-1999-209428, 1999

Newman, J. C., Jr., “A Crack Opening Stress Equation for Fatigue Crack Growth,” *International Journal of Fracture*, No. 24, 1984, pp. 131-135

APPROVED FOR PUBLIC RELEASE – DISTRIBUTION IS UNLIMITED

NASA-HDBK-5010, VOLUME 2, REVISION A

O'Brien, M.J., de la Cruz, A.R., Nguyen, E.A. "A Novel Proof Test for Silicon Nitride Balls," Journal of the American Ceramic Society, Volume 94, Issue 2, February 2011

Orange, T.W., Sullivan, T.L., and Calfo, F.D., "Fracture of Thin Sections Containing Through and Part-Through Cracks", Fracture Toughness Testing at Cryogenic Temperatures, ASTM STP 496, American Society for Testing and Materials, 1971, pp. 61-81

Rooke, D.P., and Cartwright, D.J. Compendium of Stress Intensity Factors, 1976

Koontz, E., Goyal, V.K., Mueller, D., Friedman, D. and Maghsoudy-Louyeh, S., 2018. Proof test methodology for reducing the risk of unvented honeycomb core failures in aerospace structures. In 2018 AIAA/ASCE/AHS/ASC Structures, Structural Dynamics, and Materials Conference (p. 1709).(<https://arc.aiaa.org/doi/pdfplus/10.2514/6.2018-1709>)

Reeder, J. "3D Mixed-Mode Delamination Fracture Criteria—An Experimentalist's Perspective" <https://ntrs.nasa.gov/api/citations/20060048260/downloads/20060048260.pdf>

Rome, J., Goyal, V., Patel, D. "Fatigue Fracture of AM Inconel 718: Surface Effects on Tension-Torsion Capability" 2021 AIAA SciTech Forum (AIAA-2021-1401)

Rome, J.I., Schubel, P.M., and Goyal, V.K. "Prediction of Low Velocity Impact Damage in a Composite Sandwich using a Progressive Failure Methodology," paper presented at the 22nd ASC Technical Conference

Rome, J., Soltz, B.E., Goyal, V.K. "Key Elements of the Qualification, Workmanship, and Design Verification of Additively Manufactured Parts," 2020 AIAA Scitech Forum (AIAA 2020-1474)

Rybicki, E.F., and Kanninen, M.F. "A Finite Element Calculation of Stress Intensity Factors by a Modified Crack Closure Integral," Engineering Fracture Mechanics Volume 9, Issue 4, 1977, Pages 931-938

Sagrillo, C.S., Shimizu, L., Goyal, V.K. "Elastic Plastic Fracture Mechanics Guidance and Analysis Validation," AIAA, SciTech Conference, 2022

Schubel, P.M., Luo, J.J., and Daniel, I.M. 2007. "Impact and Post Impact Behavior of Composite Sandwich Panels," Composites: Pt. A, 38: 1051-1057

Schubel, P.M., Rome, J.I., and Goyal, V.K. "Predicting Failure of Damaged Composite Sandwich Structures Using Compression- After- Impact Strength Data," 50th AIAA Structures, Structural Dynamics, and Materials Conference, Palm Springs, CA, May 4-7, 2009, (AIAA 2009-2552)

Sih, G.C., (Ed.), Mechanics of Fracture, Noordhoof International Publishing, Leyden, 1973

APPROVED FOR PUBLIC RELEASE – DISTRIBUTION IS UNLIMITED

NASA-HDBK-5010, VOLUME 2, REVISION A

Tada, H., Paris, P.C., and Irwin, G.R. The Stress Analysis of Cracks Handbook, Del Research Corp., St. Louis, Missouri, 1973

Takahashi, Y. Comprehensive Structural Integrity, 7.10 Leak Before Break

Tang, C.Y., Foerster, C., O'Brien, M.J., Hardy, B.S., Goyal, V.K., Nelson, B.A., Robinson, E.Y., Ward, P.C. "A Study on the Effects of Ball Defects on the Fatigue Life in Hybrid Bearings," The 42nd Aerospace Mechanism Symposium, Access Link - <https://ntrs.nasa.gov/api/citations/20150004053/downloads/20150004053.pdf>

Tapphorn, R.M., Test Report, Impact Damage Effects and Control Applied to Composite Overwrapped Pressure Vessels, TR-806-001, NASA Johnson Space Center, White Sands Test Facility, July 29, 1998

Underwood, et al. (ARCCB-TR-94017, Yield Before Break Fracture Mechanics Analysis of High Strength Steel Pressure Vessels, 1994)

Turon, A., Dávila, C.G., Camanho, P.P., and Costa, J. "An Engineering Solution for Mesh Size Effects in the Simulation of Delamination Using Cohesive Zone Models." Engineering Fracture Mechanics 74 (10): 1665–82. (2007)

Turon, A., González, E.V., Sarrado, C., Guillaumet, G., and Maimí, P. "Accurate Simulation of Delamination under Mixed-Mode Loading Using a Cohesive Model with a Mode-Dependent Penalty Stiffness." Composite Structures 184, No. Supplement C (January 15, 2018): 506–11 <https://doi.org/10.1016/j.compstruct.2017.10.017>

Versino, D., Mourad, H.M., Dávila, C.G., and Addessio, F.L. "A Thermodynamically Consistent Discontinuous Galerkin Formulation for Interface Separation." Composite Structures 133 (2015): 595–606. <http://dx.doi.org/10.1016/j.compstruct.2015.07.080>

Zerbst, U., Schodel, M., Webster, S., Ainsworth R. "Fitness-for-Service Fracture Assessment of Structures Containing Cracks," First Edition, Academic Press, Oxford, 2007

ECSS-E-HB-32-26A, Spacecraft Mechanical Loads Analysis Handbook (19 February 2013)

Aerospace Industries Association (AIA)/National Aerospace Standards (NAS)

AIA/NAS NAS410, NAS Certification and Qualification of Nondestructive Test Personnel

NASM1312-11, Fastener Test Methods, Method 11 Tension Fatigue

NASM1312-111, Fastener Test Methods, Metric Method 111 Tension Fatigue

APPROVED FOR PUBLIC RELEASE – DISTRIBUTION IS UNLIMITED

NASA-HDBK-5010, VOLUME 2, REVISION A

American National Standards Institute (ANSI)/American Institute of Aeronautics and Astronautics (AIAA)

ANSI/AIAA S-080-1998 and S-080A-2018, Space Systems - Metallic Pressure Vessels, Pressurized Structures, and Pressure Components

ANSI/AIAA S-081-2000, S-081A-2006, and S-081B-2018, Space Systems – Composite Overwrapped Pressure Vessels (COPVs)

ASTM International (formerly American Society for Testing and Materials)

ASTM D775-80(1986) (Withdrawn), Method for Drop Test for Loaded Boxes (Withdrawn in 1993 and replaced by ASTM D5276-98)

ASTM D895-94 (Withdrawn), Standard Test Method for Water Vapor Permeability of Packages (Withdrawn but provides appropriate test procedures)

ASTM D1083-91(1998) (Withdrawn), Standard Test Methods for Mechanical Handling of Unitized Loads and Large Shipping Cases and Crates (Provides appropriate test procedures)

ASTM D1974–98(2003), Standard Practice for Methods of Closing, Sealing, and Reinforcing Fiberboard Boxes

ASTM D4169-04, Standard Practice for Performance Testing of Shipping Containers and Systems

ASTM D5528, Standard Test Method for Mode I Interlaminar Fracture Toughness of Unidirectional Fiber-Reinforced Polymer Matrix Composites

ASTM D6115-97, Standard Test Method for Mode I Fatigue Delamination Growth Onset of Unidirectional Fiber-reinforced Polymer Matrix Composites

ASTM D7905/7905M, Standard Test Method for Determination of the Mode II Interlaminar Fracture Toughness of Unidirectional Fiber-Reinforced Polymer Matrix Composites

ASTM E399, Standard Test Method for Linear-Elastic Plane-Strain Fracture Toughness K_{Ic} of Metallic Materials

ASTM E606, Standard Test Method for Strain-Controlled Fatigue Testing

ASTM E647-15, Standard Test Method for Measurement of Fatigue Crack Growth Rates

ASTM E740/E740M, Standard Practice for Fracture Testing with Surface-Crack Tension Specimens

ASTM E1049-85, Standard Practices for Cycle Counting in Fatigue Analysis

APPROVED FOR PUBLIC RELEASE – DISTRIBUTION IS UNLIMITED

NASA-HDBK-5010, VOLUME 2, REVISION A

ASTM E1681, Standard Test Method for Determining Threshold Stress Intensity Factor for Environment-Assisted Cracking of Metallic Materials

ASTM E1820, Standard Test Method for Measurement of Fracture Toughness

ASTM E1823, Standard Terminology Relating to Fatigue and Fracture Testing

ASTM E2899-19, Standard Test Method for Measurement of Initiation Toughness on Surface Cracks Under Tension and Bending

ASTM F2094-14, Standard Specification for Silicon Nitride Bearing Balls

Battelle

MMPDS, Metallic Materials Properties Development and Standardization

BSI Group

BS7910, Guide to methods for assessing the acceptability of flaws in metallic structures

Composite Materials Handbook (CMH)

CMH-17, Composite Materials Handbook

National Aerospace Standards

NA0271, Metric Fasteners, CRES 300 Series, Externally Threaded, MJ Thread, 500 MPa F_{su} and 700 MPa F_{tu}

NAS4003, Fastener, A286 Corrosion Resistant Alloy, Externally Threaded, 160 ksi F_{tu} , 95 ksi F_{su} , 1000 °F

NASM1312-11, Fastener Test Methods - Method 11 - Tension Fatigue

NASM85604, Bolt, Nickel Alloy 718, Tension, High Strength, 125 ksi F_{su} and 220 ksi F_{tu} , High Temperature, Spline Drive

SAE International

SAE AS7468, Bolts, Cobalt-Chromium-Nickel Alloy, UNS R30035, Tensile Strength 260 ksi, Procurement Specification

APPROVED FOR PUBLIC RELEASE – DISTRIBUTION IS UNLIMITED

NASA-HDBK-5010, VOLUME 2, REVISION A

Southwest Research Institute

NASGRO® Reference Manual, Version 9.2, Southwest Research Institute, 2020

2.4 Order of Precedence

2.4.1 The guidance established in this Handbook does not supersede or waive existing guidance found in other Agency documentation.

2.4.2 Conflicts between this Handbook and other documents will be resolved by the delegated Technical Authority.

3. ACRONYMS, ABBREVIATIONS, SYMBOLS, AND DEFINITIONS

3.1 Acronyms, Abbreviations, and Symbols

ΔK_{th}	cyclic threshold stress intensity range
<	less than
>	greater than
$\sqrt{\quad}$	square root
ω	maximum operating rotational speed in radians/sec
®	registered trademark
AE	acoustic emission
AIA	Aerospace Industries Association
AIAA	American Institute of Aeronautics and Astronautics
Al	aluminum
AM	additive manufacturing; additively manufactured
ANSI	American National Standards Institute
API	American Petroleum Institute
ARC	Ames Research Center
ASME	The American Society of Mechanical Engineers
ASTM	ASTM International (formerly American Society of Testing and Materials)
atm	atmosphere
BAI	burst after impact
BBA	building block approach
BEM	boundary element model
BPVC	Boiler and Pressure Vessel Code
CAI	compression after impact
CAIB	Columbia Accident Investigation Board
CDI	cumulative damage index
CFS	critical flaw size
CLA	coupled loads analysis
cm	centimeter(s)

APPROVED FOR PUBLIC RELEASE – DISTRIBUTION IS UNLIMITED

NASA-HDBK-5010, VOLUME 2, REVISION A

CM	cage module
CMH	Composite Materials Handbook
CMOD	Crack mouth opening displacement
COPV	composite overwrapped pressure vessel
COSAP	COPV Stress Analysis Program
cp-Ti	commercially pure titanium
CR	centrifuge rotor
CRES	corrosion resistant (steel)
CZM	cohesive-decohesive zone model
D	dimensional
DCB	double cantilever beam
DFMR	design for minimum risk
DIC	digital image correlation
DLL	design limit load
DOT	Department of Transportation
DPI	dye penetrant inspection
DTA	damage threat assessment
DUL	design ultimate load
EAC	environmentally assisted cracking
EBSD	electron backscatter diffraction
ECF	environmental correction factor
ECS	environmental control system
EDM	electric discharging machining
ELS	end load split
ENF	end notch flexure
EPFCG	elastic-plastic fatigue crack growth
EPFM	elastic plastic fracture mechanics
EPRI	Electric Power Research Institute
EVA	extravehicular activity
F	Fahrenheit
F_{su}	ultimate shear strength
F_{tu}	ultimate tensile strength
F_{ty}	yield tensile strength
FAA	Federal Aviation Administration
FAD	failure assessment diagram
FAF	fatigue/fracture analysis factor
FC	fracture control
FCC	fracture control coordinator
FCP	Fracture Control Plan Fracture Control Panel
FCR	fracture control requirement
FCSR	Fracture Control Summary Report

APPROVED FOR PUBLIC RELEASE – DISTRIBUTION IS UNLIMITED

NASA-HDBK-5010, VOLUME 2, REVISION A

FEM	finite element model
FEMA	failure mode and effects analysis
FOD	foreign object debris
fps	frames per second
FS	failsafe
FSP	fluctuating surface pressure
ft	foot (feet)
ft-lb	foot-pound(s)
ft-lb-sec	foot-pound-sec (s)
G	gravity
GRC	Glenn Research Center
GSFC	Goddard Space Flight Center
HCF	high-cycle fatigue
HD	hardware developer
HDBK	handbook
hr	hour(s)
IC	impact control
ICP	impact control plan
IDC	impact damage control
IDMP	Impact Damage Mitigation Plan
IMIT	instrumented mechanical impact tester
IML	inner mold line
in	inch
IR	infrared
ISS	International Space Station
J	Joule(s)
J_c	critical J-integral fracture toughness
J_{Ic}	plane strain J-integral fracture toughness
JPL	Jet Propulsion Laboratory
JSC	Johnson Space Center
K	stress intensity factor
K_c	plane stress fracture toughness
KE	kinetic energy
K_{EAC}	stress intensity factor threshold for EAC in a specific thickness
K_{Ic}	plane strain fracture toughness
K_{Ie}	effective fracture toughness
K_{IEAC}	stress intensity factor threshold for plane strain environmentally assisted cracking
K_{ISCC}	stress intensity factor threshold for plane strain stress corrosion cracking
K_{Jic}	stress intensity factor determined from the plane strain J-integral fracture toughness
K_{SLC}	stress intensity factor threshold for sustained load cracking

APPROVED FOR PUBLIC RELEASE – DISTRIBUTION IS UNLIMITED

NASA-HDBK-5010, VOLUME 2, REVISION A

kip	kilopound
kPa	kilopascal
KSC	Kennedy Space Center
ksi	kip(s) per square inch
LaRC	Langley Research Center
lb/lbs	pound(s)
LBB	leak-before-burst
LEF	load enhancement factor
LEFCG	linear-elastic fatigue crack growth
LEFM	linear-elastic fracture mechanics
LME	liquid-metal embrittlement
m	meter(s)
M&P	materials and processes
mA	milliampere
MAFS	maximum acceptable flow size
MDCP	Mechanical Damage Control Plan
MDFC	minimum detectable flaw size
MDP	maximum design pressure
MEOP	maximum expected operating pressure
MIL	military
mm	millimeter
MMB	mixed mode bend
MMOD	micro-meteoroid and orbital debris
MMPDS	Metallic Materials Properties Development and Standardization
MPa	megapascal(s)
MPS	material property suite
MR	material review
MRB	Material Review Board
MSA	multipurpose space adapter
MSFC	Marshall Space Flight Center
MUA	Materials Usage Agreement
MWI	Marshall Work Instruction
NAS	National Aerospace Standard
NASA	National Aeronautics and Space Administration
NASGRO®	fracture mechanics and fatigue crack growth analysis software
NDE	nondestructive evaluation
NDI	nondestructive inspection
NDT	nondestructive testing
NFC	nonfracture critical
NHLBB	nonhazardous-leak-before-burst
N-m	Newton-meter (s)
N-m-s	Newton-meter-second (s)

APPROVED FOR PUBLIC RELEASE – DISTRIBUTION IS UNLIMITED

NASA-HDBK-5010, VOLUME 2, REVISION A

NPR	NASA Procedural Requirements
NSTS	NASA Space Transportation System
OD	optical density
OML	outer mold line
PBF	powder bed fusion
PE	potential energy
PFA	Predictive failure analysis
PoD	probability of detection
PRC	process specification
PSD	power spectral density
psi	pound(s) per square inch
psia	pound(s) per square inch absolute
PTC	partly through crack
QA	quality assurance
QMP	qualified material process
rev-s	revolutions per second
RFCB	Responsible Fracture Control Board
RLV	reusable launch vehicle
RPM	revolutions per minute
RQMT	requirement
RSM	reference stress method
RTD	residual threat determination
SAE	Society of Automotive Engineers
SCC	stress corrosion cracking
SEA	statistical energy analysis
SEM	scanning electron microscope
SERR	strain energy release rate
SI	Système Internationale or metric system of measurement
SIF	stress intensity factor
SLC	sustained load cracking
SLS	Space Launch System
SMA	Safety and Mission Assurance
SME	subject matter experts
SPEC	specification
sqrt	square root
SSY	small scale yielding
STA	solution treated and aged
STD	standard
Ti	titanium
TM	technical memorandum
TPFM	two parameter fracture mechanics

APPROVED FOR PUBLIC RELEASE – DISTRIBUTION IS UNLIMITED

NASA-HDBK-5010, VOLUME 2, REVISION A

TPS	thermal protection system
UT	ultrasonic testing
UTS	ultimate tensile strength
UV	ultraviolet
V	Vanadium
VAA	vibro-acoustic analysis
VCCT	virtual crack closure technique
VDT	visual damage threshold
WCC	worst-case credible

3.2 Definitions

A-Basis: A statistically calculated number that at least 99 percent of the population of values is expected to equal or exceed with a confidence of 95 percent.¹

Adhesive Bond (Bond): The joining of parts, components, or materials using a joining substance or agent.

Assembly/Assemblage: An integral arrangement of parts that make up an individual unit and that act as a whole.

B-Basis: A statistically calculated value that at least 90 percent of the population is expected to equal or exceed with a confidence of 95 percent.²

Bond: The joining of two parts through molecular attraction or through any nonmechanical means of connection.

Bonded Hardware (Structure): Hardware (structure) that is assembled using parts that are joined together with an adhesive.

Brittle Fracture: Sudden rapid fracture under stress (residual or applied) where the material exhibits little or no evidence of ductility or plastic deformation.

Building Block Approach (BBA): A development methodology often used with composites or bonded hardware that (a) starts with selecting the material system and manufacturing approach; (b) moves on to experimentation and analysis of small samples to characterize the system and quantify behavior in the presence of flaws and damage; (c) progresses to examining larger structures to examine buckling behavior, combined loadings, and built-up structures in the presence of credible damage; and (d) finally moves to complicated subcomponents and full-scale components to establish their damage tolerance strength and life. Each step along the way is

¹ See NASA-STD-6016, Standard Materials and Processes Requirements for Spacecraft; CMH-17, Composite Materials Handbook; Metallic Materials Properties Development and Standardization (MMPDS), Appendix A.2, as appropriate.

² See NASA-STD-6016; CMH-17, MMPDS (Appendix A.2), as appropriate.

NASA-HDBK-5010, VOLUME 2, REVISION A

supported by detailed analysis to validate that the behavior of these structures is well understood and predictable.

Catastrophic Event: Loss of life, disabling injury, or loss of a major national asset.

Catastrophic Failure: A failure that directly results in a catastrophic event.

Catastrophic Hazard: Presence of a risk situation that could directly result in a catastrophic event.

Component: A hardware unit considered a single entity for the purpose of fracture control. A component contains at least one part.

Composite Hardware (Structure): Hardware (structure) assembled with parts made from composite materials.

Composite Material: A combination of materials differing in composition or form on a macro scale. The constituents retain their identities in the composite; that is, they do not dissolve or otherwise merge completely into each other, although they act in concert. Normally, the constituents can be physically identified and exhibit an interface between one another. Composite material is not intended to mean an assembly of parts.

Composite or Bonded Structure: Structure (excluding overwrapped pressure vessels or pressurized components) of fiber/matrix configuration and structure with load-carrying nonmetallic bonding agents, such as sandwich structure or bonded structural fittings.

Composite Overwrapped Pressure Vessel: A pressure vessel with a composite structure fully or partially encapsulating a metallic liner. The liner serves as a fluid (gas and/or liquid) permeation barrier and may carry substantial pressure loads. The composite generally carries pressure and environmental loads.

Contained: A condition in which a suitable housing, container, barrier, restraint, etc., prevents a part or pieces thereof from becoming free bodies if the part or its supports fail.

Contamination: Any material included within or on the hardware that is not called for on the engineering drawings. Examples of contamination are dust, grease, solvent, and solid objects.

Crack or Crack-like Defect: A discontinuity assumed to behave like a crack for fracture control purposes.

Critical Stress Intensity Factor: The stress intensity factor at the initiation of crack growth in the part resulting in a catastrophic failure that is representative of the failure mode of concern for the metallic material process condition, weakest orientation, and thickness being evaluated. Examples for metallic materials may include: K_{IEAC} , the stress intensity factor threshold for plane strain environment-assisted cracking; plane strain fracture toughness (K_{Ic}) may be appropriate for

NASA-HDBK-5010, VOLUME 2, REVISION A

thick sections and/or as a lower bound value³; effective fracture toughness (K_{Ie}) is used in NASGRO® for crack growth analyses of surface or elliptical flaws; K_{JIC} calculated from J_{Ic} or a K_c calculated from J_c may be appropriate for the conditions described in ASTM E1820, Standard Test Method for Measurement of Fracture Toughness, such as evaluation of ductile tearing and instability; constraint-based assessments per ASTM E2899, Standard Test Method for Measurement of Initiation Toughness on Surface Cracks Under Tension and Bending; and/or tests may be needed for surface or other complex cracks in materials or conditions that invalidate the ability of linear-elastic fracture mechanics (LEFM) to represent crack growth.

Damage: See definitions of Flaw and Impact Damage.

Damage Threat Assessment (DTA): An evaluation of potential sources of flaws in composite or bonded hardware that includes definition, quantification, and an assessment of the residual strength sensitivity to flaws.

Damage Tolerance: Fracture control design concept under which an undetected flaw or damage (consistent in size with the flaw screening method or residual threat determination [RTD]) is assumed to exist and is shown by fracture mechanics analysis or test not to grow to failure (leak or instability) during the period equal to the service life factor times the service life.

Design Limit Load (DLL): See definition of Limit Load.

Design Ultimate Load (DUL): Limit load multiplied by the ultimate factor of safety.

Environmental Correction Factor (ECF): An adjustment factor used to account for differences between the environment (thermal and chemical) in which a part is used and the environment in which it is tested.

Environmentally Assisted Cracking (EAC): A cracking process in which the environment promotes crack growth or higher crack growth rates than would occur without the presence of the environment (see ASTM E1681, Standard Test Method for Determining Threshold Stress Intensity Factor for Environment-Assisted Cracking of Metallic Materials). An example is available in published literature (Lewis and Kenny, 1976).

Experiment: For fracture control, an arrangement or assemblage of hardware that is intended to investigate phenomena on a provisional, often human-tended, basis.

Fail-safe: A condition where a redundant load path exists within a part (or hardware), so that after loss of any single individual load path, the remaining load paths have sufficient structural capability to withstand the redistributed loads, and the loss of the load path will not cause a catastrophic hazard.

Fastener: For fracture control, any single part that joins other structural elements and transfers loads from one element to another across a joint.

³ Proof test assessments need to use upper bound fracture toughness; see section 8.1.3 of NASA-STD-5019A.

NASA-HDBK-5010, VOLUME 2, REVISION A

Flaw: For metallics, glass, or brittle materials, a crack-like defect. For composite or bonded materials, an anomaly in the hardware that has the potential for adversely affecting strength, damage tolerance life, or must-work function. Examples of flaws in metallics include cracks, deep scratches and sharp notches that behave like cracks, material inclusions, forging laps, welding incomplete fusion, penetration, and slag or porosity with a crack-like tail. Examples of flaws in composite or bonded materials may include cracks, cuts, scratches, delaminations, porosity/voids, disbonds, wrinkles, foreign object debris, impact damage, etc. Damage (used alone) and flaw are equivalent.

Fleet Leader: Articles representative of spaceflight hardware with respect to production methods, e.g., materials, manufacturing, testing, that either have accumulated (or are scheduled to accumulate) more service lifetime in typical (or more severe) environments than the remaining fleet and are monitored for indications of failure modes to provide early warning of known and unexpected risks to the remaining fleet.

Flight (Spaceflight) Hardware: Any hardware (including spares) that is approved to be part of or carried by a launch vehicle, crew module, transfer stage, landing craft, payload, etc.

Flight-like Component: A component assembled and made of parts that are of flight specifications. Flight-like components are usually intended for qualification tests. Any deviations from flight have to be insignificant with respect to test objectives.

Fracture Control Board: A project- or program-specific, multi-disciplinary group of experts responsible for implementing fracture control requirements, establishing a project- or program-specific Fracture Control Plan, and coordinating fracture control activities under the oversight of the NASA RFCB. Some programs or projects may elect to use other titles such as Panel or Committee instead of Board. Some programs or projects may also elect to have an individual serve this purpose (usually smaller payloads or hardware projects). The project- or program-specific Fracture Control Board typically functions at the prime contractor or hardware developer level.

Fracture Critical: Fracture control classification that identifies a part whose individual failure, caused by the presence of a crack, is a catastrophic hazard and requires safe-life analysis or other fracture control assessment to be shown acceptable for flight. A part is fracture critical unless it can be shown that there is no credible possibility for a flaw to cause failure during its lifetime or the part failure does not result in a credible catastrophic hazard. Assessments for fracture critical parts include damage tolerance analysis, damage tolerance test, or defined approaches for specific categories. Parts under this classification receive flaw screening by nondestructive evaluation (NDE), proof test, or process control and are subjected to traceability, materials selection and usage, documentation, and engineering drawing requirements.

Habitable Modules or Volumes: Flight containers/chambers that are designated and designed to support human occupancy.

APPROVED FOR PUBLIC RELEASE – DISTRIBUTION IS UNLIMITED

NASA-HDBK-5010, VOLUME 2, REVISION A

Hardware Developer: Organization directly responsible for design, manufacture, analysis, test, and safety compliance documentation of the hardware. This includes implementing fracture control requirements.

Hazardous Fluid: For fracture control, a fluid the release of which would create a catastrophic hazard. These types of fluids may include liquid chemical propellants, liquid metals, biohazards, and other highly toxic liquids or gases. The release of such fluids would create a hazardous environment such as a danger of fire or explosion, unacceptable dilution of breathing oxygen, an increase of oxygen above flammability limits, over-pressurization of a compartment, or loss of a safety-critical system.

Hazardous Fluid Container: Any single, independent (not part of a pressurized system) container or housing that contains a fluid the release of which would cause a catastrophic hazard and that is not classified as a pressure vessel.

Hazardous Material: For fracture control, a material the release of which would create a catastrophic hazard.

High-Cycle Fatigue (HCF): A high-frequency, low-amplitude loading condition created by structural, acoustic, or aerodynamic vibrations that can propagate flaws to failure. An example of an HCF loading condition is the vibrational loading of a turbine blade because of structural resonance.

Impact Damage: The injury or harm inflicted upon composite or bonded hardware by impingement of an object upon the hardware in question or the bumping or striking between the hardware in question and another object. Impact damage is a subset of the more general term damage (or flaw).

Impact Damage Mitigation Plan (IDMP): A plan for composite or bonded hardware to mitigate risk of impact damage to the flight hardware.

Initial Crack (Flaw) Size: The crack size that is assumed to exist at the beginning of a damage tolerance analysis, as determined by NDE or proof testing.

K_c : Plane stress fracture toughness. The value of stress intensity factor K at the tangency between a crack extension resistance curve (R-curve) and the configuration-dependent applied K curve (see ASTM E1823, Standard Terminology Relating to Fatigue and Fracture Testing). This crack extension occurs under conditions that do not approach crack-tip plane strain. The R-curve and K_c vary with the material, specimen size, and thickness. K_c is used in NASGRO® to represent fracture toughness as a function of thickness for use in crack growth calculations.⁴

⁴ See NASGRO® User Manual where the K_c symbol is defined as “critical stress intensity” and section 2.1.4 that shows K_c as a function of material thickness and describes the usage of K_c .

NASA-HDBK-5010, VOLUME 2, REVISION A

K_{EAC} : The largest value of the stress intensity factor at which crack growth is not observed for a pre-cracked through-crack specimen of specified material, environment, and thickness that is tested for a significant duration in accordance with ASTM E1681.

K_{Ic} : Plane strain fracture toughness. The crack extension resistance under conditions of crack-tip plane strain in Mode I for slow rates of loading under predominantly linear-elastic conditions and negligible plastic-zone adjustment that is measured by satisfying a standardized procedure with validity requirements (see ASTM E399, Standard Test Method for Linear-Elastic Plane-Strain Fracture Toughness K_{Ic} of Metallic Materials). Another quantity, K_{JIC} , defined for conditions with limited plasticity from J_{Ic} may also be useful (see ASTM E1820).

K_{Ie} : Effective fracture toughness for a surface or elliptically shaped crack. The toughness is based on residual strength and the original crack dimensions. This parameter is meaningful only when crack-tip plastic zones are small and stable crack growth before failure is generally absent (see ASTM E740/E740M, Standard Practice for Fracture Testing with Surface-Crack Tension Specimens, main body and section X1.2). For conditions with plastic effects and well-defined crack-tip stress fields with fracture controlled by crack initiation, an approach involving constraint may be applicable (see ASTM E2899). Testing of flaws in specimens representative of the structure is needed to determine damage tolerance for plasticity conditions when crack-tip stress fields collapse. K_{Ie} is used in NASGRO® for analyses of crack growth.⁵

K_{IEAC} : The largest value of the stress intensity factor at which crack growth is not observed for a pre-cracked through-crack specimen of specified material, environment, and thickness that is sufficient to meet requirements for plane strain and is tested for a significant duration in accordance with ASTM E1681.

K_{Isc} : K_{EAC} is often denoted as K_{Isc} in the literature.

ΔK_{th} : Threshold stress intensity factor range below which flaw growth will not occur under cyclic loading conditions.

Leak-Before-Burst (LBB): Characteristic of pressurized hardware whose only credible failure mode at or below maximum design pressure (MDP) with service life loads resulting from the presence of a potential flaw is a pressure-relieving leak at the flaw as opposed to burst or rupture at the critical stress intensity factor. As the hardware item leaks down, there is no re-pressurization or continued pressure cycles that could lead to continued crack growth. In this failure mode, the hardware will not fail in a fragmentary, catastrophic manner. Instead, only small, slow-growing leaks would develop, leaking in a controlled manner. Additional aspects of LBB assessments are described in section 6.2.4 of NASA-STD-5019A.

Life Factor: See definition of Service Life Factor.

⁵ See NASGRO® User Manual where the K_{Ie} symbol is defined as “effective fracture toughness for part-through (surface/corner) crack” and section 2.1.4 that describes how the K_{Ie} value is determined and how it is used.

NASA-HDBK-5010, VOLUME 2, REVISION A

Lifetime: See definition of Service Life. Refers to a specified life, as opposed to an analytically predicted life.

Limit Load: The maximum load expected on the hardware during its design service life, including ground handling, transport to and from orbit, including abort conditions and on-orbit operations.

Limited Life Part: Multi-mission part that has a predicted damage tolerance life that is less than the required service life factor times the complete multi-mission service life. See definition of Service Life Factor.

Load Enhancement Factor (LEF): A factor applied to the service life spectrum to satisfy a specified level of reliability and confidence with fewer cycles than would otherwise be required.

Low-Cycle Loads: A low-frequency, high-amplitude loading condition created by thermal, pressure, or structural loads that can propagate flaws to failure. An example of a low-cycle loading condition is the aerothermal loading of a turbine blade during launch.

Low-Fracture Toughness: Material property characteristic, in the applicable environment, for which the ratio is $K_{Ic}/F_{ty} < 1.66 \sqrt{\text{mm}}$ ($0.33 \sqrt{\text{in}}$). For steel bolts with unknown K_{Ic} , low-fracture toughness is assumed when material A-basis ultimate strength $F_{tu} > 1,241 \text{ MPa}$ (180 ksi). Parts made with materials of this characteristic may be at risk of a brittle fracture.

Materials Usage Agreement (MUA): A formal document showing that a noncompliant material is acceptable for the specific application identified.

Maximum Design Pressure (MDP): The highest possible operating pressure considering maximum temperature, maximum relief pressure, maximum regulator pressure, and, where applicable, transient pressure excursions. MDP for human-rated hardware is a two-failure tolerant pressure, i.e., it will accommodate any combination of two credible failures that will affect pressure. Some programs have defined MDP as a two-fault tolerant pressure.

Maximum Expected Operating Pressure (MEOP): The maximum pressure which pressurized hardware is expected to experience during its service life, in association with its applicable operating environments. MEOP includes the effects of temperature, transient peaks, vehicle acceleration, and relief valve tolerance.

Mechanism: A system of moveable and stationary parts that work together as a unit to perform a mechanical function such as latches, actuators, drive trains, and gimbals.

Mission: A major activity required to accomplish an Agency goal or to effectively pursue a scientific, technological, or engineering opportunity directly related to an Agency goal. Mission needs are independent of any particular system or technological solution (NPR 7120.5, NASA Space Flight Program and Project Management Requirements).

APPROVED FOR PUBLIC RELEASE – DISTRIBUTION IS UNLIMITED

NASA-HDBK-5010, VOLUME 2, REVISION A

Net-Section Stress or Strain: The stresses or strains computed for a hypothetical cut across a part, based on strength-of-materials theory. Possible bending loads can produce stress gradients across the net section, in which case the net-section stress is found to be the maximum combination of tension and bending stress, ignoring geometric stress concentrations. (An example of net-section stress calculation is detailed in the NASGRO® User Manual, Appendix B.)

No-Growth Threshold Strain: For a composite or bonded part, the largest strain range (where strain range is the maximum absolute value of strain in a load cycle) below which flaws compatible with the sizes established by NDE, special visual inspection, the DTA, or the minimum sizes imposed do not grow in 10^6 cycles (10^8 cycles for rotating hardware) at a load ratio appropriate to the application. Thresholds are determined on specimens with flaws for which sufficient load/cycles have been initially applied to cause flaw growth. The no-growth threshold strain is a function of the material and layup and is determined from test data in the appropriate environment for the applicable (or worst) orientation of strain and flaw for a particular design.

Nondestructive Evaluation (NDE): Examination of parts for flaws using established and standardized inspection techniques that are harmless to hardware such as radiography, penetrant, ultrasonic, magnetic particle, and eddy current. NDE is sometimes referred to as nondestructive testing (NDT) or nondestructive inspection (NDI).

Nonhazardous-Leak-Before-Burst (NHLBB): A nonfracture critical classification for metallic pressurized hardware that contains a material that is not hazardous and that exhibits the LBB failure mode in a nonhazardous manner.

Part: Hardware item considered a single entity for the purpose of fracture control.

Pressure Vessel: A container designed primarily for pressurized storage of gases or liquids and that also performs any of the following:

- a. Contains stored energy of 19,307 J (14,240 ft-lbs) or greater based on adiabatic expansion of a perfect gas.
- b. Stores a gas that will experience an MDP greater than 690 kPa (100 psia).
- c. Contains a gas or liquid in excess of 103 kPa (15 psia) that will create a catastrophic hazard if released.

Pressurized Component: A line, fitting, valve, regulator, etc., that is part of a pressurized system intended primarily to sustain a fluid pressure and fluid transfer. Any piece of hardware that is not a pressure vessel or a pressurized fluid container but is pressurized via a pressurization system.

NASA-HDBK-5010, VOLUME 2, REVISION A

Pressurized Fluid Container: A container designed primarily for pressurized storage of gases or liquids that is similar to a pressure vessel but does not satisfy the definition of a pressure vessel.

Pressurized Hardware: Any of the various hardware items that support an internal pressure.

Pressurized Structure: A hardware item designed to carry both internal pressure and vehicle structural load.

Pressurized System: An interrelated configuration of pressurized components under positive internal pressure. The system may also include pressure vessels.

Proof Test: A test on the flight article that is performed to verify structural acceptability or screen flaws. The proof test load and/or pressure level is the proof test factor times limit load and/or MDP. Proof tests may be conducted in the operational environment, or the test levels may be adjusted via an ECF. (Note that some sections in NASA-STD-5019A may specify when an ECF is optional versus when it is prescribed for the classification if the test is not conducted in the operational environment.)

Proof Test Factor: A factor that is multiplied by the limit load and/or MDP to arrive at the proof test levels. When proof tests are performed to establish structural acceptability, the proof test factor is specified. When screening for flaws with a proof test, the proof test factor is derived by fracture mechanics principles.

R Ratio: The ratio of minimum stress to maximum stress in cyclic loading.

Reflight Hardware: Hardware items that have already met the requirements in NASA-STD-5019A for service life, have flown on a flight vehicle, and are being manifested for an additional flight. Note that some fracture control categories in NASA-STD-5019A impose additional requirements that are to be satisfied before being reflown.

Residual Strength: The maximum value of load (both externally applied and internal self-equilibrating loading such as residual stresses) that a flawed or damaged part is capable of sustaining without catastrophic failure.⁶

Residual Threat Determination: An assessment that defines the worst-case credible flaw conditions that composite or bonded hardware will be designed to endure, considering all applicable flaw detection and mitigation strategies that are implemented for the flight hardware.

Responsible Fracture Control Board: A designated multi-discipline group of experts at the NASA Center that has the authority to develop, interpret, and approve fracture control requirements and the responsibility for overseeing and approving the technical adequacy of all fracture control activities at the Center.

⁶ In the NASGRO® User Manual, version 7.1.1, section 2.1.5 and Appendix O, there is discussion of a related failure condition invoked when net section stress exceeds the material flow stress.

NASA-HDBK-5010, VOLUME 2, REVISION A

Responsible NASA Center: The NASA Center acting as the sponsor and/or coordinator for the program/project developing the payload/hardware.

Rotating Hardware: Hardware that has a rotational mode of operation and devices with spinning parts such as fans, centrifuges, motors, pumps, gyros, and flywheels.

Rupture: An instance of breaking or bursting suddenly and completely.

Safe Life: See definition of Damage Tolerance.

Safety Critical: For fracture control, a part, component, or system whose failure or loss would be a catastrophic hazard.

Sealed Container: Any single, independent container (not part of a pressurized system), component, or housing that is sealed to maintain an internal nonhazardous environment and that does not meet the definition of a pressure vessel.

Service Life: Time interval for a part beginning with manufacture and extending throughout all phases of its specified mission usage. The period of time or number of cycles that includes all relevant loadings, conditions, and environments encountered during this period that will affect flaw growth, including all manufacturing, testing, storage, transportation, launch, on-orbit, descent, landing, and if applicable, post-landing events, refurbishments, retesting, and repeated flights until the hardware is retired from service.

Service Life Factor: The factor on service life required in damage tolerance analysis or testing. The service life factor is often referred to as the life factor. (Note: The service life factor is specified as 4 for metallic materials in section 7.3.2.c of NASA-STD-5019A. The service life factor is specified as the B-basis number of service lives with the corresponding LEF for composites or bonded materials in sections 7.4.7.b and 7.4.8.e of NASA-STD-5019A.)

Shatterable Materials: Any material that is prone to brittle failures during operation that could release many small pieces into the surrounding environment.

Special Visual Inspection: Close proximity, intense visual examination of localized areas of internal and/or external structure for indications of impact damage, flaws, or other structural anomalies. Appropriate access to gain proximity, e.g., removal of fairings and access doors, use of ladders and work stands, is required. High-intensity lighting, along with other inspection aids such as mirrors, magnifying lenses, and surface cleaning, are used. Special visual inspections are done independently by two inspectors. When special visual indications are found, NDE is done.

Standard NDE: NDE methods of metallic materials for which a statistically based flaw detection capability has been established. Standard NDE methods addressed by this document are limited to fluorescent penetrant, radiography, ultrasonic, eddy current, and magnetic particle.

APPROVED FOR PUBLIC RELEASE – DISTRIBUTION IS UNLIMITED

NASA-HDBK-5010, VOLUME 2, REVISION A

Sustained Load Cracking (SLC): Growth of a pre-existing crack in susceptible metallic alloys⁷ under sustained stress without assistance from an external environment. A threshold stress intensity factor can be obtained by procedures such as those in ASTM E1681 for the case of an inert or vacuum environment. One publication determines the effects of hydrogen content and temperature on SLC in Ti-6Al-4V (Boyer and Spurr, 1978).

Ultimate Factor of Safety (Ultimate Safety Factor): A specified factor to be applied to limit load. No ultimate structural failure is allowed for a load equal to the ultimate factor of safety multiplied times limit load.

Ultimate Strength (Capability): The load, stress, or strain at which collapse or rupture occurs.

Yield Strength: The stress that corresponds to a plastic axial strain of 0.002 mm/mm (0.002 in/in).

4. GENERAL GUIDANCE

4.1 Fracture Control Plan (FCP)

An FCP is crucial to the implementation of fracture control requirements by providing a roadmap for the project through the life of the hardware. FCPs will vary greatly depending on the complexity of the hardware, and it is recommended that the damage tolerance practitioner become familiar with the requirements in NASA-STD-5019A. This Handbook offers examples of FCPs for actual NASA hardware in Appendices A and C. The examples are not intended to be all inclusive and are not to be used as a copying template because the content of each FCP is unique to the application of the hardware, environments, loads, etc. In complex human-rated engineering systems such as those used in space launch systems, a complete understanding of the specific hardware is necessary to facilitate proper part classification and selection of the fracture control methodology required for each part, all of which is to be captured in the hardware-specific FCP. In auxiliary hardware applications such as experiments that may go to the International Space Station (ISS), there may be human-rated fracture control requirements because the hardware is being housed in a human-rated vehicle. In such cases, the resulting FCP sometimes implements a more generalized approach. It is easily understood that the auxiliary hardware approach, although practical for an experiment in a glovebox without posing risks, would not be applicable to or recommended for primary hardware systems such as propulsion system components that are high pressure and/or high energy.

Key elements of an FCP are generally as follows:

1. Hardware Overview:

⁷ SLC, because of the presence of interstitial hydrogen, occurs in titanium alloys, including commercially pure titanium (cp-Ti) and Ti-6Al-4V (Ti64), in both annealed and solution-treated and aged (STA) conditions. Testing is necessary to determine the threshold stress intensity for the titanium alloy metallurgical condition and interstitial hydrogen content. Other materials with different crystalline structures such as steel and aluminum alloys that do not allow interstitial hydrogen may still exhibit SLC behaviors.

NASA-HDBK-5010, VOLUME 2, REVISION A

- a. Schematics.
 - b. Purpose.
 - c. Failure Modes Effects and Analysis.
2. Hardware Operations.
 3. Fracture Control Responsibilities.
 4. Responsible Fracture Control Board.
 5. Fracture Control Implementation.
 6. Fracture Control Classification.
 7. Part Number, Drawing Number, Material Processing, and Classification
 8. Fracture Critical Identification on Drawings.
 9. Exempt Hardware.
 10. Nonfracture Critical Classifications and Rationale.
 11. Methodology for Assessing Fracture Critical Hardware.
 12. Nondestructive Evaluation Plan.
 13. Disposition of Indications.
 14. Damage Threat Assessment (e.g., impact damage source and types).
 15. Impact Damage Protection Plan.
 16. Alternate Approaches.
 17. Open Work (e.g., to be determined/to be resolved).

4.1.1 Example 1: Space Launch System (SLS) Multipurpose Stage Adaptor (MSA) Fracture Control Plan (FCP)

The MSA is an example of a dry nonpressurized thrust structure component for SLS. The FCP example provided here is intended to represent how a targeted FCP can be developed for the hardware being assessed. This example was developed for NASA-STD-5019 (Baseline), including MSFC-RQMT-3479, Fracture Control Requirements for Composite and Bonded Vehicle and Payload Structures, for composite parts. While not directly applicable to NASA-

APPROVED FOR PUBLIC RELEASE – DISTRIBUTION IS UNLIMITED

NASA-HDBK-5010, VOLUME 2, REVISION A

STD-5019A as a one-to-one comparison for the numbered requirements, it is a good representative example for how a hardware-specific FCP can be developed. Appendix A contains the MSA FCP example. Appendix B contains the fracture control assessment summary.

4.1.2 Example 2: Cubesat for Artemis 1 Fracture Control Plan (FCP)

The Artemis Program's Artemis I mission is to send an Orion spacecraft on an uncrewed loop around the moon to test lunar technologies ahead of human landings. Several cubesats are to fly on the first flight. Payloads from NASA, international partners, academia, and industry will execute a variety of experiments ranging from lunar mission to in-situ resource utilization to sustained human lunar presence, among others. The cubesats will be housed in the MSA in Artemis I. The cubesats are designed to be deployed to conduct autonomous experiments without need of human contact. By virtue of the fact they are housed and transported in a human-rated vehicle, they are required to meet fracture control requirements. The hardware developer has to demonstrate that the individual cubesats will not cause a catastrophic event that will pose a hazard to Artemis. The cubesats are subject to NASA-STD-5019 (Baseline) requirements up to the point of deployment of the cubesat from the MSA; after cubesat deployment, failure of a cubesat would not pose a hazard to the human-rated SLS vehicle or Orion spacecraft. As a result, some of the fracture control rationale provided in the example report includes a phased application of requirements and may not necessarily be applicable in all cases. Also note that the example FCP covers only the propulsion system element of the subject cubesat; a companion FCP covering the remainder of the Cubesat is not reproduced here. In general, an FCP is expected to cover the entirety of the hardware of a relevant system. Appendices C and D contain the FCP and report for this example.

4.2 Responsibilities

4.2.1 Responsible Fracture Control Board

4.2.1.1 NASA Fracture Control Organizations

Fracture organizations vary across the NASA Agency depending on the needs of the individual Center. Select Centers such as Marshall Space Flight Center (MSFC), Kennedy Space Center (KSC), and Johnson Space Center (JSC) manage human-rated programs and tend to have a formal fracture control board or panel. JPL is similarly organized in that they have a similar charter for their deep space missions that the Centers do with their large flight programs. Other Centers such as Ames Research Center (ARC), Glenn Research Center (GRC), Goddard Space Flight Center (GSFC), and Langley Research Center (LaRC) tend to have a fracture control point of contact instead of a formal fracture control organization. Each Center organizes to best suit their needs based on the programs and projects under their purview. Following are various aspects of existing fracture control organizations across the Agency.

NASA-HDBK-5010, VOLUME 2, REVISION A

4.2.1.2 Establishment of a NASA Fracture Control Board (FCB): Marshall Space Flight Center

As the Propulsion Center for human-rated space launch systems for the Agency, MSFC established an MSFC FCB in accordance with Marshall Work Instruction (MWI) 8071.1, Fracture Control Board, to comply with NASA-STD-5019.

The MSFC FCB is comprised of representatives from key technical areas as shown in Figure 4.2-1, Membership of MSFC FCB Showing Areas of Emphasis. Membership in the FCB includes subject matter experts in various areas involved in damage tolerance activities for hardware managed by MSFC. The team members perform main functions in their respective line organizations and are called upon periodically to review fracture control issues brought to the MSFC FCB. These issues may include approval of an FCP, review of an alternate approach, noncompliance of fracture control requirements, providing expert opinion on fracture control to a program office or delegated technical authority for risk assessment, etc.

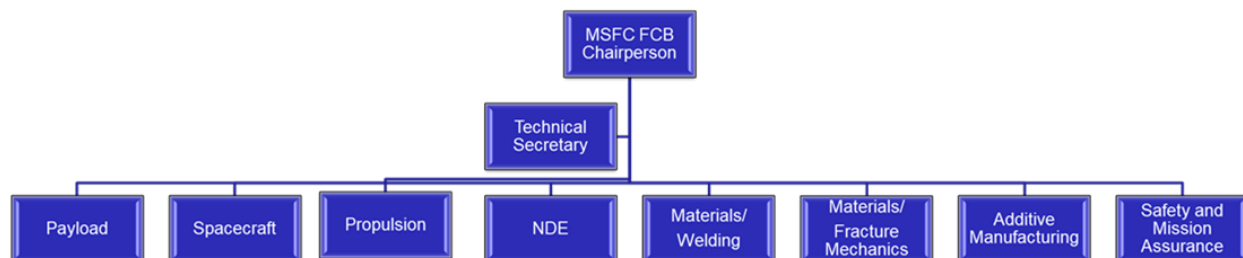


Figure 4.2-1—Membership of MSFC FCB Showing Areas of Emphasis

In Figure 4.2-2, Memorandum Establishing MSFC FCB Membership, a sample of a memorandum issued by the MSFC Engineering Director establishing membership of the MSFC FCB according MWI 8071.1 is presented.

The MSFC FCB meets regularly or on an as-needed basis to provide oversight or insight to spaceflight programs and corresponding elements. For example, in the SLS Program, the MSFC FCB provides oversight/insight regarding issues pertaining to liquid engines and solid rocket boosters. They may also provide insight to fracture control issues in connection with payloads such as cubesats that will be transported on SLS, a human-rated vehicle.

NASA-HDBK-5010, VOLUME 2, REVISION A

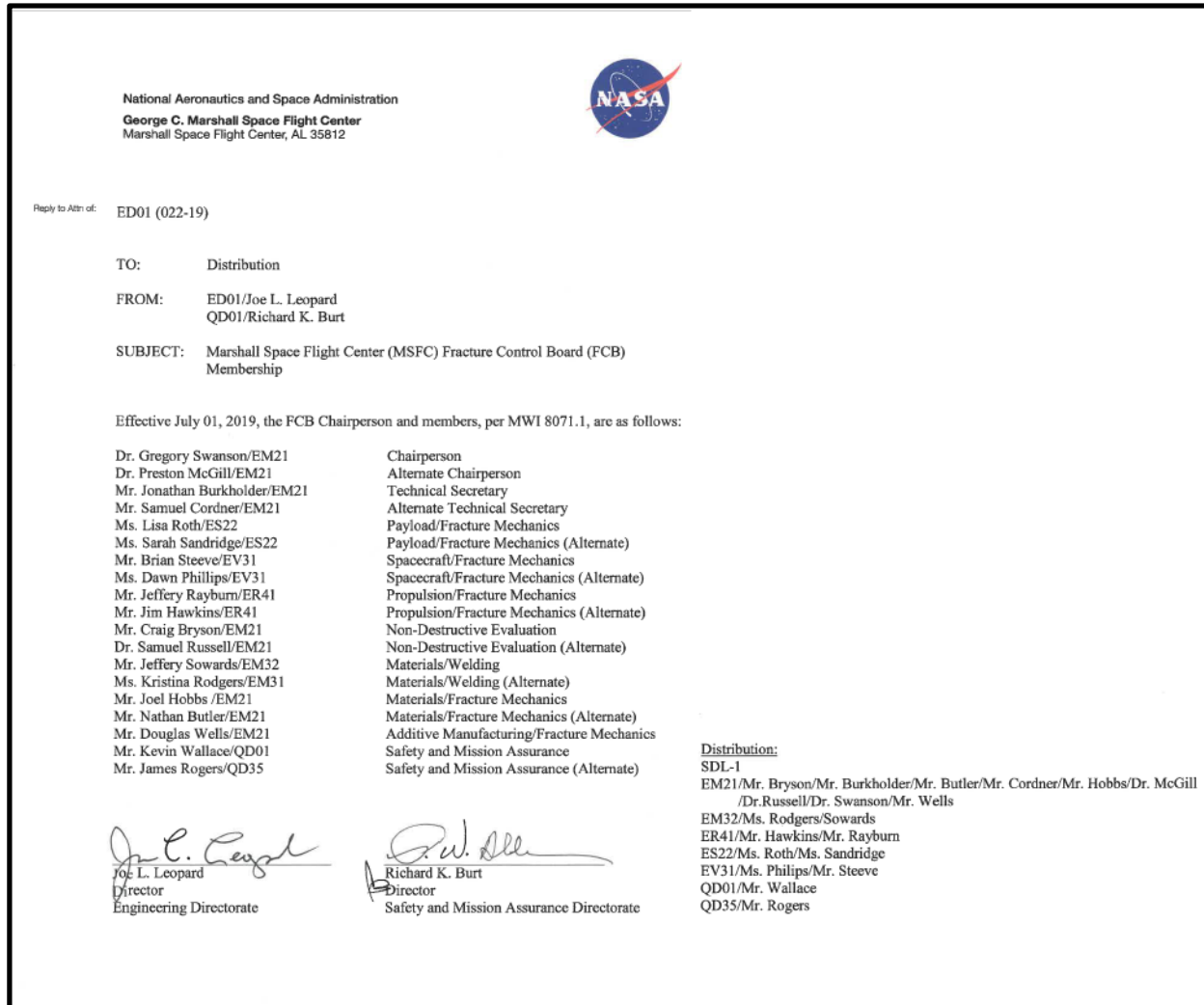


Figure 4.2-2—Memorandum Establishing MSFC FCB Membership

4.2.1.3 Example of a JPL Fracture Control Board (FCB) Charter

JPL leads deep space exploration for NASA. JPL missions have explored every planet and the Sun to gain knowledge and understanding of our universe and other ambitious quests such as the search for life beyond Earth. All of JPL's missions such as the robotic exploration of Mars by the Perseverance Rover, among numerous other notable missions, are considered national assets and may be subject to fracture control requirements. JPL established a charter for their FCB which is shown in Figure 4.2-3, JPL FCB Charter.

NASA-HDBK-5010, VOLUME 2, REVISION A

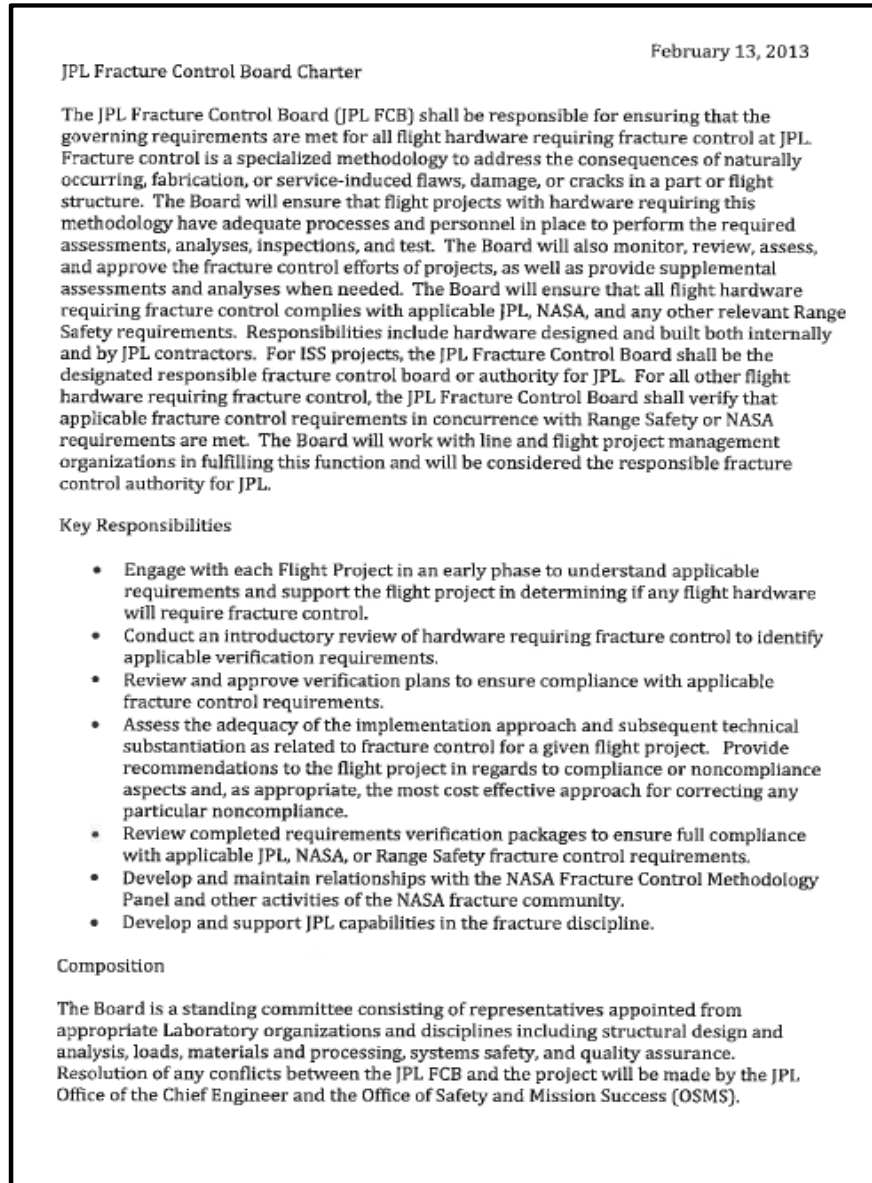


Figure 4.2-3—JPL FCB Charter

4.2.1.4 Example of a KSC Fracture Control Panel Charter

KSC Flight Operations supports a variety of missions assigned to the Center. As NASA's primary launch Center for human spaceflight and the Agency's hub for government and commercial spaceflight integration, KSC serves a critical role in enabling mission success for many of the Agency's undertakings. Human-rated spaceflight programs such as the Commercial Crew Program are under the purview of the KSC FCP. The following list shows the key elements describing the charter for this panel per KDP-KSC-F-2616A, KSC Councils, Boards, and Committees Charter:

NASA-HDBK-5010, VOLUME 2, REVISION A

1. Purpose: The KSC Fracture Control Panel (FCP) is established as the KSC authority to assure acceptability and consistency in implementation of fracture control requirements and methodology on flight hardware.

2. Applicability/Scope: This charter is applicable to all organizations at KSC that support programs or projects that implement or oversee fracture control requirements. The FCP directly supports NASA programs, NASA Engineering Review Boards, and NASA Safety Review Boards or Panels in matters of fracture control and fracture mechanics assessments.

This charter applies to all spaceflight hardware as required in NASA-STD-5019, Fracture Control Requirements for Spaceflight Hardware.

3. Functions: The Fracture Control Panel is responsible for the following:

a. Functioning as the Responsible Fracture Control Board for all human flight programs that fall under the responsibility of KSC as defined in NASA-STD-5019.

b. Supporting local Safety Review panels and/or Project Control Boards by reviewing fracture control plans and coordinating resolution strategies for fracture control issues.

c. With the establishment of appropriate multi-center agreements, supports KSC fracture control activities involving design or ground processing of hardware under the authority of another NASA Center.

4. Membership:

a. Chair - Chief, Laboratories, Development, and Testing Division or delegate. The Chief, Laboratories, Development, and Testing Division can delegate the position of Fracture Control Panel Chair.

b. Secretary: As assigned by the Chair.

c. Membership: Individuals representing the following functions: Structures, Fracture Analysis, Nondestructive Evaluation, Materials and Processes, Pressure Systems Engineering, and Safety and Mission Assurance.

Members, including any alternates, for each panel position shall be appointed by the appropriate Director or Division Chief. Membership is documented in a companion memorandum by the Panel Chair.

5. Multi-center Panels: Due to the multi-center relationships that exist for some flight programs (e.g., Commercial Crew) program-specific panels may be formed, and panel membership may be drawn from KSC or other NASA Centers. Panel membership will be coordinated with appropriate Directors of Engineering and Safety and Mission Assurance as well as the Chief Technical Authority for that applicable flight program.

6. Period of Performance: Start date and end dates are provided. Ongoing until terminated by the Director, Engineering.

APPROVED FOR PUBLIC RELEASE – DISTRIBUTION IS UNLIMITED

NASA-HDBK-5010, VOLUME 2, REVISION A

7. Deliverables: (a) The FCP will furnish opinions and recommendations on fracture control issues or questions that develop during the course of fracture control implementation. (b) The FCP will provide written recommendations to the appropriate program Chief Engineer, KSC engineering, programs, projects, boards, and panels.

8. Meeting Guidelines:

a. Meeting Frequency: The FCP will have meetings as required to meet program objectives and to assess the general status of fracture control on programs and projects. The Panel Chair may call ad hoc meetings when specific issues that must be addressed in a timely matter are identified.

b. Length of Appointment: Indefinite

c. Minutes/Agenda Requirements: The Panel Secretary is responsible for providing meeting agendas, minutes, and other documentation resulting from the meeting.

d. Voting: The FCP is a voting panel. Decisions will be made by majority vote with the Panel Chair breaking ties. In any case where there is a nonunanimous decision, all dissenting views will be included in the official minutes and will be communicated by the Panel Chair to the appropriate engineering or program customer.

e. Member Responsibilities: FCP members are responsible to represent their organizations and provide status on assigned action items and/or tasks.

Presentation Requirements: Presenters are required to create presentations and ensure proper review prior to FCP meetings.

9. Reporting to:

In this section a signature/date is required. Example as follows:

<u>/original signed by Joe Doe for/</u> Joe Doe Director, Engineering	<u>10/18/18</u> Date
---	--------------------------------

10. Applicable Requirements (KNPDs, NPDs, KNPRs, NPRs, KDPs, KCAs): Examples are provided below:

- NASA-STD-5019, Fracture Control Requirements for Spaceflight Hardware.
- NASA-STD-5009, Nondestructive Evaluation Requirements for Fracture-Critical Metallic Components.
- SSP 30558, Fracture Control Requirements for Space Station.
- SSP 52005, Payload Flight Equipment Requirements and Guidelines for Safety-Critical Structures (Safety Requirements for ISS Experiments).

APPROVED FOR PUBLIC RELEASE – DISTRIBUTION IS UNLIMITED

NASA-HDBK-5010, VOLUME 2, REVISION A

- NSTS 1700.7, Safety Policy and Requirements for Payloads Using the STS (including ISS Addendum).
- KNPR 8715.3, KSC Safety Practice Procedural Requirements.

11. Concurrence: This is usually signed by the Director of Safety and Mission Assurance.

Concurrence: */original signed by Mary Jane/on 10/31/2018/*
Director, Safety and Mission Assurance

4.2.2 Responsible Program

Human-rated spaceflight programs impose fracture control on their projects to meet the requirements of NASA-STD-5019. It is noteworthy to point out that the various programs follow different revisions of the Standard depending on the current version of the Standard at the time of the contract award. Programs like SLS are subject to NASA-STD-5019 (Baseline) and MSFC-RQMT-3479 for composite/bonded vehicle and payload structures since those were the current fracture standards at the time of contract award. NASA-STD-5019A is a more recent revision that has been imposed on the newer programs such as Gateway and Human Landing System and is the governing requirement for future NASA programs. Some of the new programs are adopting tailored or alternate requirements that meet the intent of NASA-STD-5019A. Table 4.2-1, Applicable Requirements and Handbook Documents for Different Programs, shows applicable requirements and handbooks documents for various historical and current programs.

Table 4.2-1—Applicable Requirements and Handbook Documents for Different Programs

Document/ Requirement	Historical		Current				
	Shuttle Element/ Payloads	ISS Payload/ Hardware	SLS Elements**/ Payloads (i.e. Cubesats)	Orion	Commercial Crew Program (CCP)	Gateway*	HLS*
Element Documents	✓						
MSFC-HDBK-1453	✓						
MSFC-STD-1249***	✓	✓	✓	✓	✓	✓	✓
NASA-STD-5003	✓	✓					
NASA-HDBK-5010	✓	✓	✓	✓	✓	✓	✓
NASA-STD-5007	✓	✓					
SSP 30558C		✓			✓		
SSP 30560A		✓					
NASA-STD-5019 Baseline and MSFC- RQMT-3479			✓	✓	✓		
NASA-STD-5019 A						✓	✓
NASA-STD-5009			✓	✓	✓	✓	✓
Notes:							
*Some programs are accepting tailored or alternate standards that meet intent of 5019.							
**Primary structures and propulsion systems.							
***Materials corrosion requirement							

Note: Per SSP 50808, NASA program can enforce NASA-STD-5019 or SSP 30558C. For CCP, SSP 30558C compliance is also required.

4.2.2.1 Hardware Developer Fracture Control Board (FCB)

For human-rated flight programs, it is recommended that the hardware developer (HD) establish an FCB. The FCB membership should have representation from key disciplines such as

APPROVED FOR PUBLIC RELEASE – DISTRIBUTION IS UNLIMITED

NASA-HDBK-5010, VOLUME 2, REVISION A

materials, NDE, safety, fracture, structures, and quality. Other disciplines may be necessary such as propulsion and fluids, depending on the hardware.

Not all hardware developers need to establish an FCB. For example, developers of experiments or payloads are not expected to establish their own FCB but need to coordinate with the RFCB for their project. An experiment on ISS manifest would coordinate with JSC, while a Cubesat riding on SLS would coordinate with the MSFC FCB. Manufacturers of components of propulsion systems (e.g., valve manufacturers) would not be expected to establish an FCB. Instead, the damage tolerance governance would reside at the system level. In such cases, it is expected that the hardware developer of the system would require the manufacturer to conduct the necessary damage tolerance activities and provide the documentation for their hardware to meet fracture control requirements.

In either case, whether a hardware developer's FCB is established or not, oversight and/or insight by a NASA damage tolerance organization is necessary to not only ensure fracture requirements are being met but also provide technical guidance in the implementation of fracture control. Note that RFCB located with a hardware developer requires tailoring of or a waiver to NASA-STD-5019A. An example of a Fracture Control Board is provided in Appendix E.

4.2.2.2 SLS Fracture Control Organizations

SLS is a super-heavy lift vehicle that is the backbone of the Artemis Program slated to return American astronauts to the Moon. The propulsion for SLS is comprised of a four-liquid engine RS-25 configuration for the core stage with two five-segment solid boosters. Figure 4.2-4, SLS Fracture Control Organization, shows fracture control organizations for the SLS elements. Across the various elements, some hardware developers have established FCBs and some have a technical group. Most of the elements in SLS have insight or oversight by the MSFC FCB. Some elements such as the Core Stage do not have MSFC FCB oversight but rather have insight by the MSFC damage tolerance line organization that reports to the Program.

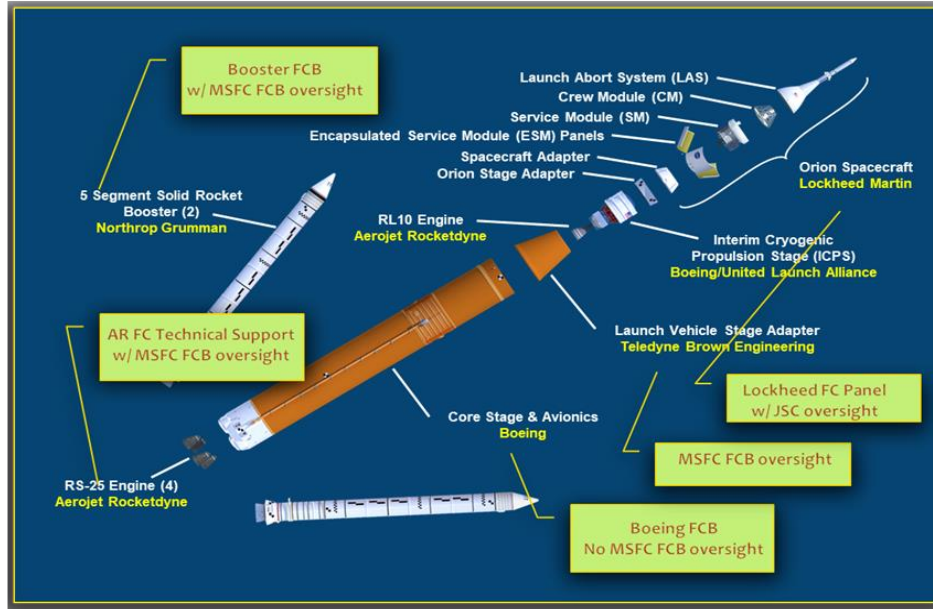


Figure 4.2-4—SLS Fracture Control Organization

4.2.2.3 Examples of a Hardware Developer’s FCB Organizations and Relationship with NASA FCBs

The traditional fracture control governance consists of a NASA FCB and a parallel hardware developer’s FCB (or technical entity). In recent years, the practical implementation has resulted in other ways to configure the fracture control organizations governing the various programs and projects. Following are schematics of possible configurations.

Historically, the Fracture Control governance resides in NASA such as the MSFC Fracture Control Board, who is responsible for approving FCPs, accepting alternative methodologies, and making recommendations to the NASA delegated Technical Authority. Figure 4.2-5, Traditional Fracture Control Governance, shows a historical or traditional governance.

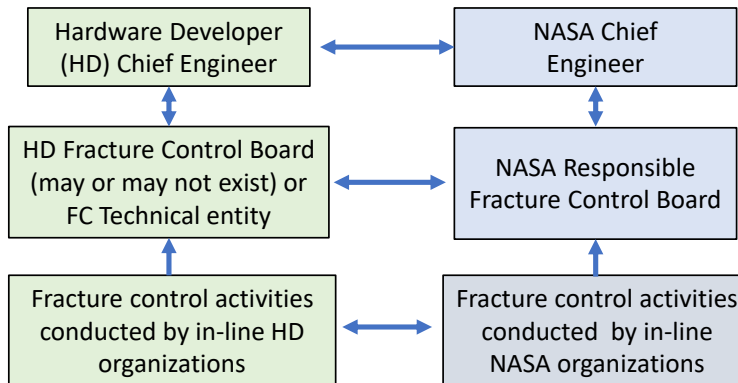


Figure 4.2-5—Traditional Fracture Control Governance

NASA-HDBK-5010, VOLUME 2, REVISION A

Fracture control is a multi-disciplinary endeavor that involves many of the following disciplines which are involved in the implementation of fracture control activities on a human-rated spaceflight hardware program:

1. Quality Assurance/Safety.
2. Materials Processes/Properties/Testing/Fracture Mechanics/Damage Control.
3. NDE/Inspection.
4. Structural/System Test/Analysis.
5. Loads/Dynamics/Environments.
6. Propulsion.
7. Process Engineering.

4.2.2.4 Example of FCB Residing with the Hardware Developer

Some programs are deviating from the historical fracture control governance in that the RFCB resides with the hardware developer. To ensure the hardware developer meets fracture control requirements for human-rated spaceflight hardware, NASA provides insight via membership in the hardware developer's FCB to identify any issues that elevate risk. NASA board members also function as the NASA Fracture Control Coordinator (FCC). This governance configuration requires extensive working knowledge of NASA's fracture standards and of the hardware developer's alternate or tailored fracture control standard. An FCC coordinates and engages the necessary team members from the NASA discipline subject matter experts (SMEs) for all fracture control issues based on the subject and components affected. Figure 4.2-6, RFCB Residing with the Hardware Developer, shows an RFCB residing with the hardware developer.

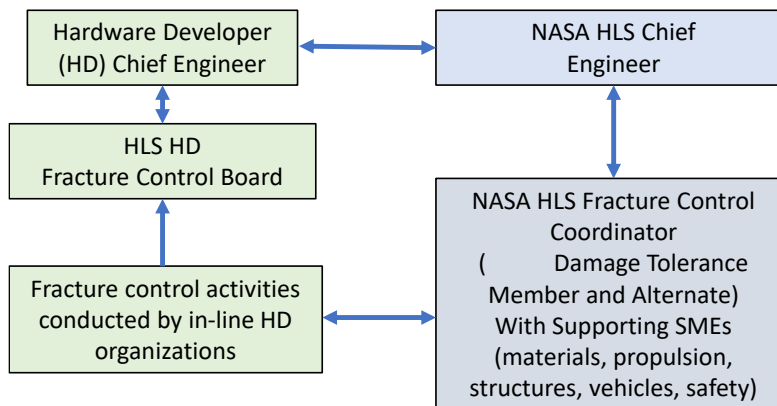


Figure 4.2-6—RFCB Residing with the Hardware Developer

4.2.2.5 Fracture Control Coordinator (FCC) Roles and Responsibilities

An FCC maintains up-to-date awareness of contractor fracture control activities and is responsible for providing information (status or updates on fracture control issues) as needed to the Program, delegated Technical Authority, line management, and discipline leads. The FCC

NASA-HDBK-5010, VOLUME 2, REVISION A

serves as primary point of contact to contractors for fracture control, serves in contractor RFCBs (as voting or nonvoting members), and in general maintains a working relationship with contractor counterparts.

In addition, the FCC coordinates internal NASA support to maintain flow of information to SMEs as deemed appropriate. The FCC may establish recurring status notes and meetings and inform team members when new data are made available. An FCC ensures that supporting SMEs are engaged when issues arise in their area of expertise. Activities may include invitations to review contractor documents, invitation to a particular FCB meeting, among others. If expertise for an issue is not currently available on the fracture control support team, the FCC works with discipline leads and line management to identify and engage an appropriate SME.

4.2.3 Fracture Control Implementation

Table 4.2-2, Checklist to Aid in Ensuring Steps for Fracture Control Implementation are Complete, is a checklist of items required for fracture control implementation and the activities that should be performed by the hardware developer/prime contractor FCB.

Table 4.2-2—Checklist to Aid in Ensuring the Steps for Fracture Control Implementation are Complete

Item	Activity	Completed?
1	Identifies group, organization, or person(s) who have fracture control responsibilities.	
2	Identifies all relevant fracture control requirements.	
3	Identifies specific fracture control activities.	
4	Identifies necessary documentation for subtier piece parts.	
5	Conducts fracture classification of parts/components.	
6	Identifies and specifies required NDE inspections or any other special requirements on fracture critical parts/components.	
7	Conducts implementation of traceability and documentation showing adherence of flight hardware to approved drawings, specifications, plans, and procedures.	
8	Conducts structural analyses, analytical, and testing methodology used in fracture control.	
9	Conducts assessments of anomalies on fracture critical parts/components and for decisions regarding questions or issues relating to fracture control.	
10	Compiles fracture control documentation and submits it to NASA FCB for approval.	
11	Ensures correct/valid material properties are used and MUAs approved.	

NASA-HDBK-5010, VOLUME 2, REVISION A

4.3 Classification of Parts and Implementation of Requirements

In this section, examples are provided on how the fracture control classification process is determined for all mission phases to determine which parts are: (a) Exempt, (b) Nonfracture Critical (NFC), and (c) Fracture Critical.

Approaches to evaluate hardware in these three categories are presented in sections 5, 6, and 7 in NASA-STD-5019A. Figure 2 of NASA-STD-5019A is the Fracture Control Classification Logic Diagram and can be used to guide the classification process.

4.3.1 Example Classifications

Classification of parts into exempt, nonfracture critical, and fracture critical will follow the logic diagram in Figure 3 of NASA-STD-5019A. Example applications are presented in sections 4.3.1.1 through 4.3.1.8.

4.3.1.1 Example: Solid Propellant, Fracture Critical

Materials exhibiting viscoelasticity can be under fracture control. Solid propellants within a solid rocket motor are generally subject to a comprehensive fracture assessment as defects within solid propellants can propagate and cause catastrophic failure modes (bore choke or burn through are two examples).

Generally, a comprehensive fracture approach is required to mitigate the risk of propellant failure. It involves a nondestructive inspection using propellant X-ray and accept/reject criteria developed by using fracture analysis and testing. Specific analysis and testing are performed to account for the viscoelastic response of propellant and insulation materials.

4.3.1.2 Example: Valve Internal Spring, Nonfracture Critical

Many moving mechanical valves contain springs that are intended to provide actuation capability. Some mechanical parts do resist loads and may not be considered exempt. Usually, these parts will be classified as nonfracture critical on the following basis: Mechanisms undergo extensive qualification and workmanship testing as part of NASA-STD-5017A, Design and Development Requirements for Mechanisms. For example, run-in testing (also known as wear-in testing) serves two purposes: (1) It acts as a screen to detect material and workmanship defects that manifest themselves early in the mechanism's life, and (2) It allows the mechanism to work through initial transient behavior and reach steady-state performance.

In this example, additional work was performed showing that the spring met the NFC low-risk criteria per section 6.2.5 of NASA-STD-5019A. Springs may undergo a rigorous piece part inspection for defects and undergo robust qualification and acceptance testing which bolsters confidence in the part.

NASA-HDBK-5010, VOLUME 2, REVISION A

4.3.1.3 Example: Structural Strut, Fracture Critical

A structural strut is assessed to resist loads. It is found that the part is a single-point failure, but it is unclear whether failure of the part can cause a catastrophic hazard. The strut does not meet any of the NFC options, so the part is classified Fracture Critical.

4.3.1.4 Example: Pressure Vessel, Fracture Critical

A pressure vessel stores working fluid for vehicle maneuvering. Pressure vessels, high energy rotating parts, hazardous fluid containers, and habitable modules are generally classified as fracture critical as they resist loads and usually a flaw can cause a catastrophic hazard. In this application, the pressure vessel wall resists load; it is found that a flaw can cause a credible catastrophic hazard. The part is classified as fracture critical.

4.3.1.5 Example(s): Composite Cover, Exempt, or Nonfracture Critical

A composite camera cover is demonstrated by stress analysis to have extremely low stresses and is judged that pre-existing defects are unlikely to cause a credible failure mode as the composite cover is fully bolted around the edges. The part has no credible potential to cause a catastrophic hazard. Consequently, the part is classified as an exempt part.

Analogously, a different program for a very similar part classified it as NFC low risk because the part met DTA in accordance with section 7.4.1, IDMP in accordance with section 7.4.2, and RTD in accordance with section 7.4.3 in NASA-STD-5019A. Additionally, since the part was determined to be contained and low-release mass, no NDE was necessary for this part.

4.3.1.6 Example: Ceramic Ball Bearings, Fracture Critical

In some applications such as silicon nitride ceramic ball bearings, the manufacturing process can result in the balls being particularly susceptible to defects. Hybrid ball bearings using silicon nitride ceramic balls with steel rings are increasingly being used in space mechanism applications due to their high wear resistance and long rolling contact fatigue life. The Ph.D. dissertation “Critical Flaw Size in Silicon Nitride Ball Bearings” by George Levesque from University of Florida demonstrates methods that can be used to determine the critical flaw size in these bearings. The critical flaw size needs to be validated through extensive life testing. In reference Tang, et al., in “A Study on the Effects of Ball Defects on the Fatigue Life in Hybrid Bearings,” characterization of defects encountered in use, generation of similar defects in a laboratory testing, and life testing was performed to understand the effects of defects on fatigue life. NDE methods and a perceptive proof test can be implemented, as the one presented in O'Brien, et al. (2011). These methods must be able to screen for the critical flaw size, or the operational stress must be limited to reduce the risk of fatigue failure.

Inspections of silicon nitride balls are performed per ASTM F2094-14, Standard Specification for Silicon Nitride Bearing Balls. Silicon nitride balls used in ball bearings and specialty applications intended for reusability applications should be inspected at an interval informed by the development and qualification program to avoid excessive wear, fatigue, or other detrimental

APPROVED FOR PUBLIC RELEASE – DISTRIBUTION IS UNLIMITED

NASA-HDBK-5010, VOLUME 2, REVISION A

degradation. This inspection, at a minimum, should involve data comparison from previous inspections collected during development and qualification testing but may also include inspection data from related inspections of flight hardware. The extent of the tests informing the inspection is sufficient to identify any out-of-family behavior and/or degradation of the bearing or ball. Additional testing is conducted if any anomaly or defect is observed during the prior flights and/or from the data comparison.

A fleet leader demonstration approach of the reliability of the design and ground testing before flight may be an acceptable alternative to establishment of the critical flaw size and corresponding inspection method for ceramic rolling elements.

4.3.1.7 Example: Fracture Control Summary List

To meet fracture control requirements for human-rated spaceflight hardware, all hardware needs to be classified. Exempt parts are documented with rationale for exemption. All remaining parts should be accounted for in a fracture control summary list. This list should be included in the fracture control summary report. The format for the summary list is optional but must include the part name and its classification. It is a good place to include other information such as part drawing number, material, and NDE flaw size and life. The summary list is assembled using the results from the fracture classification process. Detailed analysis reports for each piece of equipment are referenced along with the name of the component analyzed and the methodology used. In Table 4.3-1, Fracture Control Classification Example, the report number, component, and disposition methodology are provided along with the corresponding fracture rating.

NASA-HDBK-5010, VOLUME 2, REVISION A

Table 4.3-1— Fracture Control Classification Example

System Report Number	Component	Disposition Methodology	Fracture Rating
RAHF AW - 01769	Water Tank	Potential Energy	PE
	Support Structure	Fail Safe	FS1
	Water Tank Straps	Fracture Critical (>20 missions)	SL
RAHF AW - 01769	Water Distribution Manifolds (2)	Fail Safe	FS1
RAHF AA-3705	Monitor and Process Control System (SIR Drawer) Structure	Fail Safe	FS2
	Contents of Electronics Box	Contained Components	CR1
RAHF Cage Module Fail-Safe Analysis AA - 03828 else AW - 01769	Cage Module (CM) Structure	Fail Safe	FS2
	CM Latches	Fail Safe	FS2
	CM Contents	Contained Components	CR1
	Environmental Control System (ECS)	Contained Components (within Rack behind Cage Module)	CR1
	ECS: Bleed Air Fans	Rotating Element	KE
	ECS: Circular Fans	Rotating Element	KE
	ECS: Water Sep Fan	Rotating Element	KE

List of acronyms and definitions:

1. PE - Potential Energy: Item has stored mechanical energy. It has been shown to be below the threshold value for fracture critical hardware.
2. CR1 – Contained: Shown by engineering examination. Potential loose items and wall thickness are consistent with those used in containment test report.
3. FS1 – Failsafe: Shown by engineering examination. Multiple redundant load paths with large safety margins. Load paths are inspected between flights.
4. FS2 – Failsafe: This part has been shown to be fail safe by analysis.
5. KE – Kinetic Energy: This item has stored kinetic energy. It has been shown to be below the threshold value for fracture critical hardware.
6. SL Safe Life – Analysis is required (Parts are Fracture Critical).

APPROVED FOR PUBLIC RELEASE – DISTRIBUTION IS UNLIMITED

NASA-HDBK-5010, VOLUME 2, REVISION A

Item	Drawing	Material	Disposition	Model	Drawing	NDE	Life/4
					Thickness	Crack Size	
Sml Trq Hsn <small>www.nasa.gov</small>	96M20193	AL7075 T7351	Safe-Life	CC02	0.250	a = 0.05 c = 0.05	>50
				SC01	0.250	a = 0.05 2c = 0.20	>50
Mdm Trq Hsn <small>www.nasa.gov</small>	96M20194	AL7075 T7351	Safe-Life	CC02	0.250	a = 0.05 c = 0.05	>50
				SC01	0.250	a = 0.05 2c = 0.20	>50

4.3.1.8 Example: Fracture Summary Results

In this example, the components that require safe-life analysis, their respective NDE method, and the summarized findings are provided in Table 4.3-2, Fracture Summary Results.

Table 4.3-2—Fracture Summary Results

Item	Drawing	Material	Disposition	Model	Drawing Thickness	NDE Crack Size	Life/4
Sml Trq Hsn	96M20193	AL 7075 T7351	Safe-Life Analysis	CC02	0.25	a = 0.05 c = 0.05	>50
				SC01	0.25	a = 0.05 2c = 0.20	>50
Mdm Hrqr Hsn	96M20194	AL 7075 T7351	Safe-Life Analysis	CC02	0.25	a = 0.05 c = 0.05	>50
				SC01	0.25	a = 0.05 2c = 0.20	>50

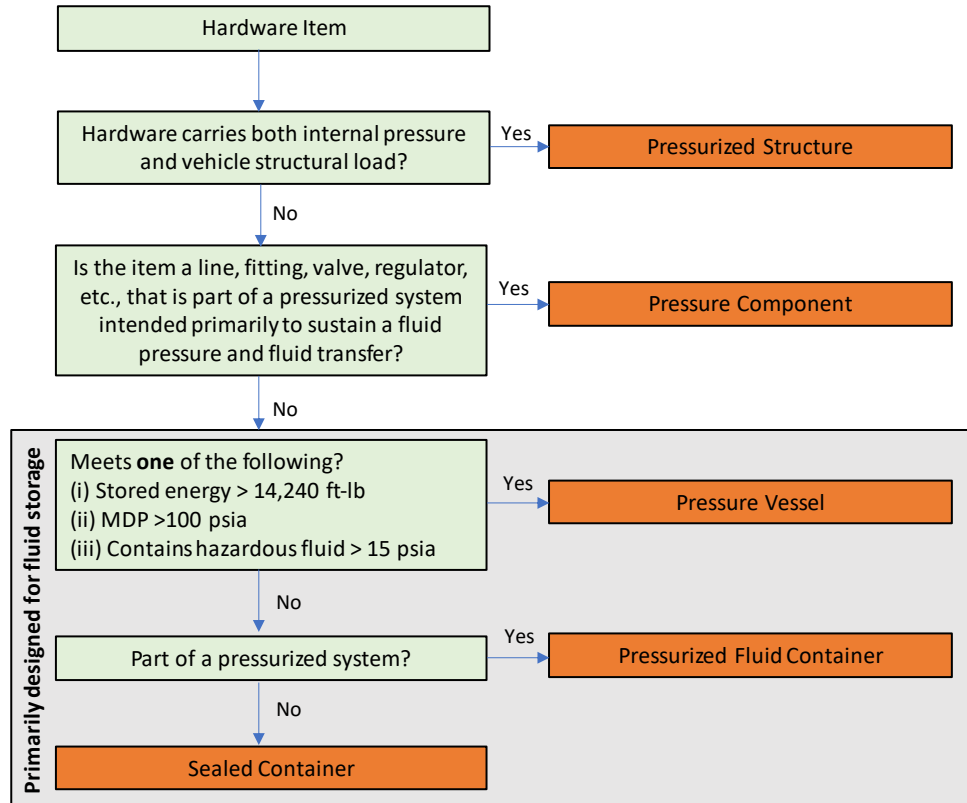
4.3.2 Classification of Pressurized Hardware

This section provides guidance on classifying the various types of pressurized hardware according to NASA-STD-5019A and provides a method for calculating the stored energy in a pressurized container. The stored energy is one of the criteria to determine if hardware is a container or a pressure vessel.

NASA-HDBK-5010, VOLUME 2, REVISION A

4.3.2.1 Pressurized Hardware Definitions and Categorization

Determining the type of pressurized hardware is critical for application of correct requirements. The flowchart in Figure 4.3-1, Flowchart to Determine Pressurized Hardware Type, can aid in classifying the pressurized hardware correctly. Table 4.3-3, Hardware Item Classification Guide and Corresponding Section in NASA-STD-5019A, is then used to classify hardware into FC or NFC. The definitions for the different types of pressure hardware are contained in section 3.2 of NASA-STD-5019A.



Note: Vehicle structural load is a primary load acting on a vehicle. Example of a pressurized structure is a Stage Tank.

Figure 4.3-1—Flowchart to Determine Pressurized Hardware Type

NASA-HDBK-5010, VOLUME 2, REVISION A

Table 4.3-3—Hardware Item Classification Guide and Corresponding Section in NASA-STD-5019A

Hardware Item Classification	FC	Criteria	Section in NASA-STD-5019A	Examples
Pressurized Structure	Always	None	7.2.6 FC Pressurized Structure	Stage Tanks
Pressure Components	Sometimes	Meets criteria in section 6.2.4 of NASA-STD-5019A	6.2.4 NFC NHLBB Lines, Fittings, and Other Pressurized Components	Valves, fittings, lines, bellows
		Does not meet criteria in section 6.2.4 of NASA-STD-5019A	7.2.4 FC Lines Fittings, and Other Pressurized Components	
Composite Overwrapped Pressure Vessel or Pressurized Fluid Container	Always	Meets ANSI/AIAA S-081A	7.2.2 FC COPVs and Composite Pressurized Fluid Containers	COPV
		Does not meet ANSI/AIAA-S-081A	7.2.3 Other FC Pressure Vessels and Pressurized Fluid Containers	
Metallic Pressure Vessel or Pressurized Fluid Container	Always	Meets ANSI/AIAA S-080-1998	7.2.1 FC Metallic Pressure Vessel	MPV
		Does not meet ANSI/AIAA S-080-1998	7.2.3 Other FC Pressure Vessels and Pressurized Fluid Containers	
Sealed Container	Sometimes	Meets criteria in section 6.1.4 of NASA-STD-5019A	6.1.4 NFC Sealed Container	Sealed electronics box
		Does not meet criteria in section 6.1.4 of NASA-STD-5019A	7.2.3 Other FC Pressure Vessels and Pressurized Fluid Containers	
Habitable modules	Always	Intended to house humans	7.2.5 Fracture Critical Habitable Modules and Volumes	Space Station Module
Hardware used in payloads or experiments	Always	Limited applicability and not part of a pressurized system	7.5.5 Hazardous Fluid Containers for Payloads and Experiments	

4.3.2.2 Calculating Stored Energy in a Vessel Under Pressure

The definitions provide straightforward language on classifying various types of pressurized hardware, which require the stored energy calculation. To decide if a vessel meets the stored energy level 19,310 J (14,240 ft-lbs) criteria for declaration as a pressure vessel, the following

APPROVED FOR PUBLIC RELEASE – DISTRIBUTION IS UNLIMITED

NASA-HDBK-5010, VOLUME 2, REVISION A

equation (Marks' Standard Handbook, Tenth Edition, pages 4-9) for reversible adiabatic (isentropic) expansion of a confined gas may be used:

$$E = \frac{P_i V}{k-1} \left[1 - \left(\frac{P_e}{P_i} \right)^{\left(\frac{k-1}{k} \right)} \right] \quad \text{(Equation 4.3-1)}$$

where:

E = stored energy

P_i = internal absolute pressure

P_e = external absolute pressure

V = gas volume or ullage in vessel

k = ratio of specific heats, C_p/C_v

C_p = specific heat at constant pressure

C_v = specific heat at constant volume

Note that the energy calculation requires consistent units. To use this criterion, the energy calculation should be verified for all conditions in which the pressurized hardware will operate (e.g., space, sea-level). Typically, there is little variation with temperature and the near room temperature (300 K) values. The gas volume of ullage in the vessel can be determined using the following calculation:

$$V = \frac{E(k-1)}{(\Delta P + P_e) \left[1 - \left(\frac{P_e}{\Delta P + P_e} \right)^{\left(\frac{k-1}{k} \right)} \right]} \quad \text{(Equation 4.3-2)}$$

where:

$\Delta P = P_i - P_e$ is the gauge pressure and other terms are as before.

Note that specific heat ratio, k , for various substances vary minimally with temperature near room temperature.

4.4 Other Requirements

This section is reserved.

NASA-HDBK-5010, VOLUME 2, REVISION A

5. EXEMPT PARTS

Exempt parts are nonstructural and have no hazardous concerns or failure modes. Nonstructural items (i.e., not required to resist loads and maintain stiffness or alignment) do not have credible fracture modes and may include small common mechanical parts that undergo traditionally strong development and rigorous quality control programs. Examples of exempt parts are insulation blankets, electrical circuit components/boards, electrical connectors and their locking devices, wire bundles, elastomeric seals, washers, nuts, fastener locking devices, and valve seats. Common off-the-shelf tools such as pliers, wrenches, etc., are generally exempt from fracture control.

Classification of parts into exempt, nonfracture critical, and fracture critical will follow the logic diagram in Figure 3 of NASA-STD-5019A. Example applications are presented below.

5.1 Example 1: Insulation Blanket, Exempt

A Mylar blanket is used for insulation on the exterior surfaces of a spacecraft for thermal control on a critical spacecraft program. The first decision gate in the part classification is to determine whether the part can be classified as exempt, which it could be if one of the following is met: (1) Nonstructural parts with no credible failure mode caused by a flaw, (2) Nonstructural parts with no credible potential for causing a catastrophic hazard, or (3) Other nonstructural parts approved by the RFCB for exempt status. In this instance, the part is nonstructural as it does not resist any loads as it is an insulator and thermal loads are unlikely to cause stresses. The presence of a flaw is very unlikely to cause any credible failures. Consequently, this part is classified as Exempt based on criteria NASA-STD-5019A FCR 6(a). Following Figure 4, the only requirement is to document the Mylar blanket as Exempt in the FCP and/or Fracture Control Summary Report (FCSR).

5.2 Example 2: Elastomeric O-ring Seal, Exempt

Elastomeric seals are generally classified as exempt. Elastomeric O-rings are often used in liquid rocket engines, valves, solid rocket motors, and other pressure sealing surfaces. Generally, elastomeric seals are considered nonstructural parts as they do not resist significant loads. It could be argued that O-rings resist load in preloaded joints which, during operations, could further compress and cause high stresses within the O-ring. In this scenario, a flaw within the O-ring can lead to a credible failure mode and the O-ring does not meet the Exempt classification. The O-ring part, at first glance, does not meet the Exempt classification. Flight confidence in these seals comes from extensive qualification experience, inspections prior to assembly, leak checks, and acceptance testing. Material tests may be performed at the lot level to ensure the material meets certification. For example, O-rings used within liquid rocket engines are rigorously inspected for any defects (e.g., nicks or dents), undergo robust quality control programs, are extensively tested through the engine qualification program, and finally acceptance tested for flight. The combination of these factors and when an O-ring is considered nonstructural could be the basis for Exempt classification per the criteria of NASA-STD-5019A

NASA-HDBK-5010, VOLUME 2, REVISION A

FCR 6(a). Following Figure 4 of NASA-STD-5019A, the only documentation required is FCP and FCSR.

Note that the material of the failed Challenger Space Shuttle Booster O-ring was a fluoroelastomer. In some cases, depending on the application, an Exempt classification would not be appropriate such as in the case of Challenger. In this case, the O-ring failure at a cold temperature was a major contributing factor that led to catastrophic failure.

6. ASSESSMENT OF NONFRACTURE CRITICAL (NFC) PARTS

This section examines the requirements and checks for classifying a part as NFC. Manufactured metallic components that meet NFC classification criteria and use nonprocess-sensitive methods do not require NDE or fracture analysis.

Material acceptance tests validating the material composition and basic mechanical properties are still required. For composites and bonded joints, an NFC classification still requires NDE and satisfying other requirements listed in section 6 of NASA-STD-5019A.

6.1 Established Approaches for Specific NFC Hardware

This section is reserved.

6.1.1 NFC Metallic Fasteners, Rivets, Shear Pins, and Locking Devices

This section is reserved.

6.1.1.1 NFC Low-Released Mass Fasteners, Rivets, and Shear Pins

This section is reserved. See section 6.2.1 in this Handbook.

6.1.1.2 NFC Contained Fasteners, Rivets, and Shear Pins

This section is reserved. See section 6.2.2 in this Handbook.

6.1.1.3 NFC Fail-Safe Rivets

This section is reserved. See section 6.2.3 in this Handbook.

6.1.1.4 NFC Low-Risk Fasteners

Use NASA-STD-5019A for NFC Low-Risk classification for fasteners. A simplified checklist is provided in Table 6.1-1, Checklist for NFC Low-Risk Fasteners, to assist in determining whether the fasteners can be classified as NFC Low-Risk. To meet this NFC category, all items in the checklist need to be met.

APPROVED FOR PUBLIC RELEASE – DISTRIBUTION IS UNLIMITED

NASA-HDBK-5010, VOLUME 2, REVISION A

**Table 6.1-1—Checklist for NFC Low-Risk Fasteners
(All requirements must be met.)**

Item	Description of Requirement	Meets (Y or N)
1	Mechanical joint with two or more fasteners	
2	Metal fasteners fabricated with high resistance to stress corrosion cracking per MSFC-STD-3029	
3	Fasteners fabricated to a military, National Aerospace Standard, or commercial aerospace specification: (a) Specification includes tensile, shear, and fatigue testing as part of lot acceptance. (b) Fasteners have traceability and are delivered with the Material Test Report; include raw material and heat-treat certifications; and document testing/processing in specification.	
4	Fasteners not made of titanium alloy	
5	The fastened joint complies with (a) Preload control in NASA-STD-5020, Requirements for Threaded Fastening Systems in Spaceflight Hardware, AND (b) No joint separation in the nominal loading configuration in NASA-STD-5020.	
6	Fasteners have rolled threads, with the rolling process occurring after all thermal treatment of the material.	
7	Fasteners have results of the mandatory lot acceptance fatigue testing to meet fatigue requirements in NASA-STD-5001, Structural Design and Test Factors of Safety for Spaceflight Hardware.	
8	Fastener types not requiring fatigue testing as part of lot acceptance, samples from the lot need to be submitted for fatigue testing in accordance with NASM1312-11, Fastener Test Methods - Method 11 - Tension Fatigue, or equivalent.	
9	The fasteners are not made from a low fracture toughness alloy.	
10	Fasteners are not reworked or custom made unless approved by RFCB.	

Fasteners that are manufactured from the following list of ductile materials show a high tolerance for typical fastener defects and flaws and are typically accepted as NFC Low-Risk fasteners. Examples of procurement specifications for these commonly accepted low-risk fastener materials are:

- Iron-based superalloy A286:** NAS4003, Fastener, A286 Corrosion Resistant Alloy, Externally Threaded, 160 ksi F_{tu} , 95 ksi F_{su} , 1000 °F; NA0026, Procurement Specification Metric Fasteners, A-286 CRES Externally Threaded, 1100 MPa Tensile, 660 MPa Shear; or equivalent.

APPROVED FOR PUBLIC RELEASE – DISTRIBUTION IS UNLIMITED

NASA-HDBK-5010, VOLUME 2, REVISION A

- **Nickel-based superalloy Inconel 718:** NASM85604, Bolt, Nickel Alloy 718, Tension, High Strength, 125 ksi F_{su} and 220 ksi F_{tu} , High Temperature, Spline Drive; or equivalent.
- **Cobalt-Chromium-Nickel-based superalloy MP35N:** SAE AS7468, Bolts, Cobalt-Chromium-Nickel Alloy, UNS R30035, Tensile Strength 260 ksi, Procurement Specification; or equivalent.
- **Austenitic Stainless Steel 300 Series CRES:** NA0271, Metric Fasteners, CRES 300 Series, Externally Threaded, MJ Thread, 500 MPa F_{su} and 700 MPa F_{tu} ; or equivalent.

6.1.1.5 NFC Fail-Safe Fasteners

The checklist in Table 6.1-2, Checklist for NFC Fail-Safe Fasteners, can assist in the evaluation of NFC for fail-safe fasteners. To meet this NFC category, all items in the checklist need to be met.

**Table 6.1-2—Checklist for NFC Fail-Safe Fasteners
(All requirements must be met.)**

Item	Description of Requirement	Meets (Y or N)
1	Assessment shows loss of load path does not result in a catastrophic hazard and that risk of loss of the structural redundancy during the service life of the structure is not a credible concern.	
2	Failure of the part does not generate pieces or debris that would violate the NFC low-released mass requirements in section 6.2.1 of NASA-STD-5019A: (a) The fracture of the part does not cause a catastrophic hazard; (b) The release of the mass does not cause a catastrophic hazard such as loss of function and impact with other hardware, equipment, spacecraft, and personnel; and (c) External released mass or parts, including those that would be subjected to aerodynamic flow, may only be classified low-released mass when the program has established an acceptable debris field criterion and the parts fall within it.	
3	After loss of any load path, structural capability remains to sustain all resulting redistributed loads and environments, including dynamic response changes until termination of the mission or until part is inspected.	
4	Reflight hardware is verified by visual inspection or other means to be intact and free of structural anomalies before being reflown.	
5	Metal fasteners fabricated with high resistance to stress corrosion cracking per MSFC-STD-3029.	
6	Fasteners are fabricated, procured, and inspected in accordance with NASA-STD-8739.14, NASA Fastener Procurement, Receiving Inspection, and Storage Practices for Spaceflight Hardware, and an	

APPROVED FOR PUBLIC RELEASE – DISTRIBUTION IS UNLIMITED

NASA-HDBK-5010, VOLUME 2, REVISION A

Item	Description of Requirement	Meets (Y or N)
	equivalent military standard, NAS, proprietary, or commercial aerospace specification.	
7	The fastened joint complies with NASA-STD-5020 without joint separation in the nominal configuration.	
8	Fasteners have rolled threads and are assessed to establish that they meet the fatigue requirements in NASA-STD-5001 (Fail-Safe section 6.2.3 of NASA-STD-5019A).	
9	The fasteners are not made from a low fracture toughness alloy as defined in section 3.2 in NASA-STD-5019A (Fail-Safe section 6.2.3 of NASA-STD-5019A).	
10	Fasteners are not reworked or custom made unless the application is approved by the RFCB (Fail-Safe section 6.2.3 of NASA-STD-5019A).	
11	Fasteners manufactured from titanium alloys require additional considerations for this classification, including risk mitigation and assessment that are approved by the RFCB (Fail-Safe section 6.2.3 of NASA-STD-5019A).	

6.1.1.6 NFC Locking Devices

This section is reserved. See section 6.2.1 in this Handbook for discussion on NFC Low Release Mass.

6.1.2 NFC Shatterable Components and Structure

This section is reserved.

6.1.3 NFC Rotating Hardware

Figure 6.1-1, Flowchart to Classify NFC Rotating Hardware, is presented to assist with determining whether rotating hardware is NFC or FC. For NFC rotating hardware, no NDE or fracture analysis is required.

NASA-HDBK-5010, VOLUME 2, REVISION A

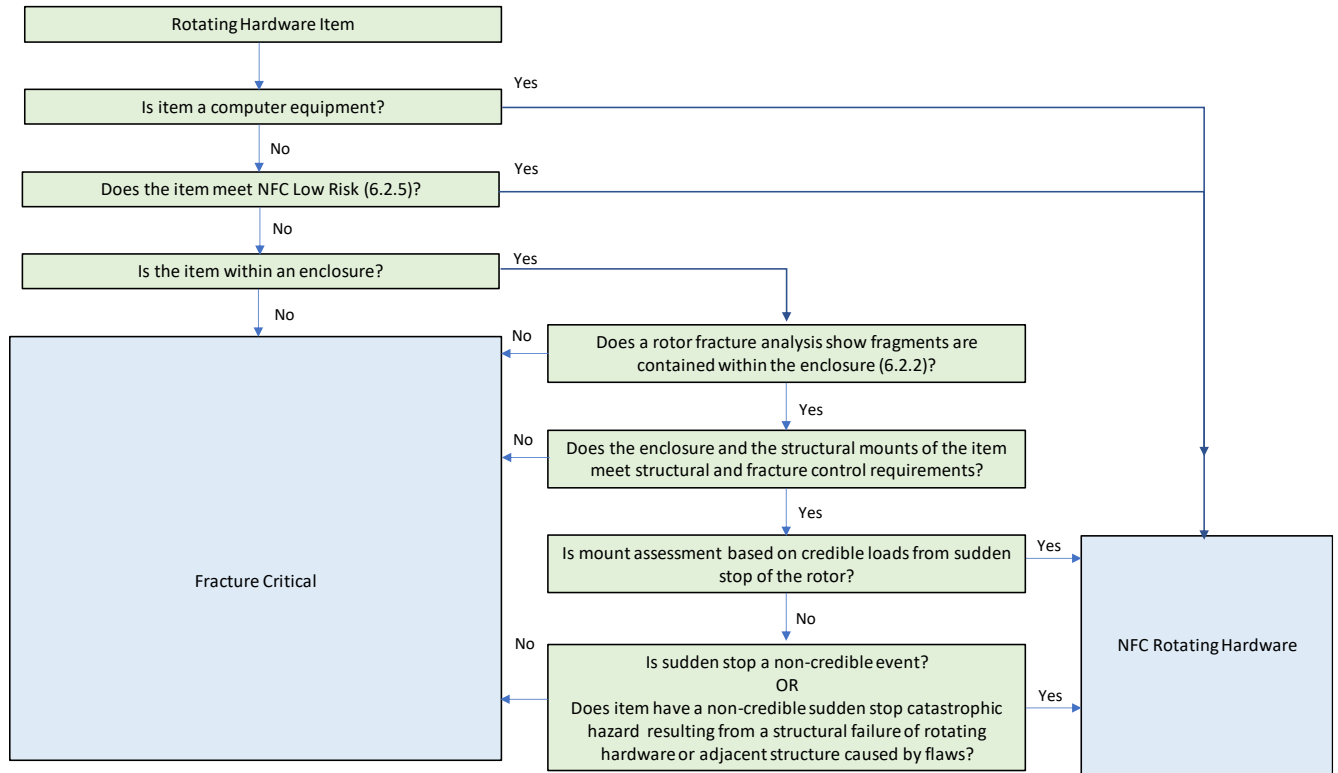


Figure 6.1-1—Flowchart to Classify NFC Rotating Hardware
(Note: Computer equipment or computer component)

6.1.3.1 Classification of Rotating Hardware with Kinetic Energy Less Than 14,240 ft-lbs

In the prior revision of this Handbook, an energy threshold of 14,420 ft-lbs was used to guide the classification of rotating hardware. This energy threshold requires more study as it can be considered quite large. Classification of rotating hardware is instead conducted with the flowchart in Figure 6.1-1 for this revision. Nonetheless, it remains informative to calculate the energy as it can be used for containment and/or impact analysis.

The Kinetic Energy (K.E.) of a rotating body is computed as $\frac{1}{2}I\omega_0^2$ where I is mass moment of inertia and ω_0 is rotational speed in radians per second. A rotating mechanical assembly is fracture critical if it has a kinetic energy of 19,310 Joules (14,240 ft-lbs) or greater (based on $\frac{1}{2}I\omega_0^2$). Rotating machinery with lower kinetic energy levels than stated above may have fracture critical components if the conditions in the flowchart in Figure 6.1-1 are met.

An example of a centrifuge inside of a locker is discussed. (See Figure 6.1-2, Picture of 8PU Locker with Centrifuge Inside).



Figure 6.1-2—Picture of 8PU Locker with Centrifuge Inside

The calculation of rotational energy is performed as follows: The weight is 5.7 lbs, the radius is 0.583 ft, and the maximum rotational speed of the centrifuge is 79.17 rev/s. The energy calculation for this system is as follows:

$$E = \frac{1}{2} I \omega^2, \text{ where: } I = \frac{1}{2} M r^2, M = \frac{W}{g} \text{ and } \omega = 2\pi N \quad (\text{Equation 6.1-1})$$

After substitution of all the values, one finds the energy as follows:

$$E = \frac{(\pi)^2 W r^2 N^2}{g} = E = \frac{(3.14159)^2 (5.7 \text{ lbs}) (0.5833 \text{ ft})^2 (79.17 \frac{\text{rev}}{\text{s}})^2}{32.2 \frac{\text{ft}}{\text{s}}} = 3726 \text{ ft} \cdot \text{lbs} \quad (\text{Equation 6.1-2})$$

This energy is far below the threshold of 14,240 ft-lbs, and the rotating equipment could be treated as low energy rotating equipment; additional requirements need to be verified per Figure 6.1-1.

Since the centrifuge is contained with an enclosure, a further assessment is required to classify the part as NFC per the flowchart presented in Figure 6.1-1. Classifying the rotating part as low energy based on this calculation is not sufficient criteria for determining part classification. For example, crack propagation may cause sudden jamming and stoppage of the rotor generating loads that could result in a catastrophic hazard.

The following sections provide examples and guidance for interpretation of fracture criticality classification and fracture control implementation of rotating machinery with kinetic energy less than 19,310 Joules (14,240 ft-lbs).

NASA-HDBK-5010, VOLUME 2, REVISION A

The centrifuge rotor example described in this section has less kinetic energy than 14,240 ft-lbs but has significant rotational momentum and fracture critical parts. The parts are classified fracture critical because they have credible structural failure modes due to crack propagation that may cause sudden jamming and stoppage of the rotor generating loads that could result in a catastrophic hazard.

6.1.3.2 Role of Jamming and Sudden Rotor Stoppage for Fracture Critical Classification

For parts to be classified as Nonfracture Critical Rotating Hardware, the following topics (in addition to the kinetic energy calculation) should be included in the assessment:

1. Rotating machinery angular momentum does not exceed a threshold based on testing or heritage data (e.g., 100 pounds-foot-seconds or 136 N-m-s) and does not present a catastrophic hazard if loads generated from a sudden jamming or stoppage of the rotor exceed structural allowable loads.
2. Credible rotor sudden-stop jamming events due to structural failure from crack propagation are not present in the mechanical assembly components.
 - a. Sudden-stop or jamming could also initiate from introduction of external jamming debris between the rotor and adjacent stationary components, or seizure of rotating mechanisms such as bearings. These hazards do not result from propagation of preexisting cracks and can be addressed through fracture control but are not the focus of this section. These types of hazards may be addressed by safety procedures such as design for minimum risk defined in Equation 6.1.3-1.
 - b. The structural loads of components in the rotating and nonrotating mechanical assembly should include normal loads (not rotor sudden-stop loads) as applicable for the hardware service life. These loads are to be utilized for fracture mechanics assessments such as crack growth safe-life calculations, structural fail-safe evaluations for fracture control, and fatigue life assessments where needed for low risk classification of parts.

The sudden rotor jamming or stoppage loads referenced in item (1) may be estimated as described in later sections. If the sudden-stop loads exceed the allowable and generate a catastrophic hazard on the mechanical assembly support structures, carrier, or vehicle, the mechanical assembly is considered potentially fracture critical. If the mechanical assembly is classified as a fracture critical assembly, all assembly parts both rotating and nonrotating should be assessed for fracture criticality.

6.1.3.3 Angular Momentum and Sudden-Stop Loads Calculation

All further examples in this Handbook regarding sudden-stop loads assume that an angular momentum of 100 foot-pounds-second is the threshold for fracture criticality, but this angular

NASA-HDBK-5010, VOLUME 2, REVISION A

momentum threshold should be based on test data. To complete the determination of hazard criticality due to rotor sudden-stop induced loads on the mechanical rotor assembly support structures, carrier, or vehicle, the impulsive sudden-stop induced loads are needed. The impulsive loads generated in a sudden-stop are directly proportional to the angular momentum, H , and inversely proportional to the speed of the sudden-stop, t . The angular momentum of a rotating body is computed as $H = I\omega_0$.

$$K.E. = \frac{1}{2}I\omega_0^2 = \frac{1}{2}(I\omega_0)\omega_0 = \frac{1}{2}H\omega_0 = 14,240 \text{ ft} - \text{lb} \quad (\text{Equation 6.1-3})$$

Note that low speed rotating machinery may have very large angular momentum and not exceed these fracture criticality criteria. The torque, T , induced during a sudden-stop into a tangential jamming spring for a rotor supported on a base is inversely proportional to the time, t , to reach the maximum torque. The equation is:

$$T = \left(\frac{\pi}{2}\right) H/t \quad (\text{Equation 6.1-4})$$

Aside from the momentum, H , the critical parameter needed to determine rotor sudden-stop loads is the time t . The time is assumed to be one second for most of the cited examples for ease of calculation and comparisons, but this value is not a generally applicable number. Loads should be computed for relevant stop times for the application. It is possible to compute a sudden-stop time for some simple rotor jamming models; but for more complex situations such as the centrifuge rotor example, more involved analyses or tests may be required.

Once the rotor sudden-stop loads are determined, they can be compared to the allowable for the rotating machinery support structures, carrier, or vehicle. Note that in addition to the dynamic torque discussed above, dynamic forces may also be generated which have to be assessed.

6.1.3.4 Rotary Mechanical Assembly Example Assessments

To help classify rotating mechanical assemblies, several examples are described in the following sections.

Steel Disk Examples

Two 8-inch diameter disks identified as A and B have only 8% and 32%, respectively, of the critical kinetic energy limit value of 14,240 ft-lbs. They represent possible shrouded or enclosed fans and require additional evaluations using the flowchart in Figure 6.1-1 before the disks can be classified as nonfracture critical.

Two other 12-inch diameter disks C and D were selected to describe hardware that exceeds the kinetic energy of 14,240 ft-lbs. After evaluation of the disks per Figure 6.1-1, it was found that these disks C and D are both fracture critical and must (1) meet the spin test and NDE requirements and (2) show adequate safe life if they are not contained.

NASA-HDBK-5010, VOLUME 2, REVISION A

Centrifuge Rotor Example

In contrast to the steel disk examples, consider a large centrifuge rotor that possesses only 45% of the kinetic energy limit value of 14,240 ft-lbs. It is determined to be a fracture critical part because (1) it has a very large angular momentum, and (2) there are credible sudden-stop events due to structural or component failures from crack propagation that can result in jamming of the rotor. The centrifuge rotor structure is then classified fracture critical as well as the attachments holding components which could jam the rotor.

There are events other than structural failure which could lead to sudden-stop hazard of the centrifuge rotor such as introduction of debris that jams the rotor or causes seizure of bearings. These hazards are controlled by special designs to meet safety requirements. The centrifuge rotor sudden-stop maximum torque is computed as 72,700 foot-pounds using a simple model. That sudden-stop torque exceeds the allowable torque of 20,500 foot-pounds for the application and results in a classification of the CR structure and other components as fracture critical even though the centrifuge rotor has only 45% of the kinetic energy limit criteria for fracture critical rotating equipment.

6.1.3.5 Simplified Models of Sudden-Stop Induced Loadings

Two types of base supported rotor sudden-stop event configurations shown in Figure 6.1-3, Sudden-Stop Simplified Models, were analyzed below with simplified models to determine loads and associated parameters. Although more complex analyses may be required for applications such as the centrifuge rotor, these simplified models are useful where applicable and can help identify the fundamental relationships of the relevant parameters.

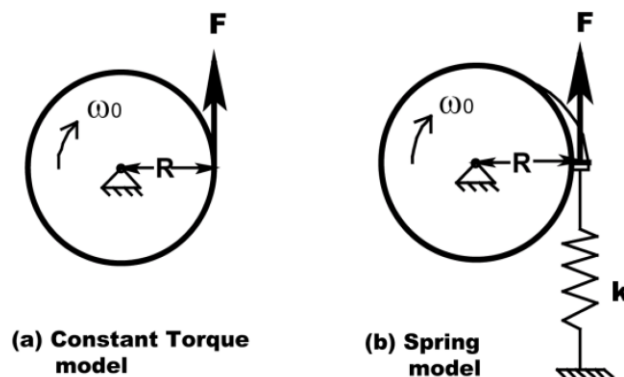


Figure 6.1-3—Sudden-Stop Simplified Models

Constant Torque Deceleration Model

In this situation, a constant torque producing a constant deceleration is assumed to act upon the rotor, which is assumed to be rotating at initial speed ω_0 about a supported central axis as shown in Figure 6.1-3(a). This situation may occur if a constant deceleration force is applied to the outer radius of a rotating body. A ball or roller bearing seizure may produce this situation if the rolling element binds with the bearing races. Bearing failures of this type have been known to continue to rotate for appreciable time until heating leads to a complete failure.

NASA-HDBK-5010, VOLUME 2, REVISION A

The conditions resulting from the case of a constant torque, T , deceleration acting for a time duration t can be computed from the equation for angular motion as follows:

$$T = I \left(\frac{d\omega}{dt} \right) \rightarrow \int d\omega = \left(\frac{T}{I} \right) \int dt \rightarrow \omega = \left(\frac{T}{I} \right) t \rightarrow T = \frac{I\omega_0}{t} = \frac{H}{t} \quad (\text{Equation 6.1-4})$$

If the time involved in a rapid stop is known, the torque can be computed from the body angular momentum and Equation 6.1-4. If the sudden-stop or deceleration is developed by loading at the body outer radius R , the associated force F is equal to T/R . The tangential force induces a force acting on the body center of gravity, with a resulting acceleration in Gs equal to the force divided by the body weight. For the case where a rotating body is presumed to possess a momentum at the fracture critical kinetic energy limit per equation (K1), and a sudden-stop time of one second, the torque T can be plotted as a function of initial rotational speed in revolutions per minute (RPM). The number of revolutions required for the body to stop can be determined from:

$$\omega = \left(\frac{d\theta}{dt} \right) = \left(\frac{T}{I} \right) t \rightarrow \int d\theta = \left(\frac{T}{I} \right) \int t dt \rightarrow \theta = \left(\frac{T}{I} \right) \frac{t^2}{2} \quad (\text{Equation 6.1-5})$$

Tangential Spring Deceleration Force Model

Another type of sudden-stop event may occur if debris or a structural failure causes a rotor jamming event at the rotor outer radius. This could be from loads transferred into a nonrotating shroud or other grounded body, which can be simulated as loading a tangential spring at the rotor outer radius as shown in Figure 6.1-3(b).

The force induced into the spring, and the dynamic loads on the body resulting from this deceleration, can be computed from the equation for angular motion. It is assumed the body remains supported at the center of rotation and does not translate. (If the body is free to translate, such as the centrifuge rotor example, additional coupled equations of motion are involved; and this simple model does not apply.) Parameters include the grounded circumferential spring stiffness k , and the circumferential spring force F due to the body rotation angle θ leading to the following equations:

$$F = k(R\theta), \quad T = -FR, \quad \text{and} \quad T = I \left(\frac{d\omega}{dt} \right) = I \left(\frac{d^2\theta}{dt^2} \right) \quad (\text{Equation 6.1-6})$$

$$I \left(\frac{d^2\theta}{dt^2} \right) + kR^2\theta = 0, \quad \left(\frac{d^2\theta}{dt^2} \right) + b^2\theta = 0 \quad \text{where} \quad b = \sqrt{kR^2/I} \quad (\text{Equation 6.1-7})$$

The solution for initial condition θ equal to zero and ω_0 angular speed is:

$$\theta(t) = (\omega_0/b) \sin(bt) \quad (\text{Equation 6.1-8})$$

By differentiation the torque is:

$$T = I \left(\frac{d^2\theta(t)}{dt^2} \right) = -I(\omega_0 b) \sin(bt) = -Hb \sin(bt) \quad (\text{Equation 6.1-9})$$

NASA-HDBK-5010, VOLUME 2, REVISION A

The peak torque is $T_{max} = Hb$, and it will occur at time t where $\sin(bt)$ is maximum at:

$$t = \frac{\pi}{2b} = \left(\frac{\pi}{2}\right) \sqrt{\frac{I}{kR^2}} \quad (\text{Equation 6.1-10})$$

$$T_{max} = \left(\frac{\pi}{2}\right) \frac{H}{t} \quad (\text{Equation 6.1-11})$$

All quantities in this simplified problem can be defined based on the rotating body characteristics, the angular momentum, and the spring constant k . The spring may be computed from the combined stiffness of rotor structures reacting the circumferential force plus stiffness of any jamming debris and stiffness of the surrounding structure to ground. Alternatively, if the sudden-stop time to the peak load t is known, the associated parameter b and spring stiffness k can be computed. The rotation at the time of maximum torque is (ω_0/b) from Equation 6.1-8.

Note from Equation 6.1-11, the maximum torque is again directly proportional to the angular momentum and inversely proportional to the sudden-stop time t to reach maximum torque. The peak torque for this model of sudden-stop acting into a spring is a factor of $(\pi/2)$ larger than the value for the constant torque deceleration example.

6.1.3.6 References

MA2-00-057, PSRP letter on Mechanical Systems Safety, September 28, 2000, in NSTS/ISS 18798b, "Interpretations of NSTS/ISS Payload Safety Requirements."

6.1.4 NFC Sealed Container

A checklist is provided in Table 6.1-3, Checklist for NFC Sealed Container, for NFC sealed containers, e.g., a sealed electronics box that is not part of a pressure system and is not a pressure vessel. For NFC sealed containers, no NDE or fracture analysis is required. To meet this NFC category, all items in the checklist need to be met.

Table 6.1-3—Checklist for NFC Sealed Container
(All requirements must be met.)

Item	Description of Requirement	Meets (Y or N)
1	Does not contain hazardous material.	
2	Loss of pressure or fluid from the container does not result in a catastrophic hazard.	
3	Container supports meet fracture control requirements.	
4	The part is manufactured from metal alloys typically used for commercially available sealed containers procured to an aerospace standard or equivalent that are not susceptible to crack extension related to EAC or SLC.	

NASA-HDBK-5010, VOLUME 2, REVISION A

5	The container satisfies the LBB definition in this document at MDP.	
6	The container does not have an impervious barrier or coating that inhibits leakage on either the interior or exterior surfaces.	
7	The container is inspected for leaks before repressurization.	
8	Reflight containers are inspected for leaks before being reflowed.	
9	Stored fluid energy < 14,240 ft-lb based on adiabatic expansion of a perfect gas.	
10	MDP is less than 44 psi.	
11	If $22 \text{ psi} < \text{MDP} < 44 \text{ psi}$, then either: (i) Positive structural margins against burst factor of $2.5 \times \text{MDP}$ is predicted OR (ii) Container is proof tested to a minimum of 1.5 times the MDP.	

Example 1. The MDP for a sealed container is less than 30 psi, the container is not proof tested, and the minimum structural margins are 12% with a burst factor of 1.5. Criteria in 10 and 11 in the checklist are not met, and the container is classified as FC.

Example 2. The container does not satisfy LBB at MDP. The container is classified as FC since criteria 5 is not met.

Example 3: The container contains hazardous material and the MDP is 50 psi. Criteria in items 10, 11, and 1 are not met; the container is classified as FC.

Example 4: Different NASA organizations (e.g., JSC) may have tailored the criteria in Table 6.1-3, but it does not imply that it will be accepted for all programs and all applications. These are typically tailored for payloads and not propulsion systems. In one program, JSC classified a hardware as NFC Sealed Container because it utilized common aerospace materials of construction and had high fracture toughness [$K_{Ic}/F_{Ty} > 0.33 \sqrt{\text{in}} (1.66 \sqrt{\text{mm}})$] as these typically demonstrate LBB failure modes per JSC 25863C, Fracture Control Plan for JSC Space-Flight Hardware.

6.1.5 NFC Tools, Mechanisms, and Tethers

This section is reserved.

6.1.6 NFC Batteries

For the battery to be classified as NFC, the battery cell and enclosure must meet both the NHLBB Pressurized Components checklist and the NFC Sealed Container checklist. Because some of the requirements are common between the two checklists, a consolidated checklist is provided in Table 6.1-4, Checklist for NFC Batteries, to assist in the NFC part classification. To meet this NFC category, all items in the checklist need to be met.

APPROVED FOR PUBLIC RELEASE – DISTRIBUTION IS UNLIMITED

NASA-HDBK-5010, VOLUME 2, REVISION A

**Table 6.1-4—Checklist for NFC Batteries
(All requirements must be met.)**

Item	Description of Requirement	Meets (Y or N)
1	Does not contain hazardous material.	
2	The leak or loss of pressure or fluid does not cause a catastrophic hazard.	
3	Battery enclosure supports meet fracture control requirements.	
4	The part is manufactured from metal alloys typically used for commercially available sealed containers procured to an aerospace standard or equivalent that are not susceptible to crack extension related to EAC or SLC.	
5	The battery cell satisfies the LBB definition in this Handbook at MDP.	
6	The battery cell does not have an impervious barrier or coating that inhibits leakage on either the interior or exterior surfaces.	
7	The battery is inspected for leaks before repressurization.	
8	Reflight batteries are inspected for leaks before repressurization and/or before being reflowed.	
9	Stored fluid energy < 14,240 ft-lb based on adiabatic expansion of a perfect gas.	
10	MDP is less than 44 psi.	
11	If 22 psi < MDP < 44 psi, then either: (i) Positive structural margins against burst factor of 2.5 x MDP is predicted OR (ii) Battery is proof tested to a minimum of 1.5 times the MDP.	
12	As the hardware item leaks down, there is no repressurization or continued pressure cycles that could lead to continued fatigue or crack growth related to EAC or SLC.	
13	The hardware is manufactured from metal alloys that are not susceptible to crack growth related to EAC or SLC	

Per section 6.1.5 in NASA-STD-5019A, the guidance indicates that “small batteries in common use such as button cells of 200 mA-hr or less and carbon-zinc or zinc-air batteries of size F or smaller are exempt from fracture control.”

Example 1: A small button cell battery of 50 mA-hr is part of a design and is considered exempt from fracture control.

Example 2: A carbon-zinc battery smaller than size F is used in a design and is considered exempt from fracture control.

APPROVED FOR PUBLIC RELEASE – DISTRIBUTION IS UNLIMITED

NASA-HDBK-5010, VOLUME 2, REVISION A

Example 3: The MDP for a battery container is less than 30 psi, the battery is not proof tested, and the minimum structural margins are 12% with a burst factor of 1.5. Criteria 11 in the checklist is not met, and the battery is classified as FC.

Example 4: The battery does not satisfy LBB at MDP. The container is classified as FC since criteria 5 is not met.

Example 5: The battery contains hazardous material and the MDP is 50 psi. Criteria 10, 11, and 1 are not met; the battery is classified as FC.

Example 6: Externally mounted batteries such as large lithium ion batteries do not fall into a strict NFC or FC category. The battery cells are not pressurized during operation but can be pressurized during thermal runaway (failure case). These batteries typically meet JSC 20793, Crewed Space Vehicle Battery Safety Requirements. There are questions as to whether the battery cells need to meet the pressure vessel requirements. The battery enclosure will trap most of the released material but can be vented. Consideration for these designs is not to treat it as a pressure vessel but rather a designed-to-leak container.

6.2 General Approaches for NFC Parts

This section is reserved.

6.2.1 NFC Low-Released Mass

An assessment of NFC Low-Released Mass can be conducted by analysis or test. Typically, a validated analysis methodology can be used in the assessment. In cases where analysis is of low confidence, a test approach is recommended. Examples are provided that utilize either an analysis approach or test.

An example is provided to illustrate the concept of NFC Low-Released mass. A nonstructural heatshield component within a liquid rocket engine cracks and releases mass that travels through the system causing no catastrophic hazard. The failure mode was exercised through six engines fires for a duration/starts equal to two times the service life per NASA-STD-5012B, Strength and Life Assessment Requirements for Liquid-Fueled Space Propulsion System Engines. None of the engines experienced an adverse event due to the released mass. Impact analysis of the released mass also showed negligible effects on the structural and system performance. Consequently, the nonstructural component was assessed as NFC Low-Released Mass.

In the following second example, a piece from a nozzle component breaks loose due to sudden pressurization. Several static fire tests and flight experience demonstrates that the loose piece does not impact system or structural performance. There is no risk of the piece impacting any part of the spacecraft or structure. The part is classified NFC Low-Released Mass.

In this third example, a zip tie attached to a bonded clip is used to attach a part to a nonpressurized composite structural interstage. The zip tie can break loose if a flaw is present,

APPROVED FOR PUBLIC RELEASE – DISTRIBUTION IS UNLIMITED

NASA-HDBK-5010, VOLUME 2, REVISION A

but analysis demonstrates that the energy is insufficient to cause damage to the structure; and there is no risk of loss of functional, structural, and performance degradation. The part is also classified as NFC Low-Released Mass.

There may be a tendency to classify a component NFC Low-Released Mass based on weight, but it is important to consider the consequences of impact of the released mass. In the case of liberated foam insulation such as in the case of the Columbia accident, although the foam was of low mass, the velocity when it struck the leading edge of the Orbiter was high. An excerpt from the Columbia Accident Investigation Board (CAIB) report stated:

"The visual evidence taken by launch cameras clearly shows the debris impact velocity was between about 500 fps and 800 fps relative to Columbia. Just prior to separating from the External Tank (ET), the foam was traveling with the orbiter at about 2300 fps. The visual evidence shows that the debris impacted the wing approximately 0.161 seconds after separating from the ET. In that time, the debris slowed down from 2300 fps to about 1500 fps, so it hit the orbiter with a relative velocity of about 800 fps. In essence, the debris slowed down and the Orbiter did not, so that the Orbiter ran into the debris. The foam slowed down rapidly because it had a low ballistic number. The ballistic number of the debris was small because the foam has a low density."

In this case, the impact of the foam on the orbiter could (and did) cause a catastrophic hazard, it should have been classified as fracture critical. Note that at that time, the ET foam insulation was not under fracture control.

6.2.2 NFC Contained

Parts that are safely confined in an enclosed volume should they become loose because of the presence of a flaw may be designated NFC via the contained category. (See Figure 6.2-1, NFC Contained Flowchart.) If the part contains hazardous materials or fluids, the containment assessment should also establish that no hazardous materials or part fragments are released that result in a catastrophic hazard. Also note that composite enclosure impact damage should be considered during fracture control classification and assessment of the enclosure.

NASA-HDBK-5010, VOLUME 2, REVISION A

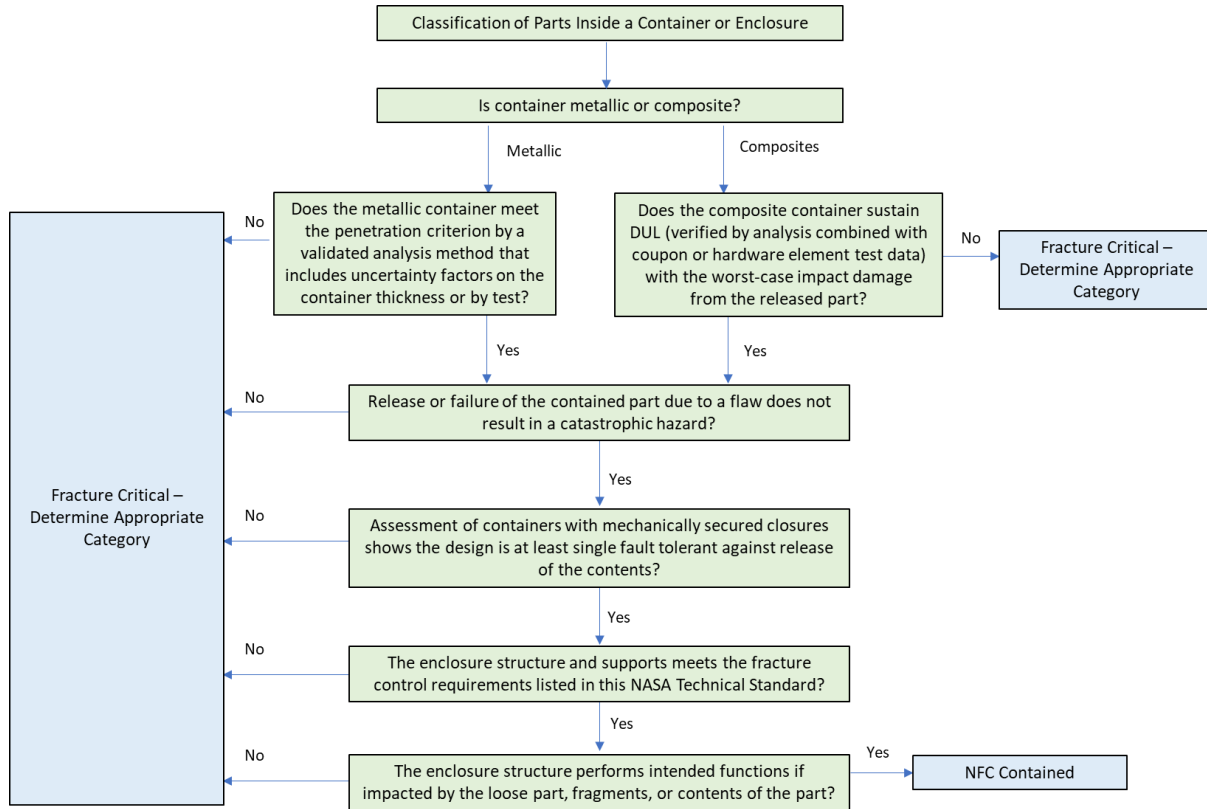


Figure 6.2-1—NFC Contained Flowchart

6.2.2.1 Containment Punch Equation Calculation

Methods to assess containments of parts that may come loose inside of “containers” such as electrical boxes during payload acceleration for launch or landing or rotation are discussed. The so-called “Punch” equation has been used in these assessments, and it is supported by very limited test data. The energy required to “punch out” various sizes of circular areas in metals with given thickness and tensile yield strength is calculated; but in general, the Punch equation is conservative. The punch equation is given as follows:

$$t = \left(\frac{M V^2}{2 \pi D F_{ty}} \right)^{1/2}$$

(Equation 6.2-1)

F_{ty} = Tensile yield strength of the container

D = Diameter of the projectile

M = Mass of projectile

t = Thickness required to contain the projectile

V = Impact velocity

An effective diameter may be used in the above equation for impact shapes other than a circle by

APPROVED FOR PUBLIC RELEASE – DISTRIBUTION IS UNLIMITED

NASA-HDBK-5010, VOLUME 2, REVISION A

calculating the diameter that will result in a perimeter of a circle equal to the perimeter length of the predicted impact area. The predicted area and shape is based on the entire frontal face of the part assumed normal to the container on impact. The diameter D is calculated by equating the perimeter of a circle of diameter D to the following example cases:

1. Perimeter of the smallest face of a rectangular object ($2 \times [\text{length} + \text{width}]$).
2. Perimeter of the circular projection when looking at a conical end.
3. The base perimeter of a cone.
4. The perimeter of the projected flat edge of a disk ($2 \times [\text{diameter} + \text{thickness}]$).

6.2.2.2 Discussion on Containment of Rotating Parts

Fracture control requirements for operational safety of rotating devices often necessitate an evaluation of containment capability of covers, rings, housings, etc., which surround a rotating part such as a fan, motor, gyroscope, etc. For extremely high rotational velocities, other additional considerations such as rubbing will likely need to be considered to help dissipate the energy. A conservative impact velocity V may be used in the Punch equation by calculating the velocity to be equal to the outer radius of the rotating part multiplied by the rotational speed of the rotating part. If the calculated thickness is larger than the actual enclosure thickness, the rotating part will not be contained in the event of fragment generation of the shape, size, and mass assessed. A rotating part, which would not be contained, must be assessed for safe life using a conventional fracture mechanics approach.

6.2.2.3 Containment Example Calculation for Rotating Hardware

A small two- (2) blade cooling fan has a diameter of $d = 3.06$ inches. The fan weighs 0.302 lb (137 grams) and rotates at $\omega = 10,000$ rpm (1047 rad/sec). The fan and its housing are made of Aluminum 6061-T6 alloy. The blades are 0.07 in thick, and the housing is 0.1 in thick. Calculations show that the rotating fan does not possess the energy level necessary (14,240 ft-lbs) to automatically require proof testing, inspection, and safe life assessment. Because of high RPM, an analysis must be made for containment.

The impact velocity can be calculated as $V = \omega d / 2 = (1.53 \times 1047) = 1602$ in/sec. The weight of the released blade from the two-blade fan is assumed to be half of the fan weight, as it is a conservative assumption: 0.151 lbs. The thickness required to contain the projectile is as follows:

$$T = \left[\frac{(0.00039 \text{ lb} - \text{sec}^2 / \text{in}) * (1602 \text{ in} / \text{sec})^2}{2 * (\pi) * (0.68 \text{ in}) * (35000 \text{ lb} / \text{in}^2)} \right]^{1/2} = 0.082 \text{ inch}$$

(Equation 6.2-2)

where:

gravitational acceleration, $g = 32.2 \text{ ft/sec}^2 = 386.4 \text{ in/sec}^2$

mass of the fan blade $0.151 / 386.4 = 0.00039 \text{ lb} - \text{sec}^2 / \text{in}$

impacting edge of the blade assumed to be 1 inch long

APPROVED FOR PUBLIC RELEASE – DISTRIBUTION IS UNLIMITED

NASA-HDBK-5010, VOLUME 2, REVISION A

perimeter of the blade calculated as $[(2 \times 1.0) + (2 \times 0.07)] = 2.14$ inches, and diameter of the circle with a circumference of 2.14 inch $= 2.14/\pi = 0.68$ inch

The wall thickness required to contain the projectile piece is 0.082 in, and the actual one is 0.1 in as provided in Figure 6.2-2, Analytical Sketch for Rotating Hardware for the Example Problem. Break-up of the fan is contained; and the part is classified as NFC Contained.

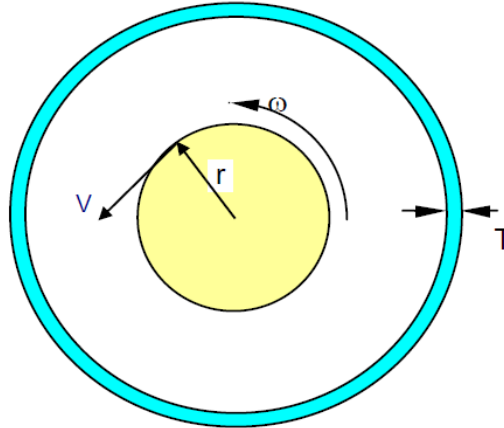


Figure 6.2-2—Analytical Sketch for Rotating Hardware for the Example Problem

6.2.2.4 General Containment Analysis

Containment analyses should consider such factors as the velocity and energy of the part, worst-case sharpness/minimum area, elastic and/or plastic deformation, and the resulting stresses on the enclosure. For containment, it must be shown that structures or parts will be contained if they become detached from the payload because of structural failure of the part or attachment fasteners. Analysis must show that no part can attain sufficient kinetic energy to escape a container, which completely encompasses the aggregate structures or parts (such that none of them or their fragments can escape the confines of their container to cause a hazard to the vehicle or crew). The velocity in the “Punch” equation is modified to include other effects associated with a preloaded fastener:

$$V = V_1 + V_0 = \sqrt{2a S_d} + \sqrt{\frac{P_0^2 L}{A E M}}$$

(Equation 6.2-3)

where V_1 is the impact velocity of the detached piece due to acceleration a , V_0 is the impact velocity due to fracture of a preloaded fastener, P_0 is the fastener preload in pounds, M is the fastener fragment mass, L is the fastener preloaded length in inches, A is the fastener cross sectional area in inches, and E is the fastener modulus of elasticity. In addition, S_d is the maximum travel distance of the projectile within the container (such as the longest diagonal in a rectangular box, minus the smallest dimension of the free part). Note that this only applies to low

APPROVED FOR PUBLIC RELEASE – DISTRIBUTION IS UNLIMITED

NASA-HDBK-5010, VOLUME 2, REVISION A

fracture toughness fasteners weighing more than 0.03 pounds; otherwise, the fastener would be considered a low-release mass.

The kinetic energy of the projectile(s) created as a result of a structural failure of contained structures or parts is determined by the mass of the detached part (M) and the velocity (V) it can attain within the confines of its container. Contributors to the projectile impact velocity that the analyst should consider are the impact velocity (V_I) due to acceleration and initial velocity (V_0) of a fastener fragment caused by the sudden release of preload. Neither the relative velocity due to the structural dynamic response of the projectile and its mounting prior to release, nor the relative velocity due to the vibration response of the impacted wall is generally considered in the velocity calculations. These components are required only for special cases of significant structural displacements sufficient to generate a whip type action propelling the projectile or wall displacements that are an order(s) of magnitude times the thickness. If the failure is that of a preloaded fastener, the initial velocity, V_0 , will be induced by the sudden conversion of stored energy (preload) to kinetic energy.

6.2.2.5 Container Fastener Analysis

Fasteners holding containers together often need to be assessed. For example, fasteners that hold the lid on a box may require analysis to show that they would not break if the lid was struck by a loose part. Both rotating and stationary parts should be assessed. This assessment would be required for containment of a relatively large mass with a relatively large contact area whose impact would not be expected to penetrate the walls, but would, nonetheless, be a significant dissipation of energy. This check may not be required for electronics and similar boxes using standard packaging designs. The analyst should coordinate with the RFCB when uncertainty exists for analyzing container fasteners. This type of analysis can be quite complex and involve several failure modes. The following needs to be evaluated:

1. Does the loose part strike at a single fastener or between fasteners?
2. Does the fastener fail in tension or extrude the fastener head through the wall thickness?
3. If a fastener fails, will adjacent fasteners carry the remaining energy?
4. If a fastener(s) fails, will the deflection of the cover remain small enough so that the loose part does not escape?
5. Does the loose part absorb significant energy itself upon impact with the container wall?

A simplified method for assessing the tensile capability assuming a loose part impacts directly upon a single fastener is given below. This is conservative since a loose part is most likely to strike in an area where the load would be shared among more than one fastener. If the fastener passes this check, a similar check would be required for extruding the fastener head through the cover wall. If both these checks are passed, the analysis would generally be considered complete; otherwise, the analyst must investigate further the type of things listed above. The approach is to assume that the kinetic energy of the loose part must be absorbed by the strain energy capability

NASA-HDBK-5010, VOLUME 2, REVISION A

of the fastener. This kinetic energy is readily available from the analysis and the following is the inequality necessary for containment:

$$1.6 \frac{1}{2} M V^2 < \frac{1}{2} \epsilon_{ult} l (P_{ty} + P_{tu})$$

(Equation 6.2-4)

where the left side of the inequality is the kinetic energy of the loose part and right side of the equation is the strain energy capability of the bolt, which depends on the length (l) of the bolt strained, ϵ_{ult} is the ultimate strain capability of the bolt material, P_{ty} is the tensile yield strength of the bolt, and P_{tu} is the ultimate strength of the bolt. The “1.6” factor in this equation is the dynamic amplification factor and, in the inequality, condition should be applied for the weakest fastener holding the container together.

6.2.3 NFC Fail-Safe

Parts with sufficient structural redundancy such that an individual element failure does not violate system performance, function, or structural capability may be designated NFC via the fail-safe category. Consider a component that is attached to a spacecraft using a four-truss system. An analysis without one of the trusses (one truss is fully cracked) shows positive structural margins of safety for the remaining trusses. A failure modes effects and analysis demonstrated no system impact and that, even if the truss cracked, the truss would not become loose or contact any composites. The truss system is classified NFC Fail-Safe.

Note that this classification only applies for structures with redundant members, i.e., the remaining members can carry the redistributed load changes due to the loss of one member without loss of structural capabilities or causing a catastrophic hazard during the mission lifetime. If inspection between reflight is not feasible, alternative rationale is required to demonstrate that the structure maintains redundancy for future flight. Possible considerations may include fatigue-based rationale, instrumentation and flight data demonstrating no member failed, and rationale that the failure of one member of the structure does not result in foreign object debris (FOD) loss of function of the structure for reflight.

6.2.4 NFC NHLBB Pressurized Component

NHLBB components are metallic pressure-bearing walls of containers, trapped volumes, lines, fittings, valves, regulators, filters, bellows, or other pressurized hardware that transfer nonhazardous fluid under pressure and that would leak down in the presence of a flaw rather than burst when used as intended. All items in the checklist in Table 6.2-1, Checklist for NFC NHLBB Pressurized Component, need to be met for a pressure component to be classified as NFC NHLBB:

NASA-HDBK-5010, VOLUME 2, REVISION A

**Table 6.2-1—Checklist for NFC NHLBB Pressurized Component
(All requirements must be met.)**

Item	Description of Requirement	Meets (Y or N)
1	The pressurized item satisfies the LBB definition in this Handbook at MDP.	
2	The leak does not cause a catastrophic hazard or release hazardous fluid.	
3	As the hardware item leaks down, there is no repressurization or continued pressure cycles that could lead to continued fatigue or crack growth related to EAC or SLC.	
4	The hardware is manufactured from metal alloys that are not susceptible to crack growth related to EAC or SLC	
5	Structure supporting pressurized hardware also meets fracture control requirements.	
6	Hardware does not have an impervious barrier, coating, etc., on either the interior or exterior surfaces that inhibits leakage.	
7	Reflight hardware is inspected for leaks before repressurization and/or before being reflown.	

Guidance is provided on the topic of NHLBB for pressure system components, which is a required evaluation listed in the first item of the checklist. Specific considerations relative to LBB are discussed in section 11 in this Handbook. When LEFM is applicable, an acceptable approach to demonstrate LBB for metallic alloys is to show by analysis that a worst-case surface crack will grow into a through-the-thickness crack without unstable crack propagation. This presumes the hardware manufacturing process has no credible risk of producing initial flaws longer than the crack, and leakage through the crack is shown to reduce pressure before loadings could grow the crack to cause fracture. The analysis, considering applied loads and residual stress effects, shows that the crack will leak and not be unstable.

The design safety factor requirements applied to typical pressurized systems and common materials of construction tend to ensure that the critical flaw size (CFS) requirements for NHLBB are met under operating conditions. NHLBB is characterized by a relatively slow leak as opposed to rapid tearing or fragmentary rupture. A general approach is to ensure that the CFS be a through flaw of length at least 10 times the thickness ($2c \geq 10t$) for the component to be NHLBB. Figure 6.2-3, Critical Flaw Size Criteria for Nonhazardous Leak Before Burst for a $2c = 10t$ Flaw, includes design curves to check for this in pressurized tubes.

To generate the design curves in Figure 6.2-3, a parametric numerical study was performed. NASGRO® was run using TC07 taking S_0 as the input rather than internal pressure, and the thick-walled cylinder stress equation was used because the thin-walled approximation does not apply for the higher thickness-to-outer diameter ratio. In the x -axis is the thickness-to-outer diameter ratio, and in the y -axis is the ratio of material fracture toughness to pressure. One design curve is provided for each outer diameter. If a point for a tube is above the respective optical density (OD) curve, the CFS is a through flaw of length at least 10 times the thickness, and the CFS requirement for NHLBB is met. If the CFS requirement for NHLBB is not met, a more

APPROVED FOR PUBLIC RELEASE – DISTRIBUTION IS UNLIMITED

NASA-HDBK-5010, VOLUME 2, REVISION A

specific fracture mechanics analysis may be conducted addressing actual component parameters and properties. When the 10t fracture analysis check is made, the analyst should make sure that any actual through cracks in the hardware will be less than 10t in length. Otherwise, an actual crack in the hardware may have grown past 10t potentially leading to an unsafe situation.

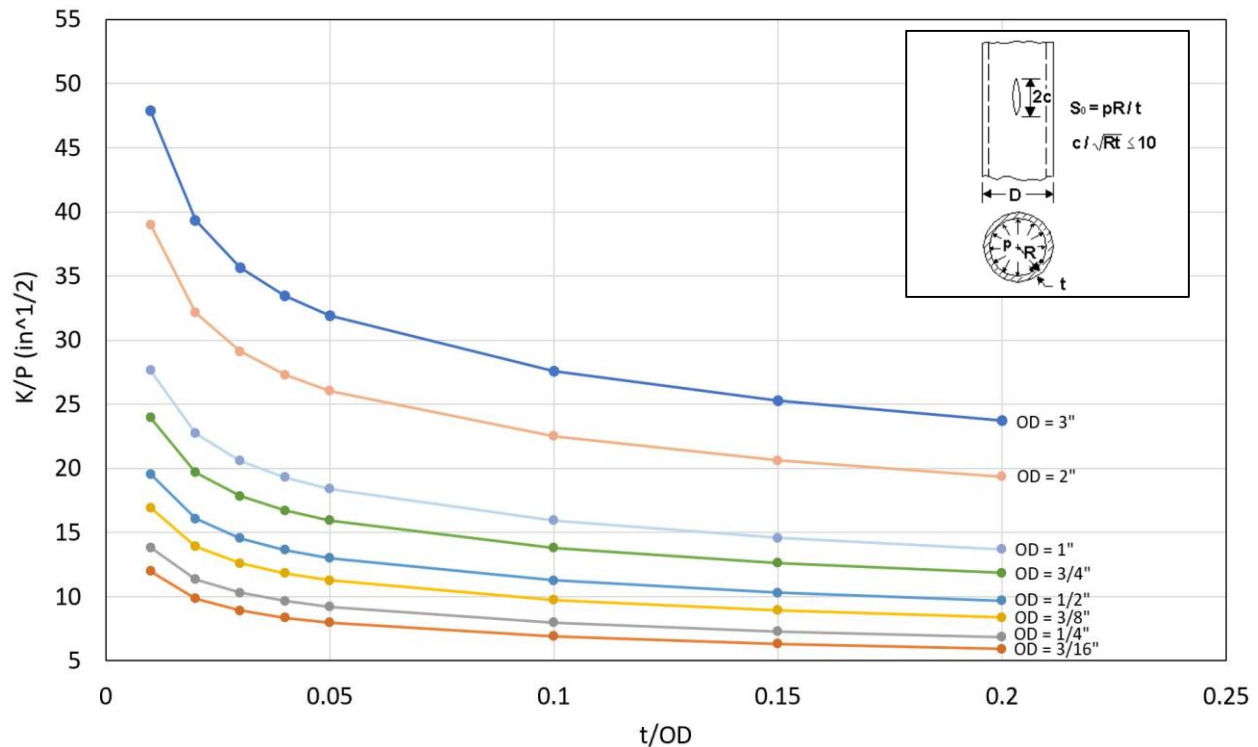


Figure 6.2-3—Critical Flaw Size Criteria for Nonhazardous Leak Before Burst for a $2c = 10t$ Flaw

(The y-axis is the ratio of fracture toughness, K , to pressure, P . The x-axis is the ratio of thickness, t , to outer diameter, OD . A pressure and geometric configuration above the curve of interest indicates the CFS requirement for NHLBB is met. Below indicates a violation of the CFS requirement.)

When the analyst or responsible engineer is uncertain about the application of the LBB analysis criteria or the prescribed flaw aspect ratios, it becomes prudent to consider the intent of LBB in the bigger context of safety, fracture control, production defects, and inspections. See the following example:

A pressure component is evaluated for NHLBB. All the criteria 1-6 are met. There are reasonable concerns based on production and inspection experience that low aspect ratio surface flaws could exist. Per section 11.1 in this Handbook, it is recognized that low aspect ratio flaws can lead to burst rather than leak, despite the analysis results suggesting an LBB failure mode. Due to this uncertainty, the pressure component is subjected to a suite of testing while containing enveloping low aspect ratio flaws (compared to production data) to show that LBB is met by test. For long surface cracks, 10t LBB criterion may be insufficient for such crack geometries.

APPROVED FOR PUBLIC RELEASE – DISTRIBUTION IS UNLIMITED

NASA-HDBK-5010, VOLUME 2, REVISION A

Alternatively, this hardware could be classified as fracture critical and receive safe-life analysis and the required NDE.

Generally, for items other than thin-walled cylinders or spheres dominated by pressure loads, it can be challenging to use a LBB justification. Complications can be caused by e.g., thicker regions, stiffeners, loads other than pressure, bending in the skin, and stress concentrations.

6.2.5 NFC Low-Risk Parts

6.2.5.1 NFC Low-Risk Metallic Parts

Metallic parts are classified as NFC Low Risk if they meet all the items in the checklist in Table 6.2-2, Checklist for NFC Low-Risk Metallic Parts. These parts are extremely unlikely to contain or develop critical flaws because of (1) extremely low likelihood of flaws being induced by manufacturing processes, environmental effects, or service events and (2) large structural margins. These parts do not require NDE or fracture analysis based on the NDE detection limit per NASA-STD-5009A, Nondestructive Evaluation Requirements for Fracture Critical Metallic Components.

**Table 6.2-2—Checklist for NFC Low-Risk Metallic Parts
(All requirements must be met.)**

Item	Description of Requirement	Meets (Y or N)
1	The part is manufactured from materials with well-characterized strength and ductility properties using processes that have been established by inspections to be extremely unlikely to produce parts with flaws and that have been shown not to fail because of brittle fracture.	
2	Metallic parts have a material property ratio of $K_{Ic}/F_{ty} \geq 1.66 \sqrt{\text{mm}}$ (0.33 $\sqrt{\text{in}}$) and do not have sensitivity to EAC, SLC, or stress corrosion cracking as defined in NASA-STD-6016.	
3	Aluminum parts are not loaded in the short transverse direction if this dimension (from the raw stock part) is greater than 7.62 cm (3 in).	
4	Parts have total net-section stresses, e.g., maximum principal or von Mises, whichever is larger, at limit load that are less than 30 percent of the ultimate strength.	
5	Fatigue analysis predicts minimum service life factor of 4 with a factor of 1.5 on local cyclic stresses. OR Damage tolerance analysis predicts minimum of 4 service lives with a factor of 1.5 on alternating stress using a 0.127-mm (0.005-in) initial crack that conservatively accounts for the effects of notches and mean stress.	

APPROVED FOR PUBLIC RELEASE – DISTRIBUTION IS UNLIMITED

NASA-HDBK-5010, VOLUME 2, REVISION A

Note that metallic welds, brazes, and castings are manufacturing processes that are likely to contain flaws, and they do not qualify as low-risk parts unless data confirms flaw sizes produced in manufacturing processes will not grow, i.e., the crack stress intensity factor is below threshold, including consideration of environment and residual stress effects. A part also does not qualify as low-risk if any section of it is considered fracture critical. Additively manufactured parts are also excluded from the NFC Low Risk category because of the likelihood of the manufacturing process to introduce defects in the material. (See NASA-STD-6030, Additive Manufacturing Requirements for Spaceflight Systems [AMR-15]. These materials are process-dependent and may not meet Item 1.

Example

Consider an Aluminum 6061-T6 bracket with the dimensions specified in Figure 6.2-4, Dimensions and Loads of the Aluminum 6061-T6 Bracket. Table 6.2-2 is used to determine if the bracket can be classified as an NFC Low-Risk metallic part.

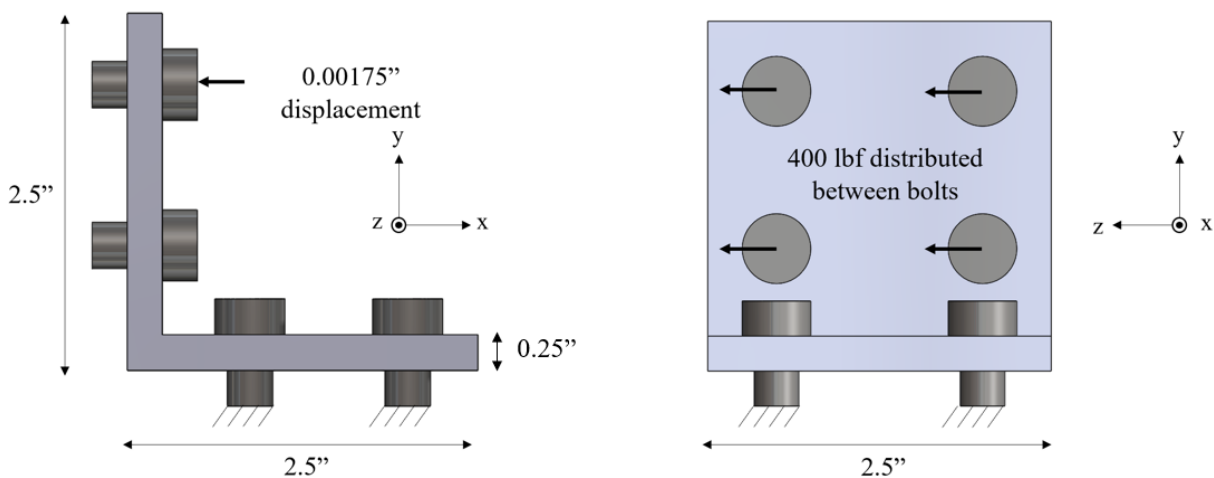


Figure 6.2-4—Dimensions and Loads of the Aluminum 6061-T6 Bracket

The requirements of item 1 from Table 6.2-2 are met because Aluminum 6061-T6 has well-characterized strength and ductility properties. Additionally, the bracket-forming process has been established by inspections to be extremely unlikely to produce parts with flaws; and the material formed using this process does not have a history of failure due to brittle fracture.

Next, item 2 of Table 6.2-2 is evaluated using the plane strain fracture toughness (K_{Ic}) and the tensile yield strength (F_{Ty}). The yield strength is 33 ksi, and the plane strain fracture toughness is 22 ksi $\sqrt{\text{inch}}$ at the operating temperature, giving a ratio of plane strain fracture toughness to yield strength (K_{Ic}/F_{Ty}) of 0.67 $\sqrt{\text{inch}}$. The ratio is greater than the minimum required value of 0.33 $\sqrt{\text{inch}}$. Additionally, Aluminum 6061-T6 does not have sensitivity to EAC, SLC, or stress corrosion cracking as defined in NASA-STD-6016. The requirements of Table 6.2-2, item 2, are met.

APPROVED FOR PUBLIC RELEASE – DISTRIBUTION IS UNLIMITED

NASA-HDBK-5010, VOLUME 2, REVISION A

Item 3 of Table 6.2-2 must be evaluated, as the bracket is made from aluminum. The bracket is constructed with an aluminum alloy sheet with a thickness of 0.25 inch in the short transverse direction, which is less than the 3-inch maximum requirement for the short transverse direction of the raw stock. The requirement of Table 6.2-2 item 3 is met.

Table 6.2-2, item 4, requires that the net section stress is less than 30 percent of the ultimate strength. The A-basis ultimate strength for Aluminum 6061-T6 at the operating temperature is 42 ksi, so the net section stress must be less than 12.6 ksi. A stress analysis was completed and determined that the maximum net section stress in the bracket is 10 ksi (average stress through-the-thickness without the crack). This is less than 30 percent of the ultimate strength, so the bracket meets the item 4 requirement. While the net section value was calculated numerically, NASGRO® provides net section stress solutions for many geometries in the user manual. The stress distribution through-the-thickness can be provided as an input to NASA.

Table 6.2-2, item 5, can be satisfied with a fatigue analysis or damage tolerance that shows a minimum of 4 service lives with a 1.5 factor on loads. In this example, a fatigue analysis is completed based on the mean S/N curve for Aluminum 6061-T6, as seen in Figure 6.2-5, Best-fit S/N Curves for Unnotched 6061-T6 Aluminum Alloy. The 10 ksi maximum net section stress is multiplied by the 1.5 load factor to get a maximum stress of 15 ksi for the fatigue analysis. The bracket undergoes fully reversible loading, so the R ratio of the bracket is -1. This corresponds to the red curve in Figure 6.2-5. The bracket is anticipated to undergo 100,000 cycles at this load during its service life. Multiplying the number of cycles in the service life by the service life factor of 4 gives a required life of 400,000 cycles. At 15 ksi, the S/N data from MMPDS indicates 5,000,000 cycles to failure. The fatigue analysis predicts more than 4 service lives with a 1.5 factor on loads, so the requirements of Table 6.2-2, item 5, are satisfied. While not illustrated here, note that all adjustment factors should be considered in the fatigue analysis to account for temperature, surface finish effects, loads, and environmental effects.

The requirements are satisfied for all five requirements of Table 6.2-2, so the bracket can be classified as an NFC Low-Risk metallic component.

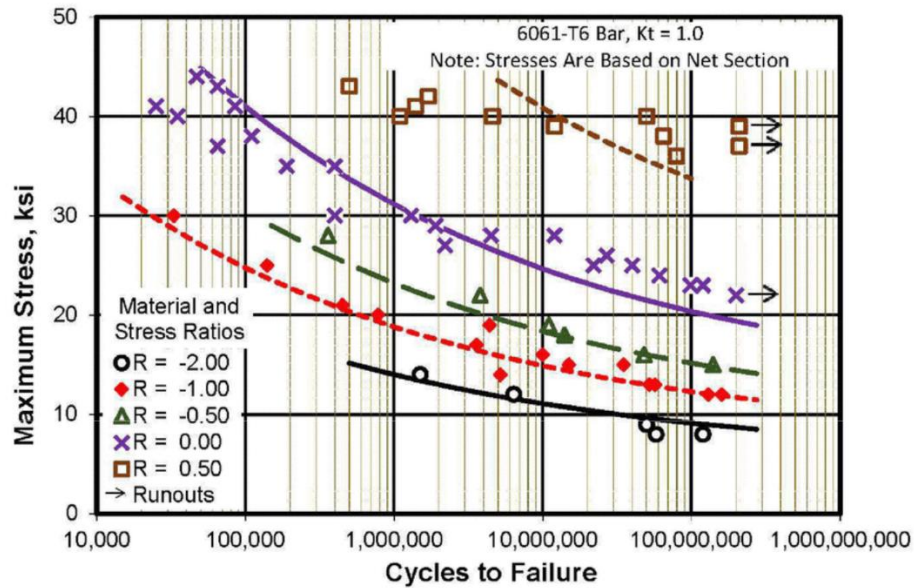


Figure 6.2-5—Best-fit S/N Curves for Unnotched 6061-T6 Aluminum Alloy (Reference MMPDS-15, page 3-480.)

6.2.5.2 NFC Low-Risk Composite Parts

Composite parts are classified as NFC Low Risk if they meet the items in the checklist in Table 6.2-3, Checklist for NFC Low-Risk Composite Parts. These parts are extremely unlikely to contain or develop critical flaws because of (1) extremely low likelihood of flaws being induced by manufacturing processes, environmental effects, or service events and (2) large structural margins.

NASA-HDBK-5010, VOLUME 2, REVISION A

**Table 6.2-3—Checklist for NFC Low-Risk Composite Parts
(All requirements must be met.)**

Item	Description of Requirement	Meets (Y or N)
1	Define the worst-case credible flaw conditions shown to be tolerated by the hardware through analysis and test, considering all flaw detection and mitigation strategies that are implemented for the flight hardware.	
2	Encompass all worst-case credible damage conditions, except the threats that are mitigated by NDE evaluations, the Impact Damage Mitigation Plan, and threats accepted by the program or project.	
3	Document the "damage states" the program chose to exclude from the design.	
4	The part residual strength with the largest Residual Threat Determination flaw based on items 1-3 can sustain Design Ultimate Loads as verified by analysis combined with coupon or hardware element test data.	
5	The part strain at limit load with the Residual Threat Determination established flaw size based on items 1-3 is below the no-growth threshold strain established by test.	
6	Reflight hardware is verified by visual inspection or other means to show the hardware is intact and free of structural anomalies before being reflown.	

If a composite part meets NFC Low Risk, it would have to comply with the following requirements in addition to the checklist above:

1. A DTA in accordance with section 7.4.1 in NASA-STD-5019A.
2. An IDMP in accordance with section 7.4.2 in NASA-STD-5019A.
3. An RTD in accordance with section 7.4.3 in NASA-STD-5019A; this is already covered in the checklist.
4. Perform NDE post-manufacturing according to section 8.1.2 of NASA-STD-5019A except for parts classified as NFC low-released mass parts and NFC contained parts.
5. Establish and maintain traceability for each fracture critical and NFC composite or bonded part by providing a unique serial number (or other method when serialization is not practical) and a complete life history, including load history, impact damage, repair, materials, manufacturing, processing, and environmental exposure.
6. Meet the material selection and usage requirement of section 8.3 in NASA-STD-5019A [FCR 22].

Example application # 1: The worst-case credible flaw condition based on flaw detection capability and potential for FOD for a composite camera cover was determined to be 2 inches. A threat analysis determined that the composite hardware is unlikely to experience impact damage; and if damage were to occur, indications on the paint can point to an impact damage event. The program decided not to exclude any damage states; all three items 1-3 have been satisfied. A full-scale test of the camera cover with 2-inch flaw survived a design ultimate load condition.

APPROVED FOR PUBLIC RELEASE – DISTRIBUTION IS UNLIMITED

NASA-HDBK-5010, VOLUME 2, REVISION A

Prior to this test, a limit load condition was applied and NDE demonstrated that there was no growth. The hardware is not designed for reflights. The camera cover is designated NFC Low Risk as items 1-6 are satisfied. The documentation for this work is cited in the FCSR where the part is listed as NFC in accordance with NASA-STD-5019A, section 9 requirements. Additional action items 1-6 are required for NFC Low-Risk composite parts.

Example application # 2: A raceway cover is inspected after manufacturing and NDE can detect flaws greater than 0.5 inch. Based on a complete damage threat analysis from manufacturing to flight, it was determined that impact events up to 75 Joules are possible. A flight representative raceway cover was subjected to the 75 Joules event, and this damage was determined to be greater than manufacturing flaws. The damaged part was immediately loaded to limit load conditions and no evidence of damage growth from this load condition was observed based on NDE. The part with the damage also survived the design ultimate load condition. The hardware is not reflown, and there are no damage states that were excluded in the evaluation. The raceway cover is designated NFC Low Risk as items 1-6 are satisfied. The documentation for this work is cited in the FCSR where the part is listed as NFC in accordance with NASA-STD-5019A, section 9 requirements. Additional action items 1-6 are required for NFC Low-Risk composite parts.

6.2.6 NFC Documented Nonhazardous Failure Mode

Note that this category is significantly different from the Exempt classification in section 5 of NASA-STD-5019A. Exempt parts are nonstructural and have no hazardous concerns or failure modes. This category may have structural or nonstructural parts that are to be addressed by a documented hazard assessment that establishes no credible catastrophic hazards exist for the failure modes identified.

An example of a situation that could be addressed by this section could be a case where a structural member cracks and loses some amount of load-carrying capability, but the consequence of the member condition is either minor or controlled such that no catastrophic hazard event could occur, and that condition is documented by engineering and safety evaluations.

Another example of a situation that may be applicable for this section may be a structure that experiences a displacement-controlled loading in a manner such that the structure/material has capability to sustain a flaw/crack that causes the loading to redistribute or reduce so that a critical crack size that results in fracture cannot be achieved.

Consider a final example involving an experiment that contains a nonhazardous liquid is on the flight manifest to ISS. The container with the liquid is triple-bagged and stowed in a locker. The levels of containment are reviewed by engineering and safety and determined to be nonhazardous.

NASA-HDBK-5010, VOLUME 2, REVISION A

6.3 Additional Activities for Composite or Bonded NFC

See section 6.2.5.2.

7. ASSESSMENT OF FRACTURE CRITICAL PARTS

7.1 Fracture Critical Parts

This section is reserved.

7.2 Established Approaches for Specific Fracture Critical Hardware Types

This section is reserved.

7.2.1 Fracture Critical Metallic Pressure Vessels

7.2.1.1 Example 1

Consider a cylindrical pressure vessel made of Ti-6Al-4V that is designed to the factors of safety in ANSI/AIAA S-080A, Space Systems - Metallic Pressure Vessels, Pressurized Structures, and Pressure Components. Assume a 10-inch radius and 2,500 psi MDP. Complete a fracture analysis to determine the predicted safe-life if it undergoes dye penetrant NDE before operation.

A pressure vessel must be designed to at least a 1.5 burst factor according to ANSI/AIAA S-080A. Assuming pressure is the only load, the maximum stress in a cylindrical pressure vessel occurs in the hoop direction. This must be less than or equal to the ultimate strength divided by the 1.5 burst factor. The ultimate strength for Ti-6Al-4V is 170 ksi, so the hoop stress must be less than or equal to 113.3 ksi. Using the thin-walled pressure vessel assumption, the minimum required thickness can be calculated as follows:

$$t \geq \frac{Pr}{\sigma_h} = \frac{(2,500 \text{ psi})(10 \text{ in})}{113,333 \text{ psi}} = 0.22 \text{ in}$$

(Equation 7.2-1)

If the thickness is at or above 0.22 inch, the pressure vessel in this example meets the 1.5 burst factor. For this demonstration, the thickness is assumed to be exactly 0.22 inch and NASGRO® was used for the fracture analysis. Two crack orientations must be considered: an axially aligned flaw (SC04 in NASGRO®) and a circumferentially aligned flaw (SC05 in NASGRO®). A depiction of these flaws and the corresponding inputs in NASGRO® can be seen in Figures 7.2-1, NASGRO® Input for an Axially Aligned Flaw in a Hollow Cylinder, and 7.2-2, NASGRO® Input for a Circumferentially Aligned Flaw in a Hollow Cylinder. An axially aligned flaw is perpendicular to the hoop direction, so hoop stresses drive crack propagation. A circumferentially aligned flaw is perpendicular to the axial direction, so axial and bending stresses drive crack propagation.

APPROVED FOR PUBLIC RELEASE – DISTRIBUTION IS UNLIMITED

NASA-HDBK-5010, VOLUME 2, REVISION A

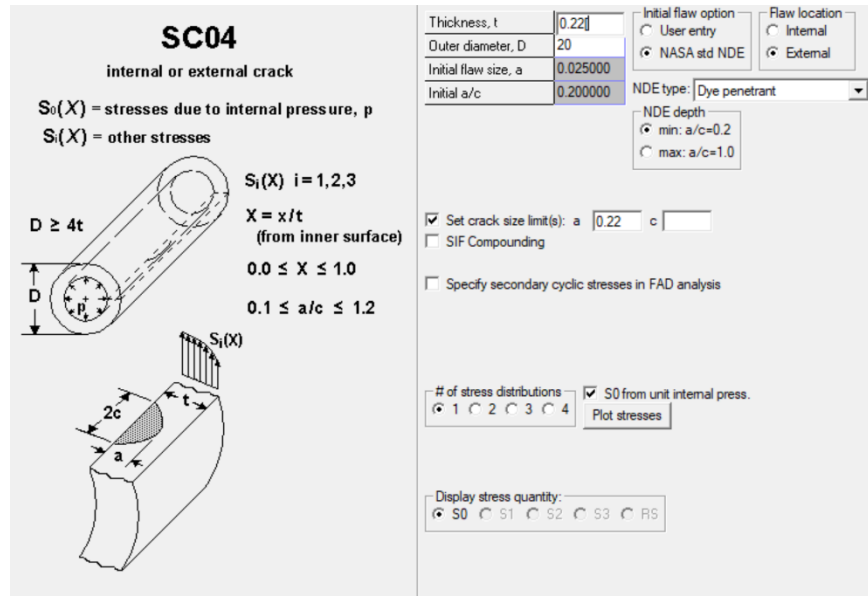


Figure 7.2-1—NASGRO® Input for an Axially Aligned Flaw in a Hollow Cylinder

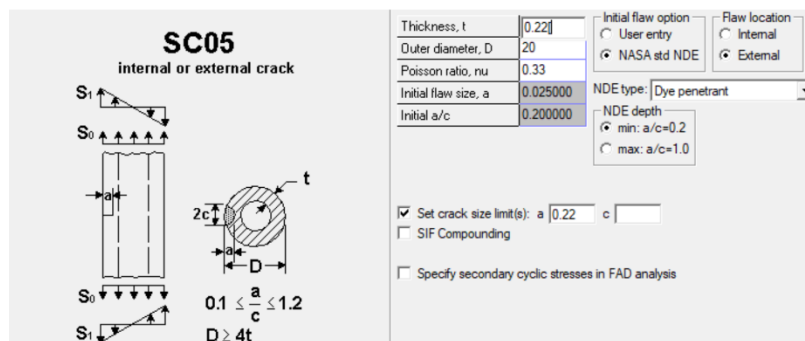


Figure 7.2-2—NASGRO® Input for a Circumferentially Aligned Flaw in a Hollow Cylinder

The “NASA std NDE” radio button within NASGRO® was chosen to allow for the entry of NDE initial flaws from NASA-STD-5009. As seen in Figures 7.2-1 and 7.2-2, dye penetrant NDE can be chosen with either the minimum or maximum dye penetrant crack aspect ratio of 0.2 and 1.0, respectively. Both aspect ratios should be evaluated. A crack size limit can also be set if a through crack is not permissible, which is often the case for pressure vessels. Note that for the axially aligned flaw (SC04), the load can be input as the internal pressure by checking the “S0 from unit internal press” option. If this option is checked, the load in the “load blocks” tab must be defined as internal pressure in the ksi units, which is 2.5 ksi in this example. For the circumferentially aligned flaw (SC05), there is no option to use the internal pressure as the load. Rather, the load must be input as the induced axial stress, which in this case can be calculated with the thin-walled pressurized cylinder assumptions as follows:

APPROVED FOR PUBLIC RELEASE – DISTRIBUTION IS UNLIMITED

NASA-HDBK-5010, VOLUME 2, REVISION A

$$\sigma_a = \frac{Pr}{2t} = 56.8 \text{ ksi}$$

(Equation 7.2-2)

The loads are input with the maximum loads as specified above and a zero R ratio. The material must also be selected in the “Material” tab. For this example, the Ti-6Al-4V alloy with the material ID of P3EA13AB1 is used. Note that it is NASA policy to change Bk to zero, or to a value such that the maximum stress intensity factor is less than or equal to the critical stress intensity factor with RFCB approval. In this example, Bk is set to zero and all other material properties are unchanged. Note Bk has no influence on the crack growth behavior as the flaw considered is a surface flaw.

The analysis was run for both crack cases with the crack aspect ratio at 0.2 and 1.0. The cycles to failure at MDP are shown in Table 7.2-1, MDP Cycles to Failure Prior to Life Factor of 4 for Different Dye Penetrant Crack Orientations and Aspect Ratios in a Hollow Cylinder. Failure occurred either due to reaching a through crack or unstable crack growth. The limiting case is 428 cycles to failure for the axial crack with a 1.0 aspect ratio. In accordance with ANSI/AIAA S080A, the life from a fracture analysis must be divided by a factor of 4 to obtain the safe life. The pressure vessel in this example has a safe life of 93 pressure cycles from zero to 2,500 psi.

Table 7.2-1—MDP Cycles to Failure Prior to Life Factor of 4 for Different Dye Penetrant Crack Orientations and Aspect Ratios in a Hollow Cylinder

Crack Orientation	Crack aspect ratio, <i>a/c</i>	Dye penetrant initial crack depth, <i>a</i>	MDP cycles to failure
Axial (SC04)	0.2	0.025”	581
Axial (SC04)	1.0	0.075”	428
Circumferential (SC05)	0.2	0.025”	8,420
Circumferential (SC05)	1.0	0.075”	6,781

7.2.1.2 Example 2

Consider a cylindrical pressure vessel designed to the factors of safety in ANSI/AIAA S-080A. Examine cases where the pressure vessel wall thickness is outside the limits for the NASGRO® built-in NASA-STD-5009 NDE flaw sizes.

NASGRO® contains built-in NDE flaw sizes based on NASA-STD-5009, but many of these flaws can only be used if a minimum thickness is met. Table 7.2-2, NASGRO® Thickness Limits for Various NDE Techniques in Hollow Cylinders, outlines the NDE inspection techniques available. The thickness must be greater than 0.05 inch for eddy current, greater than 0.075 inch for dye penetrant and magnetic particle, and greater than or equal to 0.1 inch for ultrasonic. Note that only radiographic flaws do not have a minimum thickness. This is because the radiographic crack size is a function of the thickness and does not have a minimum bound.

APPROVED FOR PUBLIC RELEASE – DISTRIBUTION IS UNLIMITED

NASA-HDBK-5010, VOLUME 2, REVISION A

Table 7.2-2—NASGRO® Thickness Limits for Various NDE Techniques in Hollow Cylinders

(EC = eddy current, P = dye penetrant, MP = magnetic particle, R = radiographic, U = ultrasonic. Taken from Table 8a of NASGRO® Main Reference Manual.)

Crack Case	NDE Inspection Technique	Thickness Range (in)	Crack Size (in)	
			a	c
SC04, SC05	EC (ext and int)	t > 0.050	0.020	0.100
			0.050	0.050
	P (ext)	t > 0.075	0.025	0.125
			0.075	0.075
	MP (ext)	t > 0.075	0.038	0.188
0.075			0.125	
R (ext and int)	t ≤ 0.107	0.7t	0.075	
	t > 0.107	0.7t	0.7t	
U (ext and int)	t ≥ 0.1	0.030	0.150	
		0.065	0.065	

Consider a Ti-6Al-4V cylindrical pressure vessel with a 10-inch radius and 500 psi MDP. If ANSI/AIAA S-080A factors are used, it must be designed to a burst factor of at least 1.5. Assuming pressure is the only load, the maximum stress in a cylindrical pressure vessel occurs in the hoop direction. This must be less than or equal to the ultimate strength divided by the 1.5 burst factor. The ultimate strength for Ti-6Al-4V is 170 ksi, so the hoop stress must be less than or equal to 113.3 ksi. Using the thin-walled pressure vessel assumption, the minimum required thickness to meet this requirement can be calculated as follows:

$$t \geq \frac{Pr}{\sigma_h} = \frac{(500 \text{ psi})(10 \text{ in})}{113,333 \text{ psi}} = 0.044 \text{ in}$$

(Equation 7.2-3)

The thickness can be as low as 0.044 inch and still meet ANSI/AIAA S-080A requirements. If the thickness is chosen to be 0.044 inch, then only a radiographic NDE flaw is available as an input in NASGRO®. This is consistent with the requirements in Table 2, as only radiographic NDE flaws are available below 0.05-inch thicknesses. Dye penetrant, eddy current, magnetic particle, and ultrasonic NDE flaw sizes are too large to use in quantitative evaluations of potential flaws for this pressure vessel.

7.2.1.3 Example 3

In this example, a simple calculation to determine period inspection levels is provided (reference Chang and Seibold [2005]). A 16-inch diameter helium bottle made of a titanium alloy (Ti-6Al-4V, STA) has a 0.15-inch membrane wall thickness and 0.25-inch-thick weld. The planned use of this helium bottle was in a reusable launch vehicle (RLV), so it will be refilled many times during its service life. The maximum expected operating pressure (MEOP) of this bottle is 4,000

APPROVED FOR PUBLIC RELEASE – DISTRIBUTION IS UNLIMITED

NASA-HDBK-5010, VOLUME 2, REVISION A

psig. To achieve safe operation and mission success, a decision was made to use a fracture control approach to determine the inspection interval after the bottle is put into use. Assume that the weld region is the most critical location on this pressure vessel. No cracks or crack-like defects were found using standard dye penetrant NDE methodology. In the fracture mechanics safe-life calculation, the initial flaw size based on probability of detection (PoD) established for a standard radiographic inspection flaw size: crack depth $a = c = 0.7t = 0.175$ in. From NASGRO® User's Manual, the fracture toughness and crack growth rate constants for this titanium alloy (Ti-6Al-4V, GTA weld) are: $K_{Ic} = 50 \text{ ksi}\sqrt{\text{in}}$, $K_{Ic} = 42 \text{ ksi}\sqrt{\text{in}}$, $C = 2.28 \times 10^{-9} \text{ (in./cycle)/(ksi}\sqrt{\text{in}})^3$, and $n = 3$.

A simple formula can be used to estimate the operating stress:

$$\sigma_{op} = \text{Pressure} \times \text{Radius} / (2 \times \text{thickness}) = 4000 \times 8/2 \times 0.25 = 64 \text{ ksi.}$$

The final crack size can be calculated using the formula of a semicircular surface flaw:

$$a_{cr} = 0.32 (K_{Ic}/\sigma_{max})^2 = 0.32 (50 \text{ ksi}\sqrt{\text{in}} / 64 \text{ ksi})^2 = 0.195 \text{ in.}$$

The total number of cycles that will be needed to fail the cracked weld region is calculated by using the simple version of the Paris Law equation:

$$(N_f - 0) = \frac{1}{C(1 - n/2)(\sigma_{op}\sqrt{\pi})^n} \left[(a_{cr})^{1 - \frac{n}{2}} - (a_0)^{1 - \frac{n}{2}} \right]$$
$$(N_f - 0) = \frac{2}{(2.28 \times 10^{-9})(2 - 3)(64\sqrt{\pi})^3} \left[(0.195)^{1 - \frac{3}{2}} - (0.175)^{1 - \frac{3}{2}} \right] = 78 \text{ cycles}$$

The inspection level can be set to 19 MEOP pressure cycles to satisfy the 4 times the service life damage tolerance requirement.

7.2.2 Fracture Critical Composite Overwrapped Pressure Vessels (COPVs) and Composite Overwrapped Pressurized Fluid Containers

COPVs are designated as fracture critical. Cracks and crack like flaws in the metallic liner are assessed using damage tolerance life assessment, which is based on either analysis or test. Many COPVs are designed with a liner that responds elastically for all pressure and combined load conditions after autofrettage and linear elastic fracture mechanics (LEFM) can be used to assess the damage tolerance life by analysis. However, additional checks beyond global elastic response of the liner are necessary to determine if LEFM is appropriate.

7.2.2.1 Limitations of LEFM

While LEFM can be used to assess damage tolerance of elastically responding liners that contain small cracks relative to the thickness, caution needs to be exercised when predicting life of part-

NASA-HDBK-5010, VOLUME 2, REVISION A

through cracks in thin metals where break-through is an end-of-life condition (e.g., COPV liners). LEFM assumptions impose limitations on the application as follows:

1. The size of the cyclic plastic zone around the crack tip is small relative to the crack size.
2. The crack-tip plasticity is surrounded by elastically responding material.
3. The material is a homogeneous continuum and governing microstructural features are small relative to the crack size.

The use of LEFM methods may not be appropriate if the liner is relatively thin compared to the inspectable crack depth. An example is a detectable crack depth of 0.025 inch in a liner that is only 0.035-inch thick, resulting in a ligament that is 0.01 inch. The crack growth rate through the ligament may be faster than that predicted by LEFM due to plasticity and microstructural features. Specifically, for plasticity, while a far-field analysis shows that thin liners are responding elastically, local plasticity in the ligament must be considered as LEFM assumes that the cracktip plastic zone is small relative to the size of the crack. Further, the ligament thickness may be on the same order as microstructural features such as grain size. The use of crack growth rate data obtained from standardized tests (such as that supplied in NASGRO®) may not be representative of crack growth in the ligament when the amount of local plasticity is not small compared to the remaining ligament. Guidance is contained in ASTM E647, Standard Test Method for Measurement of Fatigue Crack Growth Rates, on how to modify standard test procedures to characterize the growth of cracks when (1) their length is small compared to relevant microstructural dimensions (e.g., grain size), or (2) their length is small compared to the scale of local plasticity, or (3) they are merely small (e.g., < 1 mm). Note that all NASGRO® data are based on ASTM E647 but for specimens whose cracks are large compared to microstructural dimensions and large compared to the amount of local plasticity. The crack growth rate of cracks that are small compared to the amount of local plasticity can be underpredicted by da/dN data generated from tests of cracks that are large compared to the amount of local plasticity.

For COPVs with far-field plastic response, coupon or vessel testing is required per ANSI/AIAA S-081A. Such tests may be adequate to address small scale effects by test if the test captures the effects of plasticity and microstructure in the remaining ligament.

The following examples are compiled to demonstrate the cases where LEFM assumptions are inappropriate.

7.2.2.2 Guidance for Liner-to-Overwrap Debonds

Composite overwrapped pressure vessels (COPVs) with a bonded liner to composite interface are commonly used in flight programs. Liner disbonds can occur due to workmanship issues in the manufacturing process and/or due to a geometric feature in the design (e.g. as a liner thickness taper at the boss or at a weld) that causes liner and adhesive strain peaks in the bondline. Two conditions that can lead to failure as a result of liner disbond are, excess strain due to liner buckling and localization of plastic strains in the unsupported liner, similar to

APPROVED FOR PUBLIC RELEASE – DISTRIBUTION IS UNLIMITED

NASA-HDBK-5010, VOLUME 2, REVISION A

necking. Both conditions result in local strain peaks in the liner that are usually not addressed in damage tolerance analysis or test and can lead to failure of the liner at much lower pressures and fewer cycles than expected. Historically, the bond line between the COPV liner and composite is analyzed. However, this analysis is not highly reliable because bondline stresses cannot be directly validated by testing.

Disbond detection approaches include post-proof borescope inspection to detect buckles and through-composite inspection methods such as shearography, thermography, and ultrasound. However, these methods may not be 100% effective. For example, borescope is ineffective when disbonds do not form buckles or when access to the port is no longer possible. To close this gap, nondestructive evaluation (NDE) to detect disbonds through-composite would be beneficial but would require NDE validation testing to confirm that a disbond is reliably detectable.

If a buckle is found with borescope, the COPV is typically discarded. If discarding is not an option, testing would be required to establish flight rationale.

Following the detection of a disbond or if a disbond is suspected based on poor bondline process control, there are three issues that can develop: 1) liner bondline disbond growth, 2) liner buckle due to existing disbond causing liner failure, and/or 3) invalidation of damage tolerance life due to liner peak strains that occur local to the disbond. Mitigation of the first two has been accomplished through cyclic testing with disbonds for 4x service life followed by borescope inspection and NDE to confirm that no disbond growth or buckling has occurred, the liner does not leak, and the tank does not rupture. While this retires a portion of the risk, additional work to confirm damage tolerance life is required which remains after testing.

The guidance in NESC tech bulletin [NASA Engineering and Safety Center Technical Bulletin No. 21-04, "Evaluating Appropriateness of LEM Tools for COPV and Metal Pressure Vessel Damage Tolerance Life Verification] to address issue 3 is also important to retire risk associated with issues 1 and 2. Analysis that explicitly models the adhesive bondline and incorporates an elastic-plastic material model for the adhesive is required to fully predict the local strain field in the liner due to a disbond in the bondline. These local strain fields should be verified not to invalidate the damage tolerance life or LBB assessments.

7.2.2.3 Liner Inspections

An issue with COPV liners is that using the Standard NDE initial flaw sizes provided in NASA 5009 seldom results in compliance initial flaw sizes with damage tolerance life requirements. For example, the Standard dye penetrant crack size is a through-crack for all thicknesses less than 0.150" and most COPV liners are thinner than this. Therefore, Special NDE per 5009, which requires demonstration of 90/95 POD for specific inspectors, can be used to reliably detect smaller crack sizes necessary to meet damage tolerance life.

NASA-HDBK-5010, VOLUME 2, REVISION A

7.2.2.3.1 Example 1

A COPV experienced a leak due to cracking at a weld during ground operations. Analysis with a through crack demonstrated that leak before burst (LBB) criteria was met. A performance analysis indicated that leak rates predicted negligible impact for the mission to be successful. This example illustrates the use of LBB and performance analysis to demonstrate adequacy of the COPV design to complete the mission.

7.2.2.3.2 Example 2

Part of the qualification program of a COPV design requires demonstration that damage tolerance requirements are met. Machining of the flaws into the liner was performed but pre-cracking was not achieved, raising concerns that the crack-tip may not be sufficiently sharp and that the life of the COPV could be overstated. In this example, the issue was addressed by repeating the tests after pre-cracking and a thorough characterization of the flaw prior to initiating testing.

7.2.2.3.3 Example 3

Linear elastic fracture mechanics was being used to assess damage tolerance life of a liner that was plastically strained after each cycle of operation. The analysis did not include any plasticity correction factors and could produce invalid results. A full-scale test or coupon-level test was required to demonstrate adequate damage tolerance of the COPV.

7.2.2.3.4 Example 4

A hydraulic system COPV had a thickness that per NASA-STD-5009 when standard penetrant inspection was used it would require an evaluation of a through-the-thickness crack. Initially, a partly through crack (PTC) was used, but this was deemed unacceptable. The liner thickness was equal to or smaller than the crack depth when standard penetrant crack size was used. Instead, the issue was resolved by a performance analysis demonstrating that an assumed leak can be sustained to complete the mission and that the fluid leakage was nonhazardous.

7.2.2.3.5 Example 5

A COPV design had a liner thickness less than the thickness required in Table 1 of NASA-STD-5009 for standard NDE methodologies. Further, it was advised that special NDE be implemented and NASGRO® be used for the damage tolerance analysis as the liner was shown to remain linear elastic after autofrettage. The net section stress check in NASGRO® failed. While there was a push to accept the analytical results, the results could not be accepted due to the low confidence in the analysis. A full-scale test to demonstrate damage tolerance requirements was conducted with a pre-crack.

NASA-HDBK-5010, VOLUME 2, REVISION A

7.2.2.4 Best Practices Based on the NESC COPV Life Test Assessment

Any engineer working on damage tolerance assessments for COPV liners should be familiar with the work in NASA/TM–2020-5006765/Volume I, NESC-RP-16-01183, “Composite Overwrapped Pressure Vessel (COPV) Damage Tolerance Life Analysis Methodology and Test Best Practices.

Best practices were identified during the NESC COPV Life Test Assessment of elastically responding COPV liners. This effort generated:

- Data to evaluate the limitation of the LEFM computational methods used to predict crack growth behavior.
- Tests to demonstrate methodology for validating COPV damage tolerance life requirements.

In ANSI/AIAA S-081B, damage tolerance life requirements, verification, analysis, and test requirements are listed in sections 5.2.13.1, 6.2.1, 7.5.1, and 10.1, respectively. Section 7.1 addresses the selection of material properties for analysis. The best practices do not address every requirement in these sections of ANSI/AIAA S-081B:

Best Practice 1
ANSI/AIAA S-081B, Requirement 5.2.13.1
<i>“The region(s) of the COPV to which damage tolerance is applied shall be designed such that the COPV liner possesses a minimum damage tolerance life of four (4) times the service life without sustained load crack growth, detrimental deformation, leakage, or rupture.”</i>
Best Practices
<ol style="list-style-type: none">1. Demonstrate by test and/or validated elastic-plastic fracture analysis that stable tearing does not occur during the service life, including autofrettage2. Ensure margin to stable tearing is characterized.3. Margin to stable tearing can be identified by testing with larger crack sizes than NDE minimum detectable flaw or larger strains than identified COPV stress analysis.4. A minimum of ten coupons are necessary to establish the margin; five coupons should be at crack depths near the NDE minimum detectable flaw and target strain, and five coupons should be at larger crack sizes or strain levels.
Evidence Summary
Stable tearing leading to failure (i.e., crack growth to the back surface) was observed at conditions just beyond the onset of stable tearing. The stable tearing was observed to be greater at an angle of about 30 degrees to the surface rather than at the maximum depth location (90 degrees to the surface), which appears to be in agreement with the simulations based on ASTM E2899. Crack mouth opening displacement (CMOD) measurements appear to be sensitive to the onset of yielding, blunting, and stable tearing.

APPROVED FOR PUBLIC RELEASE – DISTRIBUTION IS UNLIMITED

NASA-HDBK-5010, VOLUME 2, REVISION A

Best Practice 2

ANSI/AIAA S-081B, Requirement 6.2.1

“The damage tolerance life requirement may be verified by analysis only if both of the following conditions are met: (1) The liner (or region of the liner) is shown to be elastically responding and characterized by linear elastic fracture mechanics (LEFM) throughout proof testing and the operational portion of the service life. (2) The fracture properties of the liner materials are determined in accordance with section 7.1.”

Best Practices

When NASGRO® analysis is used for damage tolerance life verification, COPV designers should address the potential violation of LEFM plasticity assumptions.

Evidence Summary

LEFM plasticity assumptions are violated before the transition from a surface crack to a through-crack (i.e., before COPV liner leakage). There is a gradual divergence between LEFM predicted behavior and measured crack behavior as cracks grow through the uncracked ligament. Measured crack growth in 0.032, 0.048, and 0.090-inch-thick AA6061-T6 sheet material (i.e., representative of COPV liner thickness) was predominantly higher than predicted by common practice LEFM-based computational methods (e.g., NASGRO®).

LEFM plasticity assumption violations are not always flagged in a NASGRO® analysis allowing users to mistakenly continue analysis. The COPV Life LEFM limit and knockdown failure criteria is a more conservative damage tolerance life analysis approach than the state-of-practice damage tolerance life analysis approach.

Best Practice 3

ANSI/AIAA S-081B, Requirement 7.1

“The test program shall include the effects of all plastic deformation throughout the service life, for example, during autofrettage (if one is performed) and any other plastic cycles.”

Best Practices

Use coupon or tank testing to characterize the amount of crack growth observed during autofrettage or plastic cycles.

Evidence Summary

1. Fracture surface (i.e., pre-crack, autofrettage crack growth, stable tearing, and post-cracking) regions were distinguished with selection of pre-cracking and post-cracking and stress ratio.
2. The amount of crack growth during autofrettage was small (i.e., < 0.002 inch) and relatively independent of crack length and strain level provided that the crack tip conditions were below the onset of stable tearing.
3. The amount of crack extension due to 4 consecutive autofrettage cycles was never

APPROVED FOR PUBLIC RELEASE – DISTRIBUTION IS UNLIMITED

NASA-HDBK-5010, VOLUME 2, REVISION A

measured to be greater than the amount of crack extension in a single autofrettage cycle, multiplied by four, provided stable tearing was not present.

4. The autofrettage cycles provided a distinct mark on the fracture surface that was used to determine the amount of crack growth.
5. CMOD measurements appear to be sensitive to the onset of yielding, blunting, and stable tearing.

Best Practice 4

ANSI/AIAA S-081B, Requirement

“Sufficient data shall be obtained either from conducting tests or other available sources so that meaningful nominal values can be established. The test program shall establish these properties for the parent metal, weld joints, and heat-affected zones, all taking into account the fluid contents, service life, and expected operating and test environments, as appropriate.”

Best Practices

1. Demonstrate by test that da/dN vs. K data from a surrogate material (i.e., rolled sheet in place of as-manufactured tank) is equivalent to or conservative to liner material. Upon modification of the material composition or processing, ensure the equivalency check is repeated.
2. Complete fatigue crack growth tests using coupons extracted from a representative COPV liner and with the minimum reliably detectable surface pre-crack.

These coupons should be extracted from a variety of regions throughout the tank, where the number of regions or extraction should be guided by electron backscatter diffraction (EBSD) or other microscopy observations. To form a baseline comparison, coupons should be extracted from the desired surrogate material (e.g., rolled sheet) with the same geometry as the liner coupons. Equivalency or conservatism can then be demonstrated by measuring fatigue crack growth rates. Fatigue crack growth testing at this scale should apply loads that induce the expected peak net section stress in the liner.

Evidence Summary

Microstructure variations are observed between different COPV liner regions, and between liner and rolled sheet material. In comparing material regions of different microstructure, fatigue crack growth tests quantified impact of damage mechanism to damage tolerance life (i.e., da/dN) while microscopy and tensile tests did not.

NASA-HDBK-5010, VOLUME 2, REVISION A

Best Practice 5

ANSI/AIAA S-081B, Requirement 7.5.1

“The analysis shall show that the COPV liner meets the damage tolerance life. The analysis may be performed using a crack growth software package.”

Best Practices

In damage tolerance life analysis, apply service lives in sequence.

Evidence Summary

The average da/dN from coupons and liners with the $4 \times$ (autofrettage & 200 MDP) load spectrum were faster than those measured from coupons and liner with the $4 \times$ autofrettage and 800 MDP load spectrum.

Best Practice 6

ANSI/AIAA S-081B, Requirement 7.5.1

“For analysis of the autofrettage cycle (if one is performed), the factor of four may be waived provided conservative crack growth properties and methodology are used in the determination of crack growth for autofrettage. EXAMPLE The autofrettage cycle might be approached through analysis of a single event predicting the potential extension in a conservative manner using a lower bound crack extension resistance curve or equivalent technique, rather than a nominal resistance curve. This extended defect size thus derived might then be used as the starting defect size in the damage tolerance life analysis.”

Best Practices

Evaluate margin to stable tearing before waiving scatter factor of four for autofrettage.

Evidence Summary

Stable tearing leading to failure (i.e., crack growth to the back surface) was observed at conditions just beyond the onset of stable tearing.

The stable tearing was observed to be greater at an angle of about 30 degrees to the surface rather than at the maximum depth location (90 degrees to the surface), which appears to be in agreement with the simulations based on ASTM E2899.

Best Practice 7

ANSI/AIAA S-081B, Requirement 7.5.1

“The analysis shall account for changes in the flaw (crack) a/c and the effects of all environment(s) on the crack growth rate.”

NASA-HDBK-5010, VOLUME 2, REVISION A

Best Practices

For flaws on the inner diameter of a COPV liner, include the contribution of pressure on inner mold line (IML) crack faces to the applied stress intensity factor in damage tolerance life analysis.

Evidence Summary

Liner IML and outer mold line (OML) crack da/dN correlated when the K solution for the IML cracks included the influence of crack face pressure.

Best Practice 8

ANSI/AIAA S-081B, Requirement 10.1.1

“The coupons shall meet the specimen configuration and size requirements of ASTM E740.”

Best Practices

Ensure the width of damage tolerance life test coupon is at least 9 times 2c to reduce edge effects.

Best Practice 9

ANSI/AIAA S-081B, Requirement 10.1.1

“Each coupon shall be pre-cracked.”

Best Practices

1. Pre-crack at $R = 0.1$ at 80% of yield or MDP whichever is lower.
2. Pre-cracks of a/c other than 0.5 can be accomplished using multiple closely-spaced notches.
3. Grow the pre-crack beyond the influence of the notch. Notches are half the size of the target pre-crack size.

Evidence Summary

Fracture surface (i.e., pre-crack, autofrettage crack growth, stable tearing, and post-cracking) regions were distinguished with selection of pre-cracking and post-cracking stress and stress ratio.

NASA-HDBK-5010, VOLUME 2, REVISION A

Best Practice 10

ANSI/AIAA S-081B, Requirement 10.1.1

“The size of each pre-crack shall be greater than or equal to the minimum flaw size associated with the NDT inspection technique(s).”

Best Practices

1. Demonstrate the pre-cracking procedure on sample coupons prior to starting test. The number of cycles required to consistently grow the pre-crack to the NDE length and depth should be demonstrated (post pre-cracking fractography) by pre-cracking and examining the pre-crack using scanning electron microscope (SEM) prior to pre-cracking the test specimens. The notch procedure for inserting a flaw from which to grow a pre-crack should also be demonstrated.
2. CMOD measurements during pre-cracking can be used to achieve target crack depth when performing low aspect ratio (i.e., $a/c < 1$) damage tolerance tests.

Evidence Summary

1. Fracture surface (i.e., pre-crack, autofrettage crack growth, stable tearing, and post-cracking) regions were distinguished with selection of pre-cracking and post-cracking stress and stress ratio.
2. Evaluating pre-crack CMOD as a function of fracture surface crack depth measurements allows for increased ability to achieve target crack depth in subsequent tests.

Best Practice 11

ANSI/AIAA S-081B, Requirement 10.1.1

“Strains equal to or greater than those associated with each load cycle, including the compressive liner strains at zero pressure, shall be tested.”

Best Practices

Use strains that represent the entire cyclic history (i.e., no truncation at zero stress). Guide plates can be used to prevent buckling during compressive strain tests.

Evidence Summary

Crack depth measurements demonstrated that the coupon that was truncated, to exclude the compressive loading following the autofrettage cycle, grew significantly slower than the coupon with the full loading history.

Guide plates provided anti-buckling support when compressive loads were applied in coupon tests, enabling testing of the full strain profile to measure accurate surface crack lengths.

NASA-HDBK-5010, VOLUME 2, REVISION A

Best Practice 12

ANSI/AIAA S-081B, Requirement 10.1.1

“Test strains and strain rate shall be verified by measurement.”

Best Practices

1. Strain measurements for uniaxial tests should be performed using physical or virtual edge extensometers or strain gages at the edge. The strain measurement location should be centered about the plane of the crack. Physical extensometers should be placed on both edges. Virtual extensometers and strain gages should be placed on both edges of both sides (i.e., four locations).
2. Identify global peak test strains using COPV analysis and set it as the target global strain for strain-controlled weld tensile damage tolerance tests.

Evidence Summary

1. The use of the weld strain from the COPV analysis as the target global strain in an autofrettage test resulted in excessive local weld strains for an undermatched weld. In a simulated autofrettage coupon test, accurate weld strains were achieved using a target global strain that resulted in the measured weld strain in tensile tests (i.e., uncracked coupons) matching the COPV analysis.

Best Practice 13

ANSI/AIAA S-081B, Requirement 10.1.1

“After completion of cyclic strain testing, the following procedures and measurements on the coupons shall be performed. (1) The crack faces will be separated in a way that will allow examination of the fracture surfaces produced during testing. (2) The fracture surface will be examined to verify that the crack has not grown The initial and final crack sizes will be measured.”

Best Practices

Identify and measure regions of notching, pre-cracking, autofrettage growth, cyclic loading, and monotonic loading to failure in the SEM. A slight microscopy is not adequate. At least a small ligament of material that failed during monotonic loading should exist between the back surface and cyclic crack growth region.

Evidence Summary

1. Multiple physical and virtual extensometers/strain gages located at the coupon edges provided consistent far-field strain measurements.
2. Fracture surface (i.e., pre-crack, autofrettage crack growth, stable tearing, and post-cracking) regions were distinguished with selection of pre-cracking and post-cracking stress and stress ratio.

APPROVED FOR PUBLIC RELEASE – DISTRIBUTION IS UNLIMITED

NASA-HDBK-5010, VOLUME 2, REVISION A

Best Practice 14
ANSI/AIAA S-081B, Requirement 10.1.2
<i>“At least two liner cracks shall be tested for each condition (location and a/c). Each location shall contain a surface crack. Each location shall be pre-cracked. The size of each pre-crack shall be greater than or equal to the minimum flaw size associated with the NDT inspection technique(s).”</i>
Best Practices Perform pre-cracking on an unwrapped liner so that crack length can be measured prior to test. Use coupons and/or a nontest liner and extract the cracks to confirm NDE minimum crack size. Use NDE (e.g., eddy current inspection) to identify IML cracks during the pre-cracking process if cracks nucleate at locations other than the notches.
Evidence Summary <ol style="list-style-type: none">1. Liner pre-cracking process via inserting EDM notches and pressure cycling was demonstrated to grow flaws to the target initial flaw size.2. Long, shallow cracks nucleating from naturally occurring IML defects in an AA6061-T6 liner were reliably detected from the OML using eddy current inspection

7.2.3 Other Fracture Critical Pressure Vessels and Pressurized Fluid Containers

See section 7.2.1 of this Handbook for examples on the application of NASGRO® analysis to metallic vessels. These approaches can be applied to pressure vessels and pressurized fluid containers.

There are questions surrounding when a post-proof test inspection is required for pressure vessels and habitable modules. The purpose of this section is to provide background and rationale for deciding when to carry out such post-proof NDE. The basis for the discussion is NASA-STD-5007, Fracture Control Requirements for Spaceflight Hardware (superseded by NASA-STD-5019), which requires that hardware that is proof tested as part of its acceptance and receives post-proof test NDE at critical welds and other critical sections. These discussions do not apply to items that are proof tested to screen for specific flaws, i.e., utilizing proof test as the flaw screening method.

Post-proof NDE of welds in pressure vessels or habitable modules can be governed by program requirements for human safety or mission assurance involving national assets. Post-proof NDE of welds is implemented depending on the mode of failure.

A pressure vessel or a module with an LBB failure mode can eventually develop a slow leak if a large enough flaw is present and enough loading cycles are applied during service. The vessel can be classified as NHLBB if the following conditions are met:

- a. The fluid is not hazardous.
- b. Slow loss of the fluid is not hazardous.

APPROVED FOR PUBLIC RELEASE – DISTRIBUTION IS UNLIMITED

NASA-HDBK-5010, VOLUME 2, REVISION A

- c. The leak unloads the vessel so further crack growth is not possible.
- d. A leak-before-burst failure mode is demonstrated by test or analysis.

The LBB designation is based on an engineering assessment of the vessel design; an NHLBB fracture control classification is based on the consequences of the leak. An NHLBB classified vessel does not require post-proof NDE based on safety, but post-proof NDE is strongly recommended.

If the design does not meet LBB criteria and fragmentary or abrupt rupture is possible, or a leak of the fluid is a hazard, or load is maintained on the vessel, failure would be hazardous and “safe life” assurance through fracture control methodology is required. These vessels are designated “safe life” designs and require that welds be inspected post proof.

Even in cases where NHLBB criteria cannot be satisfied, verifying LBB behavior is the preferred design practice, because a component that can tolerate a through flaw without rupture is inherently safer than one that cannot. LBB design practice is encouraged even for components that will have safe life inspection requirements due to their contents or operational conditions.

A habitable module whose CFS is a through flaw of length at least 10t is not classified as NHLBB because pressure within the module must be maintained during the mission. Pressure cycling in the module continues throughout the mission due to the “make up” of air can grow the crack, so the module requires safe life classification and post-proof inspection.

Post-proof NDE provides many benefits for detecting as-manufactured problems in hardware that are difficult to predict or account for. This is particularly true for unique “one of a kind” structures. The proof test enhances the NDE capability to discover problems due to:

- a. Latent defects.
- b. Weld repairs, overlaps, intersections, and porosity.
- c. Weld geometry, including peaking and mismatch.
- d. Assembly stresses.
- e. Workmanship.
- f. Effects of temporary tooling.

In summary, it is good engineering practice that all welds in habitable modules and pressure vessels receive post-proof NDE.

Nonwelded critical sections include internal and external fracture critical structure as well as fracture critical portions of the nonwelded pressure shell wall, i.e., the pressure shell base material. Technically, these areas are governed by the same NHLBB and post-proof NDE requirements as the pressure shell welds. An exception is made for pressure vessels of standard design with smooth membrane and transition areas and that are within the previous experience base. These standard design pressure vessels require only that the welds receive post-proof NDE. The NDE approach for other pressure vessels should be coordinated with the RFCB. It is recognized that strict implementation of these requirements is not always programmatically feasible; deviations must be approved by the RFCB.

APPROVED FOR PUBLIC RELEASE – DISTRIBUTION IS UNLIMITED

NASA-HDBK-5010, VOLUME 2, REVISION A

7.2.4 Fracture Critical Lines, Fittings, and Other Pressurized Components

Lines, fittings, and other pressurized components do not require any additional work if the hardware in question meets all of the criteria from Table 7.2-3, Checklist for FC Lines, Fittings, and Other Pressurized Components.

Note that AM parts are excluded from this category according to NASA-STD-6030 [AMR-15] as this category is considered insufficient to manage the process control risks inherent to AM parts.

**Table 7.2-3—Checklist for FC Lines, Fittings, and Other Pressurized Components
(All requirements must be met.)**

Item	Criteria	Meets (Y or N)
1	Pressurized component is primarily driven by pressure. For loading (stresses) to be considered pressure dominant, all other loads (stresses) should be no greater than 20 percent of the pressure loads (stresses).	
2	Hardware meets the design factors imposed by standards such as NASA-STD-5001 or ANSI/AIAA S-080.	
3	Supports, brackets, or relief loops are not subjected to significant structural loads.	
4	Parts are produced in large quantities under process controls, are identical parts, and are subjected to NDE and qualification testing to ensure the parts are reliable and present a low risk of containing detectable flaws that result in crack growth. Obtain RFCB approval that the part is manufactured using processes that have been established by reliability or by inspections of many similar parts to be extremely unlikely to produce parts with a flaw exceeding process specifications.	
5	Metallic part is not susceptible to crack extension related to EAC or SLC.	
6	100 percent inspection performed of all fusion joints in fracture critical pressure components using a qualified NDE method after proof test to inspect for the presence of unacceptable lack of penetration or other unacceptable conditions both on the surface and within the fusion joint.	
7	Final product with flaw indication(s) that do not meet specification requirements is rejected.	
8	Lines, fittings, joints, and other pressurized components or parts are proof tested to a minimum of 1.5 times the MDP during individual acceptance or at the system level.	
9	An ECF less than 1.0 is not allowed without prior approval by the RFCB.	

NASA-HDBK-5010, VOLUME 2, REVISION A

If the part does not meet 'Y' for all of the above, then the part also needs to comply with damage tolerance requirements imposed by one of the following combinations: a and b; a and c; or a, b, and c.

- a. Develop loading spectra by complying with section 7.3.1 in NASA-STD-5019A.
- b. Perform assessment by analysis to comply with section 7.3.2 in NASA-STD-5019A.
- c. Perform assessment by test to comply with section 7.3.3 in NASA-STD-5019A.

7.2.4.1 Example 1

Dynamic loads analysis of a pressure line in a liquid rocket engine revealed that the stress induced by external loads was 10 ksi, while the stress induced by internal pressure was 45 ksi. Since the stresses caused by the external load was 22% of the total load, a full damage tolerance assessment is required per NASA-STD-5019A, section 7.3.

7.2.4.2 Example 2

Tubing in a launch vehicle is exposed to cryogenic temperatures. To take advantage of the increase in strength due to cryogenic temperatures, the tubing was proof tested with an ECF less than 1.0 to take advantage of the increase in strength. A full damage tolerance assessment is required per section 7.3 of NASA-STD-5019A.

7.2.4.3 Example 3

The resistance of many materials to the initiation and growth of cracks is often substantially lower in liquid-metal, aqueous, and hydrogen environments than in inert environments. This effect is known in general terms as environmentally assisted cracking and, for specific environments, is known as liquid-metal embrittlement (LME), stress-corrosion cracking (SCC), and hydrogen-assisted cracking. The materials for a full launch vehicle design were evaluated for expected exposure and potential for EAC. After the analysis, it was found that naturally aged Aluminum 6061-T4 was used in a pressurized component. Since this material is susceptible to stress corrosion cracking, it was determined that a damage tolerance assessment per 7.3 is required.

7.2.4.4 Example 4

Forming of a tube during its manufacturing process caused linear crack indications. A dissection of a similar tube led to the conclusion that large grain sizes were present through the thin wall. While the tubes will undergo proof testing to the proof factors specified in ANSI/AIAA S-080, there are concerns that the parts may not be manufactured with a repeatable process and that the manufacturing process is likely to cause flaws in the part. A determination was made that a damage tolerance assessment per 7.3 is required; but since manufacturing was the culprit for the lack of repeatability, a test was required.

NASA-HDBK-5010, VOLUME 2, REVISION A

7.2.4.5 Example 5

Pressure components are usually component driven by pressure. There are instances where significant external loads can be present. This example illustrates the approach to assess these structures.

Consider a Ti-6Al-4V tube that is designed to the factors of safety in ANSI/AIAA S-080A. The component has a 4-inch diameter, 0.125-inch wall thickness, and 3,750 psi internal pressure. Additionally, it experiences a 15 ksi cyclic bending stress during flight. The component is intended to be reused on multiple flights. Acceptance testing, including proof and leak tests, are completed before the first flight. Cycles experienced for each reuse consist of pressurization cycles for ground operations, cyclic bending stress with constant pressure during ascent, and cyclic bending stress with constant pressure during descent. Assuming dye penetrant NDE is completed on the inner and outer surfaces, determine the number of safe flights for the tube. The tube experiences pressure only and combined bending and pressure load cases. The combined case is shown in Figure 7.2-3, Section View of a Tube, with the Pipe Running Horizontally.

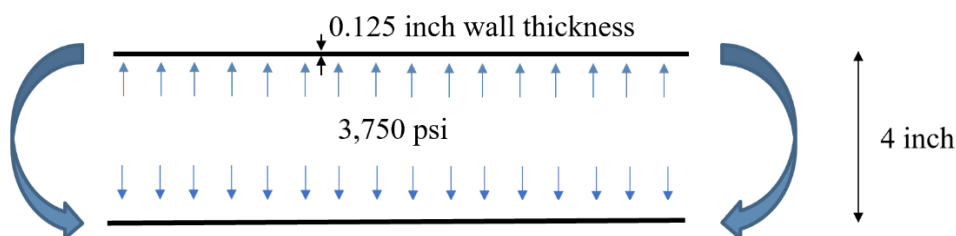


Figure 7.2-3—Section View of a Tube, with the Pipe Running Horizontally

Using the thin-walled assumption, the axial and hoop stresses during for the pressure only case were calculated as:

$$\sigma_{axial} = \frac{Pr}{2t} = 30 \text{ ksi} \quad \sigma_{hoop} = \frac{Pr}{t} = 60 \text{ ksi} .$$

(Equation 7.2-4)

Note that a proof test will be conducted with a 1.5 proof factor on MDP, as specified in ANSI/AIAA S-080A. The component is predicted to remain elastic and well below the 165 ksi yield strength, so proof testing corresponds to the axial and hoop stresses of MDP multiplied by 1.5. The bending induces a maximum stress of 15 ksi. This stress is in the axial direction and does not affect the hoop stress.

With these stresses, the load history of this component can be defined, as shown in Table 7.2-4, Load History of the Pipe. The proof test occurs once with the stresses due to MDP being multiplied by 1.5. The leak test occurs once with stresses due to MDP. These two tests occur once before the first flight. Each flight consists of ground operations, ascent, and descent. Assume ground operations have a maximum of 10 pressure cycles to MDP. Proof test, leak test, and ground operations all cycle between the unpressurized and pressurized stage. During ascent

APPROVED FOR PUBLIC RELEASE – DISTRIBUTION IS UNLIMITED


NASA-HDBK-5010, VOLUME 2, REVISION A

and descent, the tube is at constant pressure and sees cyclic bending stress with a 15 ksi amplitude. The number of cycles is determined by the frequency of loading multiplied by the duration of the event. In this case, 500 ascent cycles and 1,000 descent cycles are assumed.

Table 7.2-4—Load History of the Pipe

(Steps 1 and 2 are completed once prior to the first flight. Steps 3-5 occur on first flight and on every reuse flight.)

Event	Cycles	Hoop stress (ksi)		Axial stress (ksi)		Bending stress (ksi)	
		Min	Max	Min	Max	Min	Max
1. Proof Test	1	0	90	0	45	0	0
2. Leak Test	1	0	60	0	30	0	0
3. Ground Operations	10	0	60	0	30	0	0
4. Ascent	500	60	60	30	30	-15	15
5. Descent	1,000	60	60	30	30	-15	15

Repeat steps 3-5 for reuse flights 

To determine the safe life, the load history must be converted to load blocks for input in NASGRO®. Both axial and circumferential surface cracks must be analyzed, which corresponds to SC04 and SC05 crack types in NASGRO®. The crack geometry inputs for each can be seen in Figures 7.2-4, Input for Axially Aligned Crack in a Hollow Cylinder, and 7.2-5, Input for Circumferentially Aligned Crack in a Hollow Cylinder. Note that for SC04 a stress distribution is defined. The stress is defined to be constant through the thickness based on the thin-walled assumption. Alternatively, “S0 from unit internal press” can be selected and the internal pressure can be used for the load block.

Both the minimum and maximum crack aspect ratios of the dye penetrant NDE built-in flaws are selected. This corresponds to a/c of 0.2 and 1.0, respectively. The crack size limit is defined to be the thickness of the wall. If a through crack is permissible, this limit does not need to be defined.

NASA-HDBK-5010, VOLUME 2, REVISION A

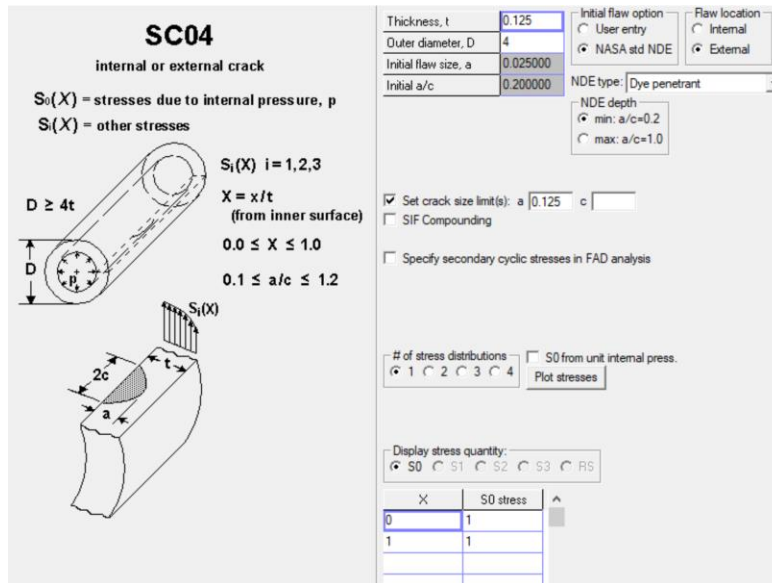


Figure 7.2-4—Input for Axially Aligned Crack in a Hollow Cylinder
 (The stress is defined to be constant through the thickness using the stress distribution.)

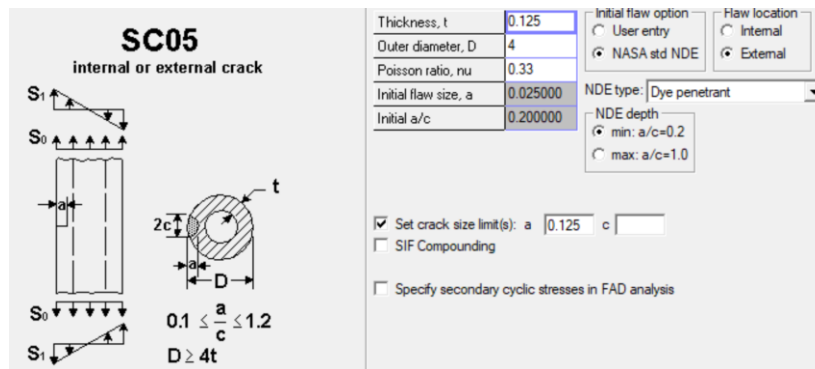


Figure 7.2-5—Input for Circumferentially Aligned Crack in a Hollow Cylinder

The material must then be selected in the “Material” tab. For this example, the Ti-6Al-4V alloy with the material ID of P3EA13AB1 is used. Note that it is NASA policy to change Bk to zero, or to a value such that the maximum stress intensity factor is less than or equal to the critical stress intensity factor with RFCB approval. In this example, Bk is set to zero and all other material properties are unchanged. Note that because this is a surface crack, there is no influence of Bk on the safe-life results.

Two load blocks must be defined: first flight, which includes single occurrence acceptance testing, and reuse flights, which only include recurring events. Table 7.2-4 is used as a guide for defining these load blocks.

The axially aligned flaw (SC04) is driven by hoop stress. The hoop stresses from Table 7.2-4 are used in the two load blocks, as seen in Figure 7.2-6, Load Blocks for Axially Aligned Crack (SC04). The cycles are multiplied by a 4x factor as required in ANSI/AIAA S-080A. The hoop

APPROVED FOR PUBLIC RELEASE – DISTRIBUTION IS UNLIMITED

NASA-HDBK-5010, VOLUME 2, REVISION A

stress is not affected by bending stress. The internal pressure is constant during flight, so the hoop stress is not cyclic, and ascent and descent can be ignored. Note that the number of cycles is multiplied by 4 because ANSI/AIAA S-080A requires the component demonstrate a minimum damage tolerance life of 4 times the service life.

The circumferentially aligned flaw (SC05) is driven by axial stress and bending stress. For SC05, NASGRO® defines axial stress as S0 and bending stress as S1. The values in Table 7.2-4 are converted to the load blocks as shown in Figure 7.2-7, Load Blocks for Circumferentially Aligned Crack (SC05). The cycles are multiplied by a 4x factor as required in ANSI/AIAA S-080A. The ascent and descent cycles are now included because of cyclic bending. Once again, a factor of 4 is applied to the cycles.

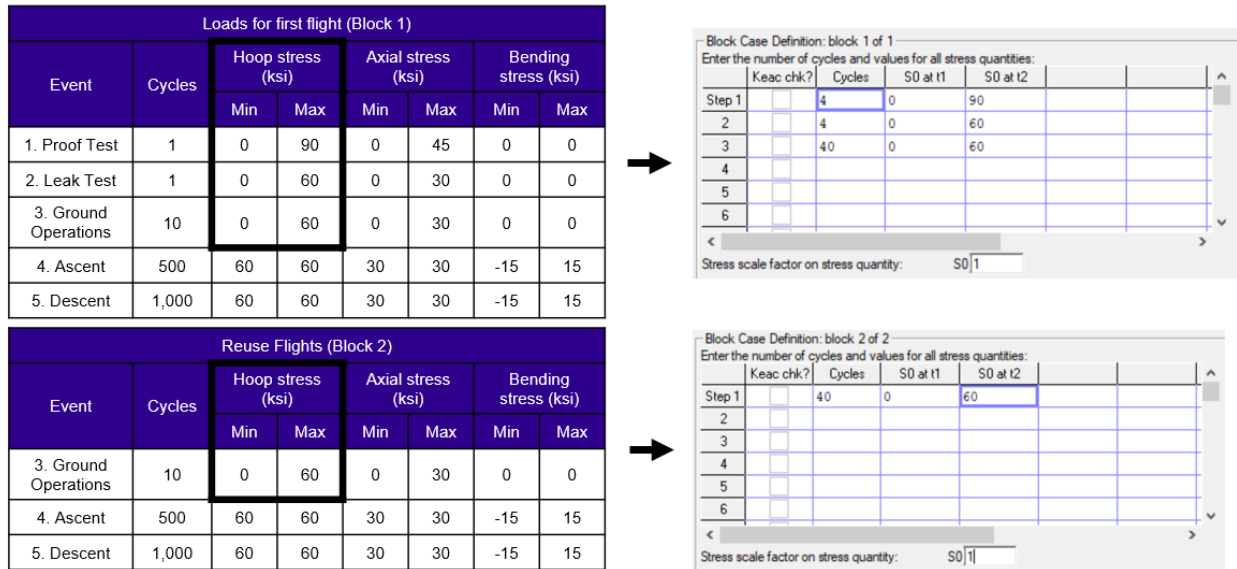


Figure 7.2-6—Load Blocks for Axially Aligned Crack (SC04)
(The cycles are multiplied by a 4x factor as required in ANSI/AIAA S-080A.)

NASA-HDBK-5010, VOLUME 2, REVISION A

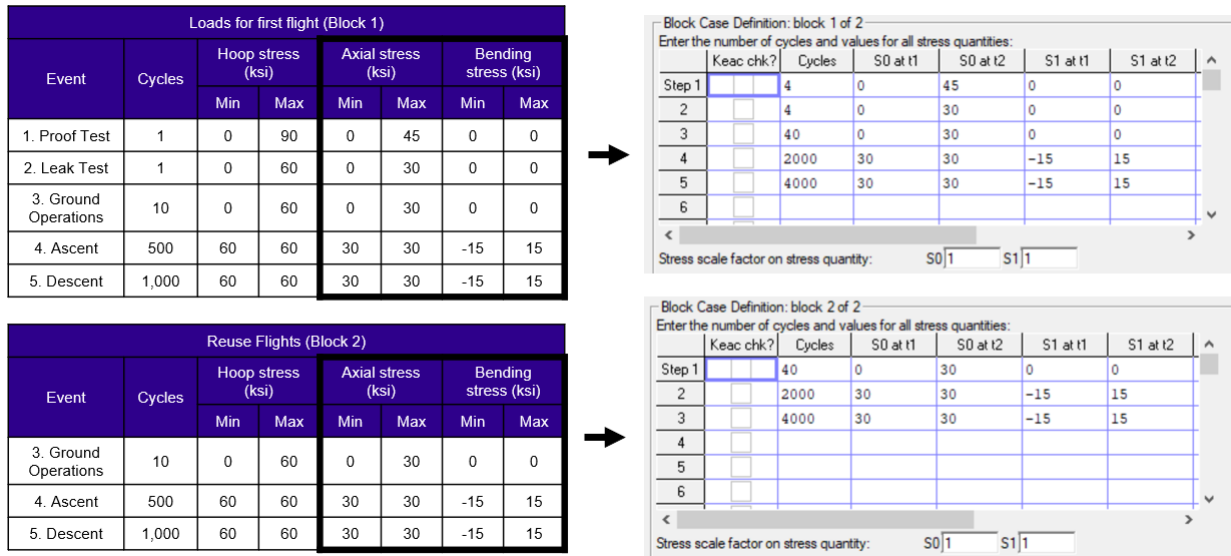


Figure 7.2-7—Load Blocks for Circumferentially Aligned Crack (SC05)
 (The cycles are multiplied by a 4x factor as required in ANSI/AIAA S-080A.)

The build schedule is applied as shown in Figure 7.2-8, Build Schedule for Initial Flight (Block 1) and Reuse Flights (Block 2). The first block, which corresponds to the first flight, is applied once. The second block, which corresponds to reuse flights, is applied as many times as the component is intended to be reflow or is set to a sufficiently large number to see the maximum number of reuse flights possible.

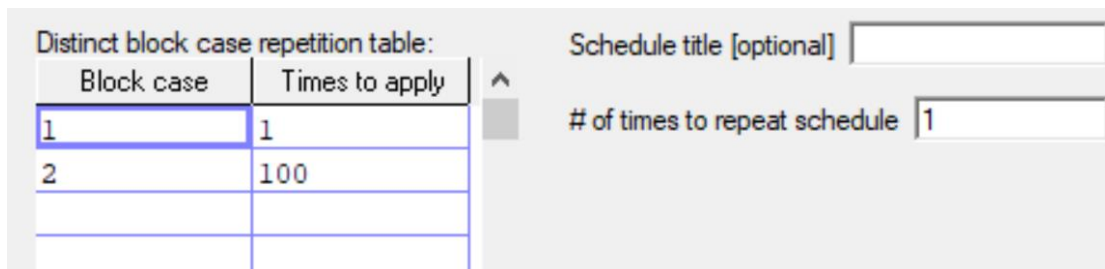


Figure 7.2-8—Build Schedule for Initial Flight (Block 1) and Reuse Flights (Block 2)

The results for a circumferential crack with a 0.2 crack aspect ratio are shown in Figure 7.2-9, Depiction of Analysis Results for a Circumferential Crack with a 0.2 Crack Aspect Ratio. The crack grew to a through crack during the fourth block. This means the component survived the first flight and two reuse flights with a factor of 4, but it failed on the third reuse flight. This case demonstrates safe life capability of 3 flights (i.e., one initial flight plus two reuse flights).

NASA-HDBK-5010, VOLUME 2, REVISION A

ANALYSIS RESULTS -----

```

FINAL RESULTS:
Crack size reached user-specified crack size limit:
# Crack size = 0.1252, user-specified limit = 0.1250
# at Cycle No. 331
# of Load Step No. 3
# of Block No. 4
# of Schedule No. 1
# Crack Sizes: a = 0.124917 , c = 0.188043 , a/c = 0.6643
# Total Cycles = 20499
    
```

Figure 7.2-9—Depiction of Analysis Results for a Circumferential Crack with a 0.2 Crack Aspect Ratio

(The crack reached a through crack during the fourth load block, indicating this crack would survive the initial flight and 2 reuse flights, including the 4x factor.)

The analysis is run for a/c of 0.2 and 1.0 for both the axial and circumferential flaws to determine the minimum number of safe flights. The results are displayed in Table 7.2-5, Safe Flights for Different Crack Orientations and Aspect Ratios in the Pipe. The safe life is defined by the configuration with the lowest life, which in this case is a circumferential flaw with a 1.0 crack aspect ratio. This component has a safe life of 2 flights (i.e., one initial flight plus one reuse flight), including the 4x factor.

Table 7.2-5—Safe Flights for Different Crack Orientations and Aspect Ratios in the Pipe

Crack Orientation	Dye penetrant crack aspect ratio, <i>a/c</i>	Safe flights (includes 4x scatter factor)
Axial (SC04)	0.2	92
	1.0	66
Circumferential (SC05)	0.2	3
	1.0	2

7.2.4.6 Bellows

The purpose of damage tolerance verification is to demonstrate that the hardware will not fail in the presence of defects during the service life. Due to a lack of confidence in analytical predictions, damage tolerance verification by analysis is not recommended for bellows convolutions. Further, verification by test is challenging. This is because it is difficult to develop crack-like flaws in bellows convolutions that are consistent in size and shape to those that can be detected with nondestructive inspections to a P90/C95 probability. Typical flaws that can occur in bellows include: disbanded seam welds, weld scratches/gouges/dents/inclusions, and convolution crown or root scratches/gouges/dents.

Per AIAA S-080A-2018, bellows must be verified to be tolerant to damage when loads other than internal pressure are significant. This applies to the complete bellows assembly; it is the bellows convolutes that pose the greatest practical challenge. To this end, an approach that can

NASA-HDBK-5010, VOLUME 2, REVISION A

be utilized in the damage tolerance verification of bellows convolutions is discussed (reference Goyal, et al. [2021]).

In the case of multi-ply bellows, demonstrating multi-ply redundancy can be a credible approach to demonstrating damage tolerance for bellows convolutions. The following criteria is provided to establish multi-ply redundancy of bellows convolutions.

Demonstration of Multi-Ply Redundancy

Life testing (i.e., pressure and external load cycling) to four times the service life and vibration qualification testing per SMC-S-016, Test Requirements for Launch, Upper-Stage, and Space Vehicles, is performed, with a fully or partially severed ply at the most critically stressed location, with the following criteria being met:

1. Bellows stiffness with severed ply remains within design requirements.
2. Failure modes associated with intrusion/entrapment of gasses or liquids are assessed and shown to be nonexistent.
3. Failure of one or more plies does not generate debris.

Multiple units (i.e., typically three) are subjected to these life tests using low-frequency loading, while the additional vibration tests at higher frequencies provide confidence in the ability of the bellows convolutions to be damage tolerant for the service life of the component.

For single-ply bellows designs, damage tolerance is much more challenging to verify. This is because small flaws may exist within the bellows convolutes that go undetected by available inspections. These flaws may then propagate through the single ply during service and introduce a leak path. As a result, the consequence of leakage in single-ply bellows designs should be deemed credible and assessed accordingly.

While fatigue testing and stringent process controls do not verify the tolerance to damage in the strictest sense, they have been used to mitigate elevated risk for bellows designs that lack adequate damage tolerance rationale. The criteria below is provided as an example of this approach.

Stringent Process Controls and Fatigue Test Requirements

After successfully completing the acceptance tests for a given bellows design, dissect a minimum of one bellows sample to verify a lack of damaging microstructural features such as pits, surface irregularities, microcracks, large grain sizes, and weld defects.

To address process variability in bellows manufacturing, perform life testing on three (3) bellows to a life factor of 4-10 times the service life and also perform vibration qualification testing per SMC-S-016. The particular life factor that is to be demonstrated is determined based on the application and program requirements.

APPROVED FOR PUBLIC RELEASE – DISTRIBUTION IS UNLIMITED

NASA-HDBK-5010, VOLUME 2, REVISION A

Prior to installation, the bellows are to be protected from damage and inadvertent deflections. This can be accomplished using protective covers and pre-installation constraints.

To minimize the potential for process drift, bellows fatigue capability is then verified at set intervals. Stiffness verification of all production units is also monitored carefully, as stiffness variation in flight bellows is usually an indicator of manufacturing variability and/or process drift.

It may also be prudent to establish a system design that has fault tolerance in lines containing bellows.

Additional requirements such as JSC-67035A, Best Practices and Guidelines (BP&G) for Thin Wall Pressure Boundaries (TWPB) for Human Spaceflight Applications, may apply to fracture critical bellows.

7.2.5 Fracture Critical Habitable Modules and Volumes

See section 7.2.1 for examples on how to perform NASGRO® analysis. These approaches can be applied to pressure vessels and pressurized fluid containers.

7.2.6 Fracture Critical Pressurized Structures

A stage tank is classified as a pressurized structure because it carries internal pressure and vehicle structural loads. Stage tanks are all proof tested. NDE (i.e., surface and volumetric) post-proof inspections were performed on a lap joint friction stir welded regions as the proof test by itself was not a sufficient screen for flaws for the service life considered. The service life definition is defined as follows: number of flights, hydro proof test, operational contingency cycles, and multiple MDP cycles. The damage tolerance analysis evaluated all load cycles after proof since the inspection was performed post-proof. The fatigue-fracture data for this alloy were available from coupon testing with and without welds. A NASGRO® configuration for this loading and geometric configuration was not available. A finite element analysis was performed to extract the stress intensity factor as a function of crack length and load, and then this analytical curve was used to integrate the Paris fatigue relationship for the alloy. The model was conservative relative to lap joint life testing, and the damage tolerance evaluation was accepted.

When NASGRO® geometry is not available, it may be possible to develop an expression for the stress intensity factor as a function of load and flaw size. The process is explained for a fatigue of a shaft with a surface flaw subject to cyclic torsional loads (reference Goyal, et al. [2018]). The following is a summary of the process:

1. Develop finite element models of the structure with various flaw depth sizes.
2. Use an approach such as the virtual crack closure technique (VCCT) to derive an analytical expression for the stress intensity factor that is a function of both flaw size and load, such that:

APPROVED FOR PUBLIC RELEASE – DISTRIBUTION IS UNLIMITED

$$K(a, P) = f(a) g(P).$$

(Equation 7.2-5)

Alternatively, instead of going through the incremental integration/approximation that follows, NASGRO's® built-in tabular stress intensity factor (K) versus crack length (a) capability could be leveraged as shown in Figure 7.2-10, Stress Intensity Factor Calculation as a Function of Pressure and Various Flaw Sizes.

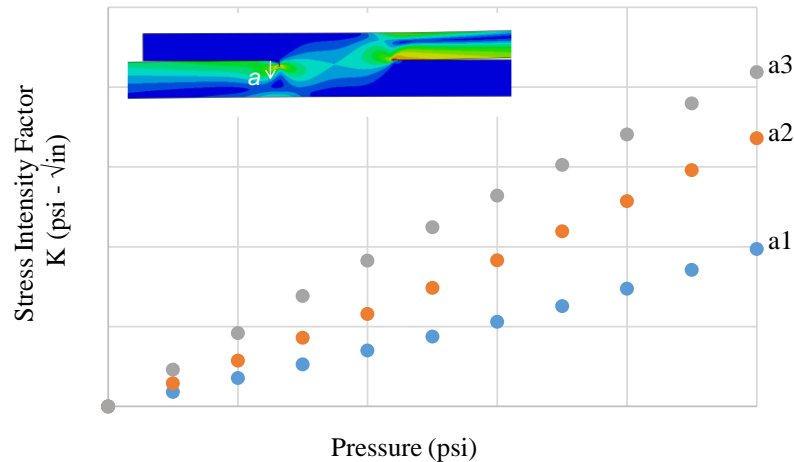


Figure 7.2-10—Stress Intensity Factor Calculation as a Function of Pressure and Various Flaw Sizes

1. Prior to proceeding, verify your analysis approach using a known flaw geometry that is present in NASGRO® to ensure the stress intensity factor calculation is accurate for that geometry.
2. Use fatigue data for the metal and the derived Mode I stress intensity factor equation to predict the fatigue life for the structure using the modified Paris equation, which is also the following equation used in NASGRO®:

$$\frac{da}{dN} = C \left(\frac{1-f}{1-R} \Delta K \right)^n \frac{(1 - \Delta K_{th} / \Delta K)^p}{(1 - K_{max} / K_c)^q} = G(a, K)$$

Crack opening function Threshold
 ↓ ↓
 Ratio Range stress intensity factor Maximum stress intensity factor Critical stress intensity factor

(Equation 7.2-6)

NASA-HDBK-5010, VOLUME 2, REVISION A

(3) Integrate the equations to determine the final flaw size given the initial flaw size:

$$\frac{da}{dN} \approx \frac{a_{N+1} - a_N}{(N+1) - N} = G(a_N, K(a_N)) \Rightarrow a_{N+1} = a_N + G(a_N, K(a_N))$$

(Equation 7.2-7)

7.2.7 Fracture Critical Rotating Hardware

Rotating hardware such as impellers and turbine wheels in liquid rocket engines are susceptible to crack growth either due to a crack initiating due to fatigue or a manufacturing flaw from processing. Damage tolerance of these components are challenging to assess using analysis approaches due to the complicated vibration environments, fluid oscillations, and centrifugal forces. For certain rotating components, the analysis may be straightforward if the boundary conditions and vibration and thermal environments are well understood; the fracture analysis can be completed starting with the initial flaw size defined by NDE. These components could include impellers and rotating shafts. As a result, a test program is used to verify actual hardware behavior and uncover errors in the assumed loading.

While proof testing of rotating components is required, the proof test is rarely sufficient to screen for flaws that can grow to failure under cyclic loads. Instead, the proof test is considered a workmanship screen for the as-built component. Turbine wheel components and other rotating components of an engine are usually vetted through full-scale engine testing at worse-case operational conditions (e.g., mixture ratio, power-level bin). The components are usually subjected to a low number of plastic strain cycles that result from engine start and stop loads, in addition to a large number of elastic strain cycles due to fluctuating pressure, vibrations, and thermal loads that occur during operation. NASA-STD-5012B requires testing up to six engine samples to two times the service life. The extensive test program is capable of surfacing vulnerabilities with the design but also vets the stability of the manufacturing program.

High energy rotating hardware such as turbine wheels need to survive challenging environments; it is often that cracks initiate prior to reaching two times the service life.

Human-rated applications designs are verified to ensure cracks do not initiate during the service life due to uncertainty in the crack growth behavior. The Space Shuttle program leveraged NSTS 07700, Volume X, Book 1, Revision M, NASA Space Shuttle-Flight and Ground System Specification-Book 1, Requirements, for the application of damage tolerance to engine components such as sections 3.2.2.1.8, 3.2.2.1.9, and 6.1.32. In the Space Shuttle Main Engine (SSME) hardware, known cracks on rotating hardware were not allowed. When a crack was discovered on rotating hardware, the life capability was defined by the last crack-free inspection.

Damage tolerance analysis for these components tends to be of lower confidence due to the complexities involving the geometry, operating conditions, and loading conditions. In some nonhuman-rated applications, a test-based approach has been used to ensure crack growth is stable and does not lead to mission ending failure. An approach successfully used is to track crack growth as the engine test program progresses to increase confidence that the flaws will

APPROVED FOR PUBLIC RELEASE – DISTRIBUTION IS UNLIMITED

NASA-HDBK-5010, VOLUME 2, REVISION A

remain stable over four times the service life of the engine component. During the test program, particular attention is required to address operations near Campbell-crossings (e.g., resonant conditions).

Note that rotating hardware is proofed by a spin test to a minimum rotational energy factor of 1.05, i.e., rotational test speed = $(1.05 \omega^2)^{1/2}$, and either NDE is performed in accordance with section 8.1 of NASA-STD-5019A before and after the spin proof test, OR it is established that the spin proof test adequately screens for flaws (i.e., section 8.1 of NASA-STD-5019A) and that this approach for flaw screening is approved by the RFCB. Generally, proof tests are usually performed in the operational environment, or the test levels are adjusted via an ECF.

7.2.8 Fracture Critical Fasteners

Fasteners classified as fracture critical need to meet several criteria. The checklist in Table 7.2-6, Checklist for Fracture Critical Fasteners, will assist in ensuring that all items have been fully evaluated. If any of the criteria below are not met, the fastener needs to comply with section 7.3 of NASA-STD-5019A; and additional discussion is required with the RFCB.

NASA-HDBK-5010, VOLUME 2, REVISION A

**Table 7.2-6—Checklist for Fracture Critical Fasteners
(All requirements must be met.)**

Item	Criteria to Meet Fracture Critical Fasteners	Completed? (Y or N)
1	Fasteners are fabricated from a metal with high resistance to stress corrosion cracking, as defined in MSFC-STD-3029.	
2	Fasteners are fabricated, procured, and inspected in accordance with NASA-STD-8739.14, and an equivalent military standard, NAS, proprietary, or commercial aerospace specification approved by the RFCB.	
3	The fastened joint complies with NASA-STD-5020 without joint separation in the nominal configuration.	
4	Fasteners have rolled threads and are assessed to demonstrate they meet the fatigue requirements in NASA-STD-5001.	
5	Fasteners manufactured from titanium alloys were coordinated with the RFCB for approval.	
6	The fasteners are not made from a low fracture toughness alloy.	
7	Fasteners are not reworked or custom made unless the application is approved by the RFCB.	
8	Include preload and its effect on flaws and cyclic stresses in the damage tolerance assessment.	
9	Inspect all fracture critical fasteners by the eddy current NDE technique or use proof testing to screen for flaws.	
10	Assume a flaw in the most critical location of a size consistent with NDE sensitivity or proof-test level in the damage tolerance analysis.	
11	Proof-load test inserts used in conjunction with fracture critical fasteners to a minimum factor of 1.2 after installation.	
12	Store and control fracture critical fasteners after inspection or testing to keep them isolated from other fasteners.	

Fasteners should be fatigue-rated. Table 7.2-6 was used to assist in an evaluation of an engine rotary component that used a single custom-made fastener. It is observed that Item 7 is not met. The fastener needs to also meet the requirements in section 7.3 of NASA-STD-5019A. Note that the custom-made bolt was the only viable option in this example, the design did not have load redundancy, and the single-bolt configuration was a key feature of the rotary design.

7.2.9 Fracture Critical Shatterable Components and Structures

An example is provided on how to approach the fracture assessment of a shatterable component. Consider a fracture critical annealed glass component made with fused silica in a human-rated space vehicle. The component is 0.25 inch thick and 12 inches wide. During flight, the component undergoes a stress with a 0.0 margin of safety for 72 hours. In this example, the component is analyzed and verified to meet the design life requirements of NASA-STD-5018, Strength Design and Verification Criteria for Glass, Ceramics, and Windows in Human Space Flight Applications, and the proof ratio needed to screen for initial flaws is determined.

APPROVED FOR PUBLIC RELEASE – DISTRIBUTION IS UNLIMITED

NASA-HDBK-5010, VOLUME 2, REVISION A

NASA-STD-5018 requires that a life factor of 4 be applied to the design life to account for scatter. For this example, an initial flaw depth of 0.0018 inch with a length to depth ratio of 20 is assumed. This is consistent with the minimum initial flaw depth and minimum length to depth ratio required in NASA-STD-5018.

An initial flaw depth is chosen for the analysis based on the manufacturing process and inspections. NASA-STD-5018 specifies that the initial total flaw depth must be at least 0.0018 inch. This corresponds to the requirement that the inspection process can identify all flaws that are at least 0.0018 inch in total depth. NASA-STD-5018 also requires that the flaw used for the structural life prediction has a length to depth ratio of at least 20.

Note that the total flaw depth is different from the visible flaw depth, as it has been shown that an invisible crack tail can extend twice the distance past visible crack depth. The inspection must identify visible flaws that are at least 0.0006 inch, which corresponds to a total flaw depth of at least 0.0018 inch. The manufacturing grinding schedule is implemented to limit flaws to less than or equal to the initial design flaw depth (see NASA-HDBK-6007, Handbook for Recommended Material Removal Processes for Advanced Ceramic Test Specimens and Components).

NASA-STD-5018 outlines two methods for verifying the life requirement of annealed glass. The first is the use of NASGRO®, which is outlined in NASA-STD-5018, section 4.7.3. The second is using hand calculations of flaw growth velocity and stress intensity factor to determine the time to failure. The procedure for the second method is outlined in NASA-STD-5018, section 4.7.4. In this example, NASGRO® is used.

The sustained stress crack growth (NASGLS) module is used, as structural degradation occurs for glass in sustained tension. A semi-elliptical surface crack in a plate (SC30) is chosen for the crack geometry. The inputs for this example are shown in Figure 7.2-11, Geometry Input for a Semi-elliptical Surface Crack in a Plate. Note that the 0.1 a/c corresponds to a length to depth ratio of 20.

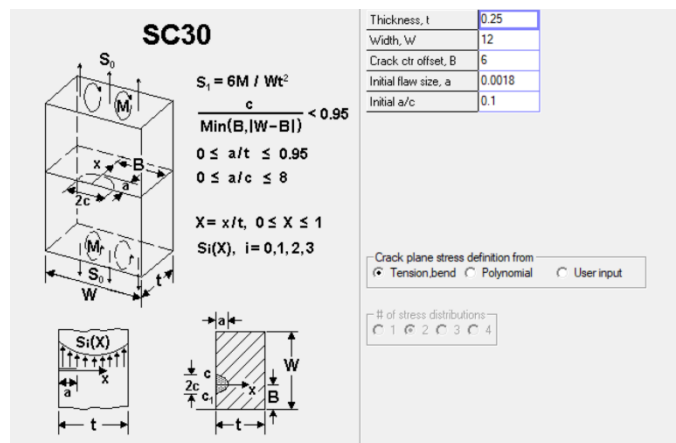


Figure 7.2-11—Geometry Input for a Semi-elliptical Surface Crack in a Plate

NASA-HDBK-5010, VOLUME 2, REVISION A

Next, the material is defined. The flaw growth properties and critical stress intensity (K_{Ic}) can either be obtained from test or from the NASGRO® built-in database. NASA-STD-5018 specifies that the exponential equation of flaw growth shall be used rather than the Paris equation. The standard also requires that the flaw growth properties should assume 100 percent moisture. Additionally, the K_{Ic} used for the life analysis should be the average K_{Ic} minus three standard deviations.

In this example, the NASGRO® built-in properties for fused silica in distilled water are used, as shown in Figure 7.2-12, Material Input for Fused Silica in Distilled Water. There is no option for using the K_{Ic} minus three standard deviations, so the database input properties are transferred to the manual input with an adjusted K_{Ic} . [Note that a 3-sigma option is being introduced with NASGRO® V10.0, in development as of this writing]. The final material properties used are displayed on the right in Figure 7.2-12.

The figure consists of two screenshots of the NASGRO software interface, showing the material input process for Fused Silica in Distilled Water.

Top Screenshot:

- # of materials (max=9): 1
- Show material: 1 (selected), 2, 3, 4, 5, 6, 7, 8, 9
- Data input mode: Database input, Manual input
- Material description: FUSED SILICA, IN DISTILLED WATER
- Choose growth equation: Paris equation: $A K^n$, Exponential equation: $V_0 \exp(BK)$
- V_0 : 0.340528D-17, B: 96.7868
- Plane strain fracture toughness K_{Ic} (mean value): 0.574
- K_{Ic} value to use: mean value, mean value - 1 sigma, mean value - 2 sigma
- [sigma = 0.018]

Bottom Screenshot:

- # of materials (max=9): 1
- Show material: 1 (selected), 2, 3, 4, 5, 6, 7, 8, 9
- Data input mode: Database input, Manual input
- Material description: FUSED SILICA, IN DISTILLED WATER
- Choose growth equation: Paris equation: $A K^n$, Exponential equation: $V_0 \exp(BK)$
- V_0 : 0.340528D-17, B: 96.7868
- Plane strain fracture toughness K_{Ic} (mean value): 0.52

Figure 7.2-12—Material Input for Fused Silica in Distilled Water

NASA-HDBK-5010, VOLUME 2, REVISION A

The top image shows the properties from the built-in NASGRO® database, which does not allow for using K_{Ic} minus three standard deviations. [Note that a 3-sigma option is being introduced with NASGRO® V10.0, in development as of this writing.] The bottom image shows the data transferred to the manual input, which keeps the same exponential equation constants but now uses K_{Ic} minus three standard deviations. The bottom input is used in this example.

After entering the material properties, the load blocks must be defined. In this example, the component undergoes stress with a 0.0 margin of safety held for 72 hours. NASA-STD-5018 requires that annealed glass is designed to a 3.0 ultimate factor of safety at the beginning of life and a 1.4 ultimate factor of safety at the end of life. Glass fails due to fracture, so the margin is calculated with stress to achieve K_{Ic} as the allowable stress. The stress intensity factor is calculated as follows:

$$K_I = 1.1 \cdot \sigma \cdot \left(\frac{\pi a}{Q}\right)^{1/2} \quad (\text{Equation 7.2-8})$$

σ is the stress, a is the flaw depth, and Q is the shape factor. Q is equal to 1 for flaws with a high length to depth ratio (length/depth ≥ 20). The allowable stress for this example can be calculated as follows:

$$\sigma_{allowable} = \frac{(K_{Ic} - 3 \cdot Std Dev)}{1.1} \cdot \left(\frac{Q}{\pi a}\right)^{1/2} = \frac{0.52 \text{ ksi} \sqrt{\text{in}}}{1.1} \cdot \left(\frac{1}{\pi \cdot 0.0018 \text{ in}}\right)^{1/2} = 6.29 \text{ ksi} \quad (\text{Equation 7.2-9})$$

The margin of safety is calculated as follows:

$$MS = \left(\frac{\sigma_{allowable}}{\sigma * 3.0}\right) - 1 \quad (\text{Equation 7.2-10})$$

The margin of safety is 0.0 when a 2.10 ksi stress is applied. This stress is applied for 72 hours.

Note that a proof test should be conducted that screens for flaws greater than that used in the life analysis, which is 0.0018 inch in this example. NASA-STD-5018 requires that the initial flaw depth screened by proof is calculated with K_{Ic} plus one standard deviation. The required minimum stress achieved in the proof to screen for flaws of at least 0.0018-inch depth is calculated as follows:

NASA-HDBK-5010, VOLUME 2, REVISION A

$$\sigma_{proof,min} = \frac{(K_{IC} + Std Dev)}{1.1} \cdot \left(\frac{Q}{\pi a}\right)^{\frac{1}{2}} = \frac{0.592 \text{ ksi} \sqrt{in}}{1.1} \cdot \left(\frac{1}{\pi \cdot 0.0018 \text{ in}}\right)^{\frac{1}{2}} = 7.16 \text{ ksi}$$

(Equation 7.2-11)

This corresponds to a proof factor of 3.41 over the stress seen during flight. NASA-STD-5018 requires that the proof factor is the larger of 3.0 or the value to screen for the initial flaw depth. This component requires a proof test that achieves a stress 3.41 times that seen in flight.

The proof test does not need to be included in the load blocks because an inspection for flaws with depths greater than 0.0018 inch is required before each flight. The load blocks consist solely of the 2.10 ksi stress applied for 72 hours. An uncertainty factor must be used on the stress based on the duration of the time life. The uncertainty factors are outlined in Table 7.2-7, Flaw Growth Analysis Uncertainty Factor Base on Design Life.

Table 7.2-7—Flaw Growth Analysis Uncertainty Factor Base on Design Life

Design Life	Uncertainty Factor
Design Life ≤ 1 week	1.4
1 week < Design Life ≤ 1 month	1.3
1 month < Design Life ≤ 1 year	1.2
Design Life > 1 year	1.1

The design life is less than 1 week, so the stress is multiplied by a 1.4 uncertainty factor to get 2.94 ksi. This is applied in the NASGRO® load block as shown in Figure 7.2-13, Load Block Definition for this Example. The block is applied 4 times to meet the required life factor.

Stress schedule description

of blocks: 4 # of steps per block (max=200): 1 Scale Factor for stress quantity: S0: 1, S1: 0

Enter info for load step: 1 Stress duration (hrs): 72 Material #: 1 Value of sustained stress: S0(t): 2.94, S1(t): 0

[actual stress = scale factor * stress qty value]

Figure 7.2-13—Load Block Definition for this Example
(Uniform tensile stress (S0) is used with the bending stress (S1) set to zero.)

With the geometry, material, and load block fully defined, the analysis can be run. The output for this example is shown in Figure 7.2-14, Analysis Results for this Example. The analysis

NASA-HDBK-5010, VOLUME 2, REVISION A

indicates that there was no failure, as the critical crack size was not reached through the 4 applied load blocks. The glass component in this example meets the design life requirements of NASA-STD-5018.

ANALYSIS RESULTS

FINAL RESULTS:

Critical Crack Size has NOT been reached.
at 72.0 hours of Load Step No. 1 of Block No. 4
Crack Size a = 0.182556E-02 , a/c = 0.101420

Figure 7.2-14—Analysis Results for this Example

(There was no failure over the 4 load blocks, indicating that the design life requirements are met.)

The output also indicates that the flaw depth increased to 0.001826 inch. Annealed glass must maintain a 1.4 factor of safety at the end of life. The stress allowable for this larger flaw is calculated in the same manner as for the original flaw, giving a value of 6.24 ksi. The end of life margin with the 1.4 factor of safety is +1.12, meeting this requirement. Note that if the material is tempered glass, a factor of safety of 3.0 is required for the duration of the design life.

Overall, this example demonstrates that this component meets the design life requirements and margin of safety requirements of NASA-STD-5018.

7.2.10 Fracture Critical Tools, Mechanisms, and Tethers

This section is reserved. See sections 7.3 and 7.4 as well as NASA-STD-5017 for guidance.

7.2.11 Fracture Critical Batteries

Design efforts should be put in place to meet NFC criteria for batteries as any leak may not be acceptable as they tend to adversely impact the mission or the leak itself tends to be hazardous. A containment could be designed to mitigate any failure modes related to a propagating flaw.

In the event that the battery cell cannot achieve the NFC criteria, a fracture critical classification is required. The approach is to develop an NDE technique that can be perceptible to flaws to a 90% probability of detection with 95% confidence. This flaw must be demonstrated to survive four times the service life of the battery.

7.3 General Approach for Fracture Critical Metallic Parts Assessment

7.3.1 Loading Spectra

See section 11.

NASA-HDBK-5010, VOLUME 2, REVISION A

7.3.2 Assessment by Analysis

Several examples are provided in this Handbook on how the damage tolerance can be performed using NASGRO® or other means. An assessment by analysis requires the following: (1) High confidence in the material properties and fracture properties; and (2) An anchored analysis methodology and software that has been validated against test data. Lack of confidence in either factor may require an assessment by test.

Generally, nominal part dimensions will suffice for fracture control analyses. An exception is for detected cracks. Worst-case dimensions, including worst-case positional tolerances, are required for analysis of detected cracks. In cases of extreme criticality, it is prudent to exercise caution; in these cases, the analyst should coordinate the dimension used with the RFCB. Actual dimensions that conservatively allow for the measurement accuracy may always be used. Table 7.3-1, Dimensions Used in the Assessment of Hardware, shows what type of conservatism should be used for each parameter in the evaluation of the hardware. Per section 8.1.5 of NASA-STD-5019A, analysis for metallic components should evaluate the following:

1. Upper bound flaw size.
2. Upper bound crack growth rate.
3. Lower bound critical stress intensity factor or residual strength.
4. Lower bound cyclic fatigue crack growth threshold stress intensity range (ΔK_{th}).

Table 7.3-1—Dimensions Used in the Assessment of Hardware

Analysis Type	Dimension For Analysis
Low Mass	Nominal
Containment	Nominal
Fail Safe	Nominal
Leak Before Burst	Nominal
Momentum	Nominal
Energy	Nominal
Fatigue	Nominal
Stress Intensity Factor	Nominal
Safe Life For Assumed Crack	Nominal
Safe Life For Detected Crack	Worst-Case Including Worst-Case Positional Tolerances
All	Actual Conservatively Adjusted For Measurement Accuracy

7.3.2.1 Assessment by Closed-Form Solution

When the closed-form solution for a flaw with known geometry and loading is available, the following blueprint provides a straightforward analytical linear elastic fracture mechanics assessment. LEFM methodology is based on a principle that assumes that fracture behavior for a homogeneous and isotropic body loaded within the linear elastic region is dominated by the crack tip stress intensity factor, K . For example, consider a panel uniformly loaded with elastic

NASA-HDBK-5010, VOLUME 2, REVISION A

tensile stress, σ , that contains a centrally located through-crack with length $2a$, the stress intensity factor can be expressed as

$$K = \beta\sigma\sqrt{\pi a} \quad (\text{Equation 7.3-1})$$

where β = geometry correction factor.

This is the so-called opening mode (Mode I) stress intensity factor, or K_I . Besides Mode I, a crack can extend in two other independent modes: shearing (a.k.a., sliding) mode, Mode II, and tearing (a.k.a., antiplane) mode, Mode III. K used without a subscript (i.e., I, II, or III) usually refers to Mode I.

For a pressure vessel, the opening mode, Mode I, is usually the predominant fracture mode. Many methods have been used to derive stress intensity factors. Among them, the finite element method is the most popular, especially for three-dimensional (3-D) cases. Quite a few stress intensity factor handbooks have been published that document various K factors with different crack geometries and loading conditions. A compendium of closed-form solutions can be found in the following references: Sih, G. C., (Ed.), *Mechanics of Fracture*, Noordhoff International Publishing, Leyden, 1973; Tada, H., P. C. Paris, and G. R. Irwin, *The Stress Analysis of Cracks Handbook*, Del Research Corp., St. Louis, Missouri, 1973; Rooke, D. P., and D. J. Cartwright, *Compendium of Stress Intensity Factors*, 1976.

For a cracked panel under cyclic elastic tensile loading, many investigators have observed that the stress intensity factor range, ΔK , is the controlling parameter. In terms of K , the stress intensity factor range can be expressed as

$$\Delta K = K_{\max} - K_{\min}, \quad (\text{Equation 7.3-2})$$

where K_{\max} and K_{\min} are the maximum and minimum stress intensity factors, respectively. They correspond to the maximum stress (σ_{\max}) and minimum stress (σ_{\min}) in a stress cycle.

More than 30 fatigue crack growth rate models have been proposed since the mid-20th century. The most popular is the "Paris Law" (reference Paris, et al. [1961]). In the early 1960s, Paris observed that for an aluminum alloy, the da/dN versus ΔK plotted in log-log scale is a straight line and can be described as follows:

$$da/dN = C(\Delta K)^n, \quad (\text{Equation 7.3-3})$$

where n = the slope of the straight line, C = intersection of the straight line with the vertical axis at $\Delta K = 1 \text{ ksi}\sqrt{\text{in}}$. Fatigue crack growth life can be determined by solving the first order differential equation. Several integration techniques can be used to provide a solution to this type of differential equation: (1) Direct integration, (2) Runge-Kutta integration, (3) Taylor series approximation, or (4) Linear approximation schemes.

NASA-HDBK-5010, VOLUME 2, REVISION A

Of the above methods, the direct integration method is the simplest. β is a function of crack size “a” and other concepts of geometry, and the application is limited to the $\beta = 1$ condition. For a center crack, with a length $2a$ contained in a wide plate subject to zero-tension constant amplitude cyclic loading, the stress intensity factor range can be expressed as:

$$\Delta K = \beta(\sigma_{\max} - \sigma_{\min})\sqrt{\pi a} = \sigma_{\max}(1 - R)\sqrt{\pi a}, \quad (\text{Equation 7.3-4})$$

where the geometry correction factor $\beta = 1$ and $\sigma_{\min} = 0$. The crack growth rate is then:

$$da/dN = C[\sigma_{\max}(1 - R)\sqrt{\pi a}]^n \quad (\text{Equation 7.3-5})$$

Through direct integration, the crack growth life is:

$$\Delta N = \frac{2}{C(2 - n)(1 - R)^n (\sigma_{\max} \sqrt{\pi})^n} [(a_f)^{1-n/2} - (a_o)^{1-n/2}], \quad (\text{Equation 7.3-6})$$

where a_o and a_f are the initial and final crack sizes, respectively.

The final crack size is usually calculated by using the fracture toughness, K_c , of the material:

$$a_{cr} = \frac{K_c^2}{\pi \sigma_{\max}^2} = 0.32 \left(\frac{K_c}{\sigma_{\max}} \right)^2 \quad (\text{Equation 7.3-7})$$

When the initial crack is known (usually determined by nondestructive inspection), the number of cycles that will be required for the crack to grow from a_o to a_{cr} can be calculated.

7.3.2.2 Assessment by Crack Growth Computer Code

Another approach is to use a crack growth computer code for flaws in metallic structures that is approved by the RFCB. NASGRO® (see NASGRO® User’s Manual) is typically the recommended fatigue crack growth application for the analytical assessment of human-rated spaceflight hardware. There are other fatigue crack growth applications that may be used, and the RFCB may recommend demonstration of equivalency with NASGRO®.

For space-flight pressure vessels, the current trend is to use NASGRO® since it contains a vast array of stress intensity factors for crack models that represent pressure vessel geometries. It also contains a large fracture and crack-growth rate (da/dN) database for materials used in fabricating pressure vessels, including titanium, corrosion-resistant steel (CRES), Inconel®, etc.

7.3.3 Assessment by Test

Typically, an assessment by test is required when the evaluation by analysis is low confidence. This situation arises when workmanship sensitivity occurs, or analysis tools are not fully validated.

NASA-HDBK-5010, VOLUME 2, REVISION A

An example of this application is discussed. There were challenges associated with evaluating the damage tolerance of friction stir welds in a pressurized structure application. A threat assessment was assembled that listed all the potential weld defects that could occur based on manufacturing of coupons, first article inspection, and several development articles. An investigation was performed to understand the cause for these flaws, and it was determined that residual stresses in the heat affected zone was the key driver for causing these flaws. There were several concerns with using an analytical approach:

- a. Geometry was not available in NASGRO®,
- b. Plasticity was expected in that region, and
- c. Residual stresses could not be fully characterized.

Only one type of flaw was deemed as critical and concerning, as the direction of the flaw was through the thickness. The flaw could propagate and cause failure of the pressure wall. First, a full-scale finite element model was used to determine the worst-case axial and azimuthal stress driving this flaw. A fatigue-life spectrum was developed based on the stress history expected during transportation, ground operations, wet rehearsals, contingency cycles, proof cycles, leak checks, and flight. The stress history was converted to a meaningful load history that could be applied to weld lap joints with worst-case manufactured flaws. In-service environments in this case only improve crack growth behavior, but these beneficial effects were not accounted for. At least twelve samples with various flaw sizes were subjected to cyclic loading based on the fatigue life spectra until the samples exhibited catastrophic failure, i.e., flaws propagated unstably. Even with the scatter observed in the fatigue crack growth test results from these tests, and using a factor greater than 4, the weld joint was verified to be damage tolerant to worst-case flaws expected during manufacturing. Further, the drawing requirement was modified to tie the initial flaw size from these tests. Due to low confidence in analysis, sections 7.3.2.c.(1) and 7.3.2.c.(2) of NASA-STD-5019A were not verified as the damage tolerance demonstration was performed by test alone.

7.4 General Approach for Fracture Critical Composite or Bonded Hardware Assessment

Fracture critical composites require undergoing an extensive evaluation. Table 7.4-1, Criteria for FC Composite Hardware, contains the criteria that need to be met for the composite hardware fracture critical classification.

Table 7.4-1—Criteria for FC Composite Hardware
(All requirements must be met.)

Item	Criteria	Completed? (Y or N)
1a	DTA 7.4.1 Provide information for residual strength sensitivity to impact damage and manufacturing flaws based on test data.	
1b	Define and quantify the flaws from any source that may occur to the hardware during its service life.	

NASA-HDBK-5010, VOLUME 2, REVISION A

Item		Criteria	Completed? (Y or N)
2a	IDMP 7.4.2	Define, document, and implement impact protection and/or detection strategies for the flight hardware to diminish the targeted damage threats identified by the DTA.	
2b		Prescribe when and how impact protection and/or detection strategies are to be used for flight hardware to mitigate credible damage or threats.	
3a	RTD 7.4.3	Define the worst-case credible flaw conditions that are shown to be tolerated by the hardware through analysis and test, considering all applicable flaw detection and mitigation strategies that are implemented for the flight hardware.	
3b		Encompass all possible worst-case credible damage conditions, except the threats that are mitigated by NDE evaluations, the IDMP, and the threats where risk is accepted by the program or project.	
3c		Document the damage states the program or project has chosen to exclude from the design.	
4	Load Spectra 7.4.4	Develop full loading spectra all the loads and the number of cycles or duration during the service life of the part at the appropriate environment are included to develop loading spectra.	
5a	DTT of Coupons 7.4.5	Perform damage tolerance tests that represent flight hardware materials, manufacturing methods, and layups.	
5b		Perform damage tolerance tests that contain induced flaws and damage that encompass the worst-case credible-flaw conditions as determined by the RTD.	
5c		Perform damage tolerance tests that represent the modes of failure expected in the flight hardware.	
5d		Perform tests in a quantity sufficient to define design values for the relevant critical failure modes, e.g., residual strength, fatigue life, using the B-basis statistical techniques as defined in CMH-17-1G or an equivalent approach approved by the RFCB.	
5e		Develop or use coupon data to establish the sensitivity of residual strength to impact and manufacturing damage	
6a	DTT of Hardware Elements 7.4.6	Damage tolerance tests of hardware elements are to include both residual strength and life-based testing.	
6b		Perform damage tolerance tests sufficient in number to guide the design and provide confidence that the tests performed encompass the worst-case credible conditions, locations, and orientations.	

APPROVED FOR PUBLIC RELEASE – DISTRIBUTION IS UNLIMITED

NASA-HDBK-5010, VOLUME 2, REVISION A

Item		Criteria	Completed? (Y or N)
7a	Strength/Life 7.4.7	Perform analysis to establish that the B-basis residual strength after 1 service lifetime is sufficient to support DUL, after which the hardware will perform as intended.	
7b		Establish that the hardware performs as intended after experiencing a B-basis number of spectrum loading service lifetimes followed by one DLL cycle.	
8a	DTT of Full-Scale 7.4.8	Perform damage tolerance tests of full-scale flight-like hardware .	
8b		Induce flaws into test hardware as specified by the RTD in the worst credible location and orientation.	
8c		Perform NDE on test hardware before test to verify that the RTD flaws have been imposed and to record any new flaws.	
8d		Account for the effects of environments and flight hardware structural conditions to simulate performances throughout the specified service lifetime. Adjusted via an ECF if not performed at operational environments.	
8e		Establish ultimate load capability in the test hardware after a minimum of 1 service lifetime loading.	
8f		Subject test hardware to a minimum of 4 service lives of spectrum loading with appropriate LEF necessary to establish B-basis reliability followed by 1 DLL cycle.	
8g		Establish that the test hardware does not experience structural failures and is capable of performing its design function after both spectrum service life testing and DUL testing (functional test or other tests) and perform NDE as part of this assessment.	
9a	BBA Evaluation 7.4.9	Evaluate any anomalies during BBA testing by evaluating unexpected flaws or unusual growth or a new failure mode observed during BBA testing.	
9b		Evaluate any anomalies during BBA testing which could drive additional actions such as test, retest, or redesign as appropriate.	
9c		Discrepancies between the anticipated and observed test responses to damage initiation or growth are reconciled.	
9d		Include RFCB involvement with all assessments and evaluations if anomalies during BBA testing occur.	
10a	NDE 8.1.2	Provide the NDE methodology and rationale in the FCP.	
10b		Perform flaw screening by NDE on all composite or bonded part regions.	
10c		For hardware that is proof tested, perform pre-proof and post-proof test NDE at critical locations identified in the	

APPROVED FOR PUBLIC RELEASE – DISTRIBUTION IS UNLIMITED

NASA-HDBK-5010, VOLUME 2, REVISION A

Item		Criteria	Completed? (Y or N)
		FCP for all hardware, i.e., critical hardware locations not screened for specific flaws with the proof test.	
11	Detected Flaws 8.1.5	Spaceflight hardware with detected flaws that is used for flight without being repaired or replaced shall have a specific detailed assessment approach documented with rationale in the FCP that contains the following: The approach and rationale provided to the RFCB for approval before implementation AND Documentation of the approved approach in the FCP.	
12a	Proof test 7.5.3	Proof test the flight article to 1.2 times the limit load using one of the following: Either conduct the proof test in the appropriate environment OR adjust the test loads using a coupon or hardware element test verified ECF.	
12b		Perform pre-proof and post-proof NDE, including special visual inspection if necessary, on the hardware.	
12c		Repair or replace hardware with indications of flaw growth or initiation that are discovered during proof test or with post-proof NDE: (1) Repeat the proof test to 1.2 times the limit load for repaired hardware. (2) Perform pre-proof and post-proof NDE, as well as special visual inspection if necessary, on the repaired regions.	
12d		Define the threats that may cause flaws from any source that may occur to the hardware during its service life, considering all applicable flaw detection and mitigation strategies that are implemented for the flight hardware.	
12e		Develop and implement an IDMP for the hardware that assures a complete record of hardware impact or damage status and mitigates the risk of undetected damage from the threats identified in section 7.5.3.d (above) for the period between post-proof NDE and launch.	
12f		Establish that the largest remaining residual threat after post-proof NDE through the remainder of the service life can create damage no larger than the flaw size screened by NDE.	
12g		Repeat the proof test, repair, or replace the hardware if any incidents of impact or other damage occur after post-proof NDE and before launch.	
12h		For reflight hardware, repeat the proof test approach activities before the hardware is reflown.	

APPROVED FOR PUBLIC RELEASE – DISTRIBUTION IS UNLIMITED

NASA-HDBK-5010, VOLUME 2, REVISION A

7.4.1 Damage Threat Assessment/Damage Protection Plan

In this section, an example of a damage threat assessment is provided. The damage threat assessment is intended to provide information for residual strength sensitivity to impact damage and manufacturing flaws based on test data. Quantity of flaws and their sources are determined that may occur to the hardware during its service.

In the DTA, information about the part should be documented and includes:

1. Part number
2. Hardware name
3. Hardware to be flown on (e.g., Ares I-X)
4. Function
5. Material constructions
6. Operating loads (e.g., pressure, temperature, loads)
7. Summary of design structural margins for all relevant failure modes
8. Summary of structural qualification tests
9. Acceptance tests (e.g., proof test, NDE, etc.)
10. Applicable/Reference standards applicable to the hardware

Many parts are susceptible to damage due to mishandling during manufacturing, handling, test, storage, transportation, in-service use, and maintenance, including integration, launch, re-entry, landing and reflight. Each phase should be assessed as to the potential damage sources and mitigations. A table as shown in Table 7.4-2, General Example of a Threat Assessment and Accompanying Protection Plan, should be developed. All the failure modes associated with the part need to be identified (failure mode and effects analyses [FMEAs]). JSC 66901, Damage Threat Assessment and Damage Control Plan Template for Composite Overwrapped Pressure Vessels, provides a useful template for developing an assessment and plan for COPVs. A generalized example template is provided in Table 7.4-2.

Table 7.4-2—General Example of a Threat Assessment and Accompanying Protection Plan

Threat	Operation	Condition	Protection Plan
Overpressurization of the component due to inadequate pressure relief or venting	Filling	Up to MDP	Fill procedure was qualified and provides fault tolerance. A relief valve prevents over-pressurization.
Contamination or debris	Filling	Up to MDP	System to be internally cleaned to X level as prescribed in the specification [Insert Here]. A filter will be installed during the filling process, and verification will be performed to ensure purity content does not exceed threshold.
Incompatible materials	Filling	Up to MDP	Material compatibility analysis and testing were performed in accordance with M&P document [Insert Here].

NASA-HDBK-5010, VOLUME 2, REVISION A

Threat	Operation	Condition	Protection Plan
Improper workmanship or assembly	Assembly	Up to MDP	The component is integrated with [Insert here] assembly per approved design and process controls. Inspections and acceptance tests in [Insert Here] will verify proper workmanship.
Handling damage	All	Up to MDP	Use of protective covers will aid in hardware protection. The hardware will be handled and transported in an approved shipping container per [Insert Here]. The hardware is protected by commercial packing material such as [Insert Here, e.g., foam, bubble wrap] or a combination of materials which is capable of absorbing the indentation and deflection damage. The shipping container will be instrumented to identify any peak forces during the shipping process.
Moisture damage	All	Up to MDP	Desiccant bags are placed to prevent moisture buildup on sensitive components during shipping process and storage.
Tool impact	All	Up MDP	All potential tools that could impact the hardware have been identified. The potential of impact damage has been minimized by removing any tools in the vicinity of the hardware per [Insert Here] procedure. The hardware and assembly are classified fracture critical and are to be handled according to manufacturer's and hardware owner's instructions [Insert Here]. All movement of COPV is covered by approved lifting and handling procedures for lifting and handling hardware [Insert Here].
External Corrosion	Handling, storage, testing, and in-service use	Up MDP	The materials used in the hardware will be subject to exterior corrosion control and maintained according to cleanliness threat mitigation in the M&P procedure [Insert Here]. The hardware will be inspected by a qualified inspector before installing protective covers per Inspection Plan [Insert Here].
Ultraviolet (UV) damage	All	Up to MDP	Assembly is kept in shipping container or is shielded from UV light until installation

APPROVED FOR PUBLIC RELEASE – DISTRIBUTION IS UNLIMITED

NASA-HDBK-5010, VOLUME 2, REVISION A

Threat	Operation	Condition	Protection Plan
			into the pressure system per Specification [Insert Here].
Interface damage and damage to the sealing surface	All	Up MDP	Inspections are performed before and after interface connections are made.
Composite surface abrasion	All	Up MDP	The hardware is restrained using manufacturer-recommended corrosion resistant mounting bracket. The structural system requires to accommodate expansion and contraction without inducing excessive loads to the bracket or causing abrasion. The nut used in the mounting bracket is not installed when the tank is pressurized.
Undetected damage	All	Up MDP	Approved and qualified inspection techniques are used. Inspections are performed and a qualified inspector at the inspection points is defined in the Inspection Plan [Insert Here].

7.4.2 Impact Damage Mitigation Plan

An impact damage mitigation plan is developed to establish strategies that ensure the hardware is not damaged beyond a level known that the hardware can tolerate during use. The plan can also include measures to identify if any damage has occurred by using damage indicators. The plan develops mitigations by addressing any damage threats identified in the damage threat assessment. The plan can utilize protection, surveillance, or inspections to accomplish those alternative goals.

7.4.2.1 Example Impact Damage Mitigation Plan for Generic Hardware

An example plan for some Hardware A is as follows:

1. Standard practice must be followed to the greatest extent possible in the manufacturing and handling of Hardware A. In the case of deviations from that practice, the induced damage must be reported and evaluated using appropriate NDE techniques. Processes used in manufacturing, handling, and shipping should include whatever measures necessary to minimize the threat of damage to the hardware.

2. Protection against impact damage from FOD is required. Document X-Y-Z provides the planning and guidance for the control of contamination and FOD for the Hardware A. That plan presents requirements for identifying the cleanliness and protection needs and for including inspections in the process planning.

APPROVED FOR PUBLIC RELEASE – DISTRIBUTION IS UNLIMITED

NASA-HDBK-5010, VOLUME 2, REVISION A

3. Hardware A must be evaluated using appropriate NDE techniques before the proof test and again after the proof test. The post-proof NDE, in conjunction with the pre-proof NDE, is intended to identify any changes in the Hardware A induced by the proof test operations. The two inspections together also serve to find and quantify any damage input prior to the respective NDE inspections.

4. Hardware A will be visually inspected upon arrival at the launch facility following Document X-Y-Z. Any significant damage arising from handling and shipping subsequent to the post-proof NDE will be found by a visual inspection upon arrival at launch facility. Hardware A has been previously shown to be tolerant to large disruptions of section, and so visual inspection to identify any potential damage should be effective for risk mitigation of undetected damage in the hardware.

5. Immediately prior to integration of Hardware A into the rocket stack, a visual inspection of the hardware is performed. After integration, the access covers will be installed; and there is no plan to access the space any further. The IDMP does not provide any guidance beyond that point, because the parts are expected to be protected in the enclosed volume. If further access is required, an appropriate IDMP for that activity should be generated. After integration, the hardware is protected in the rocket vehicle stack; no further effort should be required unless the hardware volume is accessed.

7.4.2.2 Example Impact Damage Mitigation Plan for COPVs

A set of impact damage control (IDC) procedures for COPVs has been proposed by NASA JSC White Sands Test Facility under an Air Force/NASA-funded Research and Development Program (reference Tapphorn [1998]). A more comprehensive and updated template is JSC Damage Control Plan template document (JSC 66901). An illustrative example is presented here. The specific areas covered in this set of proposed procedures are IDC plan, manufacturing IDCs, shipping IDC, COPV receiving inspection requirements, installation and system-level impact control, impact control plan (ICP) implemented with impact indicators, and ICP implemented with impact protectors.

Impact Damage Control Plan

The following are the three basic steps in the development of the IDC plan:

1. A quality assurance (QA) program, based on a comprehensive study and engineering requirements (e.g., drawings, material specifications, process specifications, workmanship standards, design review records, and fail mode analysis) for the COPV, should be established to assure that the necessary NDE and acceptance tests are effectively performed to verify that the flight article meets the requirements of the IDC Plan. The QA program should ensure that the COPVs conform to applicable drawings and process specifications; that no damage or degradation has occurred during material processing, fabrication, inspection, shipping, storage, operational use, and refurbishment; and that defects that could cause failure are detected or evaluated and corrected. Figure 7.4-1, Relationship of QA and NDE to BAI of COPVs, shows

NASA-HDBK-5010, VOLUME 2, REVISION A

how QA and NDE efforts relate to burst-after-impact (BAI) of COPVs. As a minimum, the following considerations should be included in structuring the QA program.

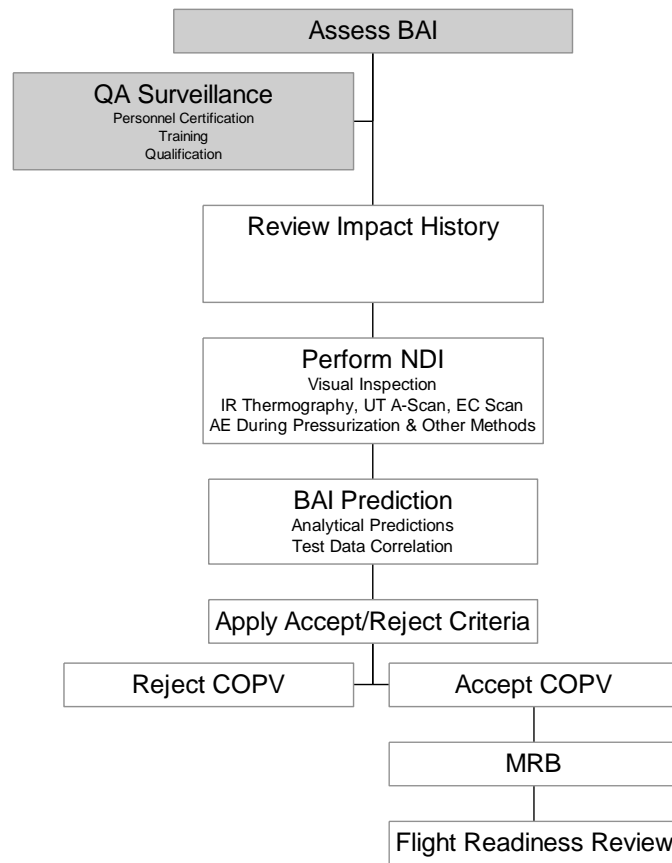


Figure 7.4-1—Relationship of QA and NDE to BAI of COPVs

2. An inspection plan should be established prior to the start of fabrication. The plan should specify appropriate inspection points and inspection techniques for use throughout the program, beginning with material procurement and continuing throughout fabrication, assembly, acceptance proof test, operation, and refurbishment, as appropriate. In establishing inspection points and inspection techniques, consideration should be given to the material characteristics, fabrication processes, design concepts, structural configuration, and accessibility for inspection of flaws.

3. *Personnel Qualifications, Training, and Certifications.* QA and NDE inspectors should be trained and certified in the visual recognition of impact damage to a COPV. For visual inspections, the inspectors should be trained to identify impact damage indentations, cuts, matrix cracking, delaminations, and fiber breakage on representative COPV surfaces prior to performing the required COPV inspection. In addition, the inspectors should also be trained to differentiate benign discontinuities (e.g., scuff marks, adhesive films, and superficial abrasions) from the detrimental defects listed above. Personnel involved in specialized NDE should be trained in the application of the technique and data interpretation. Specialized training should be

NASA-HDBK-5010, VOLUME 2, REVISION A

conducted using representative impact damage on COPVs. All personnel handling the COPV should be familiar with handling procedures associated with spaceflight hardware. At a minimum, this should include training in the damage susceptibility of the COPV and methods of preventing potential impacts during handling. Discrepancy reporting should be defined as part of the QA program and inspection plan procedures. Discrepancies in terms of impact damage, indications, overwrap or liner discontinuities, anomalies, or other flaws should be reported and dispositioned on approved forms. Jurisdictional authority should give approval prior to pressurizing the COPV to MDP levels or above.

Manufacturing Impact Damage Controls

Figure 7.4-2, Manufacturer's Impact Control Requirements, illustrates how the IDC Plan should be implemented during the manufacturing stage of the COPV. Handling procedures for manufacturing plant operations depend on the size of the COPV. For small cylindrical or spherical COPVs, manual handling should be accomplished with 100 percent QA surveillance using procedures that specify the use of gloves and foam pads to prevent scuffing of the composite overwrapped surface. For large COPVs, lifts and slings should be required to move the COPV. Prevention of COPV impact damage should be controlled procedurally with 100 percent QA surveillance when using lifts and slings.

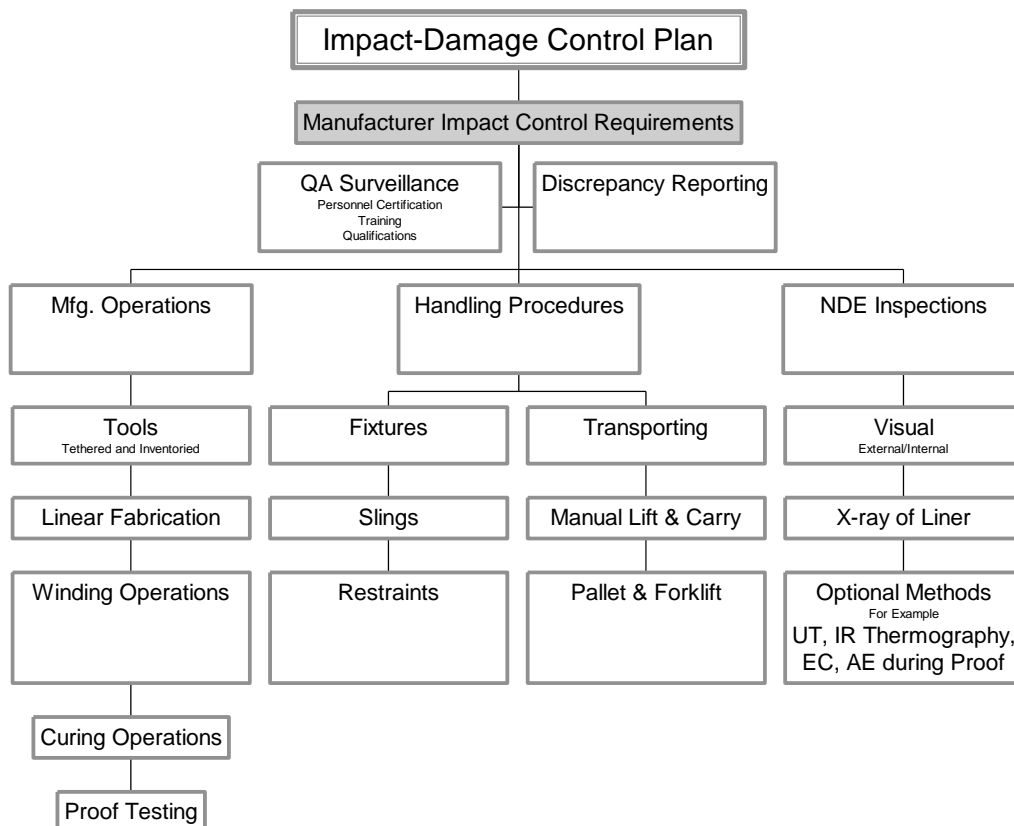


Figure 7.4-2—Manufacturer's Impact Control Requirements

NASA-HDBK-5010, VOLUME 2, REVISION A

Impact control (IC) for manufacturing operations should include the identification of tool impacts, floor drop conditions, and threat environments that could potentially contribute to or cause COPV impact damage. Since impact protective covers may not be practical for all stages of COPV manufacturing operations, the plan requires that the IDC be implemented via procedural controls with 100 percent QA surveillance. Tools in the IDC area of manufacturing plants should be inventoried and controlled by the QA program. Tethered tools on lanyards should be required for any situation that potentially may result in accidental dropping of tools that may strike the COPV during the manufacturing process. These processes include, but should not be limited to, filament winding, curing, autofrettage, leak testing, NDE, proof testing, and preparation for shipping or storage.

Impact control should include handling procedures for protective covers or fixtures used during all stages of manufacturing. The handling procedures should identify the certification requirements for lifting items such as slings, restraints, foam-padded chocks, fixtures, forklifts, or hoist assemblies. Manual handling of COPVs in manufacturing plants should be performed with surveillance QA inspectors monitoring for any floor drops or transportation collisions. Likewise, COPV transportation requiring forklift or hoist mechanical aids should be performed using a trained team of personnel to guide the COPV and avoid collision impacts with objects, walls, or floors. Protective measures, including impact protection covers, foam pads, foam-padded chocks, and foam-lined transportation containers, should be used to reduce the likelihood of anomalies or discontinuities (e.g., scuff marks or light abrasions) associated with various handling operations.

Impact Damage Controls During Shipping

Figure 7.4-3, Shipping ICP Requirements, illustrates the IDC Plan that should be implemented for COPV shipping. Handling procedures for shipping and receiving depend on the size of the COPV. For small cylindrical or spherical COPVs, handling should be performed under 100 percent surveillance using procedures that specify the use of gloves and foam pads to prevent scuffing of the composite overwrapped surface. For large COPVs, lifts and slings should be required for moving the COPV. Prevention of COPV impact damage should be controlled procedurally when using lifts and slings.

NASA-HDBK-5010, VOLUME 2, REVISION A

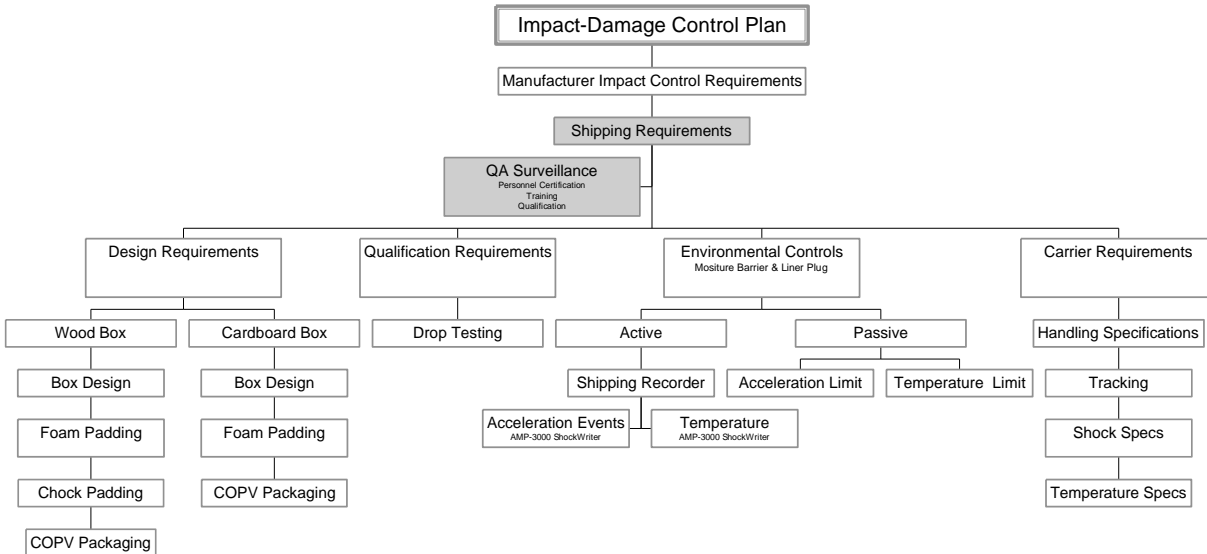


Figure 7.4-3—Shipping ICP Requirements

Transportation containers should be designed to protect the COPV from the threat environments encountered during shipping to assure that damage is not afflicted to the COPV. For small spherical COPVs, the shipping container should be foam lined per MIL-PRF-26514, Polyurethane Foam, Rigid or Flexible, for Packaging. Sufficient foam thickness is required to prevent COPV damage resulting from shipping container drops or collision impacts to the shipping container structure. The shock case defined by FED-STD-101C(4), Test Procedures for Packaging Materials, Method 5007.1, Level B, should be used to design the shipping container.

Note: FED-STD-101C(4), Test Procedures for Packaging Materials, has been cancelled and superseded by MIL-STD-3010, Test Procedures for Packaging Materials. Appendix A in MIL-STD-3010 states that Method 5007 has been superseded by American Society for Testing and Materials (ASTM) D4169-04, Standard Practice for Performance Testing of Shipping Containers and Systems. The shock test procedure in cancelled FED-STD-101C(4) is clear, detailed, and preferred. Although it has been cancelled, this document remains available on DOD's Acquisition Streamlining and Standardization Information System (ASSIST) Web site < <http://assist.daps.dla.mil/online/start/> > at no charge.

Frequently, larger or cylindrical COPV containers are suspended on foam chocks or foam-lined saddle fixtures. ASTM D1974–98(2003), Standard Practice for Methods of Closing, Sealing, and Reinforcing Fiberboard Boxes, provides standard practices for closing, sealing, and reinforcing fiberboard shipping containers of types suitable for COPVs.

Shipping containers with multiple compartments should be permitted for the shipment of a plurality of small COPVs, but each compartment should be individually lined with sufficient foam to preclude impact damage during shipment. The entire crate should be designed to survive a drop from a height consistent with the threat environment (minimum 4 ft) without inflicting damage to the COPV.

NASA-HDBK-5010, VOLUME 2, REVISION A

For large COPVs, shipping containers should be constructed to survive a minimum (4 ft) drop while protecting the COPV. This includes suspending the COPV in foam pads, chocks, or saddles. The lid of the shipping container should be secured with metal clamps held in place with banding straps. The thickness of foam required to preclude COPV damage depends on the size and weight of the COPV. Small vessels may require only 1-in thick foam, while the large vessels require foam pads up to 6 in thick or greater. The foam lining specification should be in accordance with MIL-PRF-26514. ASTM D1083-91(1998), Standard Test Methods for Mechanical Handling of Unitized Loads and Large Shipping Cases and Crates, provides appropriate test procedures, although it was withdrawn in 2001 and not replaced.

If the shipping container cannot be qualified by similarity to a previously qualified design, the new container design should be subjected to drop testing from a height consistent with the threat environment (minimum 4 ft), with the COPV installed. The results of these drop tests should demonstrate that the BAI of the COPV does not degrade to below its design burst strength. ASTM D775-80(1986), Method for Drop Test for Loaded Boxes, provides standard guidelines for drop testing loaded boxes, while ASTM D4169-04, Standard Practice for Performance Testing of Shipping Container and Systems (section E.3.1 above), provides standard guidelines for performance testing of shipping containers and systems. [Note: ASTM D775-80 was withdrawn in 1993 and replaced by ASTM D5276-98(2004), Standard Test Method for Drop Test of Loaded Containers by Free Fall.]

The shipping container should be designed to protect the COPV from environmental factors that may degrade the performance of the COPV. The COPV should be sealed in a moisture barrier with an independent port boss seal that protects both the COPV overwrap and the liner from environmental exposure to high-humidity environments or from corrosive airborne contaminants during shipping and handling. Desiccants should be permitted, provided the chemical materials are compatible with the COPV overwrap and liner. ASTM D895-94, Standard Test Method for Water Vapor Permeability of Packages, provides appropriate test procedures, although it was withdrawn in 1999 and has not been replaced.

The shipping container may also be equipped with active or passive acceleration and temperature recording devices to monitor the environmental shock conditions and temperature conditions during shipment. *In situ* health monitoring of shipping containers can be implemented with both passive and active devices. Passive monitors include shock-sensitive indicators that unload a configuration of spring-loaded balls or shock-sensitive strips that change color when the indicator has been subjected to a shock event. Active monitors include units such as the AMP-3000 ShockWriter, which is capable of storing up to several hundred events logged over a shipping duration of up to 90 days.

The shipping carrier should be qualified to ship and handle flight hardware. The shipping and handling documents should specify the acceptable ranges and limits with respect to shock, impact sensitivity, and temperature. The COPV cargo should be tracked throughout all stages of the shipping process.

APPROVED FOR PUBLIC RELEASE – DISTRIBUTION IS UNLIMITED

NASA-HDBK-5010, VOLUME 2, REVISION A

COPV Receiving Inspection Requirements

Figure 7.4-4, Receiving Inspection ICP Requirements, illustrates the ICP that should be implemented with respect to COPV receiving inspection requirements. Handling procedures for receiving inspection depend on the size of the COPV. For small cylindrical or spherical COPVs, manual handling should be accomplished with 100 percent QA surveillance using procedures that specify the use of gloves and foam pads to prevent scuffing of the composite overwrapped surface. For large COPVs, lifts and slings should be required to move the COPV. Prevention of COPV impact damage should be controlled procedurally with 100 percent QA surveillance when using lifts and slings.

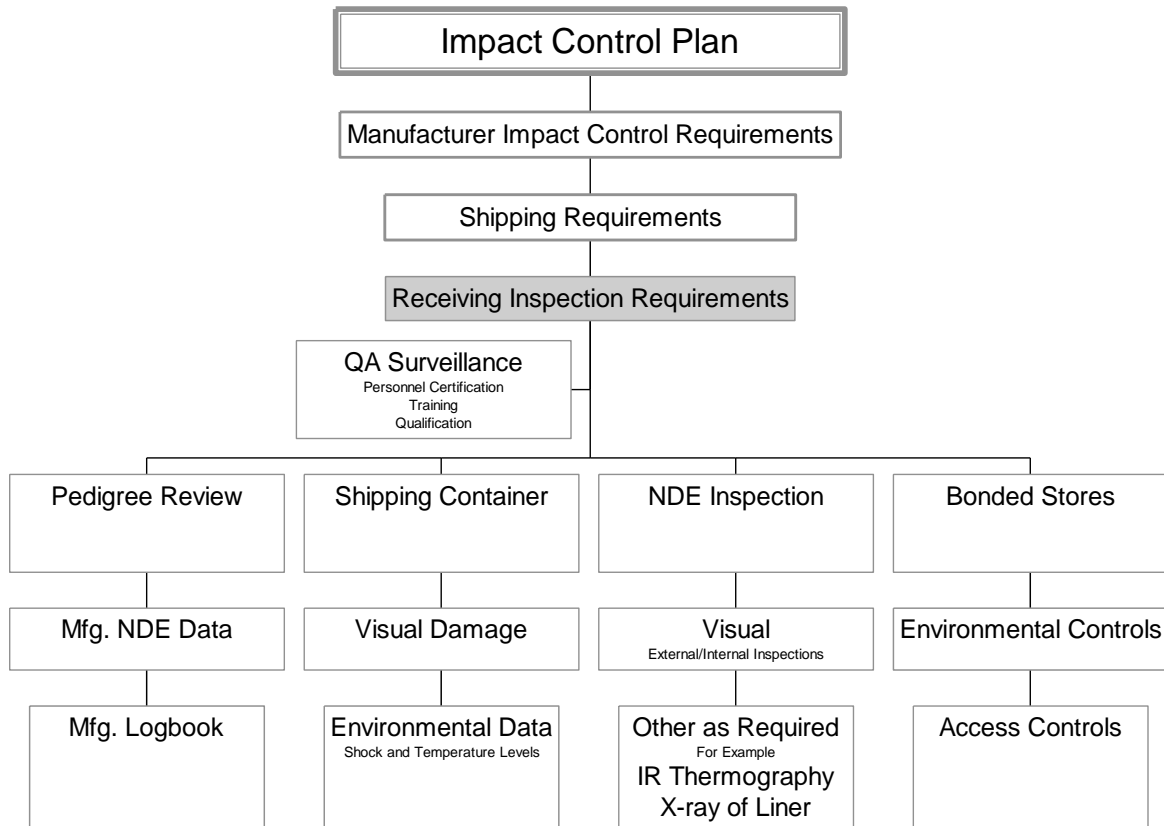


Figure 7.4-4—Receiving Inspection ICP Requirements

COPV receiving inspections should be performed to assess the integrity of the COPV as received. These inspections should include a visual inspection of the composite overwrap, a visual inspection of the COPV liner using a borescope, and an X-ray radiographic inspection of the metal liner.

Pedigree information, shipped with the COPV, should be reviewed as part of the receiving inspection process to ensure that the COPV meets the program requirements. The manufacturer's NDE data should be reviewed and compared to procurement agency requirements for the COPV and the receiving inspection NDE records. The manufacturer's COPV logbook should be reviewed to determine if any suspected impact damage conditions have been reported.

NASA-HDBK-5010, VOLUME 2, REVISION A

Visual inspection of the shipping container should be performed to determine if there are indications of a drop during shipment. Shipping container damage indications include crushed corners or impact indentations on the external surface. Internally, unusual foam deformation or compaction will provide clues of potential damage from shipping container drops. If the shipping container is equipped with active or passive shock and/or temperature monitors, data from these units should be used to assess the environmental conditions during shipment of the COPV.

All COPVs not installed on spacecraft or launch vehicle hardware should be stored in a Bonded Stores facility with access controls defined by the program QA requirements. The Bonded Stores facilities should have environmental controls to maintain the COPV within the required temperature and humidity specifications.

Installation and System-Level Impact Control

Figure 7.4-5, Installation and System-Level Procedures for Procedural-only ICP, illustrates the ICP overview that should be implemented during the installation and system-level operations of the COPV mounted on the spacecraft hardware or the launch vehicle. COPV handling procedures for the spacecraft or launch vehicle installation and test phase depend on the size of the COPV. For small cylindrical or spherical COPVs, manual handling should be accomplished using procedures that specify the use of gloves and foam pads to prevent scuffing of the composite overwrapped surface. For large COPVs, lifts and slings should be required to move the COPV. Prevention of COPV impact damage should be controlled procedurally with 100 percent QA surveillance when using lifts and slings.

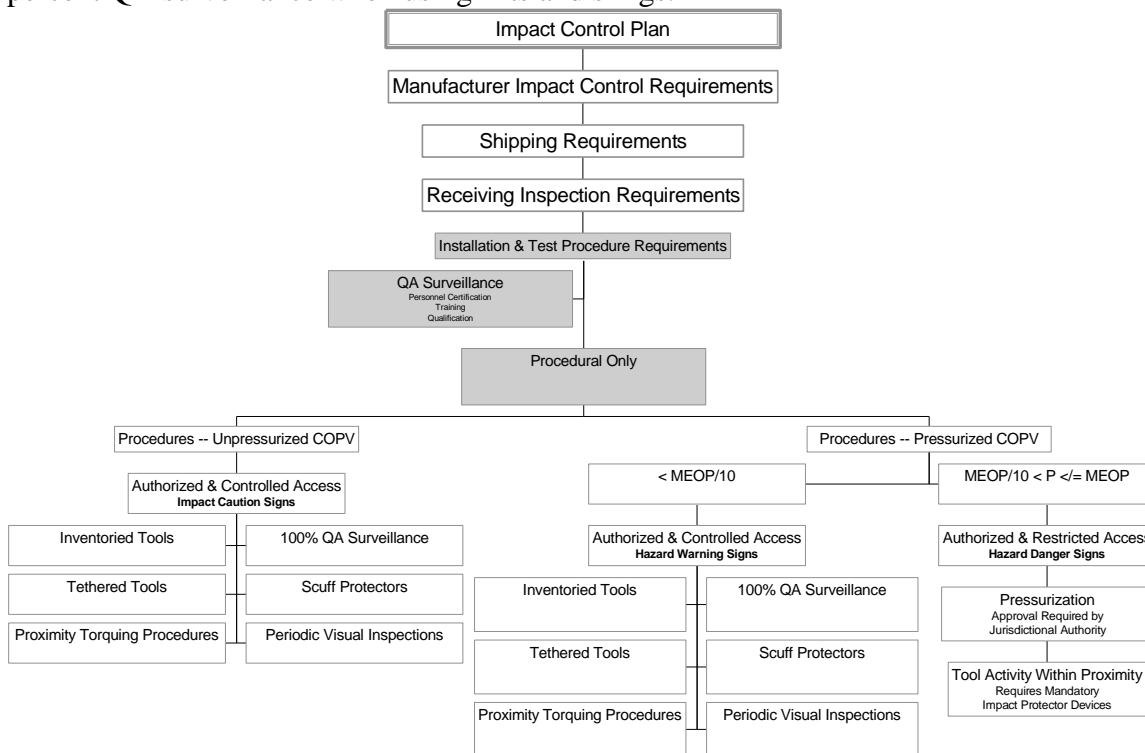


Figure 7.4-5—Installation and System-Level Procedures for Procedural-only ICP

APPROVED FOR PUBLIC RELEASE – DISTRIBUTION IS UNLIMITED

NASA-HDBK-5010, VOLUME 2, REVISION A

The following options are discussed:

1. ICP by Procedure Only: Figure 7.4-5 also illustrates the procedural-only ICP option that, if selected, should be used during the installation and test of the COPV mounted on the spacecraft hardware or the launch vehicle. Handling procedures for installation depend on the size of the COPV. For small COPV cylindrical or spherical vessels, manual handling should be accomplished using procedures that specify the use of gloves and foam pads to prevent scuffing of the composite overwrapped surface. For large COPVs, lifts and slings should be required to move the COPV. Prevention of COPV impact damage should be controlled procedurally when using lifts and slings.

2. ICP procedures for Unpressurized COPVs: Require access control and authorization by the jurisdictional authority for personnel to work within close proximity to the COPV and should be performed with 100 percent QA surveillance. Caution signs should be displayed near the COPV to make personnel aware of the impact sensitivity. Inventoried and tethered tools should be required when this work is performed. Torque or leverage tool operations within close proximity to the COPV should be performed under procedural control with 100 percent QA surveillance. Scuff-protective materials in the form of high-density foam or equivalent should be used to reduce the potential for false impact indications resulting from small tool scuffs and abrasions. Periodic inspections by trained and certified NDE inspectors should be performed prior to the installation of scuff-protective materials and after the removal thereof.

3. ICP Procedures for Pressurized COPVs: Access control for working in close proximity to a pressurized COPV ($< \text{MDP}/10$) should be controlled and authorized by the jurisdictional authority. Hazard warning signs should be displayed near the COPV to warn personnel of the impact sensitivity and the potential burst hazard of the COPV. ICP procedures for COPV pressurized to $< \text{MDP}/10$ should require inventoried and tethered tools. Torque or leverage tool operations within close proximity of the COPV should be performed under procedural control with 100 percent QA surveillance. Scuff-protective materials in the form of high-density Ensolite® foam or equivalent should be used to reduce the potential for false-positive impact indications resulting from small tool scuffs and abrasions. Periodic inspections by trained and certified NDE inspectors should be performed prior to the installation of scuff-protective materials and after the removal thereof. Pressurization of a COPV from $0.1 \times \text{MDP}$ to MDP or above should require authorization by the jurisdictional authority, and personnel access should be restricted. Hazard danger signs should be displayed near the COPV to warn personnel of impact sensitivity and the potential for catastrophic burst. In addition, any tool activity performed within proximity of the pressurized COPV should require mandatory use of impact protector devices.

ICP Implemented with Impact Indicators

Figure 7.4-6, Installation and System-Level Procedure for Implementation of ICP with Impact Indicators, illustrates the impact indicator ICP option that, if selected, should be implemented during the installation and test of the COPV mounted on the spacecraft hardware or the launch vehicle. Handling procedures for installation depend on the size of the COPV. For small cylindrical or spherical COPVs, manual handling should be accomplished using procedures that

NASA-HDBK-5010, VOLUME 2, REVISION A

specify the use of gloves and foam pads to prevent scuffing of the composite overwrapped surface. For large COPVs, lifts and slings should be required to move the COPV. Prevention of COPV impact damage should be controlled procedurally when using lifts and slings.

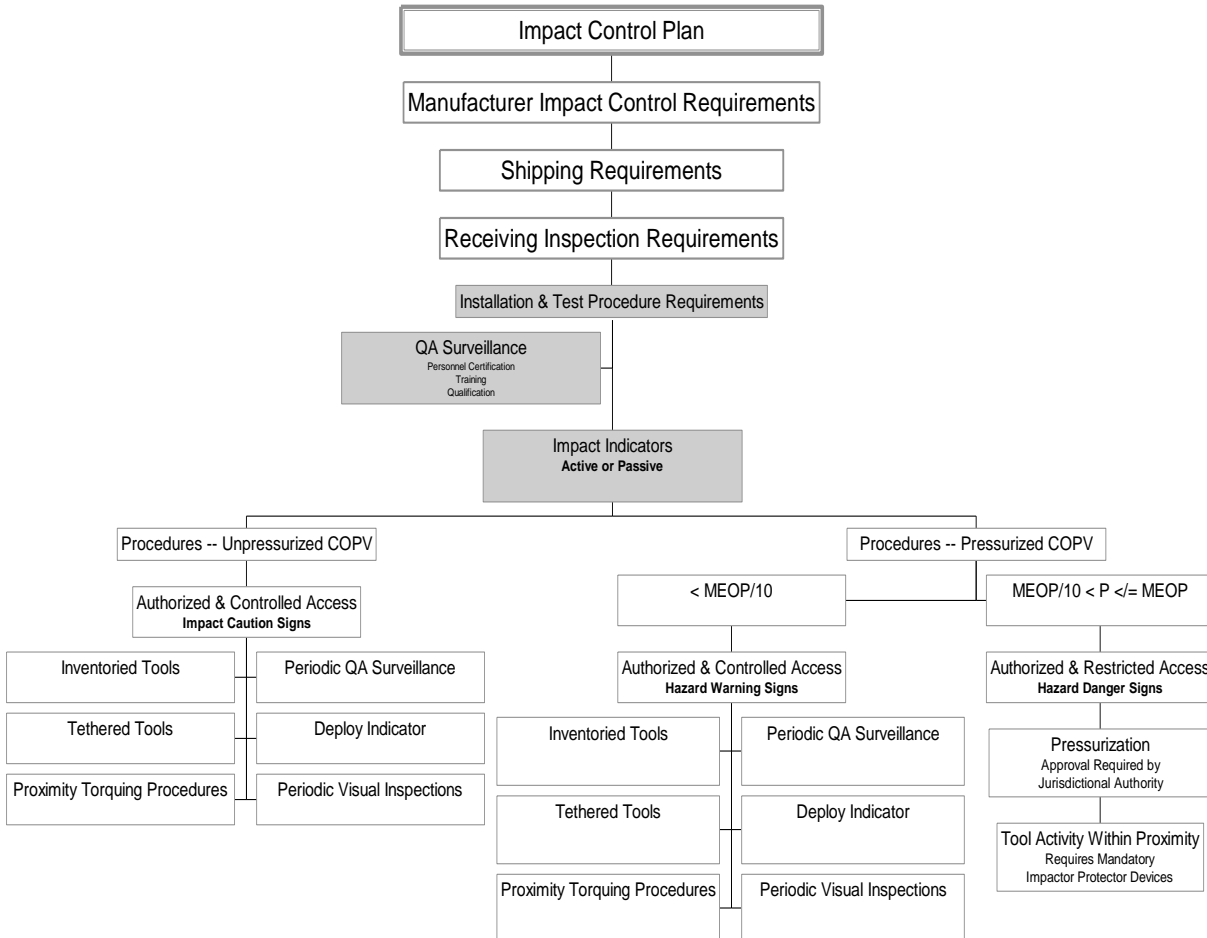


Figure 7.4-6—Installation and System-Level Procedure for Implementation of ICP with Impact Indicators

Impact indicators should be capable of detecting any impact condition that could result in a 5 percent or greater degradation of COPV nominal burst strength. Piezoresistive film, commonly used as strain and force sensors, sandwiched between two 0.25-in thick high-density Ensolite® foam layers provides an excellent active impact indicator with impact force discrimination. By using an electrical comparator circuit on the active indicator, a threshold can be set to respond only to detrimental impacts and ignore all low-energy events.

Other types of passive indicators include bubble dye wraps, pressure-sensitive films, deformable covers (e.g., metal honeycomb and polystyrene foam), and thin plexiglass or glass covers. The passive indicators should have the means for discriminating detrimental impacts from low-

NASA-HDBK-5010, VOLUME 2, REVISION A

energy events (tapping, touching, scuffing) that will not compromise the burst strength of the COPV.

ICP procedures for unpressurized COPVs using impact indicators should require access control and authorization by the jurisdictional authority to work within close proximity to the COPV. Caution signs should be displayed near the COPV to make personnel aware of the impact sensitivity. Inventoried and tethered tools should be required when this work is performed as a prudent means of avoiding impact situations that require disposition. Periodic QA surveillance should be performed to monitor the impact indicators.

Torque or leverage tool operations within close proximity to the COPV should be performed under procedural control with 100 percent QA surveillance.

Scuff-protective materials in the form of high-density Ensolite® foam used with an impact indicator should be used to reduce the potential for false impact indications. Periodic inspections by trained and certified NDE inspectors should be performed prior to the installation of the impact indicator device and after the removal of such materials. Any impact indicator device should be installed with protective high-density Ensolite® foam to preclude any scuff or abrasion marks that may have to be analyzed as suspected impact conditions.

Pressurization of a COPV from 0.1 x MDP to MDP or above should require authorization by the jurisdictional authority, and personnel access should be restricted. Hazard danger signs should be displayed near the COPV to warn personnel of impact sensitivity and the potential for catastrophic burst. In addition, any tool activity performed within proximity of the pressurized COPV should require mandatory use of impact protector devices.

ICP Implemented with Impact Protectors

Figure 7.4-7, Installation and System-level Procedure for Implementation of ICP with Impact Protectors, illustrates the impact protector ICP option that, if selected, should be implemented during the installation and system-level operations of the COPV mounted on the spacecraft hardware or the launch vehicle. Handling procedures for installation depend on the size of the COPV. For small cylindrical or spherical COPVs, manual handling should be accomplished using procedures that specify the use of gloves and foam pads to prevent scuffing of the composite overwrapped surface. For large COPVs, lifts and slings should be required to move the COPV. Prevention of COPV impact damage should be controlled procedurally when using lifts and slings.

NASA-HDBK-5010, VOLUME 2, REVISION A

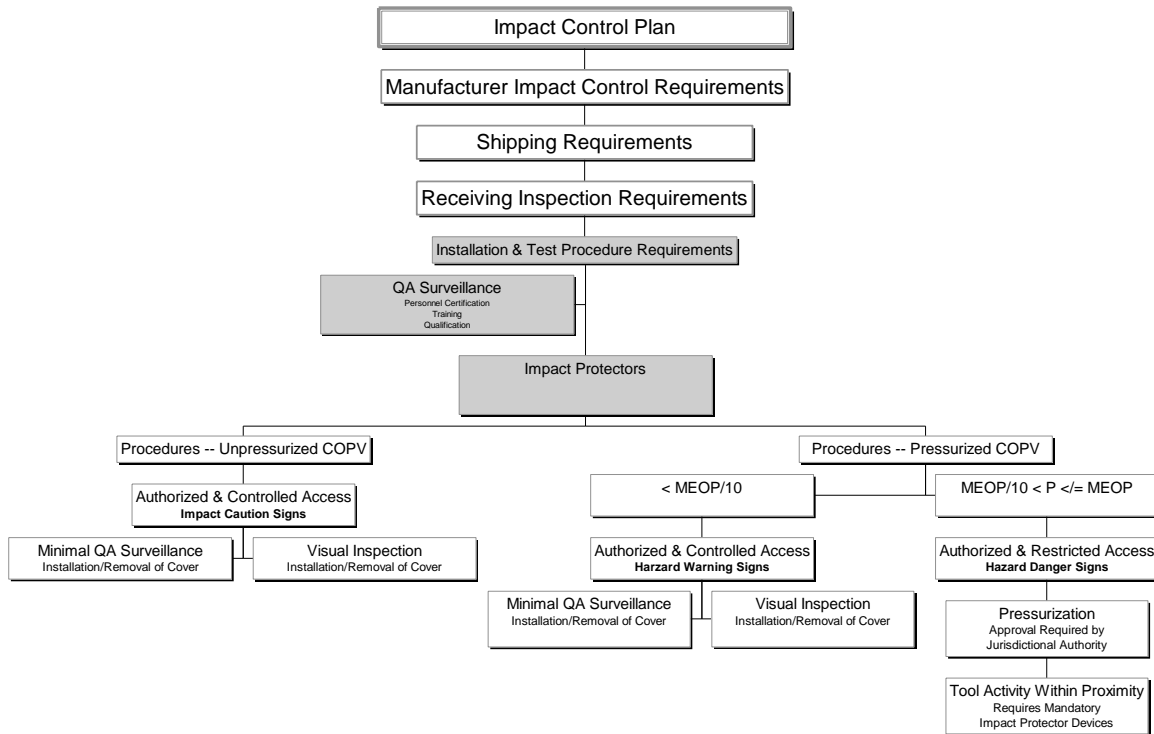


Figure 7.4-7—Installation and System-Level Procedure for Implementation of ICP with Impact Protectors

The following are considerations for design requirements for impact protectors and procedures for unpressurized and pressurized COPVs:

1. Design Requirements for Impact Protectors: Impact protectors should be capable of shielding a COPV from impact damage consistent with the threat environment or at least up to the load limits for the integral boss and mounting fixtures. An impact inflicting any damage that potentially degrades the burst strength of the COPV more than 5 percent from its nominal burst pressure is unacceptable.

The minimum design cross-section of an impact protector cover should include the shielding layers depicted in Figure 7.4-8, Cross-Section of COPV Impact Protector. The indentation damage from a credible impact should be completely absorbed by a hard shell fabricated from fiberglass/epoxy, Kevlar®/epoxy, or equivalent material sufficiently thick to absorb the indentation energy without penetration. The potential deflection damage should be mitigated by spreading the peak loading transmitted through the hard shell over an area consistent with the dimensions of the COPV. Deflection damage should be further mitigated by introducing an energy-absorbing material between the hard shell and the COPV. Aluminum mesh foam (20 pores/in, 0.5 in thick), manufactured by ERG Materials, Inc., is an example of energy-absorbing material that has been qualified for this application. Other materials with equivalent energy-absorbing properties can be qualified for this application. Finally, if an impact indicator is used in combination with the impact protector, it should be bonded to a thin (1/16-in thick) layer of interface material (e.g., fiberglass/epoxy composite or polymeric materials). The laminated

NASA-HDBK-5010, VOLUME 2, REVISION A

impact protective cover should be installed over a layer of high-density Ensolite® foam mounted directly on the COPV.

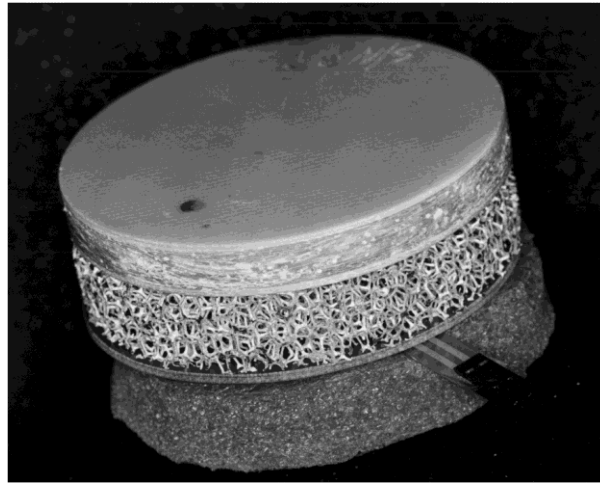


Figure 7.4-8—Cross-Section of COPV Impact Protector

The impact protector device should be qualified by testing on a representative qualification COPV to provide adequate protection up to a specified or credible impact condition (e.g., 35 ft-lb impact with a 0.5-in hemispherical tup or tool). The impact protector should then be labeled accordingly and controlled procedurally for impact protection within the specified limits. Periodic QA surveillance should be required to ensure that the impact protector is used in accordance with its specifications and that a damaged impact protector is not used for primary protection of a COPV. Any impact protector subjected to an impact that crushes or deforms the energy-absorbing material should be rejected for further use and discarded.

2. Procedures for Unpressurized COPVs: ICP procedures for unpressurized COPVs using impact protectors should require controlled access authorized by the jurisdictional authority to work within close proximity of the COPV. Caution signs should be displayed near the COPV to make personnel aware of the impact sensitivity and to utilize the impact protective covers. Periodic QA surveillance should be performed to monitor that the impact protectors are being used.

Impact protector devices should be installed with scuff-protective high-density Ensolite® foam to preclude any scuff or abrasion marks that may be mistakenly identified as a suspected impact discontinuity. Periodic inspections by trained and certified NDE inspectors should be performed prior to the installation of the impact protector device and after the removal of such materials.

3. Procedures for Pressurized COPVs: Access for working in close proximity to a COPV pressurized below MDP should be controlled and authorized by the jurisdictional authority. Hazard warning signs should be displayed near the COPV to warn personnel of the impact sensitivity and the potential burst hazard of the COPV.

APPROVED FOR PUBLIC RELEASE – DISTRIBUTION IS UNLIMITED

NASA-HDBK-5010, VOLUME 2, REVISION A

Scuff-protective materials in the form of high-density Ensolite® foam (either used directly as part of the impact protector or as additional scuff-protection measures) should be used to reduce the potential for false impact indications. Periodic inspections by trained and certified NDE inspectors should be performed prior to installation of scuff-protective materials and after removal thereof.

Pressurization of a COPV from $0.1 \times \text{MDP}$ to MDP or above should require authorization by the jurisdictional authority, and personnel access should be restricted. Hazard danger signs should be displayed near the COPV to warn personnel of impact sensitivity and the potential for catastrophic burst. In addition, any tool activity performed within proximity of the pressurized COPV should require mandatory use of impact protector devices.

7.4.3 Residual Threat Determination

In the following bonded joint example, the application of residual threat determination requirements is illustrated. The objective of the RTD is to identify flaws or damage conditions that are not screened by a combination of inspection, protection, and detection strategies. Access limitations are one reason why it may not be possible to implement an inspection in certain regions of the structure. The example consists of a bonded composite joint with an obstruction that does not permit inspection of a certain zone of the bonded joint (reference Goyal and Lundgren [2015]). The bonded joint consists of two sandwich structures that are joined by an internal prefabricated insert and external doublers; refer to Figure 7.4-9, Bonded Joint under Consideration.

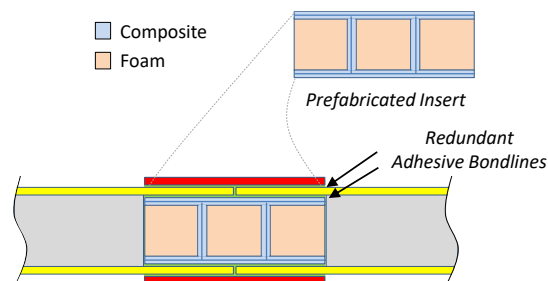


Figure 7.4-9—Bonded Joint under Consideration

The damage threat assessment and impact damage protection plan were developed. Second, various NDE techniques were evaluated through extensive studies to understand the limitations but also to select the most appropriate technique for inspecting flight hardware, shown in Figure 7.4-9. The ultrasound technique was selected as the primary inspection technique and, through many studies, the damage detection levels by nondestructive inspections were able to produce a similar level of reliability as expected from metallic fracture critical parts, which is to find a flaw with 90% probability and 95% confidence.

APPROVED FOR PUBLIC RELEASE – DISTRIBUTION IS UNLIMITED

NASA-HDBK-5010, VOLUME 2, REVISION A

After considering all applicable flaw detection and mitigation strategies implemented for the flight hardware, there was still potential for flaws that could lead to structural failure. Two types of flaws were identified for this structure: (1) A worst-case credible flaw was assumed in a region of no inspections due to access limitations (see Figure 7.4-10, Material Obstructs the Ability to Perform NDE on a Composite Joint), and (2) A worst-case credible flaw equal to the minimum detectable flaw size. The worst-case flaws were located between the external doubler and the composite sandwich structure. The size was defined by the area of no inspection. A second worst-case flaw was assumed at the edge of the external doubler and the composite sandwich structure, but this time the size was defined by the limits of the inspection capability of the NDE.

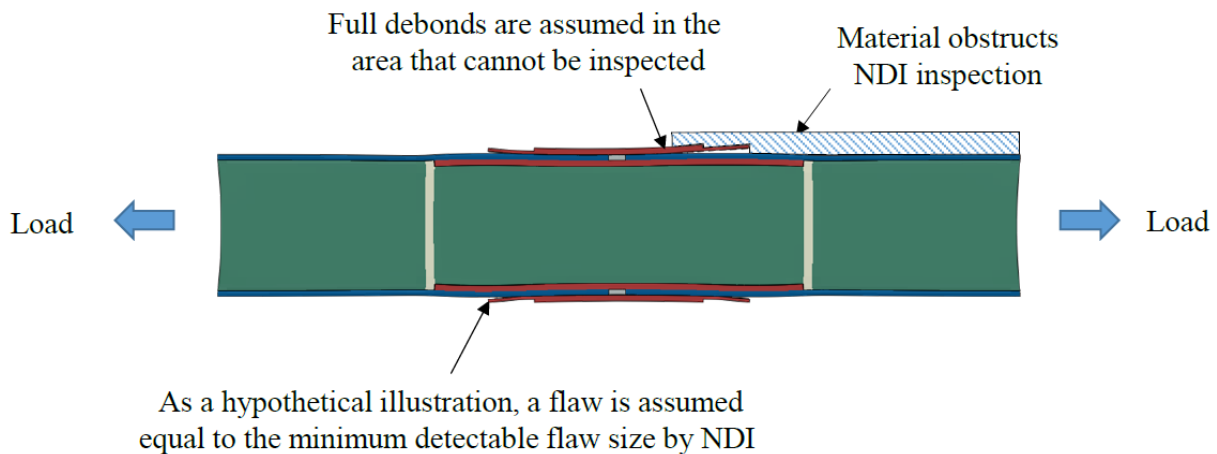


Figure 7.4-10—Material Obstructs the Ability to Perform NDE on a Composite Joint

In this bonded joint application, all possible worst-case credible damage conditions were considered except the threats mitigated by NDE evaluations and the IDMP. These worst-case flaws need to be defined as part of the RTD and the structure needs to be demonstrated to be robust to these flaws by performing damage tolerance testing.

Table 7.4-3, Evaluation of Various NDE Techniques for the Bonded Joint Application in Figure 7.4-9, provides evaluation of various NDE techniques.

NASA-HDBK-5010, VOLUME 2, REVISION A

Table 7.4-3— Evaluation of Various NDE Techniques for the Bonded Joint Application in Figure 7.4-9

NDE Technique	Coverage	Penetration	Suitable for the bonded joint in Figure 7.4-9
Ultrasound	Point-to-point	Volume	Y
Acoustic emission	Entire part	Volume	Monitoring Crack Growth
Eddy current	Point-to-point	Variable	Not for Debonds
Microwave	Point-to-point	Volume	N
X-Ray	Full-field	Volume	Tangential inspections
Thermography	Full-field	Variable	Y

7.4.4 Loading Spectra

See section 11 in this Handbook.

7.4.5 Damage Tolerance Tests of Coupons

A bonded joint system with a cross section like that shown in Figure 7.4-9 had to be demonstrated to be tolerant to worst-case credible flaws for a single-use application. A subscale coupon test geometry was designed with the intent of performing damage tolerance tests by replicating the modes of failure expected in the flight. The coupons were fabricated using flight hardware materials, manufacturing methods, and layups. The flaws inserted in the coupons were representative of the worst-case flaws as determined by the RTD. The tension limit load from the flight model was extracted, and it was calculated to be 6,200 lbs. A tension load was applied to the bonded joint coupon of the configuration shown in Figure 7.4-9. Twelve (12) coupons environmentally conditioned to flight conditions were tested in tension and were judged to be a quantity sufficient to establish high confidence that the design can tolerate worse-case flaws. Testing of all twelve coupons with the embedded flaws demonstrated no flaw growth up to a tension load of 9,600 lbs, which represents a significant margin above the limit loads expected for the structure.

For bonded joint systems such as this one, the flight hardware should undergo an inspection prior to proof test, a proof test, and a post-proof inspection to gain confidence in the workmanship of the build that no critical flaws exist and that any flaws remained stable during the proof test.

APPROVED FOR PUBLIC RELEASE – DISTRIBUTION IS UNLIMITED

NASA-HDBK-5010, VOLUME 2, REVISION A

7.4.6 Damage Tolerance Tests of Hardware Elements

Damage tolerance tests of full-scale flight hardware can be significantly expensive, so it is often preferred to demonstrate damage tolerance on subscale tests. In this example, an illustration is provided how the requirements can be applied to a hardware element rather than the full-scale structure.

A bonded joint system with a cross section like that shown in Figure 7.4-9 had to be demonstrated to be tolerant to worst-case credible flaws for a reuse application up to 100 flights. A subscale coupon test geometry was designed with the intent of performing damage tolerance tests by replicating the modes of failure expected in the flight. The coupons were fabricated using flight hardware materials, manufacturing methods, and layups. The flaws inserted in the coupons were representative of the worst-case flaws as determined by the RTD. The tension limit load from the flight model was extracted, and it was calculated to be 6,200 lbs. A twelve (12) coupons environmentally conditioned to flight conditions were tested in tension and was judged to be a quantity sufficient to establish high confidence that the design can tolerate worse-case flaws.

In this instance, damage tolerance tests to be performed at the subcomponent level were representative of the flight designs and have the properly induced RTD determined flaws. Both residual strength and life-based testing were performed as follows:

1. An NDE of all the coupons was performed before the test to verify that the RTD flaws were properly imposed.
2. Tests were performed at worse-case flight temperatures and moisture conditions so no additional ECF was applied.
3. The coupons were subjected to 1 times the service life based on the load spectra definition. In this instance 100 cycles of tension loads were applied to the joint at 6,200 lbs. The coupons were then subjected to 1.4 times the DLL.
4. The test hardware was then subjected to a minimum of 4 service lives of spectrum loading with a LEF to establish B-basis reliability. The LEF was calculated using the following equation (reference MIL-HDBK-17F and DOT/FAA/CT-86/39, Report No. NADC-87042-60):

$$\text{LEF} = \frac{\left[\Gamma\left(1 + \frac{1}{\alpha_L}\right) \right]^{\alpha_L/\alpha_R}}{\left[\frac{-\ln(\ell)N^{\alpha_L}}{\chi_{\gamma}^2(2n)/2n} \right]^{1/\alpha_R}},$$

(Equation 7.2-12)

where:

APPROVED FOR PUBLIC RELEASE – DISTRIBUTION IS UNLIMITED

NASA-HDBK-5010, VOLUME 2, REVISION A

α_L = Weibull shape parameter of the fatigue life distribution (typical value = 1.25 for composites),
 α_R = Weibull shape parameter of the residual strength distribution (typical value = 20 for composites),
 ℓ = reliability required, 0.9 for B basis, 0.99 for A basis,
 γ = confidence level, 0.95 for both A and B basis,
 N = test duration in lifetimes,
 n = sample size, i.e., the number of test articles tested,
 Γ = the gamma function, and
 $\chi^2(2n)$ = chi-squared function with $2n$ degrees of freedom at a probability of γ .

For composites, the typical values are as follows: $\alpha_L = 1.25$, $\alpha_R = 20$. The B-basis reliability is the target used in the calculation, so the value is 0.9. The test duration in lifetimes is usually selected as 4. Based on this information, the LEF can be calculated as a function of sample size and it produces Table 7.4-4, Load Enhancement Factor as a Function of Sample Size Based on the Following Assumptions: $\alpha_L = 1.25$, $\alpha_R = 20$, $\ell = 0.9$, $\gamma = 0.95$:

Table 7.4-4—Load Enhancement Factor as a Function of Sample Size Based on the Following Assumptions: $\alpha_L = 1.25$, $\alpha_R = 20$, $\ell = 0.9$, $\gamma = 0.95$

Sample Size, n	Load Enhancement Factor, LEF
1	1.21
2	1.20
5	1.18
10	1.17
15	1.17
30	1.16

It is noted that the value of LEF varies from 1.15 to 1.21 and that there is no significant influence on LEF based on the sample size. In this case, the sample size was 12; so an LEF used was 1.17. Visual inspection of the coupons after completion of the test did not reveal any damage due to the life-cycle test.

5. The coupons were subsequently subjected to 1 design limit load cycle with no evidence of damage. NDE was used to establish that the coupons were not damaged due to the cyclic tests.

7.4.7 Strength and Life Assessments

Sections 7.4.6 and 7.4.8 in this Handbook highlight the application of the requirements in this section.

NASA-HDBK-5010, VOLUME 2, REVISION A

7.4.8 Damage Tolerance Tests Full-Scale Flight-Like Hardware

Damage tolerance tests of full-scale flight hardware can be significantly expensive, so it is often preferred to demonstrate damage tolerance on subscale tests. In this example, an illustration is provided on how damage tolerance requirements are applied to a large cylindrical composite sandwich structure.

First, a comprehensive RTD assessment was performed on the cylindrical composite sandwich structure. The minimum detectable flaw sizes were determined for all the regions of the cylinder. Certain regions of the aft joint were not inspectable, so a worst-credible flaw was assumed to exist in this joint. The DTA, IDMP, and RTD revealed that there is one operation during assembly that could expose the composite sandwich structure to a tool drop in the acreage region at a 275-degree azimuth.

Based on this assessment, a flight-like cylindrical structure was manufactured with worst-case flaws near door cutouts, the acreage region, the aft joint, and forward joints of the cylindrical structure based on the comprehensive RTD assessment. After manufacturing, damage was induced to the composite in the region where tool drop could occur.

An NDE on test hardware was performed before the test to verify that the RTD flaws have been imposed. NDE revealed an additional manufacturing flaw associated with a backing paper that was left behind. Corrective action was taken to update the manufacturing planning to avoid this issue in the future.

All relevant load cases were identified, and it was determined that a compression load case could introduce the worst-case stresses to all the regions of the structure. A flight-to-test margin comparison was performed that demonstrated that the test margins were lower than flight. Because the test was performed at room temperature, an ECF was applied to the test load. The ECF was determined based on the most critical failure mode under consideration, which was delamination. The ECF was calculated as 1.2, and it was based on the ratio of the Mode I fracture toughness at room temperature to the Mode I fracture toughness at the highest flight temperature of 200 degrees F.

Prior to initiation of the test campaign, the load spectra was determined and further simplified conservatively so that compression loading could be the only load applied. The following tests were performed in sequence:

1. Thirty percent of the design compression limit load was applied to the structure to verify proper load introduction, to verify strain-gauge measurements compared to analysis, and to verify stiffness.
2. The cylindrical composite structure was subsequently subjected to 1 times the service life based on the load spectra definition.

NASA-HDBK-5010, VOLUME 2, REVISION A

3. Following the test, the cylindrical composite structure was subjected to 1.4 times the DLL. After the test, visual inspections were performed to ensure that the ultimate load capability did not cause any damage to the structure. One suspect region in the aft joint was inspected using NDE, but there were no findings.

4. The test hardware was then subjected to a minimum of 4 service lives of spectrum loading with an LEF to establish B-basis reliability. The LEF was calculated as explained in section 7.4.6 of this Handbook. In this case, the sample size was 1; so the load enhancement factor applied was 1.25 for simplicity. While more than 4 lifetimes of testing may be performed to reduce the LEF, that was not the method selected. Visual inspection of the test hardware after completion of the test did not reveal any damage due to the life-cycle test.

5. The hardware was subsequently subjected to 1 design limit load cycle with no evidence of damage. NDE was used to establish that the test hardware did not experience structural failures and could perform its design function.

7.4.9 Evaluate Flaws or Damage that Occurs during Building Block Approach (BBA) Testing

BBA is intended to increase confidence in the design evaluation as the design matures and testing of higher-level assemblies progresses. Unexpected flaws or damage, significant or unusual flaw growth, and any new failure modes observed during the BBA test program should be addressed.

For example, a bonded bracket on a spacecraft was classified fracture critical. BBA testing of the bonded bracket prior to stepping to full-scale damage tolerance testing demonstrated issues where the load at failure was significantly lower than expected. After an extensive investigation, it was found that incorrect surface treatment prior to applying the bond had caused a reduction in bondline strength. After corrective action was implemented, the bondline strength was as expected, and the BBA test program continued as expected.

7.5 Optional Approaches for Fracture Critical Parts

The purpose of section 7.5 is to offer alternatives to meet fracture critical part requirements. Examples are provided for the elements in NASA-STD-5019A, FCR 14.

7.5.1 Single-Event Fracture Critical Components

A fracture critical sandwich composite cylinder, part of a spacecraft, will be subject to single event load event. Coupled Loads Analysis demonstrated that the composite cylinder is subject to one main load event during boost phase, and there are no other cyclic loading conditions. Verifying a life factor of 4.0 to demonstrate damage tolerance is not applicable because the failure mode is driven by the single dominating load event and not fatigue. Sections 7.5.1a and 7.5.1b are satisfied. A small deviation against 7.5.1d needs evaluation by RFCB as this is not a metallic component and it was composite component. The following steps were followed:

APPROVED FOR PUBLIC RELEASE – DISTRIBUTION IS UNLIMITED

NASA-HDBK-5010, VOLUME 2, REVISION A

1. Define the rejectable/acceptable flaw size that will be utilized in the composite drawing, considering all potential locations of the defect within the thickness of the sandwich structure.
2. Identify the nature of the dominant load condition and design subscale tests with all credible flaws and apply a load factor of 1.4 to demonstrate stability of the flaw. An uncertainty factor should be applied to the flaw size, as introducing flaws can result in different flaw sizes due to potential unintended bonding surrounding the flaw perimeter.
3. Process controls were implemented to ensure the flight hardware is represented by tests conducted on identical samples

The part was demonstrated to satisfy damage tolerance requirements for the single load event via the test approach.

7.5.2 High-Cycle Fatigue (HCF) Components

Typical components subject to HCF are rotary machinery such as turbine blades, rotors, impellers, and other high-speed elements that are subject to local modes of high-frequency vibration and large numbers of loading cycles. Impeller analysis is usually of less certainty than the turbine wheel analysis. For this hypothetical example, the fatigue crack growth threshold was set based on the material used. An initial NDE flaw size was determined for the impeller, and it was located at the root of the blade. A flaw was simulated in the analytical model; and the final flaw size was calculated based on the loading spectra which was a combination of oscillating pressure, thermal gradient fluctuations, and with superimposed centrifugal forces after four lifetimes.

A safe life analysis on a fracture critical impeller is performed for an engine pump. An initial flaw forms during acceptance ground testing from starts and stops induced by thermal loading caused the initiation of the flaw. Once the flaw forms, the stress relieves, and the stress state is such that LEFM applies. The flaw could propagate during steady-state operation. It is also assumed that the impeller is made with Inconel® 718 and flaws are screened with dye penetrant.

The impeller in this example is acceptable if the flaw that exists after acceptance test loading does not grow during operational loading, as per NASA-STD-5019A, section 7.5.2. To verify this, the initial NDE flaw in the worst location and orientation should be propagated with the larger start and stop loads for 4 times the required design life. Using the final flaw size from the analysis, the stress intensity factor range from the operational loads should be calculated. If the HCF stress intensity factor range during operational loads is below the RFCB approved stress intensity factor threshold, the flaw will not grow under operational loads and the impeller is acceptable.

First, the initial flaw must be established. In this example, flaws are screened with dye penetrant NDE. The minimum detectable flaw is used in NASGRO® for the initial life analysis. A finite element model (FEM) should be used to determine the loads and worst-case flaw orientations. In

NASA-HDBK-5010, VOLUME 2, REVISION A

this example, a FEM was used to determine the mean stress state during operation as well as alternating stress states due to dynamic effects such as pump pressure oscillations. The impeller geometry is an open source design. The stress distribution for a simplified static mean pressure loading is shown in Figure 7.5-1, Stress Distribution and Critical Crack Orientation of the Impeller. The maximum principal tensile stress of 20.7 ksi occurs at the root of the leading edge. This stress state is driven by the rotational centrifugal load and uniform pressure load on the blade surfaces. A crack perpendicular to the maximum principal stress is chosen for the critical crack orientation.

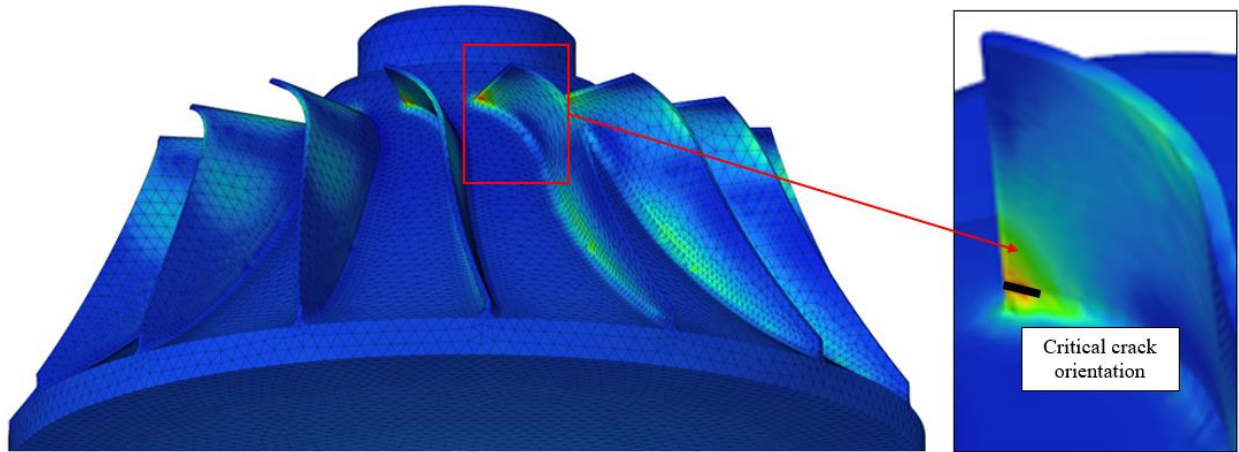


Figure 7.5-1— Stress Distribution and Critical Crack Orientation of the Impeller

The high stress location is on the leading edge of the blade at the impeller inlet, so a through crack at the edge is the critical flaw orientation. This is shown in Figure 7.5-1. This is represented by the TC12 geometry in NASGRO®. The driving stress and direction of crack propagation is more clearly shown in Figure 7.5-2, Stress Distribution at the Critical Crack Orientation. The driving stress acts in a radial direction due to the rotation of the impeller. This drives a crack parallel to the base of the impeller blade.

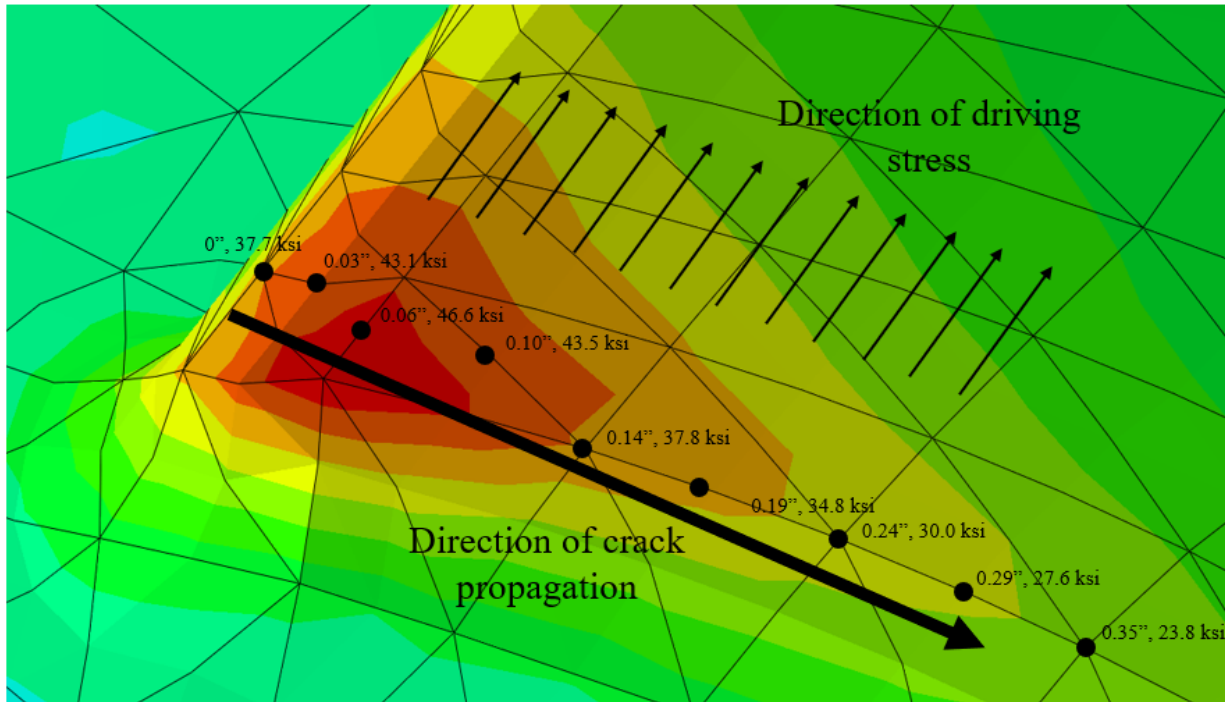


Figure 7.5-2—Stress Distribution at the Critical Crack Orientation

(The node label and stress (psi) are called out for each node along the path of the crack.)
 (Reference *Liquid Rocket Engine Turbopump Inducers*, NASA Space Vehicle Design Criteria (Chemical Propulsion), NASA SP-8052, 1971)

The geometry input for TC12 is shown in Figure 7.5-3, Geometry Input for a Through Crack at the Edge of a Plate. A large width is chosen because there is no free edge opposite the crack. The “NASA std NDE” radio button is chosen to use dye penetrant NDE initial flaws from NASA-STD-5009. The FEM results in Figure 7.5-2 show that the stress drops off away from the edge, so the “User input” option is selected to define the normalized tensile stress, S_0 , as a function of the normalized distance, x , from the edge. Note that the stress values are obtained from the FEM without a crack.

NASA-HDBK-5010, VOLUME 2, REVISION A

TC12

$0 \leq \frac{c}{W} \leq 0.9$

$X = \frac{x}{W}$

$i = 0, 1, 2, 3$

$0.0 \leq X \leq 1.0$

Width, W	2	Initial flaw option <input type="radio"/> User entry <input checked="" type="radio"/> NASA std NDE
Thickness, t	0.075	
Initial flaw size, c	0.150000	

NDE type: Dye penetrant

Set crack size limit(s):

SIF Compounding

Specify secondary cyclic stresses in FAD analysis

Crack plane stress definition from
 Tension/bend Polynomial User input

of stress distributions: 1 2 3 4

Shakedown choice: None Automatic Full cyclic

Optimize point spacing Include residual stress

Input stresses from file Plot stresses

Display stress quantity:
 S0 S1 S2 S3 RS Tens/Comp stress gradients
 t1/2 stress gradients

X	S0 stress
0	0.81
0.015	0.92
0.03	1.00
0.05	0.93
0.07	0.81
0.095	0.75
0.12	0.64

Figure 7.5-3—Geometry Input for a Through Crack at the Edge of a Plate

The values obtained are outlined in Table 7.5-1, Stress Distribution from the FEM and the Corresponding Normalized NASGRO® Input. The distance from the edge is normalized by the maximum width specified in the TC12 input, which is 2 inches. The stress is normalized by the peak value seen, which is 20.7 ksi. During the analysis, the normalized stress values are multiplied by the inputs in the load blocks in the analysis.

NASA-HDBK-5010, VOLUME 2, REVISION A

Table 7.5-1—Stress Distribution from the FEM and the Corresponding Normalized NASGRO® Input

(Reference Blach, Harry., *Turbo Charger Impeller*, GrabCAD, 2020,
<https://grabcad.com/library/turbo-charger-impeller-2>)

Obtained from FEM		Input into NASGRO®	
Distance from edge (inch)	Stress normal to crack (ksi)	Normalized distance, x	Normalized stress, S_0
0	16.7	0	0.81
0.03	19.1	0.015	0.92
0.06	20.7	0.03	1.00
0.1	19.3	0.05	0.93
0.14	16.8	0.07	0.81
0.19	15.5	0.095	0.75
0.24	13.3	0.12	0.64
0.29	12.3	0.145	0.59
0.35	10.6	0.175	0.51
0.4	8.3	0.2	0.40
2	8.3	1	0.40

Next, the relevant material properties for Inconel® 718 are assigned in the “Material” tab. These should be representative of the behavior at the operating temperature of the impeller. Note that it is NASA policy to change B_k to zero, or to a value such that the maximum stress intensity factor is less than or equal to the critical stress intensity factor with RFCB approval. Since B_k scales down K_{Ic} when is nonzero, this policy ensures that results for a through-crack are conservative with respect to unstable crack growth in Region III of the Paris Law.

After assigning the material, the start and top load cycles must be defined in the “Load Blocks” tab and consider the starts and stops during ground testing and the initial start for flight. For this example, assume that the impeller undergoes 25 start and stop cycles before operational loading. The stress normal to the crack goes from 0 ksi to 20.7 ksi during these cycles. The minimum stress is 0 ksi because a portion of the load is driven by rotation, which can only induce a tensile load normal to the crack. These loads are input into NASFLA as shown in Figure 7.5-4, Load Blocks Input, with a factor of 4.0 applied to the number of cycles.

NASA-HDBK-5010, VOLUME 2, REVISION A

Block Case Definition: block 1 of 1
Enter the number of cycles and values for all stress quantities:

	Keac chk?	Cycles	S0 at t1	S0 at t2			
Step 1	<input type="checkbox"/>	100	0	20.7			
2	<input type="checkbox"/>						
3	<input type="checkbox"/>						
4	<input type="checkbox"/>						
5	<input type="checkbox"/>						
6	<input type="checkbox"/>						

Stress scale factor on stress quantity: S0 1

Figure 7.5-4—Load Blocks Input

With the input fully defined, the analysis can now be run. The output for this example is shown in Figure 7.5-5, Output of 4 × Life Analysis of Low-Cycle Loading. The critical crack size was not reached during the impeller start and stop loads. The crack had little growth during the application of 4x the start and stop loads, with the final calculated crack size of 0.150 inch.

ANALYSIS RESULTS

```
FINAL RESULTS:
Critical Crack Size has NOT been reached.
# at Cycle No.          100
# of Load Step No.     1
# of Block No.         1
# of Schedule No.      1
# Crack Size c =       0.150060
# Total Cycles =       100
```

Figure 7.5-5—Output of 4 × Life Analysis of Low-Cycle Loading

Now, it must be demonstrated that the operational loads do not lead to propagation of the crack after the start and stop loads. The crack will not propagate if the stress intensity factor range is below the RFCB approved stress intensity factor threshold.

The NASSIF module in NASGRO® can be used to calculate the stress intensity factor at the maximum and minimum stress states. Note that NASFLA can also be used to check for an exceedance of crack growth threshold during operational loads, but special care should be taken to ensure that the threshold is properly calculated by NASGRO® in the analysis.

As previously discussed, the mean stress is 20.7 ksi. During operation, the impeller experiences an additional 4.1 ksi alternating stress from a 20% pressure load oscillation (see Figure 7.5-2).

NASA-HDBK-5010, VOLUME 2, REVISION A

During operation, the stress normal to the crack oscillates between maximum values of 16.6 ksi and 24.8 ksi.

The NASSIF geometry input matches the input previously used in NASFLA, as shown in Figure 7.5-6, NASSIF Geometry Input for Through Crack at the Edge of a Plate. In the “Output Options” tab, the material yield stress, the applied stress S_0 , and the crack size c are entered. These are shown in Figure 7.5-7, Output Options for NASSIF. After defining the inputs, the analysis can be run. The outputs for the minimum and maximum stress intensity factor cases are shown in Figure 7.5-8, Results of NASSIF for the Minimum (Left) and Maximum (Right) Stress Intensity Factors.

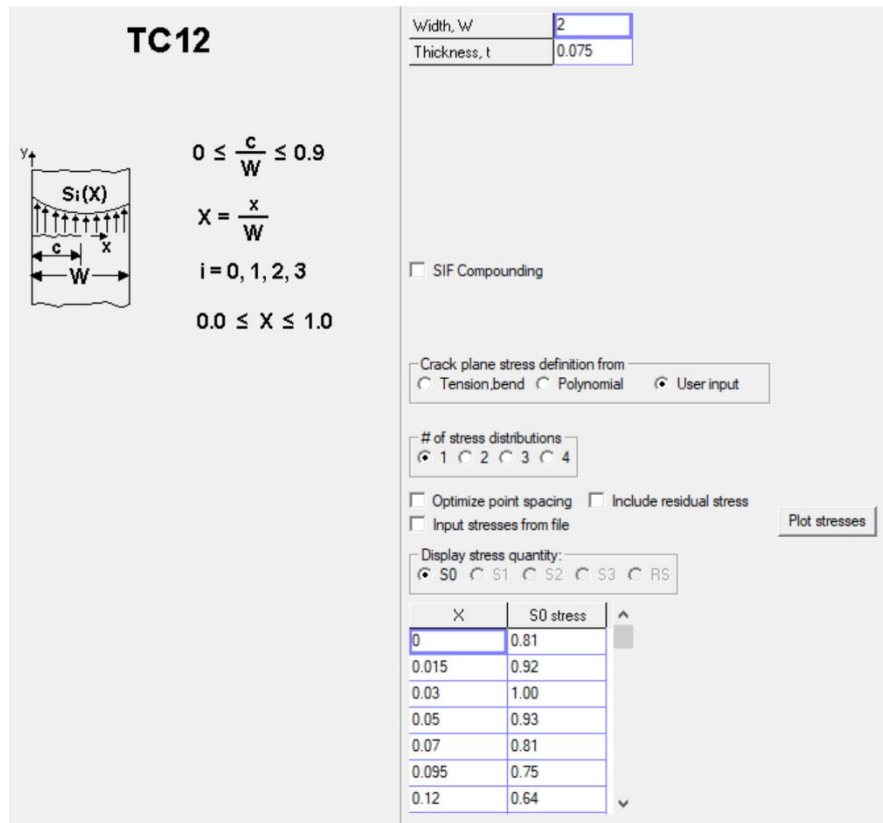


Figure 7.5-6—NASSIF Geometry Input for Through Crack at the Edge of a Plate

NASA-HDBK-5010, VOLUME 2, REVISION A

The screenshot shows the NASSIF software interface with the following elements:

- Problem title [optional]:** An empty text input field.
- Problem description [optional]:** A large empty text area with a scroll bar.
- Select which to compute:** Two radio buttons: Stress Intensity Factors and Correction Factors.
- Material yield stress:** Two input fields. The first is labeled "Material yield stress" and contains the value "67". The second is labeled "S0" and contains the value "16.6".
- Select output format:** Two radio buttons: Tabulate solutions and Plot solutions.
- Flaw Sizes, c [max = 2000 comma- or space-delimited entries in table]:** A large text area containing the value "0.150060".
- Auto-fill c:** A button located to the right of the Flaw Sizes input area.

Figure 7.5-7—Output Options for NASSIF

<p>S0: tress Distribution #1 S0 = 16.60</p> <p>Material Yield Stress = 67.00</p> <p style="text-align: center;">STRESS INTENSITY FACTORS AND NET SECTION STRESS</p> <p style="text-align: center;">-----</p> <table border="1" style="width: 100%; border-collapse: collapse; text-align: center;"> <thead> <tr> <th style="width: 12.5%;">c</th> <th style="width: 12.5%;">K</th> <th style="width: 12.5%;">Sn</th> <th style="width: 12.5%;">Sn/Sy</th> </tr> </thead> <tbody> <tr> <td>0.1501</td> <td>11.995</td> <td>9.773</td> <td>0.146</td> </tr> </tbody> </table>	c	K	Sn	Sn/Sy	0.1501	11.995	9.773	0.146	<p>S0: tress Distribution #1 S0 = 24.80</p> <p>Material Yield Stress = 67.00</p> <p style="text-align: center;">STRESS INTENSITY FACTORS AND NET SECTION STRESS</p> <p style="text-align: center;">-----</p> <table border="1" style="width: 100%; border-collapse: collapse; text-align: center;"> <thead> <tr> <th style="width: 12.5%;">c</th> <th style="width: 12.5%;">K</th> <th style="width: 12.5%;">Sn</th> <th style="width: 12.5%;">Sn/Sy</th> </tr> </thead> <tbody> <tr> <td>0.1501</td> <td>17.920</td> <td>14.600</td> <td>0.218</td> </tr> </tbody> </table>	c	K	Sn	Sn/Sy	0.1501	17.920	14.600	0.218
c	K	Sn	Sn/Sy														
0.1501	11.995	9.773	0.146														
c	K	Sn	Sn/Sy														
0.1501	17.920	14.600	0.218														

Figure 7.5-8—Results of NASSIF for the Minimum (Left) and Maximum (Right) Stress Intensity Factors

The results indicate that during operational, the crack undergoes a minimum and maximum stress intensity factor of 12.0 and 17.9 ksi sqrt(in), respectively. This corresponds to a stress intensity factor range of 5.9 ksi sqrt(in). For this particular material and loading environment, the stress intensity factor threshold (ΔK_{th}) is 6.46 ksi sqrt(in).

NASA-HDBK-5010, VOLUME 2, REVISION A

The stress intensity factor for the impeller example is below the threshold value, so the crack does not propagate during operational loading. With this analysis, the fracture critical impeller meets the requirements of NASA-STD-5019A, section 7.5.2, for HCF fracture critical components.

7.5.3 Proof Test Approach for Composite or Bonded Hardware

Example: A component is bonded to the wall of the structure. An ultimate strength test on a dedicated hardware unit that will not be flown was performed to establish a 1.5 greater capability on limit load, thus providing margin against potential for damage during proof test, which is conducted on a 1.2x limit load.

An ambient proof test load of 1.2x limit load is applied to the component to verify for workmanship, and an additional environmental load correction factor is applied to account for the 12% strength reduction found through bondline testing at ambient versus at the maximum bondline temperature in flight of 120 °F. Pre-proof inspection found a flaw; and during post-proof inspection, the flaw was found to be slightly larger. A repair was performed by reinforcing the through-the-thickness direction with a pre-loaded fastener. The proof test was repeated, and the flaw did not grow based on post-proof examination. While a full DTA is not required, it was performed. It was concluded that no additional threats after proof test would be a detriment to the hardware. An IDMP was constructed regardless to prevent any detrimental contact events (e.g., impact) on the bonded component. Since no remaining residual threats were determined to be present, the hardware was acceptable for one flight. Since the hardware needs to be reflown, all the proof test activities were repeated prior to the next flight.

7.5.4 Fleet Leader Testing

The Fleet Leader Testing classification is typically applied for highly complicated problems where damage tolerance predictions are low confidence and the use of fracture analysis, discrete fracture test, or increased proof test levels may not be able to provide evidence that the hardware is sufficiently robust against flaws. As discussed in section 7.2.7 of this Handbook, the turbine wheel components and other rotating components of an engine are usually vetted through full-scale engine testing at worse-case operational conditions (e.g., mixture ratio, power-level bin).

Example #1: Human-rated applications designs are verified to ensure cracks do not initiate during the service life due to uncertainty in the crack growth behavior. When a crack was discovered on rotating hardware, the life was set by the last crack-free inspection.

For nonhuman-rated application, the approach outlined has been utilized in the assessment of turbine wheels. An example application for a fleet leader test is demonstrated for an engine turbine wheel. Frequently, turbine wheel blades experience flaws from either manufacturing issues or from operation. Here is an example step-by-step process explaining the general approach on how a fleet leader test may look like:

NASA-HDBK-5010, VOLUME 2, REVISION A

1. Types of flaws that were found during manufacturing or during the engine test program were fully characterized.
2. Root-cause investigation identified the nature and cause of the flaws.
3. Defined the service life of the engine to include acceptance tests and flight duration, starts, and stops.
4. Inspections during the engine test program characterized flaws as a function of duration and starts/stops.
5. Selected the engine with the worse-case flaws at 2 times the service life, then established an engine test program to exercise the flaws such that the environments are bounding to expected operation.
6. Performed extended duration and starts/stops testing.
7. Performed periodic inspections during extended duration testing.
8. Measured flaws as a function of duration and starts/stops to assess stability of flaw growth.
9. Assessed data and determined fleet leader testing sufficiently demonstrated damage tolerance of the engine against flaws.
10. Established reject/accept flaw acceptance criteria based on test/inspection results.

Typically for human-rated applications, the fleet leader approach is utilized to prevent the initiation of cracks because of the uncertainty in the crack growth rates and impact to the mission.

Example #2: Thermal protection systems (TPS) experience challenging environments and are usually constructed of materials that exhibit high variability and can make it very difficult to assess damage tolerance. TPS are used in the rocket nozzles, on the exterior of launch vehicles, and on heatshields. In these instances, accumulated flights can be used to establish confidence in the hardware relative to damage tolerance. An approach that has been adopted is to develop an acceptance criterion tied to manufactured flaws into the TPS, fly the worse-case trajectories relative to thermal and mechanical loads, and then inspect the flaws post-recovery. The flight unit that has been reflown several times becomes the fleet leader for the design that will be flown. Ideally, the fleet leader has experienced flights that are four times the service life of the vehicle that will be flown.

NASA-HDBK-5010, VOLUME 2, REVISION A

7.5.5 Hazardous Fluid Containers for Payloads and Experiments

A checklist is provided in Table 7.5-2, Hazardous Fluid Containers for Payloads and Experiments Checklist, for hazardous fluid containers on payloads and experiments to assist the engineer in the evaluation.

Table 7.5-2—Hazardous Fluid Containers for Payloads and Experiments Checklist
(All requirements must be met.)

Item	Requirement	Meet (Y or N)
1	The container is limited to an MDP of 152 kPa (22 psi, 1.5 atm) and a maximum volume of 0.05 m ³ (1.76 ft ³).	
2	Analysis shows positive margin against burst with a factor of 2.5 on MDP.	
3	Performed proof test to 1.5 MDP.	
4	Verified that no damage or detrimental deformation exists after the proof test.	
5	Establish damage tolerance against rupture and leak by satisfying sections 8 and 9, section 7.3 for metallic parts, section 7.4 for composite or bonded parts in NASA-STD-5019A, and by test or analysis as approved by the RFCB for other materials.	
6	In addition to section 8 requirements in NASA-STD-5019A, perform an NDE inspection of all fusion joints in the container after proof test to determine acceptable conditions both on the surface and within the fusion joint.	
7	Performed a leak test to 1.0 times the MDP.	

In instances where NDE is not feasible, the manufacturer may employ a process-control program that assures the quality of the uninspectable welds and obtain approval of the RFCB. Proof tests are usually performed in the operational environment, or the test levels are adjusted via an ECF. Inertial load effects (including attach points) may necessitate additional assessments beyond the items in this category.

Note that each NASA Center or program may have alternate approaches to satisfy this requirement. An alternate approach is provided in JSC 25863C, section 6.2.2, for hazardous fluid containers: “A container that has a pressure less than 22 psia (151.7 kPa), a minimum factor of 2.5 times MDP on burst pressure, and is proof tested to a minimum proof factor of 1.5 X MDP can be classified nonfracture critical.”

8. FLAW SCREENING, TRACEABILITY, AND MATERIAL SELECTION

This section is reserved.

APPROVED FOR PUBLIC RELEASE – DISTRIBUTION IS UNLIMITED

NASA-HDBK-5010, VOLUME 2, REVISION A

8.1 Flaw Screening

The purpose of this section of the Handbook is to ensure the responsible design engineers and analysts recognize the interconnectedness of fracture critical classifications and the role that NDE plays in the assessments of fracture critical hardware. A fracture assessment cannot even begin without mutual involvement from NDE experts and a baseline understanding of the inspection techniques eligible to the parts in question. NASA-STD-5009B was developed to establish NDE requirements for metallic hardware where fracture control is a requirement (NASA-STD-5019 A, [FCR 16] and [FCR 17]). NASA-STD-5009B requires an NDE Plan which allows for proper planning, especially for complex engineering systems.

Parts classified as Fracture Critical must undergo testing or analysis with the associated initial flaw sizes based on the NDE technique used to inspect the parts after production. Because part durability and structural life are directly affected by the quality and presence of build defects, the assurance that production parts are of a certain quality is paramount to their safety and longevity. Further, fracture critical parts that are verified by analysis are subject to errors in the life predictions if incorrect NDE defect sizes are used in the analysis. As such, NDE must be involved in the fracture critical assessments to ensure correct methods and flaw sizes are being employed.

8.1.1 NDE for Metallic Parts

Section 7.2 of this Handbook presents examples of fracture critical metallic hardware undergoing assessments to meet fracture control requirements. These examples leverage NDE flaw sizes associated with those set forth by Figure 8.1-1, Minimum Detectable Crack Sizes for Fracture Analysis Based on Standard NDE Methods [NASA-STD-5009B], and Figure 8.1-2, Assumed Flaw Geometries, as established in NASA-STD-5009B. Some NDE methods are more conducive to certain types of hardware. For example, it is generally not feasible to conduct dye penetrant NDE on the inner surface of a spun formed pressure vessel dome. This is because the penetrant must be wiped away to reveal the surface defects, and access to removing the penetrant is not possible on the inside of the vessel after forming.

NASA-HDBK-5010, VOLUME 2, REVISION A

U. S. CUSTOMARY UNITS (inches)

Crack Location	Part Thickness, t	Crack Type	Crack Dimension, a*	Crack Dimension, c*
<u>Eddy Current NDE</u>				
Open Surface	$t \leq 0.050$	Through PTC ¹	t	0.050
	$t > 0.050$		0.020	0.100
			0.050	0.050
Edge or Hole	$t \leq 0.075$	Through Corner	t	0.100
	$t > 0.075$		0.075	0.075
<u>Penetrant NDE</u>				
Open Surface	$t \leq 0.050$	Through Through PTC	t	0.100
	$0.050 < t < 0.075$		t	$0.150 - t$
	$t > 0.075$		0.025	0.125
			0.075	0.075
Edge or Hole	$t \leq 0.100$	Through Corner	t	0.150
	$t > 0.100$		0.100	0.150
<u>Magnetic Particle NDE</u>				
Open Surface	$t \leq 0.075$ $t > 0.075$	Through PTC	t	0.125
			0.038	0.188
			0.075	0.125
Edge or Hole	$t \leq 0.075$ $t > 0.075$	Through Corner	t	0.250
			0.075	0.250
<u>Radiographic NDE</u>				
Open Surface	$t \leq 0.107$ $t > 0.107$	PTC PTC Embedded	$0.7t$	0.075
			$0.7t$	$0.7t$
			$2a=0.7t$	0.7t
<u>Ultrasonic NDE</u> Comparable to a Class A Quality Level (ASTM-E-2375)				
Open Surface	$t \geq 0.100$	PTC Embedded**	0.030	0.150
			0.065	0.065
			0.017	0.087
			0.039	0.039

Figure 8.1-1—Minimum Detectable Crack Sizes for Fracture Analysis Based on Standard NDE Methods [NASA-STD-5009B]

NASA-HDBK-5010, VOLUME 2, REVISION A

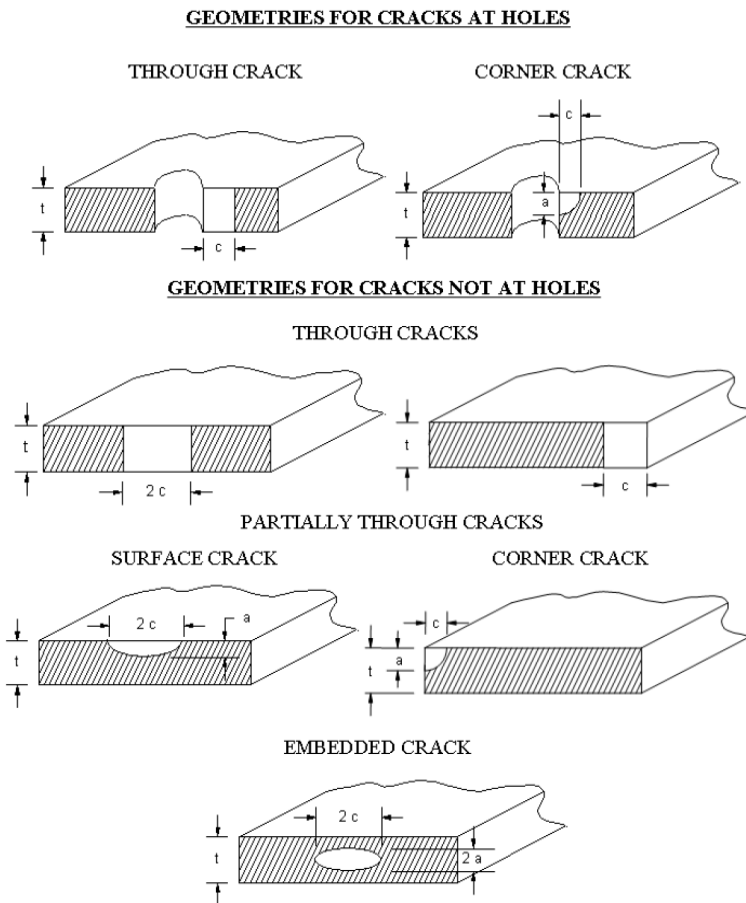


Figure 8.1-2—Assumed Flaw Geometries

In other situations, the fracture analysis may demonstrate adequate capability for only a certain NDE initial flaw size but not for the remainder of techniques. If the NDE technique is not practical or not feasible for the part manufacturing process or dimensionality, it may be prudent to redesign the part or manufacturing order to accommodate a different NDE method that is more compatible with verification using fracture analysis.

To successfully design and analyze a fracture critical part, an overall understanding of the recommendations in this Handbook and the requirements from NASA-STD-5019A and NASA-STD-5009B is needed.

The NDE flaw sizes in NASA-STD-5009B are provided in NASGRO®. Care must be taken to ensure that NASGRO®-provided values are consistent with NASA-STD-5009B and that the orientation of the flaws is consistent with the application. This is particularly important for corner cracks where NASGRO® could assume a particular aspect ratio that may be inconsistent with the actual application. It is recommended that even though the flaw sizes are provided within NASGRO® in the module, that the users always verify consistency and applicability. Otherwise, the users should override the inputs that are automatically provided by NASGRO®.

APPROVED FOR PUBLIC RELEASE – DISTRIBUTION IS UNLIMITED

NASA-HDBK-5010, VOLUME 2, REVISION A

8.1.2 NDE for Composite or Bonded Parts

To perform a composite damage tolerance assessment, characterization of the inspectable flaw sizes is needed. In this section, guidance is provided regarding NDE of composite structures.

NDE reference standard(s) should be representative of the part and should have known sizes of representative flaws (e.g., programmed delaminations or disbonds) at various depths through-the-thickness locations and in-plane spatial locations. Representative flaws in the laminate sections must be located at minimum 3 depths providing adequate coverage for flaws within the laminate thickness. Typically, in laminates, flaws should be on the nearside, middle, and farside of the reference standard. Nearside and farside flaws may be between the second and third ply from the nearside and farside laminate surfaces, respectively. For thinner laminate thicknesses, where more than two to three plies of separation between flaw depths is not possible, less than three depths of flaws may be used. Representative disbonds should be located on both sides of the film or paste adhesive for bonded parts. Pull tabs may be used for core structures. The representative flaws should be spaced so that they do not overlap in the plane of the laminate. A minimum of six (6) target size flaws and a minimum of six (6) size flaws smaller than the target sizes are recommended for each flaw type domain. Flaws used for validation of NDE procedures may be located on one or multiple physical test specimens.

Both target flaws and the smaller flaws should provide adequate and uniform flaw detectability (i.e., indication size and signal response). Flaws with out-of-family flaw indications caused by either bonding of flaw partially or wholly should not be used in the validation. Flaws with out-of-family flaw indications that are larger than the expected area of the indications should not be used in the validation.

Application Example of NDE Techniques for COPVs

Six NDE methods suitable for assessing impact damage to COPVs are discussed below (reference Johnson and Nokes [1998]) and Chang and Seibold [2005]). They are visual inspection, ultrasonic inspection, shearography, thermography, eddy current, and acoustic emission. Details about these techniques are discussed in the following sections.

1. Visual Inspection: The easiest method for inspecting COPVs for mechanical damage is to perform a visual inspection. The outside of the COPV can be examined for signs of fiber damage using the unaided eyes. There is no quantitative reliability and confidence level associated with visual inspection capability. The impact energy level producing a damage state that cannot be detected by visual inspection is often called visual damage threshold (VDT).

The capability for visual inspection can be enhanced using magnification loupes. Also, the use of dye penetrant or alcohol wipes can sometimes accentuate indications. With a borescope, the inside liner of the COPV can be visually inspected for dents caused by impact. All these visual inspection techniques are hampered by any circumstances that limit visual access to the surface in question and by the poor surface contrast that typifies graphite/epoxy COPVs.

NASA-HDBK-5010, VOLUME 2, REVISION A

2. Ultrasonic Inspection: Ultrasonic inspection has been used in the aerospace industry for many years for detecting delamination or debonding of composite structures. Two ultrasonic techniques that can be used for detecting mechanical damage, including impact, are through-transmission and pulse-echo. With the through-transmission technique, a sound pulse generated by one transducer is received by a second after passing completely through the pressure vessel. With the pulse-echo technique, a reflection rod is inserted into the center of the vessel. Figure 8.1-3, Pulse-Echo C-Scan of a COPV Subjected to a 7.5 ft-lb Impact, shows a C-scan representation of a COPV after a 7.4 ft-lb impact. The impact left no visible indication on the surface of the COPV; the impact site can be clearly identified by the dark region in the scan.

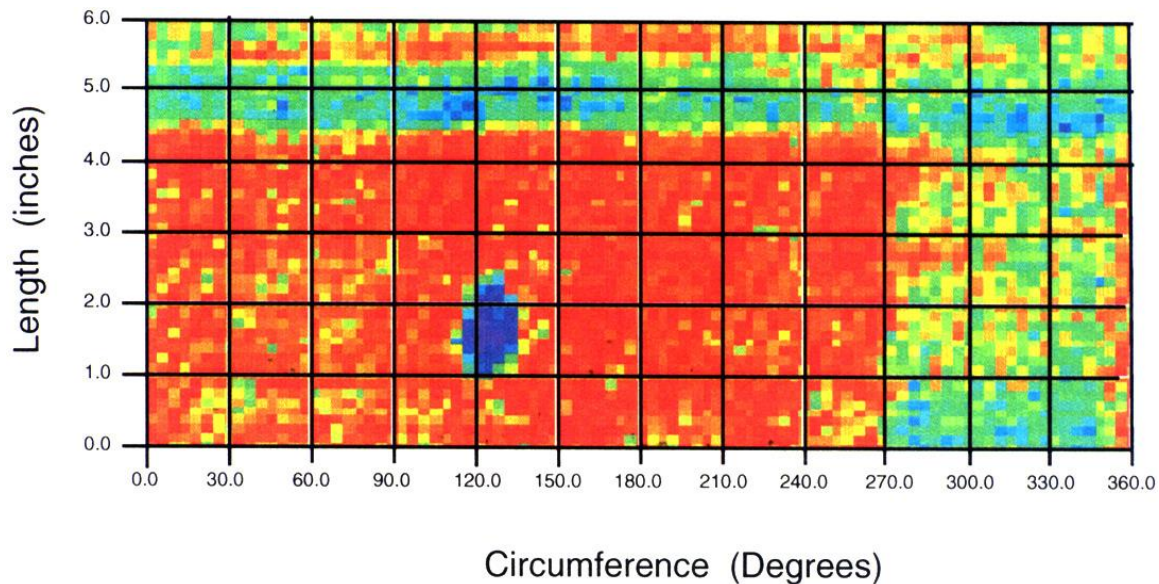


Figure 8.1-3—Pulse-Echo C-Scan of a COPV Subjected to a 7.5 ft-lb Impact

3. Shearography: Electronic shearography is a noncontact interferometric method for measuring changes in the out-of-plane slope of a surface. The application of shearography to COPVs requires an initial image of the vessel to be acquired and stored in the digital memory of a computer. After storing the initial image, a small load is applied to the vessel. Best results can be achieved by pressurizing the vessel to some small amount of pressure. A second image of the loaded or slightly deformed vessel is acquired and subtracted from the initial image. The result is a family of high contrast fringes indicative of the deformation due to the pressure differential. Mechanical damage such as impact to vessels can cause subtle changes in load-carrying characteristics and, hence, the contours of the vessel that are effectively detected using shearography.

The shearography inspection technique is particularly effective in detecting impact in spherical COPVs because of the relatively uniform stress field, as shown in Figures 8.1-4(a), Initial Shearography Image. The fringes presented in Figure 8.1-4(a) represent the nominal deformation of a spherical COPV under 40-psi pressure. These fringes can be contrasted with the fringes in Figure 8.1-4(b), Post-Impact Shearography Image, that clearly indicate the location of a 15 ft-lb

NASA-HDBK-5010, VOLUME 2, REVISION A

impact. A drawback to the use of the shearography in this application is the need for a matted surface to scatter the laser, creating the necessary speckle pattern. During testing, the vessels might have to be prepared using either a strippable paint or a spray powder. This approach should be evaluated for specific space applications.

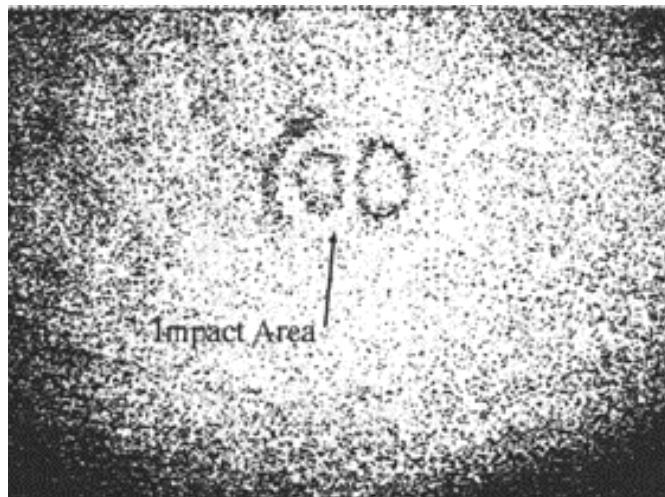


Figure 8.1-4—(a) Initial Shearography Image (b) Post-Impact Shearography Image

4. Thermography is an NDE technique for measuring the surface temperature of an object based on the emission of infrared (IR) radiation. Using an IR camera, the complete temperature profile of a target can be recorded at video frame rates (30 Hz). Variation in the surface temperature profile can occur as the result of internal discontinuity of flaws within the hardware. Flaws that produce localized variation in the thermal properties of a composite such as delamination or porosity can often be easily detected via thermography.

APPROVED FOR PUBLIC RELEASE – DISTRIBUTION IS UNLIMITED

NASA-HDBK-5010, VOLUME 2, REVISION A

For a COPV, one possible consequence of an impact event is the creation of a disbond between the liner and overwrap of the impact site. In the damage area, significantly high thermal impedance can be formed. An increase of thermal impedance translates to higher surface temperature when the COPV is exposed to a transient heat source. The location of surface hot spots can then be mapped using an IR camera. Evaluation of IR data showed a bruised area to be as much as 4-degree F hotter than surrounding areas shortly after transient heating with a quartz lamp. Images obtained during the thermography inspection of a cylindrical COPV with both 11 ft-lb (13 J) and 25 ft-lb (20 J) impact sites are shown in Figure 8.1-5, Thermography Indications on a COPV Subjected to Two Impact Levels.

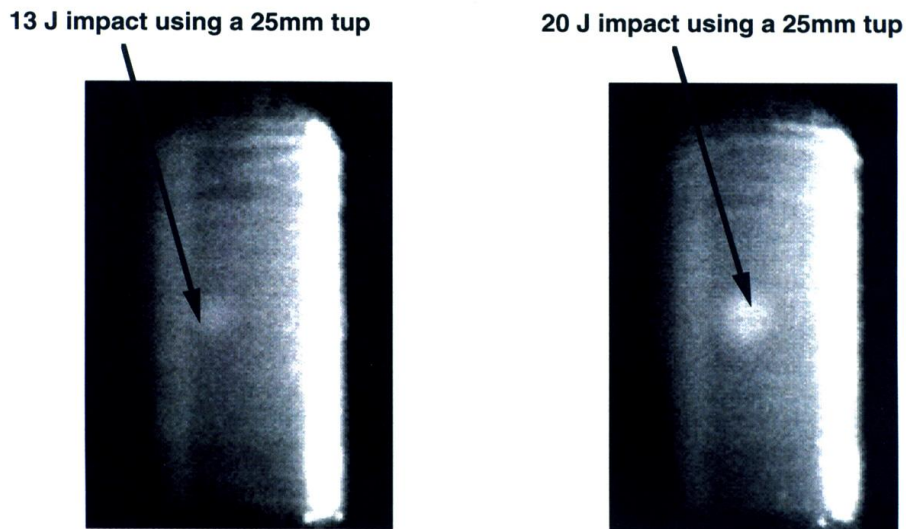


Figure 8.1-5—Thermography Indications on a COPV Subjected to Two Impact Levels

5. Eddy Current Inspection: Eddy current inspection is a commonly used NDE technique for detecting cracks in metallic parts of hardware. While the graphite fibers are conductive, the Gr/Ep COPVs are essentially transparent to the eddy current probes at standard inspection frequencies (i.e., less than 1 MHz). Within the COPV composite overwrap and metal liner, the overwrap acts as a spacer between the probe and the metal liner. Eddy currents that are very sensitive to the gap between the probe and the liner can be used to detect impact-induced

NASA-HDBK-5010, VOLUME 2, REVISION A

dents in the liner. A simple eddy current image is shown in Figure 8.1-6, Eddy Current Image of a COPV Subjected to Various Impact Levels.

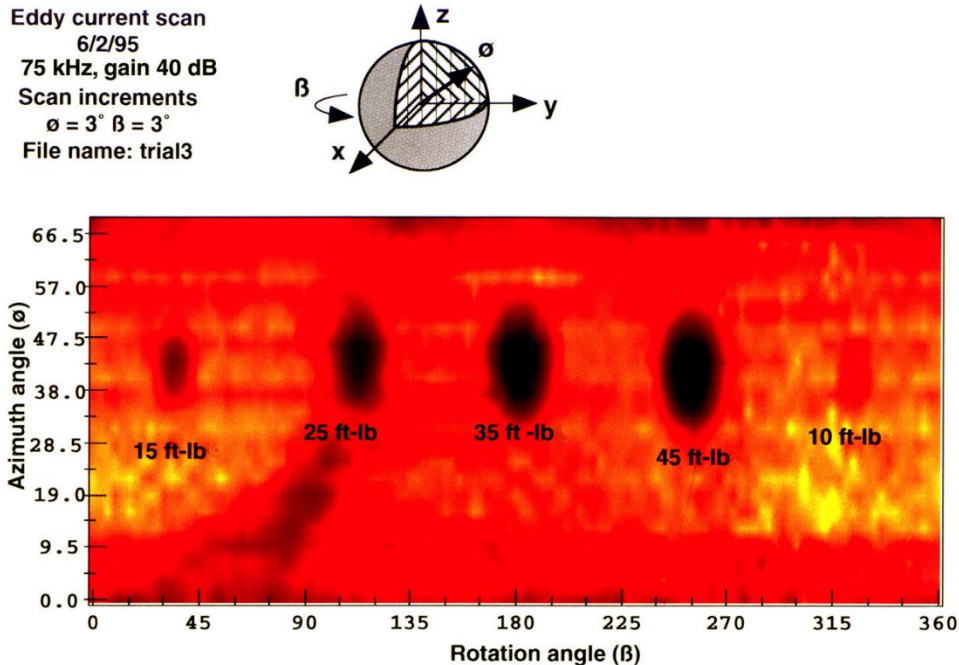


Figure 8.1-6—Eddy Current Image of a COPV Subjected to Various Impact Levels

6. Acoustic Emission Inspection: Loaded structures typically produce sound as the materials and components within the structure respond to the load. For composite hardware, matrix cracking or fiber breaking produces this sound. Acoustic emission (AE) monitoring is a method for evaluating the structural integrity of a structure based on the generation of sound during loading of the structure.

To detect impact damage that occurred in a COPV, the COPV can be subjected to an initial AE screening and then pressurized again after being subjected to an impact. Changes in the acoustic activity are noted, with the COPV exhibiting significantly more AE after impact above a given threshold. The energy threshold required for AE monitoring to detect impact varies significantly between and among COPV types. Figure 8.1-7, Acoustic Emission Data: (a) Before Impact and (b) After Impact, demonstrates change activity that occurred after a 25 ft-lb impact on a cylindrical COPV.

NASA-HDBK-5010, VOLUME 2, REVISION A

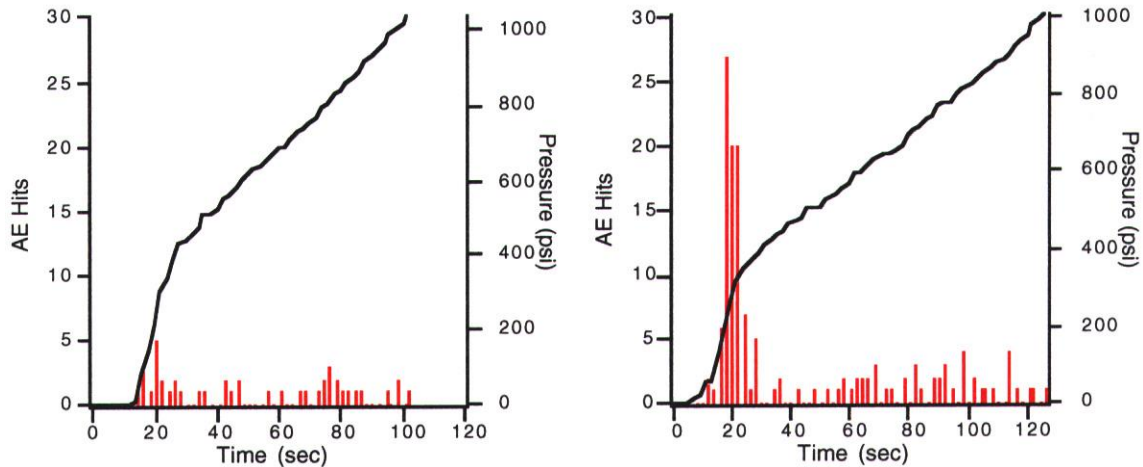


Figure 8.1-7—Acoustic Emission Data: (a) Before Impact and (b) After Impact

In summary, a number of NDE techniques have been shown to be effective for detecting impact damage sites of Gr/Ep COPVs even if the impact energy is below VDT. Selection of the most appropriate technique(s) depends on a number of factors, including:

- a. Specific type (size, shape, material thickness, coatings, etc.) of COPV to be inspected,
- b. Accessibility constraints during inspection, and
- c. Required sensitivity.

Anytime inspection methods are developed for a COPV, a guide similar to Figure 8.1-8, COPV Example Comparisons of Various NDE Methods, can be helpful in guiding inspection methods. In the figure, “whole field” refers to how the data are taken: point-by-point as in a scan versus whole field as in an acquired image. “Flaw characterization” is an assessment of how well the flaw is sized. “COPV preparation” refers to what must be done to the COPV to enable it to be inspected (e.g., coating the surface). “Field use” refers to how amenable the technique is to deployment in the field.

NASA-HDBK-5010, VOLUME 2, REVISION A

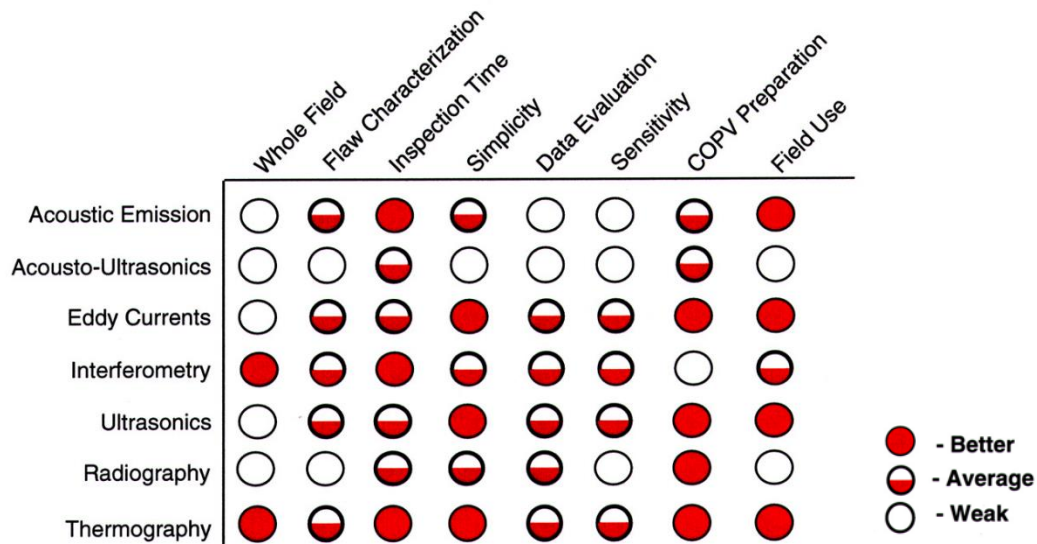


Figure 8.1-8—COPV Example Comparisons of Various NDE Methods

8.1.3 Proof Test

See discussion in Section 11.2.

8.1.4 Process Control

Reserved.

8.1.5 Detected Flaws

See Section 7.3 of this Handbook.

8.2 Traceability for Fracture Control

Reserved.

8.3 Material Selection and Usage for Fracture Critical Parts

Reserved.

9. FRACTURE CONTROL DOCUMENTATION AND VERIFICATION

9.1 Fracture Control Documentation

The primary documentation in fracture control is the FCP and the FCSR (see sections 9.1.1 and 9.1.3 of NASA-STD-5019A). Additional documentation is maintained by the hardware developer in support of fracture control activities such as analysis to demonstrate a part is nonfracture critical or damage tolerance analysis for a fracture critical part. Other documentation

APPROVED FOR PUBLIC RELEASE – DISTRIBUTION IS UNLIMITED

NASA-HDBK-5010, VOLUME 2, REVISION A

would include a load history log of a fracture critical pressurized component. See Table 9.1-1, Load History Log for a Pressurized Component such as a Valve on an Upper Stage Engine, for an example.

Table 9.1-1—Load History Log for a Pressurized Component such as a Valve on an Upper Stage Engine

Sequence	Pressure	Cycles*
Proof test	1.5 x MDP	2
Leak test	MDP	2
Engine acceptance firing tests	MDP	<i>M</i>
Launch	MDP	<i>N</i>

*Includes contingency cycles for re-proofing, and *M* and *N* depend on program requirements and number of firings expected during ground and flight operations.

9.1.1 Fracture Control Plan (FCP)

Two examples of FCPs are presented in Appendices A and C.

9.1.2 Engineering Drawings

Figure 9.1-1, Drawing for a Fracture Critical Part with a Note Providing the Expected Inspections and Associated Acceptable Flaw Size, offers an example of an engineering drawing with notes tagging the part as Fracture Critical and providing the NDE requirement in the notes section. Fracture critical parts typically have a unique serialization.

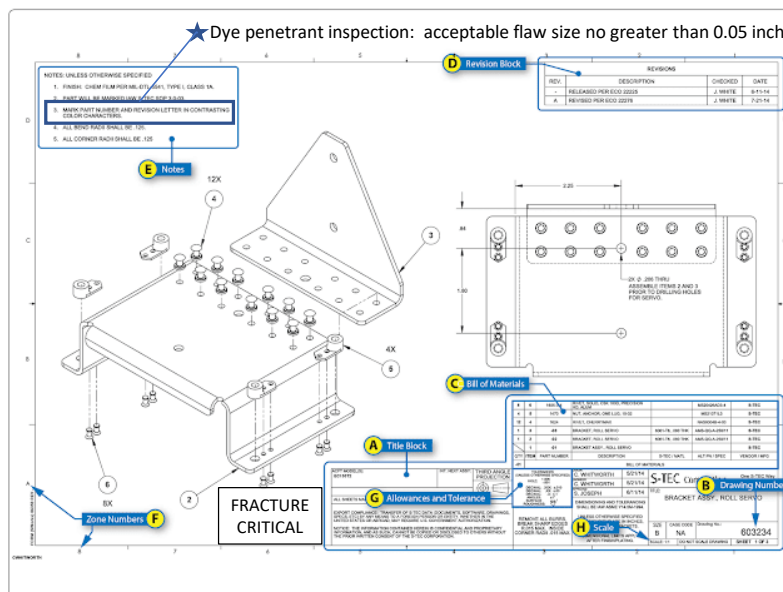


Figure 9.1-1—Drawing for a Fracture Critical Part with a Note Providing the Expected Inspections and Associated Acceptable Flaw Size

NASA-HDBK-5010, VOLUME 2, REVISION A

9.1.3 Fracture Control Summary Report

Two examples of FCSRs are presented in Appendices B and D. Although the FCSR summarizes what activities have been performed to meet fracture control requirements, a whole set of activities and documentation in support of these activities should be available to the Technical Authority and RFCB. The FCSR would contain a parts list, their fracture control classification, and describe how fracture control requirements have been met. Additional supporting documentation would include, but is not limited to, structural analysis reports, fracture analyses such as NASGRO® runs, test results, checklist as presented in this Handbook for various NFC and FC categories of hardware, NDE certifications (such as AIA/NAS NAS410), NDE inspection results, load history logs, among others.

10. ALTERNATIVES

Alternative approaches that meet the intent of NASA-STD-5019A can be developed and submitted to the fracture control board for approval. Examples are provided to illustrate alternative approaches for composite structures damage tolerance assessments.

10.1 Example 1: Impractical Full-Scale Testing

The following example is from “Damage Tolerance Approach for Composite Space Structures with Curved Bends” (<https://arc.aiaa.org/doi/abs/10.2514/6.2020-1214>). In this example, it was found to be impractical to perform cyclic testing on a large-scale composite space structure containing complicated geometries such as bends with small-radii. Further, inspecting these features using traditional NDE techniques was not feasible. The following approach was utilized to increase confidence in the composite design and reduce risk of a flaw propagating to failure:

- a. A pre-proof NDE of all the inspectable regions was implemented, a flight-enveloping proof test was performed, and post-proof NDE was performed to determine whether any flaws in uninspectable areas propagated into inspectable regions and exceeded acceptance flaw criteria.
- b. Acceptance criteria for flaws were established with a combination of a simple analytical tool validated by test, full-scale finite element models, and global-local models, thus reducing the necessity for a costly and uncertain full-scale damage tolerance test program for composite systems containing such features.
- c. Subscale cyclic tests were designed to mimic flight conditions and to demonstrate robustness of the design to manufacturing flaws.
- d. An impact damage threat assessment was made and, because of protective measures that were implemented, no additional testing associated with impact damage was performed.

APPROVED FOR PUBLIC RELEASE – DISTRIBUTION IS UNLIMITED

NASA-HDBK-5010, VOLUME 2, REVISION A

10.2 Example 2: Proof Test of Full-Scale Composite Structures

The following example is from “Proof Test Methodology for Reducing the Risk of Unvented Honeycomb Core Failures in Aerospace Structures”

(<https://arc.aiaa.org/doi/pdfplus/10.2514/6.2018-1709>). Trapped air in unvented honeycomb core and the surrounding environment can induce a pressure differential across the facesheet during launch ascent. Combined with the presence of a defect, the pressure differential across a facesheet in combination with external loads can cause facesheet failure or unstable facesheet debond growth. The following activities aided in the mitigation of concerns associated with this failure mode:

- a. Because of the honeycomb construction, impact damage was of concern for this design. The worst-case credible damage was imposed on representative samples that were subsequently subjected to cyclic loading, and then followed by an ultimate load.
- b. Nondestructive inspection techniques were developed to detect flaws between the facesheet and the honeycomb core; and then a pre-proof NDE was implemented to detect any manufacturing flaws.
- c. Subscale tests with detectable flaws subjected to a combination of internal pressure and external loads mimicking flight conditions were performed to demonstrate robustness of the design.
- d. Since the number of expected ground-to-air cycles was expected to be less than one hundred (100), cyclic testing was not expected to reveal the limiting failure mode. Regardless, testing was performed that demonstrated robustness of the design to cyclic loading (“Composite Damage Tolerance Approach for Reusable Launch Vehicle Applications.” AIAA 2021-1166).

10.3 Example 3: Thermal Protection System Challenges

The bondline attaching a TPS to the composite was deemed fracture critical, as bondline failure could cause TPS detachment and potential burn-through. The following activities were performed to gain confidence in the design’s damage tolerance:

- a. All potential damage threats were identified, and measures were taken to protect the hardware from the identified threats. Further, the design was such that any contact such as impact would produce an indication on the surface paint. The only concern remaining was manufacturing flaws or weak bonds.
- b. The loading spectra was fully characterized, and it was determined through extensive dynamic/thermal analysis that only a few load events would be critical for the bondline so that fatigue (i.e., cyclic testing) was less of a concern.
- c. Extensive materials and fracture testing via coupon-level tests were performed to characterize the fracture toughness to cover the full temperature range.

APPROVED FOR PUBLIC RELEASE – DISTRIBUTION IS UNLIMITED

NASA-HDBK-5010, VOLUME 2, REVISION A

d. Extensive analyses were performed to determine the critical bondline flaw sizes across the heatshield design and analysis that demonstrated the critical flaw size was greater than the detectable size using NDE.

e. NDE performed before and after a proof test that mimicked flight-like stresses at the bondline was implemented to ensure manufacturing flaws did not grow in size.

f. Thermomechanical tests that replicated flight conditions were performed to validate the design robustness with flaws.

A combination of acceptance testing, extensive coupon/subscale testing, development of NDE procedures to inspect for flaws, and analysis helped to reduce the risk that a bondline flaw could cause catastrophic failure.

10.4 Example 4: Catastrophic Composite Failure Risk Mitigation

A composite design for a launch vehicle is designed for significant load cycling. The following activities were performed to reduce the risk that a flaw could cause catastrophic failure:

a. The composite structure was designed to be robust against open hole allowable strengths, which enveloped any strength reduction from composite impact damage from all potential identified damage threats.

b. NDE was developed to enable detection of manufacturing flaws.

c. Full-scale testing with no flaws was performed to validate the predicted load paths by the analytical models.

d. Subscale cyclic tests with flaws greater than the NDE minimum detectable flaw size were performed, followed by an ultimate load condition, demonstrating robustness of the design to manufacturing flaws.

e. An acceptance proof test was implemented to verify the manufacturing.

The combination of NDE, acceptance testing, test-validated analysis to guide subscale tests, subscale cyclic testing, and design robustness to impact damage reduced risk of a flaw leading to a failure event.

10.5 Example 5: Composite Damage Tolerance – Analysis Validated by Test

Due to geometric complexities of a human-rated structural component, Figure 10.5-1, Complicated Sandwich Structure is Subject to Internal Core Pressure during Ascent, shows the stress field in this structure is complicated and damage tolerance of the component was

NASA-HDBK-5010, VOLUME 2, REVISION A

challenging to perform. The spacecraft panel consisted of a sandwich construction with a carbon-fiber/cyanate-ester fabric facesheet and aluminum Flexcore® that was unvented.

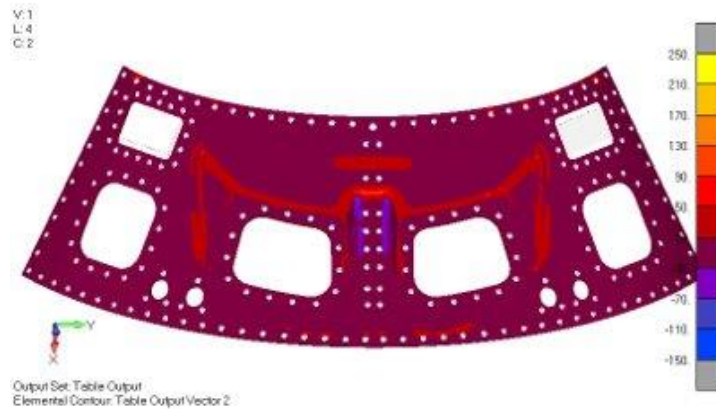


Figure 10.5-1—Complicated Sandwich Structure is Subject to Internal Core Pressure during Ascent

(The stress field in this structure is complicated.)

Damage tolerance analysis of composite or bonded hardware is generally considered insufficiently mature to certify flight hardware without the support of a test program and a mature BBC. When a test-verified approach exists and is applicable, an analysis approach that minimizes some of the testing detailed below may be submitted to the RFCB for consideration and approval. The structural component was covered in thermal tiles during service so any damage during service would be visible. The fabrication was tightly controlled and verified through multiple audits that identified issues and corrective actions. Finally, the system was under a comprehensive impact damage protection plan.

A residual threat determination found that the only flaw of concern during service was core-to-facesheet debonds. The primary concern is that core pressure coupled with a manufacturing flaw can cause the facesheet to detach from the core. Due to the complexity in the design, structural testing would be challenging to implement. Rather, the approach was to implement an NDE procedure that could identify flaws with a high-degree of confidence and to determine the acceptable flaw sizes by an analysis approach that was validated by test. The acceptable flaw size was determined to be 0.5-inch in diameter for the facesheet-core debonds failure mode. A finite element model, the VCCT, and an estimated value of fracture toughness determined through testing were used to assess the structure. The testing for feature-specific fracture toughness consisted of a test where the structure was pressurized until failure occurred, representing a pseudo “burst test.” A finite element model was used to perform a virtual test of the experimental configuration to estimate the fracture toughness that was present in test. This fracture toughness was then utilized to develop the acceptable flaw sizes in the structural spacecraft component for the flight analysis case. While this test was not typical test standard to measure toughness, it was a practical approach to validate the acceptable flaw size. Note that “test verified” analysis is permitted in NASA-STD-5019A to aid in fracture control implementation, but it does require RFCB approval for the approach.

APPROVED FOR PUBLIC RELEASE – DISTRIBUTION IS UNLIMITED

NASA-HDBK-5010, VOLUME 2, REVISION A

10.6 Example 6: Delaminations in Composite Overwrapped Pressure Vessels

Delaminations occasionally occur in COPVs. The objective of this section is to describe a method used to evaluate these defects by using a pre-processor in conjunction with progressive failure analysis. An example is used to illustrate this approach for a typical COPV. COPVs store highly pressurized gases in launch vehicles and spacecraft. Typical COPV construction consists of high-strength fiber composites wrapped around a thin metal liner. The purpose of the liner is to act as a leakage barrier while the composite carries most of the load from pressurization. This combination leads to lighter weight designs for the same pressure capability, which is valuable for space applications.

Structural integrity and conformance to safety requirements demand accurate stress, fatigue, and fracture mechanics analyses. Typically, netting analysis has been used as a design tool for COPVs but is a highly simplified method that cannot always be used to evaluate the structural integrity of a discrepant COPV. Accurate analysis is particularly important since the consequences of a local defect propagating can lead to catastrophic failure and possibly complete mission loss.

In this example, damage tolerance evaluation of a COPV is illustrated. This case study was taken from Goyal and Rome (2021).

The COPV Stress Analysis Program (COSAP), began in the 1990s under Air Force and NASA sponsorship. COSAP is primarily comprised of pre-processing software code that was designed to work with Abaqus™ commercial finite element software. COSAP is flexible enough to model various vessel configurations, winding patterns and peculiar situations resulting from manufacturing considerations, including delaminations. COSAP was validated through experiments (reference Goyal and Rome [2012]). Although COSAP was designed for analysis of COPVs, it may also be used for analysis of other filament-wound vessels such as composite solid rocket motor cases.

COSAP was designed to handle the complicated features such as the continuously changing local wrap angle and thickness resulting from the filament winding process. Although the local wrap angle changes as a function of axial position, it is self-consistent circumferentially which enables the convenient use of analysis by 2D axisymmetry. As such, COSAP was designed to automatically generate an axisymmetric finite element model for a COPV, while calculating the effective three-dimensional composite material properties. The input file requires major dimensions, basic material properties and definition of the winding pattern. The dome geometry can be specified by the user directly or optimized by the pre-processor. Depending upon the winding method (e.g., geodesic or planar), COSAP will automatically determine the local wrap angle and thicknesses of composite layers based on the input data and then generate the finite element mesh. To limit the total number of elements, groups of composite layers defined at a sublaminar level can be incorporated into a row of elements.

NASA-HDBK-5010, VOLUME 2, REVISION A

COSAP generates a finite element model suitable for analysis with Abaqus™. Abaqus™ can then be used to perform a multi-step analysis that may include fabrication, sizing, and burst cycles. Sizing or autofrettage is part of a typical manufacturing process, whereby the COPV is pressurized to yield the metal liner and, as a result, the liner retains compressive residual stresses at lower operating pressures. This increases the number of cycles the tank can sustain before leaking. Upon completion of the multi-step analysis, the results are processed to evaluate burst pressure capability, fatigue life, and the leak-before-burst failure mode. Prediction of the burst pressure is based upon progressive failure analysis. The ultimate failure of the COPV is often fiber breakage. Preceding the global failure, delaminations may propagate into the boss region or into other regions, resulting in decreased capability.

Damage may propagate along the plies, either as delaminations between adjacent composite plies or as disbonds between the liner and the overwrap. While different techniques may be used to model this sort of damage growth, usage of cohesive elements with embedded fracture mechanics properties holds a particular advantage; since the path of delamination growth can be established *a priori* and cohesive elements can be readily inserted along these boundaries.

In the example described here, each layer or ply of composite is modeled by one solid element through the thickness. A layer of zero-thickness cohesive elements can be inserted between any two layers, either during the initial creation of the COPV model using software like COSAP that automates the process, or with standard finite element modeling tools. Alternatively, if multiple ply layers are grouped together as sublaminates within a given element, cohesive elements can only be placed between these elements. Cohesive elements may not be placed within a sublaminate, so care must be taken to ensure that likely delamination interfaces are modeled.

Fracture and strength properties of the composite are embedded into the material properties of the cohesive elements to predict delaminations. The interlaminar tensile and shear strength of the composite are used to establish when failure initiates, while the Mode I and Mode II fracture toughness are used to predict fracture growth. For standard material systems, these values are often available. Likewise, the fracture and strength properties of the adhesive can be embedded in those cohesive elements along the liner-to-overwrap interface. Since these properties are dependent upon the surface preparation, liner material, adhesive and composite, good data are seldom available and must instead be measured experimentally. If that is not practical, using bounding estimates is the next best course of action.

The objective of this section is to demonstrate how COSAP or equivalent tools can be used to evaluate the burst strength reduction due to the presence of a delamination. A typical COPV with a 20-inch diameter and alternating hoop and helical plies with a total thickness of up to 0.5 inch is analyzed is shown in Figure 10.6-1, A Typical COPV with Boundary Conditions. In this example, the model development consisted of the following steps:

1. The liner contour was found by digitizing the available drawings and using software to determine the exact shape.

NASA-HDBK-5010, VOLUME 2, REVISION A

2. Ply thickness and initial ply angle at the tangent point were specified in the winding program, which then generated the remaining ply angle and thickness throughout.
3. The modeling also considered the inclusion of ply drop-off geometry and location. Data were obtained from a cross section of a fabricated component.
4. Candidate delamination locations were identified in critical ply interfaces as shown in Figure 10.6-2, Delamination Location for this Example.
5. With the above geometric information, COSAP was used to generate an axisymmetric finite element model with cohesive elements located at candidate locations, including the liner-to-overwrap interface.

The analysis was performed in Abaqus™ and included elastic-plastic material properties of the metallic liner, and contact modeling was used to prevent delaminated surfaces from penetrating. Three load steps were required to evaluate the COPV: (1) load to autofrettage pressure of 4000 psi, (2) unload to 0 psi, and then (3) load to MEOP at 3000 psi. Progressive failure analysis was active during these analysis steps. To build confidence in the model, strain gauge data were gathered and found to be in good agreement with the predicted strains from the model. Calculated axial and radial growth values were also found to be in agreement with measurements from the autofrettage cycle.

Two failure modes that could result from an initial delamination were evaluated. The first failure mode was a decreased burst capability due to a hypothetical fiber defect occurring directly above the delamination as shown in Figure 10.6-3, Hypothetical Fiber Defect near Delamination. The concern was that the delamination growth could amplify the effects of local fiber damage. The fiber defect was modeled by substantially reducing the elastic modulus in the hoop direction. The analysis showed that while the fiber defect itself could substantially reduce the burst capability, the addition of a delamination near this hypothetical fiber damage resulted in a strength reduction of less than 5%. Based on previous experience, the effects of delamination can be much larger than in this example, arising from multiple factors.

The second failure mode examined was delamination propagation towards the boss as shown in Figure 10.6-4, Direction of Delamination Growth in this Example. A delamination in this region could have uncertain effects due to the large external loads that exist in this region. Progressive failure analysis was used to predict delamination growth. Fracture toughness properties were not available from test data, so values that varied between 1.0 and 5.0 lb/in were assumed. The analysis predicted delamination growth in the ply drop-off region, which can be explained by the high transverse shear stresses present in this region. Once the delamination grew outside of the drop-off region, the delamination growth rate slowed substantially. Further, results showed that this growth was insensitive to the fracture toughness chosen as shown in Figure 10.6-5, Predicted Delamination Growth for Low and High Fracture Toughness Values. Based on previous experience, delamination growth characteristics are driven by multiple factors; and this example should not be used for the assessment of any other structure, especially considering that delamination growth to the boss is plausible.

APPROVED FOR PUBLIC RELEASE – DISTRIBUTION IS UNLIMITED

NASA-HDBK-5010, VOLUME 2, REVISION A

In summary, an example was used to demonstrate how progressive failure analysis in conjunction with state-of-the-art pre-processing tools can be used to evaluate delaminations in COPVs. A limitation of this example is that not all failure modes were considered. While these tools can be used as part of an assessment of other failure modes, additional analysis may be required. Particular to liner buckling, analysis tools need to be improved and validated through a program that consists of testing, NDE, and analysis.

In nonaxisymmetric problems where a delamination does not run the full circumference, using an axisymmetric assumption may be too conservative. In these situations, a wedge model or a three-dimensional approach may be more acceptable.

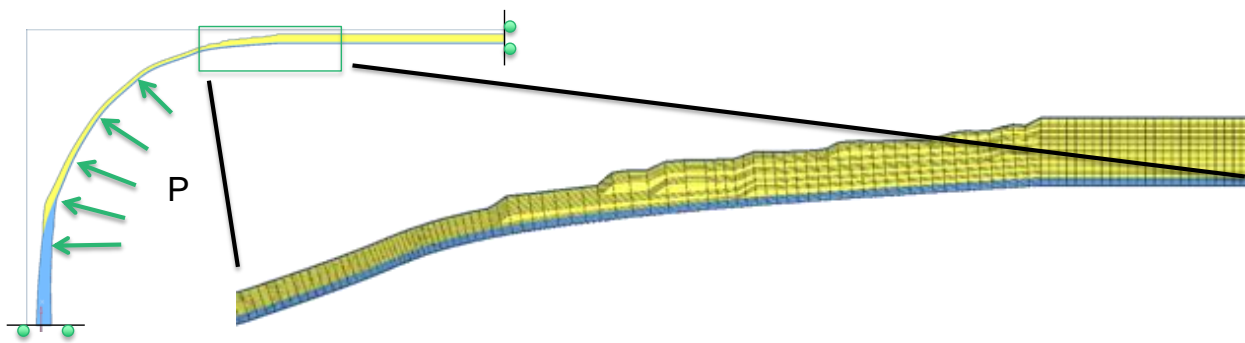


Figure 10.6-1—A Typical COPV with Boundary Conditions

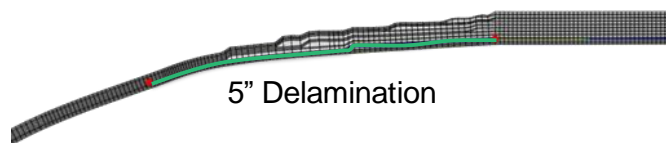


Figure 10.6-2—Delamination Location for this Example

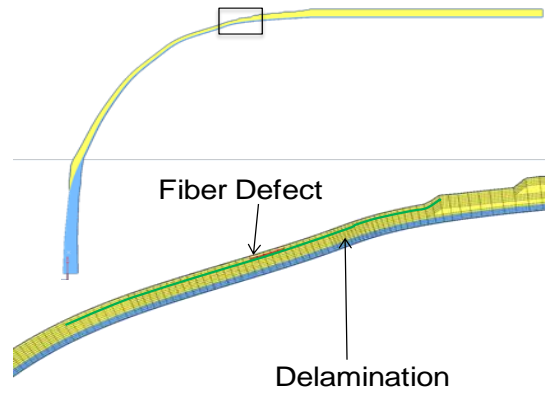


Figure 10.6-3—Hypothetical Fiber Defect near Delamination

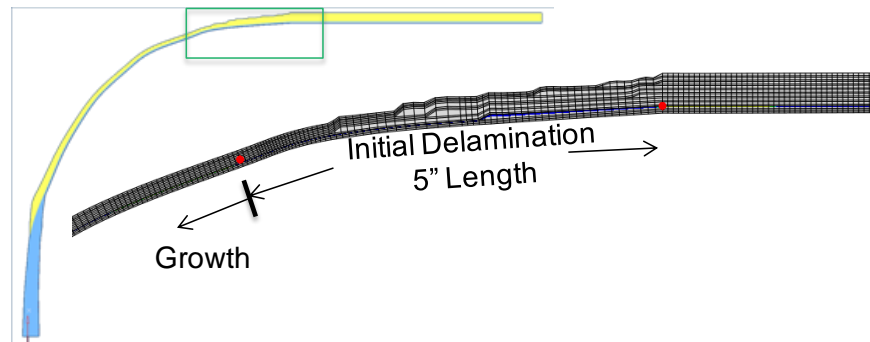


Figure 10.6-4—Direction of Delamination Growth in this Example

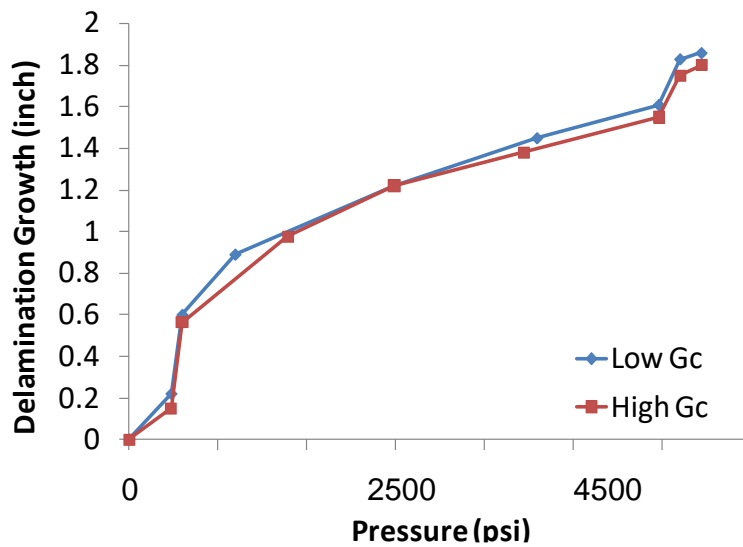


Figure 10.6-5—Predicted Delamination Growth for Low and High Fracture Toughness Values

NASA-HDBK-5010, VOLUME 2, REVISION A

10.7 Impact Damage of Composite Structures

Composite failure analysis is complicated and requires validation by test. Many software packages exist that can simulate impact damage; but in general, validation by test is required due to complexities related to the impactor, the composite system, and other considerations. In practice, the potential damage events are assessed via the damage threat analysis; and those are generally simulated in a test program. Analysis can help guide the test program, especially when the analysis has been validated with an initial set of tests.

10.7.1 General Impact Damage Approach

The damage tolerance design approach that is generally used for many space vehicles may be summarized as follows (reference NASA/TM-2003-2 12420).

1. Identify fracture critical components.
2. Determine the possible damage states that could exist in the fracture critical component.
3. Determine the size of damage that could be missed (i.e., is undetectable) by the initial manufacturing quality assurance inspection and by subsequent in-service inspections. This process sets the design allowable damage limit values.
4. Assume that the undetectable damage is present in each fracture critical component at the most critical location.
5. Determine the residual strength of the structure with undetectable damage that is required at the design limit load condition and the associated critical damage state.
6. Determine the extent to which the undetectable damage may grow during the service life of the vehicle and the point in life when the damage becomes critical for design limit loads. This process sets the critical damage threshold. The vehicle with critical damage may also need to survive a discrete source damage event such as an uncontained rotor burst.
7. Develop an in-service inspection program (i.e., method and inspection intervals) that will detect the damage before it reaches the critical damage threshold so that the structure can be repaired and restored to its original strength.

10.7.2 Compression-After-Impact Strength Testing

Typically, tests can be performed to determine the compression-after-impact (CAI) strength reduction due to various energy levels and diameter impactor sizes as shown in Figure 10.7-1, Compression-After-Impact Test Data Shows Reduction in Residual Strength due to Foreign Object Impact Damage. The CAI strength reductions are typically characterized through testing. There can be instances where the strength reduction is significant when impact damage is not

NASA-HDBK-5010, VOLUME 2, REVISION A

visible. An impact damage protection plan to avoid any impact damage in those instances should be implemented, or mitigation approaches such as redesigns should be pursued.

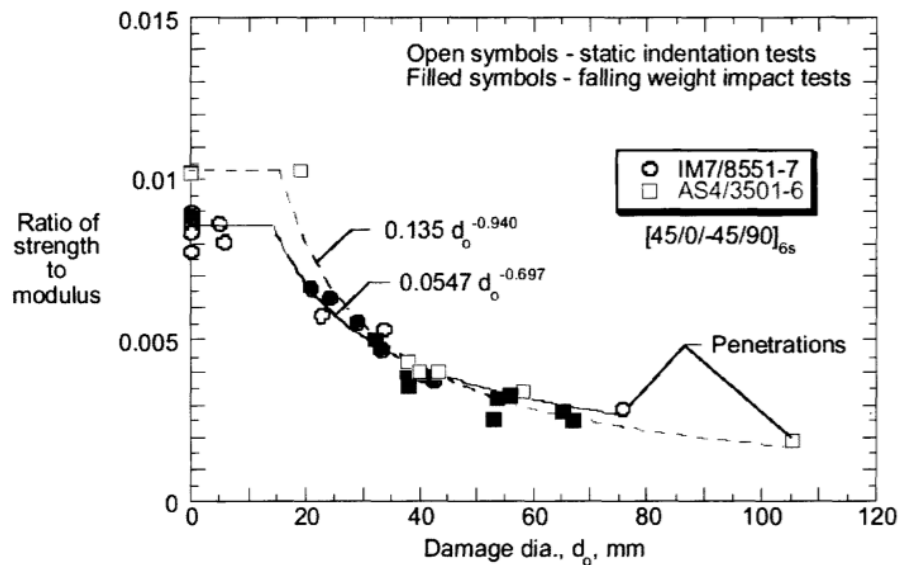


Figure 10.7-1—Compression-After-Impact Test Data Shows Reduction in Residual Strength due to Foreign Object Impact Damage

10.7.3 Burst-After-Impact COPV Testing

An example is provided based on the work in “Impact Damage Effects on Gr/Ep Composite Overwrapped Pressure Vessels,” AIAA-99-132. It is presented to illustrate a test program aimed at understanding the effects of impact energies on the strength reduction of composites. In this particular study, a research, development, test, and evaluation funded jointly by the Air Force and NASA entitled “Enhanced Technology for Composite Overwrapped Pressure Vessels” was conducted by a government-industry team led by The Aerospace Corporation (Aerospace). One of the primary objectives of this research, development, test, and evaluation effort was to study the impact damage effects on Gr/Ep COPVs. More than one hundred Gr/Ep COPVs were tested. The test parameters included COPV configuration, impact energy level, impactor size and shape, impact location, pressure level during impact, and the type of pressurized mediums. The experimental program included impact test procedures, post-impact inspection, and post-impact burst testing. Impact tests were carried out by using flight qualified cylindrical COPVs as test specimens to determine the critical parameters that have the most effect on the burst strength.

Typical parameters studied in an impact damage composite program include: (1) impact energy level, (2) impactor geometry, (3) vessel geometry/size, (4) impact location, (5) internal pressure level during impact, and (6) pressure media (i.e., gas or liquid).

After each impact, the fluid in the vessel is typically discharged; and the vessel is inspected visually by several trained inspectors. This also provides an excellent opportunity to study NDE techniques and determine how well each technique can detect damage. Adding acoustic emission

NASA-HDBK-5010, VOLUME 2, REVISION A

sensors can be beneficial in identifying damage occurring during pressurization. After the inspections, these vessels are pressurized in a test chamber until burst failure occurs.

COPVs were fabricated by overwrapping Aluminum 6061-T62 liners with graphite fibers and epoxy resins. COPVs were designed to have a MEOP of 6,000 psi and a minimum design burst pressure of 9,000 psi. The impact testing was conducted at WSTF using a Dynatup® Model 8250 drop tower type Instrumented Mechanical Impact Tester (IMIT). The load cell located in the impact tup has a maximum load range of 10,000 lb. The tip of the impact tup is hemispherical with a diameter of 0.5 or 1 inch. The impactor weight was varied and dropped from different heights to achieve different levels of impact energy. The specimens were secured at the end bosses, and the impact was applied in the membrane region. A total of 15 cylindrical COPVs were impacted under various conditions and subsequently burst tested to determine their BAI levels. Some of the results are shown in Table 10.7-1, Comparison of Burst Strengths for Cylindrical COPV. The data can be used in conjunction with the impact damage protection plan and residual threat determination to determine whether additional mitigations are required to prevent an in-flight failure.

Table 10.7-1—Comparison of Burst Strengths for Cylindrical COPV

Impact Energy	Test Results	
	Burst Pressure	Degradation
0 ft-lb (0 Joule)	10,700 psi (73.7 MPa)	-
5 ft-lb (7 Joule)	9,800 psi (67.6 MPa)	8.4%
10 ft-lb (14 Joule)	8,884 psi (61.2 MPa)	17.0%
15 ft-lb (20 Joule)	8,246 psi (56.9 MPa)	22.9%
15 ft-lb (20 Joule)	8,377 psi (57.8 MPa)	21.7%
15 ft-lb (20 Joule)	9,257 psi (63.8 MPa)	13.5%
20 ft-lb (27 Joule)	7,681 psi (53.0 MPa)	28.2%

In general, a comprehensive test program should be developed after the residual threat determination assessment is completed. The following are important test characteristics that need to be included in a general impact damage tolerance test program:

- a. Fully characterize the maximum level of impact energy that can be induced into the part via the residual threat determination.

APPROVED FOR PUBLIC RELEASE – DISTRIBUTION IS UNLIMITED

NASA-HDBK-5010, VOLUME 2, REVISION A

- b. Determine the characteristics of the composite system in the area where damage could occur.
- c. Determine the types of impactors that could impact the composite and their characteristics (e.g., blunt, hammer, etc.)
- d. Design an experimental program using initial impact analysis to bound all the characteristics of the impact damage event.

The testing is performed to predict the strength reduction due to the impact damage which is then compared against the allowables used in the design. The key is to ensure that barely visible impact damage does not cause a significant strength reduction to the extent that the design could fail service with that damage.

10.7.4 Impact Damage of Sandwich Panels

In this final example, Schubel, et al. (2009) is leveraged to illustrate that damage not visible to the human eye can cause a significant strength reduction, and that it is important to understand damage characteristics after impact and the causes for those characteristics.

A square panel with facesheets made from woven carbon fabric/epoxy laminates (AGP370-5H/3501-6S) and a closed-cell core made of PVC foam (Divinycell H250) was subjected to a low velocity impact caused by a free-falling blunt impactor (see Figure 10.7-2, Sandwich Structure Impacted by a Free-Falling Mass). Visually, the damage was not visible. After an ultrasonic C-scan image, a ring-shape delamination was observed (see Figure 10.7-3, Ultrasonic C-Scan Image of Impacted Panel Showing Delamination Damage). Subsequent testing of a portion of the panel containing the damage demonstrated a significant reduction in strength due to the damage (reference Schubel, et al. [2007]). This illustrates that the presence of damage that can occur in service can degrade the strength significantly even when not visible to the naked eye.

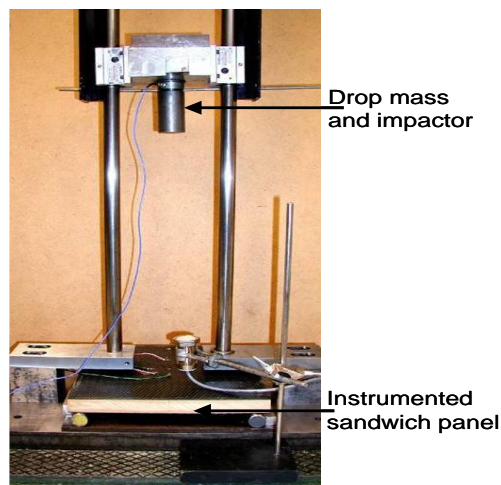


Figure 10.7-2—Sandwich Structure Impacted by a Free-Falling Mass

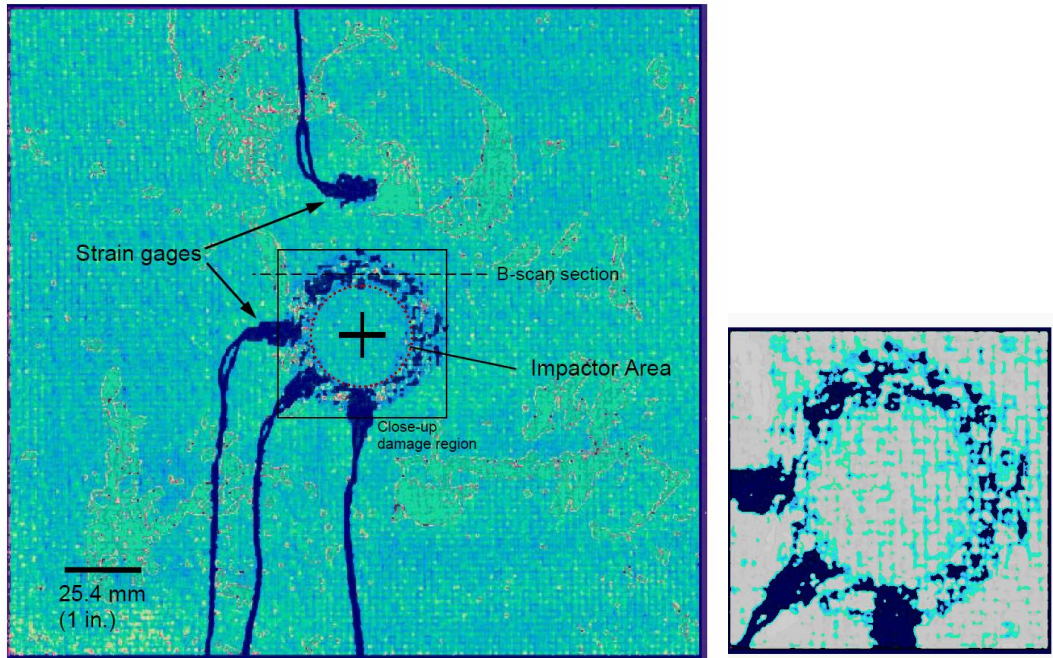


Figure 10.7-3—Ultrasonic C-Scan Image of Impacted Panel Showing Delamination Damage

(Reprinted with permission of Patrick Schubel [Schubel, P.M. 2007. “Three-Dimensional Failure Modes and Criteria of Textile Composites and Sandwich Structures,” PhD Thesis, Northwestern University, Evanston, Illinois.])

Because the shape of the delamination was a ring, decohesion elements were used to develop an analytical understanding of the damage induced into the panel. The predicted delaminations were ringed shape, extended outwards from just the circular edge of the impactor, and were located in the midplane of the upper facesheet. The predictions compared well with ultrasonic scanning of the failed test specimen (see Figure 10.7-4, Strain Response at Bottom Facesheet of the Sandwich Structure). The predicted global response of the sandwich structure was in reasonable agreement with the tests (see Figure 10.7-5, Delamination Predicted by Analysis Compared Well with the Test). This example was also selected because there were two unexpected characteristics of the failure analysis that were instrumental in achieving a good correlation with test data:

- a. Incorporating a separate damage model for the foam core to properly simulate the extent and shape of delamination.
- b. Including beneficial effects of the increase in interlaminar shear strength and Mode II fracture toughness when the composite is subject to transverse compression loads (reference J. I. Rome, et al. [2007]).

The failure analysis was also able to predict a decrease in load-carrying capability caused by delamination growth, which was also observed in compression testing. When a validated model is developed and the damage characteristics are well-understood through a physical

NASA-HDBK-5010, VOLUME 2, REVISION A

understanding of the system, it is possible to use analytical methods to predict the CAI strength with caution and to guide impact damage protection plans to ensure that invisible damage to the human eye does not cause a catastrophic failure in-service.

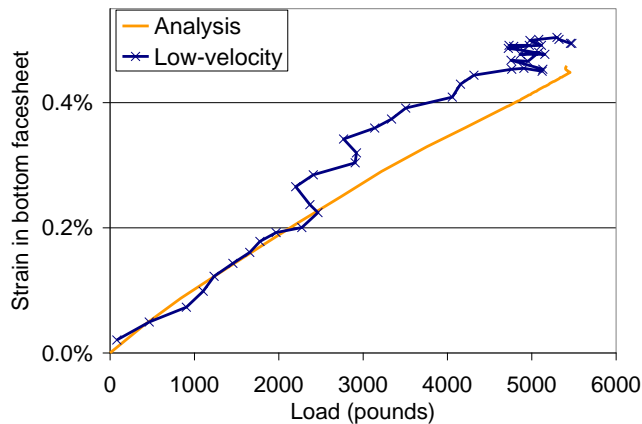


Figure 10.7-4—Strain Response at Bottom Facesheet of the Sandwich Structure

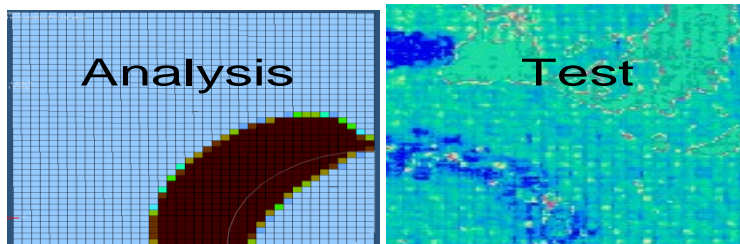


Figure 10.7-5—Delamination Predicted by Analysis Compared Well with the Test

11. SPECIAL TOPICS

This NASA Technical Handbook, Volume 2, was developed such that examples presented in each section mirrors the corresponding sections in NASA-STD-5019A. Section 11 is a new section for which it does not have a corresponding section in NASA-STD-5019A. Section 11 covers special topics such as additive manufacturing materials, composite analysis, leak before burst, proof test logic, and many other special topics associated with damage tolerance.

11.1 Leak Before Burst

11.1.1 Background and Introduction

For metallic pressure vessels and elastic response metal liners of COPVs, the LBB demonstration can be done by either a fracture mechanics-based analysis or by an LBB test. For plastic response COPV metal liners, testing is the only acceptable method to demonstrate the LBB failure mode.

APPROVED FOR PUBLIC RELEASE – DISTRIBUTION IS UNLIMITED

NASA-HDBK-5010, VOLUME 2, REVISION A

LBB is often oversimplified for pressure vessels. S-080 and S-081 require it to be demonstrated everywhere, yet LBB is frequently only demonstrated in the mid-cylinder or acreage region. Areas where the pressure vessel or COPV are thicker, contain welds, or are mixed-mode are neglected. When LBB is the only demonstration of robustness to the existence of a crack, such as a Category 2 metallic pressure vessel, gaps in LBB rationale can exist since thicker regions, welds, and mixed mode fracture can be worse-case compared to mid-cylinder or acreage locations. Testing or analysis at multiple locations in a pressure vessel is usually necessary to demonstrate LBB in a pressure vessel.

S-080A and S-081B require that:

The worst case location(s) shall be determined based on an analysis that establishes the greatest potential for a flaw to grow to critical size. The analysis shall incorporate the material properties/microstructure, stress/strain state of the pressurized hardware, residual stresses, and orientation.

All embrittling effects from manufacturing processing, or other toughness reduction factors shall be included. The assessment may involve multiple candidate worst-case locations, including the boss region. If this LBB requirement applies to a portion of the pressurized hardware, sufficient analysis or assessment shall be performed to fully characterize the applicable region and transitional zones to other regions. The rationale for the determination of this worst-case location(s) shall be documented.

Once the locations for test or analysis are chosen, then either analysis or test can be used to demonstrate it, depending on the applicability of LEFM. When analysis or coupon testing is used, a crack of “10t” length ($2c=10t$) must be shown to be stable under pressurized conditions. For a full-scale or subscale pressure vessel test, leak from a crack of any crack length is sufficient.

The “10t” requirement for LBB verification was introduced in NASA fracture control requirements for Space Station (NASA-SSP-30558, Rev. B, 1994). This length requirement is consistent with the condition that a surface flaw with a crack shape $(a/2c) = 0.1$ will not fail as a partial-through crack before it grows through the wall thickness, i.e., when $a = t$. At this condition, the length of crack is $2c = 10t$. For a typical spaceflight metallic pressure vessel, wall thickness is around 0.05 in. Thus, a through-thickness crack with a total length, $2c = 0.5$ in., was considered large enough to cause the fast release of stored fluids, especially helium gases.

The LBB failure mode can be demonstrated by analysis employing the principles of LEFM, i.e., the fracture behavior can be characterized by the stress intensity factor, K , a parameter derived from LEFM. The analysis should show that a surface flaw with a crack shape $(a/2c)$ ranging from 0.1 to 0.5 would not fail as a part-through crack. This implies that all critical regions of a metallic pressure vessel should be shown to have the stress intensity factor calculated for a partial-through crack (i.e., surface flaw), K_{ptc} , with depth “a” equal to thickness t (i.e., $a = t$), is less than or equal to the surface flaw fracture toughness, K_{Ic} . In simple mathematical terms, the first condition can be expressed as:

APPROVED FOR PUBLIC RELEASE – DISTRIBUTION IS UNLIMITED

NASA-HDBK-5010, VOLUME 2, REVISION A

$$K_{ptc} \text{ (for } a = t) < K_{Ie}.$$

The second condition is to show the stress intensity factor of a through-crack

$$K \text{ (for } 2c = 10t) \leq K_c,$$

where K = stress intensity of a through-crack in the opening mode, Mode I,
 $2c$ = total length of the assumed through-crack,
 t = thickness of the hardware, and
 K_c = material's fracture toughness (i.e., most likely mixed-mode fracture toughness).

For metallic pressure vessels, the LBB demonstration can be also done by test. This is usually done when a new material or heat treat condition is used where there is no reliable fracture toughness database. The test specimens used in the LBB demonstration testing can be either coupons or a full-scale article. When coupons are used, their material and fracture properties should be representative of the parent metals, weld-region, and heat-affected zone. The thickness of the test coupons should be also identical to the thickness of the critical regions, determined based on maximum stress and corresponding thickness. The induced surface flaws with various $a/2c$ ratios, ranging from 0.5 to 0.1, should be fabricated using an electric discharge machining (EDM) or equivalent notching process. Pre-cracking procedures should be applied to assure that a fatigue crack has been initiated from the induced notch. Fatigue stress cycles from zero stress to the maximum stress corresponding to MDP based on stress analysis should be applied to the specimen until the surface flaw grows through the thickness of the specimen and becomes a through-thickness crack. Test specimens should be continuously cycled at the same minimum and maximum stresses until $2c \geq 10t$. At this crack size, the specimen should be loaded at maximum stress for a minimum of 5 minutes. If the crack remains stable after a 5-minute hold time, LBB is successfully demonstrated. The LBB test is a fracture test, not a crack-life test; the number of cycles that are applied to the specimens is not a part of the success criteria.

If a full-scale vessel is to be used for testing, the initial flaws are better fabricated on the outer surface of the vessel for easy monitoring of the crack growth. should be placed at the location of peak strain. Usually, the maximum strain occurs at the inner wall, so initial notches should be placed there (perhaps notching the interior of the liner prior to final machining). If the inner and outer wall strains are close, it may be possible to notch the outer wall instead. The cyclic stresses in test will be induced by internal pressure. Charge and discharge of each cycle should be maintained at an appropriate rate. After the surface flaw penetrates the thickness of the metallic pressure vessel, leakage may develop, and the internal pressure of the vessel may drop very fast. When leakage occurs at the crack, then before the crack length propagates to ten times the wall thickness, internal pressure should be maintained by pumping the vessel with more test fluid. If the pump rate increased to its maximum allowable rate and leakage continues without rupture, the test should be discontinued. Under this condition, the LBB failure mode is considered to have been demonstrated. Note that it is not necessary to grow the crack to $10t$ for a full-scale vessel test. Demonstration that leakage has occurred is sufficient evidence of LBB.

When metallic material is in the elastic range, linear elastic fracture mechanics should be used in the failure mode evaluation, i.e., $K \text{ (for } 10t) < K_c$. Here K_c is the plane strain fracture toughness of the material. When plane stress fracture toughness is used, it should correspond to the

APPROVED FOR PUBLIC RELEASE – DISTRIBUTION IS UNLIMITED

NASA-HDBK-5010, VOLUME 2, REVISION A

thickness of interest in the actual application and be approved by the RFCB. Due to lack of reliable toughness data at the small values of thickness for many pressurized components, it has become NASA policy to employ K_{Ic} unless acceptable K_c data exist and have been approved by the RFCB.

For plastically responding metal liners of COPVs, the LBB demonstration should be conducted at the strain levels determined by elastic-plastic analysis for the undamaged state.

If a full-scale COPV is to be used, the initial flaws are better fabricated on the outer surface of the liner using an EDM process before it is overwrapped with composite materials. If there is a large enough opening in the port area for the EDM process, the initial flaws can be fabricated on the inner surface of the liner after the liner is overwrapped.

The initial size and shape of the EDM prefabricated flaws should be carefully selected so that fatigue pre-cracking cycles can be applied to initiate the sharp fatigue crack at the tip of the EDM notch. If a full-scale COPV is used as the test specimen, crack growth should be closely monitored. After the part-through crack penetrates the thickness of the COPV, leakage may develop and the internal pressure of the vessel may drop very fast. Before the crack length reaches ten times the wall thickness, internal pressure should be maintained by pumping the vessel with more test fluid. If the pump rate is increased to its maximum allowable and leakage continues without rupture, the test should be discontinued. Under this condition, LBB is considered to have been demonstrated.

11.1.2 Leak Before Burst Limitations and Considerations

Many pressure vessels are designed to satisfy LBB criteria to allow a vessel to depressurize from a leak safely before catastrophic rupture occurs. Typically, LBB criteria involves the demonstration of sufficient residual strength capability to tolerate a through-the-thickness crack of length $10t$ without rupturing. More specifically, LBB requirements are used to verify that a through-the-thickness crack of length $10t$ remains stable with stress intensities sufficiently below the fracture toughness of the material during its operating environments.

In addition to LBB criteria, proof tests are performed on pressure vessels to screen out hardware with significant defects. Proof testing helps to open material flaws and can relieve crack-closure mechanisms, thus making it easier to detect defects in test and afterwards when performing inspections.

The following considerations for LBB criteria and proof testing are highlighted to increase awareness that catastrophic rupture can occur in pressure vessels, even when LBB and proof test requirements are satisfied. These considerations are introduced here at a top-level and then described in greater detail in the upcoming paragraphs:

1. Verifying residual strength for a through-the-thickness crack of length $10t$ protects for some but not all initial flaws sizes and geometries. As a result, there are defect sizes and aspect ratios that can produce a burst failure even when LBB criteria are satisfied.

APPROVED FOR PUBLIC RELEASE – DISTRIBUTION IS UNLIMITED

NASA-HDBK-5010, VOLUME 2, REVISION A

Catastrophic failure can occur at lower load levels under some nonuniform stress fields.

2. If inspections are not performed after proof testing, there is a potential for flaws with small aspect-ratios ($a/c < 0.2$) to go undetected and result in catastrophic rupture during the life of the vessel.
3. Typical LBB criteria in spaceflight applications are missing the requirement to determine the leak rate for the through-the-thickness crack and to verify that leak can be detected before exceeding the residual strength of the vessel. This is of particular importance if the vessel will be repressurized/refilled during ground operation or in flight, when it will be subjected to dynamic loads afterwards, or when e.g., timely switch to a back-up system is required.

11.1.3 Initial Flaw Sizes, Geometries, and Failure Modes

A crack-like defect that extends across the surface and some depth into the cross section is the most common geometry assessed for pressure vessel defects. The crack half-length is defined as c , where $2c$ is the total crack length. The crack depth is defined as a . The ratio of the crack depth to the crack half-length, a/c , describes the shape of the surface crack and refers to the crack's aspect ratio. The depth of a surface crack when normalized by the thickness refers to the amount of the cross section penetrated by the surface crack, a/t .

A first order approximation can be made to estimate the sizes and shapes of cracks that are covered by the $10t$ residual strength requirement. When $a = t$ and $2c = 10t$, the aspect ratio of the crack is $a/c = t/5t = 0.2$ (see Figure 11.1-1, Illustration of Full Through-Crack of $10t$ Length (shown in blue), and Elliptical Part Through-Crack of $2c = 10t$ (shown in orange)).

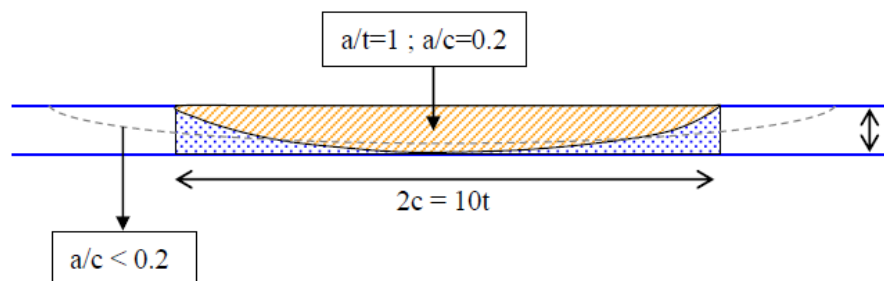


Figure 11.1-1—Illustration of Full Through-Crack of $10t$ Length (shown in blue), and Elliptical Part Through-Crack of $2c = 10t$ (shown in orange)

One interesting issue with the assessment of crack growth and verification of leakage or burst failure mode is the relationship of the failure mode to the initial crack aspect ratio. Orange, et al., performed cryogenic tests of aluminum and titanium alloy tensile coupons and observed that there are certain geometries of surface cracks that can rupture at a lower load than a through-the-thickness crack of the same length. From the coupon testing performed, a crack's aspect ratio can be used to infer the failure mode that would occur in thin cross-sections and when a failure mode

NASA-HDBK-5010, VOLUME 2, REVISION A

would shift from leakage to rupture. The analyst must be cognizant that LBB assumptions do not always guarantee an LBB failure mode, and that this depends on the crack's aspect ratio. In addition, researchers that studied size and shape of initial flaws were able to produce burst failures prior to leakage (see NASA/CR-1999-209427).

The following examples from the literature are consistent with Orange, et al.'s observations that failure mode can transition from leak to burst in actual hardware for cracks with low aspect ratios:

1. Pressure testing was performed on three retired SSME high pressure oxidizer ducts made of Inconel®-718 with initial flaws with low aspect ratio surface cracks. All three test units failed with a burst failure mode, even though stability of a through-the-thickness crack of 10t limit was predicted (see NASA/CR-1999-209427).
2. Underwood, et al. (1994), observed that deep cracks with short lengths (cracks with high aspect ratios) exhibited LBB failure modes in test.
3. Burst failure modes were observed in pipe sections when subjected to internal pressure and externally loaded using a 4-point bend configuration and when circumferential flaws with low aspect ratios were present (see Comprehensive Structural Integrity, 7.10 Leak Before Break, Y. Takahashi].
4. Initial defect sizes and shapes that produce a burst response instead of a leak in pipes with circumferentially oriented flaws have been published in German nuclear industry documents, echoing the propensity for low aspect ratio cracks to result in a burst failure mode (see Comprehensive Structural Integrity, 7.10 Leak Before Break, Y. Takahashi].
5. A metallic-lined COPV with low aspect ratio cracks in the liner was filled with water and pressure tested; and the study is based on the Orbiter case study RCS COPV S/N-021. An instantaneous failure of the liner and an instantaneous loss of the pressurized contents were observed. Although the composite overwrap remained intact, possibly due to the low stored energy of the compressed liquid, one could overzealously conclude that the COPV had exhibited an LBB failure mode. It is not known whether the composite overwrap would remain intact under the increased stored energy of a pneumatic application. Recall that an LBB failure mode typically consists of stable crack propagation through the pressure containment wall, followed by a controlled leak that is detectable prior to failure. The burst failure of the liner was consistent with Orange, et al.'s observation for low aspect ratio flaws. Since the leak rate did not permit intervention to mitigate collateral damage and/or loss of a mission critical subsystem, the COPV would not conform to the standard definition of LBB behavior and would need to be accepted based on a dedicated rationale.
6. A demonstration of the 10t LBB requirement in a cryogenically formed spherical tank is provided in Cotter, Leak-Before-Burst Criteria Applied to Cryoformed Pressurant Tanks,

APPROVED FOR PUBLIC RELEASE – DISTRIBUTION IS UNLIMITED

NASA-HDBK-5010, VOLUME 2, REVISION A

AIAA-86-1503. Here, the 301-series stainless steel tank had a nominal diameter of 23 inches with a weldment effective thickness of 0.314 inch. The crack size at leakage was with a large aspect ratio (i.e., $\sim 4.3t$) that led to a leak instead of burst, which was accepted as sufficient instead of $10t$.

11.1.4 Uniform versus Nonuniform Stress Fields

Initial flaw sizes with both $a/t < 1$ and $a/c \leq 0.2$ are bounded by the $10t$ through-the-thickness crack. Figure 11.1-1 provided that 100% of cyclic loading is under tensile stress (i.e., $R \geq 0$, where R is the ratio of minimum stress over maximum stress in the loading cycle). Tensile stresses are common in pressure vessels subjected predominately to internal pressure. In addition, it is common for pressure vessels to have uniform in-plane stress at the crack location and through the thickness of the vessel. Tensile loading and uniform far-field stress tends to promote crack growth in the direction of crack depth, a , instead of the direction of crack length, $2c$. As a result, it is less common for a flaw to grow and transition into a low-aspect ratio configuration that could result in a catastrophic burst failure mode. Note that tensile residual stresses, when present, increase damage accumulation and reduce the residual strength of the vessel, especially when uniform tensile stress fields are present.

The presence of $R \geq 0$ loading in most pressure vessels, combined with compressive residual stresses being more common in metallic liners, helps to explain why the existing LBB requirement has been largely successful to date in traditional pressure vessels. Under these conditions, shifts in failure modes from leakage to rupture due to changes in crack aspect ratio are less likely. Large static strength factors of safety, the absence of undetected rogue defects, proof test requirements, and the low duty cycle nature of most spaceflight applications are additional contributors that have helped to mitigate catastrophic failures.

Now consider nonuniform stresses through the thickness. In these cases, initial flaws with low aspect ratios may be less common but should still be considered in the fracture mechanics assessment. In addition, the shape of cracks (i.e., aspect ratio) can change as a crack propagates, especially when a nonuniform stress field is present at the flaw. It is possible for a flaw to start with a larger aspect ratio and transform to a smaller aspect ratio as the flaw grows which can make catastrophic fracture more possible. Nonuniform stress gradients through the thickness that promote changes in flaw aspect ratio can arise from stiffness discontinuities that result from welding, geometric mismatches and offsets, nonuniform residual stress fields, and/or shape changes (e.g., cylinder/dome transition). A demonstration of how fatigue crack growth changes crack aspect ratio as a function of applied loading and stress gradients has been published (see NASA/TM-102165, Behavior of Surface and Corner Cracks Subjected to Tensile and Bending Loads in Ti-6Al-4V Alloy, 1990). Changes in failure modes as cracks grow has also been identified by the American Petroleum Institute (API) as a limitation in leak before burst requirements. Even though nondestructive inspections performed after proof testing can help to verify the vessel quality and reduce the uncertainty in flaw size and shapes assumed during LBB verification, the effects of nonuniform stress fields and other crack geometry should be evaluated to prevent catastrophic rupture.

NASA-HDBK-5010, VOLUME 2, REVISION A

In cases of significant nonuniform stress and through-thickness variations, a finite element analysis should be used to extract directional stresses and gradients. Fracture codes such as NASGRO® can readily accept stress gradients as part of their inputs and provide a more robust approach than one that relies on the simplifying assumptions of uniform stress (e.g., no spatial and thickness variation), especially in conditions where the stress gradients are known to be nonuniform.

11.1.5 Proof Testing at $1.25 \times \text{MDP}$

Often pressure vessels are proof tested to at least 1.25 times the MDP. Proof tests screen for flaws by either targeting a failure of a particular critical flaw size or opening embedded flaws to be more readily observed through NDE post-test. This test has the potential to screen initial defects that are relatively deep (i.e., a/t approaching 1) even when low aspect ratios (i.e., $a/c < 0.2$) are present. These low aspect ratios are of interest because they can cause failure modes to more readily transition from leakage to burst. Note that static proof testing does not always prevent the cyclic propagation of cracks in service. In addition, one of the challenges with relying on proof testing to screen for flaws is that the presence of residual stresses and local stress gradients can prevent the definitive determination of the flaw sizes that were screened out by the proof test. In addition, variability in fracture toughness properties and the potential for stable tearing responses at flaws in higher toughness materials can make it difficult for flaws to be detected at a macro level. Comprehensive inspections, when performed after proof testing, serve to mitigate the proof test uncertainty by ruling out unacceptable flaws, thus increasing confidence in the vessel's structural integrity for in-service applications.

A successful proof test at $1.25 \times \text{MDP}$ provides a sound measure of vessel quality and has contributed to the success of pressure vessels to date. It does not fully ensure leakage will occur prior to burst, especially when a large number of cycles or nonlinear stress gradients are present.

11.1.6 Leakage Detection

The use of LBB requirements to provide a measure of safety requires that the fluid contents of the pressure vessel be nonhazardous to people and property if a leak were to occur. Even for designs with nonhazardous fluids, an important operational consideration is whether the system is sufficiently monitored so that leakage can be detected prior to vessel failure. To enable closed-loop monitoring without causing a safety hazard for inspectors, the leak rate for unacceptable flaws would need to be understood and able to be detected by the system. Plots of leakage or burst behavior relative to crack size, and whether leak rates are detectable are illustrated in Figure 11.1-2, Schematic Representation of (a) an LBB Response with Detectable Leakage and (b) a Non-LBB Response with Burst Failure Occurring Prior to Leakage Detection. Note that when the critical crack size that causes the pressure vessel to burst is smaller than the crack size of when leakage can be detected, the design does not achieve the level of safety that LBB requirements were intended to provide. Conversely, when the leak rate is sufficiently large and is sufficiently detectable prior to a through-the-thickness crack reaching its critical size for fracture, the vessel can be operated in a safe manner.

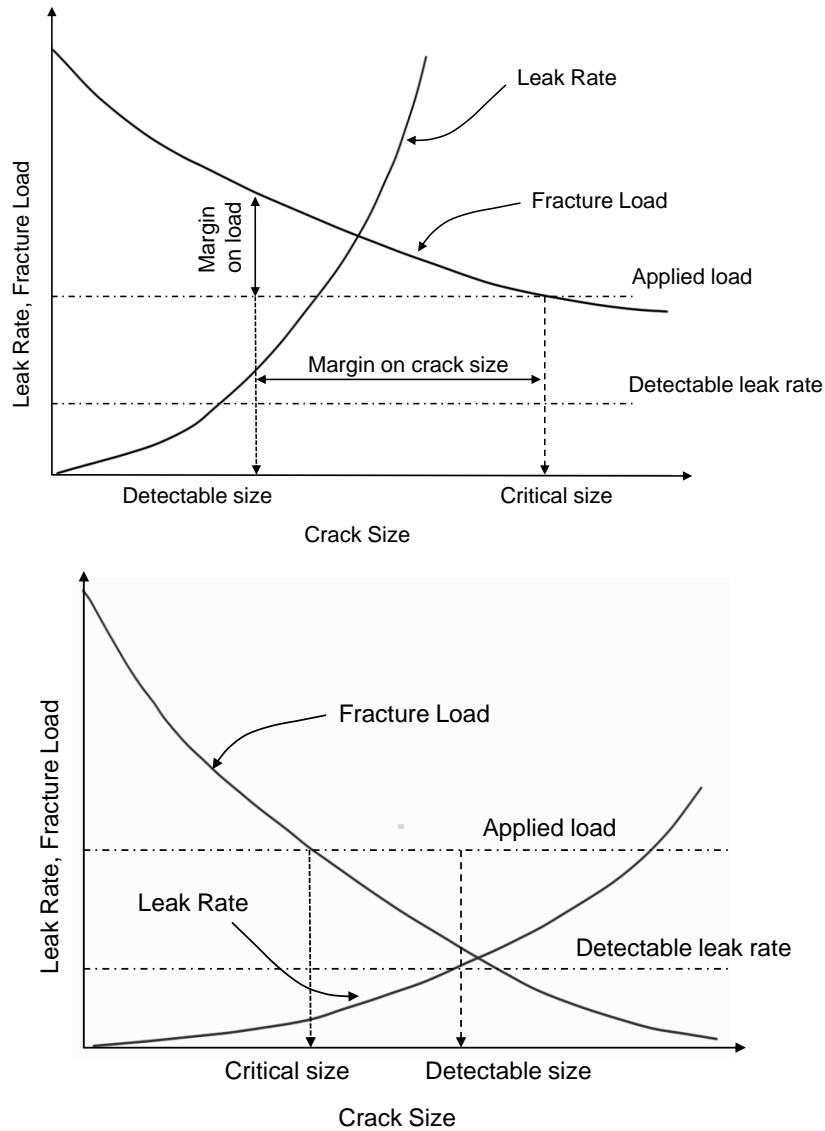


Figure 11.1-2—Schematic Representation of (a) an LBB Response with Detectable Leakage and (b) a Non-LBB Response with Burst Failure Occurring Prior to Leakage Detection

11.1.7 Summary

This section highlighted scenarios when the LBB requirements and the $10t$ criteria need to be applied with caution. These observations are consistent with API recommendations regarding the applicable range of the LBB methodology. API emphasizes that safety of the vessel in LBB designs is achieved through (a) being able to detect leaks, (b) evaluating and mitigating conditions that will cause low aspect ratio cracks from becoming critical under fatigue loading, (c) avoiding through-the-thickness crack leakage scenarios near the unstable region of the material’s fracture toughness (i.e., vertical asymptote of fatigue crack growth curve), and (d)

NASA-HDBK-5010, VOLUME 2, REVISION A

limiting LBB verification to pressure vessels that contain nonhazardous fluids. These factors need to be considered when relying on LBB behavior to ensure system safety.

11.1.8 LBB Examples

11.1.8.1 Example 1: Sharp-Notched Features

In this example, a cylinder containing a sharp notch associated with a partially fusing weld is considered. This example illustrates the implications that sharp-notched features may have on LBB (and also crack-growth).

Consider an aluminum pipe or pressurized cylindrical container, $D_{cyl} = 200$ mm, $t_{cyl} = 10$ mm. It has a partially fusing circumferential weld, with fusion depth $t_{weld} = 2.5$ mm. The question is whether the sharp notch at the weld root (depth $a_{notch} = t_{cyl} - t_{weld} = 7.5$ mm) can act as a crack-like defect and affect the LBB classification of the weld when the cylinder is subjected to uniform axial stress S_{0cyl} . The NASGRO[®] software is used to perform an assessment. The relatively simple NASGRO models have some limitations but can be used to illustrate the fundamentals. See Figure 11.1-3, Welded Aluminum Cylinder with Unfused Depth a ($= a_{notch}$), for the geometry under consideration.

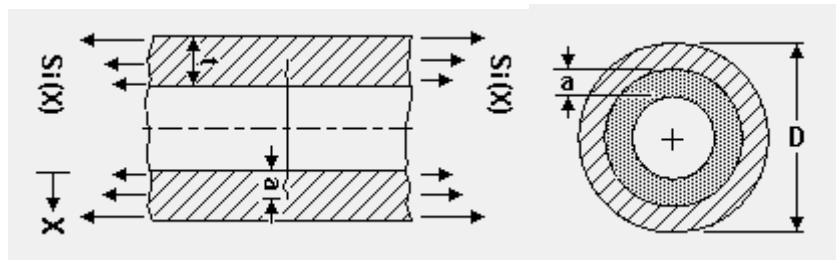


Figure 11.1-3—Welded Aluminum Cylinder with Unfused Depth a ($= a_{notch}$).

For the LBB assessment, a through-thickness crack in the fused, net section, weld thickness t_{weld} is assumed. For the through-thickness crack in the net section of the weld, the axial stress will be dominant. The hoop stress will be maximum of the order of 50% of the axial net section weld stress (in the case that the axial load is caused by internal overpressure only).

The cylinder is designed such that the critical through-thickness crack length, $2c$, is $10t_{weld}$, i.e., 25mm. Using NASGRO[®] model TC08 (see Figure 11.1-4, Through-Thickness Crack in Cylinder Representing the Fused Thickness t_{weld}), with $t = t_{weld} = 2.5$ mm, the net section stress level is determined as $S_{0weld} = 101.5$ MPa, as follows.

The critical crack size $2c = 25$ mm is confirmed by crack-growth analysis using the NASFLA module of NASGRO[®] (with arbitrary starting crack size of 2.5mm and arbitrary stress spectrum), as shown in Figure 11.1-5, Material Definition: Al 2219-T87, GTA Weld (Bk is set to 0, Conservatively), and 11.1-6, Stress Spectrum: $S_{0weld} = 101.5$ MPa (Obtained by Manual Iteration), $R = 0$. This is one of the ways the critical crack size can be determined.

APPROVED FOR PUBLIC RELEASE – DISTRIBUTION IS UNLIMITED

NASA-HDBK-5010, VOLUME 2, REVISION A

TC08

$$S_0 = \frac{P}{2\pi R t}$$

$$S_1 = \frac{4M}{\pi R^3} \frac{1 + \frac{1}{2} \frac{t}{R}}{\left(1 + \frac{1}{2} \frac{t}{R}\right)^4 - \left(1 - \frac{1}{2} \frac{t}{R}\right)^4}$$

$c = \alpha R$
 $R = \text{mean radius} = (D - t)/2$
 $2\alpha = \text{total angle (radians)}$
 $0 < 2\alpha < 3\pi/2 \text{ radians} = 270 \text{ degrees}$
 $\text{Minimum cylinder length} = 2R\sqrt{R/t}$

Outer diameter, D	200	Initial flaw option <input checked="" type="radio"/> User entry <input type="radio"/> NASA std NDE
Thickness, t	2.5	
Poisson ratio, nu	0.3	
Initial flaw size, c	2.5	

Set crack size limit(s):
 SIF Compounding
 Specify secondary cyclic stresses in FAD analysis

Figure 11.1-4—Through-Thickness Crack in Cylinder Representing the Fused Thickness t_{weld}

Material properties: ID M2IFB1AB1, 2219-T87 Plt & Sht; GTA, GMA & PA Welds (2219 filler) Par								
UTS	Yield	K1e	K1c	Ak	Bk	a0	Kth(s)/Kth(l)	
289.6	137.9	973	695	1.	0	0.0381	0.2	
Crack growth parameters: equation constants								
C	n	p	q	DK1	Cth	Cth-	Alpha	Smax/Flow
2.48e-13	3.80	0.25	0.5	34.75	0.0	0.1	2.0	0.3
<input type="checkbox"/> Suppress closure								
<input checked="" type="radio"/> Cth <input type="radio"/> Rth <input checked="" type="radio"/> 0 throughout <input type="radio"/> input cell value throughout								
Threshold Alpha Smax/Flow <input type="text" value="2"/> <input type="text" value="0.3"/>								

Figure 11.1-5—Material Definition: Al 2219-T87, GTA Weld (Bk is set to 0, Conservatively)

Block Case Definition: block 1 of 1						
Enter the number of cycles and values for all stress quantities:						
	Keac chk?	Cycles	S0 at t1	S0 at t2	S1 at t1	S1 at t2
Step 1	<input type="checkbox"/>	100	0	1	0	1
2	<input type="checkbox"/>					
3	<input type="checkbox"/>					
4	<input type="checkbox"/>					
5	<input type="checkbox"/>					
6	<input type="checkbox"/>					
Stress scale factor on stress quantity: S0 <input type="text" value="101.5"/> S1 <input type="text" value="0"/>						

Figure 11.1-6—Stress Spectrum: $S_{0\text{weld}} = 101.5\text{MPa}$ (Obtained by Manual Iteration), $R = 0$

The critical crack size Crack Size $c = 12.5 \text{ mm}$ (i.e., $2c = 25 \text{ mm} = 10t_{\text{weld}}$) is reached after 11158 cycles.

NASA-HDBK-5010, VOLUME 2, REVISION A

Using NASGRO® model SC05, again with $t = t_{\text{weld}} = 2.5$ mm and $S_{0\text{weld}} = 101.5$ MPa, a spot check is performed to confirm that an (arbitrary) initial shallow surface crack of depth $a = 0.635$ mm and aspect ratio $a/c = 0.2$ will not grow to length $2c > 25$ mm before becoming a through-thickness crack. Relevant details are provided in Figure 11.1-7, Surface Crack in Cylinder Representing the Fused Thickness Weld.

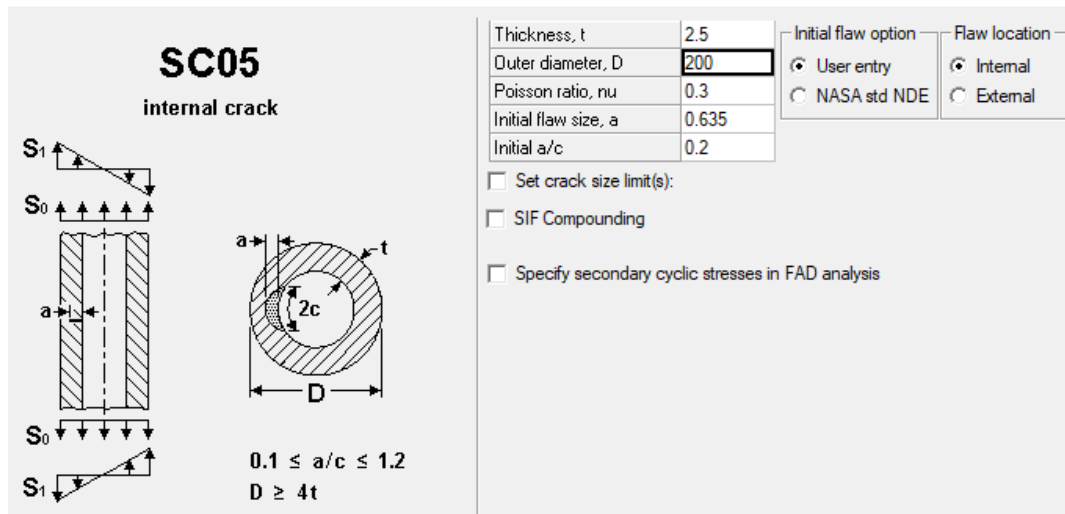


Figure 11.1-7—Surface Crack in Cylinder Representing the Fused Thickness Weld

The material and load spectrum definitions used in NASFLA are the same as used for TC08 above.

The plot of Figure 11.1-8, Results Plot of Crack Sizes (a and c) and Aspect Ratio (a/c) as Function of Load Cycles, shows that the aspect ratio a/c is predicted to increase monotonically, and the crack will break through the surface at length $2c < 10t_{\text{weld}} = 25$ mm. The transition to through-thickness crack (TC08) is for this initial crack size and shape predicted at $c = 4.03$ mm, with $a/c = 0.63$, after 40800 cycles. The critical crack size $c = 12.5$ mm is reached after 45767 cycles.

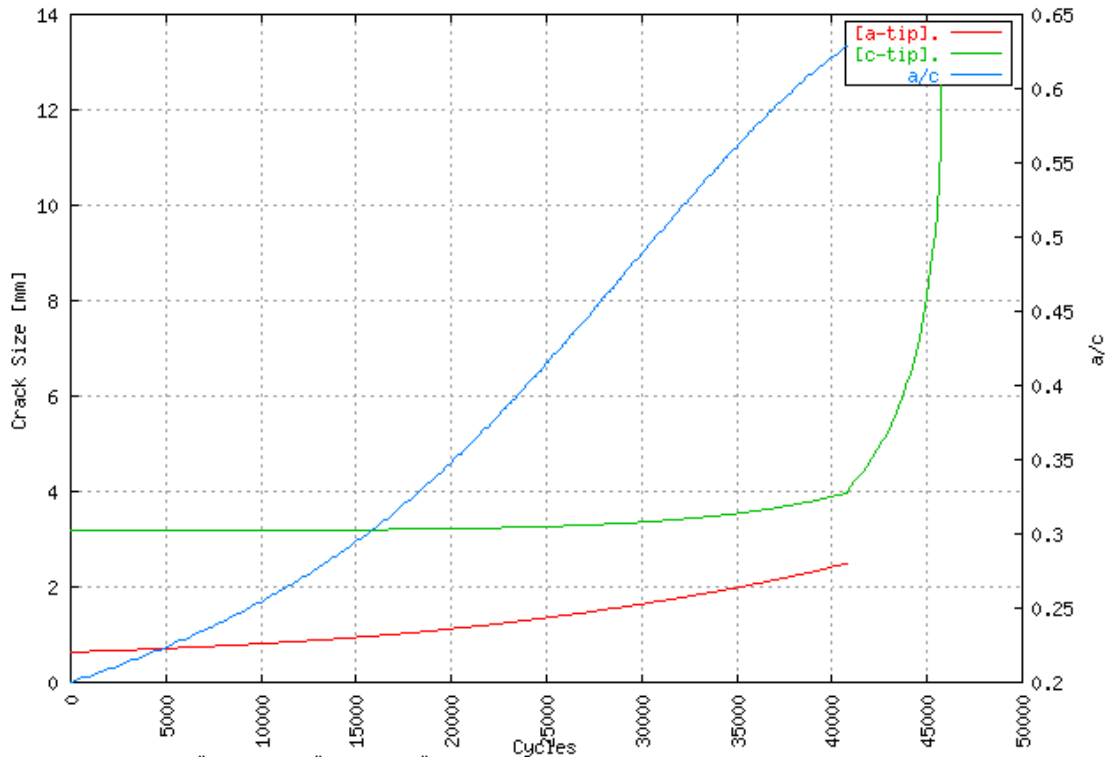


Figure 11.1-8—Results Plot of Crack Sizes (a and c) and Aspect Ratio (a/c) as Function of Load Cycles

The NASSIF module of NASGRO® predicts for the initial crack of $a = 0.635$ mm, $a/c = 0.2$: $K(a) = 161 \text{ MPa}\sqrt{\text{mm}}$ (depth), $K(c) = 87 \text{ MPa}\sqrt{\text{mm}}$ (surface). This confirms the tendency to grow in thickness faster than in circumferential direction.

The above assessment could lead to the conclusion that the weld can be considered LBB. It cannot be excluded that the sharp notch at the root of the weld will develop into a crack tip and grow in radial direction, or otherwise affect the growth of the surface crack, especially by accelerating growth along the surface (c-direction). To assess whether this could invalidate the LBB assessment, an assessment is performed as recommended by flaw assessment procedures like FITNET™ and the British standard BS7910, Guide to methods for assessing the acceptability of flaws in metallic structures. See Figure 11.1-9, Example Characterization of a Complex Flaw.

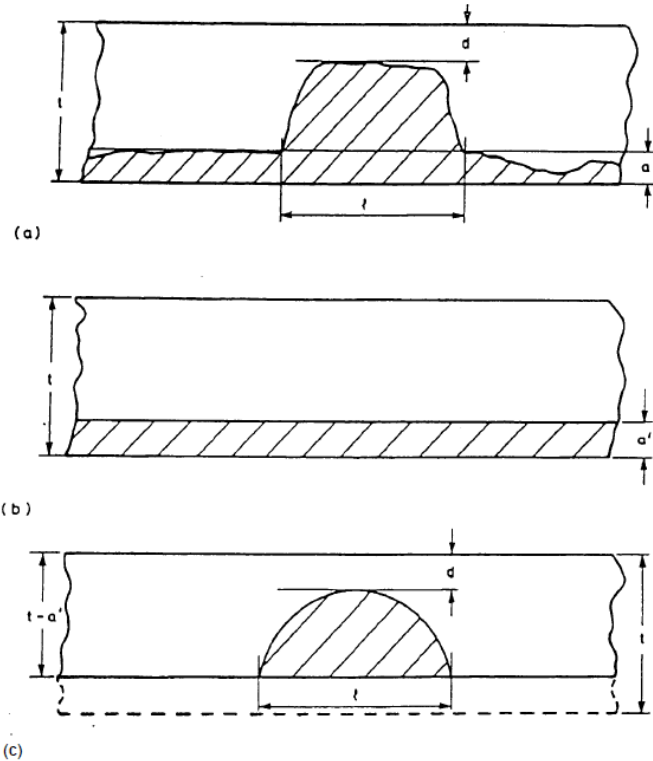


Figure 11.1-9—Example Characterization of a Complex Flaw

(The complex flaw in (a) may be separately assessed as the two simple flaws in (b) and (c). Assessment of flaw (c) is performed, using SC05, although that model may underestimate secondary bending in the weld due to the notch. Flaw (b) can be assessed using NASGRO® model SC06.)

The sharp notch created by the partial fusion can start to act as a crack front, that can be modeled as SC06, applying $S_{0\text{tube}} = 26.37 \text{ MPa}$ (this creates a net section stress of $S_{0\text{weld}} = 101.5 \text{ MPa}$ for $a_{\text{notch}} = 7.5 \text{ mm}$, i.e., the stress applied to flaw type [b]). Relevant details are provided in Figure 11.1-10, Part-Through Crack in Cylinder Representing a Sharp Notch in the Wall Thickness t_{cyl} .

NASA-HDBK-5010, VOLUME 2, REVISION A

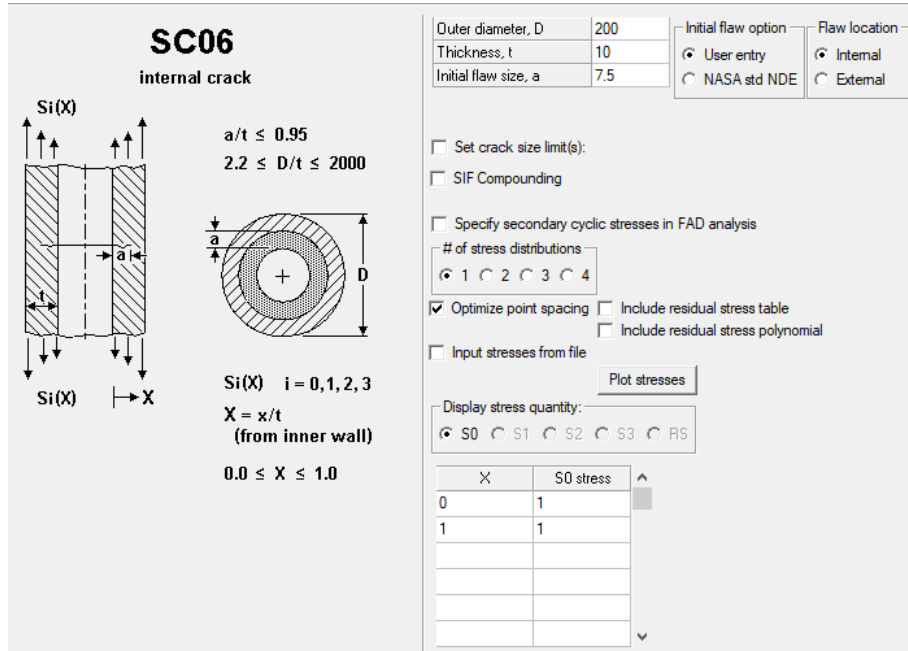


Figure 11.1-10—Part-Through Crack in Cylinder Representing a Sharp Notch in the Wall Thickness t_{cyl}

The material definition used in NASFLA is the same as used for TC08 and SC05 (see Figure 11.1-11, Stress Spectrum: $S_{0tube} = 26.37$ MPa, $R = 0$).

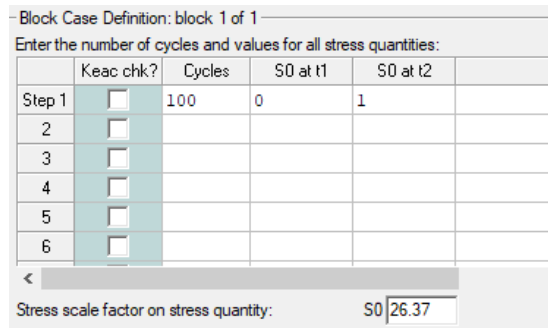


Figure 11.1-11—Stress Spectrum: $S_{0tube} = 26.37$ MPa, $R = 0$

For SC06, NASSIF predicts for $a_{notch} = 7.5$ mm: $K = 315 \text{ MPa}\sqrt{\text{mm}}$. This K, for flaw type ‘(b)’, is much higher than for the surface crack, flaw type ‘(c)’, assessed using SC05 previously. In case crack growth occurs in such situation, there is significant risk that the elliptical crack is at least partially “absorbed” by the developing straight crack front represented by SC06, for which the predicted critical crack size is $a_{crit} = 8.83$ mm (plastic failure mode). This is before leakage is predicted. The predicted number of cycles to failure after developing an effective crack tip is 3497 cycles, i.e., this tends to be much shorter than the life to leakage predicted for the surface crack analysis described above.

NASA-HDBK-5010, VOLUME 2, REVISION A

The LBB failure mode is questionable, unless there are complementary considerations that make it plausible, or make the risk of failure otherwise acceptable. Some additional considerations relevant to LBB verification in the presence of a sharp root notch are:

Fracture software like NASGRO® offers limited options to assess quantitatively the effect of sharp notches that are not yet cracks at the root of a weld. But some additional trends can be investigated using, e.g., the SC27 model as shown in Figure 11.1-12, Input Data for the NASSIF Module of NASGRO®. The symmetric SC27 option is used in this assessment rather than SC26 because it limits secondary bending moments in the net section ($W - 2(d + r)$), more similar to what may happen in a cylinder. The smallest notch tip radius possible within the parameter ranges allowed by the model is selected ($r = 0.3\text{mm}$). Note that the definition of surface crack dimensions a and c is reversed in this model with respect to SC05. Relevant details are provided below in Figure 11.1-13, Surface Cracks (Symmetric) at a (Sharp) Central Notch in a Plate, Approximating a Surface Crack in the Partially Fusing Cylindrical Weld of Thickness t_{weld} , and 11.1-14, Stress Spectrum: $S_{0\text{tube}} = 26.37\text{ MPa}$, $R = 0$.

Select which to compute: Material yield stress

Stress Intensity Factors 137.9

Correction Factors S0

26.37

Select output format: Flaw Sizes, a [max = 2000 comma- or space-delimited entries in table]

Tabulate solutions 7.5

Plot solutions

Figure 11.1-12—Input Data for the NASSIF Module of NASGRO®

NASA-HDBK-5010, VOLUME 2, REVISION A

SC27

$$0.05 \leq \frac{d+r}{B} \leq 0.75$$

$$0.25 \leq \frac{2(d+r)}{t} \leq 2$$

$$0 \leq \frac{d}{r} \leq 24$$

$$B = \frac{W}{2}$$

$$0 \leq \frac{c}{B-d-r} \leq 0.8$$

$$0.5 \leq \frac{a}{c} \leq 10$$

$$0.1 \leq \frac{T}{t} \leq 0.9$$

$$0 \leq \text{Max}\left(\frac{a}{T}, \frac{a}{t-T}\right) \leq 0.9$$

$$X = \frac{x}{B-d-r}$$

$$0.0 \leq X \leq 1.0$$

$$i = 0.1, 2, 3$$

Thickness, t	60
Width, W	20
Hole half-width, d	7.2
Notch tip radius, r	0.3
Hole ctr offset, B	10
Crack ctr offset, T	30
Initial flaw size, a	3.175
Initial a/c	5

Initial flaw option

 User entry
 NASA std NDE

Embedded hole shape

 Straight-edge slot
 Elliptical hole

Set crack size limit(s):
 SIF Compounding

Two symmetric cracks at a centered hole under symmetric stressing

Crack plane stress definition from

 Remote tension Tabular input

of stress distributions

 1 2 3 4

Shakedown choice

 None Automatic

Figure 11.1-13—Surface Cracks (Symmetric) at a (Sharp) Central Notch in a Plate, Approximating a Surface Crack in the Partially Fusing Cylindrical Weld of Thickness t_{weld}

-Block Case Definition: block 1 of 1-

Enter the number of cycles and values for all stress quantities:

	Keac chk?	Cycles	S0 at t1	S0 at t2
Step 1	<input type="checkbox"/>	100	0	1
2	<input type="checkbox"/>			
3	<input type="checkbox"/>			
4	<input type="checkbox"/>			
5	<input type="checkbox"/>			
6	<input type="checkbox"/>			

Stress scale factor on stress quantity: S0

Figure 11.1-14—Stress Spectrum: $S_{0tube} = 26.37$ MPa, $R = 0$

This crack-growth analysis cannot be run until the leaking through-thickness crack due to limitations in the SC27 solution (crack depth $c < 80\%$ of ligament size). The analysis stops at $c = 2.0$ mm (depth), $a = 7.16$ mm (half length), $c/a = 0.280$ after 5861 cycles (see Figure 11.1-15, Results Plot of Crack Sizes (a and c) and Aspect Ratio (a/c) as Function of Load Cycles).

APPROVED FOR PUBLIC RELEASE – DISTRIBUTION IS UNLIMITED

216 of 527

NASA-HDBK-5010, VOLUME 2, REVISION A

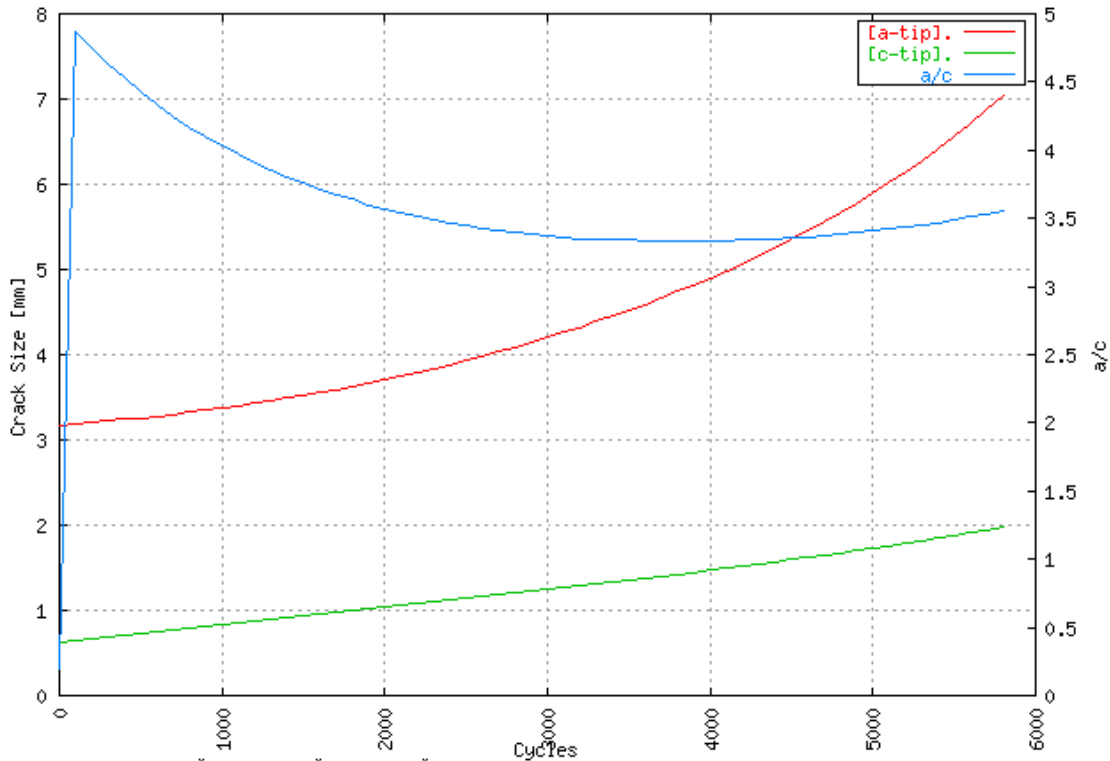


Figure 11.1-15—Results Plot of Crack Sizes (a and c) and Aspect Ratio (a/c) as Function of Load Cycles

This plot illustrates that the aspect ratio c/a is no longer monotonically increasing, as was the case for the SC05 model, and stays closer to 0.2 (or a/c close to 5). There is a tendency to grow more in length before growing through the thickness. This analysis may not be quantitatively valid for the cylinder analyzed above, but it allows to make some observations that support the doubts on LBB validity expressed above.

Figure 11.1-16, Results Plot of $K(a)$ (Surface) and $K(c)$ (Depth) as Function of Load Cycles, shows the plot of $K(a)$ (surface) and $K(c)$ (depth) as function of load cycles. The K -ratio ($K[\text{depth}]/K[\text{surface}]$) indicates the tendency for shape change during fatigue crack growth. An increasing ratio indicates a stronger trend to grow from aspect ratio 0.2 toward 1.0, i.e., semi-circular crack, while growing through the thickness. When a/c drops below 0.2, there is a risk that the crack will grow longer than $10t$ before growing through the thickness, putting the LBB verification in question.

NASA-HDBK-5010, VOLUME 2, REVISION A

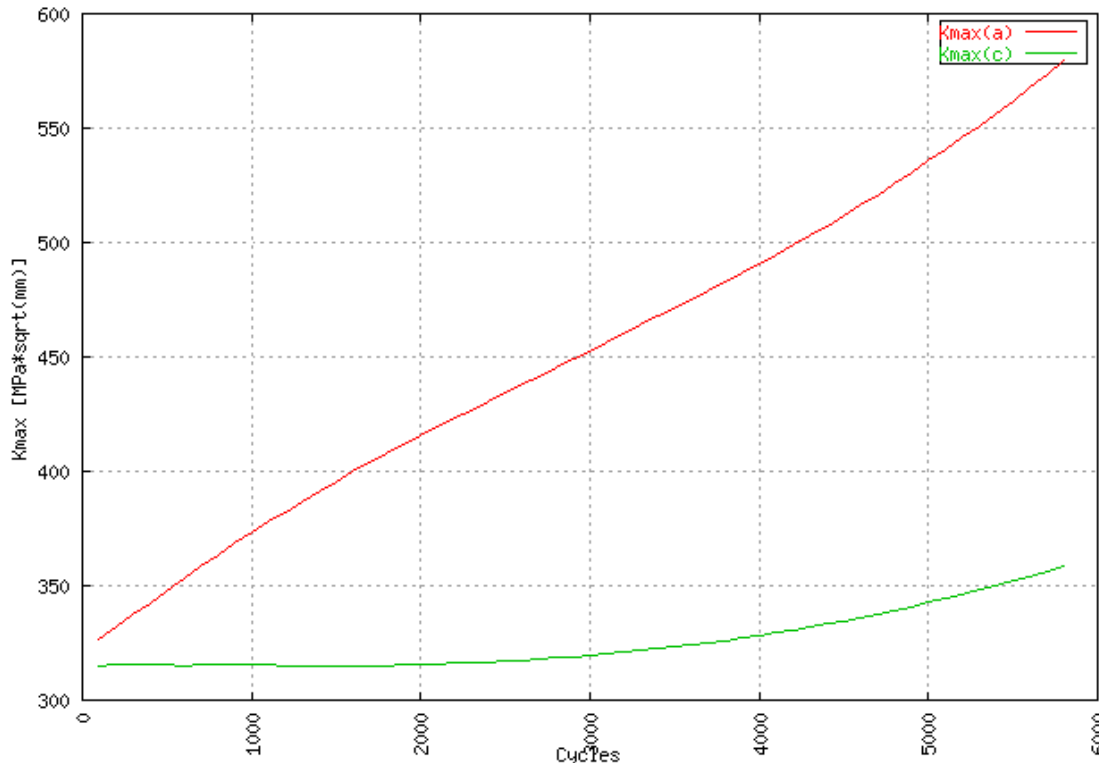


Figure 11.1-16—Results Plot of K(a) (Surface) and K(c) (Depth) as Function of Load Cycles

In this example based on SC27, the initial K-ratio is $314/321 = 0.98$, providing a slight (initial) tendency to remain above $a/c = 0.2$.

For less sharp notches with same depth, but radius different from 0.3mm, the K-ratio tends to increase, as expected: from 0.98 ($r = 0.3$ mm) via 1.47 ($r = 2.5$ mm) to 1.66 ($r = 7.5$ mm, i.e., semi-circular notch). It can be noted that at the same time the number of cycles to reach $c = 2$ mm crack depth increases from 5861 cycles ($r = 0.3$ mm) via 7069 cycles ($r = 2.5$ mm) to 12482 cycles ($r = 7.5$ mm).

For the SC05 analysis reported above, which essentially ignores some consequences of the presence of the notch, the corresponding K-ratio is much higher: $161/87 = 1.85$. It can be noted that the predicted cycle life until 2mm crack depth is 35200 cycles, i.e., much longer (even if not fully comparable).

11.1.8.2 Example 2: LBB Issues with Secondary Bending

In this example, LBB issues in the presence of significant secondary bending is discussed. This example illustrates further implications that sharp notched features may have for LBB verification.

The fact that significant nonuniform stress and through-thickness variations can cause cracks to grow shallower than assumed in the traditional LBB verification can be illustrated as follows, using the SC26 model of the NASGRO® software.

APPROVED FOR PUBLIC RELEASE – DISTRIBUTION IS UNLIMITED

NASA-HDBK-5010, VOLUME 2, REVISION A

Consider a pressurized container that has a flat aluminum wall with a stress concentrator, a notch similar to the previous cylindrical example. Potential limitations of the traditional LBB verification can be highlighted using the SC26 model of the NASGRO® software. In this example, when compared with the previous cylindrical example with notch, higher secondary bending stresses will be introduced into the notched net section ($W - (d + r)$) in addition to the stress concentration due to pure tension. Relevant details are provided below. See Figures 11.1-17, Surface Crack at a (Sharp) Edge Notch in a Plate, 11.1-18, Material Definition: Al 7075-T7351 (B_k is set to 0, conservatively), and 11.1-19, Stress Spectrum: $S_{0plate} = 10$ MPa, $R = 0$.

SC26

$0 \leq \theta \leq 75^\circ$

$0 < \frac{d+r}{W} \leq 0.75$

$0 \leq \frac{d}{r} \leq 24$

$\frac{c}{W-d-r} \leq 0.95$

$0.1 \leq \frac{T}{t} \leq 0.9$

$\frac{a}{T} \leq 0.95$

$\frac{a}{t-T} \leq 0.95$

$0 < \frac{c}{a} \leq 8$

$X = \frac{x}{W-d-r}$

$0.0 \leq X \leq 1.0$

$i = 0, 1, 2, 3$

Thickness, t	1000
Width, W	10
Notch depth, d	7.2
Notch tip radius, r	0.3
Crack ctr offset, T	500
Initial flaw size, a	3.175
Initial a/c	5

Initial flaw option

 User entry
 NASA std NDE

Notch shape

 Angular Elliptical

Set crack size limit(s):
 SIF Compounding

Crack plane stress definition from

 Tension, bend Polynomial Tabular input

of stress distributions

 1 2 3 4

Shakedown choice

 None Automatic

Figure 11.1-17—Surface Crack at a (Sharp) Edge Notch in a Plate

Material properties: ID M7HH11AB1, 7075-T7351 Plt; L-T; LA/DA

UTS	Yield	K1e	K1c	Ak	Bk	a0	Kth(s)/Kth(l)
503.3	434.4	1529	1112	1.	0	0.0381	0.2

Crack growth parameters: equation constants

C	n	p	q	DK1	Cth	Cth-	Alpha	Smax/Flow
1.899e-1	2.90	0.5	0.5	24.32	2.00	0.1	2.0	0.3

Suppress closure

Threshold fanning exponent

 Cth Pth

Cth value used in analysis

 0 throughout
 input cell value throughout

Threshold

Alpha	Smax/Flow
2	0.3

Figure 11.1-18—Material Definition: Al 7075-T7351 (B_k is set to 0, Conservatively)

NASA-HDBK-5010, VOLUME 2, REVISION A

Enter the number of cycles and values for all stress quantities:

	Keac chk?	Cycles	S0 at t1	S0 at t2	S2 at t1	S2 at t2
Step 1	<input type="checkbox"/>	100	0	1	0	1
2	<input type="checkbox"/>					
3	<input type="checkbox"/>					
4	<input type="checkbox"/>					
5	<input type="checkbox"/>					
6	<input type="checkbox"/>					

<

Stress scale factor on stress quantity: S0 S2

Figure 11.1-19—Stress Spectrum: $S_{0plate} = 10 \text{ MPa}$, $R = 0$

This crack-growth analysis cannot be run until through-thickness crack, due to limitations in the SC26 solution (crack depth $c < 95\%$ of ligament size). The analysis stops at $c = 2.38 \text{ mm}$ (depth), $a = 20.3 \text{ mm}$ (half length), $c/a = 0.117$ after 4960 cycles. The crack length $2a = 40.6 \text{ mm}$ is already well beyond $10t_{notch} = 25 \text{ mm}$.

The plot in Figure 11.1-20, Results Plot of Crack Sizes (a and c) and Aspect Ratio (a/c) as Function of Load Cycles, illustrates that the aspect ratio c/a is not monotonically increasing, and drops significantly below 0.2 (i.e., a/c increases beyond 5), so there is a strong tendency to grow more in length before growing through the thickness. This analysis supports the doubts on LBB validity at sharp stress raisers expressed before.

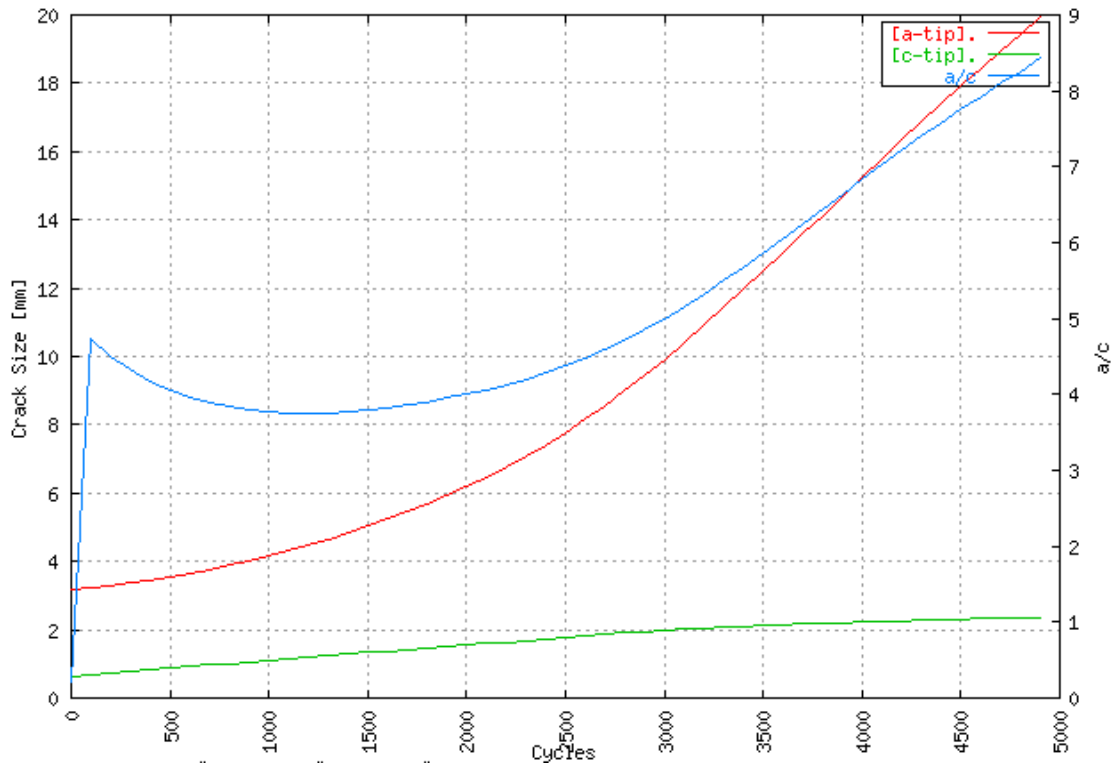


Figure 11.1-20—Results Plot of Crack Sizes (a and c) and Aspect Ratio (a/c) as Function of Load Cycles

In this example based on SC26, the initial K-ratio is $503/575 = 0.87$, which will further decrease during crack growth as the gap between K(a) and K(c) widens (see Figure 11.1-21, Results Plot of K(a) (Surface) and K(c) (Depth) as Function of Load Cycles). This confirms the predicted trend for the crack to grow shallower.

NASA-HDBK-5010, VOLUME 2, REVISION A

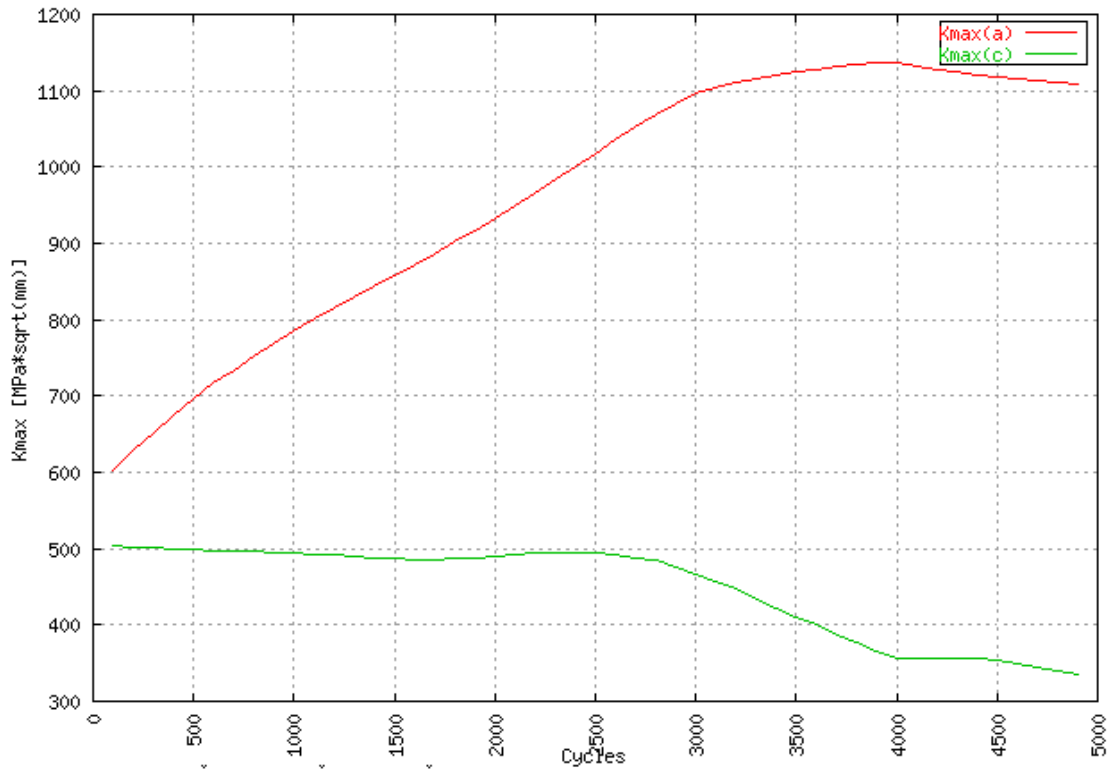


Figure 11.1-21—Results Plot of $K(a)$ (Surface) and $K(c)$ (Depth) as Function of Load Cycles

11.1.8.3 Example 3: LBB Issues with Stiffened Plates

Figure 11.1-22, Through-Thickness Crack in Flat Wall of Thickness t_{plate} , with Stiffeners Omitted, illustrates the implications that stiffeners (or more generally: nonuniform thickness) may have on LBB verification.

Consider a pressurized container that has a flat aluminum wall with integral blade stiffeners. This can be idealized as a wide plate, $W = 1000$ mm, of thickness $t_{plate} = 5$ mm and with a stiffener of $h_{stiff} = 30$ mm and $t_{stiff} = 5$ mm on top of the plate.

LBB verification becomes challenging if it has to be considered that the crack may originate in the stiffener, and the stiffener may be fully cracked prior to development of a crack and leakage of the skin.

NASA-HDBK-5010, VOLUME 2, REVISION A

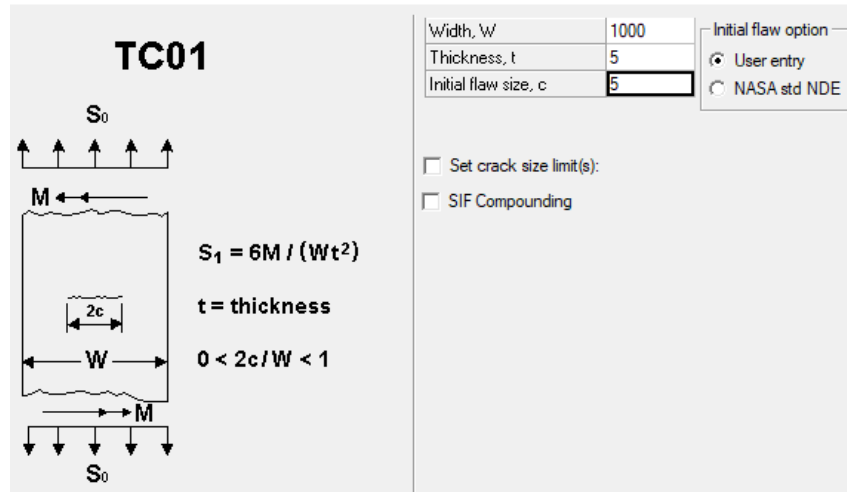


Figure 11.1-22—Through-Thickness Crack in Flat Wall of Thickness t_{plate} , with Stiffeners Omitted

In locations away from the stiffener, the uniform stress that allows a stable through-thickness crack of length $2c = 10 = 50$ mm is $S_{0LBB} = 125$ MPa. Note that this is $125/503.3 = 25\%$ of the ultimate tensile strength (UTS) provided in the NASGRO® database (nominal strength value). (See Figure 11.1-23, Stress Spectrum: $S_{0LBB} = 125$ MPa (Obtained by Manual Iteration), $R = 0$).

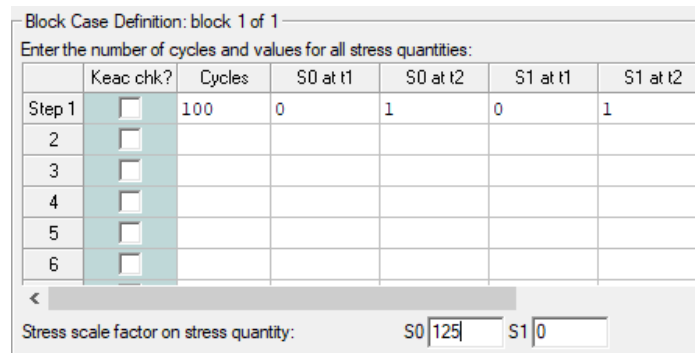


Figure 11.1-23—Stress Spectrum: $S_{0LBB} = 125$ MPa (Obtained by Manual Iteration), $R = 0$

For assessment of plate cracks caused by a cracked integral stiffener, crack-growth software based on relatively simple cracked geometries, like NASGRO® and similar, offers limited options currently. For example, the NASGRO® model TC39 (T-section) cannot handle a fully cracked stiffener at this time.

The simplest way to represent the effect of the stiffener is then to use the TC11 model of the NASGRO® software (see Figure 11.1-24, Through-Thickness Crack in a Plate, Allowing Local Introduction of the Stiffener Load). This model allows to apply to the crack faces a stress that represents the load contained in the broken stiffener. The stress is distributed over a width equal to the stiffener thickness $t_{stiff} = 5$ mm. This will provide a simplified assessment that may provide reasonable results if, e.g., bending effects (including secondary bending as a result of cracking) can be considered minor (which may not be the case). It assumes that the force inside the stiffener is applied directly to opposite crack surfaces.

NASA-HDBK-5010, VOLUME 2, REVISION A

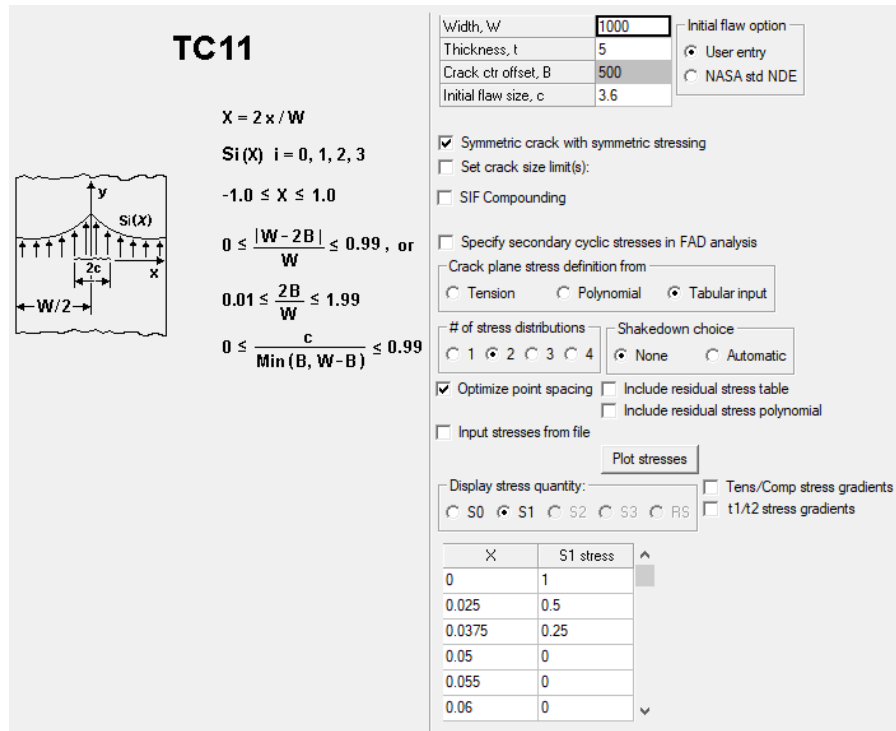


Figure 11.1-24—Through-Thickness Crack in a Plate, Allowing Local Introduction of the Stiffener Load

The force contained in the stiffener is $P = S_{0LBB} \cdot h_{stiff} \cdot t_{stiff} = 18750 \text{ N}$. When distributed over an area of $t_{stiff} \cdot t_{plate} = 5 \text{ mm} \cdot 5 \text{ mm}$ the equivalent stress to be applied is: $S_{1stiff} = 18750 / (5 \times 5) = 750 \text{ MPa}$. This is added to the uniform $S_{0LBB} = 125 \text{ MPa}$. Simply distributing the stiffener load over the stiffener width of 5 mm predicts a high peak in K at the edge of the stiffener at $c = 2.5 \text{ mm}$, exceeding considerably the one considered for the initial LBB assessment—more than double the toughness of Al 7075 plate. See Figure 11.1-25, Plot of K as Function of Crack Length, TC11, Uniform Stiffener Stress Distribution S₁ over $t_{stiff} = 5 \text{ mm}$. The highest risk is predicted for relatively small crack length, as the stiffener crack grows into the plate.

NASA-HDBK-5010, VOLUME 2, REVISION A

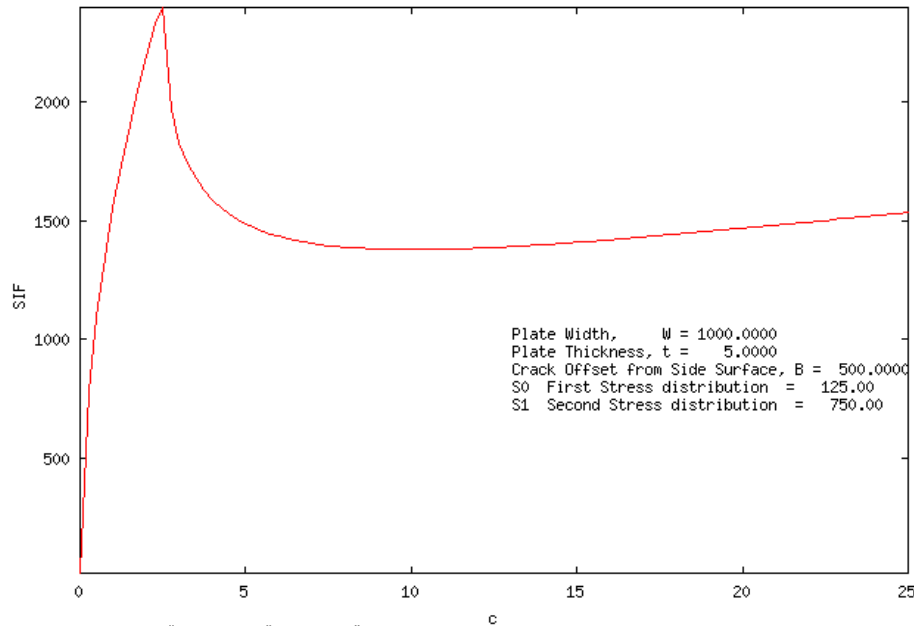


Figure 11.1-25—Plot of K as Function of Crack Length, TC11, Uniform Stiffener Stress Distribution S_1 over $t_{\text{stiff}} = 5$ mm

A knockdown factor of 0.456 on S_{OLBB} is calculated, resulting in an allowable LBB stress of 57 MPa that allows to survive the predicted peak in K.

In fact, this is likely to be conservative, as a fully cracked stiffener will start to shed some of its load into the skin before reaching the crack flange. As stated before, it ignores possible secondary bending effects due to a cracked stiffener, which could make the situation significantly worse.

To assess whether a reduction of the predicted peak in K can be justified, an additional assessment is made, considering a less severe triangular distribution (S_1) of the stiffener load over the LBB crack length of $2c = 10t_{\text{plate}} = 50$ mm. The peak stress level for S_1 is then $18750 / (0.5 * (50 * 5)) = 150$ MPa. The corresponding uniform plate stress remains $S_{OLBB} = 125$ MPa. (See Figure 11.1-26, Stress Distribution Plot: Triangular Distribution S_1 of Stiffener Load over $2c = 10t_{\text{plate}} = 50$ mm Crack Length (Left Half not Shown)).

NASA-HDBK-5010, VOLUME 2, REVISION A

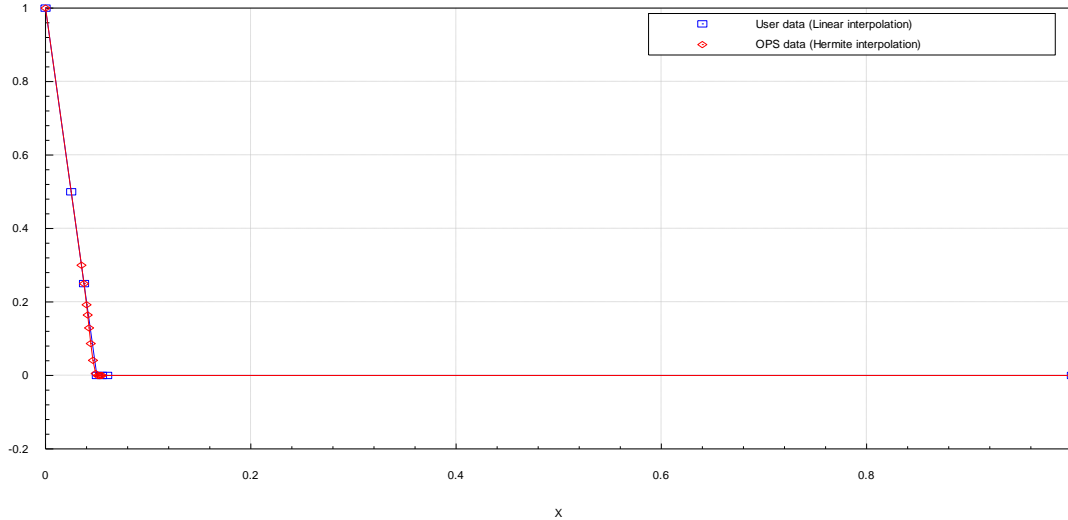


Figure 11.1-26—Stress Distribution Plot: Triangular Distribution S_1 of Stiffener Load over $2c = 10t_{plate} = 50$ mm Crack Length (Left Half not Shown)

The NASFLA module of NASGRO® is again used iteratively to determine a factor on the previously determined ‘LBB stress’ $S_{0LBB} = 125$ MPa. (See Figure 11.1-27, Stress Spectrum: Factor on Stress that Allows Crack-Growth of $2c$ up to ‘ $10t_{plate}$ ’, $R = 0$).

Block Case Definition: block 1 of 1

Enter the number of cycles and values for all stress quantities:

	Keac chk?	Cycles	S0 at t1	S0 at t2	S1 at t1	S1 at t2
Step 1	<input type="checkbox"/>	100	0	125	0	150
2	<input type="checkbox"/>					
3	<input type="checkbox"/>					
4	<input type="checkbox"/>					
5	<input type="checkbox"/>					
6	<input type="checkbox"/>					

< Stress scale factor on stress quantity: S0 S1

Figure 11.1-27—Stress Spectrum: Factor on Stress that Allows Crack-Growth of $2c$ up to ‘ $10t_{plate}$ ’, $R = 0$

The resulting knockdown factor to account for the possibility of a cracked stiffener is now 0.702, i.e., 154% of the factor defined based on the assumption of more concentrated stiffener load application. This results in an allowable LBB stress of 88 MPa.

Figure 11.1-28, Plot of K as Function of Crack Length, TC11, Triangular Stiffener Stress Distribution over ‘ $10t_{plate}$ ’, indicates that this assumption predicts a monotonically increasing K and does not predict any risk of failure at shorter crack lengths.

NASA-HDBK-5010, VOLUME 2, REVISION A

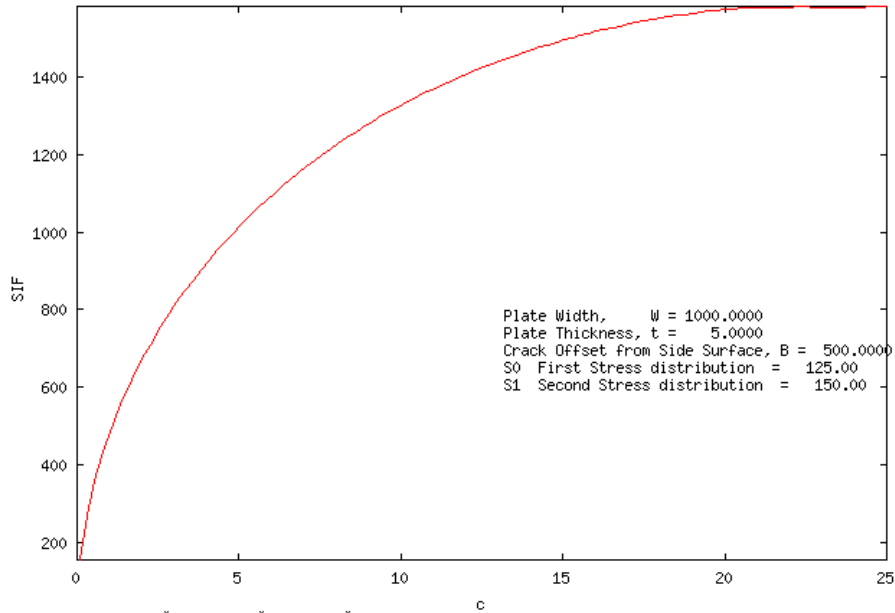


Figure 11.1-28—Plot of K as Function of Crack Length, TC11, Triangular Stiffener Stress Distribution over ‘10t_{plate}’

Another approach to predict the allowable LBB stress for a stiffened plate can be attempted using the TC23 model of the NASGRO software, Figure 11.1-29, Through-Thickness Crack from a Loaded Hole in a Plate, Allowing Local Introduction of the Stiffener Load. It can also deliver the load contained in the stiffener at the crack plane.

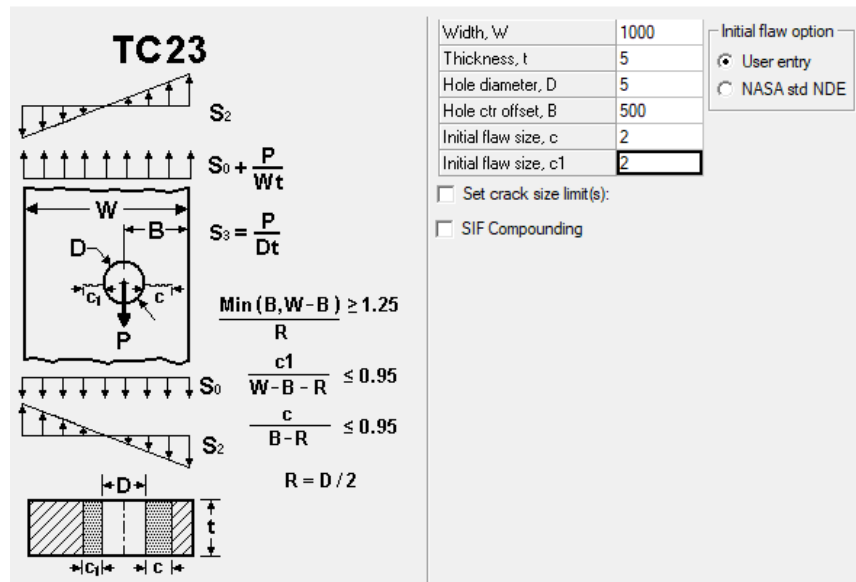


Figure 11.1-29—Through-Thickness Crack from a Loaded Hole in a Plate, Allowing Local Introduction of the Stiffener Load

NASA-HDBK-5010, VOLUME 2, REVISION A

The TC23 model will predict a $K = 0$ at the edge of the hole, which will not be fully representative of the cracked plate at the stiffener, but which will rapidly increase similar to the first analysis using TC11.

The stiffened plate can be simulated by a superposition of a number of elementary cases (see Figure 11.1-30, The Plate with a Cracked Stiffener can be Addressed by the Superposition of 3 Crack Cases [Item a], where the 2 Pin Load Cases Provide Identical K [Item b]), which can all be represented by the TC23 model. The LBB crack length is $c + c1 + D = 10t_{plate} = 50$ mm. $c = c1 = 22.5$ mm. TC23 will represent the through-thickness crack with remote loading S_0 for c of sufficient size with regard to D : typically when $c/(c + D/2) > 0.3$, in this case $c > (0.3D/2)/0.7 = 1.1$ mm (reference Janssen, Zuidema & Wanhill, "Fracture Mechanics," 2nd ed, 2002).

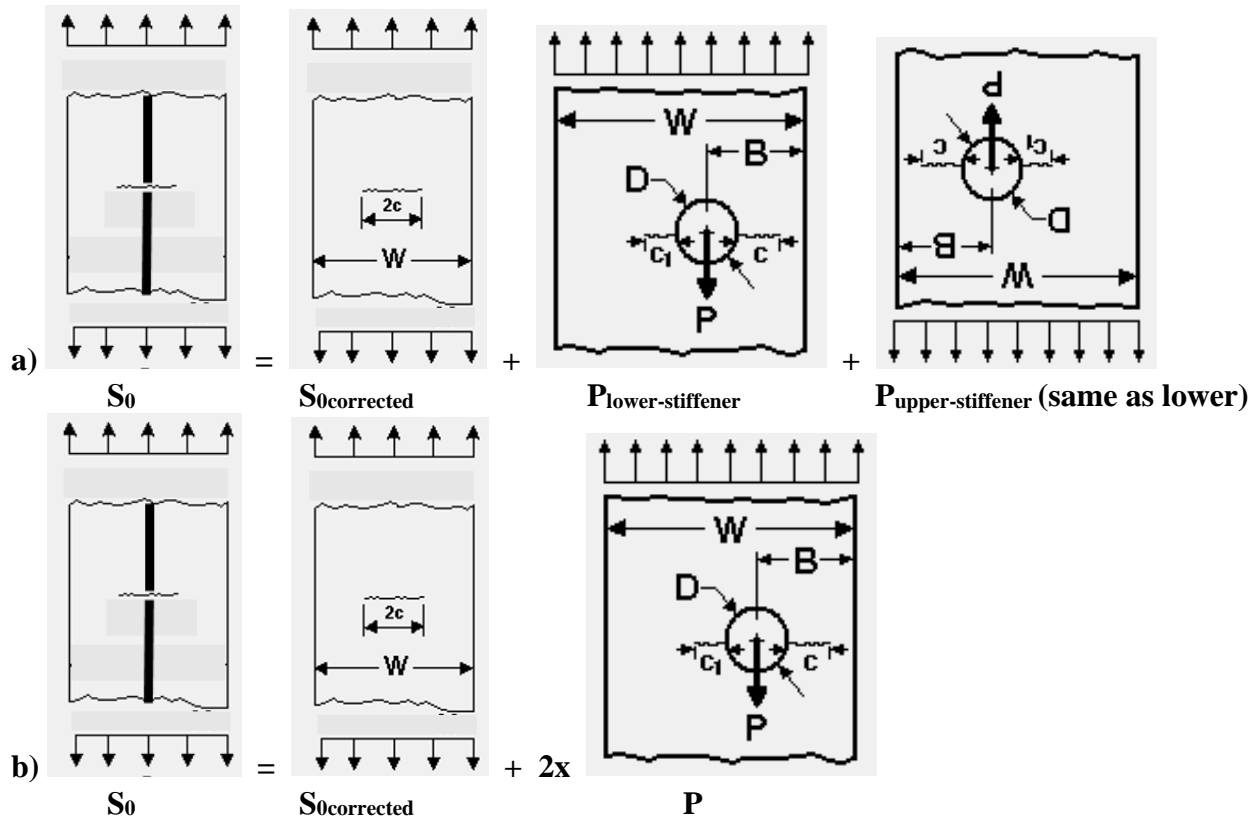


Figure 11.1-30—The Plate with a Cracked Stiffener can be Addressed by the Superposition of 3 Crack Cases (Item a), where the 2 Pin Load Cases Provide Identical K (Item b)

$S_{0LBB} = 125$ MPa is applied to both plate and stiffener. In this superposition, it is assumed that the forces contained in the stiffener ($P = S_0 * h_{stiff} * t_{stiff} = 18750N$), are applied directly to the crack faces, separately for the upper and lower stiffener. This requires a correction of the stress applied to the plate loading: $S_{0corrected} = S_0 - P/(W * t_{plate})$. $P = P_{lower-stiffener} = P_{upper-stiffener}$.
 $S_{0corrected} = 121.25$ MPa.

NASA-HDBK-5010, VOLUME 2, REVISION A

$S_3 = 2P/Dt_{plate} = 2S_0 * h_{stiff} * t_{stiff} / Dt_{plate} = 1500 \text{ MPa}$ (this includes a factor 2 to cover upper and lower stiffeners). (See Figure 11.1-31, Stress Spectrum: Representative of $S_{0panel} = 125 \text{ MPa}$, $R = 0$.)

The critical crack size is predicted as $c = 0.16 \text{ mm}$ (determined using the NASCCS module of NASGRO®). This is smaller than the validity limit of $c > 1.1 \text{ mm}$ (as derived below).

The evolution of K with crack length c is shown in Figure 11.1-32, Plot of K as Function of Crack Length (Add 2.5 mm Offset due to Pin Radius), the K is always above the critical value of $1112 \text{ MPa}\sqrt{\text{mm}}$. For c between 1.1-22.5 mm, the results are not very sensitive to the size assumed for the pin. Investigated are pin diameters 0.1 mm-5 mm, as well as the theoretical solution for discrete forces on opposite crack flanges (note that the theoretical solution for discrete forces on opposite crack flanges tends to go to infinity for crack length approaching zero (reference Janssen, Zuidema & Wanhill, "Fracture Mechanics," 2nd ed, 2002).

Block Case Definition: block 1 of 1

Enter the number of cycles and values for all stress quantities:

	Cycles	S0 at t1	S0 at t2	S2 at t1	S2 at t2	S3 at t1	S3 at t2
Step 1	100	0	1	0	1	0	1
2							
3							
4							
5							
6							

Stress scale factor on stress quantity: S0 | 121.25 | S2 | 0 | S3 | 1500 |

Figure 11.1-31—Stress Spectrum: Representative of $S_{0panel} = 125 \text{ MPa}$, $R = 0$

NASA-HDBK-5010, VOLUME 2, REVISION A

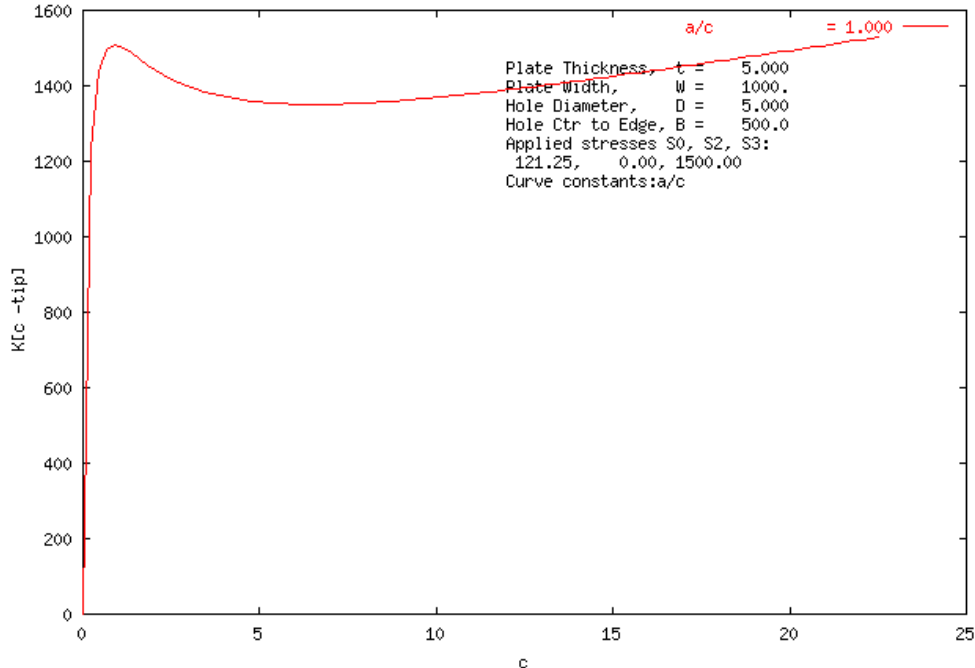


Figure 11.1-32—Plot of K as Function of Crack Length (Add 2.5mm Offset due to Pin Radius)

The NASFLA module of NASGRO is used iteratively to determine a factor on the previously determined ‘LBB stress’ $S_{0LBB} = 125 \text{ MPa}$. (See Figure 11.1-33, Stress Spectrum: Factor that Allows Crack-Growth from $2c = 1.1 \text{ mm}$ to ‘ $10t_{plate}$ ’, $R = 0$).

Block Case Definition: block 1 of 1

Enter the number of cycles and values for all stress quantities:

	Cycles	S0 at t1	S0 at t2	S2 at t1	S2 at t2	S3 at t1	S3 at t2
Step 1	100	0	121.5	0	1	0	1500
2							
3							
4							
5							
6							

Stress scale factor on stress quantity: S0 [0.726] S2 [0] S3 [0.726]

Figure 11.1-33—Stress Spectrum: Factor that Allows Crack-Growth from $2c = 1.1 \text{ mm}$ to ‘ $10t_{plate}$ ’, $R = 0$

The resulting knock-down factor to account for the possibility of a cracked stiffener is 0.726. The corrected ‘LBB stress’ is then $S_{0LBB} = 0.726 * 125 = 91 \text{ MPa}$. It cannot really be concluded that the peak at small c could not be higher, as is suggested by the assessment based on the TC11 model. This transition is not well represented by the pin load model where the crack starts at the pin hole. In reality, there is no pin hole; and the plate material in that area will be cracked also.

A simple 2D boundary element model, using the NASBEM module of NASGRO®, see Figure 11.1-34, SIF Results Based on a Simple 2D NASBEM Model of the Stiffened Plate, indicates

NASA-HDBK-5010, VOLUME 2, REVISION A

that the actual result could be in between the direct crack face loading approach using TC11, and the pin load approach using TC23. This model may also lack accuracy for c approaching 2.5 mm. The model considers the stiffener as zones of increase stiffness. It predicts steep gradients in K near the stiffener, and the results will be sensitive to details of the model.

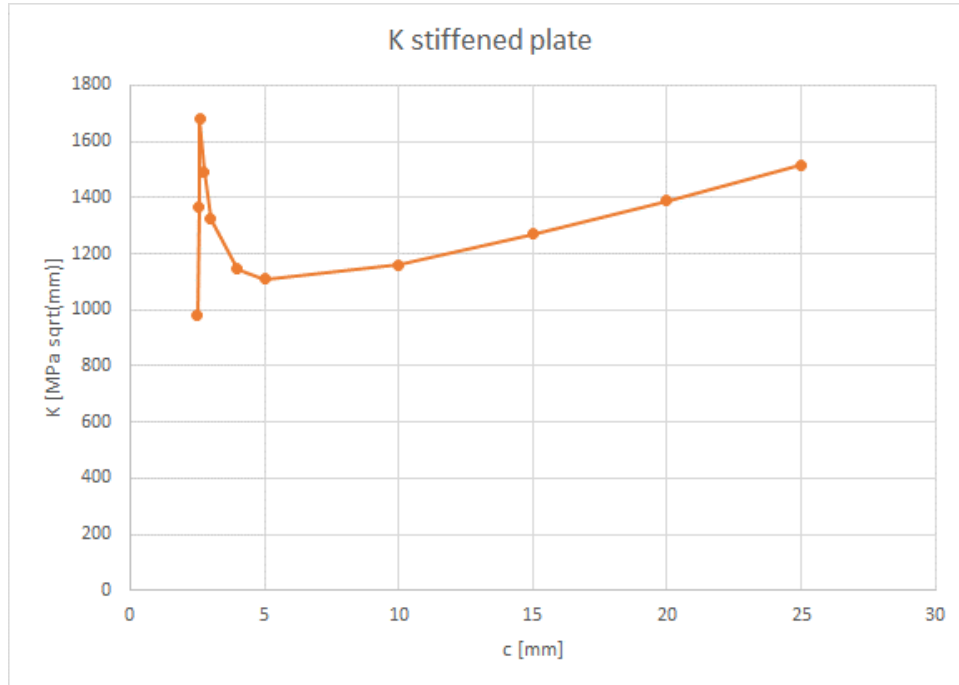


Figure 11.1-34—SIF Results Based on a Simple 2D NASBEM Model of the Stiffened Plate

It can be noted that, for this particular example, all assessment methods provide similar results for the LBB crack length of 50 mm.

In case of marginal results based on the simple approaches offered by TC11 with localized crack face loading, it can be appropriate to model a cracked stiffener in FEM, or other mathematical approaches like the boundary element model (BEM). Either by disconnecting nodes in the stiffeners and feeding the resulting stress distribution of the plate into TC11 as crack-plane stress, or by performing the complete fracture analysis by FE model. The latter especially in case bending effects are judged to be significant.

In practice, there may be more convenient alternative ways to show that stiffeners are sufficiently uncritical, and do not need to be considered in LBB assessments, including:

1. Low risk: the 'LBB stress' in this example is below $0.3 \times UTS$, which is an important prerequisite for the application of the low-risk classification.
2. Damage tolerance: inspection of the stiffeners and verification by crack-growth assessment can allow not having to consider completely cracked stiffeners as part of the LBB assessment of the skin.

NASA-HDBK-5010, VOLUME 2, REVISION A

11.1.8.4 Example 4: LBB Issues with Plate Dominated by Bending Loads

In Figure 11.1-35, Through-Thickness Crack in Flat Wall of Thickness t_{plate} , Submitted to Uniform Tension, LBB issues for a plate dominated by bending loads is discussed. This example illustrates the implications of bending loads on the LBB demonstration. It is mentioned in this section that bending loads can cause shallow crack growth that may affect LBB verification. This can be illustrated using a conventional crack-growth software (NASGRO®) with the example of a flat wall of a pressurized container that is subjected predominantly by bending loads (as can be the case between stiffeners).

Consider that one may assume “conservatively” that the LBB failure mode can be demonstrated as follows: using the peak, outer fiber stress as uniform stress, and demonstrating a critical crack size $> 10t$. Consider an arbitrarily wide aluminum plate $W = 600\text{mm}$ of thickness $t_{plate} = 2.5\text{ mm}$ with a through-thickness crack:

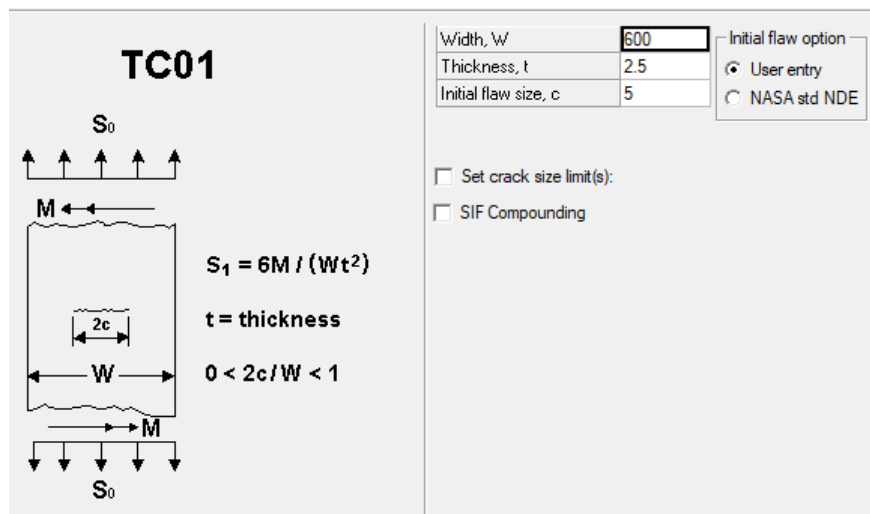


Figure 11.1-35—Through-Thickness Crack in Flat Wall of Thickness t_{plate} , Submitted to Uniform Tension

Two materials are considered in this example: Al 7075 plate and Al 2219 welded based on crack-growth calculation and manual iteration, the following uniform stresses will result in critical crack size of $2c = 10t_{plate} = 25\text{ mm}$: Al 7075 plate: $S_{0LBB} = 177\text{ MPa}$, and Al 2219 weld: $S_{0LBB} = 111\text{ MPa}$.

If, in reality, the loading would be predominantly pure bending, $S_1 = S_{0LBB}$, the question is whether this could result in violation of the LBB demonstration. The critical crack size will increase, but the crack will tend to grow with lower aspect ratio.

To investigate this, plates with initial surface cracks defined by NASA-STD-5009 (arbitrary initial crack size) with aspect ratio $a/c = 0.2$ are subjected to a pure bending spectrum with $S_1 = S_{0LBB}$. (See Figure 11.1-36, Surface Crack in Flat Wall of Thickness t_{plate} , Submitted to Bending, and Figure 11.1-37, Stress Spectrum: Factor on Stress Applied S_{0LBB} as Pure Bending (S_1). $R = 0$.)

APPROVED FOR PUBLIC RELEASE – DISTRIBUTION IS UNLIMITED

NASA-HDBK-5010, VOLUME 2, REVISION A

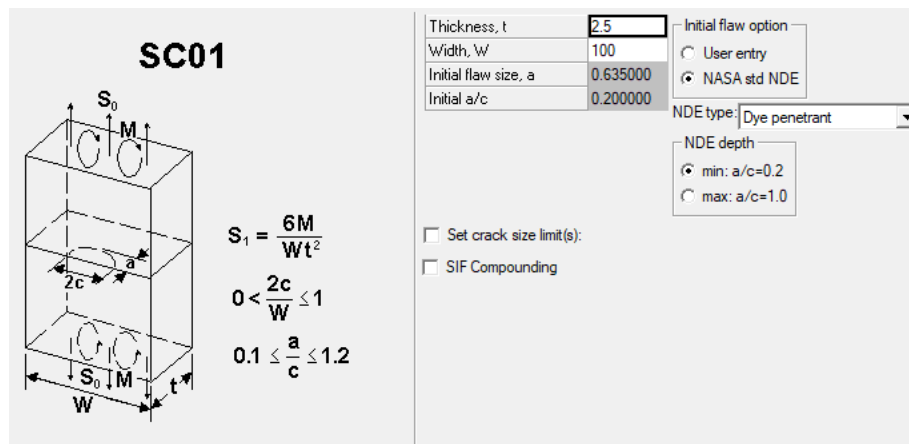


Figure 11.1-36—Surface Crack in Flat Wall of Thickness t_{plate} , Submitted to Bending

Block Case Definition: block 1 of 1

Enter the number of cycles and values for all stress quantities:

	Keac chk?	Cycles	S0 at t1	S0 at t2	S1 at t1	S1 at t2
Step 1	<input type="checkbox"/>	100	0	1	0	1
2	<input type="checkbox"/>					
3	<input type="checkbox"/>					
4	<input type="checkbox"/>					
5	<input type="checkbox"/>					
6	<input type="checkbox"/>					

Stress scale factor on stress quantity: S0 S1

Figure 11.1-37—Stress Spectrum: Factor on Stress Applied S_{0LBB} as Pure Bending (S_1). $R = 0$

For the Al 7075 plate, the following result is obtained:

1. The surface crack becomes a through-thickness crack at length $2c = 73.1$ mm at $a/c = 0.0684$, i.e., much longer than $10t_{plate} = 25$ mm. Stability is still predicted when subjected to pure bending.
2. Instability is predicted for a through-thickness crack of length $2c = 97.4$ mm.
3. Whether this can be actually considered to fulfil LBB requirements may depend on additional risk mitigating considerations. For example: Occasional loads of different nature, like tension, could cause failure of a crack that has grown beyond length $2c = 10t$, before the transition to a through-thickness crack. Note that in the case of a 1:1 ratio of bending and tension stress, NASGRO® predicts breaking through the thickness at crack length $2c = 11.9$ mm at $a/c = 0.4217$, i.e., well within $10t_{plate}$. Instability is predicted for a through-thickness crack of length $2c = 44.6$ mm.

APPROVED FOR PUBLIC RELEASE – DISTRIBUTION IS UNLIMITED

NASA-HDBK-5010, VOLUME 2, REVISION A

For the Al 2219 weld, the following result is obtained:

1. The software indicates that there is a risk that surface crack fails when the remaining ligament becomes plastic, prior to leaking, at depth $a = 2.48$ mm and length $2c = 96.7$ mm at $a/c = 0.0513$, i.e., much longer than $10t_{\text{plate}} = 25$ mm.

Note: The associated warning in the NASGRO® software is ‘ADVISORY: Crack depth + Yield zone > thickness’

2. Validity of the LBB assessment is even more questionable in this case, unless additional risk mitigating considerations apply.

11.2 Proof Test Logic

A damage tolerance assessment is performed using the maximum initial flaw size in a component such that the component passes proof test. The adequacy of the component is determined by calculating the amount of sub-critical crack growth incurred during service due to mechanisms such as fatigue, environmental attack, and creep, and up to a critical service flaw size. Proof test logic relaxes inspection requirements because the proof test acts as a flaw screening. Due to the relaxation in inspection requirements performed on the component, it is important to ensure that the proof test is comprehensive. The proof test level can be set such that the maximum initial flaw size can meet four times the service life.

A successful proof test supported by fracture mechanics analysis enables hardware to enter service with a degree of confidence that no flaw will propagate to failure during its service life. Although proof test logic approach should be used with caution, it can be effective in screening critical flaws for the entire service life of the component.

When using proof test logic, the following considerations should be accounted for:

a. *Analysis.* Analysis methodology and material properties should have a high degree of confidence because proof test logic places greater reliance on analysis than on inspections. Note that some stress intensity factor (SIF) solutions may not be conservative in the proof test analysis. For example, NASGRO® SC08 assumes conservatively that the crack is exactly at the stress concentration at the entry of the nut, but that may not be conservative for the proof test analysis when a pre-existing flaw may not be at that same location.

b. *As-Built.* Caution should be exercised in using proof test logic for cases where the material is process sensitive, as one cannot ensure that as-built properties are consistent with the properties used in the proof test logic analysis.

c. *Environmental Factors.* If proof test logic were to be used, proof test load levels should be adjusted to account for environmental differences based on the fracture toughness.

APPROVED FOR PUBLIC RELEASE – DISTRIBUTION IS UNLIMITED

NASA-HDBK-5010, VOLUME 2, REVISION A

d. *Statistics.* Because materials exhibit a degree of variability, the upper-bound fracture toughness should be used in establishing the maximum initial flaw size; if not available, use a value of at least 1.3 x fracture toughness.

e. *Coverage:* All locations need to be sufficiently loaded during proof test, which can be challenging. Overtesting the part in question and those adjacent to the part needs to be considered and judged to be acceptable.

Note: A crack-like flaw can pass proof test, go through engine hot fire, and fail in flight. This is a classic low-cycle fatigue and high-cycle fatigue problem in ductile materials. The larger the proof test factor, the more likely critical flaws will be screened. The lower the proof factor, the more likely a crack can pass proof test and later propagate to a critical flaw size assuming similar crack-growth during the service life.

A limitation of proof test logic relative to wall thickness is discussed. There exists a threshold flaw that will pass proof test without fracturing completely through-the-thickness and without causing a leak. If proof test logic holds, the entire four times service lives can be applied to this initial flaw; and it will not propagate through-the-thickness during the component's entire service life. For thin-walled structures, proof test logic is typically not successful when the proof test factor needs to be unreasonably high to screen critical flaws. Also note that ***proof test logic is not permitted for specific hardware safe-life verifications, including COPVs, metallic pressure vessels, and not recommended for bellows. Usage outside of what is required by the standards requires approval by the FCB.***

The reader is also referred to NASA/CR-1999-209427, Guidelines for Proof Test Analysis, for additional considerations relative to proof test logic.

11.2.1 Example 1

Consider a metallic pipe that has a 4-inch diameter, 0.125-inch wall thickness, and undergoes a 7,500 psi internal pressure during proof testing. During flight, internal pressure is the only significant load on the pipe. In this example, it is evaluated whether proof test can be used as a flaw screening technique. The procedure on how to derive the flaw size and orientation used for the life analysis will also be illustrated. For pipes using proof test as flaw screening, RFCB approval is required.

NASA-STD-5019A permits using a proof test to screen for flaws in certain fracture critical parts. For metallic components, an appropriate proof test followed by a visual inspection can replace other NDE techniques to establish the initial flaw in a life analysis. The initial flaw corresponds to the largest flaw in a critical location that can survive the proof test without unstable crack growth or yielding. If a larger flaw existed, it would lead to failure during the proof test. It can be assumed that any flaw in the hardware after proof is less than or equal to the size of the critical flaw. If there are multiple critical locations and orientations, multiple critical flaws should be characterized and used in the life analysis.

NASA-HDBK-5010, VOLUME 2, REVISION A

It should be noted that few components are easily proof tested. For a fracture critical part, an approach for flaw screening with a proof test must be documented in the FCP and approved by the RFCB. Multiple complexities must be accounted for to accept proof as the only flaw screening method, including environmental effects, temperature, test fixtures, inertial loads, and others. The proof test must load the component such that the entire assembly undergoes stresses that are at least the stress during operation multiplied by the appropriate proof factor. In this example, internal pressure is the only significant load during flight, so a proof test that matches the flight loads is easily conducted with only internal pressure.

The proof test is conducted with the MDP multiplied by a 1.5 proof factor and an ECF. ANSI/AIAA S-080A requires a 1.5 proof factor for lines and fittings. The ECF is based on the knockdown of the strength at the temperature seen by the pipe during flight. For additional requirements of the proof test requirements, see ANSI/AIAA S-080A. In this case, the MDP multiplied by the 1.5 proof factor and the ECF is assumed to give a proof pressure of 7,500 psi.

To determine the largest flaw that can survive proof, the NASCCS module in NASGRO® can be used. The representative geometry and worst-case flaw orientation are chosen. If the worst-case flaw orientation is not clear, multiple flaw orientations should be studied. In this case, the stresses are due to internal pressure. Using the thin-walled assumption for a pressurized cylinder, it can be calculated that the hoop stress is twice the magnitude of the axial stress. The hoop stress drives an axial crack, so only an axial crack (SC04) must be evaluated in this example. Crack aspect ratios of 0.2 and 1.0 and internal and external flaws must be examined. The crack aspect ratios correspond to the minimum and maximum crack aspect ratios for various NDE techniques.

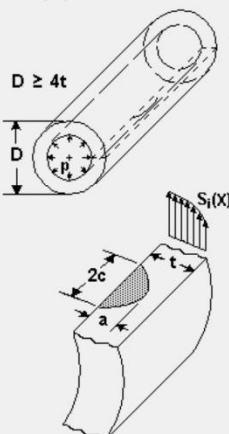
The geometry input for SC04 is shown in Figure 11.2-1, Input for the NASCCS Module to Determine the Critical Crack Size for an Axial Crack in a Hollow Cylinder (SC04). The input for a 0.2 crack aspect ratio is shown, and the internal flaw location is chosen. Both the 0.2 and 1.0 crack aspect ratio were checked for internal and external cracks. The “S0 from unit internal press” option was selected. This allows for the internal pressure to be used as the input to determine the hoop stress in the cylinder. The internal pressure is defined as 7.5 kilo pounds per square inch (ksi).

NASA-HDBK-5010, VOLUME 2, REVISION A

SC04

internal or external crack

$S_0(X)$ = stresses due to internal pressure, p
 $S_i(X)$ = other stresses



$D \geq 4t$

$S_i(X) \quad i = 1, 2, 3$

$X = x/t$
(from inner surface)

$0.0 \leq X \leq 1.0$

$0.1 \leq a/c \leq 1.2$

Thickness, t	0.125	Flaw location <input checked="" type="radio"/> Internal <input type="radio"/> External
Outer diameter, D	4	
a/c	0.2	

of stress distributions: 1 2 3 4

S_0 from unit internal press. Plot stresses

Display stress quantity: S_0 S_1 S_2 S_3 R_S

Internal pressure: 7.5

Figure 11.2-1—Input for the NASCCS Module to Determine the Critical Crack Size for an Axial Crack in a Hollow Cylinder (SC04)

(A 0.2 crack aspect ratio, a/c , is assigned, and the internal location is chosen. Additionally, the stress is defined from internal pressure, which is 7.5 ksi in this case.)

The output options also must be defined, as shown in Figure 11.2-2, Output Options Input for NASCCS. The “Max K” radio button is chosen such that the maximum stress intensity factor and net section yielding are considered to determine the critical crack size. Note that “Max K and NSY” were not selected because NSY is physically incapable of reliably producing a proof-screened flaw size.

This requires the input of the fracture toughness and the yield stress. The applied stresses do not require an input because the internal pressure is already defined. Note that when using proof test to screen for flaws, the upper bound fracture toughness must be used to determine the initial flaw size for the life analysis. This upper bound fracture toughness must be included in the FCP and approved by the RFCB.

NASA-HDBK-5010, VOLUME 2, REVISION A

The screenshot shows a software interface with two main sections. The first section is titled "Basis for calculating critical crack size" and contains six radio button options: "Max K and NSY", "Max K only" (which is selected), "K at a-tip only", "K at c-tip only", "NSY only", and "Fatigue crack growth threshold". The second section is titled "Critical material properties" and contains a text input field labeled "Fracture toughness" with the value "50" entered.

Figure 11.2-2—Output Options Input for NASCCS

The output for the 0.2 crack aspect ratio for an interior flaw is shown in Figure 11.2-3, Results of Critical Crack Size Analysis (NASCCS) for an Interior Axial Surface Crack in a Hollow Cylinder with Crack Aspect Ratio of 0.2. The critical interior flaw with a 0.2 crack aspect ratio that would survive proof has a depth, a , of 0.039 inches and a width, c , of 0.193 inches. In this case, the critical crack is controlled by stress intensity factor rather than yielding, as indicated in the output.

```
Critical crack size (CCS):  
a = 3.8550E-02  
c = 1.9275E-01  
CCS determination is based on Kmax only.
```

Figure 11.2-3—Results of Critical Crack Size Analysis (NASCCS) for an Interior Axial Surface Crack in a Hollow Cylinder with Crack Aspect Ratio of 0.2

The crack sizes for the different combinations of crack aspect ratio and position are shown in Table 11.2-1, Critical Crack Depth for Axial Flaws in a Hollow Cylinder for Combinations of Crack Aspect Ratios and Positions in the Cylinder. The crack sizes can be verified in the NASSIF module of NASGRO® to ensure that the cracks correspond to a stress intensity that meets the upper bound fracture toughness. These flaws can then be used as the initial flaws for a life analysis on the pipe. This corresponds to four separate life analyses, one for each flaw. The lowest predicted life controls the life of the pipe. The NDE flaw sizes can now be replaced with the initial flaw sizes screened by the proof test.

NASA-HDBK-5010, VOLUME 2, REVISION A

Table 11.2-1—Critical Crack Depth for Axial Flaws in a Hollow Cylinder for Combinations of Crack Aspect Ratios and Positions in the Cylinder

Crack aspect ratio, a/c	Crack position	Critical depth, a (inches)	Critical width, c (inches)
0.2	Interior	0.039	0.193
0.2	Exterior	0.042	0.211
1.0	Interior	0.079	0.079
1.0	Exterior	0.087	0.087

In the case of welds, flaw screening may be driven by cracks in welds in the circumferential direction resulting in lower life despite the lower stresses. Loading spectra may generate a greater number of stress cycles in those directions. For example, circumferential weld flaws may experience higher number of cycles in the axial direction due to bending from random vibration, compared to the hoop stress from internal pressure, which tends to be much fewer in the number of cycles for a press/prop system. Further, residual stresses can be significant and may need to be considered as part of the mean stress.

11.2.2 Example 2

In this example, a proof test screening method is used to validate damage tolerance of a bracket. The bracket has a 5-inch width, 0.25-inch wall thickness, and a net section stress of 85 ksi during flight. In this example, the validity of a proof test as a flaw screening technique is checked, and flaw size and orientation that should be used for the life analysis is derived.

NASA-STD-5019A permits using a proof test to screen for flaws in certain fracture critical parts. For metallic components, an appropriate proof test followed by a visual inspection can replace other NDE techniques to establish the initial flaw in a life analysis. The initial flaw corresponds to the largest flaw in a critical location that can survive the proof test without unstable crack growth or yielding. If a larger flaw existed, it would lead to failure during the proof test, so it can be assumed that any flaw in the hardware after proof is less than or equal to the size of the critical flaw. If there are multiple critical locations and orientations, multiple critical flaws should be characterized and used in the life analysis.

It should be noted that few components are easily proof tested. For a fracture critical part, an approach for flaw screening with a proof test must be documented in the FCP and approved by the RFCB. Multiple complexities must be accounted for to accept proof as the only flaw screening method, including environmental effects, temperature, test fixtures, inertial loads, and others. The proof test must load the component such that the entire assembly undergoes stresses that are at least the stress during operation multiplied by the appropriate proof factor.

In this example, assume that the bracket is loaded in the same manner as flight. The proof test is conducted with the MDP multiplied by the proof factor and an ECF. An elevated proof factor of 1.5 is chosen to better screen for flaws. The ECF is based on the knockdown of the fracture toughness or strength at the temperature seen by the pipe during flight. The highest ECF calculated based on the fracture toughness and strength knockdowns should be used. For

NASA-HDBK-5010, VOLUME 2, REVISION A

additional requirements of the proof test requirements, see ANSI/AIAA S-080A. In this case, the net section stress multiplied by the 1.5 proof factor and the ECF is assumed to give a maximum net section stress of 130 ksi.

To determine the largest flaw that can survive proof, the NASCCS module in NASGRO® is used. The representative geometry and worst-case flaw orientation were chosen. If the worst-case flaw orientation is not clear, multiple flaw orientations should be studied. In this case, it was assumed that a semi-elliptical surface crack in a plate is the worst-case orientation. Crack aspect ratios of 0.2 and 1.0 must be examined. The crack aspect ratios correspond to the minimum and maximum crack aspect ratios for various NDE techniques. The geometry input for SC30 with a 0.2 crack aspect ratio is shown in Figure 11.2-4, Input for the NASCCS Module to Determine the Critical Crack Size for a Semi-elliptical Surface Crack in a Plate (SC30).

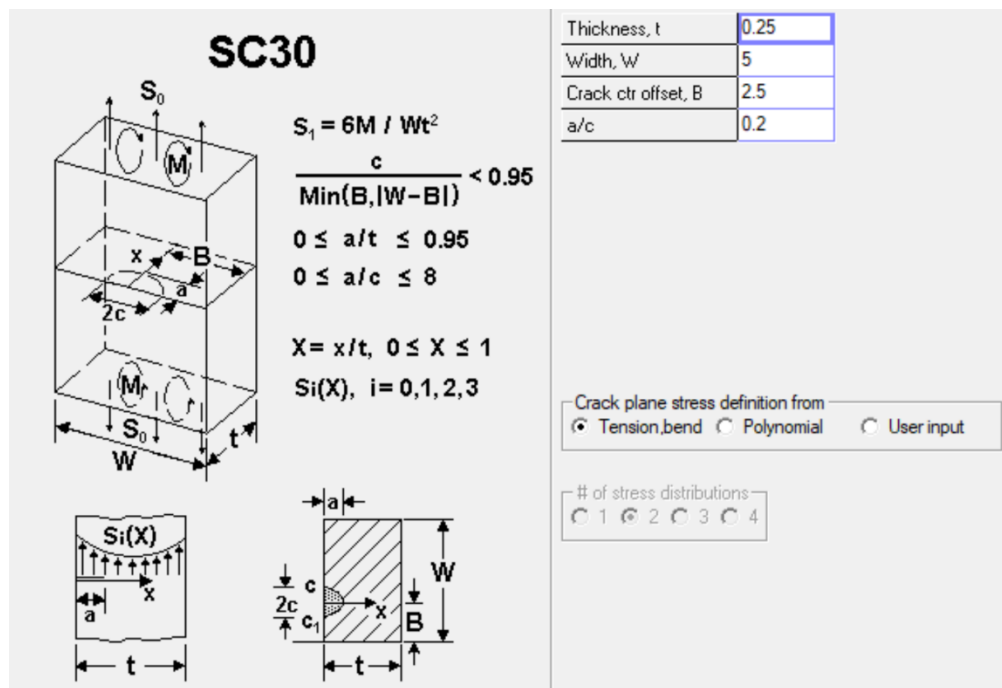


Figure 11.2-4—Input for the NASCCS Module to Determine the Critical Crack Size for a Semi-elliptical Surface Crack in a Plate (SC30)
(A 0.2 crack aspect ratio, a/c , is assigned.)

The output options also must be defined, as shown in Figure 11.2-5, Output Options Input for NASCCS. The “Max K” radio button is chosen such that the maximum stress intensity factor and net section yielding are considered to determine the critical crack size. Note that “Max K and NSY” were not selected because NSY is physically incapable of reliably producing a proof-screened flaw size. This requires the input of the fracture toughness and the yield stress. Note that when using proof test to screen for flaws, the upper bound fracture toughness must be used to determine the initial flaw size for the life analysis. This upper bound fracture toughness must be included in the FCP and approved by the RFCB. The fracture toughness is defined in the units of ksi sqrt(in), and the stresses are defined in the units of ksi.

APPROVED FOR PUBLIC RELEASE – DISTRIBUTION IS UNLIMITED

NASA-HDBK-5010, VOLUME 2, REVISION A

Basis for calculating critical crack size

Max K and NSY

Max K only

K at a-tip only

K at c-tip only

K at c1-tip only

NSY only

Fatigue crack growth threshold

Critical material properties

Fracture toughness

85

Applied stresses

S0	S1
130	0

Figure 11.2-5—Output Options Input for NASCCS

The output for the 0.2 crack aspect ratio is shown in Figure 11.2-6, Results of Critical Crack Size Analysis (NASCCS) for a Surface Crack in a Plate with Crack Aspect Ratio of 0.2. The critical flaw with a 0.2 crack aspect ratio that would survive proof has a depth, a , of 0.085 inch and a width, c , of 0.424 inch.

```
Critical crack size (CCS):
a = 8.4866E-02
c = 4.2433E-01
CCS determination is based on Kmax only.
```

Figure 11.2-6—Results of Critical Crack Size Analysis (NASCCS) for a Surface Crack in a Plate with Crack Aspect Ratio of 0.2

The critical crack sizes for both the 0.2 and 1.0 crack aspect ratios are shown below in Table 11.2-2, Critical Crack Depth for Axial Flaws in a Hollow Cylinder for Combinations of Crack Aspect Ratios and Positions in the Cylinder. The crack sizes can be verified in the NASSIF module of NASGRO® to ensure that the cracks correspond to a stress intensity that meets the upper bound fracture toughness. These flaws can then be used as the initial flaws for a life analysis on the bracket. This corresponds to two separate life analyses, one for each flaw. The lowest predicted life controls the life of the pipe. The NDE flaw sizes can now be replaced with the initial flaw sizes screened by the proof test.

Table 11.2-2—Critical Crack Depth for Axial Flaws in a Hollow Cylinder for Combinations of Crack Aspect Ratios and Positions in the Cylinder

Crack aspect ratio, a/c	Critical depth, a (inches)	Critical width, c (inches)
0.2	0.085	0.424
1.0	0.168	0.168

NASA-HDBK-5010, VOLUME 2, REVISION A

The example presented here is a simple approach that should be accepted on a case-by-case basis to ensure that the analysis is sufficiently conservative. In the case of problems where yield is the driving failure mode, sizing the proof factor may not be conservative if the net section yield/flow stress failure prediction is used. A conservatism in crack-growth predictions is not necessarily a conservatism in the failure prediction for a proof test. To determine the maximum flaw size that passes proof test, typically an upper bound fracture toughness (e.g., $1.3 \times K_{Ic}$) is used in the assessment.

Elastic plastic fracture mechanics (EPFM) should be considered in cases where yielding is predicted and LEFM is known to be unconservative.

11.3 Guidelines for LEFM and EPFM Assessments

Damage tolerance requirements can be verified either by test or analysis. When analysis is used, an analysis methodology anchored to test data generally provides the highest confidence.

In space vehicle applications, there are many components that experience large cyclic stresses that cannot be evaluated using LEFM. In these instances, alternate paths exist using EPFM that can allow for a high confidence damage tolerance verification.

To this end, this section provides guidance with respect to demonstration of damage tolerance using LEFM and EPFM. In particular, determination of the appropriate damage tolerance assessment is discussed. Limitations for LEFM and EPFM assessments are also highlighted.

11.3.1 Limitations of LEFM Assessments

LEFM is easy to implement and, when coupled with an appropriate scatter factor, is widely accepted for damage tolerance assessments. LEFM has limitations, and it is up to the responsible engineer to verify that LEFM is appropriate. LEFM is generally applicable when small scale yielding (SSY) prevails at the crack-tip.

LEFM without SSY can result in unconservative results, as plasticity can drastically affect resistance to crack instability and crack growth rate. This concept is illustrated in Figure 11.3-1, Comparisons of LEFM and EPFM FCG Curves for Al 2014-T6: $R = -1$, $a = 0.025$ inch, $a/c = 0.2$, $w = 10$ inches, $t = 0.1$ inch, Failure Represents Unstable Crack Growth or Plastic Collapse, where linear elastic fatigue crack growth (LEFCG) and elastic plastic fatigue crack growth (EPFCG) are plotted as a function of fully reversed, constant amplitude cycles for an Al 2014-T6 surface crack specimen. The curve in Figure 11.3-1 was generated using NASGRO®, flaw type SC30, and LEFM properties built-in within NASGRO.

NASA-HDBK-5010, VOLUME 2, REVISION A

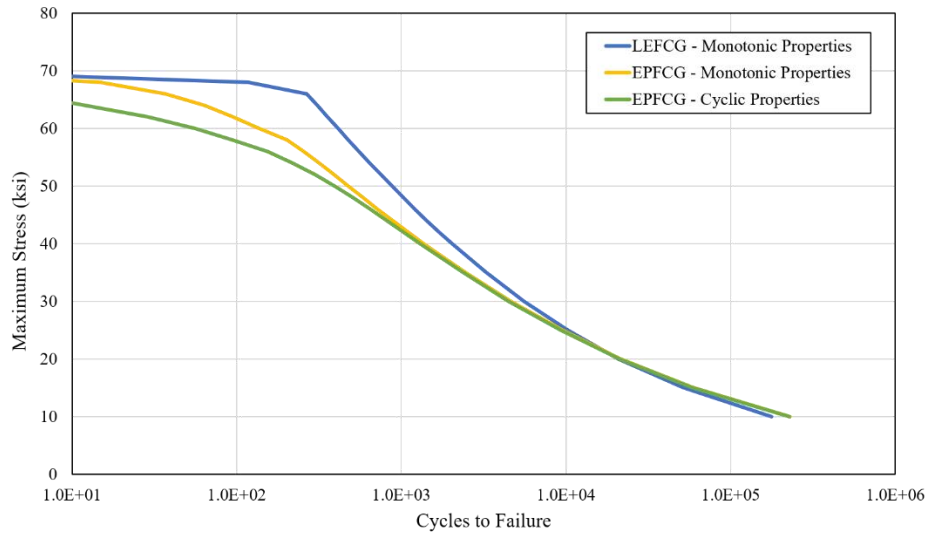


**Figure 11.3-1—Comparisons of LEFM and EPFM FCG Curves for Al 2014-T6:
R = -1, a = 0.025 inch, a/c = 0.2, w = 10 inches, t = 0.1 inch,
Failure Represents Unstable Crack Growth or Plastic Collapse**

As plasticity increases, the number of cycles to failure are increasingly overpredicted by the LEFM solution, which is especially true when stresses approach the material yield strength. Because Al 2014-T6 exhibits cyclical softening behavior, the EPFM assessment with monotonic material properties is unconservative compared to an EPFM assessment with cyclic properties.

The trends in Figure 11.3-1 have been noted for other alloys such as titanium and steel, where EPFM and LEFM match for lower magnitude stress cycles but begin to diverge above ~50% of yield strength. A figure such as this one can provide guidance on when to apply LEFM versus EPFM.

11.3.2 Determination of the Appropriate Damage Tolerance Assessment

Using the appropriate damage tolerance assessment is critical to avoid unconservative life predictions. The flowchart in Figure 11.3-2, Flowchart to Determine Validity of LEFM Assessments, is provided to assist the analyst in determining a bounding damage tolerance assessment.

NASA-HDBK-5010, VOLUME 2, REVISION A

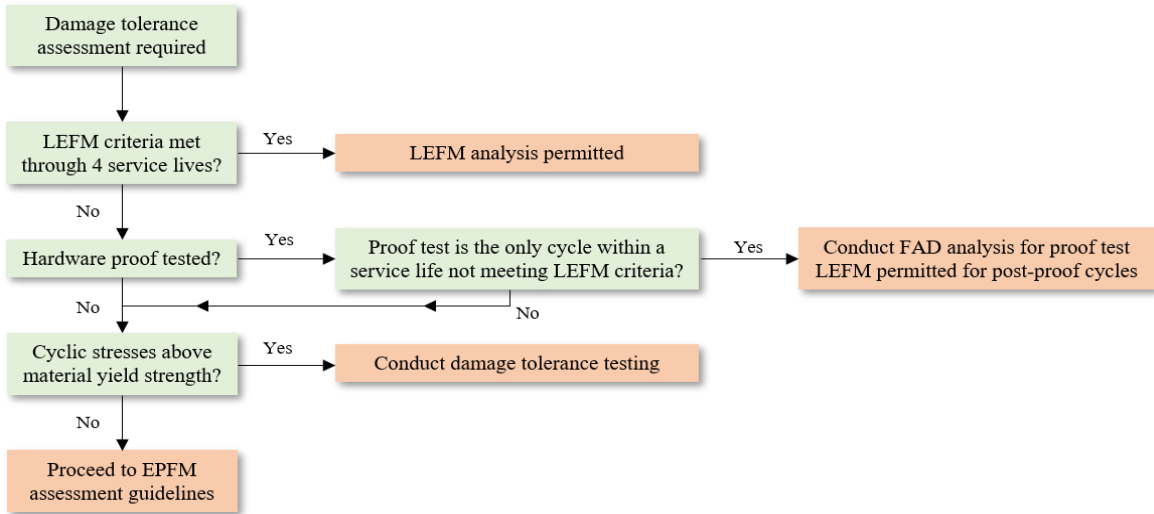


Figure 11.3-2—Flowchart to Determine Validity of LEFM Assessments.

For an LEFM analysis to be permitted, it is recommended that the LEFM criteria provided below be met throughout four service lives:

For surface, corner, and embedded cracks, the following criteria derived from ASTM E2899-19, is recommended [11.3-1]:

$$\sigma_{NS} < 0.9\sigma_{ys} \quad \text{and} \quad r_{\phi a}, r_{\phi b} \geq \frac{E}{\sigma_{ys}} \left(\frac{J_K}{\sigma_{ys}} \right) \quad \text{for all } \phi \text{ from } \phi = 0^\circ \text{ to } \phi = 90^\circ, \quad (\text{Equation 11.3-1})$$

where for linear elastic plane strain:

$$J_K = \frac{K_I^2(1-\nu^2)}{E}, \quad \text{and} \quad r_{\phi a}, r_{\phi b} \geq (1-\nu^2) \left(\frac{K_I}{\sigma_{ys}} \right)^2, \quad (\text{Equation 11.3-2})$$

and for linear elastic plane stress:

$$r_{\phi a}, r_{\phi b} \geq \left(\frac{K_I}{\sigma_{ys}} \right)^2. \quad (\text{Equation 11.3-3})$$

For through-cracks, the following criteria derived from ASTM E647-15, is provided as a LEFM threshold [11.3-2]:

$$(t - a), \quad \text{where} \quad a \geq \frac{4}{\pi} \left(\frac{K_I}{\sigma_{ys}} \right)^2 \quad (\text{Equation 11.3-4})$$

Any exceptions to the above LEFM criteria, should be reviewed and approved by the appropriate governing authority for fracture control.

NASA-HDBK-5010, VOLUME 2, REVISION A

The following are additional considerations relative to damage tolerance assessments associated with the LEFM criteria in Equations 11.3-1–11.3-4 and Figure 11.3-2:

1. While the requirements established in ASTM E2899-19 require a LEFM validity check for surface cracks to be performed solely at the critical crack initiation angle, the criteria must be broadened for general applications. This is because there are applications where fatigue crack growth must be accurately characterized across the entire crack front. The ASTM E2899-19 criteria has been expanded to apply to all ϕ in the range of 0-degrees to 90-degrees; it was noted that for many applications, a validity check at $\phi = 0, 90$ degrees alone is sufficient.

2. When the ligament in front of a crack-tip becomes small, elastic constraint decreases. Elastic constraint quantifies the degree of triaxial stress present at a given crack-tip. While lower constraint can lead to lower crack growth rates, quantification of this requires the use of two parameter fracture mechanics (TPFM). If TPFM data are available, it may be possible to reduce conservatism within a given LEFM or EPFM assessment.

3. When a proof test is the only cycle within a service life that does not meet the LEFM criteria, it is recommended that the proof test be evaluated using a failure assessment diagram (FAD) (see Figure 11.3-3, Surface Crack Cross-Section. FAD analyses can be performed using either the NASFAD module in NASGRO®, version 9.20, or by using the NASFLA module in earlier versions of NASGRO®. FAD assessments account for the detrimental effects of plasticity on crack instability. They generally do not account for EPFCG. FAD analyses should be restricted to static assessments.

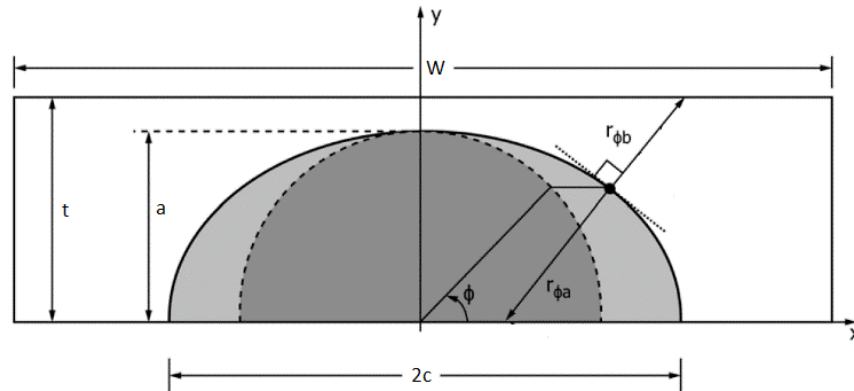


Figure 11.3-3—Surface Crack Cross-Section

4. When low amplitude cycles are preceded by an overload event that does not cause gross yielding, crack growth retardation generally occurs. If the post-proof test cycles meet the aforementioned LEFM criteria, then an LEFM analysis for the post-proof test cycles will be conservative so long as the post-proof flaw size is appropriately characterized. There are exceptions noted where the presence of a compressive underload reduces or eliminates the retardation effects, and may even accelerate crack growth rate, if the overload event results in significant plastic deformation. Research activities are ongoing to solidify these assertions.

NASA-HDBK-5010, VOLUME 2, REVISION A

5. As cyclic stresses within the service life approach the yield strength of the material, EPFM assessments are encouraged. When yielding is predicted within the service life, it is recommended that damage tolerance testing be considered. This is because EPFM analyses may not capture other failure modes associated with detrimental yielding.

11.3.3 EPFM Assessment Guidelines

Care must be taken to avoid unconservative results when using LEFM and EPFM assessments. To this end, the EPFM assessment criteria in Table 11.3-1, EPM Assessment Criteria, provides a means to ensure results using EPFM analysis are bounding.

Table 11.3-1—EPFM Assessment Criteria

EPFM Assessment Criteria	Criteria Met (Y/N)?
characterization tests?	

When all EPFM criteria are met, an EPFM analysis is permissible. While some material properties for an EPFM assessment can be difficult to obtain, assessments that do not permit ductile tearing are much more tractable. Ductile tearing defines a state of stable crack growth that can occur in materials beyond J_{Ic} . In general, interactions between ductile tearing and other sub-critical flaw growth mechanisms are not well understood. It is recommended that ductile tearing not be permitted with other sub-critical flaw growth mechanisms.

For an EPFM analysis that does not model ductile tearing, the following material properties are required:

1. Monotonic and cyclic stress-strain curve(s).
2. Critical value of J.
3. Elastic-plastic fatigue crack growth rate parameters.

When the above EPFM properties are unavailable at the appropriate environmental conditions, it is possible to derive them from LEFM properties using the following relationships:

For the critical value of J:

$$J_{crit} = \frac{K_{crit}^2}{E'} , E' = \frac{E}{(1-\nu^2)} \text{ (for plane strain) and } E' = E \text{ (for plane stress),}$$

(Equation 11.3-5)

where K_{crit} is the critical stress intensity factor relevant to the application (e.g., K_{Ic} , K_c , K_{Ie}).

APPROVED FOR PUBLIC RELEASE – DISTRIBUTION IS UNLIMITED

NASA-HDBK-5010, VOLUME 2, REVISION A

To develop an elastic-plastic fatigue crack growth formulation, one starts with the Paris equation:

$$\frac{da}{dN} = C_0(\Delta K)^{m_0} .$$

(Equation 11.3-6)

Then introduce the crack closure correction factor U_0 associated with the applicable fatigue crack growth (FCG) testing, as well as the effective stress intensity factor ΔK_{eff} :

$$\frac{da}{dN} = \frac{C_0}{U_0^{m_0}} (\Delta K_{eff})^{m_0} \text{ and } \Delta K_{eff} = U\Delta K = K_{max} - K_{open} ,$$

(Equation 11.3-7)

where ΔK_{eff} is the stress intensity factor range corrected for crack closure and U is the general crack closure correction factor for the particular application. Note that $U = U_0$ when Equation 11.3-7 is applied to the applicable fatigue crack growth testing.

Finally, recast Equation 11.3-7 in terms of the effective J integral range, as defined by McClung, et al. [11.3-4]:

$$\frac{da}{dN} = \frac{C_0(E')^{m_0/2}}{U_0^{m_0}} (\Delta J_{eff})^{m_0} .$$

(Equation 11.3-8)

The following are considerations relative to EPFM assessments described in Table 11.3-1:

1. Elastic constraint plays a significant role in all fracture mechanics assessments. For EPFM assessments, one must be especially cautious. Elastic constraint quantifies the degree of triaxial stress present at a given crack-tip. When da/dN and crack instability characterization is performed using geometry with greater triaxial stress than the application, analytically predicted crack instability and crack growth rate will be conservative.

2. Unlike LEFM, where overload events lead to crack retardation, overload events under large strain cycling can result in crack growth acceleration. EPFM analyses with variable amplitude cycles must be evaluated carefully to ensure that crack growth is accurately modeled. If the variable amplitude cycles can be approximated using the maximum stress within the spectrum for cycles that do not meet LEFM requirements, uncertainty associated with crack growth acceleration can be eliminated provided that all cyclic stresses are below the material yield strength.

3. In many cases, EPFM analyses are derived from fully plastic fracture mechanics solutions. Examples include Electric Power Research Institute (EPRI) handbook solutions and reference stress method (RSM) solutions. If EPFM analyses do not contain fully plastic solutions, an EPFM validity check may be warranted.

APPROVED FOR PUBLIC RELEASE – DISTRIBUTION IS UNLIMITED

NASA-HDBK-5010, VOLUME 2, REVISION A

11.3.4 EPFM Using NASGRO®: Benchmarks and Examples

This section contains EPFM benchmarks and examples using NASGRO®. Each example contains step-by-step information for a particular aspect of the analysis: development of EPFM properties (section 11.3.4.1), using the NASGRO® EPFM module (section 11.3.4.2), and interpreting EPFM results in NASGRO® (section 11.3.4.3). Lessons learned from the benchmarks are also provided in section 11.3.4.4. The examples presented here are based on Sagrillo, et al. (2022).

11.3.4.1 Validation of EPFCG Properties Derived from LEFCG Properties

This benchmark was taken from McClung, et al. (1999) [11.3-4]. This 1999 paper developed the original NASGRO® EPFM module, and the test data therein was used for verification purposes. McClung, et al., found very good agreement between test predictions and test results. This benchmark is not intended to verify the EPFM module, but rather is intended to validate the derivation of the EPFCG parameters from available da/dN vs ΔK curves and published engineering stress-strain curves.

The testing by McClung, et al., was completed using STA Inconel® 718 through crack, surface crack, and corner crack specimens. The tests covered a wide range of crack-tip conditions, including SSY, large scale yielding, and severe plasticity. Fully reversing, fluctuating, and repeating cyclic stress ratios were also considered. Many specimens were not taken to failure, but instead, the cycles to reach a certain crack size were recorded. Subsequently, the benchmarks completed by McClung, et al., were intended to verify the EPFM module's ability to predict EPFCG rate, more so than elastic-plastic crack instability. A summary of the specimens and conditions tested are included in Table 11.3-2, Test Specimens and Conditions from McClung, et al. [11.3-4].

NASA-HDBK-5010, VOLUME 2, REVISION A

Table 11.3-2—Test Specimens and Conditions from McClung, et al. [11.3-4]

Specimen #	Crack Geometry	Specimen Width (W)	Specimen Thickness (t)	Crack Depth (a)	Half-crack Width (c)	Stress Ratio (R)	Max. Stress (σ_{max})	Test Cycles (N)
DI	Through	1.25	0.5	-	0.15	0.1	56.4	9,820
SD1		1.25	0.2	-	0.15	0.1	55.8	13,470
SD2		1.25	0.2	-	0.15	0.1	20	270,118
S7	Surface	1.25	0.2	0.01	0.01	-1	135	5,900
S33		1.25	0.2	0.01	0.01	0	135	44,900
S25		1.25	0.2	0.149	0.163	0	145	385
S29		1.25	0.2	0.164	0.184	0	135	378
S11		1.25	0.2	0.146	0.152	-1	165-157	4
S13		1.25	0.2	0.129	0.134	-1	158-138	32
S44	Corner	0.5	0.5	0.034	0.034	-1	135	2,950

Note: Dimensions for stress are in ksi, and dimensions for length are in inches.

In evaluating the test conditions for each specimen with respect to the validity of LEFM, it was found that all surface crack specimens in this study exceeded and did not satisfy the ASTM E2899-19 derived validity criteria in section 11.3.2. For the corner crack specimen, the LEFM criteria derived from ASTM E2899-19 was also exceeded. For all through crack specimens, the criteria derived from ASTM E647-15 was satisfied and LEFM is applicable under the given test conditions. Table 11.3-3, LEFM Validity Checks for McClung, et al., Tests [11-3-4], provides the details of each LEFM validity check.

Table 11.3-3—LEFM Validity Checks for McClung, et al., Tests [11.3-4]

Specimen #	Results at Test Start				Results and Test Completion			
	σ_{NS} (ksi)	$\sigma_{NS} < 0.9\sigma_{ys}$	K_I (crit) (ksi $\sqrt{\text{in}}$)	$r_{\phi a}, r_{\phi b} > \text{LEFM Limit}$	σ_{NS} (ksi)	$\sigma_{NS} < 0.9\sigma_{ys}$	K_I (crit) (ksi $\sqrt{\text{in}}$)	$r_{\phi a}, r_{\phi b} > \text{LEFM Limit}$
DI	74.21	Yes	40.15	Yes	86.47	Yes	50.42	Yes
SD1	73.42	Yes	39.73	Yes	93.88	Yes	55.54	Yes
SD2	26.32	Yes	14.24	Yes	31.47	Yes	18.45	Yes
S7	135.27	Yes	17.34	No ($r_{\phi a}$)	-	-	-	-
S33	135.27	Yes	17.34	No ($r_{\phi a}$)	-	-	-	-
S25	198.24	No	-	-	-	-	-	-
S29	194.82	No	-	-	-	-	-	-
S11	219.93	No	-	-	-	-	-	-
S13	199.39	No	-	-	-	-	-	-
S44	137.41	Yes	31.98	No ($r_{\phi a}$)	-	-	-	-

Net section stresses in several tests also exceed the Inconel® 718 STA material yield strength of 171 ksi. For applications subjected to these conditions, the guidelines established in section 11.3.2 would not recommend the use of EPFM analysis for qualification purposes. Instead, damage tolerance testing would be recommended.

APPROVED FOR PUBLIC RELEASE – DISTRIBUTION IS UNLIMITED

NASA-HDBK-5010, VOLUME 2, REVISION A

To perform EPFCG analysis in NASGRO®, several material properties are required. These include constants for the Ramberg-Osgood (R-O) stress-strain curve description, mechanical properties, crack growth rate properties, and the critical value of the J-integral. The complete list of EPFCG analysis inputs required by NASGRO® are shown in Figure 11.3-4, EPFCG Analytical Inputs Required by NASGRO®.

Figure 11.3-4—EPFCG Analytical Inputs Required by NASGRO®

The following are the steps to define the properties in Figure 11.3-4:

Step 1: Define stress-strain properties

Material properties for Inconel® 718 STA were obtained from MMPDS-13, Table 6.3.5.0(c1) [11.3-6]. Properties for 1.000-inch to 1.499-inch bar stock were chosen; as the test specimens were machined from 1.250-inch bar stock. Modulus of elasticity was found to be 29,400 ksi, Poisson’s ratio was 0.29, and the B-basis tensile ultimate strength was 199 ksi. A Ramberg-Osgood relationship was then used to mathematically describe the MMPDS-13, Figure 6.3.5.1.6(b1), stress-strain curve [11.3-6]:

$$\frac{\varepsilon}{\varepsilon_0} = \frac{\sigma}{\sigma_0} + \alpha_{R-O} \left(\frac{\sigma}{\sigma_0} \right)^n, \quad (\text{Equation 11.3-9})$$

where σ_0 was chosen as the material yield stress with a 0.2% offset (171 ksi), and ε_0 was the elastic strain at yield. Then, α_{R-O} and n were defined as follows:

$$\alpha_{R-O} = \frac{E}{\sigma_0} (0.002) \quad \text{and} \quad n = \frac{\ln\left(\frac{\varepsilon_{PL,1}}{0.002}\right)}{\ln\left(\frac{\sigma_1}{\sigma_0}\right)} \quad \text{and} \quad \varepsilon_{PL,1} = \varepsilon_1 - \frac{\sigma_1}{E}, \quad (\text{Equation 11.3-10})$$

where E is the elastic modulus, $\varepsilon_{PL,1}$ is the plastic strain at an arbitrary point in the plastic region, σ_1 is the corresponding engineering stress, and ε_1 is the corresponding total strain. From these equations, α_{R-O} was found to equal 0.343 and $n = 17.16$.

For conditions where $R < 0$, cyclic material properties are recommended. Cyclic-stress curve properties can be measured using ASTM E606, Standard Test Method for Strain-Controlled Fatigue Testing, and procedures described in Landgraf, et al. (1969). The cyclic stress strain curve describes how the stress-strain curve of a material work-hardens or work-softens under

NASA-HDBK-5010, VOLUME 2, REVISION A

plastic cyclic loads. McClung, et al., published R-O material properties for such a curve [11.3-4], including:

$$\sigma_0 = 158.3 \text{ ksi}, \alpha_{R-O} = 1.0, \text{ and } n = 6.15.$$

Step 2: Determine crack closure corrected LEFCG properties

For Inconel® 718 STA LEFCG properties, material Q3LE13AB1 from the NASGRO® material database was utilized. This corresponds to Inconel® 718 solution treated to 2,000 °F and aged at 1,325 °F for 4 hours, followed by 1,150 °F for 16 hours. The applicable product form is sheet/plate, and the test conditions are ambient. LEFCG properties for stress ratios of 0.05 and 0.7 are available with Q3LE13AB1, as shown in Figure 11.3-5, LEFCG Curves in NASGRO® for Q3LE13AB1.

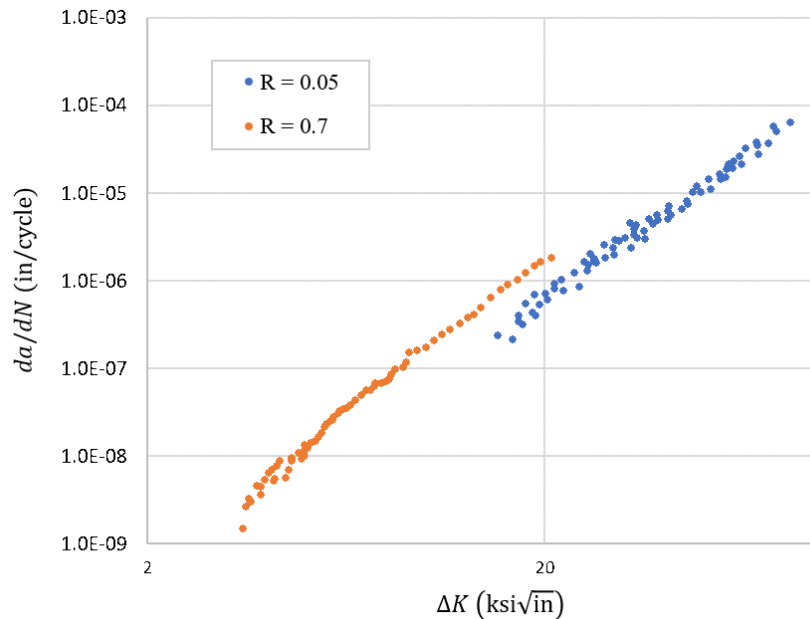


Figure 11.3-5—LEFCG Curves in NASGRO® for Q3LE13AB1

Given that the stress ratios of interest for this study vary, it is of value to normalize the da/dN data using the approach defined by Newman in “A Crack Opening Stress Equation for Fatigue Crack Growth” [11.3-7]. By correcting the da/dN data for crack closure, a relationship between effective stress intensity and crack growth rate can be determined. This relationship will be the same for all stress ratios. When the data is corrected for crack closure, the da/dN curves taken at different stress ratios collapse into a single unified curve.

To utilize this approach, one must calculate the constant U_0 for each R ratio using the following equations:

$$U_0 = \frac{1 - K_{open}/K_{max}}{1 - R}$$

APPROVED FOR PUBLIC RELEASE – DISTRIBUTION IS UNLIMITED

NASA-HDBK-5010, VOLUME 2, REVISION A

$$\frac{K_{open}}{K_{max}} = \begin{cases} A_0 + A_1R + A_2R^2 + A_3R^3 & R \geq 0 \\ A_0 + A_1R & -2 \leq R < 0 \end{cases}$$

$$A_0 = (0.825 - 0.34\alpha_c + 0.05\alpha_c^2) \left[\cos\left(\frac{\pi \sigma_{max}}{2 \sigma_{flow}}\right) \right]^{1/\alpha_c}$$

$$A_1 = (0.415 - 0.071\alpha_c) \frac{S_{max}}{S_{flow}}, \quad A_2 = 1 - A_0 - A_1 - A_3, \quad A_3 = 2A_0 + A_1 - 1$$

(Equation 11.3-11)

First, S_{max}/S_{flow} is set to 0.3 because this value is close to an average value obtained from fatigue crack growth tests using various specimen types. Further, it has been shown to produce acceptable results for positive stress ratios, where its effects on the crack opening function are small [11.3-8].

Next, an initial guess for the constraint factor α_c is required. To start, α_c is assumed to equal 2.5. This results in the following initial guesses:

For $R = 0.05$: $U_0 = 0.76$; For $R = 0.7$: $U_0 = 0.99$

Using these results, $\Delta K_{eff} = U_0 \Delta K$ is calculated for every data point of each curve. The value α_c is iterated until the correlation regression coefficient (R-squared) is maximized such that a linear function fits the linear portion of the da/dN curves, which represents maximum collinearity in the ΔK_{eff} domain (see Figure 11.3-6, Closure Corrected LEFCG Curves for Q3LE13AB1).

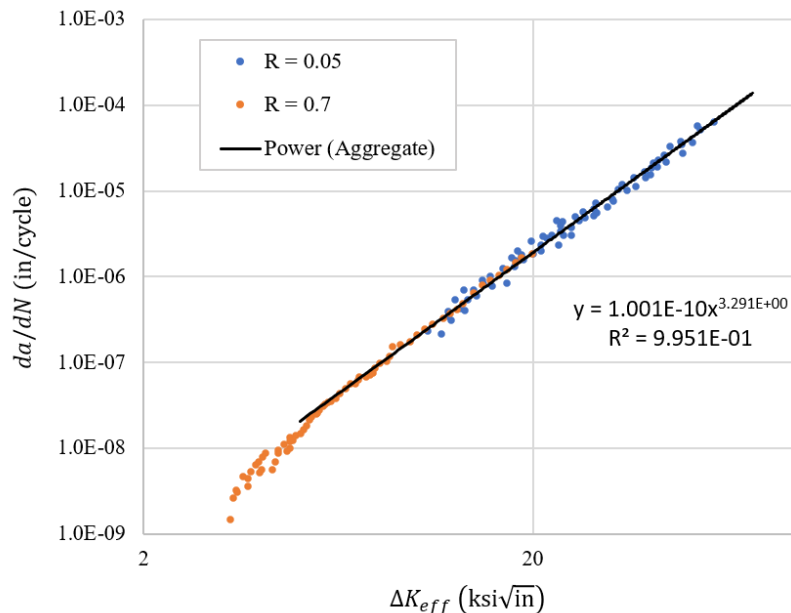


Figure 11.3-6—Closure Corrected LEFCG Curves for Q3LE13AB1

NASA-HDBK-5010, VOLUME 2, REVISION A

From Figure 11.3-6, the closure corrected LEFCG formulation was found to be:

$$\frac{da}{dN} = 1.00 \times 10^{-10} (\Delta K_{eff})^{3.291},$$

where, $C_0 = 1.00 \times 10^{-10}$, $m_0 = 3.291$, and $U_0 = 1$.

It is important to note that C_0 and m_0 differ from the crack growth constants in NASGRO®. This is because the NASGRO® LEFCG equation includes additional terms to make corrections in the near-failure and near-threshold regimes. As a result, the curve's slope everywhere is greater than n when plotted on log-log axes, which means that the n reported by NASGRO® will be lower than the m_0 obtained through curve-fitting the data and is unconservative.

Step 3: Derive EPFCG properties from LEFCG properties

Once C_0 , m_0 , and U_0 are estimated, EPFCG properties are derived from LEFCG properties using Equation 11.3-12:

$$\frac{da}{dN} = \frac{C_0 (E')^{m_0/2}}{U_0^{m_0}} (\Delta J_{eff})^{m_0/2}$$

$$E' = \frac{E}{(1-\nu^2)} \text{ (For Plane Strain) and } E' = E \text{ (For Plane Stress)}$$

(Equation 11.3-12)

where ΔJ_{eff} is the J-Integral range corrected for crack-closure. Interestingly, the EPFCG constants in this particular formulation are equivalent to those obtained from a LEFCG analysis that is corrected for crack closure:

$$\frac{da}{dN} = \frac{C_0}{U_0^{m_0}} (\Delta K_{eff})^{m_0}, \quad \Delta K_{eff} = U_0 \Delta K = K_{max} - K_{open}$$

(Equation 11.3-13)

where ΔK_{eff} is the stress intensity factor range corrected for crack-closure. For additional information on the NASGRO® EPFCG formulation, refer to the NASGRO® EPFM user manual [11.3-8].

Step 4: Define J_{crit}

Next, the critical value of J is required. Given that the testing conducted by McClung, et al., covers different crack geometries, J_{crit} is calculated using equation 11.3-14:

$$J_{crit} = \frac{K_{crit}^2}{E'} , \quad E' = \frac{E}{(1-\nu^2)} \text{ (for plane strain) and } E' = E \text{ (for plane stress)}$$

(Equation 11.3-14)

APPROVED FOR PUBLIC RELEASE – DISTRIBUTION IS UNLIMITED

NASA-HDBK-5010, VOLUME 2, REVISION A

Where K_{crit} is the critical stress intensity factor relevant to the application (e.g., K_{Ic} , K_c , K_{Ie}).

This form of J_{crit} does not allow for ductile tearing. Ductile tearing defines a state of stable crack growth that can occur in materials beyond J_{Ic} . In general, interactions between ductile tearing and other sub-critical flaw growth mechanisms are not well understood. As a result, the provided formulation of J_{crit} is both conservative and practical in that additional capability may be present beyond J_{crit} , but also the complex interactions between multiple sub-critical flaw growth mechanisms are avoided. Analyses that permit ductile tearing also require definition of a resistance curve, which in many cases, is not readily available.

For surface and corner crack cases, J_{crit} is calculated from $K_{Ie} = 125 \text{ ksi}\sqrt{\text{in}}$ (from NASGRO® material database) to be $0.5315 \text{ ksi} \cdot \text{in}$.

For through-crack cases, K_c was calculated from:

$$K_c = K_{Ic} \left(1 + B_k e^{-\left(A_k \frac{t}{t_0} \right)^2} \right), \quad t_0 = 2.5 \left(\frac{K_{Ic}}{\sigma_{ys}} \right)^2$$

(Equation 11.3-15)

Where K_{Ic} , A_k , and B_k are taken from the NASGRO® material database.

$K_c = 136.56 \text{ ksi}\sqrt{\text{in}} \rightarrow J_{crit} = 0.5810 \text{ ksi} \cdot \text{in}$ (for plane strain),

$J_{crit} = 0.6343 \text{ ksi} \cdot \text{in}$ (for plane stress)

While K_c and K_{Ie} are used in this example for benchmarking purposes, these parameters should be used with caution in practice. This is because the equations to approximate K_c and K_{Ie} in NASGRO® are empirical equations and may not be valid for all materials. It is also known that deviations from these solutions occur for small cracks [11.3-8]. In NASGRO®, an assessment can be forced to use K_{Ic} by setting B_k equal to 0 for through cracks, or by selecting ‘Constant K_c ’ in the ‘ K_c values at tips used in analysis’ field for surface cracks, noting that for through crack geometries, NASGRO® will default to K_c , and for corner crack and surface crack geometries, NASGRO® will default to K_{Ie} .

Step 5: Define constraint alpha (α_c) for the application

Lastly, the constraint alpha (α_c) for the application needs to be defined. The constraint alpha for the application, which is input into the EPFM material module, differs from the constraint alpha used to define the degree of elastic constraint present in the fatigue crack growth test results. In general, elastic constraint quantifies the degree of triaxial stress present at a given crack-tip. While it is known that elastic constraint varies as a function of several inputs, Newman’s crack closure model assumes that this parameter is constant.

As described in the NASGRO® Manual, α_c typically varies from 1 to 3, with 1 corresponding to plane stress conditions, and 3 to plane strain conditions. The NASGRO® manual also recommends using a 2.55 constraint alpha for interior crack tips and a 1.15 constraint alpha for

NASA-HDBK-5010, VOLUME 2, REVISION A

surface crack tips [11.3-8]. To understand the broader impact of α_c , analyses in this benchmark were completed with $\alpha_c = 1$ and $\alpha_c = 3$.

The completion of all five steps above fully defines the EPFCG parameters required by the NASGRO® EPFM module. A summary of the key equations associated with defining EPFCG parameters is provided in Table 11.3-4, Key Equations Associated with Deriving EPFCG Properties in NASGRO®.

Table 11.3-4—Key Equations Associated with Deriving EPFCG Properties in NASGRO®

Steps to Derive EPFM Properties for use in NASGRO®	Key Equations
Step 1: Define Stress-Strain Properties	$\frac{\epsilon}{\epsilon_0} = \frac{\sigma}{\sigma_0} + \alpha \left(\frac{\sigma}{\sigma_0}\right)^n$
Step 2: Determine Crack Closure Corrected LEFCG Properties	$\frac{da}{dN} = \frac{C_0}{U_0^{m_0}} (\Delta K_{eff})^{m_0}$
Step 3: Derive EPFCG Properties from LEFCG Properties	$\frac{da}{dN} = \frac{C_0 (E')^{m_0/2}}{U_0^{m_0}} (\Delta J_{eff})^{m_0/2}$
Step 4: Define J_{crit}	$J_{crit} = \frac{K_{crit}^2}{E'}$
Step 5: Define Constraint Alpha (α_c) for the Application	$\alpha_c = 1$ (plane stress) $\alpha_c = 3$ (plane strain)

With all EPFCG parameters fully defined, the EPFM module material inputs can be established. The surface and corner crack material inputs for $R > 0$ are shown in Figure 11.3-7, EPFCG Material Inputs for Surface and Corner Cracks, $R > 0$, Constraint Alpha Evaluated at a Value of both 1 and 3.

Material properties: [Ramberg-Osgood eqn: Eps/Eps0 = Sigma/Sigma0 + alpha*(Sigma/Sigma0)**n]

Modulus	Poisson ratio	R-O eqn alpha	Sigma0 n	Yield	UTS
<input type="text" value="29.4E3"/>	<input type="text" value="0.29"/>	<input type="text" value="0.343"/>	<input type="text" value="171"/>	<input type="text" value="17.16"/>	<input type="text" value="171"/>

Crack growth parameters:

C0	m0	U0	Constraint Alpha	Jmat
<input type="text" value="1.00E-10"/>	<input type="text" value="3.291"/>	<input type="text" value="1"/>	<input type="text" value=""/>	<input type="text" value="0.5315"/>

Figure 11.3-7—EPFCG Material Inputs for Surface and Corner Cracks, $R > 0$, Constraint Alpha Evaluated at a Value of both 1 and 3

Using the specimen geometry and loading conditions from Table 11.3-2, EPFCG predictions were calculated in NASGRO®, whereby the cycles to achieve the corresponding final test condition were determined. The critical value of J was included as a limiting threshold using EPFCG for all test cases except S11 and S13. For these test specimens, ductile tearing was noted by McClung, et al., during the first test cycle. It is expected that analysis of S11 and S13 test conditions would terminate at the initial cycle. To compare NASGRO® EPFCG predictions with test for S11 and S13, J_{crit} was set to an arbitrarily large value. Figure 11.3-8, NASGRO® EPFCG Predictions vs. Test Cycles, provides a comparison of EPFCG predictions versus test for all specimens.

NASA-HDBK-5010, VOLUME 2, REVISION A

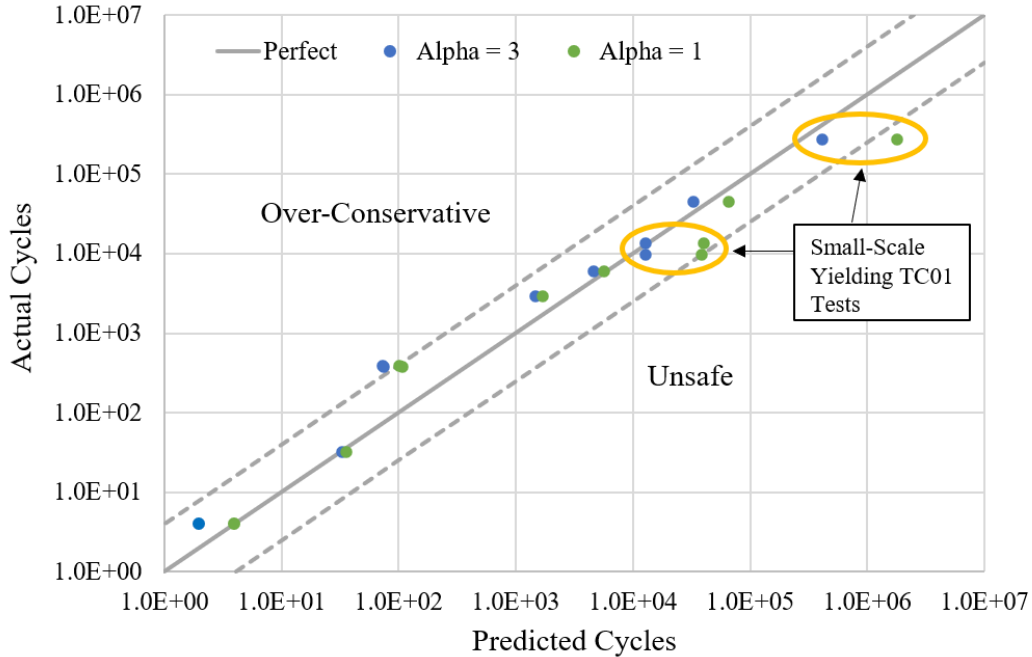


Figure 11.3-8—NASGRO® EPFCG Predictions vs. Test Cycles

In Figure 11.3-8, the solid line represents perfect agreement between prediction and test. Anything that lies above the solid line is conservative, and anything below the solid line is unconservative. The dashed lines in Figure 11.3-8 were constructed by applying a four times service life against the solid line on either side of the curve. The results fall within the dashed bands, except for test case SD2 and S25; whereby an $\alpha_c = 1$ for SD2, and $\alpha_c = 3$ for S25, resulted in larger deviations from test. The corresponding data in tabular form is provided below in Table 11.3-5, NASGRO® EPFCG Predictions vs. Test Cycles.

Table 11.3-5—NASGRO® EPFCG Predictions vs. Test Cycles

Specimen #	Crack Geometry	Cycles @ alpha = 1	Cycles @ alpha = 3	Test Cycles (N)
D1	Through	38,832	12,841	9,820
SD1		40,628	12,911	13,470
SD2		1,806,635	412,250	270,118
S7	Surface	5,700	4,600	5,900
S33		65,364	32,858	44,900
S25		101	73	385
S29		107	75	378
S11		2	4	4
S13		36	33	32
S44	Corner	1,700	1,460	2,950

NASA-HDBK-5010, VOLUME 2, REVISION A

The reason for the deviation with test case S25 can likely be explained by the definition of the critical value of J . The chosen definition of J_{crit} represents the point at which stable ductile tearing can occur, so long as stability conditions associated with the applicable R-curve are met. Given that additional cycles may be permitted in an analysis that allows for ductile tearing, it makes sense that the NASGRO® EPFCG results would underpredict cycles to failure for both S25 and S29; noting that both specimens represent testing of deep cracks cycled to failure.

In contrast to the over-conservative results for S29, the unconservative result for SD2 is more concerning. In this case, as well as the other SSY tests (e.g., D1 & SD1), results with an alpha constraint of 1 overpredict cycles to failure by an appreciable amount. The reason for this is likely due to the high degree of elastic constraint present in the samples. Given that crack-tip plasticity is small in these test cases relative to the specimen geometry, the stress state at the crack-tip is likely dominated by triaxial stress. This is supported by the fact that results for an alpha constraint of 3 are very close to the test results. Subsequently, when the degree of elastic constraint in a given application is uncertain, the use of a constraint alpha of 3 is prudent.

Overall, the NASGRO® EPFCG predictions are in reasonable agreement with test. The NASGRO® EPFM module successfully predicted EPFCG beyond the conditions for which section 11.3.2 allows. This increases confidence in the use of EPFM for applications with moderate plasticity. It also suggests that with EPFCG model correlation to test, it may be permissible to use EPFM beyond the material yield strength.

Finally, the results suggest that it is possible to derive EPFCG parameters from LEFCG parameters. One must be cautious when selecting the LEFCG fatigue crack growth properties as material composition, product form, and environments all play a significant role in fatigue crack growth properties.

11.3.4.2 EPFM Benchmark – Al 6061-T6 Elastic-Plastic Coupon Testing

The fatigue crack growth tests in this study were taken from the NASA/TM-2020-5006765/Volume I, NESC-RP-16-01183, “Composite Overwrapped Pressure Vessel (COPV) Damage Tolerance Life Analysis Methodology and Test Best Practices. The results from these tests were used to evaluate the predictions of the NASGRO® EPFM module.

The fatigue crack growth tests were conducted on Aluminum 6061-T6 rolled sheet specimens with surface cracks. Tests were completed with a 0.1 R ratio on 2-inch-wide specimens. The crack width and depth were determined from the fracture surfaces. A relationship between CMOD and crack depth were obtained from fractographic measurements and the digital image correlation (DIC) surface measurements of CMOD. The test geometry, loads applied, and results are displayed in Table 11.3-6, Fatigue Crack Growth Measurement Test Results for Surface Cracks in Aluminum 6061-T6 Rolled Sheet [11.3-9].

NASA-HDBK-5010, VOLUME 2, REVISION A

Table 11.3-6—Fatigue Crack Growth Measurement Test Results for Surface Cracks in Aluminum 6061-T6 Rolled Sheet [11.3-9]

Test ID	Material Orientation	Thickness (in)	Max Stress Applied (ksi)	Initial Crack Depth (in)	Initial Crack Width (in)	Initial Aspect Ratio	Final Crack Depth (in)	Final Crack Width (in)	Final Aspect Ratio	Cycles
FL-LT-032-11	LT	0.032	35	0.0195	0.0213	0.9155	0.0264	0.0303	0.8713	3,502
FL-LT-032-13	LT	0.032	40	0.0202	0.02	1.011	0.027	0.0299	0.903	2,502
FL-LT-032-18	LT	0.032	35	0.02	0.0209	0.9569	through	0.0372	--	5,302
FL-LT-032-20	LT	0.032	40	0.0208	0.0233	0.8927	0.0278	0.0327	0.8494	1,752
FL-LT-050-02	LT	0.048	30	0.0335	0.0345	0.9705	0.0458	0.0494	0.9278	3,002
FL-LT-050-03	LT	0.048	30	0.0205	0.0216	0.946	0.0405	0.0442	0.9154	24,002
FL-LT-050-04	LT	0.048	40	0.0203	0.0209	0.9713	0.037	0.037	1	3,502
FL-LT-050-07	LT	0.048	40	0.0267	0.0283	0.9435	0.0427	0.0472	0.9047	1,702
FL-LT-050-12	LT	0.048	35	0.0318	0.0292	1.0905	0.0423	0.0451	0.939	2,502
FL-LT-050-13	LT	0.048	35	0.0192	0.0201	0.9576	0.0359	0.0383	0.9373	8,202
FL-LT-050-16	LT	0.048	35	0.0251	0.027	0.9314	0.0461	0.0494	0.9332	6,002
FL-TL-032-01	TL	0.032	30	0.0195	0.0201	0.9701	through	0.0372	--	12,002
FL-TL-032-06	TL	0.032	30	0.0167	0.0195	0.8564	0.0183	0.021	0.8714	4,002
FL-TL-032-08	TL	0.032	30	0.0192	0.0205	0.9366	0.0261	0.0291	0.8969	8,514
FL-TL-032-09	TL	0.032	30	0.0176	0.0203	0.867	0.0187	0.0218	0.8578	3,000
FL-TL-032-10	TL	0.032	30	0.0191	0.0205	0.9317	0.0299	0.0347	0.8617	10,002
FL-TL-032-15	TL	0.032	30	0.0184	0.0197	0.934	0.0249	0.0284	0.8768	10,002
FL-TL-032-17	TL	0.032	35	0.0195	0.0209	0.933	0.028	0.0316	0.8861	5,202
FL-TL-032-19	TL	0.032	40	0.0181	0.0201	0.9005	through	0.0422	--	4,202
FL-TL-050-01	TL	0.048	40	0.0311	0.0305	1.0197	0.0447	0.049	0.9122	1,602
FL-TL-050-03	TL	0.048	30	0.0265	0.0267	0.9895	0.0444	0.0489	0.9091	8,002
FL-TL-050-10	TL	0.048	30	0.0198	0.0205	0.9657	0.0374	0.0376	0.9925	17,002
FL-TL-050-12	TL	0.048	40	0.0236	0.0221	1.0679	0.0368	0.0392	0.9388	2,502
FL-TL-050-17	TL	0.048	35	0.025	0.024	1.0438	0.0444	0.0446	0.9955	5,502
FL-TL-090-19	TL	0.09	20	0.0199	0.0203	0.9803	0.0757	0.0861	0.8792	186,502
SC-LT-032-01	LT	0.032	30	0.0195	0.0195	1	0.025	0.026	0.9615	8,000
SC-LT-032-02	LT	0.032	30	0.022	0.0215	1.0233	0.028	0.0305	0.918	8,000
SC-LT-032-04	LT	0.032	30	0.0218	0.0218	1	0.03	0.0357	0.8389	12,000
SC-LT-090-04	LT	0.09	30	0.02	0.02	1	0.05	0.0485	1.0309	36,000
SC-LT-090-06	LT	0.09	30	0.019	0.02	0.95	0.043	0.0425	1.0118	32,000
SC-LT-090-08	LT	0.09	30	0.02	0.0205	0.9756	0.0564	0.056	1.0071	36,000
SC-LT-090-09	LT	0.09	30	0.02	0.02	1	0.031	0.03	1.0333	16,000
SC-LT-090-10	LT	0.09	30	0.021	0.0205	1.0244	0.065	0.0665	0.9774	27,500
SC-LT-090-12	LT	0.09	30	0.0223	0.02	1.1155	0.0758	0.0755	1.0038	26,000
SC-LT-090-13	LT	0.09	35	0.021	0.019	1.1082	0.0376	0.0336	1.119	9,000
SC-LT-090-14	LT	0.09	35	0.021	0.0218	0.9642	0.0607	0.0614	0.9894	12,000
SC-LT-090-15	LT	0.09	35	0.023	0.0243	0.9453	0.057	0.0564	1.0115	7,000
SC-LT-090-16	LT	0.09	35	0.025	0.0231	1.0823	0.0602	0.0563	1.0702	11,000
SC-LT-090-18	LT	0.09	35	0.0302	0.0264	1.1461	0.076	0.0789	0.9632	10,000
SC-LT-090-19	LT	0.09	35	0.0252	0.0229	1.0992	0.0628	0.0606	1.0355	11,000

In the NASA TM, NASGRO® LFM predictions for each test are provided. In Volume 1 of the report, it was found that LFM underpredicts the amount of crack growth in 82% of the tests [11.3-9]. LFM is only applicable when small-scale yielding occurs at the crack-tip, the crack-tip plastic zone is surrounded by elastically responding material, and the microstructural features are small relative to the crack size. DIC was used during test to identify when plastic strains reached the back side of the specimens. At that point, the LFM assumption of a crack-tip plastic zone surrounded by elastically responding material is violated. Plastic strains were observed on the back side when the crack depth reached around 75%, 80%, and 90% for the 30 ksi, 35 ksi, and 40 ksi applied loads, respectively.

To further quantify LFM violations, a check was performed using the criteria in section 11.3.2. Table 11.3-7, LFM Limit Checks for the Initial Crack and Loading Condition for the Tests

NASA-HDBK-5010, VOLUME 2, REVISION A

Outlined in Table 11.3-6, contains the LEFM limit checks for the initial crack and loading condition, and Table 11.3-8, LEFM Limit Checks for the Final Crack and Loading Condition for the Tests Outlined in Table 11.3-6, contains the LEFM limit checks for the final crack and loading conditions. If Equation 11.3-3 is violated for r_a or r_b at 0 or 90 degrees, then the LEFM limits are violated for that case. The equation for r_a and r_b at 0 and 90 degrees is provided in the tables. The stress intensity factor, K_I , was calculated at 0 and 90 degrees using standard equations for a stress intensity factor in a plate with a centered surface crack. Red highlighted cells in Tables 11.3-7 and 11.3-8 indicate that the condition in Equation 11.3-3 was not passed for that characteristic length. Only 0 and 90 degrees are checked as these cases envelope the other crack front angle checks.

NASA-HDBK-5010, VOLUME 2, REVISION A

Table 11.3-7—LEFM Limit Checks for the Initial Crack and Loading Condition for the Tests Outlined in Table 11.3-6
(W Corresponds to the Specimen Width, and B Corresponds to the Specimen Thickness. All Characteristic Lengths and LEFM Checks are in Inches.)

Test ID	Thickness (in)	Max Stress Applied (ksi)	Initial Crack Geometry		Characteristic Length at $\phi = 0^\circ$		Check at $\phi = 0^\circ$	Characteristic Length at $\phi = 90^\circ$		Check at $\phi = 90^\circ$	LEFM Limits Violated for Initial Crack?
			Crack Depth (in)	Crack Aspect Ratio	$r_a = c_0$	$r_b = W/2 - c_0$	$\left(\frac{K_{I0}}{\sigma_{ys}}\right)^2$	$r_a = a_0$	$r_b = B - a_0$	$\left(\frac{K_{I90}}{\sigma_{ys}}\right)^2$	
FL-LT-032-11	0.032	35	0.0195	0.9155	0.0213	0.9787	0.03	0.0195	0.0125	0.0216	Yes
FL-LT-032-13	0.032	40	0.0202	1.011	0.02	0.98	0.0396	0.0202	0.0118	0.0255	Yes
FL-LT-032-18	0.032	35	0.02	0.9569	0.0209	0.9791	0.0306	0.02	0.012	0.0209	Yes
FL-LT-032-20	0.032	40	0.0208	0.8927	0.0233	0.9767	0.044	0.0208	0.0112	0.0317	Yes
FL-LT-050-02	0.048	30	0.0335	0.9705	0.0345	0.9655	0.0404	0.0335	0.0145	0.0258	Yes
FL-LT-050-03	0.048	30	0.0205	0.946	0.0217	0.9783	0.0193	0.0205	0.0275	0.0151	No
FL-LT-050-04	0.048	40	0.0203	0.9713	0.0209	0.9791	0.0336	0.0203	0.0277	0.0256	Yes
FL-LT-050-07	0.048	40	0.0267	0.9435	0.0283	0.9717	0.0502	0.0267	0.0213	0.0364	Yes
FL-LT-050-12	0.048	35	0.0318	1.0905	0.0292	0.9708	0.0473	0.0318	0.0162	0.0276	Yes
FL-LT-050-13	0.048	35	0.0192	0.9576	0.0201	0.9799	0.024	0.0192	0.0288	0.0187	Yes
FL-LT-050-16	0.048	35	0.0251	0.9314	0.0269	0.9731	0.0352	0.0251	0.0229	0.0264	Yes
FL-TL-032-01	0.032	30	0.0195	0.9701	0.0201	0.9799	0.0207	0.0195	0.0125	0.0141	Yes
FL-TL-032-06	0.032	30	0.0167	0.8564	0.0195	0.9805	0.017	0.0167	0.0153	0.0139	No
FL-TL-032-08	0.032	30	0.0192	0.9366	0.0205	0.9795	0.0205	0.0192	0.0128	0.0146	Yes
FL-TL-032-09	0.032	30	0.0176	0.867	0.0203	0.9797	0.0184	0.0176	0.0144	0.0146	Yes
FL-TL-032-10	0.032	30	0.0191	0.9317	0.0205	0.9795	0.0204	0.0191	0.0129	0.0146	Yes
FL-TL-032-15	0.032	30	0.0184	0.934	0.0197	0.9803	0.0192	0.0184	0.0136	0.0139	Yes
FL-TL-032-17	0.032	35	0.0195	0.933	0.0209	0.9791	0.0287	0.0195	0.0125	0.0203	Yes
FL-TL-032-19	0.032	40	0.0181	0.9005	0.0201	0.9799	0.0337	0.0181	0.0139	0.0255	Yes
FL-TL-050-01	0.048	40	0.0311	1.0197	0.0305	0.9695	0.0596	0.0311	0.0169	0.0376	Yes
FL-TL-050-03	0.048	30	0.0265	0.9895	0.0268	0.9732	0.0264	0.0265	0.0215	0.0183	No
FL-TL-050-10	0.048	30	0.0198	0.9657	0.0205	0.9795	0.0177	0.0198	0.0282	0.0136	No
FL-TL-050-12	0.048	40	0.0236	1.0679	0.0221	0.9779	0.0384	0.0236	0.0244	0.0256	Yes
FL-TL-050-17	0.048	35	0.025	1.0438	0.024	0.976	0.0323	0.025	0.023	0.0216	Yes
FL-TL-090-19	0.09	20	0.0199	0.9803	0.0203	0.9797	0.007	0.0199	0.0701	0.0057	No
SC-LT-032-01	0.032	30	0.0195	1	0.0195	0.9805	0.0212	0.0195	0.0125	0.014	Yes
SC-LT-032-02	0.032	30	0.022	1.0233	0.0215	0.9785	0.0255	0.022	0.01	0.0156	Yes
SC-LT-032-04	0.032	30	0.0218	1	0.0218	0.9782	0.0254	0.0218	0.0102	0.0159	Yes
SC-LT-090-04	0.09	30	0.02	1	0.02	0.98	0.0163	0.02	0.07	0.0131	No
SC-LT-090-06	0.09	30	0.019	0.95	0.02	0.98	0.0156	0.019	0.071	0.0132	No
SC-LT-090-08	0.09	30	0.02	0.9756	0.0205	0.9795	0.0164	0.02	0.07	0.0135	No
SC-LT-090-09	0.09	30	0.02	1	0.02	0.98	0.0163	0.02	0.07	0.0131	No
SC-LT-090-10	0.09	30	0.021	1.0244	0.0205	0.9795	0.0171	0.021	0.069	0.0133	No
SC-LT-090-12	0.09	30	0.0223	1.1155	0.02	0.98	0.0179	0.0223	0.0677	0.0127	No
SC-LT-090-13	0.09	35	0.021	1.1082	0.0189	0.9811	0.0228	0.021	0.069	0.0164	Yes
SC-LT-090-14	0.09	35	0.021	0.9642	0.0218	0.9782	0.0236	0.021	0.069	0.0195	Yes
SC-LT-090-15	0.09	35	0.023	0.9453	0.0243	0.9757	0.0262	0.023	0.067	0.022	Yes
SC-LT-090-16	0.09	35	0.025	1.0823	0.0231	0.9769	0.0279	0.025	0.065	0.0203	Yes
SC-LT-090-18	0.09	35	0.0302	1.1461	0.0264	0.9736	0.0341	0.0302	0.0598	0.0229	Yes
SC-LT-090-19	0.09	35	0.0252	1.0992	0.0229	0.9771	0.028	0.0252	0.0648	0.0201	Yes

NASA-HDBK-5010, VOLUME 2, REVISION A

Table 11.3-8—LEFM Limit Checks for the Final Crack and Loading Condition for the Tests Outlined in Table 11.3-6

(W Corresponds to the Specimen Width, and B Corresponds to the Specimen Thickness. All Characteristic Lengths and LEFM Checks are in Inches.)

Test ID	Thickness (in)	Max Stress Applied (ksi)	End of Test Crack Geometry		Characteristic Length at $\phi = 0^\circ$		Check at $\phi = 0^\circ$ $\left(\frac{K_{I,0}}{\sigma_{ys}}\right)^2$	Characteristic Length at $\phi = 90^\circ$		Check at $\phi = 90^\circ$ $\left(\frac{K_{I,90}}{\sigma_{ys}}\right)^2$	LEFM Limits Violated for Final Crack?
			Crack Depth (in)	Crack Aspect Ratio	$r_a = c_f$	$r_b = \frac{W/2 - c_f}{W/2}$		$r_a = a_f$	$r_b = \frac{B - a_f}{B}$		
FL-LT-032-11	0.032	35	0.0264	0.8713	0.0303	0.9697	0.0524	0.0264	0.0056	0.0335	Yes
FL-LT-032-13	0.032	40	0.027	0.903	0.0299	0.9701	0.0701	0.027	0.005	0.0426	Yes
FL-LT-032-18	0.032	35	through	--	0.0372	0.9628	through	--	--	through	Yes
FL-LT-032-20	0.032	40	0.0278	0.8494	0.0327	0.9673	0.0765	0.0278	0.0042	0.0484	Yes
FL-LT-050-02	0.048	30	0.0458	0.9278	0.0494	0.9506	0.0739	0.0458	0.0022	0.0394	Yes
FL-LT-050-03	0.048	30	0.0405	0.9154	0.0442	0.9558	0.0588	0.0405	0.0075	0.0352	Yes
FL-LT-050-04	0.048	40	0.037	1	0.037	0.963	0.0842	0.037	0.011	0.0491	Yes
FL-LT-050-07	0.048	40	0.0427	0.9047	0.0472	0.9528	0.1164	0.0427	0.0053	0.0677	Yes
FL-LT-050-12	0.048	35	0.0423	0.939	0.045	0.955	0.0857	0.0423	0.0057	0.0484	Yes
FL-LT-050-13	0.048	35	0.0359	0.9373	0.0383	0.9617	0.0632	0.0359	0.0121	0.0401	Yes
FL-LT-050-16	0.048	35	0.0461	0.9332	0.0494	0.9506	0.1015	0.0461	0.0019	0.0536	Yes
FL-TL-032-01	0.032	30	through	--	0.0372	0.9628	through	--	--	through	Yes
FL-TL-032-06	0.032	30	0.0183	0.8714	0.021	0.979	0.0195	0.0183	0.0137	0.0152	Yes
FL-TL-032-08	0.032	30	0.0261	0.8969	0.0291	0.9709	0.0358	0.0261	0.0059	0.0225	Yes
FL-TL-032-09	0.032	30	0.0187	0.8578	0.0218	0.9782	0.0203	0.0187	0.0133	0.0159	Yes
FL-TL-032-10	0.032	30	0.0299	0.8617	0.0347	0.9653	0.0474	0.0299	0.0021	0.0278	Yes
FL-TL-032-15	0.032	30	0.0249	0.8768	0.0284	0.9716	0.0332	0.0249	0.0071	0.022	Yes
FL-TL-032-17	0.032	35	0.028	0.8861	0.0316	0.9684	0.056	0.028	0.004	0.0338	Yes
FL-TL-032-19	0.032	40	through	--	0.0357	0.9643	through	--	--	through	Yes
FL-TL-050-01	0.048	40	0.0447	0.9122	0.049	0.951	0.1221	0.0447	0.0033	0.0677	Yes
FL-TL-050-03	0.048	30	0.0444	0.9091	0.0488	0.9512	0.0679	0.0444	0.0036	0.038	Yes
FL-TL-050-10	0.048	30	0.0374	0.9925	0.0377	0.9623	0.0468	0.0374	0.0106	0.0273	Yes
FL-TL-050-12	0.048	40	0.0368	0.9388	0.0392	0.9608	0.0833	0.0368	0.0112	0.0519	Yes
FL-TL-050-17	0.048	35	0.0444	0.9955	0.0446	0.9554	0.0877	0.0444	0.0036	0.0449	Yes
FL-TL-090-19	0.09	20	0.0757	0.8792	0.0861	0.9139	0.0484	0.0757	0.0143	0.0301	Yes
SC-LT-032-01	0.032	30	0.025	0.9615	0.026	0.974	0.033	0.025	0.007	0.0199	Yes
SC-LT-032-02	0.032	30	0.028	0.918	0.0305	0.9695	0.0419	0.028	0.004	0.0243	Yes
SC-LT-032-04	0.032	30	0.03	0.8389	0.0358	0.9642	0.0502	0.03	0.002	0.0301	Yes
SC-LT-090-04	0.09	30	0.05	1.0309	0.0485	0.9515	0.051	0.05	0.04	0.0339	Yes
SC-LT-090-06	0.09	30	0.043	1.0118	0.0425	0.9575	0.0413	0.043	0.047	0.0293	No
SC-LT-090-08	0.09	30	0.0564	1.0071	0.056	0.944	0.0623	0.0564	0.0336	0.0403	Yes
SC-LT-090-09	0.09	30	0.031	1.0333	0.03	0.97	0.0268	0.031	0.059	0.0199	No
SC-LT-090-10	0.09	30	0.065	0.9774	0.0665	0.9335	0.0805	0.065	0.025	0.0498	Yes
SC-LT-090-12	0.09	30	0.0758	1.0038	0.0755	0.9245	0.105	0.0758	0.0142	0.0571	Yes

APPROVED FOR PUBLIC RELEASE – DISTRIBUTION IS UNLIMITED

NASA-HDBK-5010, VOLUME 2, REVISION A

Test ID	Thickness (in)	Max Stress Applied (ksi)	End of Test Crack Geometry		Characteristic Length at $\phi = 0^\circ$		Check at $\phi = 0^\circ$	Characteristic Length at $\phi = 90^\circ$		Check at $\phi = 90^\circ$	LEFM Limits Violated for Final Crack?
			Crack Depth (in)	Crack Aspect Ratio	$r_a = c_f$	$r_b = \frac{W/2 - c_f}{c_f}$		$\left(\frac{K_{I0}}{\sigma_{ys}}\right)^2$	$r_a = a_f$		
SC-LT-090-13	0.09	35	0.0376	1.119	0.0336	0.9664	0.0451	0.0376	0.0524	0.0299	Yes
SC-LT-090-14	0.09	35	0.0607	0.9894	0.0614	0.9386	0.0966	0.0607	0.0293	0.0614	Yes
SC-LT-090-15	0.09	35	0.057	1.0115	0.0564	0.9436	0.0861	0.057	0.033	0.0551	Yes
SC-LT-090-16	0.09	35	0.0602	1.0702	0.0563	0.9437	0.0914	0.0602	0.0298	0.0539	Yes
SC-LT-090-18	0.09	35	0.076	0.9632	0.0789	0.9211	0.1472	0.076	0.014	0.0833	Yes
SC-LT-090-19	0.09	35	0.0628	1.0355	0.0606	0.9394	0.0999	0.0628	0.0272	0.0596	Yes

It was found that 72.5% of the tests violated the ASTM-E2899 derived LEFM limits at the test start, and 95% of tests violated LEFM limits at the end of testing. Despite significant ligament plasticity, net section stresses for all tests fell below the material yield strength. As a result, the guidelines established in section 11.3.2 would allow for the use of EPFM analysis for qualification of damage tolerance.

The following steps were undertaken to execute the EPFM analysis:

Step 1: Module selection

To evaluate the NASGRO® EPFM module, analyses were completed and compared to the NASA TM test results in Table 11.3-6. To do this, the NASFLA fatigue crack growth module was chosen, and the elasticity type was switched to “elastic-plastic” under options (see Figure 11.3-9, Accessing NASGRO® EPFM Module).

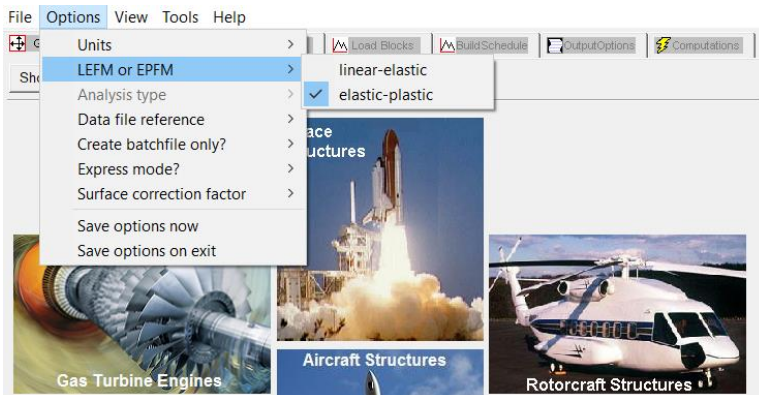


Figure 11.3-9—Accessing NASGRO® EPFM Module

Step 2: Crack geometry

The semi-elliptical surface crack in a plate (SC01) geometry was selected as it is representative of the test coupon geometry. The width was 2 inches for all tests. The thickness, initial flaw depth, and initial crack aspect ratio were input for each test. For surface cracks that propagated

NASA-HDBK-5010, VOLUME 2, REVISION A

through the thickness, the analysis was continued with a through crack in the center of a plate (TC01).

As shown in Figure 11.3-10, Relevant EPFM Crack Geometries, the TC01 crack geometry in the EPFM module included two methods to estimate the J-integral—the EPRI formulation as defined by Kumar et al. [11.3-10] and the RSM as defined by Ainsworth, et al. [11.3-11]. Both methods produce nearly identical results in the NASGRO® EPFM module. In theory the RSM formulation allows for evaluation of materials that do not follow a Ramberg-Osgood, or a power law relationship. With the proper assumptions, the RSM formulation also allows for a relationship to be defined between K and J for materials with small strain hardening exponents. Unfortunately, NASGRO®, v9.2, has limited the EPFM module to a few crack geometries and requires R-O constants regardless of the chosen estimation scheme. The benefits of the RSM formulation are currently unavailable in NASGRO®.

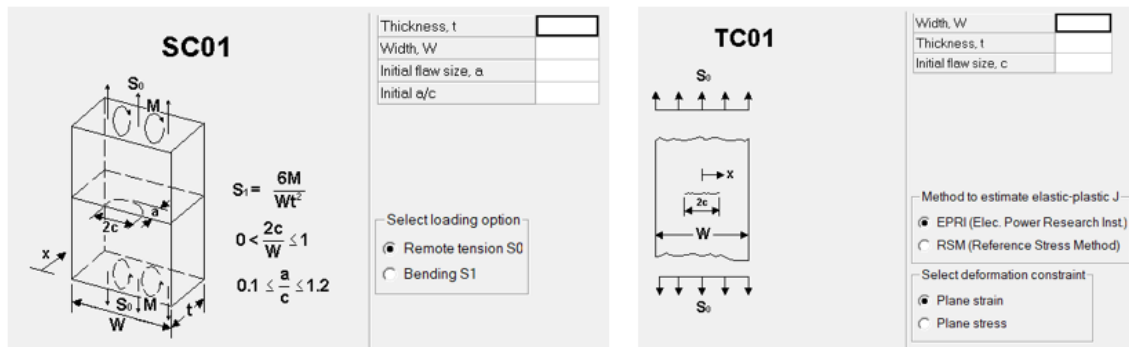


Figure 11.3-10—Relevant EPFM Crack Geometries

Step 3: Material properties

The EPFM module does not have a built-in material database. Consequently, all material properties must be input by the analyst. To define the material properties for this study, tensile test results from Volume 2 of the NASA TM were used [11.3-9]. The modulus of elasticity, yield strength, and ultimate tensile strength were all taken from the stress-strain curve. A Poisson ratio of 0.3 was also determined from testing. Note that both the LT and TL material orientations were tested for Aluminum 6061-T6. These have slightly different properties based on the stress-strain results in the report.

The stress-strain curves were then fit to the Ramberg-Osgood equation:

$$\frac{\epsilon}{\epsilon_0} = \frac{\sigma}{\sigma_0} + \alpha_{R-O} \left(\frac{\sigma}{\sigma_0} \right)^n.$$

(Equation 11.3-16)

σ_0 was defined to be the material yield stress with a 0.2% offset, and the ultimate strength and elongation at failure were used as follows to determine α_{R-O} and n :

APPROVED FOR PUBLIC RELEASE – DISTRIBUTION IS UNLIMITED

NASA-HDBK-5010, VOLUME 2, REVISION A

$$\alpha_{R=0} = \frac{E}{\sigma_0} (0.002) \quad n = \frac{\ln\left(\frac{\epsilon_{PL,f}}{0.002}\right)}{\ln\left(\frac{\sigma_{UTS}}{\sigma_0}\right)} \quad \epsilon_{PL,f} = \epsilon_f - \frac{\sigma_{UTS}}{E}$$

(Equation 11.3-17)

Where E is the elastic modulus, $\epsilon_{PL,f}$ is the plastic strain at ultimate failure, σ_{UTS} is the ultimate tensile strength, and ϵ_f is the total strain at ultimate failure.

Step 4: Crack growth parameters

Next, the crack growth parameters were derived. For this study, the da/dN curves in the NASGRO® LEM material database for Aluminum 6061-T6 (M6AB13AB1) were utilized. This material has da/dN curves for R ratios of 0.1, 0.5, and 0.75. Newman’s approach as defined in section 11.3.4.1 was used to correct for crack closure and normalize the fatigue crack growth curves [11.3-7]. Given that the NASA testing was conducted solely at an R ratio of 0.1, a crack closure corrected fatigue crack growth formulation for $R = 0.1$ alone could have been utilized. In this case, U_0 will not equal 1, but instead will be specific to a stress ratio of 0.1.

To assist in the calculations, the values for α_c and S_{max}/S_{flow} from the applicable NASGRO® material database can be leveraged (see Figure 11.3-11, Material-Specific Parameters Available to Determine EPFCG Parameters when a Single da/dN Curve Exists). Then, a power law relationship can be fit to the linear region of the da/dN data to determine C_0 and m_0 . As stated in section 11.3.4.1, C_0 and m_0 differ from the NASGRO® parameters C and n . When multiple da/dN curves are available, it is recommended that Newman’s approach be utilized.

Material properties: ID M6AB13AB1, 6061-T6 Plt; T-L							
UTS	Yield	K1e	K1c	Ak	Bk	a0	Kth(s)/Kth(l)
45.	41.	36.	27.	1.	0.75	0.0015	0.2
Crack growth parameters: equation constants							
C	n	p	q	DK1	Cth	Cth-	Alpha
7.0E-8	2.30	0.5	0.5	1.31	1.50	0.1	2.0
							Smax/Flow
							0.3

Figure 11.3-11—Material-Specific Parameters Available to Determine EPFCG Parameters when a Single da/dN Curve Exists

Step 5: Select constraint alpha parameter

For semi-elliptical surface cracks, setting the constraint alpha to 3 is conservative. In Appendix V of the NASGRO® manual, it is recommended to use a 2.55 constraint alpha for the interior crack-tip and a 1.15 constraint alpha for the surface crack-tip [11.3-8]. The EPFM material property inputs in NASGRO® only allow for one constraint alpha to be defined. To evaluate the effects of constraint alpha at both extremes, the analyses were run with both the 1.15 and 2.55 values.

Step 6: Calculation of J_{crit}

For the critical value of J, the following equations were utilized:

APPROVED FOR PUBLIC RELEASE – DISTRIBUTION IS UNLIMITED

NASA-HDBK-5010, VOLUME 2, REVISION A

$$J_{crit} = \frac{K_{crit}^2}{E'}, \text{ where } E' = \frac{E}{(1-\nu^2)} \text{ (for plane strain) and } E' = E \text{ (for plane stress)}$$

(Equation 11.3-18)

Where K_{crit} is the critical stress intensity factor relevant to the application (e.g., K_{Ic} , K_c , K_{Ie}).

This formulation of J_{crit} does not allow for ductile tearing. Ductile tearing defines a state of stable crack growth that can occur in materials beyond J_{crit} . In general, interactions between ductile tearing and other sub-critical flaw growth mechanisms are not well understood. As a result, the provided formulation of J_{crit} is both conservative and practical in that additional capability may exist beyond J_{crit} , but also the complex interactions between multiple sub-critical flaw growth mechanisms are avoided. Analyses that permit ductile tearing also require definition of a resistance curve, which in many cases, is not readily available.

For the surface crack (SC01), K_{Ie} was used as K_{crit} , and for the through crack (TC01), K_c was used as K_{crit} . Fracture toughness properties were not stated in the NASA TM, so the values for Aluminum 6061-T6 from the NASGRO® LEMM material database (ID M6AB13AB1) were used. K_{Ie} was taken directly from the database, and K_c was calculated from the following NASGRO® equation:

$$K_c = K_{Ic} \left(1 + B_k e^{-\left(A_k \frac{t}{t_0} \right)^2} \right), \quad t_0 = 2.5 \left(\frac{K_{Ic}}{\sigma_{ys}} \right)^2$$

(Equation 11.3-19)

Where K_{Ic} , A_k , and B_k are taken from the NASGRO® material database.

While K_c and K_{Ie} are used in this example for benchmarking purposes, these parameters should be used with caution in practice. This is because the equations to approximate K_c and K_{Ie} in NASGRO® are empirical equations and may not be valid for all materials. It is also known that deviations from these solutions occurs for small cracks [11.3-8]. In NASGRO®, an assessment can be forced to use K_{Ic} by setting B_k equal to 0 for through cracks, or by selecting ‘Constant K_c ’ in the ‘ K_c values at tips used in analysis’ field for surface cracks, noting that for through crack geometries, NASGRO® will default to K_c ; and for corner crack and surface crack geometries, NASGRO® will default to K_{Ie} .

From the derivations above, the material properties shown in Table 11.3-9, Material Properties used for the NASGRO® EPFCG Analysis for the LT and TL Orientations of Aluminum 6061-T6, were obtained.

NASA-HDBK-5010, VOLUME 2, REVISION A

Table 11.3-9—Material Properties used for the NASGRO® EPFCG Analysis for the LT and TL Orientations of Aluminum 6061-T6

Property	Symbol	LT Orientation	TL Orientation
Elastic modulus	E	10,033 ksi	10,173 ksi
Poisson's ratio	ν	0.3	0.3
Ramberg-Osgood alpha constant	α	0.4560	0.4542
Ramberg-Osgood Sigma0	σ_0	44.0 ksi	44.8 ksi
Ramberg-Osgood n constant	n	26.22	26.17
Yield stress	σ_{ys}	44.0 ksi	44.8 ksi
Ultimate tensile strength	σ_{us}	51.3 ksi	52.0 ksi
Paris Law C coefficient, corrected for crack closure	C_0	3.207E-08 (in/cycles)(ksi $\sqrt{\text{in}}$) ^{-m0}	
Paris Law exponential m coefficient, corrected for crack closure	m_0	2.969	
Crack closure correction factor	U_0	1	
Constraint alpha	α_c	1.15 or 2.55	
Critical J-integral (for SC01)	J_{mat}	0.1175 ksi-in	0.1159 ksi-in
Critical J-integral (for TC01)	J_{mat}	0.2204 ksi-in	0.2172 ksi-in

Step 7: Definition of the load spectra (blocks)

Load blocks were established based on the maximum stress and number of cycles for each test in Table 11.3-6. For every test, an R ratio of 0.1 was used, and tensile stresses were defined using S0 max and S0 min (see Figure 11.3-12, Load Block for Test Case FL-LT-032-11). The same maximum stress was applied during every cycle.

Block Case Definition: block 1 of 1

Enter the number of cycles and values for all stress quantities:

	Cycles	S0 max	S0 min				
Step 1	3502	35	3.5				
2							
3							
4							
5							
6							
7							

Stress scale factor on stress quantity:

Figure 11.3-12—Load Block for Test Case FL-LT-032-11

After completion of all the steps to setup the analysis, the following strategy was used to execute the EPFM analysis. The EPFM analyses were run until reaching the test cycle count. If a through crack developed prior to reaching the test cycle count, the analyses were continued using TC01 geometry. In such instances, the half-crack width when a through crack developed was used as the initial half-crack width in the through crack analysis. Table 11.3-10, Comparison of the Test Results with the NASGRO® EPFM Predictions; Crack Predictions that are not Conservative are

NASA-HDBK-5010, VOLUME 2, REVISION A

Highlighted in Red, contains the NASGRO® EPFM prediction of the final crack depth and width for each test. The results are presented with both a 1.15 and 2.55 constraint alpha.

Table 11.3-10—Comparison of the Test Results with the NASGRO® EPFM Predictions; Crack Predictions that are not Conservative are Highlighted in Red

Test ID	Thickness (in)	Max Stress Applied (ksi)	Final Test Results			NASGRO EPFM 1.15 Constraint Alpha Results			NASGRO EPFM 2.55 Constraint Alpha Results		
			Cycles	Final Crack Depth (in)	Final Crack Width (in)	Cycles	Final Crack Depth (in)	Final Crack Width (in)	Cycles	Final Crack Depth (in)	Final Crack Width (in)
FL-LT-032-11	0.032	35	3,502	0.0264	0.0303	3,502	0.02971	0.03607	3,502	through	0.0675
FL-LT-032-13	0.032	40	2,502	0.027	0.0299	2,502	through	0.0684	2,502	through	0.119
FL-LT-032-18	0.032	35	5,302	through	0.0372	5,302	through	0.136	4,667	through	0.031
FL-LT-032-20	0.032	40	1,752	0.0278	0.0327	1,752	through	0.0451	1,752	through	0.0578
FL-LT-050-02	0.048	30	3,002	0.0458	0.0494	3,002	0.0413	0.047	3,002	through	0.0713
FL-LT-050-03	0.048	30	24,002	0.0405	0.0442	16,412	through	0.438	9,772	through	0.0554
FL-LT-050-04	0.048	40	3,502	0.037	0.037	3,502	0.041	0.0488	3,502	through	0.211
FL-LT-050-07	0.048	40	1,702	0.0427	0.0472	1,702	0.0394	0.0462	1,702	through	0.0632
FL-LT-050-12	0.048	35	2,502	0.0423	0.0451	2,502	0.0427	0.0489	2,502	through	0.0888
FL-LT-050-13	0.048	35	8,202	0.0359	0.0383	8,202	through	0.094	6,236	through	0.0551
FL-LT-050-16	0.048	35	6,002	0.0461	0.0494	6,002	through	0.298	4,334	through	0.0553
FL-TL-032-01	0.032	30	12,002	through	0.0372	12,002	through	0.192	4,399	through	0.0365
FL-TL-032-06	0.032	30	4,002	0.0183	0.021	4,002	0.0207	0.0238	4,002	0.0255	0.0294
FL-TL-032-08	0.032	30	8,514	0.0261	0.0291	8,514	through	0.0459	4,404	through	0.0368
FL-TL-032-09	0.032	30	3,000	0.0187	0.0218	3,000	0.0207	0.0237	3,000	0.0241	0.0276
FL-TL-032-10	0.032	30	10,002	0.0299	0.0347	10,002	through	0.0742	4,436	through	0.0369
FL-TL-032-15	0.032	30	10,002	0.0249	0.0284	10,002	through	0.0564	4,860	through	0.0369
FL-TL-032-17	0.032	35	5,202	0.028	0.0316	5,202	through	0.0986	2,501	through	0.0367
FL-TL-032-19	0.032	40	4,202	through	0.0422	3,529	through	0.2581	1,802	through	0.0369
FL-TL-050-01	0.048	40	1,602	0.0447	0.049	1,602	0.0458	0.0557	1,199	through	0.0538
FL-TL-050-03	0.048	30	8,002	0.0444	0.0489	8,002	0.0448	0.0539	4,631	through	0.0549
FL-TL-050-10	0.048	30	17,002	0.0374	0.0376	17,002	through	0.208	7,727	through	0.0553
FL-TL-050-12	0.048	40	2,502	0.0368	0.0392	2,502	0.0367	0.0416	2,322	through	0.0543
FL-TL-050-17	0.048	35	5,502	0.0444	0.0446	5,502	through	0.0732	3,262	through	0.0544
FL-TL-090-19	0.09	20	186,502	0.0757	0.0861	119,671	through	0.6569	45,775	through	0.106
SC-LT-032-01	0.032	30	8,000	0.025	0.026	8,000	0.031	0.0374	8,000	through	0.323
SC-LT-032-02	0.032	30	8,000	0.028	0.0305	8,000	through	0.0734	7,037	through	0.438
SC-LT-032-04	0.032	30	12,000	0.03	0.0357	10,780	through	0.438	7,026	through	0.438
SC-LT-090-04	0.09	30	36,000	0.05	0.0485	25,666	through	0.438	14,255	through	0.438
SC-LT-090-06	0.09	30	32,000	0.043	0.0425	26,346	through	0.438	14,602	through	0.438
SC-LT-090-08	0.09	30	36,000	0.0564	0.056	25,359	through	0.438	14,091	through	0.438
SC-LT-090-09	0.09	30	16,000	0.031	0.03	16,000	0.0428	0.0455	14,255	through	0.438
SC-LT-090-10	0.09	30	27,500	0.065	0.0665	24,714	through	0.438	13,763	through	0.438
SC-LT-090-12	0.09	30	26,000	0.0758	0.0755	24,187	through	0.438	13,509	through	0.438
SC-LT-090-13	0.09	35	9,000	0.0376	0.0336	9,000	0.0457	0.0488	8,461	through	0.343
SC-LT-090-14	0.09	35	12,000	0.0607	0.0614	12,000	through	0.163	7,916	through	0.343
SC-LT-090-15	0.09	35	7,000	0.057	0.0564	7,000	0.0465	0.0503	7,000	through	0.25
SC-LT-090-16	0.09	35	11,000	0.0602	0.0563	10,922	through	0.343	7,027	through	0.343
SC-LT-090-18	0.09	35	10,000	0.076	0.0789	9,010	through	0.109	5,891	through	0.343
SC-LT-090-19	0.09	35	11,000	0.0628	0.0606	10,909	through	0.109	7,022	through	0.343

As shown in Table 11.3-10, EPFM predictions with a 1.15 constraint alpha were conservative for all but 4 tests. The 4 tests that the EPFM predictions were not conservative for are highlighted in red. EPFM predictions with a 2.55 constraint alpha were conservative for every test. The tests were not run to failure, but the EPFM analyses predicted failure before the cycles seen in test for multiple cases. EPFM with a 1.15 constraint alpha predicted unstable crack growth earlier than 12 of 40 tests, while EPFM with a 2.55 constraint alpha predicted unstable crack growth in 29 of 40 tests. Early failure predictions can likely be attributed to the fact that ductile tearing is not accounted for beyond J_{crit} .

The NASGRO® EPFM predictions are compared to NASGRO® LEM predictions in Figure 11.3-13, Percent of Predictions that were Conservative Compared to Aluminum 6061-T6 Fatigue

NASA-HDBK-5010, VOLUME 2, REVISION A

Crack Growth Test Results for Different Analysis Methods. The analysis is considered conservative if the analysis predicts a larger crack size than that seen in test. The NASGRO® LEFM and LEFM penalized results come from analysis presented in Volume 1 of the NASA TM. In the NASGRO® LEFM penalized analysis, a knockdown is applied that scales with the magnitude of deviation from LEFM assumptions [11.3-9]. As seen in Figure 11.3-13, the NASGRO® LEFM analysis was conservative for only 18% of tests, while the NASGRO® LEFM penalized analysis was conservative for 81% of test. The NASGRO® EPFM analyses bounded 90% of the tests with a 1.15 constraint alpha and bounded all the test data with a 2.55 constraint alpha.

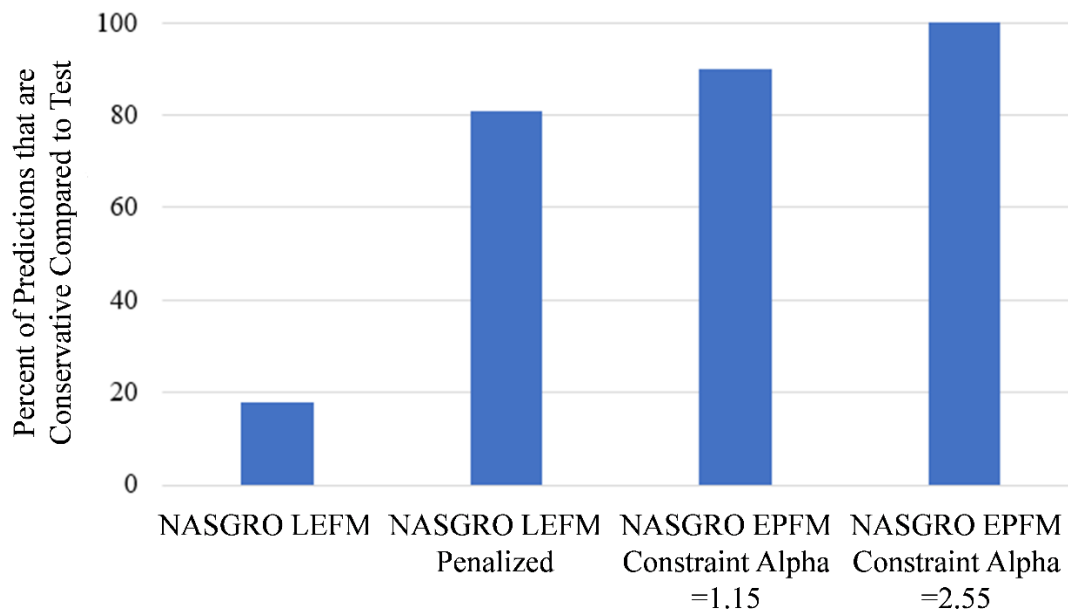


Figure 11.3-13—Percent of Predictions that were Conservative Compared to Aluminum 6061-T6 Fatigue Crack Growth Test Results for Different Analysis Methods

Of the 40 tests, 28 included data on the crack size as a function of cycles for both the test and the NASGRO® LEFM prediction. For these tests, the number of cycles for the crack to reach a 75% through-thickness depth was determined. Analyses were then conducted to the same crack depth to establish predictions for comparison. The LEFM predictions were found to be unconservative for most tests, with an average of 37.7% more cycles predicted than test. The EPFM prediction with a 1.15 constraint alpha had the most accurate results, with an average of only 11.5% less cycles than test. The EPFM prediction with a 2.55 constraint alpha was overly conservative in this case, with an average of 46.7% less cycles than test.

Based on these results, the EPFM predictions with a 1.15 constraint alpha are the best candidate for accurately predicting the crack growth in these test coupons. This can be attributed to low elastic constraint in the test specimens, and the low yield strength of Al 6061-T6. Without test data to support the use of a low constraint alpha, it would be difficult to justify selection of $\alpha_c =$

NASA-HDBK-5010, VOLUME 2, REVISION A

1. 15. Additional investigation into generally determining the appropriate α_c by analysis alone is warranted.

11.3.4.3 EPFM Benchmark – Ti-6Al-4V Elastic-Plastic Coupon Testing

Fatigue crack growth tests on annealed Ti-6Al-4V specimens with notches were performed, and the results were compared to the predictions using the NASGRO® EPFM module. A milling operation on the samples resulted in a notch opening equal to 0.005 inch, with a 10-degree taper from the notch opening to its final depth. Pre-cracking of the specimens was not conducted. It was unknown when sharp cracks initiated during the test, as inspections were not conducted before final failure. While the test specimens represent nontraditional samples, the testing is applicable to situations where the hardware does not contain sharp cracks.

Notch penetration was large in all tests and ranged from 81–94 percent of the specimen thickness. The tests were completed with a 0.1 R ratio and targeted tensile net section stresses slightly below the material yield strength (133 ksi). Detailed information on the test specimens and test conditions are provided in Table 11.3-11, Test Specimens and Test Conditions for Notched Ti-6Al-4V Coupons.

Table 11.3-11—Test Specimens and Test Conditions for Notched Ti-6Al-4V Coupons

Specimen ID	Notch Penetration (%)	Specimen Thickness (in)	Specimen Width (in)	Flaw Depth (a, in)	a/c	Maximum Stress (ksi)	Net Section Stress (ksi)
2	94	0.036	0.4	0.0338	0.636	76.39	105.86
3	86			0.031	0.504	88.54	130.49
5	86			0.031	0.564	91.53	128.62
6	90			0.0324	0.583	76.39	107.84
7	89			0.032	0.555	86.81	124.42
8	84			0.0302	0.538	91.81	130.00
9	84			0.0302	0.572	93.75	129.64
10	81			0.0292	0.549	94.31	130.60

Given the depth of the notched surface cracks, the LFM criteria in section 11.3.2 is not expected to be met. To confirm this, net section stresses (σ_{NS}) and the mode I stress intensity factor (K_I) were calculated using the initial flaw depth, aspect ratio, and applied stress. The criteria from section 11.3.2 was then utilized to check the validity of EPFM:

As a first screen, the net section stresses were checked for each specimen. With $0.9\sigma_{ys} = 119.7 \text{ ksi}$, specimens 3, 4, 7, 8, 9, and 10 are found to violate the LFM criteria. Next, the crack size and ligament length, represented by $r_{\phi a}$ and $r_{\phi b}$, were evaluated (see Figure 11.3-3). While the criteria for $r_{\phi a}$ and $r_{\phi b}$ are required from phi equals 0° to phi equals 90° , the small ligament length at phi equals 90° is a logical first check. For specimens 2 and 6, $K_I(a)$ is found to equal $23.09 \text{ ksi}\sqrt{\text{in}}$ and $23.78 \text{ ksi}\sqrt{\text{in}}$, respectively. Due to the thinness of these specimens, plane stress conditions are evaluated against the ligament length as follows:

APPROVED FOR PUBLIC RELEASE – DISTRIBUTION IS UNLIMITED

NASA-HDBK-5010, VOLUME 2, REVISION A

Specimen 2: $\left(\frac{K_I}{\sigma_{ys}}\right)^2 = 0.030 \text{ inches} > 0.002 \text{ inches}$

Specimen 6: $\left(\frac{K_I}{\sigma_{ys}}\right)^2 = 0.032 \text{ inches} > 0.0036 \text{ inches}$

Where the ligament length is calculated using the thickness and flaw depth for each specimen.

As expected, the crack-tip is not surrounded by elastically responding material, and the LEFM criteria is not met for any of the specimens.

For problems with different loading and geometric conditions, a more comprehensive LEFM validity check through the entire load spectra and across the entire flaw surface may have been warranted. In these instances, ASTM E2899-19 provides an approximation for K_I as a function of ϕ [11.3-1]. ASTM E2899-19 also provides a means to calculate the critical crack initiation angle. This angle may not correspond to the critical angle for LEFM validity for fatigue crack growth conditions; whereby crack growth occurs in every direction.

Net section stresses are slightly below the material yield strength at the beginning of all tests, and prior to failure, net section stresses grow to values in excess of the material yield strength for many of the specimens. In these instances, the recommendations in section 11.3.2 would not warrant EPFM analysis alone for qualification purposes.

Before conducting fatigue crack growth tests, tensile testing was conducted on the annealed Ti-6Al-4V sheet stock. The yield and ultimate strengths of the material were found to be 133 ksi and 138 ksi, respectively. Modulus of elasticity was determined to equal 16,700 ksi. Using these properties as an initial basis, MMPDS-13 was utilized to find a similar stress-strain curve. Ramberg-Osgood parameters were calculated from the stress-strain curve (see Figure 11.3-14, Ramberg-Osgood Plasticity Model for Ti-6Al-4V).

NASA-HDBK-5010, VOLUME 2, REVISION A

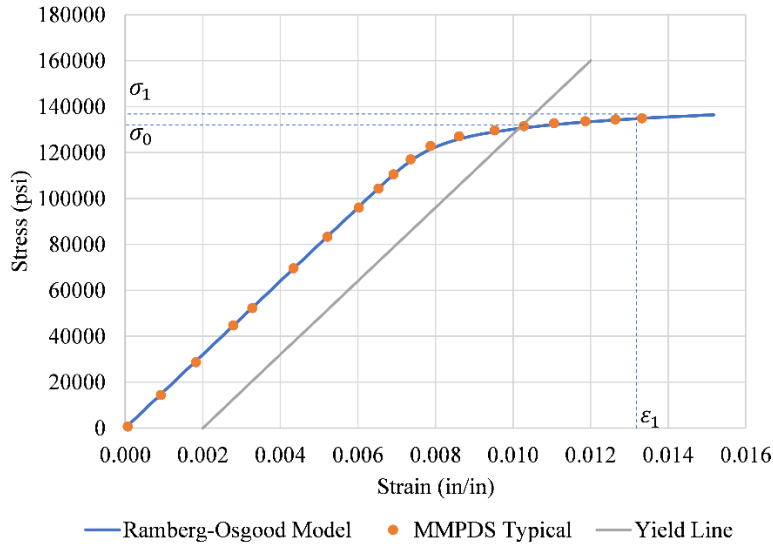


Figure 11.3-14—Ramberg-Osgood Plasticity Model for Ti-6Al-4V

$$E = 16,000 \text{ ksi}, \quad \sigma_0 = 130.5 \text{ ksi}, \quad \sigma_1 = 134.9 \text{ ksi}, \quad \varepsilon_1 = 0.0133$$

$$\varepsilon_{PL,1} = \varepsilon_1 - \frac{\sigma_1}{E} = 0.00489, \quad \alpha_{R-O} = \frac{E}{\sigma_{ys}} (0.002) = 0.2452, \quad n = \frac{\ln\left(\frac{\varepsilon_{PL,1}}{0.002}\right)}{\ln\left(\frac{\sigma_1}{\sigma_0}\right)} = 27.172$$

For EPFCG properties, the NASGRO® material database was leveraged. Mill annealed properties (P3EA13AB1) were chosen based on a comparison between the material certifications and available material properties in NASGRO®; da/dN data at several stress ratios are available for P3EA13AB1; each was obtained through testing of 0.25 inch plate (see Figure 11.3-15, da/dN Test Data Available in Mill Annealed Ti-6Al-4V. Given that the test specimens in question are much thinner, it is expected that the inherent elastic constraint in the fatigue crack growth tests bounds the elastic constraint for the application.

NASA-HDBK-5010, VOLUME 2, REVISION A

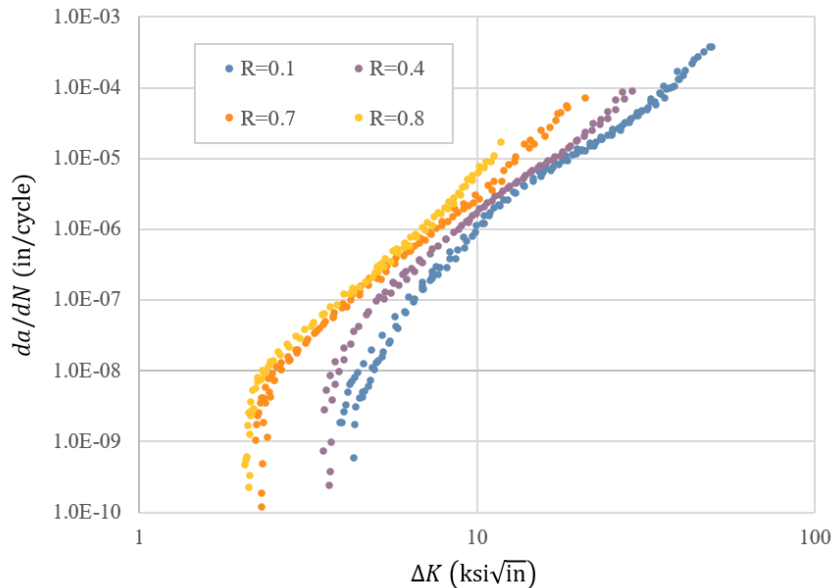


Figure 11.3-15—da/dN Test Data Available in Mill Annealed Ti-6Al-4V

Using the data shown in Figure 11.3-15, the methodology and iterative process described in section 11.3.4.1 were used to calculate ΔK_{eff} , and subsequently, the necessary fatigue crack growth parameters C_0 , m_0 , and U_0 . The critical value of the J-integral for the surface cracks was obtained from K_{Ic} and was found to equal $0.229 \text{ ksi} \cdot \text{in}$. Constraint alpha (α_c) was varied from 1.15 to 2.55 to determine sensitivity to this parameter. Figure 11.3-16, EPFCG Properties used to Analyze Ti-6A-4V Surface Cracks, provides the complete set of properties used to define the EPFCG model for the notched surface cracks.

Material properties: [Ramberg-Osgood eqn: $Eps/Eps0 = Sigma/Sigma0 + alpha*(Sigma/Sigma0)^n$]						
Modulus	Poisson ratio	R-O eqn alpha	Sigma0	n	Yield	UTS
16000	0.31	0.2452	130.5	27.172	133	138
Crack growth parameters:						
C0	m0	U0	Constraint Alpha	Jmat		
6.48E-10	3.6772	1	2.55	0.22868		

Figure 11.3-16—EPFCG Properties used to Analyze Ti-6A-4V Surface Cracks

The primary objective of the laboratory testing was to determine the propensity for a through crack to develop. To this end, dye penetrant was applied to the notched surface and dye penetrant inspection (DPI) of the back surface was conducted. To determine when a through crack developed, a fluorescent sensitive camera was utilized. Figure 11.3-17, Dye Penetrant Inspection of Specimen 6 Back Surface at Breakthrough of Surface Crack, shows development and detection of a through crack in specimen 6 using the outlined approach.

NASA-HDBK-5010, VOLUME 2, REVISION A

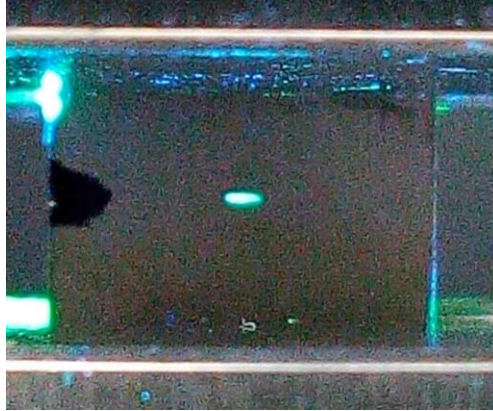


Figure 11.3-17—Dye Penetrant Inspection of Specimen 6 Back Surface at Breakthrough of Surface Crack

For each test specimen, an initial monotonic load equal to the maximum stress from Table 11.3-11 was applied. Upon unloading, DPI was conducted. Thereafter, the specimens were cycled at $R = 0.1$ to the maximum stress from Table 11.3-11. DPI was conducted every 10 cycles, until either a through crack was observed, or 100 cycles were reached. All specimens exhibited through cracks before 100 cycles except specimen 6. After reaching 100 cycles, specimen 6 was cycled at 86.81 ksi with a stress ratio of 0.1 for three additional cycles, at which point a through crack was observed.

In the EPFM module, the geometry for each specimen was specified using the SC01 crack geometry. The load block for each analytical prediction included a single initial cycle at $R = 0$, followed by 100 cycles at $R = 0.1$. The analytical model for specimen 6 included additional cycles at 86.81 ksi. The number of cycles to reach a through crack were determined from the NASGRO® EPFM output as shown in Figure 11.3-18, Cycles to a Through Crack for Specimen 2 with a Constraint Factor of 1.15 as Reported in the NASGRO® EPFM Module.

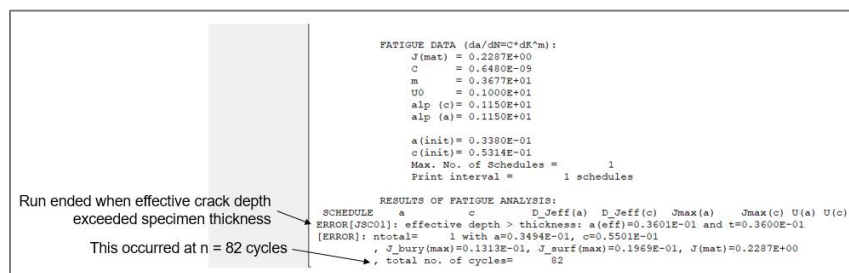


Figure 11.3-18—Cycles to a Through Crack for Specimen 2 with a Constraint Factor of 1.15 as Reported in the NASGRO® EPFM Module

Test results, EPFM, and LEFM predictions for all specimens are provided in Table 11.3-12, Test Results and Analytical Predictions for Ti-6Al-4V Specimens. As shown in Table 11.3-12, the EPFM predictions with a constraint factor of 1.15 are in good agreement with test data. While some of the predictions using $\alpha_c = 1.15$ are unconservative, these are all within 10% of the test

NASA-HDBK-5010, VOLUME 2, REVISION A

results. With a constraint factor of 2.55, all EPFCG predictions are conservative—some by an appreciable amount. The appropriate constraint factor for these test conditions is closer to 1.15, but likely falls between 1.15 and 2.55.

Table 11.3-12—Test Results and Analytical Predictions for Ti-6Al-4V Specimens

Specimen Details				Cycles Until Through-Crack			
Specimen ID	Notch Penetration (%)	a/c	Maximum Stress (ksi)	Test	EPFM ($\alpha_c = 1.15$)	EPFM ($\alpha_c = 2.55$)	LEFM
2	94	0.636	76.39	81-90	82	45	23
3	86	0.504	88.54	91-100	56	44	77
5	86	0.564	91.53	81-90	71	53	84
6	90	0.583	76.39	103	114	80	92
7	89	0.555	86.81	51-60	62	44	66
8	84	0.538	91.81	61-70	76	59	99
9	84	0.572	93.75	91-100	85	64	103
10	81	0.549	94.31	81-90	95	73	122

Note: LEFM predictions terminate at 95% of the specimen thickness and do not represent a through-crack condition.

Like the EPFM predictions, LEFM predictions were also in general agreement with test data. While this was initially unexpected, one of the reasons for this can be attributed to the fact that the LEFM surface crack model SC30 in NASGRO® terminates LEFM analyses when a crack reaches 95% of the specimen thickness. This can be seen in Table 11.3-12 for specimen 2, where the initial notch penetration was 0.94t, and subsequently, the cycles to a through crack totaled 23. The tested flaws were notches and not sharp cracks. As a result, the cycles to reach a through crack are likely inflated. In other words, had notches been pre-cracked to equivalent crack sizes, the cycles to reach a through crack would be smaller. Despite this, the EPFM predictions are relatively accurate, which suggests that the large net section stresses that were targeted, may have resulted in formation of sharp cracks quickly. In many applications, the flaw tip characteristics may not be sharp; in these cases, the approach is practical. Sharp cracks are likely to initiate early in the cyclic test, but it is unknown when this would occur without removing the specimen and performing inspections.

Testing was continued until failure on a subset of the specimens. This includes specimens 7, 8, 9, and 10. For these tests, the same maximum stresses and stress ratios were prescribed. To establish an initial flaw size for EPFM predictions, the half-crack width when a through crack developed was extracted from the NASGRO® output as shown in Figure 11.3-19, Half-Crack Width When a Through Cracked Developed for Specimen 2 with a Constraint Factor of 1.15.

NASA-HDBK-5010, VOLUME 2, REVISION A

```

RESULTS OF FATIGUE ANALYSIS:
SCHEDULE  a      c      D_Jeff(a)  D_Jeff(c)  Jmax(a)    Jmax(c)  U(a)
ERROR[JSC01]: effective depth > thickness: a(eff)=0.3601E-01 and t=0.3600E-01
[ERROR]: ntotal=      1 with a=0.3494E-01, c=0.5501E-01
          , J_bury(max)=0.1313E-01, J_surf(max)=0.1969E-01, J(mat)=0.2287E+00
          , total no. of cycles=      82
    
```

Figure 11.3-19—Half-Crack Width When a Through Cracked Developed for Specimen 2 with a Constraint Factor of 1.15

From the EPFM module, the TC01 through crack geometry was chosen. The EPRI J integral estimation scheme was selected; it is noted that similar results are obtained with both the EPRI and RSM. The critical value of the J-integral was then calculated for a through crack using the following equations:

$$J_{crit} = \frac{K_c^2}{E'} \quad \rightarrow \quad K_c = K_{Ic} \left(1 + B_k e^{-\left(A_k \frac{t}{t_0} \right)^2} \right) \quad \rightarrow \quad t_0 = 2.5 \left(\frac{K_{Ic}}{\sigma_{ys}} \right)^2$$

(Equation 11.3-20)

$$A_k, B_k = 1.0, \quad E' = E = 16,000 \text{ ksi}, \quad K_{Ic} = 50 \text{ ksi}\sqrt{\text{in}}$$

In the NASGRO® EPFM module, specimen failure is identified when $J_{max} > J_{crit}$. This does not necessarily represent unstable crack growth, but rather that J_{crit} had been exceeded. Given the complexities involved with analyses that permit ductile tearing, J_{crit} is used as a conservative threshold. For reference, an example EPFM module output at specimen failure is shown in Figure 11.3-20, Cycles to Exceedance of J_{crit} for Specimen 2, where J_{crit} and J_{mat} are identical.

	RESULTS OF FATIGUE ANALYSIS:
	SCHEDULE c D_Jeff(c) Jmax(c) U(c)
Reason the analysis ended:	Results: one-D, J(max)=0.6252E+00 J(mat)=0.5926E+00
Crack size at failure:	with c=0.8641E-01 after 0-th schedule,
Cycles to failure:	total no. of cycles= 101

Figure 11.3-20—Cycles to Exceedance of J_{crit} for Specimen 2

In addition to a change in J_{crit} for the through crack assessments, the constrain factor (α_c) was fixed at 1.15. This is because in the through crack configuration, plane stress conditions dominate around the crack-tip. Lastly, the strain hardening exponent for the R-O relationship was updated from 27.172 to 20, noting that 20 is the maximum strain hardening exponent allowed with the TC01 geometry in NASGRO®.

With all material and geometric inputs established, LEFM and EPFM analyses were conducted in NASGRO®. Test results for the through cracked specimens taken to failure, as well as EPFM and LEFM predictions are provided in Table 11.3-13, Test Results and Analytical Predictions for Ti-6Al-4V Through Crack Specimens Taken to Failure.

NASA-HDBK-5010, VOLUME 2, REVISION A

Table 11.3-13—Test Results and Analytical Predictions for Ti-6Al-4V Through Crack Specimens Taken to Failure

Specimen Details			Post-Through Crack Cycles to Failure		
Specimen ID	Initial Notch Penetration (%)	Maximum Stress (ksi)	Test	EPFM ($\alpha_c = 1.15$)	LEFM
7	89	86.81	174	101	322
8	84	91.81	64	59	251
9	84	93.75	42	58	260
10	81	94.31	37	50	240

As shown in Table 11.3-13, the EPFM predictions are relatively accurate; once again, the cycles to failure for some specimens were slightly unconservative, while others were slightly conservative. To look at these differences from the perspective of elastic constraint, the following equation from NASGRO®, Appendix V, for through cracks was examined.

$$\mathbf{a}_t = 1.15 + 1.4e^{-n}, \quad n = 0.95 \left(\frac{K_{max}}{\sigma_{flow}\sqrt{t}} \right)^{1.5}$$

(Equation 11.3-21)

where \mathbf{a}_t is the constraint coefficient used in the NASGRO® Willenborg retardation models [11.3-8].

Calculating \mathbf{a}_t for the conditions at the start of each test, one finds similar values for each set of conditions; with an \mathbf{a}_t value of 1.37, 1.33, 1.34, and 1.33 for specimens 7, 8, 9, and 10, respectively. This supports the notion that a constraint factor larger than 1.15 may be warranted for these coupons, but it does not explain the apparent and random deviations from test. Subsequently, the slightly unconservative, and slightly conservative EPFM results could simply be attributed to scatter in the test data. In contrast to the EPFM results, cycles to failure are consistently overpredicted by LEFM with a minimum error of 185 percent and a maximum error of 650 percent.

Lastly, the results tend to suggest that little-to-no ductile tearing occurred in these specimens. This is supported by the fact that the EPFM results did not consistently predict early failures. To an extent, this is also supported by the fact that the LEFM results consistently overpredict cycles to failure. This example shows that even under conditions where net section stresses exceed the material yield strength, the EPFM module in NASGRO® can produce reliable results, particularly when using the appropriate constraint alpha.

NASA-HDBK-5010, VOLUME 2, REVISION A

11.3.5 EPFM Benchmarks and Examples – Lessons Learned

Through benchmarking of the EPFM module in NASGRO®, several lessons learned were established. First, the derivation of EPFCG properties from LEFCG properties was shown to be possible for the evaluated specimens. In some instances, cyclic stresses in test exceeded the yield strength of the material, which violates the criteria established in Figure 11.3-2. Even under these conditions, the EPFCG properties appeared to be acceptable. Despite this, it is recommended to conduct damage tolerance testing for applications that experience large cyclic stresses.

Second, the EPFM results demonstrated reasonable correlation to test data. Figure 11.3-21, Predicted EPFM Cycles Versus Test Cycles for all Three Tests, provides a comparison of the analysis predictions and test results for all benchmarks and examples.

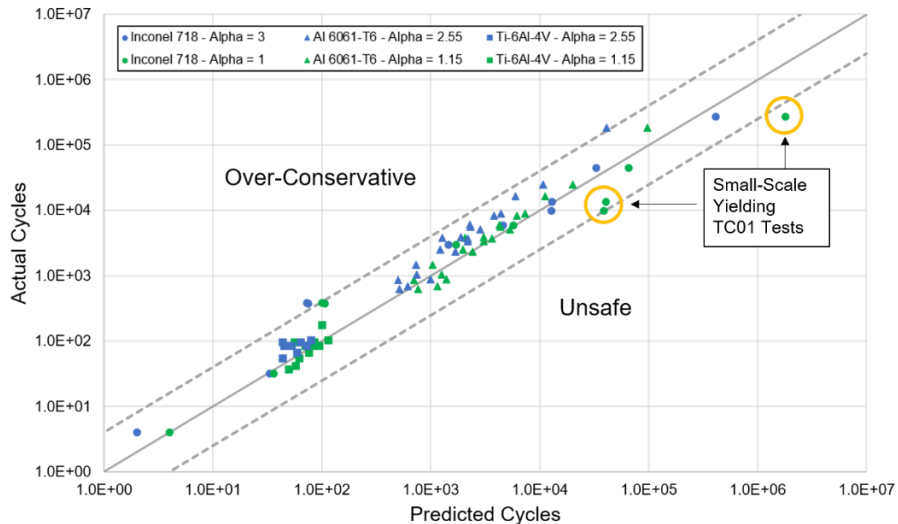


Figure 11.3-21—Predicted EPFM Cycles Versus Test Cycles for all Three Tests

For applications with low elastic constraint, a constraint alpha of 1.0 – 1.15 generally resulted in accurate predictions of crack growth. For applications with high elastic constraint, a constraint alpha of 2.55–3.0 was shown to be necessary to adequately predict test results. In particular, SSY tests of through cracks revealed that a small constraint alpha can grossly overpredict cycles to failure. If there is a lack of analysis or test data to substantiate the presence low elastic constraint in a given application, a constraint alpha value of 3.0 is recommended.

Finally, LEFM predictions in many instances were unconservative with respect to predicting elastic-plastic crack growth and elastic-plastic crack instability (see Figure 11.3-22, Predicted LEFM and EPFM Cycles Versus Test Cycles for all Three Tests).

NASA-HDBK-5010, VOLUME 2, REVISION A

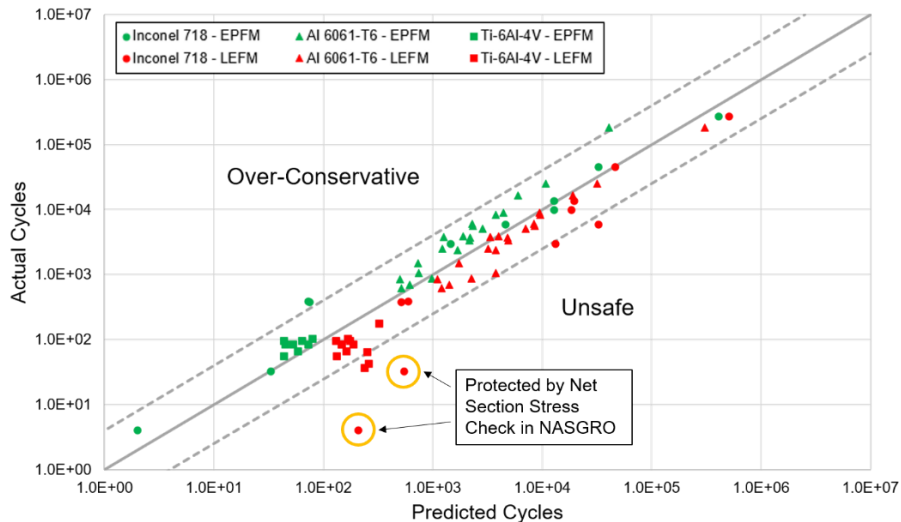


Figure 11.3-22—Predicted LEFM and EPFM Cycles Versus Test Cycles for all Three Tests

As shown in Figure 11.3-22, LEFM predictions conservatively bound the test data in very few instances. For the most egregious errors shown, NASGRO® includes net section stress criteria that can prevent such deviations. These checks may be lacking if the application includes a large net section, at which point, termination of the analysis may not occur before reaching severe EPFCG conditions. In general, LEFM analysis should only be used when SSY prevails at the crack-tip. Use of LEFM when SSY is lost can result in unconservative damage tolerance assessments.

11.4 Damage Tolerance for Additive Manufacturing Parts

As of this writing, NASA-HDBK-5026 providing guidance on strength, fatigue, and fracture control of additive manufacturing (AM) is forthcoming. In case of conflict between this Handbook and NASA-HDBK-5026, NASA-HDBK-5026 takes precedent.

NASA-STD-6030 assigns classifications to AM components depending on the component consequences of failure, structural demand, and AM risk. The AM part classifications are complimentary to, but not replacements for, fracture control classifications. For example, AM parts that are Fracture Critical are, by definition, associated with a catastrophic failure mode, and thus are, by definition, Class A AM components. NASA-STD-6030 imposes rigorous process control measures on Class A components intended to ensure high material quality for these components with high criticality. Components that are nonfracture critical may be Class A or Class B, depending on the specifics of the application. Note also that NASA-STD-6030 specifically prevents AM parts from classification as nonfracture critical, low risk, or as fracture critical lines, fittings, and other pressurized components.

The qualification requirements for AM parts are determined primarily from the application and mission, with some modifications to account for features unique to AM. These modifications are derived from two distinctions: AM is a relatively new process, and each build may be considered the entire material lot. Since each build is a unique lot, the importance of minimizing and

NASA-HDBK-5010, VOLUME 2, REVISION A

tracking process variability becomes more evident. A robust damage tolerance rationale for AM parts is based on a three-part foundation. First, the part design is qualified to existing structural standards. Second, the AM process, including feedstock specification, machine operation, and part post-processing, is developed and qualified per NASA-STD-6030 and defined in a Qualified Material Process (QMP). Finally, rigorous process controls are in place, per NASA-STD-6030 and NASA-STD-6033, Additive Manufacturing Requirements for Equipment and Facility Control, to ensure that production processes maintain similarity with the qualification material. (Reference Rome, et al. (2020)). The importance of developing an appropriate understanding of the AM process and resulting material and ensuring rigor in the process controls for the production of fracture critical spaceflight hardware cannot be overstated. Such development activities are foundational to any fracture control rationale for an AM component.

There is no authoritative source for AM material properties. Mechanical properties, including modulus, strength, ductility, and fatigue life can vary considerably from wrought materials of the same chemical specification and heat treatment. The variations are driven mostly by the differences on the microstructural level, including characteristics like grain size, grain orientation, porosity, and crystalline phase. That microstructure, and in turn the mechanical properties, are dependent upon the machine, machine parameters, raw material characteristics, environment, post-processing, and more variables. Each manufacturer will typically qualify a material process in accordance with NASA-STD-6030, which consists of defining and controlling the critical aspects of the AM process in a QMP. Following the process defined in the QMP, material characterization coupons are manufactured and tested to establish an initial Material Property Suite (MPS), which is a controlled and documented set of material property data that is used to establish design values, material allowables, and statistical process control limits for the AM process. The properties in the MPS are expected to include those properties necessary for the evaluation of the parts produced using the applicable QMP. For parts subject to cyclic loading, fatigue testing is also required. This concept extends to the full range of expected operating conditions; liquid engine parts often require testing at elevated or cryogenic temperatures, and if so, material testing for a bounding range of temperatures would be required.

Thin-walled AM parts may behave differently than thicker parts. This has been demonstrated for fatigue loading, as the transition from plane stress to plane strain can affect the ductile zone near the crack-tip (see Figure 11.4-1, Effects on Cycles to Failures for Various Conditions). Coupon-level testing should be performed using processing (e.g., heat treatment) consistent with flight. Damage tolerance testing with different processing parameters can help the designer select the best processing for the hardware.

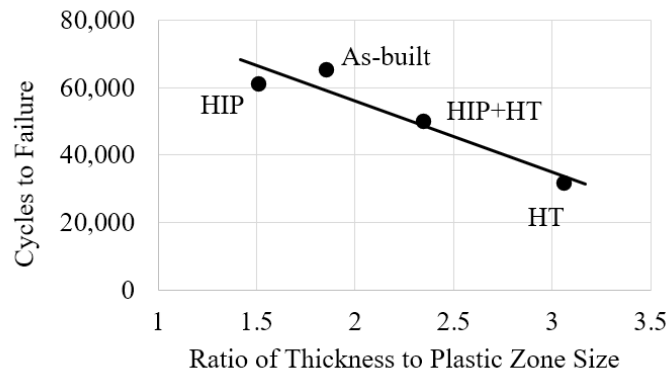


Figure 11.4-1—Effects on Cycles to Failures for Various Conditions

(“Fracture Behavior of Thin-Walled Inconel® 718 Manufactured with Selective Laser Melting,” F. S. Golinveaux, C. S. Lynch, C. N. Sagrillo, K. B. Rivera, J. Rome, T. D. McLouth and J. R. Lohser, AIAA 2020-1473].

The material properties of AM components may also be affected by aspects unique to the AM build process, including build orientation, surface finish, microstructural segregation, and thin-wall features. Relevant AM influence factors should be accounted for in any AM component analysis.

11.4.1 Example 1: AM Component with Machined Surface

Consider a rotating engine part subjected to torsional fatigue loads. The Inconel® 718 part is AM using powder bed fusion (PBF) to a near-net shape, and all surfaces are machined to the final shape. It is made using a QMP, characterized in accordance with NASA-STD-6030, and that process is maintained. An approach is described to qualify the part using a damage tolerance approach.

Once the material has been characterized, a damage tolerance assessment can proceed following standard procedures. Since all surfaces are machined, the surfaces can be readily inspected using a variety of methods such as liquid penetrant inspection and/or volumetric inspection as applicable. One approach would be to use analysis to determine the maximum acceptable flaw size for 4X life. Then develop an inspection plan that can reliably detect those flaws.

Once a part is qualified with an inspection plan in place, it is essential that the process remains under control. For AM, this means maintaining the qualified process: machines, parameters, raw material, post-processing, etc. Deviations from a qualified process must be evaluated to determine if there is any impact on the material properties.

Witness coupons must be manufactured and tested with every part build. The minimum number of witness coupons is determined in accordance with NASA-STD-6030. Specifically, AM parts with high consequence of failure (Class A) and parts with a low consequence of failure but high structural demand and AM risk (Class B1) are required to have fatigue witness coupons to

NASA-HDBK-5010, VOLUME 2, REVISION A

monitor the AM process for deviations that might be detrimental to the fatigue properties of the material. For metal additive processes, surface finish is the feature most likely to degrade fatigue capability while not affecting tensile strength. Witness testing results that deviate from the expected values are indicative of a process issue. In that case, parts from that build should be evaluated; and a review should be held to determine if there was an important or unexpected change in the manufacturing process.

11.4.2 Example 2: AM Rotating Part

This example illustrates the benefit of employing a damage tolerance approach to assess an AM part. Fatigue life of parts can be challenging to predict for AM hardware as it may be affected by many processing parameters but also on the surface finish and near-surface defects. Damage tolerance can be employed as an effective substitute to fatigue life assessment.

Consider a rotating engine part subjected to torsional fatigue loads. The Inconel® 718 part is AM using PBF to the final shape. A few spots are machine finished for interface issues. Other surfaces are left as built; external surfaces are shot-peened while interior surfaces are not finished. There are several areas of down skins, with angles ranging from 10-45 degrees. There are also vertical, horizontal, and down skin surfaces. An approach is described to qualify the part using a damage tolerance approach.

For mechanical and strength characterization, all the points from Example 1 apply. For fatigue characterization, the assessment and qualification approach are more challenging since the surface finish will affect fatigue performance. Generally, a rougher surface finish will lead to decreased fatigue life due to larger initial defects. But that does not always hold for AM parts, especially when the measured surface roughness does not necessarily correlate with the size of microcracks. For example, on downskins, a high surface roughness measurement may be due to partially sintered powder rather than inherent roughness. Below, an approach to characterize the fatigue performance for the full variety of surface finishes is described.

The simple, very time-consuming approach would involve a full fatigue characterization of each type of surface finish. Then, the critical flaw size for each could be determined, and inspections for each area would be based upon the surface finish. This may be effective, but the testing campaign would be costly and impractical.

An alternative process is proposed in two steps. First, conduct a pilot study to evaluate fatigue for the surfaces suspected to have the worst performance. Those selections should be based on published research and prior work. The pilot study should also include samples that have been machined surface finishes. At its conclusion, the worst performing surface finish is chosen for the second step.

An approach has been demonstrated which may reduce the quantity of fatigue life characterization testing when used in conjunction with a damage tolerant methodology (reference Rome, et al. (2021)). In this approach, flight loads were used to predict local stresses using finite element modeling. Then, the known or predicted fatigue spectra (corresponding to 4x

NASA-HDBK-5010, VOLUME 2, REVISION A

life) was applied to estimate the maximum acceptable flaw size using NASGRO®, while the final determination requires further testing. The initial prediction may use published data for a similar alloy and surface finish but will be later validated using data included in the MPS for a particular AM process. There are multiple material models available in NASGRO®, or the data could be found in published literature. If a custom material model is used, the input data include da/dN vs. delta K, ultimate tensile strength, yield strength, and fracture toughness. A detailed walk-through of the NASGRO® software implementation is included in the next section. See Figure 11.4-2, Approach to Determine Whether As-built Surface Finishes Require Full Fatigue Characterization.

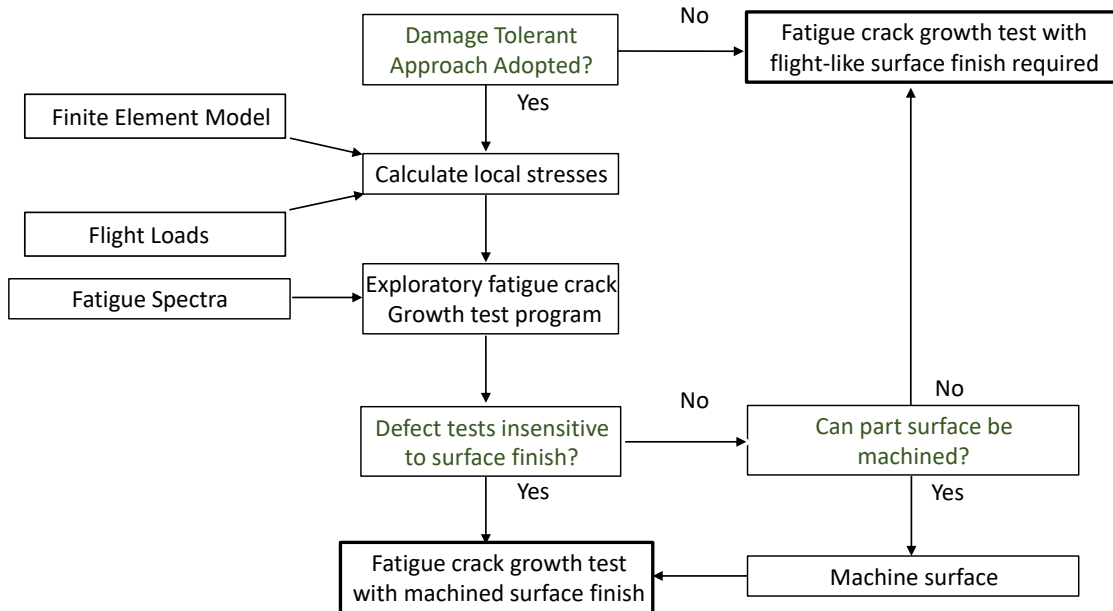


Figure 11.4-2—Approach to Determine Whether As-built Surface Finishes Require Full Fatigue Characterization

An exploratory test program is then adopted to evaluate fatigue for the machined surface finish (best performance) and the surface finish with the worst fatigue performance. This test series should include both defect-free samples, and samples with pre-existing manufactured flaws corresponding to the maximum acceptable flaw size (see Figure 11.4-3, Penny-Shaped Cracks in Cylindrical Samples at 10% and 30% Depth). It is recommended that intermediate defect sizes be tested as well, since the estimate maximum acceptable flaw size may be reduced after the full test campaign.

NASA-HDBK-5010, VOLUME 2, REVISION A

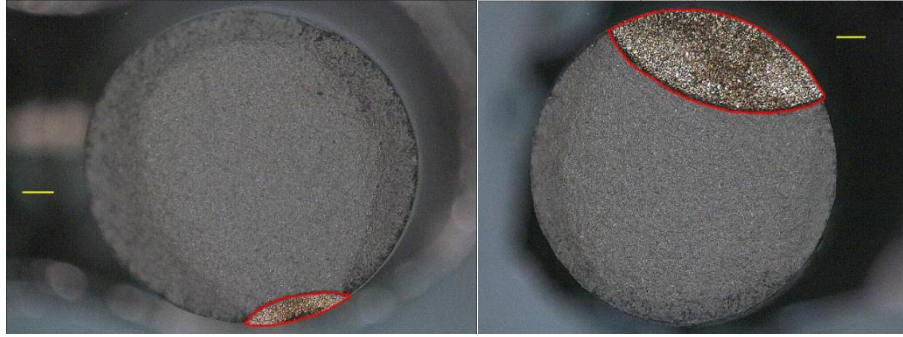


Figure 11.4-3—Penny-Shaped Cracks in Cylindrical Samples at 10% and 30% Depth

The machined coupons without the notches are expected to have the longest fatigue life for a given load spectra. It was confirmed in testing that the machined samples survived more than 5 times as many cycles without failure compared to the as-built samples, Figure 11.4-4, Tests Demonstrated that Fatigue Life was Sensitive to Surface Finish (Circles); with Prescribed Flaws, the Fatigue Life was Similar Regardless of Surface Finish (Exes and Triangles). Further examination revealed that the machined coupons with the smaller pre-existing defects exhibited about 95% reduction in fatigue life compared to machined specimens without defects. Fatigue testing of the as-built coupons took about the same number of cycles to fail as the machined samples with the smaller pre-existing defects.

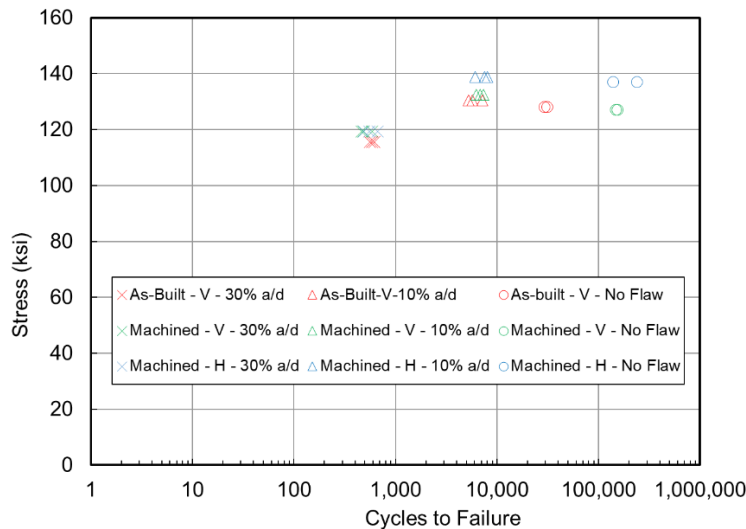


Figure 11.4-4—Tests Demonstrated that Fatigue Life was Sensitive to Surface Finish (Circles); with Prescribed Flaws, the Fatigue Life was Similar Regardless of Surface Finish (Exes and Triangles)

For that study, the machined samples with defects bounded the fatigue life of the as-built coupons without defects and had similar fatigue life of as-built coupons with defects. With that result, it could be concluded that the fatigue life with those defects was insensitive to the surface finish for the material tested analysis should be performed with the fully characterized fatigue crack-growth data to determine the maximum flaw size. This will follow the same process

APPROVED FOR PUBLIC RELEASE – DISTRIBUTION IS UNLIMITED

NASA-HDBK-5010, VOLUME 2, REVISION A

referenced earlier; the key difference is that the material properties and NASGRO® parameters are determined based upon the characterization campaign.

Of course, the inspection program will need to demonstrate the ability to locate defects that size on all types of surface finish, including interior surfaces which are not inspectable by many methods. Generally, dye-penetrant inspections are not a good match for as-built AM surfaces, which could affect the minimum detectable flaw size.

The qualification program could be complicated if the fatigue life with prescribed defects is sensitive to surface finish. In that case, fatigue testing would be required of several types of surface finish. Even then, full characterization can be avoided. The maximum acceptable flaw size would then be estimated for each type of surface finish. If the poor surface finish correlates to an area of low stress, the exploratory test program could be repeated using the larger defect size to determine fatigue sensitivity to a defect of that size. Ultimately, there is no guarantee that this approach will work; and a full characterization of multiple surface finishes may be required, accompanied by NASGRO® analysis specific to that stress environment and fatigue capability.

There is also the possibility that the maximum acceptable flaw size (MAFS) is smaller than the minimum detectable flaw size (MDFS). If that occurs, location specific analysis can be pursued to determine the MAFS and MDFS in each area of the part. The outcome could be that the MAFS cannot be detected in some locations. Options at that point include redesign, or additional post-processing to improve the inspectability or fatigue capability. There is also the option of using higher fidelity inspection techniques.

11.4.3 Additive Manufacturing (AM) Damage Tolerance Evaluation

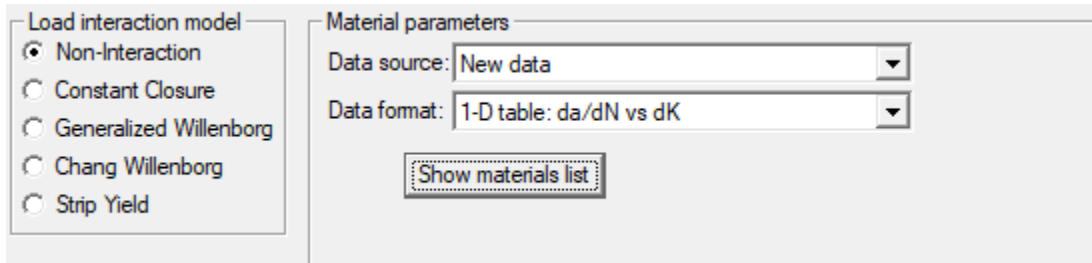
An approach is described on how to analyze an AM part made with an Inconel® alloy using NASGRO®.

AM materials have significant variation in material properties, so material characterization tests are often required for the analysis of AM components. Material properties obtained from AM coupon tests need to be generated. The battery of tests should include all possible processing parameters expected during service life of the part and the test coupons should contain representative features (e.g., pores). Note that these properties should be derived from tests that load the material in the appropriate direction, as AM structures are anisotropic due to the layering process. The effects of coupon orientation relative to the flight configuration is an important consideration, as AM parts can exhibit a degree of orthotropic behavior. The data are then collected, and an enveloping da/dN curve is generated and inputted into the NASGRO® software for safe-life analysis.

To complete a safe-life analysis, the NASFLA module in NASGRO® can be used. After choosing the appropriate geometry, the material must be defined. Rather than choosing a material from the NASGRO® database, custom material properties can be input. To do this, “New data” can be chosen as the data source in the Material input tab, as shown in Figure 11.4-5, Material Parameters Selection to Define Material Properties Based on a da/dN curve.

NASA-HDBK-5010, VOLUME 2, REVISION A

Alternatively, a user material file can be used if available. If the “New data” source is selected, the data can be entered in a variety of formats. If a crack growth measurement test was conducted to obtain a da/dN curve, then it is recommended to use either “1-D table: da/dN vs dK ” or “2-D table: da/dN vs dK and R .” The 2-D table should be used if data for multiple R values is required. In this example, the 1-D table is chosen.



The image shows a software interface for material parameter selection. On the left, under 'Load interaction model', there are five radio button options: 'Non-Interaction' (selected), 'Constant Closure', 'Generalized Willenborg', 'Chang Willenborg', and 'Strip Yield'. On the right, under 'Material parameters', there are two dropdown menus: 'Data source' is set to 'New data' and 'Data format' is set to '1-D table: da/dN vs dK'. Below these dropdowns is a button labeled 'Show materials list' which is highlighted with a dashed border.

Figure 11.4-5—Material Parameters Selection to Define Material Properties Based on a da/dN Curve

After specifying the data format, the material must be defined by clicking “Show materials list.” The material alloy and group can be chosen to best match the alloy used in the AM part. In this case, “Inconel alloys” is chosen from the “NI ALLOYS/SUPERALLOYS”. This defines the first 2 characters of the material code, which is used by NASGRO® to identify the material used. The remaining 6-8 characters can be any combination of characters defined by the user. The material code entered in this example is set to Q3AB1234, as seen in Figure 11.4-6, Input of Custom Material Data into NASGRO® Crack Growth Module. The yield strength, ultimate strength, critical stress intensity factor, and da/dN data are all required inputs.

NASA-HDBK-5010, VOLUME 2, REVISION A

Material parameters

Data source: New data Save data to user file

Data format: 1-D table: da/dN vs dK

Show materials list 1-char category code: Q description: NI ALLOYS/SUPERALLOYS
1-char group code: 3 description: Inconel alloys

2-character alloy code: AB description:
4-6 char form/orient/env code: 1234 description:
 da/dN multiplier?

Through crack toughness computed from
 value entered directly K1c, Ak, Bk equation Kc v. thickness table

K1c	Ak	Bk
90	1	0

Material properties: ID code = Q3AB1234

UTS	Yield	K1e
125	75	110

Crack growth parameters - 1D table

da/dN	dK
106.103	0.001854972
93.8158	0.000926332
77.9764	0.000437938
64.783	0.000223634
53.7937	1.18E-04
44.6401	6.28E-05
37.0157	3.38E-05
30.665	1.83E-05
25.3752	9.93E-06

Interpolation type
 Linear Hermite Plot

Figure 11.4-6—Input of Custom Material Data into NASGRO® Crack Growth Module

Two critical stress intensity factors are defined: the through-crack toughness and the effective fracture toughness for a surface crack (K_{Ie}). There are multiple input options for the through-crack toughness. The through-crack toughness can be entered directly with the first radio button; this should either be the plane strain fracture toughness (K_{Ic}) or a toughness obtained from tests on the AM material with a thickness that matches the application. Alternatively, the plane strain fracture toughness (K_{Ic}) can be input with the “ K_{Icx} , A_k , B_k equation” radio button under the through-crack toughness. A_k and B_k are constants are required with K_{Ic} . These correspond to an increase in toughness as plane stress dominates with decreasing thickness. Unless there is test data to characterize the effects of decreasing thickness, B_k must be set to zero. Setting B_k to zero eliminates the increase of toughness with decreasing thickness, which is conservative. For more details on tests for the plane strain fracture toughness, see ASTM E399. Additionally, the through-crack toughness can be input in a table based on thickness with the “ K_c v. thickness table” radio button.

Next, the UTS, yield strength, and K_{Ie} are all input. These values are determined from tests on the AM material. For more details on the test for K_{Ie} , see ASTM E740/E740M, Annex X1.2, or ASTM E2899.

The final input required is the da/dN curve, which is entered in the “Crack growth parameters” table. The da/dN column represents the change in crack growth during a cycle, and the dK column represents the range of stress intensity factor during a cycle. These data are obtained with a fatigue crack growth measurement test. For more information on this test, see ASTM E647-15E1. Example data is shown in Figure 11.4-7, Example da/dN Data to be Entered in the Crack Growth Parameters Table of the NASGRO® New Data Material Input.

APPROVED FOR PUBLIC RELEASE – DISTRIBUTION IS UNLIMITED

NASA-HDBK-5010, VOLUME 2, REVISION A

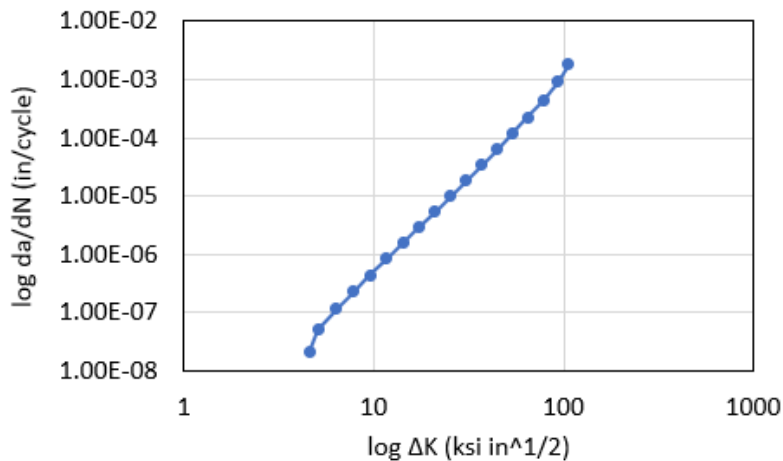


Figure 11.4-7—Example da/dN Data to be Entered in the Crack Growth Parameters Table of the NASGRO® New Data Material Input

The da/dN data is input into the crack growth parameters table to complete the material definition. The material properties for this example were constructed for illustrative purposes.

After defining the material, the life analysis can be completed as demonstrated in previous NASGRO® examples.

11.5 Heatshield Damage Tolerance

Damage tolerance for ablative or thermally insulative structures represent a multi-disciplinary challenge. These components such as heat shields, external insulators, and nozzle liners are primarily intended to protect an underlying component from hostile thermal environments. As such, tolerance to damage must address not only potential structural failure modes, but also interactions with the thermal functionality of these components.

Types of damage will vary depending on materials. For ablative composites used in typical nozzle applications, the most common defect will be a delamination. Bondline cracks or voids between components, and cracking of other materials (ceramics, metals, carbon-carbon, etc.), must also be considered. The defects may be caused during manufacturing but can also be induced during storage, aging, or operation. Operational testing such as static fire for nozzles, or simulated heating tests for heat shields, can reveal propensity for cracking, typically in heat affected zones. Cracks leading into nonheat-affected regions found after test need special attention and review to understand if these formed and propagated during the test, or afterwards during cooldown.

Regardless of type or cause, two aspects should be considered to evaluate defects in these components. The first is stability or maximum extent of damage. The loading environments on these components are a combination of mechanical and thermal stresses, which change and evolve over time, and may drive growth of flaws. Fracture analysis is needed to determine the maximum extent of the defect for the remaining service life of the part after the flaw is observed,

APPROVED FOR PUBLIC RELEASE – DISTRIBUTION IS UNLIMITED

NASA-HDBK-5010, VOLUME 2, REVISION A

or for the maximum size flaw that could not be observed through NDE. Test demonstration for growth or stability is often not feasible since one cannot achieve duration margins with these components sufficient to account for potential material scatter. Proof test acceptance logic is also often not feasible, since internal thermally induced stresses are usually not replicated through mechanical means with high confidence. For hardware where proof test does induce bounding stresses at the flaw location, pre- and post-test NDE and analysis of worst-shaped flaws could be used to determine stability. To conduct analysis, fracture testing of the materials is needed at the relevant thermal conditions. These tests would determine critical strain energy release rate allowables to use in fracture analysis with appropriate factors of safety, to determine stability or maximum growth extent of the flaws. Finally, at the maximum extent of the defect, the remaining structure must maintain structural integrity to stay intact and provide the primary functionality of these components.

The second aspect to consider is the consequence of the maximum extent defect on the thermal performance. This is itself a multidisciplinary endeavor, as potential flow into and around the defect must be considered. The amount of thermal energy available is highly dependent on whether there can be a sustaining flow of hot gas into the defect (i.e., either as a passage to a lower pressure location, or back into the flow). If similar defects are present during representative testing such as hot fire, this may be inferred through post-test observation of the hardware. The effect of these temperatures on nearby materials must be taken into account and the impacts to structural integrity evaluated. The defect itself may also change the effective thermal conductivity, which then must also be assessed for the thermostructural integrity of the component. The consequences of impacts to thermal performance could thus impose limitations on location or extent of flaws.

As an example, a delamination present in the nozzle may be found after manufacturing during routine X-ray inspection. If it is predicted that the delamination grows but does not intersect the exposed surface after accounting for uncertainties in erosion, hot gas could not intrude into this defect. If the remaining structural margins are positive with this defect such that ejection of nozzle components are not a possibility, this might be found to be acceptable for flight. If a delamination is found that is predicted to grow and intersect an exposed surface, additional analyses would be necessary to address potential flow into the defect and the subsequent thermostructural response.

11.6 Thrust Chamber Liner Damage Tolerance

Thrust chamber liners should be designed to prevent fatigue and crack-growth failure modes during operation. It is common to encounter thrust chamber cracks during the qualification program due to pressure loads, cyclic temperature environments, thermal gradients, and challenges associated with manufacturing complexities.

Propulsion requirements are usually prioritized over structural requirements in the design process of engines, making it challenging to prevent cracks late in the design process. The qualification program in combination with a FMEA are used to determine the adequacy of the design.

APPROVED FOR PUBLIC RELEASE – DISTRIBUTION IS UNLIMITED

NASA-HDBK-5010, VOLUME 2, REVISION A

NASA-STD-5012B requires six engines to be tested to at least 2 times the service life. The extensive amount of testing at multiple operating conditions will likely expose weaknesses in the manufacturing and design. If a crack were to form during qualification or production, a good understanding of the root cause of these flaws is required.

Best practices for the damage tolerance philosophy of thrust chamber liner are presented below:

Option 1: The maximum acceptable flaw size should be shown through qualification test experience to be stable over four times the service life.

Option 2. A damage tolerance analysis methodology anchored to test is required to demonstrate stability of the maximum acceptable flaw over four times the service life.

Option 3: No damage tolerance is required if a through-crack of maximum size based on geometric limits is assumed to exist and found to be acceptable.

In all cases, any flaws found during qualification should be investigated and root-cause understood.

For all three options, a FMEA must be conducted if the maximum acceptable flaw or assumed flaw allows a through-crack:

1. A through-crack of maximum size in length cannot have a detrimental impact to the functional performance of the engine, and
2. A through-crack of maximum size in length cannot lead to other detrimental system-level failure modes.

A multi-disciplinary assessment involving multiple subject matter experts is required to determine whether the functional consequences of a leak are benign. The functional consequence of through-cracks in a thrust chamber liner can be either minor or significant. Pressure in the cooling channels is typically higher than the pressure in the combustion chamber; the colder fuel from within the cooling channels can migrate into the combustion volume when a through-the-thickness crack is present.

For single-burn engine applications, the functional effect of fluid migration from the cooling channel side of a liner to the combustion chamber side is that localized cooling will occur on the liner in the vicinity of the crack. This localized cooling can result in a change in the thrust efficiency or specific impulse (Isp) of the engine. The consequences of the maximum crack size should be evaluated. When the impact on thrust efficiency is small and mission performance requirements can still be met, the single-burn engine can tolerate cracks in the liner without compromising the mission.

In contrast with multiple-burn applications such as upper stage engines and reusable applications, engines shutdown and re-ignite during the mission. The performance impact due to

APPROVED FOR PUBLIC RELEASE – DISTRIBUTION IS UNLIMITED

NASA-HDBK-5010, VOLUME 2, REVISION A

the presence of a flaw during the first burn of the engine may be small. When the engine shuts down and there is a period before re-igniting, the fuel can continue to inadvertently migrate into the combustion chamber. In this scenario, the extra fuel in the combustion chamber can cause a detonation or overpressure event when re-igniting the engine, which can result in hardware damage or rupture. There may also be noticeable time between engine burns where fuel continues to leak from the cooling channels throughout the mission. When too much fuel is lost through the liner leak, a mission performance shortfall can occur. In the context of an upper stage, the spacecraft may not reach the intended orbit due to loss of performance and in the context of reusability, or landing may not be possible. Similar to the single-burn example, if the mission objectives can be met with the maximum flaw size, the liner can tolerate cracks without compromising the mission.

11.7 Loading Spectra

11.7.1 Relevance to Damage Tolerance Assessments

The load spectra definition is a necessary aspect that requires attention in the damage tolerance evaluation of fracture critical space components. Often, simplifying assumptions can be made that lead to conservatism in the fracture mechanics analysis. It is important for the analyst to understand underlying assumptions made in the loading spectra. The loading spectra can be often generated by the “Dynamics” or “Dynamics Environments” disciplines.

In certain instances, the assumptions made for simplification of safe-life analysis (e.g., fully reversing (i.e., $R = -1.0$) or fully unloading stress cycles (i.e., $R = 0$), constant amplitude loading, or max-on-max stresses) can result in unnecessary over-conservatism that cannot meet design verification requirements. In such cases, the next level of analysis refinement includes the development and analysis of a loading spectrum related to the expected hardware environments. The estimation of stress amplitude versus number of cycles and their respective sources is both a science and an art form and often blends the use of analytical methods, test data, flight experience, flight data, signal processing, and empirical methods.

A complete load spectrum can be used with standard fracture analysis software techniques as “load block” inputs with which the crack growth and overall life estimates can be performed. The load spectrum typically represents a single service life that can be used to demonstrate conformance with the design verification requirement (e.g., four service lives, ten service lives).

11.7.2 Spectra Calculation Overview

This section presents five examples of load spectrum generation, each representing a unique but related case generally separated and grouped by load source. The method of spectrum generation is dependent on loading type and the various methods can be combined when the structure is subject to multiple loads. To effectively use these examples, an analyst can use Figure 11.7-1, Example Cases for Load Spectra Development, to determine which example may offer the most assistance. In general, each example effectively builds from the previous example, so refer to the

NASA-HDBK-5010, VOLUME 2, REVISION A

first case with each load type for the most detail on the generation of spectra specific to that load type.

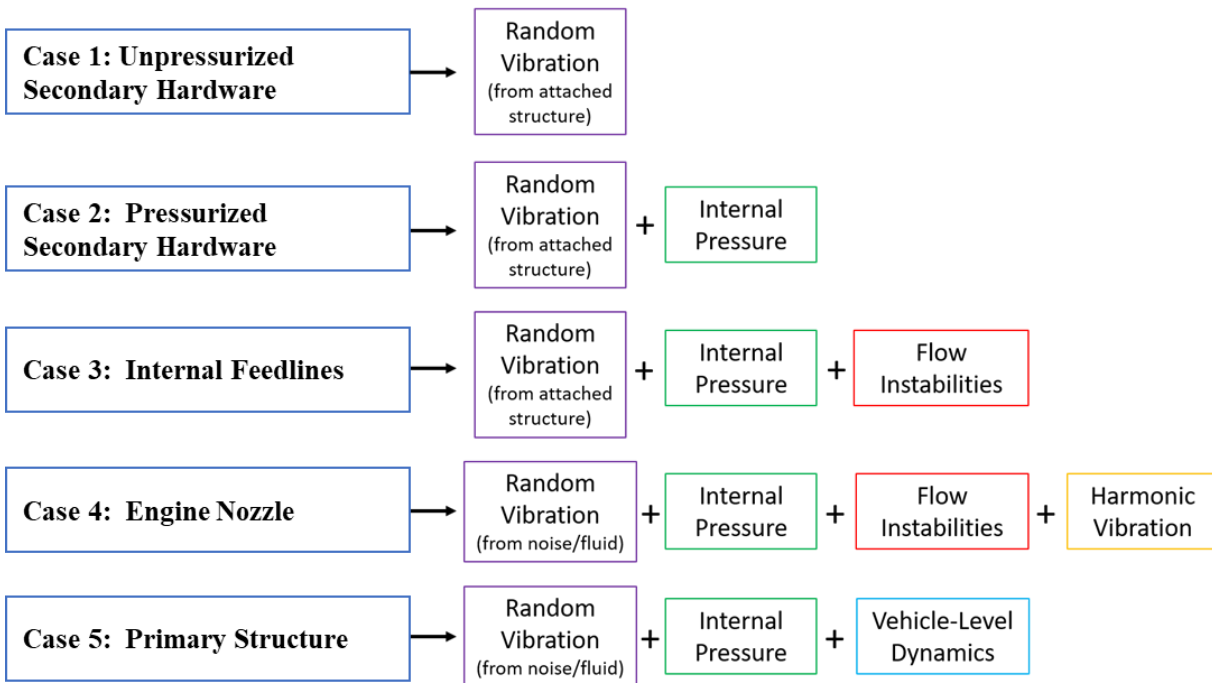


Figure 11.7-1—Example Cases for Load Spectra Development

These examples are meant to provide an analyst with insight into how stress and/or strain spectra are developed and are not intended to be used as a standard for developing them. Development of these load spectra are often the responsibility of SMEs in Structural Dynamics and/or Loads and Environments groups, and typically not the structural analyst performing the fatigue and/or fracture analyses. Loads can also develop from thermal stress, installation, or deformations of adjacent components. ECSS-E-HB-32-26A (19 February 2013), Spacecraft Mechanical Loads Analysis Handbook, Section 12, Fatigue and Fracture control, provides guidance relative to this aspect.

Care should be taken to ensure accurate prediction of load spectra and that they are used correctly when applied to structural analysis; these examples provide insight into the process to help assist with communication between the relevant disciplines.

11.7.3 Case 1: Unpressurized Secondary Hardware

Example Hardware: Instrumentation shelves, mounting brackets, trays

Load Source: Structure is subject to inertial/acceleration loading driven by the parent structure to which it is attached. This is commonly referred to as structure-borne vibration.

Stress Generation: Multiple methods presented:

NASA-HDBK-5010, VOLUME 2, REVISION A

Acceleration Power Spectral Densities (PSD) from flight instrumentation or predictions near attachment points may be used as inputs for a base-drive analysis. For an example of how predictions of the acceleration PSD may be made from Statistical Energy Analysis, see section 11.7.7 Case 5: Primary **Structure**. Each mission event may be analyzed separately. Stress PSD results are extracted from location(s) of interest. The stress PSD is used to directly calculate the RMS value of stress and the apparent frequency of vibration. The stress PSD is used along with mission event duration(s) to determine peaking factor(s). The limit stress is equal to Peaking Factor*Stress RMS and is calculated for each mission event analyzed.

This means of excitation is simpler but can be unrealistic erring on the very conservative side due to compliance differences between the flight mounting structure and the base-drive analysis. Spatial variability of accel input should be considered when using a spectrum from what is effectively a point source. A transfer function may be developed using instrumentation on secondary hardware to ensure a reasonable response. Alternately, a response-limiting procedure may be developed to ensure compliance differences are accounted for.

Forcing functions may be applied to parent structure in a global model, with *acceleration PSD* results extracted at secondary hardware CG. Acceleration PSD results are used to directly calculate the RMS value of acceleration and the apparent frequency of vibration. Acceleration PSD results are used along with mission event duration(s) to determine peaking factor(s). Limit acceleration load is equal to Peaking Factor*Acceleration RMS. A breakout model of the hardware is used to conduct a static analysis using the limit acceleration load. Limit stress is extracted at location(s) of interest for each mission event analyzed.

In this case, if the secondary hardware is modeled as a lumped element in the parent structure model, the extracted fundamental frequency may be higher than the range of significant forcing/primary structure response. If the secondary structure is being modeled explicitly (even at a simplified level) in the primary structure model, the CG location from which the response is extracted should be picked judiciously to represent a “dynamic CG” that is representative of overall motion through frequency. A comparison of interface or reaction force between the dynamic and static models of the secondary structure could be used to help dial this in, although it may be overly iterative.

Forcing functions may be applied to the parent structure in a global model, with *stress PSD* results extracted at location(s) of interest from a detailed model of the secondary hardware attached to the parent structure. The stress PSD is used to directly calculate the RMS value of stress and the apparent frequency of vibration. The stress PSD is used along with mission event duration(s) to determine peaking factor(s). The limit stress is equal to Peaking Factor*Stress RMS and is calculated for each mission event analyzed.

Zonal acceleration PSD predictions may be used with Mile’s equation for a quick, alternative approach. A modal analysis is conducted for the secondary hardware and the frequency of vibration is selected as the fundamental frequency of the secondary hardware. This frequency and a conservative quality factor may be used to determine the quasi-static acceleration loading

NASA-HDBK-5010, VOLUME 2, REVISION A

of the structure to be applied during a static analysis. A breakout model of the hardware is used to conduct a static analysis using the limit acceleration load. Limit stress is extracted at location(s) of interest for each mission event analyzed. In this case, the fundamental frequency should be selected judiciously, per a review of the modal participation factors in the degrees of freedom most relevant to directions where loading would cause significant stress in the secondary structure.

Spectrum Generation: Random vibration input is assumed to be Gaussian, and a Rayleigh distribution of fully reversed load cycles is assumed for the response. The peak cyclic stress is selected as the limit stress scaled by any desired Fatigue/Fracture Analysis Factors (FAF), with the shape of the Rayleigh distribution being determined by selection of desired probability/confidence level. The total number of cycles is determined by apparent frequency of vibration multiplied by the duration.

For conservatism, the maximum limit stress determined across all mission events and the maximum apparent frequency determined across all mission events is used with the total mission duration.

For reduced conservatism, event-consistent stress, apparent frequency, and duration may be used to calculate a load spectrum for each event. Per Miner's rule of accumulative fatigue damage, these spectra can be applied separately, and the damage combined linearly.

Example Calculation: A stress PSD is calculated for two events, Ascent and Descent, and separate stress spectra are derived and then combined.

The peak cyclic stress, including peaking factors and fatigue analysis factors, is determined to be 20 ksi for Ascent, with an apparent frequency of vibration of 100 Hz. The duration of the event is 100 seconds, giving a total cycle count of 40,000 cycles, including a 4x scatter factor ($40,000 = 100 * 100 * 4$). A Rayleigh distribution is assumed, and the stress cycles are organized into bins with a width of 2.5 ksi. The peak cyclic stress, including peaking factors and fatigue analysis factors, is determined to be 25 ksi for Descent, with an apparent frequency of vibration of 200 Hz. The duration of the event is 150 seconds, giving a total cycle count of 120,000 cycles, including a 4x scatter factor ($120,000 = 200 * 150 * 4$). A Rayleigh distribution is assumed, and the stress cycles are organized into bins with a width of 2.5 ksi. A cumulative stress cycle spectrum is then constructed by combining the Ascent and Descent spectra, shown in Figure 11.7-2, Combined Stress Spectrum.

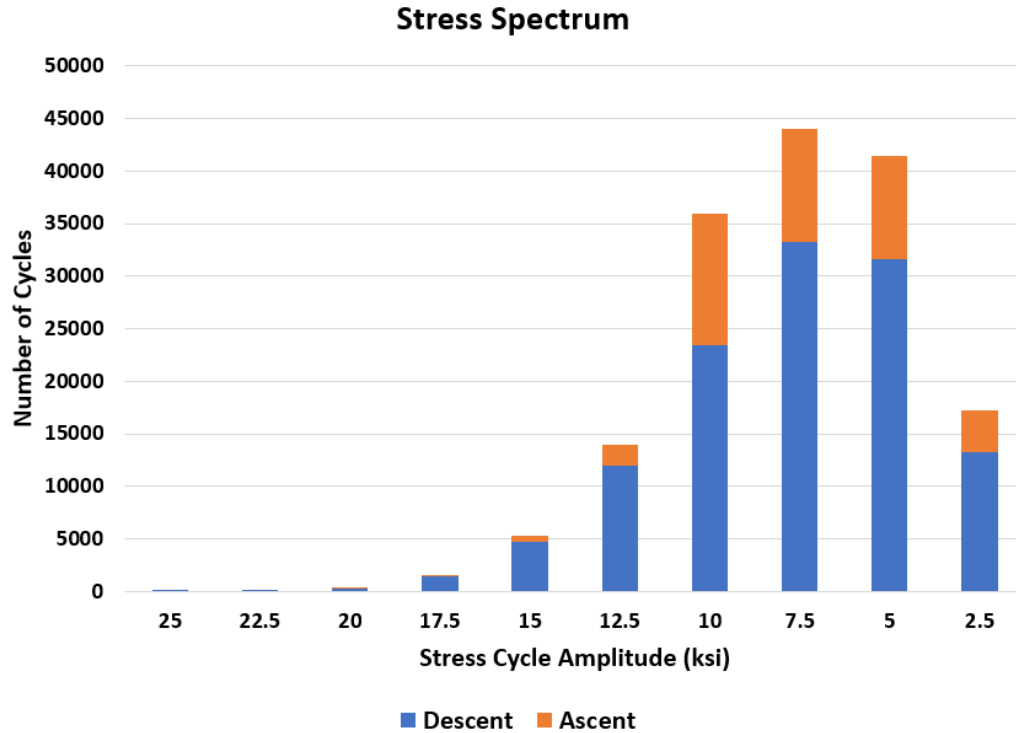


Figure 11.7-2—Combined Stress Spectrum

If multiple ascents and descents are to be analyzed, the number of cycles in the final cycle spectrum shown directly above may be multiplied by the number of missions. For example, if 5x missions are to be analyzed, ~175,000 cycles at 10 ksi is a conservative, yet appropriate, estimate for the number of cycles in that bin is (175,000 = 35,000*5). This estimate is conservative due to the consideration that 5 missions at maximum predicted (i.e., limit load) levels is not statistically probable. If conservatism is to be removed from this multiple mission analysis, consideration should be given to either reducing the load or reducing the total duration per statistical considerations of probable vibration environments vs enveloping vibration environments. If the duration or load level is decreased, this same sequence of steps may be followed to derive new stress spectra.

11.7.4 Case 2: Pressurized Secondary Hardware

Example Hardware: Plumbing lines, COPVs, valves

Load Source: Structure is subject to inertial/acceleration loading driven by the parent structure it is attached to (i.e., structure-borne vibration) and internal pressure.

Stress Generation: Same methods as for nonpressurized secondary hardware, but effects of pressure are included, e.g., pressure-stiffening effects included in static and/or vibration analyses.

Spectrum Generation: Same method as for nonpressurized secondary structures, but pressure-stress cycles are included for the operational lifetime of plumbing (e.g., operational pressure and

NASA-HDBK-5010, VOLUME 2, REVISION A

fill/flow cycles). Per Miner's rule of accumulative fatigue damage, the inertial acceleration and pressure-driven stress spectra can be applied separately, and the damage combined linearly.

11.7.5 Case 3: Engine Feedlines

Example Hardware: Flex joints, bellows, inlet/outlet plumbing

Load Source: Structure is subject to inertial/acceleration loading driven by the parent structure to which it is attached (i.e., structure-borne vibration), internal pressure, and flow-instability effects.

Stress Generation: For structure-borne, inertial acceleration, and pressure-driven stresses, use the same methods as for pressurized secondary hardware. For flow-instability effects, Finite Element Analysis, closed-form solutions, or test data may be used to determine stress and/or strain spectra.

Spectrum Generation: Same method as for pressurized secondary hardware, with additional stress cycles as determined from flow-instability effects. Per Miner's rule of accumulative fatigue damage, these additional cycles can be applied separately from the inertial acceleration and pressure-driven stress spectra, if the analyses were performed separately. The flow-instability effects must be considered separately if the inertial acceleration-driven stress spectrum is to be generated from a Rayleigh distribution. This is because the flow-instability input spectra should not be assumed to be a Gaussian distribution, and the structural response from the loading cannot be assumed to be a Rayleigh distribution.

If the effects of all three loading sources are to be considered simultaneously, a transient analysis may be conducted for time segments representative of various mission events. Load cycles from the transient analysis may be counted using the rainflow algorithm for direct computation of stress and/or strain spectra. Similarly, test data may be used to determine time histories for use with the rainflow algorithm.

Example Calculation: Fluid lines are subjected to short duration and high-amplitude internal pressure spikes from water-hammer effects that result from actuation valves for the controlling engine position. A rainflow counting algorithm is employed to determine the resulting strain spectrum.

In addition to the standard flight pressure transducers, strain gages and high-sample rate pressure transducers were placed on the return lines during testing. The resultant strain on the hardware was measured and correlated with the pressure spike magnitude, as shown Figure 11.7-3, Pressure Spike Amplitude to Strain Correlation. The higher sample rate pressure recordings indicated that the standard flight transducers that sampled at a low rate did not adequately capture the peak pressure cycles and that the higher sample rate was necessary to capture this dynamic behavior.

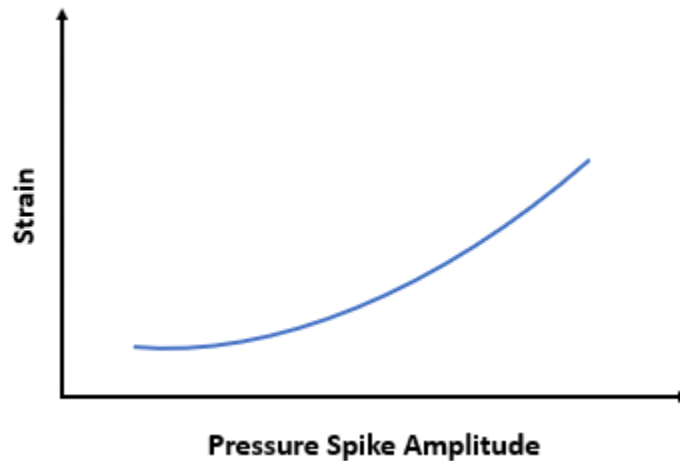


Figure 11.7-3—Pressure Spike Amplitude to Strain Correlation

During operation of the engine, the pressure in the return line was measured. The rainflow counting algorithm as detailed in ASTM E 1049-85, Standard Practices for Cycle Counting in Fatigue Analysis, was employed. The algorithm is available as a standard part of Matlab's Signal Processing Toolbox or as a download from the Mathworks File Exchange. The algorithm is illustrated in Figure 11.7-4, Rainflow Counting Example, and Figure 11.7-5, Binning of Pressure Spikes, and more information can be found at the following link:

<https://www.sciencedirect.com/science/article/pii/B9780123852045000033>. The first plot shows a representative time history due to the pressure spikes. In the second plot, the first plot is rotated so that the time axis is vertical. A trace is run along each line mimicking rain flowing off a pagoda style roof. The method counts cycles based on taking the local maximum and minimum points and assigns a half-cycle for each instance of the following: (1) It reaches the end of the time history, (2) It merges with a flow that started at an earlier *tensile peak*, or (3) An opposite *tensile peak* has greater magnitude.

NASA-HDBK-5010, VOLUME 2, REVISION A

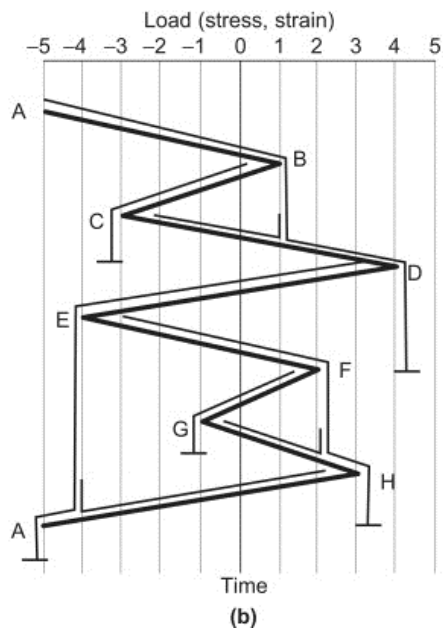
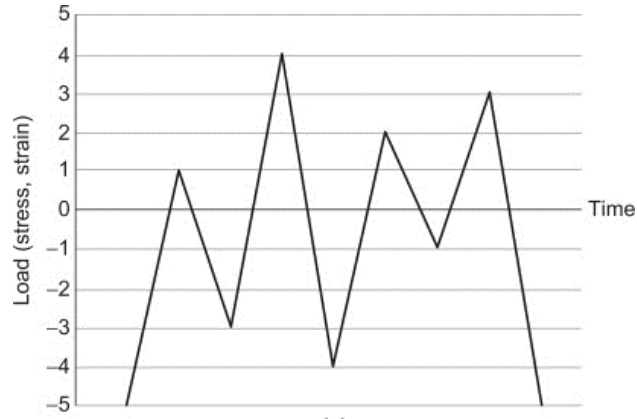


Figure 11.7-4—Rainflow Counting Example

NASA-HDBK-5010, VOLUME 2, REVISION A

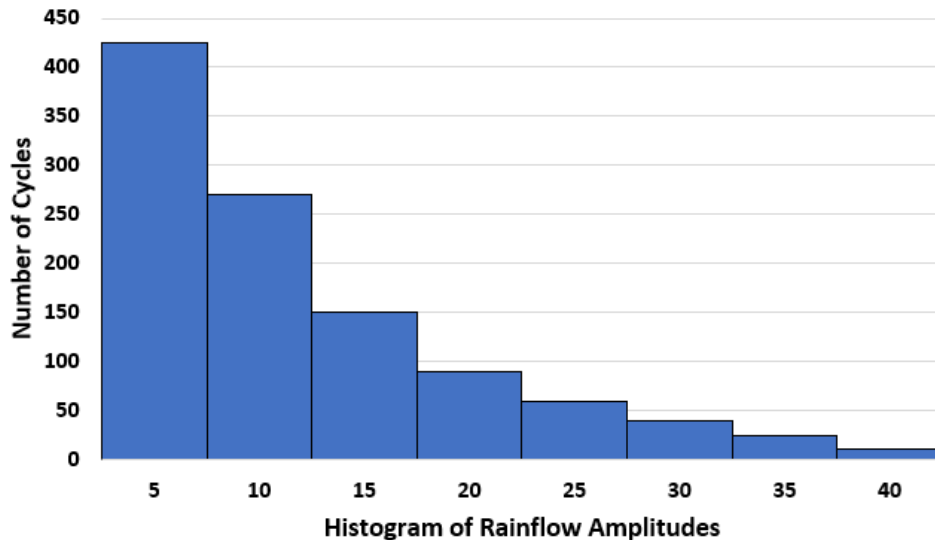


Figure 11.7-5—Binning of Pressure Spikes

For example, considering the points A-B-C-D-E-F-G-H Figure 11.7-4, the first trace “flows” from A to B and then to D. This counts as a half-cycle with magnitude equal to D-A. The next tensile half cycle is from E to H with a magnitude equal to H-E again. On the compressive side, one half-cycle is from B to C with a magnitude of C-B, with another D to A with magnitude of D-A. After running through the complete pressure spike history of the engine test the number of cycles and corresponding magnitudes are tallied. This is then binned into several groups. In this study, the pressure spikes were separated into 10 bins of equal width (e.g., 0 to 5 atm, 5-10 atm, 10-15 atm, etc..) as shown in Figure 11.7-5.

From the empirical relation determined from the prior testing the pressure bins are converted into bins of strain. While the illustration here was performed for low cycle fatigue assessment, the same approach can be utilized to predict crack-growth behavior with NASGRO® by using load blocks. The load spectra were used here for a fatigue analysis, but it can just easily be applied to a damage tolerance evaluation.

In the literature, a strain-life curve for the metal alloy that covers failure due to Low and High Cycle Fatigue failure modes is shown in Figure 11.7-6, Strain to Cycles to Failure Correlation.

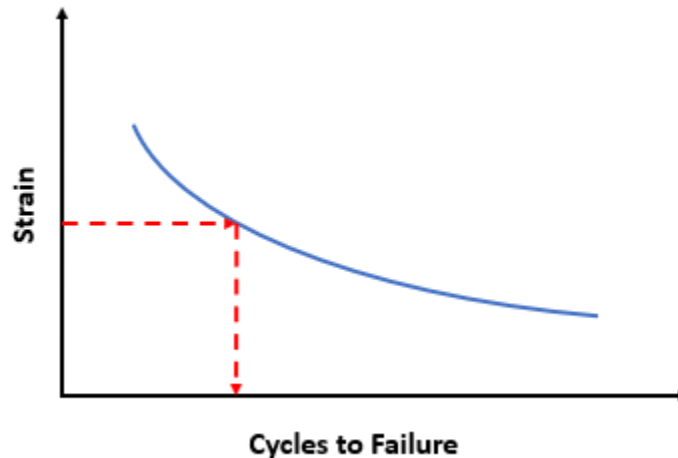


Figure 11.7-6—Strain to Cycles to Failure Correlation

Using this curve, the number of cycles to failure was calculated for each discrete strain bin using the maximum value of the bin range. The amount of life debited from the cycles in each bin is calculated as the number of cycles in the bin divided by the cycles to failure for the corresponding strain. The total Cumulative Damage Index (CDI) is then calculated as the sum across all bins. For design verification purposes, the maximum allowable value for the CDI is often taken to be 0.25 (a value of 1 indicating failure has been reached, divided by a life design factor of 4), but can vary based on program-specific requirements. In other cases, the allowable CDI is equal to unity divided by the life design factor which may also be equal to unity. As an example, say a pressure range of 20 to 25 atm had 1,000 cycles. Based on the test data, this pressure range equates to a strain range of 0.9 to 1%. Looking up 1% strain range on the Low Cycle Fatigue curve, this equates to 10,000 cycles to failure. The 1,000 cycles from this bin uses 0.1, or 10%, of the life of this part. This process is then repeated for all bins and CDI is a sum of all bins.

11.7.6 Case 4: Engine Nozzle

Load Source: Structure is subject to inertial acceleration loading driven by attached engine components (i.e., structure-borne vibration) and acoustic loading driven by internal and external fluctuating surface pressures (FSP).

Stress Generation: The forcing from the acoustic loading is assumed to be random and Gaussian in nature, so a Rayleigh response assumption is appropriate. The forcing from the structure-borne vibration will likely be harmonic due to the rotating turbomachinery, so is analyzed as a separate load case.

For the acoustic-borne vibration, a Vibro-Acoustic Analysis (VAA) may be conducted using the FEM. The internal FSPs, representative of the free-flow exhaust plume, are applied as a pressure PSD to the inside surface of the nozzle across spatially correlated acoustic patches per axial and radial decay functions formulated per the internal loads. The external FSP, representative of any

NASA-HDBK-5010, VOLUME 2, REVISION A

aerodynamic effects or ground effects, are applied as a pressure PSD to the external surface of the nozzle across spatially correlated acoustic patches per axial and radial decay functions formulated per the external loads. A frequency response analysis is conducted for each desired mission event, with the stress PSD used to calculate event-specific apparent frequencies and RMS values. The stress PSD is used along with event durations to determine the peaking factor. Limit stress is equal to Peaking Factor*Stress RMS and is calculated for each mission event analyzed.

The structure-borne vibration levels from the engine turbomachinery at the nozzle interface is used as a harmonic force distributed over the interface in the FEM. A frequency response analysis is conducted for each desired mission event, with the stress PSD used to calculate event-specific apparent frequencies and RMS values.

Spectrum Generation: Random vibration input is assumed to be Gaussian, and a Rayleigh distribution of fully reversed load cycles is assumed for the response. The harmonic cycles from the turbomachinery are calculated separately.

For the acoustic loading, the peak cyclic stress is selected as the limit stress scaled by any desired Fatigue Analysis Factors, with the shape of the Rayleigh distribution being determined by selection of desired probability/confidence level. The mean stress as calculated from a static equivalent mean nozzle pressure may be applied and considered as part of a mean stress correction. The total number of cycles is determined by apparent frequency of vibration multiplied by the duration.

For conservatism, the maximum limit stress determined across all mission events and the maximum apparent frequency determined across all mission events is used with the total mission duration.

For reduced conservatism, event-consistent stress, apparent frequency, and duration may be used to calculate a load spectrum for each event. Per Miner's rule of accumulative fatigue damage, these spectra can be applied separately, and the damage combined linearly.

For the structure-borne vibration, the peak cyclic stress is selected as the RMS stress scaled by any desired Fatigue Analysis Factors. All cycles are assumed to be at this peak cyclic stress. The total number of cycles is determined by apparent frequency of vibration multiplied by the duration.

Per Miner's rule of accumulative fatigue damage, the spectra from the random vibration and the harmonic excitation can be applied separately and the damage combined linearly.

11.7.7 Case 5: Primary Structure

Example Hardware: Stage tanks and interstage assemblies

Load Source: Structure is subject to acoustic loading driven by external fluctuating surface pressures, internal and/or external pressure loading, and vehicle-level compression and tension.

NASA-HDBK-5010, VOLUME 2, REVISION A

Stress and Spectrum Generation: In this case, the vehicle-level compression and tension loads induce the most significant stress, and the life of the hardware is not likely to be driven by high-frequency dynamics.

A time-consistent analysis is conducted using net section load outputs from Coupled Loads Analysis (CLA) and the rainflow algorithm is used to calculate the load spectrum. A structural FEM is used to calculate the stress at location(s) of interest from a unit compression/tension cycle and the rainflow count is scaled to produce a stress spectrum. If net section loads are determined to induce significant strain in the structure, a low-cycle fatigue model should be considered.

If effects of high-cycle fatigue from the acoustic loading are to be considered, a separate VAA can be conducted. The same FEM used for the CLA can be used for the VAA, or a separate SEA can be conducted. It is not common to use the VAA or SEA results solely to derive loading spectra for the primary structure. Rather, these methods are often used to predict the motion and/or response of secondary hardware or units attached to the parent structure. Please note that the determination of loading spectra for primary structure is generally the responsibility of an organization's Structural Dynamics group, and expert technical skill is required to determine accurate spectra. The details here and in the following example discussing SEA are meant to provide insight and are not intended to provide guidelines for how this analysis is to be conducted. With FEM-based VAA or SEA, the external acoustic loading, representative of any aerodynamic effects or ground effects, are applied as pressure PSD to the external surface of the structure. An analysis is conducted for each desired mission event, with the stress PSD used to calculate event-specific apparent frequencies and RMS values. The stress PSD is used along with event durations to determine the peaking factor. Limit stress is equal to Peaking Factor*Stress RMS and is calculated for each mission event analyzed. This random vibration input is assumed to be Gaussian, and a Rayleigh distribution of fully reversed load cycles is assumed for the response. The peak cyclic stress is selected as the limit stress scaled by any desired Fatigue Analysis Factors, with the shape of the Rayleigh distribution being determined by selection of desired probability/confidence level. The total number of cycles is determined by apparent frequency of vibration multiplied by the duration.

If the load spectrum from the net section loads is to be considered along with the load spectrum from the acoustic-borne random vibration spectrum, a fatigue model considers low-cycle and high-cycle fatigue failure modes may be necessary.

Example Calculation: A force time history is used to calculate a stress spectrum for a primary structure.

Coupled Loads Analysis is used to determine a force time history for various mission events. Figure 11.7-7, Example Time History, shows an example time history.

NASA-HDBK-5010, VOLUME 2, REVISION A

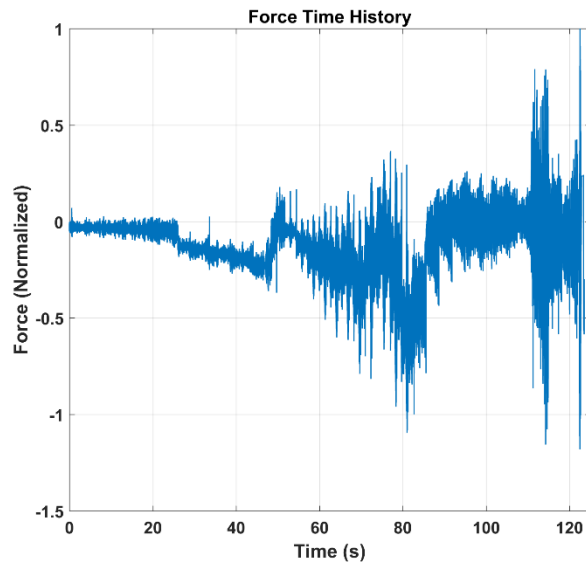


Figure 11.7-7— Example Time History

The rainflow counting algorithm was used to determine the force spectrum. In this case, a Matlab function was downloaded from the Mathworks File Exchange to compute the spectrum. For more information on the rainflow counting algorithm, see section 11.7.5, Case 3: Engine Feedlines. The resulting histogram, showing the number of load cycles for combinations of mean and alternating stress, is shown in Figure Example Force Spectrum.

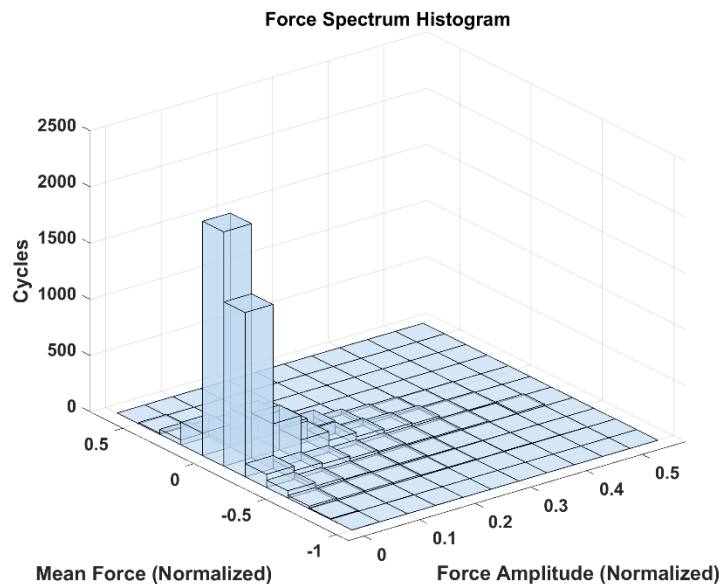


Figure 11.7-8—Example Force Spectrum

A FEM of the structure is used to determine the amount of stress induced from 1 kip of axial force applied as a net section load. If the units of the spectrum shown in the histogram above are taken to be 100 kips, then the final stress spectrum has the same number of mean/alternating

APPROVED FOR PUBLIC RELEASE – DISTRIBUTION IS UNLIMITED

NASA-HDBK-5010, VOLUME 2, REVISION A

cycles as the spectrum above, with magnitudes being 100 times the stress determined from the FEM. In the literature a strain-life curve covering low and high-cycle fatigue failure modes for the material was found. Using this curve, the number of cycles to failure was calculated for each discrete strain range bin using the maximum value of the bin range. The amount of life debited from the cycles in each bin was calculated as the number of cycles in the bin divided by the cycles to failure for the corresponding stress. The total CDI was then calculated as the sum across all bins. As an example, there are around 2,000 cycles with a mean of 0 kips and an amplitude of 5 kips (0.05×100 kips). The FEM predicts a stress of 5 ksi for every kip, so these 2,000 cycles at 5 kips induce 2,000 cycles at 25 ksi. Looking up 25 ksi on the fatigue curve, this equates to 100,000 cycles to failure. The 2,000 cycles from this bin use 0.02, or 2%, of the life of this part. This process is then repeated for all bins and CDI is a sum of all bins.

Statistical Energy Analysis: Some concepts of SEA for use with predicting the response of a primary structure are included below. There are several commercially available SEA software options, and the following simple example was put together using Wave6.

In SEA, a system is split into a set of coupled subsystems and statistical wave mechanics methods are used to describe the input, storage, transmission, and dissipation of vibro-acoustic energy throughout the system. It provides benefits over traditional FEA when accurate predictions may be computationally expensive such as for large, complex structures in a frequency range of interest that can include thousands to millions of natural modes of vibration. While both SEA and FEA solve a system of equations to determine a structural response, the number of equations involved in an SEA solution can be orders of magnitude less than the same structure solved with FEA. This is largely due to SEA discretizing the structure into subsystems with similar dynamic properties, resulting in fewer degrees of freedom than an FEA that discretizes the structure into elements.

A common analogy is that of two water tanks, as shown in Figure 11.7-9, Water Tank Analogy for SEA. In this analogy, water is stored in each tank, representing the energy in each system. The size of each tank is representative of its storage capacity, and the total energy stored in each subsystem is a function of its modal density, i.e., how many natural modes are available to absorb vibrational energy. Water flows from Tank A to Tank B, which represents the energy transmission between the two subsystems. The amount of energy transferred is a function of the coupling between the two subsystems and the difference in energies between them, similar to how the flow of water between the two tanks is proportional to the difference in pressures. Water is being poured into Tank A, which represents the source supplying energy into the system. Both tanks have small outlets from which water is leaving the system, representing the losses in the system which often occur through damping.

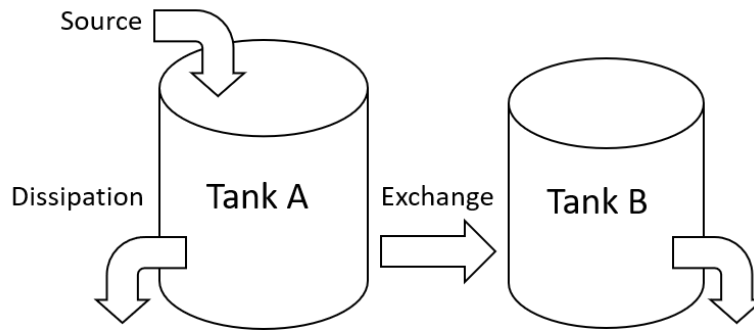


Figure 11.7-9—Water Tank Analogy for SEA

A simple cylinder with an annular shelf was constructed in Wave6, as shown in Figure 11.7-10, Example SEA Model. The system in Figure 11.7-9 is modeled as three connected subsystems using Statistical Energy Analysis.

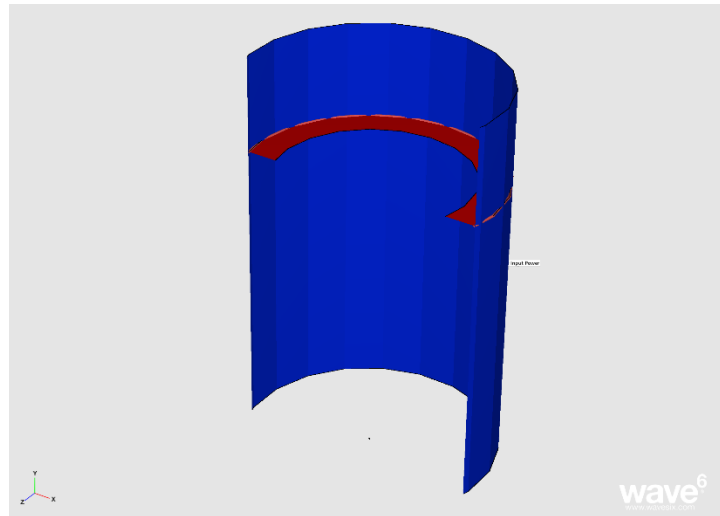


Figure 11.7-10—Example SEA Model

This model contains three connected subsystems: The cylinder (i.e., representing the primary/parent structure), the shelf, and the acoustic cavity inside the cylinder. One percent damping was included for all subsystems and an arbitrary flat power spectrum was input to the surface of the cylinder. The model was solved in 1/3 proportional octave bands from 30 Hz to 8 kHz. The acceleration PSD results for the shelf are shown in blue in Figure 11.7-11, Example SEA Results. An analyst intending to develop a load spectrum for secondary hardware on the shelf could use these results to inform their approach per Case 1. The acceleration PSD results for the cylinder are shown in black in Figure 11.7-11. These results can be used by an analyst intending to develop a load spectrum for either secondary hardware attached to the cylinder or for the cylinder itself, although the latter approach is not common due to vehicle-level dynamics governing the load spectrum for a primary structure and SEA more commonly being used for attached secondary structures.

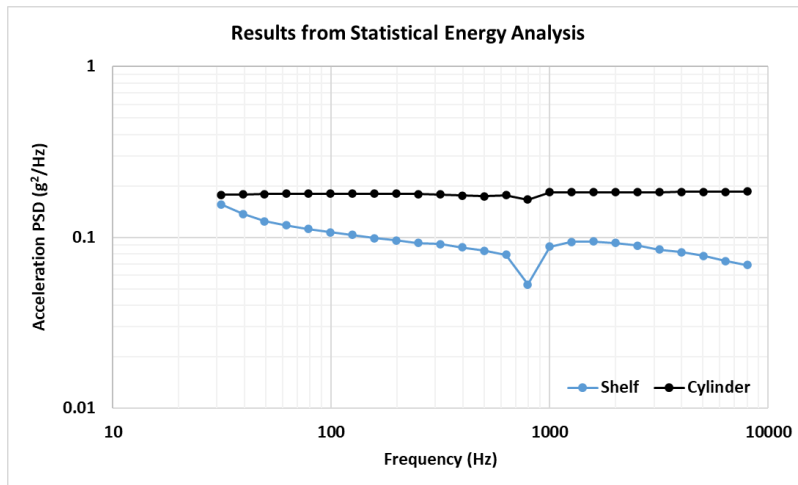


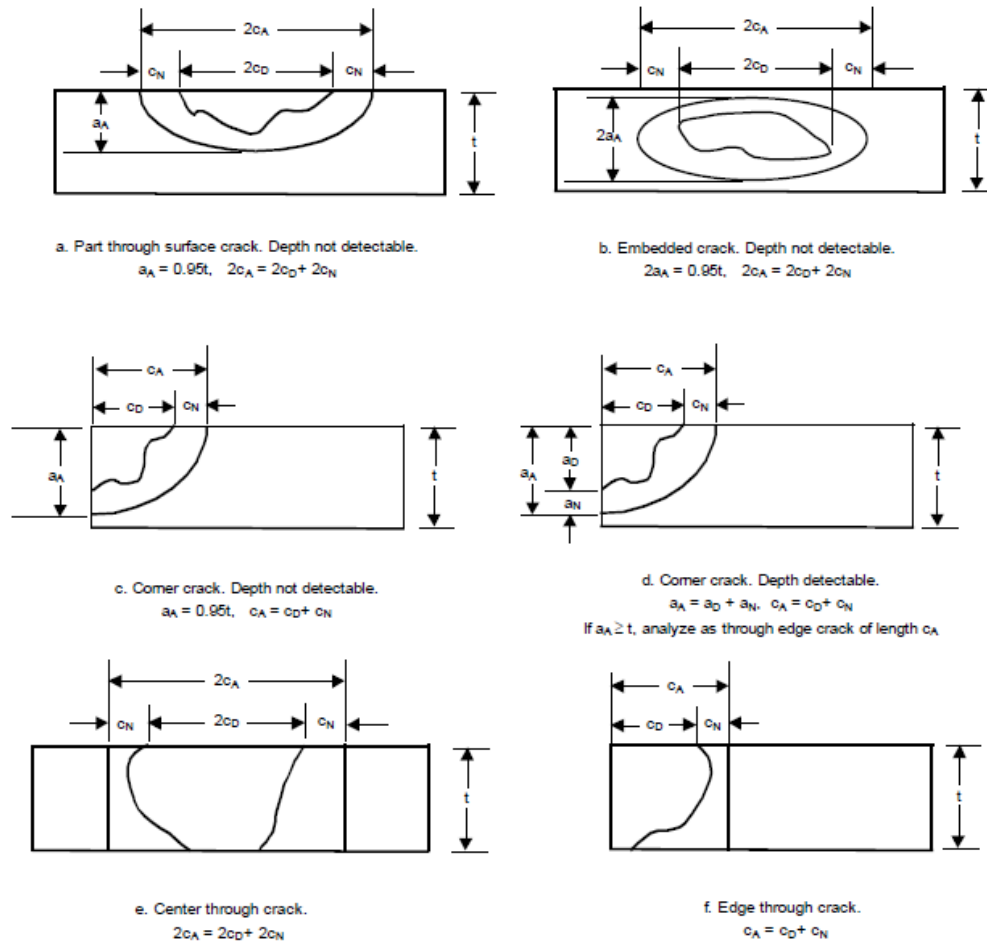
Figure 11.7-11—Example SEA Results

11.8 Analysis Conservatism

The crack size used for analysis must conservatively bound the actual physical size of detected cracks and any possible nondetected adjacent cracks and/or crack tip extensions that will add to the effective length of the detected cracks. The enveloping size to be used should be compatible with the particular NDE method utilized for the crack detection.

Figure 11.8-1, Analysis Crack Sizes for Detected Cracks, presents analysis crack sizes for various detected crack cases. The recommended approach is to add the detected crack size to the particular crack type and NDE method inspection limit based on NASA-STD-5009B. That is, for a crack detected on the surface, the analysis length would be taken as the detected length plus the NDE capability. If no information is available on the depth other than it is not a through crack, the analysis depth should be taken to be 95 percent of the thickness. If a detected embedded flaw, cannot be verified as truly embedded, i.e., does not break through to the surface, it should be considered as a through crack. If it can be verified only for one surface that it does not break through, it should be considered as a surface crack.

NASA-HDBK-5010, VOLUME 2, REVISION A



Definitions

- a Crack depth or half the crack depth
- c Crack length or half the crack length
- t Part thickness

Subscripts

- A Indicates crack dimension used for analysis
- D Indicates detected crack dimension
- N Indicates the capability of the NDE method used to detect the crack

Figure 11.8-1—Analysis Crack Sizes for Detected Cracks

The stresses computed at the detected crack location must be determined for the worst-case limit loads expected during the mission (i.e., upper bound load induced stresses). All additional stresses such as residual stresses must also be appropriately combined in the analysis.

The fracture toughness used for the analysis must be a lower bound fracture toughness, based on available material data. If fewer than seven values of material toughness data are available, the lower bound must be taken as the lower value of the following two cases: (a) the lowest value of all available applicable data, or (b) the average of the available applicable data divided by the factor 1.20. The crack growth rate material data used for the analysis of known cracks should be upper bound. Upper bound data may be estimated by enveloping the growth rate data, including the lower and upper tail regions available in NASGRO®. This envelope should be compared

NASA-HDBK-5010, VOLUME 2, REVISION A

with any other known data points to make certain that it does indeed envelope the data. Several methods exist for establishing the upper bound growth curve, ranging from statistical $+3\sigma$ bounding to hand drawn curves. Figure 11.8-2, Analysis Crack Sizes for Detected Cracks, shows an example of a da/dN versus ΔK curve with mean and upper bound curves. The analyst should contact the RFCB and associated materials group for approval of upper bound properties before analyzing the cracked hardware. In the absence of any other known data, the analyst may use the NASGRO® data as is (i.e., the average) and apply an appropriate increase to the service life factor. Because this multiplying factor can range from 2 to beyond five (5) times, the analyst should seek guidance from the RFCB in selecting a final service life factor. In general, material data will be required for an RFCB to approve use of cracked hardware.

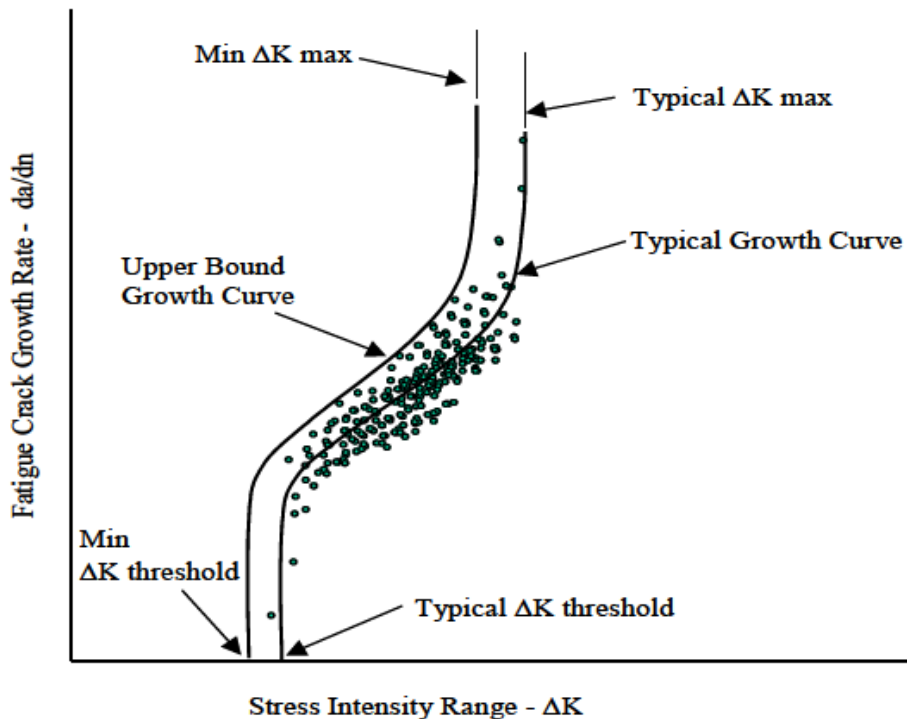


Figure 11.8-2—Analysis Crack Sizes for Detected Cracks

The analysis must show, as a minimum, that the component has a service life factor of four (4) based on the conservatively bounded crack sizes, applied stresses, fracture toughness, and upper bound crack growth rate. For especially critical applications, the RFCB may require a larger service life factor. To protect against cracks near instability, it is necessary to impose a safety factor to provide margin against limit load fracture. In addition to the service life factor, the analysis also must show a fracture safety factor of 1.4 as follows: $(K_c/K) > 1.4$. Here, K_c is the appropriate lower bound fracture toughness, K is the stress intensity at limit load for the crack size computed to exist at the end of one service life. This “end of one service life” crack size should be calculated using the initial crack size determined from Figure 11.8-1, the upper bound crack growth rate, and the load spectrum for one service life.

NASA-HDBK-5010, VOLUME 2, REVISION A

Finally, load sequence can accelerate crack growth. The load spectrum should be reviewed for scenarios such as compressive overloads that may result in tensile residual stresses that could accelerate crack growth. Any potential accelerated crack growth should be accounted for in the analysis of detected cracks.

11.9 Composites Damage Tolerance: Delamination

One of the most common failure modes for composite structures is interlaminar failure or delamination. In space hardware, flaws are bound to occur due to FOD, impact damage, or poor compaction. The use of fracture mechanics to evaluate these delaminations is common practice. An approach to evaluating these delaminations involves the total strain energy release rate which is the rate at which energy is transformed as a material undergoes fracture. The energy release rate is expressed as the decrease in total potential energy per increase in fracture surface area and is thus expressed in terms of energy per unit area.

The total strain energy release rate, G_T , the mode I component due to interlaminar tension, G_I , the mode II component due to interlaminar sliding shear, G_{II} , and the mode III component due to interlaminar scissoring shear, G_{III} , need to be calculated for a given geometry, material system, and loading scheme. The three modes, including Modes I, II, and III of crack growth, are shown in Figure 11.9-1, Three Modes of Fracture. To predict delamination onset or growth, these calculated G components are compared to measured interlaminar fracture toughness properties, often given as a function of mixed-mode ratio G_{II}/G_T . Failure is expected when the calculated total energy release rate, G_T , exceeds the measured interlaminar fracture toughness, G_c . The Composite Materials Handbook-17 is an extensive document that can be used to guide the analyst in the assessment of delaminations in composite hardware.

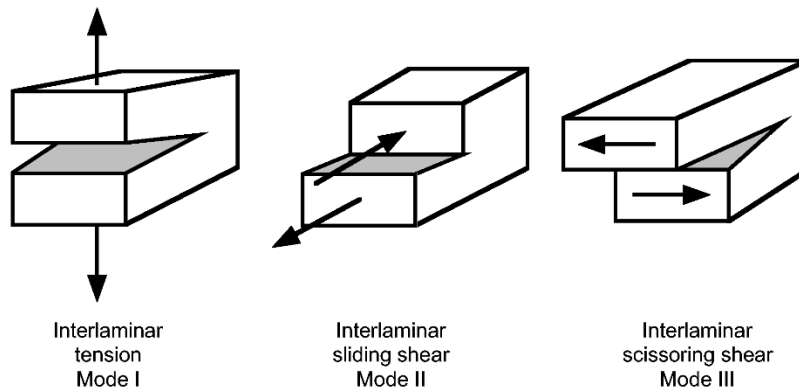


Figure 11.9-1—Three Modes of Fracture

Typical steps in evaluating delaminations in composite structures were adapted from Goyal and Lundgren (2015) and are generally as follows:

1. Establish processing parameters: A baseline must be established for the relevant surface cleaning agents, abrasive media used for surface preparation, and the cure cycle.

APPROVED FOR PUBLIC RELEASE – DISTRIBUTION IS UNLIMITED

NASA-HDBK-5010, VOLUME 2, REVISION A

Traceability is required for manufacturing coupon test specimens, subcomponent test specimens, qualification hardware, and production hardware.

2. Characterization of fracture properties: Fundamental properties, including fracture toughness, need to be characterized for the material systems employed in the joint design. The Double Cantilever Beam (DCB) measures the Mode I critical energy release rate and the End Notch Flexure (ENF) measures the Mode II critical energy release rate. Fracture tests should consider environmental degradation due to temperature and moisture, geometric sensitivity (e.g., adhesive thickness), and processing parameters (e.g., surface preparation and cure cycle). As an alternative to the ENF and DCB tests, fracture toughness may be estimated from tests similar in configuration to the flight hardware. These tests will be discussed later.

3. Determining acceptable flaw size: With known maximum operating loads, finite element models or tests can be used to establish critical flaw sizes, which may vary depending upon the location within the joint. In space applications, factors of safety are used to define the acceptable flaw size relative to the critical flaw size. These acceptable flaw sizes require fracture analysis using analytical methods described later.

4. Identifying inaccessible bondlines: A recommendation is to assume that the portion of a bondline that is inaccessible to inspection is debonded. Fracture mechanics must be used to demonstrate that the structure is adequate under the maximum service loads and assumed flaw condition.

5. Establishing minimum detectable flaw size: Appropriate NDE techniques need to be deployed to inspect for flaws in a joint to an acceptable POD defined by the program. The sensitivity of the inspection is limited by several factors, among them accessibility, accuracy, and repeatability. Consequently, a minimum detectable flaw size must be defined from NDE studies using flight-like coupons with various known flaw sizes.

6. Accepting the design: If NDE can determine that there are no flaws larger than the acceptable flaw size and the structure is tolerant to debonds in areas obstructed from inspection, the structural joint can be considered robust and reliable. Otherwise, the structural joint should be redesigned.

For practicality, LEFM is generally used to assess when delamination progression is expected based on the strain energy release rate (SERR) calculation. The virtual crack closure technique to be described later is a common fracture analysis method used in the evaluation of flaws in a composite structure.

Benchmarking is required to gain confidence in the software tools used. Benchmarking highlights the issues associated with the input of a particular code. Once the parameters have been identified, they may be used with confidence to model more complex configurations. Benchmark cases must be simple and independent of software used. The BBA ensures that the fracture analysis methodology is adequate and can be applied with confidence in assessing the

NASA-HDBK-5010, VOLUME 2, REVISION A

full-scale hardware (see Figure 11.9-2, Building Block Approach for Damage Tolerance Evaluations). The BBA can be found in the Composites Materials Handbook-17.

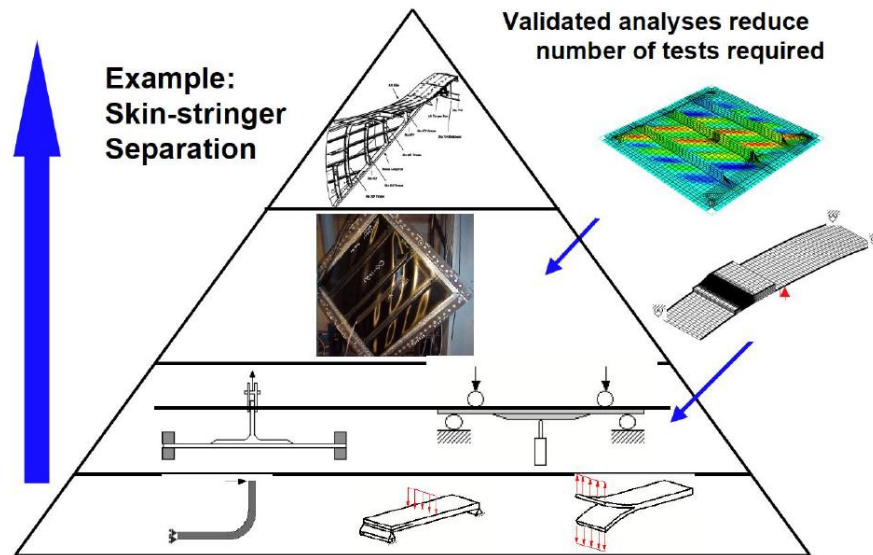


Figure 11.9-2—Building Block Approach for Damage Tolerance Evaluations
("Development of benchmark examples for quasi-static delamination propagation and fatigue growth predictions." Ronald Krueger SIMULIA Community Conference, Providence, RI, May 14-17, 2012)

11.9.1 Fracture Toughness Characterization

Mode I testing is performed using the DCB specimen using the procedures in ASTM D5528, Standard Test Method for Mode I Interlaminar Fracture Toughness of Unidirectional Fiber-Reinforced Polymer Matrix Composites. An initial delamination is fabricated in the sample using Teflon™ inserts. Loading hinges are bonded to the top and bottom surfaces for tensile loading the specimen's delaminated end. During the test, the displacement rate is held constant, and the applied load, crosshead displacement and delamination length are recorded as stable delamination growth occurs. Edges are coated with white paint and markers to track the delamination tip. The initial delamination is achieved by incorporating a Teflon™ film at the midplane of the laminate layup prior to curing. There are issues pertaining to the test specimen layup. With these test specimens, the delamination front may not be straight due to uneven distribution of the energy release rate across the width of the beam. This uneven distribution is caused by the anticlastic bending effect. Secondly, the main delamination may branch into multiple cracks that may follow the fiber-matrix interfaces. This situation may lead to Mode II loading. In addition, the phenomenon of fiber bridging caused by fiber nesting in 0-degree composites can lead to variations of the critical energy release rate. A complex fracture behavior involving fiber breakage, ply jumping, and fiber bridging often occurs when arbitrary orientation in ply angles is considered in the design of DCB test specimen. The delamination branches to interfaces away from the midplane which leads to larger values of fracture toughness.

APPROVED FOR PUBLIC RELEASE – DISTRIBUTION IS UNLIMITED

NASA-HDBK-5010, VOLUME 2, REVISION A

Researchers have investigated if the complex fracture behavior is a function of the test rather than an intrinsic property of the material. They developed a DCB test method to suppress crack jumping and fiber bridging effects. To achieve pure Mode I delamination in a layup other than 0-degrees, the arms of the DCB specimen were designed such that these are balanced and symmetric so as to eliminate the stretching-shearing and stretching coupling effects. In addition, the layup of the angle ply laminate was designed to minimize the bending-twisting effects. The tests were designed to ensure there was no curvature or shear distortion of the laminate due to thermal stresses from curing.

For Mode II testing, the three-point ENF test was standardized as ASTM D7905/7905M, Standard Test Method for Determination of the Mode II Interlaminar Fracture Toughness of Unidirectional Fiber-Reinforced Polymer Matrix Composites. Because delamination growth can be unstable, compliance data for calibration are obtained at low loads. The specimen is shifted in the fixture to produce three delamination lengths. The Mode II fracture toughness is obtained for the onset of growth from the implanted insert and a natural precrack. The critical energy release rate for Mode II can also be determined using the End Load Split (ELS), mixed mode bending apparatus, or the four-point end notch flexure. In the ENF test, if the delamination length is less than approximately 35 percent of the total length, the test specimen undergoes unstable delamination. The ELS test configuration is clamped at one end and a load is applied at the other end. For this test configuration, the delamination growth is unstable for short delamination lengths that are less than 55 percent of the length of the specimen. In both test configurations, Mode II loading is promoted by the relative sliding of the upper surface of the lower lamina with respect to the lower surface of the upper lamina. The relative sliding occurs due to the rotation of the upper and lower arms. The practical difficulties in measuring the Mode II fracture toughness with these test configurations is the choice of starter defect, the stability of the test, and frictional effects between the crack faces. Using a film insert as a starter defect leads to a larger fracture toughness than a test specimen with a precrack. The main problem encountered with the Mode II tests is that determining fracture toughness can be challenging due to the potential delamination instability of short cracks.

The Mixed Mode Bend (MMB) test method, standardized as ASTM D6671/6671M-13, Standard Test Method for Mixed Mode I-Mode II Interlaminar Fracture Toughness of Unidirectional Fiber Reinforced Polymer Matrix Composites, is able to introduce Mode I and Mode II loadings via loading hinges bonded to the delaminated end and attached to the fixture base and the upper loading lever. The ratio of Mode I to Mode II can be varied by adjusting the position of a loading saddle. Mode I to Mode II ratio is increased by loading away from the specimen's delaminated end. ASTM D6671 provides equations for calculating the Mode I and Mode II components (G_I and G_{II}) and total fracture toughness, G_c . For most composite materials, G_c increases as the percentage of Mode II loading increases. The end goal is to develop a mixed-mode fracture criterion for delamination propagation.

These three tests can play an important role in the evaluation of damage tolerance of composites containing delaminations. A summary of test configurations is provided in Table 11.9-1, Summary Table for Fracture Test Configurations. The derivations for test geometries that can lead to unstable crack growth are provided in Goyal, et al. (2004).

APPROVED FOR PUBLIC RELEASE – DISTRIBUTION IS UNLIMITED

NASA-HDBK-5010, VOLUME 2, REVISION A

Mixed mode fracture criterion for the progression of delamination should be determined based on characterization testing using the MMB configuration. As an example, the linear interaction between Mode I and Mode II is as follows:

$$\frac{G_I}{G_{Ic}} + \frac{G_{II}}{G_{IIc}} + \frac{G_{III}}{G_{IIIc}} = 1;$$

where the Mode I, II, and III energy release rates are G_I , G_{II} , and G_{III} , respectively; and the critical Mode I, II, and III energy release rates are G_{Ic} , G_{IIc} , and G_{IIIc} , respectively. The constitutive law that governs the delamination process typically follows the onset and growth criteria per the preceding equations. The power law criterion is:

$$\left(\frac{G_I}{G_{Ic}}\right)^\alpha + \left(\frac{G_{II}}{G_{IIc}}\right)^\beta = 1$$

where α and β are the mixed-mode interaction parameters. The B-K mixed-mode criterion is as follows:

$$G_c = G_{Ic} + (G_{IIc} - G_{Ic}) \left(\frac{G_{II}}{G_I + G_{II}}\right)^\eta$$

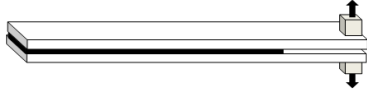
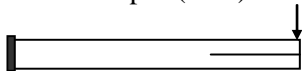
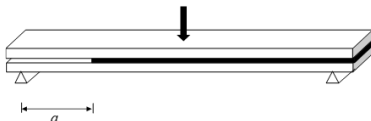
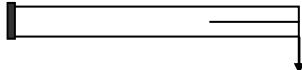
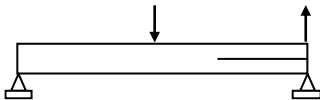
and is the η is the B-K mixed mode parameter. The choice of the mixed mode criterion depends on correlation mixed mode data from the MMB test configuration.

The fracture toughness, G_c , is mode-dependent, which implies that the propagation criterion must be a function of the pure mode fracture toughnesses and a mixed mode ratio. The interaction between fracture modes is usually fitted from experimental data of different mixed-mode tests. In the treatise by J. Reeder, mixed mode fracture criteria are discussed (see J. Reeder, “3D Mixed-Mode Delamination Fracture Criteria—An Experimentalist’s Perspective,” <https://ntrs.nasa.gov/api/citations/20060048260/downloads/20060048260.pdf>).

Conservative assumptions can be made such as not taking advantage of the additional capability provided by the R-curve or using Mode I fracture toughness alone to assess the hardware.

NASA-HDBK-5010, VOLUME 2, REVISION A

Table 11.9-1—Summary Table for Fracture Test Configurations

Test Configuration	Failure Modes	Failure Description
<p>1. Double cantilever beam (DCB) Layups: [0]₂</p> 	Mode I	<p>(1) Delamination front may be curved. (2) For short cracks, delamination is dominated by strength, while for long cracks delamination is dominated by fracture energy. Unstable delamination growth occurs under load control.</p>
<p>2a. End Load Split (ELS)</p>  <p>2b. End Notch Flexure (ENF)</p> 	Mode II	<p>(1) Unstable delamination growth occurs either under displacement or load control if the crack length to specimen length ratio is 0.55 for the ELS and 0.35 for the ENF. (2) The energy dissipated due to friction is negligible compared to the fracture dissipation. Frictional forces can cause temporary crack arrest.</p>
<p>3a. Fixed Ratio Mixed Mode (FRMM) Layups: [0]₂</p>  <p>3b. Mixed Mode Bending (MMB)</p> 	Mixed-mode failure	<p>(1) Delamination may be governed by G_I and G_{II}. (2) The delamination growth is unstable under either load or displacement control if the crack length to specimen length ratio is 0.4 for the FRMM and 0.35 for the MMB.</p>

11.9.2 Virtual Crack Closure Technique

A fundamental paper to the Virtual Crack Closure Technique is “A Finite Element Calculation of Stress Intensity Factors by a Modified Crack Closure Integral” by Rybicki and Kanninen.

The VCCT (reference Krueger, R. [2004]) is a widely-used method for computing energy release rates based on results from continuum two-dimensional (2D) and solid three-dimensional (3D) finite element analyses, which allows the calculation of the individual mode components required when using the mixed-mode fracture criterion. Often the application of this fracture mechanics-based approach is referred to as “performing a VCCT analysis” to distinguish it from other approaches. Strictly speaking, VCCT calculates the mixed-mode energy release rates based on the computed forces and displacements obtained from a finite element analysis. VCCT allows

NASA-HDBK-5010, VOLUME 2, REVISION A

the calculation of the total strain energy release rate, G_T ; the mode I component due to interlaminar tension, G_I , the mode II component due to interlaminar sliding shear, G_{II} ; and the mode III component due to interlaminar scissoring shear, G_{III} . These calculated G components are compared to measured interlaminar fracture toughness properties, often given as a function of mixed-mode ratio G_{II}/G_T . Failure is expected when the calculated total energy release rate, G_T , exceeds the measured interlaminar fracture toughness, G_c .

The VCCT is a method that has been extensively validated and used widely to evaluate delaminations in composite hardware, especially to disposition nonconforming conditions. The work by Krueger, R. (2004) provides history of the method, provides the theoretical background, and provides application examples. The paper provides equations for two dimensional and three-dimensional elements; modifications for the use of the method with geometrically nonlinear finite element analysis and corrections required for elements at the crack tip with different lengths and widths; and problems that could be encountered when delaminations propagate between different materials.

The VCCT has been implemented in commercial codes, although it is suggested that whenever VCCT is employed it be benchmarked against known analytical solutions and literature data. Delamination assessments should be accompanied by building block test data validation. Abaqus, MARC™, NASTRAN™ and ANSYS® now include VCCT capability. The following codes also have similar capabilities: SAMCEF™, GENOA™, and ESRD StressCheck®. Automatic propagation analysis and fatigue crack growth is possible.

11.9.2.1 Virtual Crack Closure Technique Modeling Overview

The modified crack closure integral, as VCCT is called in the original publication, is primarily based on Irwin's crack closure integral where it is assumed that the energy required to extend a crack by Δa is identical to the work required to close it to its original length. In the context of finite element analysis, the energy ΔE released when a crack of length a is extended by one element from a to $(a + \Delta a)$ is identical to the energy required to close the crack ahead of the crack tip. The work ΔE required to close this crack along one element side can be calculated by multiplying the shear and opening forces calculated at the nodal points at its closed state with the respective differences in shear and opening nodal displacements when the crack is open. This analysis requires two steps and is often referred to "crack closure method", "two-step crack closure technique" or "2-step VCCT" (Krueger, 2004). To avoid performing two analyses, self-similar crack growth is assumed such that a crack extension of Δa from a to $(a + \Delta a)$ does not significantly alter the state at the crack tip. The energy ΔE released when the crack is extended by Δa from $(a + \Delta a)$ to $(a + 2\Delta a)$ is identical to the energy required to close the crack. Thus, the work ΔE required to close the crack along one element side can simply be calculated in one step by multiplying the shear and opening forces.

A top-level mathematical overview of VCCT is provided. For convenience, only a section of the delaminated area which is modeled with eight-node three-dimensional solid elements is illustrated in Figure 11.9-3, VCCT Applied to a Delamination Modeled with Three-Dimensional

NASA-HDBK-5010, VOLUME 2, REVISION A

Eight-Noded Solid Elements. The mode I, mode II, and mode III components of the strain energy release rate, G_I , G_{II} , and G_{III} are calculated as

$$\begin{aligned}G_I &= -\frac{1}{2\Delta A} F'_{zLi} (w'_{L\ell} - w'_{L\ell^*}) \\G_{II} &= -\frac{1}{2\Delta A} F'_{xLi} (u'_{L\ell} - u'_{L\ell^*}) \\G_{III} &= -\frac{1}{2\Delta A} F'_{yLi} (v'_{L\ell} - v'_{L\ell^*})\end{aligned}$$

with $\Delta A = \Delta a \cdot b$ as shown in Figure 11.9-4, Three-Dimensional Eight-Noded Solid Elements VCCT Nomenclature.

Here, ΔA is the area virtually closed, Δa is the length of the elements at the delamination front, and b is the width of the elements. For better identification in this and the following figures, columns are identified by capital letters (L) and rows by lower case letters (i, k, ℓ) as illustrated in the top view of the upper surface. Hence, F'_{xLi} , F'_{yLi} and F'_{zLi} denote the forces in the local system at the delamination front in column L , row i . The corresponding displacements behind the delamination at the top face node row ℓ are denoted $u'_{L\ell}$, $v'_{L\ell}$ and $w'_{L\ell}$ and at the lower face node row ℓ^* are denoted $u'_{L\ell^*}$, $v'_{L\ell^*}$ and $w'_{L\ell^*}$. All forces and displacements are obtained first from the finite element analysis with respect to the global system. The forces and displacements are then transformed with respect to the local crack tip coordinate system (x' , y' , z') that defines the normal and tangential coordinate directions at the delamination front in the deformed configuration, as discussed earlier for two-dimensional elements. Equations for higher order elements, further details, and additional references are provided in an overview paper by Krueger.

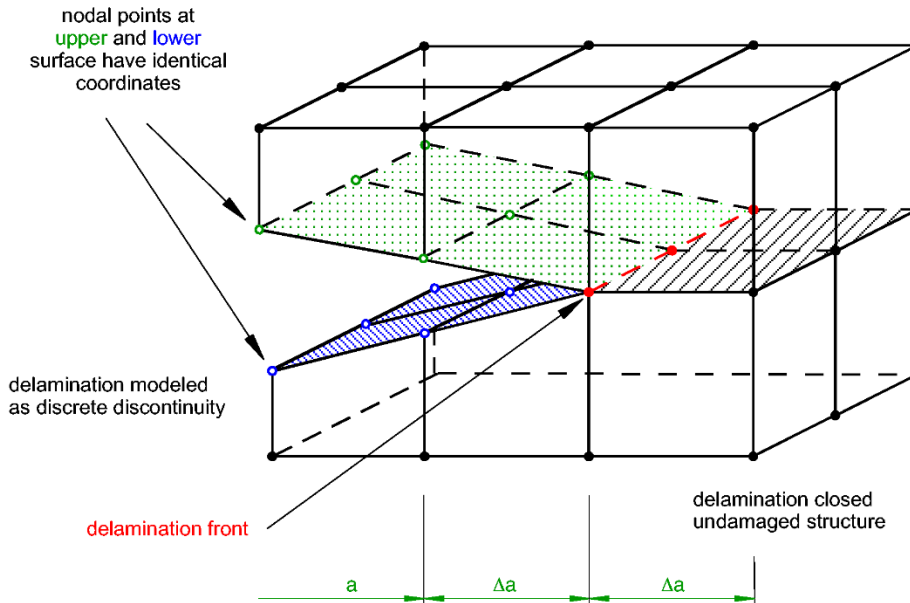


Figure 11.9-3—VCCT Applied to a Delamination Modeled with Three-Dimensional Eight-Noded Solid Elements

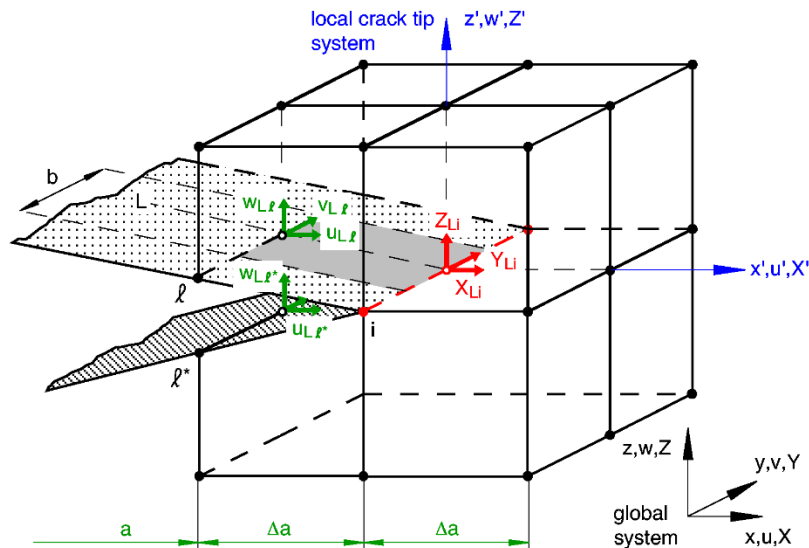


Figure 11.9-4—Three-Dimensional Eight-Noded Solid Elements VCCT Nomenclature

Very large 3D finite element models may require extensive modeling and computational effort. The use of a shell-to-solid submodeling techniques offers great potential for saving modeling and computational effort because only a relatively small section in the vicinity of the delamination front needs to be modeled with solid elements. Large built-up structures such as aircraft fuselage and wing components are traditionally modeled and analyzed using plate or shell finite elements

NASA-HDBK-5010, VOLUME 2, REVISION A

to keep the modeling and computational effort affordable. Often, beam elements are used to represent the stiffeners and shell elements are used to model the skin. It may appear appealing to apply VCCT to cases where the delamination is located at an interface between different element types.

When mixed-mode conditions exist, the computations of the relative contribution of the strain energy release rate components (G_I , G_{II} , and G_{III}) may not be reliable. This problem is likely related to the bi-material interface problem. The relative contribution of the individual modes can depend on element order, shear deformation assumptions, kinematic constraints in the neighborhood of the delamination front, continuity of material properties, and section stiffness in the vicinity of the disbond when delaminations or disbonds are modeled with plate or shell finite elements.

For example, mesh refinement studies showed that computed values of G_I , G_{II} , and G_{III} did not converge when the structure above and below the plane of delamination was modeled with plate elements with different section properties (thickness or layup) (reference Glaessgen, et al. [2002]). A comparison of computed mixed-mode strain energy release rates obtained from plate models with values computed from three-dimensional models showed differences in results near the free edges of the structure where the stress state is three-dimensional (reference König, et al. [2000]). Currently, the community at large has not yet reached a consensus on an approach or a set of approaches that provide a practical solution to this problem. New methodologies need to provide analysis tools to determine the mixed-mode fracture parameters along an arbitrarily shaped crack or delamination front located at a bi-material interface in a three-dimensional solid modeled with any combination of elements.

Oscillatory due to the mathematical singularity at the delamination front due to two dissimilar materials at the interface will not be mitigated by using a three-dimensional model. In composite materials nonconvergence of the individual modes results, total energy release rate can converge.

11.9.2.2 Fracture Margin Assessment Using the Virtual Crack Closure Technique (VCCT)

An example is provided on how the structural margins using VCCT can be predicted. The modeling is performed in two dimensions, so the G_{III} mode is not computed and assumed to be negligible compared to the total energy release rate. This approach has been successfully used in several NASA programs. The mode I and mode II fracture toughness for the material or the interface material in question should be calculated. Next the best fit to mixed mode fracture data from a test like MMB test configuration should be determined.

If it was found that the mixed-mode Power Law for flaw propagation

NASA-HDBK-5010, VOLUME 2, REVISION A

$$\sqrt{\left(\frac{G_I}{G_{Ic}}\right)^2 + \left(\frac{G_{II}}{G_{IIc}}\right)^2} = 1$$

was the best fit, then the structural margins of safety (MS) for a design can be calculated using the following formula:

$$MS = \frac{G_c}{FS \times (G_I + G_{II})} - 1 = \frac{1 + m}{\sqrt{\left(\frac{1}{G_{Ic}}\right)^2 + \left(\frac{m}{G_{IIc}}\right)^2}} - 1$$

where $m = G_{II}/G_I$ is the mixed-mode ratio, FS is the factor of safety, and G_I and G_{II} are Mode I and Mode II energy release rates at the delamination front. The mixed-mode Power Law for flaw propagation was used in Equation 1.

Many spaceflight programs have used a Factor of Safety (FS) of 2.0 and it protects for variability in fracture toughness properties and uncertainty with analysis. The acceptable flaw size is such that $MS = 0$ and $FS = 2.0$, while the critical flaw size is such that $MS = 0$ and $FS = 1.0$. The choice of FS of 2.0 can be explained as follows: The 2.0 FS on fracture energy is nearly equivalent to 1.4 in the load space, as the fracture energy is typically proportional to the square of the load. The factor of 1.4 is used in most NASA human spaceflight programs.

11.9.2.3 Example # 1: Application of VCCT to a Composite Joint

In this example, a durable composite joint (referred to as DRJ) that incorporates a 2.8-inch-long preformed insert was analyzed and assessed using a damage tolerance analysis approach. The insert is made of the same layup and materials as the doubler system. The insert core is Rohacell 200WF, Figure 11.9-5, Schematic of the Composite Joint Configuration. The examples presented in this section are from Goyal and Lundgren (2015).

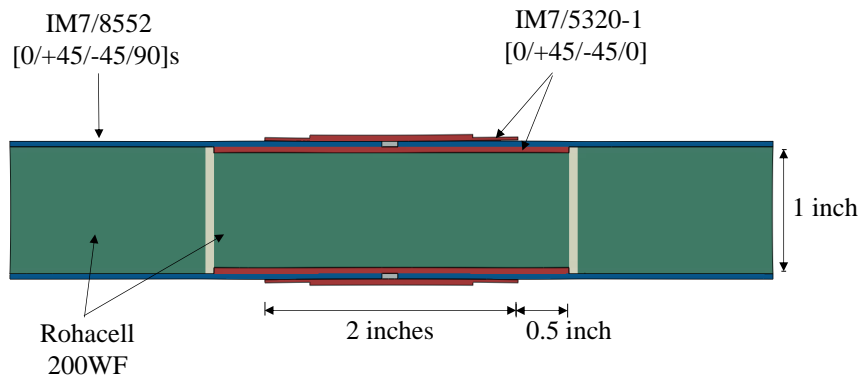


Figure 11.9-5—Schematic of the Composite Joint Configuration

APPROVED FOR PUBLIC RELEASE – DISTRIBUTION IS UNLIMITED

NASA-HDBK-5010, VOLUME 2, REVISION A

The critical energy release rates, while typically measured from Mode I and Mode II tests, were estimated as $G_{Ic} = 2.8 \text{ lb}_f/\text{inch}$ and $G_{IIc} = 5.6 \text{ lb}_f/\text{inch}$ based on fracture toughness characterization. The Power Law is used as the mixed mode fracture criterion as an example application using the Equations in section 11.9.2.2. Following fracture methodology best practices, the surface preparation of the composite joint samples is consistent with fracture toughness characterization samples.

Using the VCCT available in Abaqus® and finite element models with material properties in Table 11.9-2, Mechanical Properties for the Material Systems used in the Composite Joint, the following cases were examined: (1) Analysis of minimum detectable flaw size, (2) No inspection of a portion of the bondline due to a physical obstruction, and (3) Acceptable flaw sizes per bondline zone. The DRJ design will be subject a maximum tension load of 12,900 lb_f . DRJ bondlines are inspected with handheld ultrasound, and it is assumed that the corresponding minimum detectable flaw size is 0.25 inch.

Table 11.9-2—Mechanical Properties for the Material Systems used in the Composite Joint

Material	Model Region	E_{11} (Msi)	$E_{22} = E_{33}$ (Msi)	$\nu_{12} = \nu_{13}$	ν_{23}	$G_{12} = G_{13}$ (Msi)	G_{23} (Msi)
^a IM7/5320-1	Doublers	22.2	1.31	0.370	0.400	0.78	0.47
^b IM7/8552	Sandwich Panel Facesheets	23.8	1.70	0.316	0.400	0.86	0.50
^a Foam	Sandwich Panel Core & Insert Core	0.056	0.056	0.230	0.230	0.23	0.23
^b Adhesive	Foam Splices	0.30	0.30	0.400	0.400	0.11	0.11
^c Teflon	Facesheet Gaps	0.001	0.001	0.400	0.400	0.00036	0.00036

^a Test

^b Literature

^c Assumed

A flaw size equal to the minimum detectable flaw size (i.e., 0.25 inch) was introduced on all four edges of the bonded doublers (see Figure 11.9-6, Edge Flaws were Assumed between the Facesheet and the Doublers), since stresses peak at reentrant corners of a bonded joint design. At the crack-tip, the energy release rates were calculated as $G_{II} = 1.26 \text{ lb}_f/\text{inch}$ and $G_I = 0.51 \text{ lb}_f/\text{inch}$, and the MS using Equation 1 was calculated as +0.71. A larger flaw, 1.0 inch, greater than the minimum detectable flaw size was simulated in the middle of the joint between the insert and the facesheet (see Figure 11.9-7, A Large Flaw is Assumed to be Located between the Facesheet and the Insert (Bottom) Away from the Reentrant Corners of the Joint, and Another Large Flaw is Assumed to be Located between the Facesheet and the Doubler (Top). The MS for this simulation was greater than +1000.0 ($G_{II} = 0.02 \text{ lb}_f/\text{inch}$, $G_I = 0. \text{ lb}_f/\text{inch}$). In another simulation, a 1.0-inch flaw was simulated in the middle of the joint between the doubler and the facesheet. The MS for this simulation was greater than +5.0 ($G_{II} = 0.42 \text{ lb}_f/\text{inch}$, $G_I = 0.01 \text{ lb}_f/\text{inch}$). As expected, the larger flaws were not critical away from the reentrant corners of the joint. In summary, for the maximum expected loads, the design is tolerant to flaws equal or

APPROVED FOR PUBLIC RELEASE – DISTRIBUTION IS UNLIMITED

NASA-HDBK-5010, VOLUME 2, REVISION A

below the minimum detectable flaw size. Interestingly, a designer may optimize the spew fillet; but this design step becomes redundant if the minimum detectable flaw size is 0.25 inch (since a flaw must be assumed at the edge of the joint).

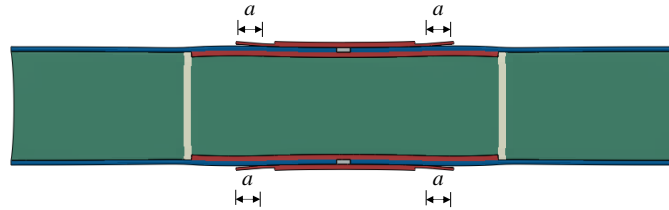


Figure 11.9-6—Edge Flaws were Assumed between the Facesheet and the Doublers

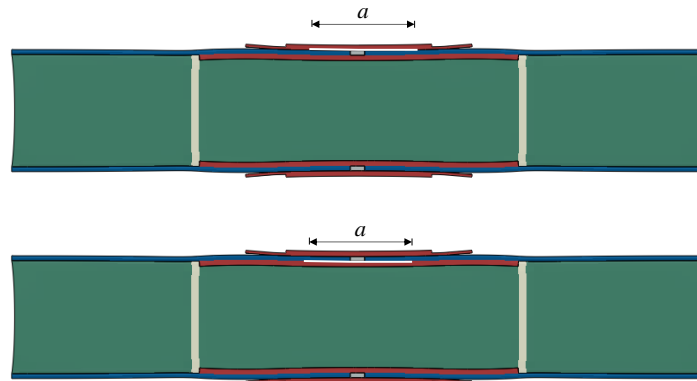


Figure 11.9-7—A Large Flaw is Assumed to be Located between the Facesheet and the Insert (Bottom) Away from the Reentrant Corners of the Joint, and Another Large Flaw is Assumed to be Located between the Facesheet and the Doubler (Top)

A hypothetical situation of an obstruction preventing inspection of the doubler-to-facesheet bondline is now considered. An edge flaw 0.7 inch is simulated across the uninspectable zone. It is assumed that prior inspections did not indicate defects at the insert-to-facesheet bondline. The MS is +0.58 ($G_{II} = 1.4 \text{ lb}_f/\text{inch}$, $G_I = 0.53 \text{ lb}_f/\text{inch}$); the design is tolerant to a flaw in the portion of the bondline where inspection was not possible.

Acceptable flaw sizes per bondline zone were estimated such that the margin of safety was 0.0 with a safety factor of 2.0. This required several simulations varying the flaw size. Only edge flaws were considered because flaws away from the edges were demonstrated to be structurally benign. The acceptable flaw size for an edge flaw between the doubler and the facesheet was determined to be 0.9 inch (see Figure 11.9-8, Margin of Safety for an Edge Flaw between the Facesheet and the Doubler.) The acceptable flaw size for an edge flaw between the insert and the facesheet was determined to be 0.45 inch (see Figure 11.9-9, Margin of Safety for a Flaw between the Facesheet and the Insert). These acceptable flaw sizes are detectable by NDE techniques.

APPROVED FOR PUBLIC RELEASE – DISTRIBUTION IS UNLIMITED

NASA-HDBK-5010, VOLUME 2, REVISION A

In summary, as an illustration of the bonded joint analysis methodology, the design acceptability of the DRJ design subject to the maximum expected tension load of 12,900 lb_f was investigated. This illustration demonstrated that the design is tolerant to flaws greater than the minimum detectable flaw size of 0.25 inch. Acceptable flaw sizes were determined for the facesheet-to-doubler bondline and insert-to-facesheet bondline. These acceptable flaw sizes are greater than the minimum detectable flaw size and can be found through inspection. Finally, the design was demonstrated to be robust in the presence of a flaw across the region of the bondline that is not inspectable.

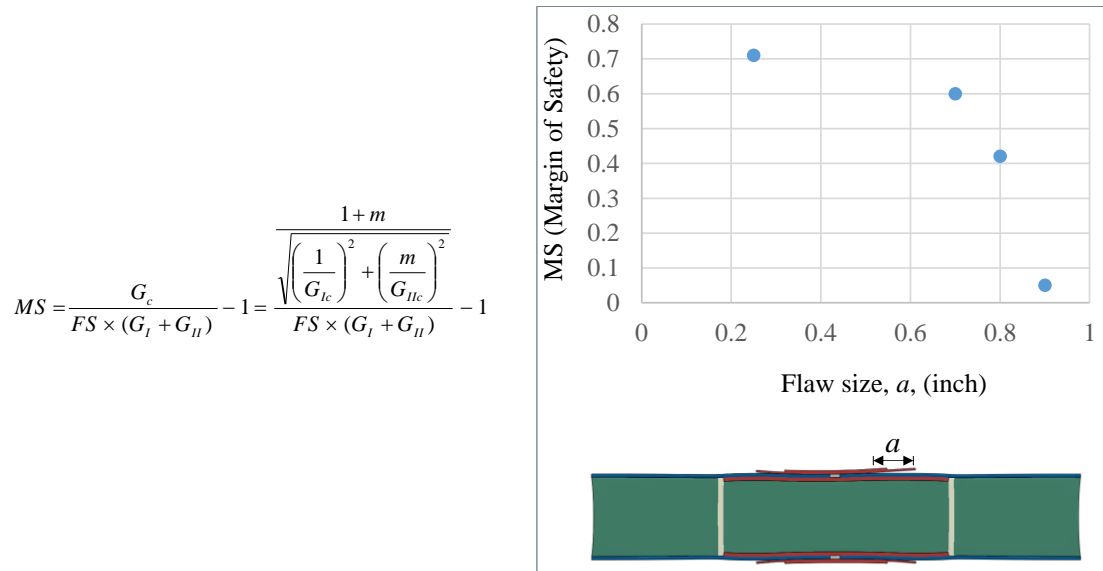


Figure 11.9-8—Margin of Safety for an Edge Flaw between the Facesheet and the Doubler

$$MS = \frac{G_c}{FS \times (G_I + G_{II})} - 1 = \frac{1+m}{\sqrt{\left(\frac{1}{G_{Ic}}\right)^2 + \left(\frac{m}{G_{IIc}}\right)^2}} - 1$$

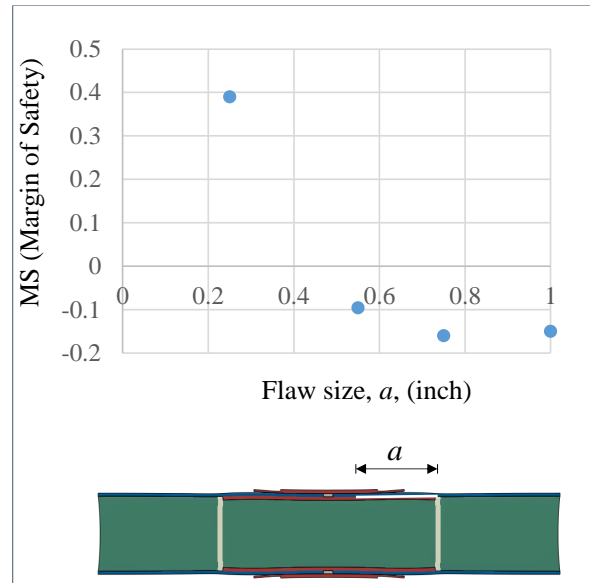


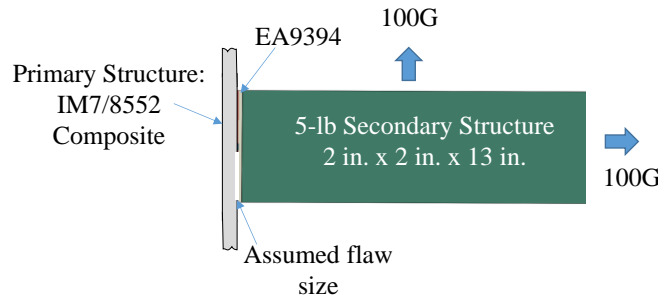
Figure 11.9-9—Margin of Safety for a Flaw between the Facesheet and the Insert

11.9.2.4 Example # 2: Application Using the Virtual Crack Closure Technique

There are many applications where it is necessary to adhesively attach secondary structures. Accessibility may be limited, which may prohibit NDE inspection. Unless access can be gained, these bondlines cannot be inspected using NDE. It would be impractical to assume a fully debonded interface. The following discussions are limited to situations where the bondline cannot be inspected. The design must be shown to be tolerant to flaws of sufficient size such that under load, visual inspection can detect an edge debond. The fracture toughness of the bonded joint system must be determined from coupon tests using pertinent material systems. Once the adequacy of the design is demonstrated for the loads expected in service, a workmanship screen is necessary for accepting the manufactured hardware. A proof test with loads higher than service loads can be used as an effective workmanship screen.

In the following hypothetical illustration, a 2-inch by 2-inch by 13-inch secondary structure, weighing 5 lbs, is bonded to a primary composite structure and the assembly is subject to 100G's in the axial and lateral directions (see Figure 11.9-10, Margin of Safety for a Flaw between the Facesheet and the Insert). With the characteristic element size of 0.01 inch at edge of the bonded joint, and under these load conditions, the peel stress alone (i.e., 8,000 psi) exceeds the strength capability of the adhesive. The problem is revisited using a fracture mechanics approach. Energy release rates for a 0.25-inch by 2.0-inch edge flaw, a 0.6-inch by 2.0-inch edge flaw, and a 1-inch by 2-inch centered flaw were calculated using Abaqus® and VCCT to be less than 1.0 lb_f/inch. These calculated energy release rates are significantly lower than the critical energy release rates that result in crack growth in EA9394, and this design is considered adequate. While the design is acceptable, a proof test is still required to ensure that the structural integrity of the bondline can be maintained during flight conditions.

NASA-HDBK-5010, VOLUME 2, REVISION A



Flaw Configuration	G_I (lbf/inch)	G_{II} (lbf/inch)
0.25-inch flaw	0.4	2.0e-4
0.6-inch flaw	0.44	4.2e-4
1-inch middle flaw	1.6e-2	1.0e-4

Figure 11.9-10—Margin of Safety for a Flaw between the Facesheet and the Insert

11.9.3 Cohesion-Decohesion Elements

Cohesive-decohesive zone models, referred to as CZM, are generally used to predict the initiation and progression of delamination. The prediction of initiation of delamination tends to be of lower confidence than the prediction of delamination progression, as the initiation of delamination can be influenced by the mesh size. These approaches are used with caution in practical application and are usually employed with extensive experimental testing. Further, significant knowledge is required on how these techniques operate to interpret the results accurately.

To provide more background, delaminations stemming from unbonds or debonds require careful evaluation due to their potential detrimental effects on the structural integrity of the part. In practice, acceptance criteria for these types of defects are generally developed and substantiated using coupon-level and subscale-level tests. When defects violate the drawing criteria, these defects are assessed and repaired. In special cases, subscale-tests may not be able to fully capture the load paths in the full-scale structure. In these instances, VCCT can be used to formulate a test program and establish loads such that the predicted energy release rates in sub-scale tests envelop the energy release rates predicted in the full-scale configuration. To increase confidence, structural margins for the defect are generally assessed using analytical techniques such as VCCT, as it provides a straightforward calculation against the fracture limits of the material.

In practice, a delamination that progresses is not an acceptable failure mode in structural applications because it could lead to unknown events; the benefits of utilizing CZM diminish from this perspective. CZM can be highly beneficial in (1) the support of anomaly investigations, (2) supporting the definition of test programs, (3) supporting the design and analysis of more complex structural components, (4) demonstrating that a potential flaw could arrest with no additional adverse consequence to the structure, and (5) demonstrating stability of an irregular-shaped flaw.

NASA-HDBK-5010, VOLUME 2, REVISION A

There are many other practical applications where CZMs have been used to study flaws in COPVs (Goyal and Rome [2012]), bolted joints (Goyal and Rome [2006]), solid rocket nozzles (Goyal, et al. [2008]), hypersonic applications (Goyal, V.K. [2015]), and studying the burst pressure of cylinders with wrinkles (Goyal, et al. [2005]).

Since its inception nearly 30 years ago, CZM has matured through academic and industry research and has been incorporated in finite element commercial codes (e.g., Abaqus® and ANSYS®). This has made the use of CZM more practical and more accessible to end users. It is discussed in this Handbook because it can be a valuable addition to the toolbox of a practitioner. Any time CZM is used, it should be validated against coupon-level test data and preferably with subscale-testing.

CZM is an alternative to modeling technique VCCT, and it is described in Goyal, et al. (2004). Many formulations have been developed but all the formulations have similar features. CZM models material degradation due to failure processes between plies using a simplified constitutive representation that governs the behavior between two separating surfaces that are initially coincident. The interfacial constitutive behavior is described in terms of the separation across the surfaces between the two initially coincident surfaces that are tied by a continuous distribution of “breakable” nonlinear springs (see Figure 11.9-11, Interface Element Consists of a Continuous Distribution of Breakable Springs).

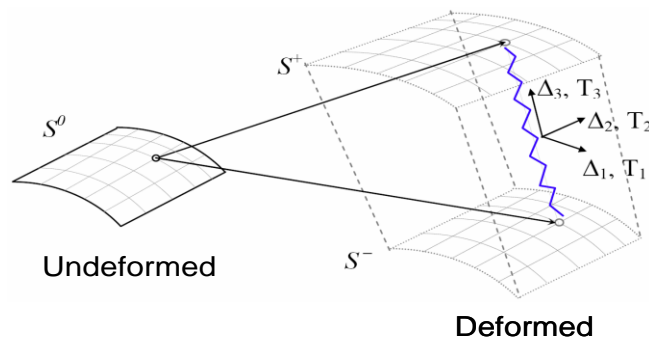


Figure 11.9-11—Interface Element Consists of a Continuous Distribution of Breakable Springs

11.9.3.1 Traction-Separation Constitutive Law

At a high-level, the traction-separation constitutive law is used with cohesive elements as shown in Figure 11.9-12, Traction-Displacement Constitutive Relationship of a Cohesive Element, and placed between adjacent elements representing plies as shown in Figure 11.9-13, Decohesion Elements Placed between Laminates (Gray Solid Elements).

NASA-HDBK-5010, VOLUME 2, REVISION A

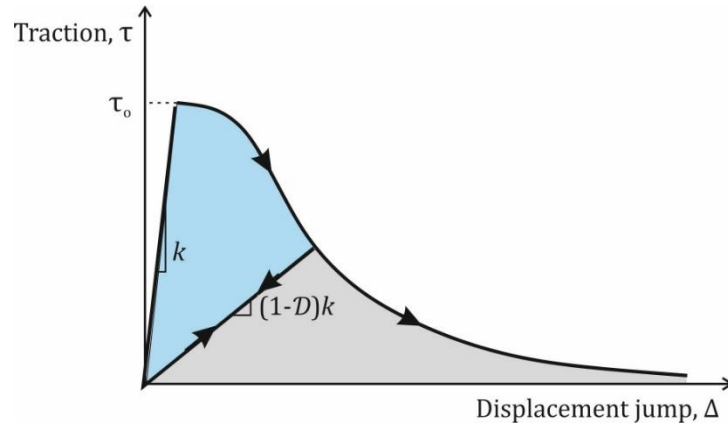


Figure 11.9-12—Traction-Displacement Constitutive Relationship of a Cohesive Element

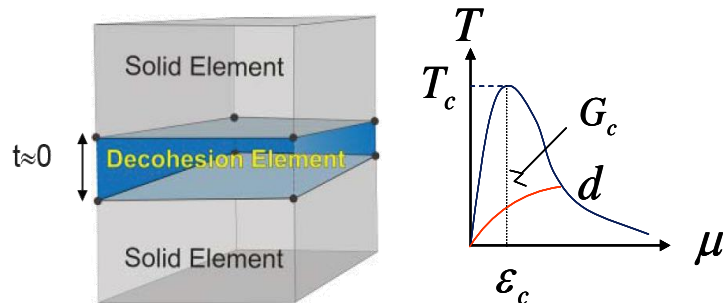


Figure 11.9-13—Decohesion Elements Placed between Laminates (Gray Solid Elements)

The constitutive law governing the failure process has the following features:

1. Initial high penalty stiffness (K): Simulates a rigid connection between the two initially coincidental surfaces and prevents the surfaces from penetrating. After delamination occurs, the high penalty stiffness simulates contact between the two surfaces.
2. Interfacial strength (τ_o): The fracture process at a point initiates when the traction across the two surfaces reaches the interfacial strength, strength, τ_o .
3. Fracture toughness (G_c): Fracture occurs at an interfacial material point when the fracture energy equates the G_c . This is the amount of energy dissipated per unit of newly created crack and represents the area under the curve.
4. Shape of the softening curve and process zone: Can be any shape such as linear or exponential, and it is considered a material property. For a relatively large process zone (e.g., fiber bridging), the shape of the softening function should be characterized by experiment; but for small process zones, the shape of the curve has little effect on the fracture response.

APPROVED FOR PUBLIC RELEASE – DISTRIBUTION IS UNLIMITED

NASA-HDBK-5010, VOLUME 2, REVISION A

5. Damage variable D : Ensures that interfacial damage is not restored. As the relative displacement increases, the maximum interfacial traction is reduced; and the energy dissipated is irrecoverable. $D = 0$ corresponds to no damage and $D = 1$ equates to complete fracture.

To model the interaction between interlaminar tension and shear, a delamination initiation and interaction failure criterion such as the following can be used:

$$\left(\frac{T_3}{S_{3t}}\right)^2 + \left(\frac{T_1}{S_1}\right)^2 + \left(\frac{T_2}{S_2}\right)^2 = 1, T_3 \geq 0,$$
$$\left(\frac{T_3}{S_{3c}}\right)^2 + \left(\frac{T_1}{S_1 - \eta T_3}\right)^2 + \left(\frac{T_2}{S_2 - \eta T_3}\right)^2 = 1, T_3 < 0;$$

where T_1 and T_2 are the interfacial traction components associated with shear, and S_1 and S_2 are the interfacial shear strengths. T_3 is the normal interfacial traction component, S_{3t} is the tensile interfacial normal strength, and S_{3c} is the compressive interfacial normal strength. The quadratic failure criterion includes a “friction coefficient” that incorporates the apparent increase in shear strength due to transverse compression. The constitutive law must also satisfy the mixed mode fracture criterion for the particular material of interest.

11.9.3.2 Validation Cases

The cohesion-decohesion models should be validated against closed form solutions and test data prior to assessing hardware. As an example, Goyal, et al. (2004) presents validation against Mode I double cantilever beam (see Figure 11.9-14, Predictions by Predictive Failure Analysis (PFA) of the Double Cantilever Beam Compare Well to Experimental Data and Analytical Solutions), Mode II end load split (see Figure 11.9-15, Predictions by PFA for the End Load Split Compare Well to Analytical Solutions), Mode II end notched flexure (see Figure 11.9-16, Predictions by PFA for the End Notch Flexure Compare Well to Analytical Solutions), mixed mode bending (see Figure 11.9-17, Predictions by PFA for the Fixed Ratio Mixed Mode Compare Well to Analytical Solutions), and additional validation against experimental data (see Figure 11.9-18, CZM Predicted Load-Displacement Response for Double Cantilever Beam and End Load Split Accurately). These figures show the numerical structural response compared to test data or analytical results. The structural response is given in terms of reaction force as a function of either opening displacement or tip-displacement.

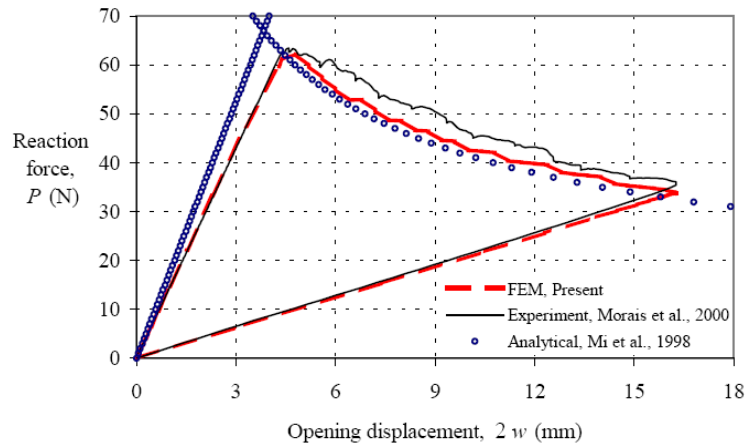


Figure 11.9-14—Predictions by Predictive Failure Analysis (PFA) of the Double Cantilever Beam Compare Well to Experimental Data and Analytical Solutions

(Reference V. K. Goyal, E. R. Johnson, C. G. Davila, “Irreversible constitutive law for modeling the delamination process using interfacial surface discontinuities,” Composite Structures 65 [2004], pp 289-305)

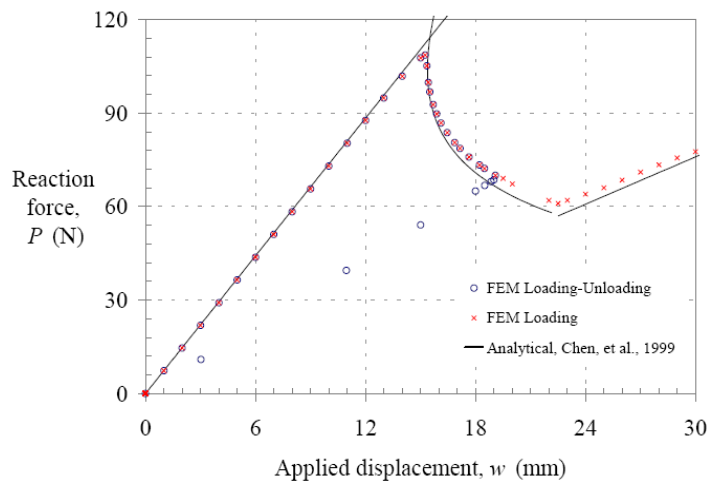


Figure 11.9-15—Predictions by PFA for the End Load Split Compare Well to Analytical Solutions

(Reference V. K. Goyal, E. R. Johnson, C. G. Davila, “Irreversible constitutive law for modeling the delamination process using interfacial surface discontinuities,” Composite Structures 65 [2004], pp 289-305)

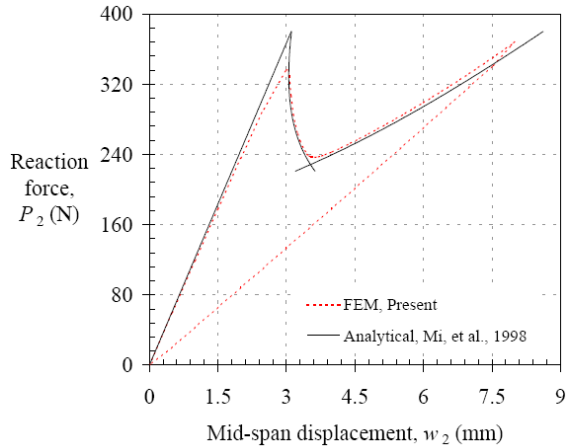


Figure 11.9-16—Predictions by PFA for the End Notch Flexure Compare Well to Analytical Solutions

(Reference V. K. Goyal, E. R. Johnson, C. G. Davila, “Irreversible constitutive law for modeling the delamination process using interfacial surface discontinuities,” Composite Structures 65 [2004], pp 289-305)

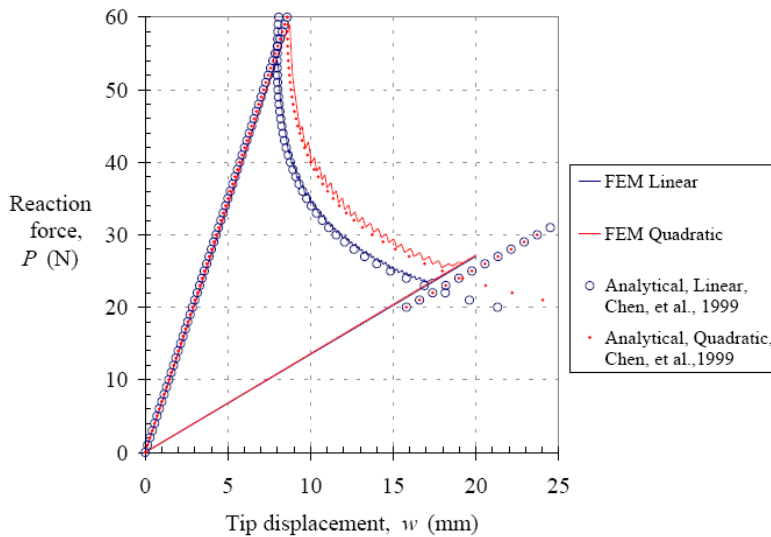


Figure 11.9-17—Predictions by PFA for the Fixed Ratio Mixed Mode Compare Well to Analytical Solutions

(Reference V. K. Goyal, E. R. Johnson, C. G. Davila, “Irreversible constitutive law for modeling the delamination process using interfacial surface discontinuities,” Composite Structures 65 [2004], pp 289-305)

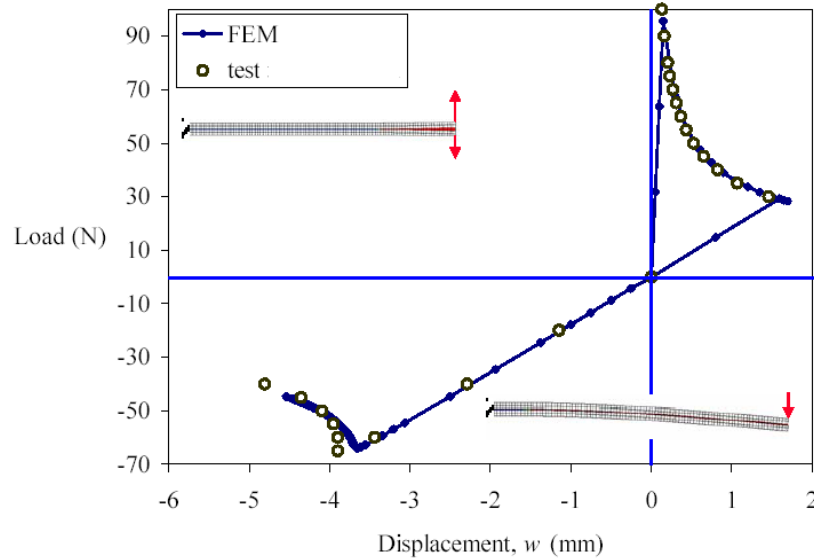


Figure 11.9-18—CZM Predicted Load-Displacement Response for Double Cantilever Beam and End Load Split Accurately

(Reference V. K. Goyal, E. R. Johnson, C. G. Davila, “Irreversible constitutive law for modeling the delamination process using interfacial surface discontinuities,” *Composite Structures* 65 [2004], pp 289-305)

Additional validation examples can be found in NASA/CR-2012-217347.

Bonded joints can also be analyzed using CZM, but an appropriate failure criterion is needed to ensure accurate prediction of propagation. In V. K. Goyal, et al. (2008), the CZM model was validated against experimental data prior to using it to assess flight hardware for a bonded joint application. The CZM model compared well against test data of a single lap joint made of woven carbon epoxy fabric and epoxy-acrylate adhesive (see Figure 11.9-19, Failure and Response of the Single Lap Joint Test Configuration). The CZM model performed well against test data of a double cantilever beam made of an Aluminum 6061-T6 with a thermoplastic acrylic polymer adhesive (see Figure 11.9-20, Failure and Response of a Double Cantilever Beam Test). Finally, in a third validation example, the predicted failure and response of the crack lap shear test configuration compared well with experimental data (see Figure 11.9-21, Failure and Response of a Crack Lap Shear Test).

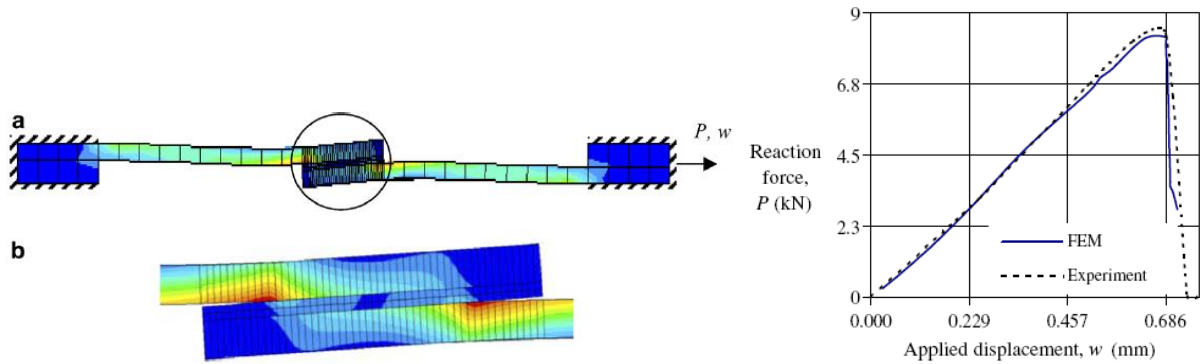


Figure 11.9-19—Failure and Response of the Single Lap Joint Test Configuration
 (Reference V. K. Goyal, E. R. Johnson, and V. K. Goyal, “Predictive Strength – Fracture Model for Composite Bonded Joints,” Composite Structures 82 [2008], pp 434-446)

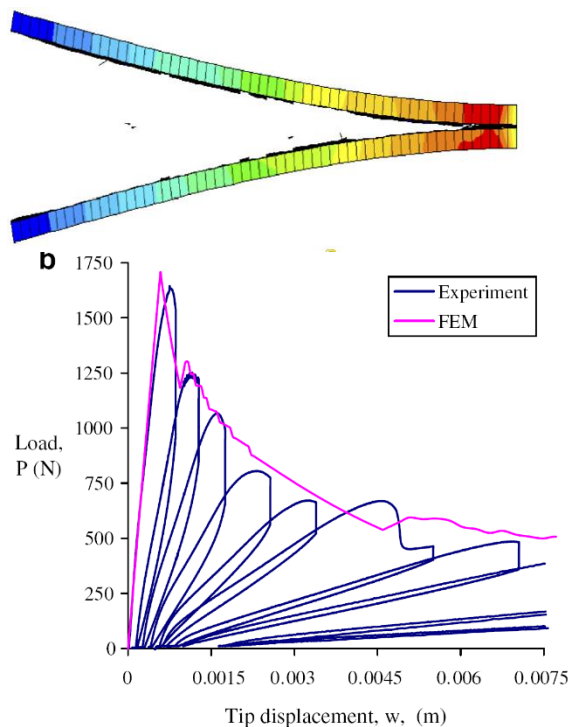


Figure 11.9-20—Failure and Response of a Double Cantilever Beam Test
 (Reference V. K. Goyal, E. R. Johnson, and V. K. Goyal, “Predictive Strength – Fracture Model for Composite Bonded Joints,” Composite Structures 82 [2008], pp 434-446)

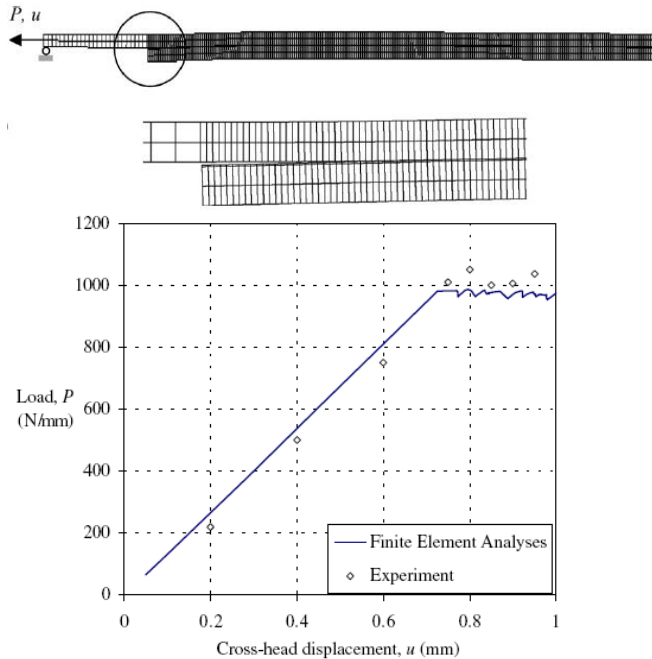


Figure 11.9-21—Failure and Response of a Crack Lap Shear Test

(Reference[V. K. Goyal, E. R. Johnson, and V. K. Goyal, “Predictive Strength – Fracture Model for Composite Bonded Joints,” Composite Structures 82 [2008], pp 434-446])

Cohesive models for the prediction of delamination have been extensively validated by analysis and experimental test data for the DCB and mixed mode bending (MMB) (see NASA/TM-2002-211737 and Versino, et al. [2015]). Sub-element testing such as separation of skin/stiffener in flexure loading, including the behavior in the postbuckling regime, was accurately captured by cohesive zone models (see Bisagni, et al. [2011]) and NASA/TP-2020-220584. These methods were also successfully applied to composite bonded joints with complicated failure modes (see Leone, et al. (2015)).

11.9.3.3 Cautions

Some of the basic requirements for an accurate cohesive analysis are:

1. The mesh sufficiently is refined and at least 3-5 elements are employed in the process zone.
2. Penalty stiffness is set high enough to avoid introducing unwanted compliance and low enough to avoid numerical issues.
3. Accurate knowledge of strengths and critical energy release rates is important. When linear elastic fracture mechanics conditions prevail, i.e., the critical dimensions, including crack length, are much larger than the length of the process zone, the analysis solution becomes less dependent on the value of the cohesive strengths selected.

NASA-HDBK-5010, VOLUME 2, REVISION A

These issues are discussed in Turon, et al. (2007).

The following are cautions that need to be taken when utilizing cohesion-decohesion elements:

Caution 1: Given the singularity at a crack tip, the load required to initiate damage is mesh dependent. The definition of crack “initiation” should correspond to the point where the initial crack tip initially opens ($D = 1$), not when damage first starts ($D > 0$).

Caution 2: Softening laws often cause convergence difficulties in the load incrementation procedure, which are accompanied by the appearance of negative eigenvalues, cuts in the load increment, and followed by a termination of the analysis. The most severe convergence difficulties are the result of unstable crack growth, i.e., when more elastic energy is released by an infinitesimal amount of crack propagation than is needed for creating new fracture surfaces. Procedures to achieve convergence include dynamics analysis, viscoelastic regularization of the damage rate, or modification of the tangent stiffness matrix. See Dávila, et al. (2008) and; Goyal (2002).

Caution 3: Fracture in composites is most often composed of a number of interacting micromechanical events such as delamination, transverse matrix cracking, fiber bridging, delamination migration, and surface delving. These mechanisms build up in the wake of the crack front and cause blunting, bridging, and an effective increase in the critical energy release rate for propagation. Standard characterization protocols may define the critical energy release rate at the first point of nonlinearity and may not consider the resistance effects. Cohesive analyses based on conservative values of the energy release rate will underpredict the propagation curves. Techniques exist to represent R-curves with cohesive elements such as by superposition of bilinear laws (reference Airoidi, et al. [2012]).

Caution 4: Changes in mode mixity can occur during loading. All fracture problems where mixed mode is induced by flexure (e.g., MMB specimen or skin/stiffener separation) exhibit local variations of mode mixity, where the damage starts predominantly in mode II, and it evolves towards mode I. The material science needed to account for different mode histories has not been developed. Nevertheless, thermodynamically consistent cohesive models have predicted energy release rates and mode mixities that are consistent with standard material characterization procedures (reference Turon, et al. [2018]).

11.9.4 Analytical Fatigue Assessments

Note that the community at large has not yet reached a consensus on an approach for characterizing fatigue driven delamination growth under mixed-mode conditions and research is ongoing. Most models are phenomenological, based on the observed macro-scale behavior of test specimens, and it is suggested that a more physics-based approach that focuses on clarifying the mechanisms involved is required to come to a full understanding of the problem of delamination growth.

NASA-HDBK-5010, VOLUME 2, REVISION A

The number of cycles to delamination onset, N_D , can be obtained from a delamination onset curve ASTM D6115-97, Standard Test Method for Mode I Fatigue Delamination Growth Onset of Unidirectional Fiber-reinforced Polymer Matrix Composites. This onset curve (solid line) is a power law fit

$$G = m_0 \cdot N_D^{m_1}$$

of the experimental data (i.e., open circles) obtained from a DCB test using ASTM D6115-97.

Note that standards for mode II and mixed-mode I/II delamination onset currently do not exist; the test methods for static fracture toughness testing have been used to generate onset curves. As additional information, an example of a mixed-mode I/II failure surface is provided to guide the analyst who is seeking input data for performing a mixed-mode fatigue onset analysis using commercial codes.

To perform a delamination onset analysis using VCCT, only one quasi-static analysis to determine G_{max} , and the mixed-mode ratio, G_{II}/G_I , are required. The number of cycles to delamination onset, N_D , can then be determined directly from the experimental data. A time-dependent analysis is not required.

The number of cycles during stable delamination growth, N_G , can be obtained from a fatigue delamination propagation relationship. The delamination growth rate (solid line) can be expressed as a power law function (Paris Law)

$$\frac{da}{dN} = c \cdot G_{max}^n$$

where da/dN is the increase in delamination length, da , per cycles, dN , and G_{max} is the maximum energy release rate at the front at peak loading. The factor c and exponent n were obtained by fitting the curve to the experimental data obtained from DCB tests.

Since composites do not exhibit the same threshold behavior commonly observed in metals, considerable research effort has been spent recently to develop a fatigue delamination threshold criterion. If not provided, a cutoff value, G_{th} , below which delamination growth is assumed to stop, may need to be chosen by the analyst for analysis input.

To perform a delamination fatigue growth analysis using VCCT, only a series of quasi-static analyses to determine, G_{max} , (and the mixed-mode ratio, G_{II}/G_I) are required. The increase in delamination length, da , is determined by the element length at the crack tip Δa . The number of cycles, dN , can be determined directly from the Paris Law. The implemented procedure to move the mesh or release nodal constraints to advance the front remain the same as for the static case. As the delamination advances, the number of cycles, dN , for each incremental growth are

NASA-HDBK-5010, VOLUME 2, REVISION A

summarized to obtain the total number of cycles of stable delamination growth, N_G . A time-dependent analysis is not required to perform this type of analysis. Implementation of algorithms in commercial codes to perform delamination growth analysis under cyclic loading is ongoing and has not yet reached the maturity of automated quasi-static delamination propagation.

Examples where cohesive-decohesive model formulations have shown effectiveness of predicting the fatigue delamination behavior in composites include:

1. Clamped tapered beam: see Liang, et al. (2021).
2. Three-point bend doubler skin/stiffener configuration: see NASA/TP–2020-220584.
3. DCB and MMB test configurations: see NASA/TP–2020-220584.

APPENDIX A

SPACE LAUNCH SYSTEM (SLS)

**MULTIPURPOSE STAGE ADAPTOR (MSA) FRACTURE
CONTROL PLAN (FCP) AND ACCOMPANYING FORM 1676**



National Aeronautics and
Space Administration

SLS-SPIO-PLAN-017

REVISION B

EFFECTIVE DATE: JANUARY 8, 2020

**SPACECRAFT AND PAYLOAD INTEGRATION AND
EVOLUTION OFFICE (SPIE) MSA FRACTURE
CONTROL PLAN**

Approved for Public Release. Distribution is Unlimited.

*The electronic version is the official approved document.
Verify this is the correct version before use.*

Revised: 11/01/2011

APPROVED FOR PUBLIC RELEASE – DISTRIBUTION IS UNLIMITED

NASA-HDBK-5010, VOLUME 2, REVISION A

Space Launch System (SLS) Program/Project	
Revision: B	Document No: SLS-SPIO-PLAN-017
January 8, 2020	Page: 2 of 54
Title: SPIE MSA Fracture Control Plan	

REVISION AND HISTORY PAGE

Status	Revision No.	Change No.	Description	Effective Date
Draft	–		Draft	07/31/12
Baseline			Baseline (Reference SPIE ECBD SV3-03-0326, dated 12/19/14); CR SLS-SPIE-0120. MSFC Fracture Control Board Memo EM20-14-FCB-014.	12/23/14
Update	A		MSFC Fracture Control Board Memo referenced in baseline revision table entry; various places within the document, changed from doghouse, access port, secondary payload platform and forward electrical panel to housing, access hatch or access cover, secondary payload bracket, and electrical interface panel, respectively; modified text to indicate the housing to diaphragm joint has become a bolted connection, changed from 12 to 14 secondary payload brackets, removed reference to a camera, and updated the SPIO to SPIE (see acronyms list); Provided editorial changes throughout the document to improve clarity; Section 1.0: removed EM-2 effectivity; Section 1.1: removed reference to an EFT-1 update; Section 1.2: removed reference to XP50-14-011; Section 1.3: updated OPR to EM20; updated CM Plan Document; Section 2.0: added MSA Cable Attachment SAR; added NASA-STD-5001, added SLS-SPIE-SPEC-004, and changed the reference to the CM Plan Document; added two bolt specifications and the (EFT-1) MPCV Diaphragm Strength and Stability Report; and removed the SPIE ISPE Integrated Test Plan; inserted reference to the MSFC fracture control board memo regarding secondary payload fracture control; Throughout Section 3.0: improved and updated description of hardware to match current configuration and clarified design authorities for the components; Section 3.2: changed title from Access Port Covers; Section 3.4: modified wiring harness provider to MSFC Engineering, added descriptions and figure describing the electrical	

*The electronic version is the official approved document.
Verify this is the correct version before use.*

APPROVED FOR PUBLIC RELEASE – DISTRIBUTION IS UNLIMITED

NASA-HDBK-5010, VOLUME 2, REVISION A

Space Launch System (SLS) Program/Project	
Revision: B	Document No: SLS-SPIO-PLAN-017
January 8, 2020	Page: 3 of 54
Title: SPIE MSA Fracture Control Plan	

			<p>wiring harnesses and mounting for the secondary payloads system, and modified the discussion to remove old configuration language; Section 3.5: changed title from Forward Electrical Panel; Section 3.7: added to discuss secondary payload avionics configuration; Sections 3.7 and 3.8 become 3.8 and 3.9; Section 3.9: updated the diaphragm electrical connector plates to be consistent with the current design and materials; Section 4.0: clarified hardware operations; Section 5.0: clarified contents of classification tables and responsibilities for working fracture control; Table 5-1, added the machine-drilled assembly (MSA), removed the wiring harness mounting hardware to Table 5-2, and added the -001 extension to drawing numbers; Sections 5.2.2, 5.4.1, and 5.4.5: removed shall wording; Section 5.2.2.5: clarified the applicability of the IDPP; 5.3.2: clarified the significance of the critical initial flaw size; Section 5.4: updated text to reflect the current state of fracture control classification; identified the limitation of further fracture control effort required for NFC parts; Table 5-2, corrected the part numbers for the electrical interface brackets and added the threaded nodes of the MSA barrel panels to the non-fracture critical classification list, added secondary payload brackets and wiring harnesses and cable attach bracket, spacer and bolts, and avionics and avionics mounting, and removed reference to camera mounting hardware and added the -001 extension to drawing numbers; Section 5.4.4, removed text about gasket and inserted text about tape; inserted Section 5.4.5, Contained Hardware; Section 5.4.6 adding rationale for the electrical plates; Section 5.4.7 updated rationale regarding the classification of the threaded nodes of the MSA barrel panels; Section 5.4.8 discussed the rationale for fail-safe access cover bolts; added Section 5.4.9: low-risk part rationale for loop clamp (p-clamp) bolts; added Section 5.4.10: low-risk fastener cable attach bracket bolts. Appendix A: Added</p>	
--	--	--	--	--

*The electronic version is the official approved document.
Verify this is the correct version before use.*

APPROVED FOR PUBLIC RELEASE – DISTRIBUTION IS UNLIMITED

NASA-HDBK-5010, VOLUME 2, REVISION A

Space Launch System (SLS) Program/Project	
Revision: B	Document No: SLS-SPIO-PLAN-017
January 8, 2020	Page: 4 of 54
Title: SPIE MSA Fracture Control Plan	

Update	B	<p>more acronyms to the list. Appendix C: updated the DTA to reflect operations at the MSA diaphragm vendor; removed Appendix C. MSFC Fracture Control Board Memo EM20-17-FCB-007_encls.pdf</p> <p>Revision B (Reference SPIE ECBD SV3-03-1531, dated 10/13/19; CR SPIE-0367; PCN SP01420 MSFC Fracture Control Board Memo referenced in Revision A table entry; changed wording in numerous places to identify effectivity to Artemis II and beyond, removing references to EFT-1 where appropriate; updated text in numerous places to new secondary payload (SPL) configurations, quantity sixteen with eleven 12U SPLs; added two new threaded inserts for isogrid nodes to Table 5.2; changed the OPR from EM20 to EM21 to reflect an organizational change, provided editorial updates to improve readability.</p>	1/8/2020
--------	---	--	----------

*The electronic version is the official approved document.
Verify this is the correct version before use.*

APPROVED FOR PUBLIC RELEASE – DISTRIBUTION IS UNLIMITED

NASA-HDBK-5010, VOLUME 2, REVISION A

Space Launch System (SLS) Program/Project	
Revision: B	Document No: SLS-SPIO-PLAN-017
January 8, 2020	Page: 5 of 54
Title: SPIE MSA Fracture Control Plan	

TABLE OF CONTENTS

PARAGRAPH	PAGE
1.0 INTRODUCTION	8
1.1 Purpose.....	8
1.2 Scope.....	8
1.3 Change Authority/Responsibility.....	8
2.0 DOCUMENTS.....	9
2.1 Applicable Documents.....	9
2.2 Reference Documents	9
3.0 HARDWARE OVERVIEW	11
3.1 Barrel Segments	14
3.2 Access Covers.....	14
3.3 Forward and Aft Rings.....	14
3.4 Electrical Cables	14
3.5 Electrical Interface Brackets 1 and 2	16
3.6 Secondary Payload Brackets.....	17
3.7 Secondary Payload Avionics	19
3.8 MSA Diaphragm.....	19
3.9 MSA Diaphragm Electrical Connector Plates	20
4.0 HARDWARE OPERATIONS.....	22
5.0 FRACTURE CONTROL CLASSIFICATIONS	23
5.1 Fracture Critical Hardware	23
5.2 MSA Diaphragm Fracture Control Approach.....	25
5.2.1 Planned Efforts for the Diaphragm	25
5.2.2 Impact Damage Protection Plan (IDPP).....	26
5.3 Processing of Fracture Critical Hardware.....	27
5.3.1 Fracture Critical Identification on Drawings.....	27
5.3.2 Methodology for Assessing Fracture Critical Hardware.....	28
5.3.3 Nondestructive Evaluation	28

*The electronic version is the official approved document.
Verify this is the correct version before use.*

APPROVED FOR PUBLIC RELEASE – DISTRIBUTION IS UNLIMITED

NASA-HDBK-5010, VOLUME 2, REVISION A

Space Launch System (SLS) Program/Project	
Revision: B	Document No: SLS-SPIO-PLAN-017
January 8, 2020	Page: 6 of 54
Title: SPIE MSA Fracture Control Plan	

5.3.4 Disposition of Significant Indications	28
5.4 Non-Fracture Critical Hardware	29
5.4.1 Low Risk Metallic Hardware	34
5.4.2 Fail-Safe Metallic Hardware	34
5.4.3 Low Released-Mass Hardware.....	35
5.4.4 Exempt Hardware.....	35
5.4.5 Contained Hardware.....	35
5.4.6 Alternative Approach for Electrical Connector Plates	36
5.4.7 Alternate Approach for the Threaded Nodes of the Barrel Panels.....	37
5.4.8 Fail-Safe Approach for Access Cover Bolts	38
5.4.9 Loop Clamp Bolts Alternate Non-Fracture Critical Low Risk Part Classification.....	40
5.4.10 Non-Fracture Critical Low-Risk Cable Attach Bracket Bolts.....	42
6.0 FRACTURE CONTROL RESPONSIBILITIES.....	43
6.1 Responsible Fracture Control Board.....	43
6.2 Fracture Control Implementation.....	43

APPENDIX

APPENDIX A ACRONYMS AND ABBREVIATIONS AND GLOSSARY OF TERMS	44
APPENDIX B OPEN WORK	47
APPENDIX C MSA DIAPHRAGM DAMAGE THREAT ASSESSMENT	48

TABLE

TABLE 5-1. FRACTURE CONTROL CLASSIFICATIONS, GROUP 1, FRACTURE CRITICAL PARTS	24
TABLE 5-2. FRACTURE CONTROL CLASSIFICATIONS, GROUP 2, NON-FRACTURE CRITICAL PARTS	29
TABLE B1-1. TO BE DETERMINED ITEMS	47
TABLE B2-1. TO BE RESOLVED ISSUES	47
TABLE C-1. DTA SCENARIO TABLE, MSA DIAPHRAGM/HOUSING ASSEMBLY	51

*The electronic version is the official approved document.
Verify this is the correct version before use.*

NASA-HDBK-5010, VOLUME 2, REVISION A

Space Launch System (SLS) Program/Project	
Revision: B	Document No: SLS-SPIO-PLAN-017
January 8, 2020	Page: 7 of 54
Title: SPIE MSA Fracture Control Plan	

FIGURE

FIGURE 3-1. ISPE CONFIGURATION.....	11
FIGURE 3-2. CROSS-SECTION OF THE MSA	13
FIGURE 3-3. SCHEMATIC OF ISOGRID RIBS MACHINED INTO THE INTERIOR SURFACES OF THE BARREL PANELS	13
FIGURE 3-4. FABRICATION OF THE MSA	13
FIGURE 3-5. CABLE MOUNTING P-CLAMPS	15
FIGURE 3-6. A) CABLE ATTACH BRACKET ASSEMBLY, ALSO SHOWING THE P- CLAMP, AND B) CABLE ATTACH SPACERS (SHORT AND TALL)	16
FIGURE 3-7. ATTACHMENT OF THE ELECTRICAL INTERFACE BRACKETS TO THE MSA.	17
FIGURE 3-8. CONFIGURATION OF THE MSA ELECTRICAL INTERFACE BRACKETS ..	17
FIGURE 3-9. SECONDARY PAYLOAD BRACKETS, (A) PLACEMENT IN THE MSA (ARTEMIS I CONFIGURATION), (B) LOCATION OF 12U BRACKETS (ARTEMIS II), (C) PICTORIAL OF THE 6U BRACKET ASSEMBLY, AND (D) 12U BRACKET WITH A SECONDARY PAYLOAD.	18
FIGURE 3-10. AVIONICS ASSEMBLY	19
FIGURE 3-11. CROSS-SECTIONAL VIEW OF THE MSA SHOWING THE HOUSING ATTACHED TO THE DIAPHRAGM	20
FIGURE 3-12. DIAPHRAGM ELECTRICAL CONNECTOR PLATE 1	20
FIGURE 3-13. DIAPHRAGM ELECTRICAL CONNECTOR PLATE 2	21
FIGURE 5-1. IMAGE OF AN ISOGRID NODE	37
FIGURE C-1. DAMAGE THREAT ASSESSMENT (DTA) TASKS AND FLOW.....	50

*The electronic version is the official approved document.
Verify this is the correct version before use.*

APPROVED FOR PUBLIC RELEASE – DISTRIBUTION IS UNLIMITED

NASA-HDBK-5010, VOLUME 2, REVISION A

Space Launch System (SLS) Program/Project	
Revision: B	Document No: SLS-SPIO-PLAN-017
January 8, 2020	Page: 8 of 54
Title: SPIE MSA Fracture Control Plan	

1.0 INTRODUCTION

This document is an update to Revision A for the Spacecraft and Payload Integration and Evolution office (SPIE) MSA Fracture Control Plan (SLS-SPIO-PLAN-017), and it applies to all SLS Block-1 missions using an MSA. MSA is an acronym identifying the Orion Multipurpose Crew Vehicle Stage Adapter, also identified now as the Orion Stage Adapter, or OSA. Revision A updated requirements and activities for Artemis I¹, principally adding secondary payloads. Revision B updates the fracture control planning to consider the hardware configuration to be used for the second exploration mission, Artemis II and beyond. This configuration will be essentially identical to that used for the Artemis I, but the fourteen secondary payload brackets from Artemis I increased to as many as eighteen, with up to eleven of those secondary payload brackets changed to brackets to accommodate larger, 12U-sized secondary payloads.

1.1 Purpose

Among the requirements levied by SLS-SPIO-RQMT-001, SLS Spacecraft Payload Integration and Evolution Office (SPIE) Data Requirements List (DRL), and SLS-SPIO-RQMT-002, SPIE ISPE Requirements Document is the need for the MSA to meet requirements defined by NASA-STD-5019, Fracture Control Requirements for Spaceflight Hardware and MSFC-RQMT-3479, Fracture Control Requirements for Composite and Bonded Vehicle and Payload Structures. This document addresses the fracture requirements by establishing the plan for fracture control activities for the MSA, which is a component of the Integrated Spacecraft and Payload Element (ISPE).

1.2 Scope

The ISPE consists of four components, but this document will only discuss fracture control of the MSA in detail. Attachment hardware for integration of the MSA to the Multi-Purpose Crew Vehicle (MPCV) and to the Interim Cryogenic Propulsion System (ICPS) are not a part of the MSA, and fracture control of those items is not discussed herein. The MSA will conform to NASA requirements and to the specific SLS and SPIE requirements cited above. This document identifies the planned activities and deliverables required to establish fracture control on the MSA, and it is consistent with NASA-STD-5019, Fracture Control Requirements for Spaceflight Hardware and MSFC-RQMT-3479, Fracture Control Requirements for Composite and Bonded Vehicle and Payload Structures.

1.3 Change Authority/Responsibility

The NASA Office of Primary Responsibility (OPR) for this document is EM21. Proposed changes to this document will be submitted by an SPIE change request (CR) to the SPIE Engineering Review Board (ERB) for disposition. All such requests will adhere to the SLS-SPIO-PLAN-032, SPIE Configuration Management Plan.

¹ Artemis is an updated naming from the exploration missions (EM), where sequentially, EM-1, EM-2, *et cetera*, become Artemis I, Artemis II, *et cetera*.

*The electronic version is the official approved document.
Verify this is the correct version before use.*

NASA-HDBK-5010, VOLUME 2, REVISION A

Space Launch System (SLS) Program/Project	
Revision: B	Document No: SLS-SPIO-PLAN-017
January 8, 2020	Page: 9 of 54
Title: SPIE MSA Fracture Control Plan	

2.0 DOCUMENTS

2.1 Applicable Documents

The specifications, standards and handbooks in the Applicable Documents table below form a part of this document to the extent specified herein. The user shall refer to SLS-SPIO-RPT-039, SPIE Element Baseline and Applicable Documents List, for the version incorporated into the SPIE baselines, which defines the requirements for the design, development, test, and evaluation of ISPE hardware. In most cases, the latest revision is used, unless otherwise stated in SLS-SPIO-RPT-039. The released Program documents can be found in the ICE Windchill "Category 1 CM-Controlled Items" folder. Released Element documents can be found in the ICE Windchill location "SLS SPIE CMDM Limited Rights, 002-CM Library" folder.

MSFC-RQMT-3479	Fracture Control Requirements for Composite and Bonded Vehicle and Payload Structures
NASA-STD-5019	Fracture Control Requirements for Spaceflight Hardware
SLS-SPIO-RQMT-001	SLS Spacecraft Payload Integration and Evolution Office (SPIE) Data Requirements List (DRL)
SLS-SPIO-RQMT-002	SPIE ISPE Requirements Document
SLS-SPIO-RPT-013	SPIO MSA Fracture Control Summary Report
SLS-SPIO-RPT-038	SPIO MSA Structural Assessment Report

2.2 Reference Documents

The following documents contain supplemental information to guide users in the application of this document.

Ares-USO-SE-25753	Upper Stage Damage Threat Assessment for Composite and Bonded Structures
EM20-17-FCB-001	Fracture Control Board Memo: Responsible Fracture Control Board for SLS Secondary Payloads
EV31-002-AR-162-2016	MSA Cable Attachment Structural Assessment Report
NAS1953	National Aerospace Standard: BOLT, SHEAR, HEXAGON HEAD, 108 KSI SHEAR, LONG THREAD
NAS4003	National Aerospace Standard: FASTENER, A286 CORROSION RESISTANT ALLOY, EXTERNALLY THREADED, 160 KSI Ft _u , 95 KSI F _{su} , 1000 °F
NASA-STD-5001	STRUCTURAL DESIGN AND TEST FACTORS OF SAFETY FOR SPACEFLIGHT HARDWARE

*The electronic version is the official approved document.
Verify this is the correct version before use.*

APPROVED FOR PUBLIC RELEASE – DISTRIBUTION IS UNLIMITED

NASA-HDBK-5010, VOLUME 2, REVISION A

Space Launch System (SLS) Program/Project	
Revision: B	Document No: SLS-SPIO-PLAN-017
January 8, 2020	Page: 10 of 54
Title: SPIE MSA Fracture Control Plan	

NASA-STD-5009	Nondestructive Evaluation Requirements for Fracture-Critical Metallic Components
SLS-SPIO-EFT1-PLAN-004	EFT-1 MSA Fracture Control Plan
SLS-SPIE-PLAN-032	SPIE Configuration Management Plan.
SLS- SPIO-PLAN-018	SPIO Nondestructive Evaluation Plan
SLS-SPIO-PLAN-020	SPIE ISPE Contamination and Foreign Object Debris (FoD) Control Plan.
SLS- SPIO-RPT-039	SPIO Element Baseline and Applicable Documents List
SLS-SPIE-SPEC-004	PROCESS SPECIFICATION FOR FABRICATION OF THE MPCV STAGE ADAPTER COMPOSITE DIAPHRAGM
STSB-2012-015	MPCV Diaphragm Strength and Stability Report.
WAD-QE-MSA-0001	Work Plan - MSA Receiving Inspection

*The electronic version is the official approved document.
Verify this is the correct version before use.*

APPROVED FOR PUBLIC RELEASE – DISTRIBUTION IS UNLIMITED

NASA-HDBK-5010, VOLUME 2, REVISION A

Space Launch System (SLS) Program/Project	
Revision: B	Document No: SLS-SPIO-PLAN-017
January 8, 2020	Page: 11 of 54
Title: SPIE MSA Fracture Control Plan	

3.0 HARDWARE OVERVIEW

A notional depiction of the SLS Block 1 vehicle ISPE configuration is shown in Figure 3-1. Moving upwards in the stack, the ISPE sub-elements of the Block 1 configuration consist of the Launch Vehicle Stage Adapter (LVSA), Separation System (SS), Interim Cryogenic Propulsion Stage (ICPS), and the Multi-Purpose Crew Vehicle Stage Adapter (MSA).

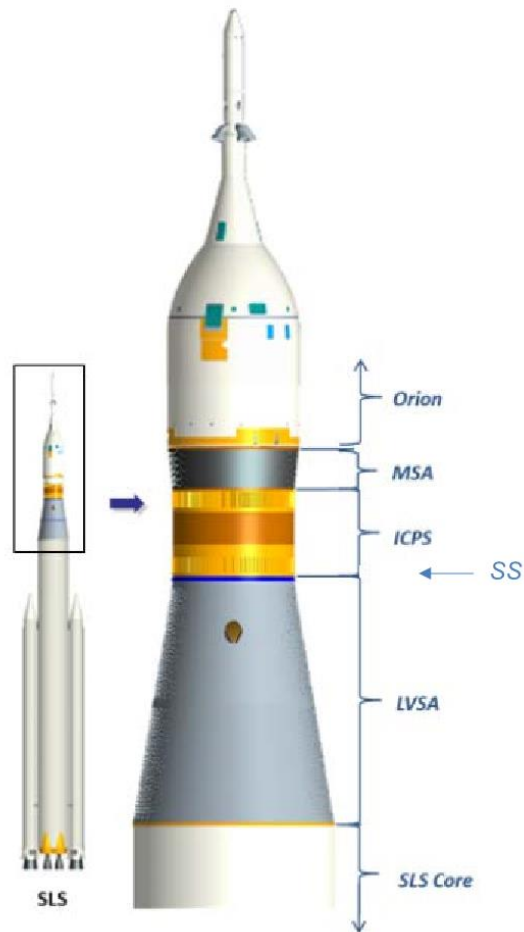


Figure 3-1. ISPE Configuration

*The electronic version is the official approved document.
Verify this is the correct version before use.*

NASA-HDBK-5010, VOLUME 2, REVISION A

Space Launch System (SLS) Program/Project	
Revision: B	Document No: SLS-SPIO-PLAN-017
January 8, 2020	Page: 12 of 54
Title: SPIE MSA Fracture Control Plan	

The ICPS and SS are existing Delta IV launch vehicle systems modified for use on SLS, and a manufacturing vendor will provide the LVSA. Fracture control will be the responsibility of the vendors who manufacture the components.

The MSA is a segment of primary structure that connects the MPCV to the ICPS. The MSA will accomplish the functions of providing structural support, separation of the respective, internal MPCV and ICPS environments, and provision of features to pass electrical interfaces from the MPCV to the ICPS. In addition, secondary payload brackets will be provided to attach seventeen secondary payloads and an associated avionics unit, for a total of eighteen brackets.

The interface joint fasteners for the MPCV-to-MSA joint are the responsibility of the MPCV designers, and the interface joint fasteners for the MSA-to-ICPS joint are the responsibility of the ICPS designers.

The MSA primary structure was designed to SLS loads during the First Exploration Flight Test (EFT-1) effort. Plies were added to the diaphragm for SLS to accommodate a slightly higher differential pressure. MSFC will deliver the flight MSA for integration into the SLS.

The MSA is dry structure with the larger diameter of the conical frustum shape located forward, and it is an assembly that includes the MSA diaphragm, secondary payload brackets, electrical interface brackets, electrical wiring harnesses, and harness mounting brackets. The conical barrel sections are manufactured from 2195 aluminum-lithium alloy by machining an isogrid patterned pocket structure (Figure 3-2 and Figure 3-3) that retains much of the stiffness of the original plate while lightening the structure dramatically. These panels are formed into a conical segment and are then joined together using the conventional friction-stir welding (C-FSW) process, and then circular aluminum flanges, made of continuous rolled-ring 2219 aluminum forgings, are joined to the ends of the conical barrel (Figure 3-4) using the self-reacting friction-stir welding (SR-FSW) process. The flanges are drilled to provide a bolted joint at the MSA attachment flanges. The diaphragm is a dome-shaped composite that is bolted to the aft ring of the MSA and is included to insure separation of the ICPS environment from that of the MPCV. The MSA volume is purged prior to launch, but the volume is not sealed. Externally, the assembled flight MSA will be painted, but there is no plan to apply a thermal protection system (TPS).

Electrical wiring harnesses will pass through the MSA along the wall in the longitudinal direction. These harnesses provide communications between the MPCV and the portion of the stack that is below the MSA and will be mounted to the MSA using holes with threaded inserts at the isogrid nodes. Electrical interface brackets support the electrical wiring harness connections. These brackets are attached using the threaded inserts, as well. The secondary payload brackets and associated electrical wiring harnesses are also mounted using holes with threaded inserts at the isogrid nodes.

*The electronic version is the official approved document.
Verify this is the correct version before use.*

APPROVED FOR PUBLIC RELEASE – DISTRIBUTION IS UNLIMITED

NASA-HDBK-5010, VOLUME 2, REVISION A

Space Launch System (SLS) Program/Project	
Revision: B	Document No: SLS-SPIO-PLAN-017
January 8, 2020	Page: 13 of 54
Title: SPIE MSA Fracture Control Plan	

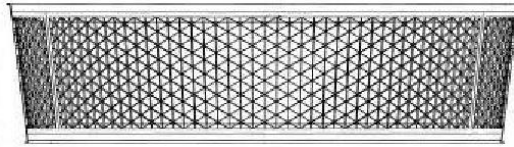


Figure 3-2. Cross-Section of the MSA

Note isogrid rib pattern of the panels.

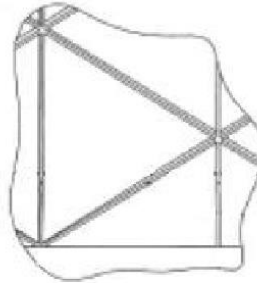


Figure 3-3. Schematic of Isogrid Ribs Machined into the Interior Surfaces of the Barrel Panels

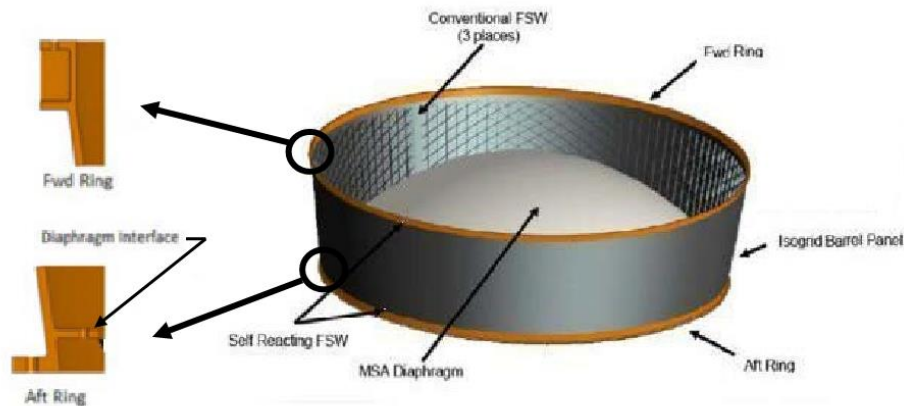


Figure 3-4. Fabrication of the MSA

*The electronic version is the official approved document.
Verify this is the correct version before use.*

NASA-HDBK-5010, VOLUME 2, REVISION A

Space Launch System (SLS) Program/Project	
Revision: B	Document No: SLS-SPIO-PLAN-017
January 8, 2020	Page: 14 of 54
Title: SPIE MSA Fracture Control Plan	

3.1 Barrel Segments

The barrel section of the MSA will be made of panels with conical curvature, but with the vertex removed, leaving the frustum of the cone. This section will be produced from three panels that have been machined to produce an isogrid-rib stiffening structure. Panels will be bump-formed into the curved shape and processed into the final –T8M4 temper. MSFC will perform C-FSW to assemble the panels into a barrel assembly. Nodes are drilled and tapped to allow mounting of hardware along the IML. Threaded inserts are assembled to the threaded holes in the nodes. The solid-wall inserts used for the Artemis I will be changed to staked, solid-wall inserts for Artemis II and beyond.

Two circular access hatches are provided to allow connection of electrical cabling. The portals through the barrel segments will use thickened bosses, relative to the skin thickness of the isogrid, and these will be drilled, with threaded inserts installed to facilitate attachments of the access covers.

3.2 Access Covers

The access hatches will require covers, and these will be made of 2219 aluminum and will be bolted to the barrel segments using aerospace-grade bolts with 180-ksi strength.

3.3 Forward and Aft Rings

The forward and aft rings will serve as mounting flanges for the MSA, and these will be nominally 18.0 and 16.5 feet in diameter and will be machined from continuous-rolled ring forgings using 2219 aluminum that will be processed to –T851 temper. MSFC will perform SR-FSW to assemble the rings into the barrel assembly.

3.4 Electrical Cables

Two, redundant, electrical wiring harnesses will follow the inner mold line of the MSA in a longitudinal orientation, mounted to the MSA barrel using p-clamps (Figure 3-5 and Figure 3-6) attached to threaded inserts located in the primary MSA structure at the isogrid nodes. The cable connections are supported by cable attach brackets (Figure 3-6). The wiring harnesses are a design provided by MSFC Engineering, and they will provide communications between the MPCV and the portion of the stack that is below the MSA. The electrical wiring harnesses associated with the secondary payloads are located and mounted similarly.

*The electronic version is the official approved document.
Verify this is the correct version before use.*

NASA-HDBK-5010, VOLUME 2, REVISION A

Space Launch System (SLS) Program/Project	
Revision: B	Document No: SLS-SPIO-PLAN-017
January 8, 2020	Page: 15 of 54
Title: SPIE MSA Fracture Control Plan	

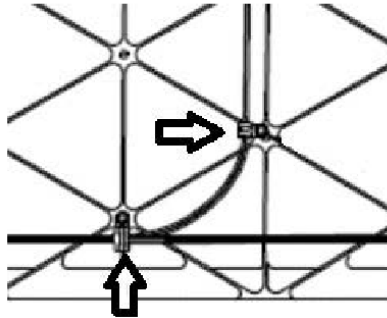


Figure 3-5. Cable Mounting p-clamps

*The electronic version is the official approved document.
Verify this is the correct version before use.*

APPROVED FOR PUBLIC RELEASE – DISTRIBUTION IS UNLIMITED

NASA-HDBK-5010, VOLUME 2, REVISION A

Space Launch System (SLS) Program/Project	
Revision: B	Document No: SLS-SPIO-PLAN-017
January 8, 2020	Page: 16 of 54
Title: SPIE MSA Fracture Control Plan	

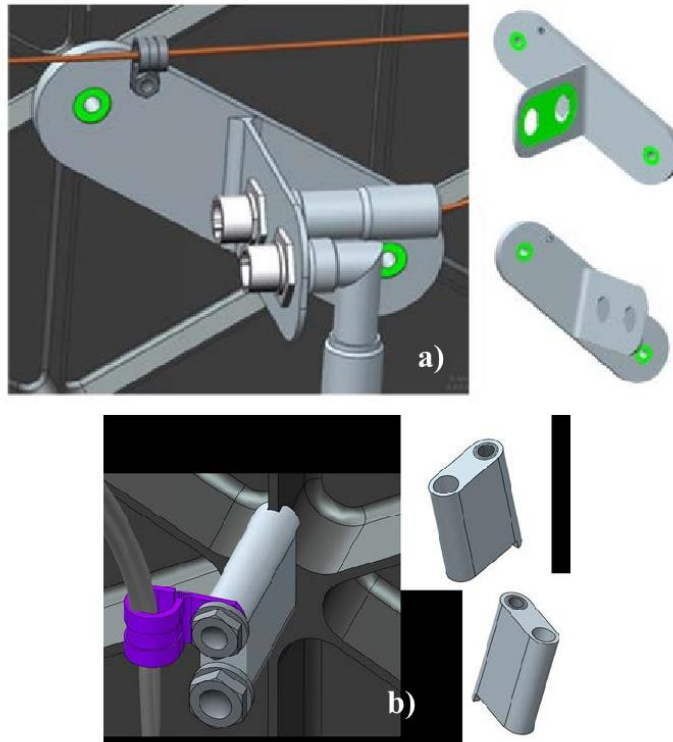


Figure 3-6. a) Cable Attach Bracket Assembly, also showing the p-clamp, and b) Cable Attach Spacers (short and tall)

3.5 Electrical Interface Brackets 1 and 2

Two electrical interface brackets are attached to the inside of the MSA using threaded inserts installed at appropriate nodes of the isogrid. These are located immediately below the access hatches as shown in Figure 3-7. These will provide points of attachment for the electrical cable connections. The brackets are bolted assemblies made of 2219 aluminum, as depicted in Figure 3-8.

*The electronic version is the official approved document.
Verify this is the correct version before use.*

NASA-HDBK-5010, VOLUME 2, REVISION A

Space Launch System (SLS) Program/Project	
Revision: B	Document No: SLS-SPIO-PLAN-017
January 8, 2020	Page: 17 of 54
Title: SPIE MSA Fracture Control Plan	



Figure 3-7. Attachment of the Electrical Interface Brackets to the MSA.

Note the circular access hatches and note the position of the brackets.

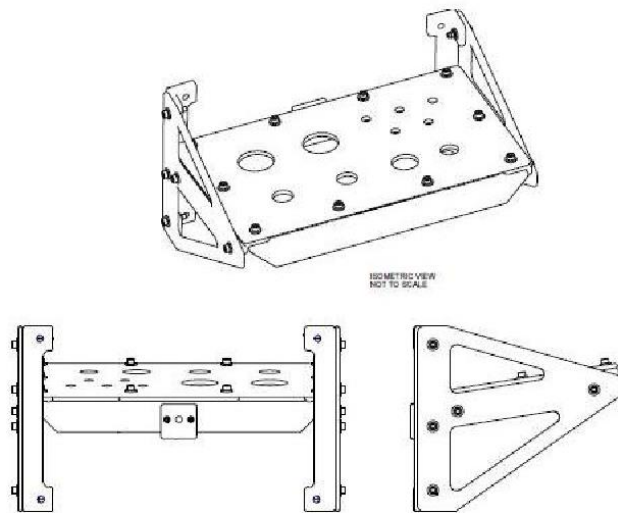


Figure 3-8. Configuration of the MSA Electrical Interface Brackets

3.6 Secondary Payload Brackets

For Artemis I, fourteen secondary payload brackets will be used with a configuration as shown in Figure 3-9c. These will affix and support thirteen secondary payloads and an avionics unit. Beginning with Artemis II, the configuration will change, and as many as eighteen secondary payload brackets will be used, and these will support up to seventeen secondary payloads and an

*The electronic version is the official approved document.
Verify this is the correct version before use.*

NASA-HDBK-5010, VOLUME 2, REVISION A

Space Launch System (SLS) Program/Project	
Revision: B	Document No: SLS-SPIO-PLAN-017
January 8, 2020	Page: 18 of 54
Title: SPIE MSA Fracture Control Plan	

avionics unit. The payloads are provided by vendors, along with the vibration isolation units and dispensers for each payload. Secondary payload brackets (SPB) will be fixed to the MSA within the upper volume using threaded inserts installed at appropriate nodes of the isogrid, as depicted in Figure 3-9. Two different sized brackets will be used, and these accommodate 6U and 12U sized secondary payloads. These will allow for the attachment of payloads and avionics secondary to the primary flight mission. These are fabricated from 2219 aluminum, and attached at the nodes of the isogrid, similarly to the electrical interface brackets.

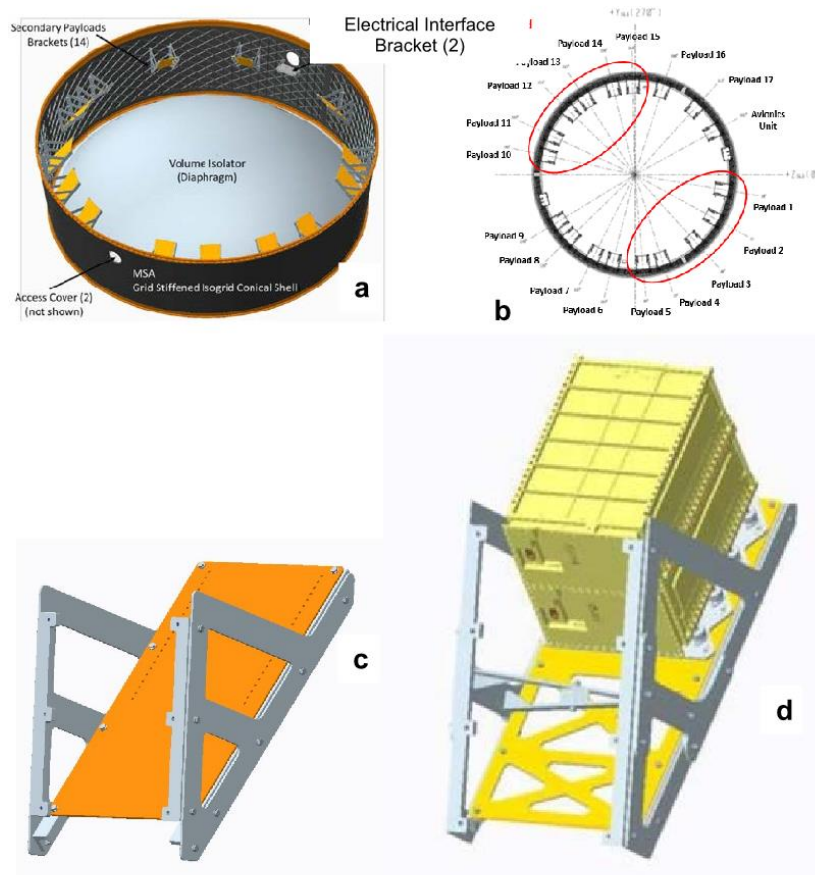


Figure 3-9. Secondary Payload Brackets, (a) placement in the MSA (Artemis I configuration), (b) location of 12U brackets (Artemis II), (c) pictorial of the 6U bracket assembly, and (d) 12U bracket with a secondary payload.

Note: The bracket assemblies are scaled approximately to each other.

*The electronic version is the official approved document.
Verify this is the correct version before use.*

NASA-HDBK-5010, VOLUME 2, REVISION A

Space Launch System (SLS) Program/Project	
Revision: B	Document No: SLS-SPIO-PLAN-017
January 8, 2020	Page: 19 of 54
Title: SPIE MSA Fracture Control Plan	

3.7 Secondary Payload Avionics

An avionics box is mounted on one of the SPB's. This avionics assembly is a commercial, off-the-shelf device, and an image appears in Figure 3-10.

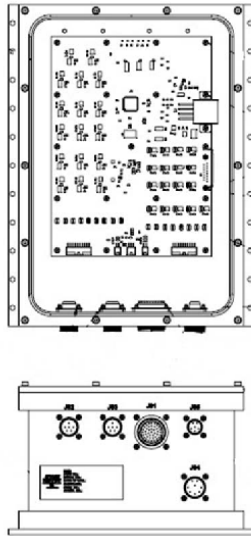


Figure 3-10. Avionics assembly

3.8 MSA Diaphragm

The MSA diaphragm is installed in the MSA assembly to provide a barrier between the ICPS environment and that of the MPCV. The diaphragm is a composite laminate that is dome-shaped, and it is bolted to the aft ring of the MSA (Figure 3-4). The upper and lower MSA volumes are purged prior to launch, but the volumes are not sealed. The diaphragm is penetrated by wiring harnesses that pass through two holes that have five-inch diameters and are located near the edges of the diaphragm. Communication of the gases from one side of the diaphragm to the other at the holes will be minimized by two box structures, called housings, which are bolted to the diaphragm. These are schematically represented in Figure 3-11.

*The electronic version is the official approved document.
Verify this is the correct version before use.*

NASA-HDBK-5010, VOLUME 2, REVISION A

Space Launch System (SLS) Program/Project	
Revision: B	Document No: SLS-SPIO-PLAN-017
January 8, 2020	Page: 20 of 54
Title: SPIE MSA Fracture Control Plan	

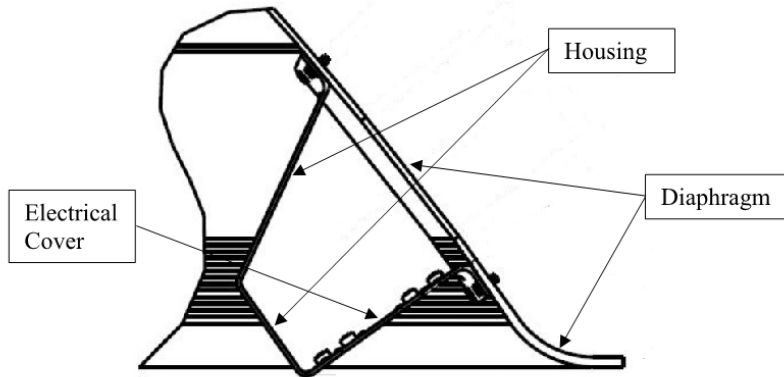


Figure 3-11. Cross-Sectional View of the MSA Showing the Housing Attached to the Diaphragm

3.9 MSA Diaphragm Electrical Connector Plates

Two electrical connector plates are screwed to the housings using riveted nut-plates to better separate the upper chamber from the lower one. The connector plates can be seen in Figure 3-12 and Figure 3-13, and they are approximately 16-inches-by-5.5-inches and are made of titanium plate. Twelve 0.2-inch diameter holes along the perimeter secure the plates to the housing, and there are numerous pass-through holes for electrical cabling. The largest hole is nominally 1-5/8-inches diameter.

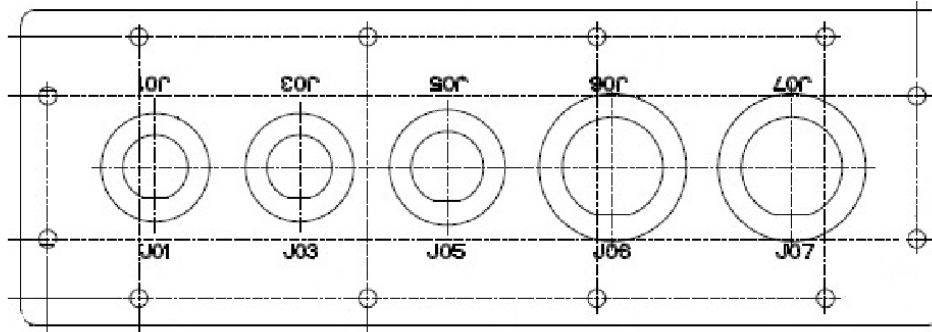


Figure3-12. Diaphragm Electrical Connector Plate 1

*The electronic version is the official approved document.
Verify this is the correct version before use.*

NASA-HDBK-5010, VOLUME 2, REVISION A

Space Launch System (SLS) Program/Project	
Revision: B	Document No: SLS-SPIO-PLAN-017
January 8, 2020	Page: 21 of 54
Title: SPIE MSA Fracture Control Plan	

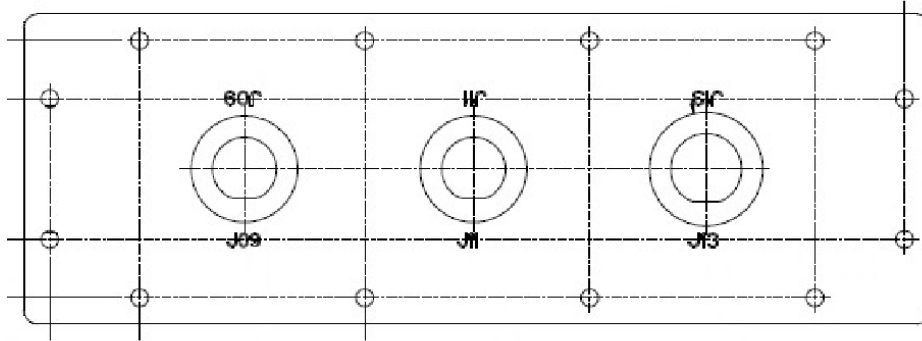


Figure 3-13. Diaphragm Electrical Connector Plate 2

*The electronic version is the official approved document.
Verify this is the correct version before use.*

NASA-HDBK-5010, VOLUME 2, REVISION A

Space Launch System (SLS) Program/Project	
Revision: B	Document No: SLS-SPIO-PLAN-017
January 8, 2020	Page: 22 of 54
Title: SPIE MSA Fracture Control Plan	

4.0 HARDWARE OPERATIONS

The MSA provides the structural attachment between the MPCV and the ICPS. The MSA contains a diaphragm that separates the volumes in the top and bottom of the MSA and facilitates the independent purging of those volumes. The purges and subsequent usage of the MSA likely will produce a slight differential pressure above or below the diaphragm. Secondary payload brackets will allow payloads beyond the primary function of the MSA to be fixed to the MSA and launched with the SLS spacecraft. For Artemis I, fourteen SPBs designed to support thirteen secondary payloads and an avionics unit will be attached to the nodes of the isogrid. For Artemis II and beyond, up to eighteen secondary payload brackets will be installed, and these brackets support up to five 6U and eleven 12U payloads and dispensers and an avionics unit controller and power supply. Electrical cabling is installed on the MSA inner mold line to feed signals to the secondary payloads, and the electrical circuits are inert until after separation from the Orion crew vehicle.

*The electronic version is the official approved document.
Verify this is the correct version before use.*

APPROVED FOR PUBLIC RELEASE – DISTRIBUTION IS UNLIMITED

NASA-HDBK-5010, VOLUME 2, REVISION A

Space Launch System (SLS) Program/Project	
Revision: B	Document No: SLS-SPIO-PLAN-017
January 8, 2020	Page: 23 of 54
Title: SPIE MSA Fracture Control Plan	

5.0 FRACTURE CONTROL CLASSIFICATIONS

Fracture control requirements are specified in NASA-STD-5019, Fracture Control Requirements for Spaceflight Hardware and MSFC-RQMT-3479, Fracture Control Requirements for Composite and Bonded Vehicle and Payload Structures, and these are listed as required in SLS-SPIO-RQMT-002, SPIE ISPE Requirements Document.

The ISPE consists of four components: MSA, LVSA, ICPS, and separation system, but this document will discuss fracture control of only the MSA in detail. Fracture control of the other components is covered by the respective vendors. Attachment hardware for integration of the MSA to the Multi-Purpose Crew Vehicle (MPCV) and to the Interim Cryogenic Propulsion System (ICPS) are not a part of the MSA and fracture control of those items is not discussed herein. The interface joint fasteners for the MPCV-to-MSA joint are the responsibility of the MPCV designers, and the interface joint fasteners for the MSA-to-ICPS joint are the responsibility of the ICPS designers.

Two tables of the components of the MSA appear below along with fracture control classifications: Table 5-1, fracture critical and Table 5-2, non-fracture critical (including exempt). Fracture control planning and execution for the MSA was completed for Artemis-I with the fracture control classifications evaluated to the SLS loads. The results can be found in SLS-SPIO-RPT-038, SPIO MSA Structural Assessment Report. The diaphragm was designed by MSFC and MSFC will be responsible for the manufacture of it. The fracture control classification for the diaphragm remains fracture critical. The fracture control summary report² (FCSR) will discuss the approach relevant to each component and summarize the results, discussion, and conclusions associated with fracture control for the MSA assembly.

Fracture control of secondary payload brackets (SPB) and wiring harnesses associated with secondary payloads and avionics is discussed in this document. . The secondary payload providers will be responsible for fracture control for their equipment: secondary payloads plus vibration isolators and dispensers. Fracture control documentation for secondary payloads, vibration isolators and dispensers will be reviewed by the MSFC fracture control board.

5.1 Fracture Critical Hardware

Fracture critical parts will be identified as such on the engineering drawings to alert all who use the drawings as to the criticality of the part. Section 5.3.1, below, lists additional requirements for drawings associated with fracture critical parts.

The metallic components identified as fracture critical in Table 5-1 (all but the last of the items listed) will need to be processed per NASA-STD-5019. This includes

- Safe-life assessment
- NDE evaluation

² SLS-SPIO-RPT-013, *SPIO MSA Fracture Control Summary Report*

*The electronic version is the official approved document.
Verify this is the correct version before use.*

NASA-HDBK-5010, VOLUME 2, REVISION A

Space Launch System (SLS) Program/Project	
Revision: B	Document No: SLS-SPIO-PLAN-017
January 8, 2020	Page: 24 of 54
Title: SPIE MSA Fracture Control Plan	

- Serialization of parts
- Traceability of records of manufacture:
 - Design and Analysis
 - Hardware Configuration
 - Materials
 - Manufacturing

The last item in Table 5-1, the MSA diaphragm, is a composite and bonded structure that has been classified as fracture critical, and it will need to meet MSFC-RQMT-3479 requirements, including the following:

- Damage Threat Assessment (DTA)
- Impact Damage Protection Plan (IDPP)

Fracture control-related processing of the MSA diaphragm appears next in the subsection that follows this table.

Table 5-1. Fracture Control Classifications, Group 1, Fracture Critical Parts

Drawing Number(s)	Part Description	Material or Process	Classification
MSA Components			
97M62121-001, 97M62122-001, 97M62123-001	MSA barrel panels 1, 2, and 3, respectively	2195-T8M4	Fracture Critical (§5.3)
97M62124-001	MSA barrel welds	conventional longitudinal FSW 2195-T8M4 plate to 2195-T8M4 plate	
97M62125-001	MSA forward ring	2219-T851 rolled ring forging	
97M62127-001	MSA aft ring	2219-T851 rolled ring forging	
97M62124-001	MSA flange to barrel welds (fore- and aft-)	self-reacting circumferential FSW 2195-T8M4 plate to 2219-T851 rolled ring forging	
97M62120-001	Machine-drilled assembly (MSA)	Weldment (2195 and 2219, per above)	Fracture Critical (§5.3)
97M62140-001	MSA diaphragm	laminar composite dome, (Newport NB321-3K70P)	Fracture Critical (§§5.2 & 5.3)

*The electronic version is the official approved document.
Verify this is the correct version before use.*

NASA-HDBK-5010, VOLUME 2, REVISION A

Space Launch System (SLS) Program/Project	
Revision: B	Document No: SLS-SPIO-PLAN-017
January 8, 2020	Page: 25 of 54
Title: SPIE MSA Fracture Control Plan	

5.2 MSA Diaphragm Fracture Control Approach

The MSA diaphragm is a laminar, polymer-matrix composite dome oriented in a concave-down configuration. The diaphragm separates the environment below the MPCV from that above the ICPS, and the diaphragm is subjected to inertial loads, changes of temperature, and potentially a net differential pressure. This pressure differential can produce a net pressure above the diaphragm, creating a buckling-type loading, or below the diaphragm, creating a burst-type loading. The housings are bolted to the diaphragm dome, and the bolted joint will be subjected to a peel-type loading when the diaphragm is subjected to flight loads. The bolted joint is fail-safe.

The diaphragm design allows for a nominal leakage area, and this suggests that some leakage of fluid would not be an issue. Because the consequences of buckling or burst failure modes are not known, the MSA diaphragm has been conservatively classified as fracture critical.

Non-metallic fracture critical components are required by MSFC-RQMT-3479 to be shown to be under fracture control by either a damage tolerant approach or a proof test approach, and the latter has been adopted. This approach is straight forward, requiring that flight articles be proofed in excess of the anticipated flight loads (MSFC-RQMT-3479, Section 5.3.1). The part must be evaluated using nondestructive testing before and after the proof test, and this will include the acreage of the dome, the flange, the housings, and the transition region where the dome curves into the flange.

Potential damage sources must be identified per damage threat assessment (DTA) task 1, and an impact damage protection plan (IDPP) must be put into place to insure that any damage inflicted after the proof test is either benign or is at least known to have occurred.

5.2.1 Planned Efforts for the Diaphragm

A brief listing of the planned efforts to establish fracture control for the MSA diaphragm follows:

- The diaphragm assembly will be subjected to a proof loading of 1.2 times the limit load times a correction factor (ECF).

$$Proof\ Load = 1.2 \times ECF \times Design\ Limit\ Load$$

The correction factor will be used to account for the difference between the properties in the proof test environment relative to the flight environment. The proof test will be required by drawing 97M62140-001.

- The proof test will use differential pressure to evaluate the diaphragm against a buckling load.
- The level of proof will be shown to not exceed the 80-percent of ultimate strength requirement as identified in MSFC-RQMT-3479.

*The electronic version is the official approved document.
Verify this is the correct version before use.*

NASA-HDBK-5010, VOLUME 2, REVISION A

Space Launch System (SLS) Program/Project	
Revision: B	Document No: SLS-SPIO-PLAN-017
January 8, 2020	Page: 26 of 54
Title: SPIE MSA Fracture Control Plan	

- The design of the diaphragm is driven by the potential for buckling, and this is believed to be the principal failure mode. This is true except in the flange area, which is contained and non-fracture critical. Buckling will be the failure mode of interest for the proof test.
- The proof test will be conducted at room temperature, and the diaphragm flange will be bolted to a fixture that maintains the bolt circle diameter. This is necessary to avoid overstressing the flange.
- The effectiveness of the proof test will be evaluated by the diaphragm design and analysis team. This will include evaluations in the acreage of the diaphragm, as well as in the flange, the transition from acreage to flange, and the wiring harness pass-through holes. Thereby, all areas of concern are properly proof tested.
- The diaphragm will be inspected for flaws pre- and post-proof (NDE and visual inspection). The inspection criteria will be specified on the drawing and will be reported in the SLS-SPIO-RPT-013, SPIO MSA Fracture Control Summary Report (FCSR).
- A damage threat assessment (DTA) of the diaphragm, specifically task 1, has been conducted, and it appears in Appendix C. This exercise was performed to identify damage threats for all of the service life following the post-proof NDE inspection. The DTA is an adaptation from a draft that was developed for use in the Ares upperstage composite and bonded structures.
- An impact damage protection plan (IDPP) is required, and the details of that IDPP follow in the next section.

5.2.2 Impact Damage Protection Plan (IDPP)

The MSA diaphragm has been classified as fracture critical, and an impact damage protection plan is essential. The IDPP is developed to either (1) establish strategies to ensure that the hardware is in good shape when it is used, i.e., there is no damage inflicted beyond the level that can be tolerated by the structure in use, or (2) at least identify that any induced damage is known to have occurred. The IDPP addresses any damage threats identified in the damage threat assessment (DTA) that has been included in Appendix C. The IDPP can utilize protection, surveillance, or inspections to accomplish those alternative goals. The approach identified is, as follows:

1. Standard practice must be followed to the greatest extent possible in the manufacturing and handling of the MSA diaphragm. In case of deviations from that practice, the potential for damage must be minimized. Any activities or circumstances that might induce damage must be reported and evaluated using appropriate nondestructive evaluation (NDE) techniques.

Rationale: Processes used in manufacturing, handling, and shipping should include whatever measures necessary to minimize the threat of damage to the diaphragm. Many of the processes used are standard practice.

*The electronic version is the official approved document.
Verify this is the correct version before use.*

NASA-HDBK-5010, VOLUME 2, REVISION A

Space Launch System (SLS) Program/Project	
Revision: B	Document No: SLS-SPIO-PLAN-017
January 8, 2020	Page: 27 of 54
Title: SPIE MSA Fracture Control Plan	

2. Protection against impact damage from foreign-object debris (FOD) is required, and the SPIE ISPE Contamination and Foreign Object Debris Control Plan, SLS-SPIO-PLAN-020, provides planning and guidance for the control of contamination and FOD for the MSA. That plan presents requirements for identifying the cleanliness and protection needs and for including inspections in the process planning.
3. Consistent with MSFC-RQMT-3479, the diaphragm must be evaluated using appropriate NDE techniques before the proof test and again after the proof test.

Rationale: The post-proof NDE, in conjunction with the pre-proof NDE, is intended to identify any changes in the diaphragm induced by the proof test operations. The two inspections together also serve to find and quantify any damage input prior to the respective NDE inspections.

4. The diaphragm will be visually inspected upon arrival at the Kennedy Space Center (KSC) by EGS per document WAD-QE-MSA-0001, MSA Receiving Inspection.

Rationale: Any significant damage arising from handling and shipping subsequent to the post-proof NDE will be found by a visual inspection upon arrival at KSC. The diaphragm has been shown to be tolerant to fairly large disruptions of section, and so visual inspection to identify any potential damage should be effective for risk mitigation of undetected damage in the hardware.

5. Immediately prior to integration of the MSA assembly into the rocket stack, a visual inspection of the diaphragm must be performed, and after integration, the access covers will be installed, and there is no plan to access the space any further. The IDPP does not provide any guidance beyond that point, because the MSA parts are expected to be protected in the enclosed volume. If further access is required, then an appropriate IDPP for that activity should be generated.

Rationale: After integration, the diaphragm is protected in the rocket vehicle stack, and so no further effort should be required, unless the MSA volume is accessed.

5.3 Processing of Fracture Critical Hardware

The following sub-sections discuss various aspects associated with special treatment of hardware identified as fracture critical.

5.3.1 Fracture Critical Identification on Drawings

The drawings of parts and assemblies classified as fracture critical must be marked as such, and this should include the following note types:

- Part (or Assembly) will be identified as Fracture Critical.
- NDE techniques that will be used and criteria for acceptance/rejection will be identified.

*The electronic version is the official approved document.
Verify this is the correct version before use.*

NASA-HDBK-5010, VOLUME 2, REVISION A

Space Launch System (SLS) Program/Project	
Revision: B	Document No: SLS-SPIO-PLAN-017
January 8, 2020	Page: 28 of 54
Title: SPIE MSA Fracture Control Plan	

- The method of serialization of components produced will be identified, including details of the serialization process.
- Requirements for traceability records will be established and implemented, including the establishment of what information should be retained and any redundancy/backup requirements.

5.3.2 Methodology for Assessing Fracture Critical Hardware

For fracture critical metallic hardware, a safe-life assessment will be performed, where appropriate, using the flaw sizes from NASA-STD-5009, Nondestructive Evaluation (NDE) Requirements for Fracture-Critical Metallic Components: the document contains lower limit flaw sizes that can be found with high reliability for all of the planned NDE techniques. For the welds, the critical initial flaw sizes were found to be larger than the 0.25-inch through flaws inspection criterion, and this will be used for the weld assessments.

For the diaphragm assembly, analysis has indicated that flaws with five-inch diameters could be tolerated without buckling—buckling is the failure mode of concern. Rejection criteria that are much smaller, i.e., NDE indications that rise to the level of a reportable flaw, will be used for the acceptance of the diaphragm, and these will address the following criteria

- Maximum individual flaw size,
- Minimum distance between flaws,
- Maximum accumulation of flaws in a region, and
- Maximum accumulation of flaws overall.

Similar acceptance criteria will be developed for the diaphragm flange and for the electrical cabling pass-through holes. These criteria will be established by the MSA diaphragm design and analysis team and will be included on the relevant drawings.

The assessment of the fracture-critical hardware, results, discussion, and conclusions will be referenced or else provided in the SLS-SPIO-RPT-013, ISPE Fracture Control Summary Report.

5.3.3 Nondestructive Evaluation

NDE methods to be used appear in the SLS-SPIO-PLAN-018, SPIO Nondestructive Evaluation Plan. Techniques that are capable of reliably finding the critical initial flaw sizes identified for each component or assembly will be defined within that plan.

5.3.4 Disposition of Significant Indications

All NDE indications will be verified and recorded, and all fracture-critical hardware with relevant indications exceeding acceptance criteria will be assessed by the Material Review Board. The assessment methodology for metallic hardware will include an NDE evaluation to estimate the size of any detected defect and a fracture analysis that incorporates a bounding defect size, upper bound crack growth rate, lower bound fracture toughness, and lower bound

*The electronic version is the official approved document.
Verify this is the correct version before use.*

NASA-HDBK-5010, VOLUME 2, REVISION A

Space Launch System (SLS) Program/Project	
Revision: B	Document No: SLS-SPIO-PLAN-017
January 8, 2020	Page: 29 of 54
Title: SPIE MSA Fracture Control Plan	

fatigue crack growth threshold values to demonstrate no predicted failure at four times the service life. The acceptability of detected defects in non-metallic parts will be based on the criteria developed per the process described in Section 5.3.2.

5.4 Non-Fracture Critical Hardware

Table 5-2 contains all of the non-fracture critical and exempt hardware of the MSA. This includes various fasteners, the secondary payloads and associated hardware, the wiring harness mounting hardware. Components in Table 5-2 have been assessed per NASA-STD-5019 requirements and are identified as non-fracture critical, and brief descriptions of the approaches used appear in the sub-sections below Table 5-2. Further details can be found in SLS-SPIO-RPT-013, SPIO MSA Fracture Control Summary Report and in SLS-SPIO-RPT-038, SPIO MSA Structural Assessment Report.

Table 5-2. Fracture Control Classifications, Group 2, Non-Fracture Critical Parts

Drawing Number	Part Description	Material or Process	Classification	Notes
NAS1954C11	diaphragm attach bolts	aerospace bolts, 1/4-28, 108 ksi, passivated	failsafe and low released mass (§§5.4.2 – 5.4.3)	
NAS1291C4M	diaphragm attach barrel nuts	aerospace nuts 1/4-28, dry lube	failsafe and low released mass (§§5.4.2 – 5.4.3)	
97M62144-001	diaphragm housing	3K70P/NB321 Carbon Plain Weave Fabric	fail-safe (§5.4.2)	
NAS1953C6	housing to diaphragm bolts	aerospace bolts, A286, #10-32, 108 ksi	fail-safe (§5.4.2)	
NAS1291C3M	housing to diaphragm nuts	corrosion resistant steel, #10-32, MoS dry lube	fail-safe (§5.4.2)	
97M62117-001, 97M62118-001	connector plate 1 and 2, respectively	Ti-6Al-4V sheet, annealed to AMS4911	alternate approach: non-fracture critical documented non-hazardous failure modes (§5.4.6)	
NAS1954C5	housing to connector plate bolt	aerospace bolts, A286, ¼-28, 108 ksi	failsafe and low released mass (§§5.4.2 – 5.4.3)	
MS20426AD3-6A	Rivet, solid, countersunk, connector plate mount	AL-2117-T4, anodized	failsafe and low released mass (§§5.4.2 – 5.4.3)	

*The electronic version is the official approved document.
Verify this is the correct version before use.*

NASA-HDBK-5010, VOLUME 2, REVISION A

Space Launch System (SLS) Program/Project	
Revision: B	Document No: SLS-SPIO-PLAN-017
January 8, 2020	Page: 30 of 54
Title: SPIE MSA Fracture Control Plan	

Drawing Number	Part Description	Material or Process	Classification	Notes
NAS1773C3M	1/4-20 self-locking nut plate, connector plate mount	CRES: A286 PER AMS5525, AMS5732 OR AMS5737, silver plated	failsafe and low released mass (§§5.4.2 – 5.4.3)	
Called out on 97M62112-001	exterior and interior coating	MIL-DTL5541, Class 3, chemical conversion coating	exempt (§5.4.4)	
Called out on 97M62112-001	primer, exterior and interior coating	MSFC-SPEC-3615, primer	exempt (§5.4.4)	
Called out on 97M62112-001	paint, white	SLS-SPIE-SPEC-006	exempt (§5.4.4)	
97M62111-001	access cover	2219-T87 plate	low risk (§5.4.1)	
NAS1954C5	access cover mount bolts	aerospace bolts, A286, ¼-28, 108 ksi	fail-safe, low risk (§5.4.8)	
M45932/1-13DL	access cover mounting inserts	NAS A286 CRES solid-wall inserts, ¼-28, dry lube	exempt (§5.4.4)	
97M62115-001, 97M62116-001	electrical interface brackets 1 and 2, respectively	2219-T81 or -T87 aluminum alloy assembly	failsafe (§5.4.2)	
NAS1954C7	electrical interface bracket fasteners to MSA, bolt, hex head	aerospace bolts, A286, 108 ksi	fail-safe (§5.4.2)	
NAS1587-4C NAS1587-4	washer, electrical interface bracket to MSA and housing to electrical plate and diaphragm to MSA	CORROSION RESISTANT STEEL PER AMS5510 (UNS S32100), AMS5512 (UNS S34700) OR PER AMS-QQ-S-763. CLASS 321 (UNS S32100) OR 347 COND A (UNS S34700), (75,000 PSI UTS MIN).	no credible failure mode	
97M62145-101	bracket, connector (cable attach bracket)	2219-T851	low risk (§5.4.1)	
97M62166-101 97M62167-101	spacer, short and spacer, tall (cable attach spacers)	CRES A286	low risk (§5.4.1)	
MS14181-05008	cable attach bracket bolt	Inconel 718	low risk fasteners and rivets (§5.4.10)	

*The electronic version is the official approved document.
Verify this is the correct version before use.*

APPROVED FOR PUBLIC RELEASE – DISTRIBUTION IS UNLIMITED

NASA-HDBK-5010, VOLUME 2, REVISION A

Space Launch System (SLS) Program/Project	
Revision: B	Document No: SLS-SPIO-PLAN-017
January 8, 2020	Page: 31 of 54
Title: SPIE MSA Fracture Control Plan	

Drawing Number	Part Description	Material or Process	Classification	Notes
MS14181-05024 MS14181-05008	cable attach spacer bolt	Inconel 718	low risk part (§5.4.9)	
NAS1715C6KH NAS1715C7KH NAS1715C8KH NAS1715C9KH NAS1715C10KH NAS1715C11KH NAS1715C12KH NAS1715C13KH NAS1715C14KH	clamp, loop	CRES - 304 (UNS S30400) PER AMS5513, OR 321 (UNS S32100) PER AMS5510, OR 302 (UNS S30200) PER AMS5516	contained (§5.4.5)	
39111	avionics unit		contained (§5.4.5), exempt (§5.4.4)	
NAS1351N3-16	avionics mounting screw	heat resistant steel	fail-safe (§5.4.2)	
NAS1587A3C	Avionics mounting washer	A286	no credible failure mode	
NAS9104	bolt, loop clamp mount	A286	low risk (§5.4.9)	
NAS1587A3C	washer, countersink, housing to diaphragm	CORROSION RESISTANT STEEL PER AMS5510 (UNS S32100), AMS5512 (UNS S34700) OR PER AMS-QQ-S-763. CLASS 321 (UNS S32100) OR 347 COND A (UNS S34700), (75,000 PSI UTS MIN).	no credible failure mode	
NAS620C10L	washer, flat, housing to diaphragm	CORROSION-RESISTANT STEEL SHEET OR STRIP IN ACCORDANCE WITH ASTM A240/A240M, ANY OF THE 300 SERIES, CONDITION A, FINISH 2D OR 2B (FOR SHEET), FINISH 2 (FOR STRIP).	no credible failure mode	

*The electronic version is the official approved document.
Verify this is the correct version before use.*

APPROVED FOR PUBLIC RELEASE – DISTRIBUTION IS UNLIMITED

NASA-HDBK-5010, VOLUME 2, REVISION A

Space Launch System (SLS) Program/Project	
Revision: B	Document No: SLS-SPIO-PLAN-017
January 8, 2020	Page: 32 of 54
Title: SPIE MSA Fracture Control Plan	

Drawing Number	Part Description	Material or Process	Classification	Notes
97M62171-001	MSA secondary payload brackets (SPB), 6U	2219 aluminum alloy assembly	fail-safe (§5.4.2)	
97M62290-001	MSA secondary payload brackets (SPB), 12U	2219 aluminum alloy assembly	fail-safe (§5.4.2)	
NAS1954 ³	bolt, SPB assembly	aerospace bolt, A286, 108 ksi, passivated	failsafe and low released mass (§§5.4.2 – 5.4.3)	
MS14181-05008	bolt, 12U SPB assembly	Inconel 718, 220 ksi	failsafe and low released mass (§§5.4.2 – 5.4.3)	
NAS1805 ³	nut/insert, SPB assembly	NAS insert, A286, passivated	failsafe and low released mass (§§5.4.2 – 5.4.3)	
MS14183L-C4	washers, SPB assembly	A286, 220 ksi. passivated	no credible failure mode	
MS14183L-C5	washer, 12U SPB assembly countersunk	Inconel 718, 220 ksi	no credible failure mode	
NAS1149 ³	washer, SPB	A286, passivated	no credible failure mode	
MS14181-05008	bolt tension 220 ksi--SPB to MSA	NICKEL ALLOY 718 WITH CHEMISTRY OF AMS5662 (UNS N07718), AMS5663 (UNS N07718) OR AMS5962 (UNS N07718).	failsafe and low released mass (§§5.4.2 – 5.4.3)	
NASM14183L-C5	washer, countersunk, passivated--SPB to MSA	NICKEL ALLOY 718 (UNS N07718) CONFORMING TO THE CHEMISTRY OF AMS5596, AMS5597 OR AMS5662.	no credible failure mode	

³ Several places in this table, the part number that fully describes the fastener description is shortened. This has been done because the 12-U SPBs have not yet been designed. Any changes in the hardware from the pieces shown in this table will be identified in the fracture control summary report, SLS-SPIO-RPT-013, and compliance with the final fracture classification will be confirmed therein.

*The electronic version is the official approved document.
Verify this is the correct version before use.*

NASA-HDBK-5010, VOLUME 2, REVISION A

Space Launch System (SLS) Program/Project	
Revision: B	Document No: SLS-SPIO-PLAN-017
January 8, 2020	Page: 33 of 54
Title: SPIE MSA Fracture Control Plan	

Drawing Number	Part Description	Material or Process	Classification	Notes
97M43361-001 97M43362-001 97M43372-001 97M43345-001 97M43341-001 97M43343-001 97M43371-001	MSA PF-1 WIRE HARNESS ASSEMBLIES - W361, -W362, - W372, -W345, - W341, -W343, - W371	Electrical Cables	NFC contained	
MIL-I-19166	fiberglass tape, wrap wiring harnesses	fiberglass tape	exempt (§5.4.4)	
MS20995C32	safety wire		exempt (§5.4.4)	
NAS1057W4-150 NAS1057W4-075	spacer, wiring harness mount	A286 - CRES (UNS S66286) PER AMS5731	fail-safe (§5.4.2)	
MIL-PRF-16173 CL 1 G3	thread lubricant, wiring harness mount	lubricant	exempt (§5.4.4)	
MolyKote	thread lubricant, wiring harness mount	lubricant	exempt (§5.4.4)	
TYZ2XM	cable tie wrap	nylon	exempt (§5.4.4)	
97M62129-001	Threaded nodes on MSA barrel panels (to mount the electrical interface brackets and the SPB's)	2195-T8M4	alternate approach: low risk (§5.4.7)	
M45932/1-13DL M45932/1-17DL EFFECTIVITY: ARTEMIS I	threaded inserts, for mounting SPB, electrical interface brackets, and wiring to the MSA structure	NAS solid-wall inserts, A286 CRES	exempt (§5.4.4)	
MS51831CA202LMS5 1831CA203L EFFECTIVITY: ARTEMIS II AND BEYOND	threaded inserts, for mounting SPB, electrical interface brackets, and wiring to the MSA structure	NAS keyed inserts, A286 CRES	exempt (§5.4.4)	

Whereas a classification of fracture critical invokes a series of analyses and controls, the non-critical fracture classifications also require certain activities to assure that the classification is appropriate. Those parts that are identified as non-fracture critical are designated as complying with the requirements of fracture control without further activity beyond conventional aerospace

*The electronic version is the official approved document.
Verify this is the correct version before use.*

APPROVED FOR PUBLIC RELEASE – DISTRIBUTION IS UNLIMITED

NASA-HDBK-5010, VOLUME 2, REVISION A

Space Launch System (SLS) Program/Project	
Revision: B	Document No: SLS-SPIO-PLAN-017
January 8, 2020	Page: 34 of 54
Title: SPIE MSA Fracture Control Plan	

verification and quality assurance procedures. The following sections enumerate the classifications and requirements for establishing non-fracture criticality for the components in Table 5-2.

5.4.1 Low Risk Metallic Hardware

The following is a listing of the requirements and characteristics of hardware listed as low-risk:

- It will be constructed from a commercially available material procured to an aerospace standard or equivalent.
- Aluminum parts will not be loaded in the short transverse direction if this dimension is greater than three inches.
- A part whose failure directly results in a catastrophic hazard will be excluded from being classified low risk, except when the total (unconcentrated) stresses in the part at limit load are less than 30 percent of the ultimate strength for the material used, and
- If the part contains metallic materials, it will be fabricated from a well characterized metal that is not sensitive to stress corrosion cracking
- Metallic parts will have a material property ratio,

$$\frac{K_{Ic}}{F_{ty}} > 0.33 \text{ in}^{1/2}$$

Where K_{Ic} is the plane strain fracture toughness and F_{ty} is the tensile yield strength.

- Processes that do not have significant probability of introducing flaws will be used to fabricate the parts.
- At a minimum, the parts will receive an inspection for surface defects prior to assembly. Any defects that could affect part life will be cause for rejection of the low-risk classification.
- In addition, A maximum stress that does not exceed the endurance limit or

$$S_{max} < \frac{F_{tu}}{4\{1 - 0.5R\}}$$

where S_{max} is the local concentrated stress, F_{tu} is the ultimate tensile strength, and R is the ratio of minimum stress to maximum stress in a fatigue cycle or a damage tolerance analysis from a 0.005-in initial crack that conservatively accounts for the effects of notches and mean stress and shows a minimum of four (4) complete service lives with a factor of 1.5 on alternating stress.

5.4.2 Fail-Safe Metallic Hardware

Hardware can be identified as fail safe when it meets the following criteria:

*The electronic version is the official approved document.
Verify this is the correct version before use.*

NASA-HDBK-5010, VOLUME 2, REVISION A

Space Launch System (SLS) Program/Project	
Revision: B	Document No: SLS-SPIO-PLAN-017
January 8, 2020	Page: 35 of 54
Title: SPIE MSA Fracture Control Plan	

- The structure remaining after complete part failure will withstand all redistributed loads with a minimum ultimate safety factor of 1.0 on limit load.
- For fasteners, use the highest load and the lowest margin to evaluate the fail safe condition.
- Structural failure will not release a potentially catastrophic mass.

Details of the analysis will appear in SLS-SPIO-RPT-038, SPIO MSA Structural Assessment Report.

5.4.3 Low Released-Mass Hardware

- Released mass internal to the structure will not be able to achieve 35 ft/sec with a limit of momentum of 1.24 ft-lbm/sec.
- Fasteners preloaded in tension that have low fracture toughness will be limited to 0.03-lbm of potential free mass. Low fracture toughness is defined, as follows:

$$\frac{K_{Ic}}{F_{ty}} < 0.33 \text{ in}^{1/2}$$

Where K_{Ic} is the plane strain fracture toughness and F_{ty} is the tensile yield strength.

5.4.4 Exempt Hardware

NASA-STD-5019 describes a variety of hardware that are considered exempt:

“...exempt hardware typically includes non-structural items such as flexible insulation blankets, enclosed electrical circuit components/boards, electrical connectors (including locking devices), wire bundles, and seals. Small mechanical parts, such as bearings and valve seats, that have been developed and qualified through required test programs and rigorous process control to demonstrate their reliability, and whose failure does not directly lead to a catastrophic hazard, may be exempt from fracture control with the approval of the FCB.”

The tape between the diaphragm and the MSA is classified as exempt.

5.4.5 Contained Hardware

A failed part confined in a container or housing or otherwise positively restrained from free release that does not result in a catastrophic hazard can be classified as non-fracture critical.

- (a) Pressurized components or rotating devices within stowed or contained hardware must be assessed independently, as provided in this standard, to ensure safe application against catastrophic failure of the container/compartment.
- (b) Containment of rotating devices must consider the combined effect of rotational speed and potential for mass release to determine classification.

*The electronic version is the official approved document.
Verify this is the correct version before use.*

NASA-HDBK-5010, VOLUME 2, REVISION A

Space Launch System (SLS) Program/Project	
Revision: B	Document No: SLS-SPIO-PLAN-017
January 8, 2020	Page: 36 of 54
Title: SPIE MSA Fracture Control Plan	

- (c) Guidance for calculating containment of high-energy rotating devices is given in NASA-HDBK-5010.
- (d) Contained hardware must also be examined for potential damage effects of single-point mass releases inside the confinement itself.
- (e) Release of masses (of any size) within a container that could credibly defeat an internal safety-critical function need to be precluded by appropriate technical measures, which can include compliance with requirements for low-risk part classification (see section 5.4.1, above), or other techniques approved by the MSFC FCB.
- (f) Enclosures with openings must only be assessed for containment of parts larger than accessible openings.
- (g) When containment is furnished by a compartment with doors or other hardware designed to open, the closure design must be one failure tolerant of accidentally opening; i.e., hinges, latches, and other mechanisms must be redundant for keeping a door closed in the event one device fails.

Typical electronic boxes and related equipment such as radios, cameras, recorders, personal computers, and similar close-packed and enclosed hardware can be regarded as acceptable containers of internal parts without further assessment.

Release of a free mass from a fastener that is mechanically constrained (e.g., safety wired) can be assumed to be contained. All constrained fasteners can be classified non-fracture critical if failure does not result in a catastrophic hazard due to loss of structural integrity of the fastener or loss of a safety-critical function.

5.4.6 Alternative Approach for Electrical Connector Plates

Alternative approaches are acceptable for fracture control, and this requires approval of the responsible fracture control and safety authorities. In addition, the request for approval of an alternative approach is required immediately upon identification of the need.

The diaphragm electrical connector plates fit this category. Consideration of the failure modes of the electrical connector plates suggests that the parts are very robust for the application (the plates are the mounting surfaces for electrical connectors) and are nominally 16" x 5.5" x 0.125". Multiple holes accommodate the connectors, and if a flaw were to lead to cracking of a plate, then the result would only be the reduction of support of one or two of the connectors. This is thought to be insignificant. There are no credible catastrophic hazards resulting from failure of the plates due to a flaw.

This approach was brought before the MSFC FCB and to the safety authority for approval for the EFT-1 flight hardware and was accepted by both (FCB Memo EM20-14-FCB-003_signed and CR SPIO-0087).

*The electronic version is the official approved document.
Verify this is the correct version before use.*

NASA-HDBK-5010, VOLUME 2, REVISION A

Space Launch System (SLS) Program/Project	
Revision: B	Document No: SLS-SPIO-PLAN-017
January 8, 2020	Page: 37 of 54
Title: SPIE MSA Fracture Control Plan	

5.4.7 Alternate Approach for the Threaded Nodes of the Barrel Panels

The fracture classification of the threaded nodes of the MSA barrel panels was re-examined after it was found that an eddy current inspection was removed from the drawing. The isogrid nodes are the regions where six ribs converge, as depicted in Figure 5-1. They are characterized by a relative wide region of material formed by the radii between the ribs. Each node has a flat bottom hole in the center that is threaded to accept a threaded insert. The MSA secondary payload brackets are bolted to these inserts at prescribed locations around the inside of the MSA. Two sources of loads are reacted by the nodes: the MSA primary structure loads introduced by the stress in each rib and the bolt loads introduced by the bolted connections of the secondary payload hardware, the electrical interface brackets, and the secondary payload wiring harness mounting hardware.

The SPB and electrical interface brackets bolted connections to the MSA have been shown to be fail safe. Therefore, the MSA nodes would be fail-safe relative to the failure to secure the SPB and electrical interface brackets to the MSA.

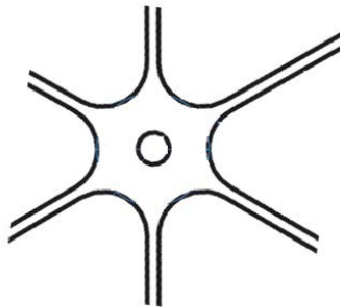


Figure 5-1. Image of an isogrid node

The cable attach brackets are only bolted to the MSA in one or two nodes, so they cannot be fail-safe for these locations.

The nodes are classified as non-fracture critical by an alternative low risk classification for the primary shell and cable bracket loadings. The details appear below.

- The nodes are much thicker than the ribs, producing a relatively low stress. A preliminary analysis suggests that the peak stress associated with the primary loading is about 10-percent of the typical yield strength.
- Damage tolerance analysis of an initial flaw of 0.005-inches must show an excess beyond four complete service lives at a factor of 1.5 on the alternating stress.

*The electronic version is the official approved document.
Verify this is the correct version before use.*

NASA-HDBK-5010, VOLUME 2, REVISION A

Space Launch System (SLS) Program/Project	
Revision: B	Document No: SLS-SPIO-PLAN-017
January 8, 2020	Page: 38 of 54
Title: SPIE MSA Fracture Control Plan	

- For the 2195-T8M4 temper, the ratio of $K_{Ic}/\sigma_{ys} = 0.34\text{-}\sqrt{\text{in}}$ at room temperature, and $K_{Ic}/\sigma_{ys} = 0.31\text{-}\sqrt{\text{in}}$ at -110F. NASA-STD-5019 requires a minimum of $0.33\text{-}\sqrt{\text{in}}$, and the assessment of the ratio at -110F is below, but still close to the requirement.
- After rolling, the plate material used is subjected to ultrasonic testing that would find flaws parallel to the surface of the plate. After threading, an insert is installed that would bridge any flaw parallel to the plate.
- During manufacturing, the nodes are pilot-drilled and threads are cut, then a plug is inserted to ensure the hole holds its shape while the panels are bump formed. After bump forming, the plugs are removed, and the isogrid is subjected to fluorescent dye-penetrant testing (PT), and this would identify any cracks open to the plate surface. The detectable surface crack (POD) for this method is 0.075-inches radius.
- The inserts are assembled into the tapped holes at the nodes, essentially acting as a go/no-go thread gauge. The depth of the inserts is also verified. For the Slimserts installed around the access ports, they are subjected to inspection using a go/no-go thread gauge.

The details of this will be provided in SLS-SPIO-RPT-013, SPIO MSA Fracture Control Summary Report.

5.4.8 Fail-Safe Approach for Access Cover Bolts

The access cover bolts are classified as fail-safe, and the logic of this classification is presented, below. The fail-safe classification is discussed in section 5.4.2, above. The third bullet in that section identifies that Structural failure will not release a potentially catastrophic mass. This can be by containment (section 5.4.5) or by low-released mass (section 5.4.3). The bolts are external to the MSA, and are not contained. The bolts meet the relevant requirements of low-released mass:

- (a) The access cover bolts are external.
- (b) Released mass external to a vehicle shall be shown to present acceptable risk after impact upon all potential impact surfaces if applicable. This requires the following:
 - (1) Process controls verified by lot testing of components or structures have provided A Basis static and dynamic strength properties.
 - (2) The service of the bolts is for a single mission.
 - (3) The access cover bolts have been shown to have a factor of four on life and 1.4 on strength, while reliably accounting for the effects of manufacturing and/or service-induced flaws.
- (c) The fasteners are torqued to see tension, and the fracture toughness is $K_{Ic}/F_{ty} = 55/85 = 0.64\text{-}\sqrt{\text{in}} \gg 0.33\text{-}\sqrt{\text{in}}$. The fastener is not a low-toughness material.

*The electronic version is the official approved document.
Verify this is the correct version before use.*

NASA-HDBK-5010, VOLUME 2, REVISION A

Space Launch System (SLS) Program/Project	
Revision: B	Document No: SLS-SPIO-PLAN-017
January 8, 2020	Page: 39 of 54
Title: SPIE MSA Fracture Control Plan	

(d) Release of the bolt head frees a mass of about 0.08-lbm and this would be a single-point failure. The specification of low-released mass in this case is unknown. As a result, the part must meet the requirements of containment or a low-risk classification. As stated earlier, it is not contained. Low-risk requires the following:

- (1) The access cover bolts are made of A286, a nickel chromium steel.
- (2) It is unknown if the failure of the bolt would result in a catastrophic hazard, and so further requirements are applied:
 - i. The design factor of safety is 2.0, and a margin of 1.78 exists for the design. This results in an overall factor of safety of 5.56. The ratio of the total unconcentrated stress at limit load to the ultimate tensile strength is the reciprocal of this: $1/5.56 = 18$ percent \ll 30 percent. The bolts are lightly loaded relative to the strength.
 - ii. The bolts are A286, which is well-characterized and not sensitive to stress corrosion cracking.
 - iii. A286 is tough, with a toughness ratio

$$K_{Ic} = 55 \text{ ksi}\sqrt{\text{in}}, F_{ty} = 85 \text{ ksi}$$

$$\frac{K_{Ic}}{F_{ty}} = 0.64 > 0.33 \text{ in}^{1/2}$$

- iv. The bolts are not fabricated using a process that has a significant probability of introducing flaws, and the threads are rolled.
- v. A damage tolerance analysis with a 0.005-inch initial flaw was conducted, and the bolt completed four service lives with a factor of 1.5 on alternating stress. Per the NAS1953 standard, all bolts receive a visual inspection, and a representative sample receive inspection at 10X magnification. In addition to this, the bolts are subject to NAS4003, which requires liquid fluorescent dye-penetrant inspection on a sample from each lot. This technique is specified to be either Method B or D, and the sensitivity level is specified to be 2, 3, or 4. Metallurgical evaluation is performed for discontinuities at between 50X and 100X magnification, and for microstructure at 100X to 150X magnification on a sample of each lot. No cracks are allowed, and other discontinuities are limited to at most 0.005-inches or less.

The list above identifies full compliance to the relevant requirements for fail-safe classification of external parts, and therefore, the access cover bolts are fail-safe.

*The electronic version is the official approved document.
Verify this is the correct version before use.*

NASA-HDBK-5010, VOLUME 2, REVISION A

Space Launch System (SLS) Program/Project	
Revision: B	Document No: SLS-SPIO-PLAN-017
January 8, 2020	Page: 40 of 54
Title: SPIE MSA Fracture Control Plan	

5.4.9 Loop Clamp Bolts Alternate Non-Fracture Critical Low Risk Part Classification

Low-risk fasteners and shear pins are subject to the following requirements:

1. Fastener shall be in a local pattern of two or more similar fasteners.
2. Fastener and joint shall be within the Shuttle or International Space Station experience base.
3. Fastener shall be fabricated and inspected in accordance with military standard, national aircraft standard, or equivalent commercial aerospace specifications.
4. Fasteners shall be procured and have positive back-off prevention consistent with their criticality using NASA-STD-(I)-6008, NASA Fastener Management and Control Practices.
5. Fasteners used in multi-cycle applications shall have rolled threads and be fatigue rated.
6. Fastener shall be fabricated from a metal not sensitive to stress corrosion cracking as defined in NASA-STD-(I)-6016, Standard Materials and Processes Requirements for Spacecraft.
7. If used in tension applications, the fastener shall not be made from a low fracture-toughness alloy as defined in section 3.2 or, specifically, Ti-6Al-4V STA titanium.
8. Fasteners shall meet appropriate preloads and stress requirements with no joint gapping (gapping is allowed under fail-safe and/or emergency conditions).
9. Reworked or custom-made fasteners shall require MSFC FCB approval.

The loop-clamp bolts meet the low-risk fasteners and shear pins requirements, except that the wiring bracket mountings are attached to the isogrid nodes with single bolts, not a pattern of two or more. The bolts are procured with a fatigue rating.

The subject bolts meet all of the low-risk part requirements:

- It will be constructed from a commercially available material procured to an aerospace standard or equivalent. **This is true.**
- Aluminum parts will not be loaded in the short transverse direction if this dimension is greater than 3 in. **Aluminum is not used.**
- A part whose failure directly results in a catastrophic hazard will be excluded from being classified low risk, except when the total (unconcentrated) stresses in the part at limit load are less than 30 percent of the ultimate strength for the material used,

Limit load stress is less than 30 percent of ultimate strength.

and

*The electronic version is the official approved document.
Verify this is the correct version before use.*

NASA-HDBK-5010, VOLUME 2, REVISION A

Space Launch System (SLS) Program/Project	
Revision: B	Document No: SLS-SPIO-PLAN-017
January 8, 2020	Page: 41 of 54
Title: SPIE MSA Fracture Control Plan	

- If the part contains metallic materials, it will be fabricated from a well characterized metal that is not sensitive to stress corrosion cracking

The material is not sensitive to stress corrosion cracking.

- Metallic parts will have a material property ratio,

$$\frac{K_{Ic}}{F_{ty}} > 0.33 \text{ in}^{1/2}$$

Where K_{Ic} is the plane strain fracture toughness and F_{ty} is the tensile yield strength.

This is true.

$$K_{Ic} = 55 \text{ ksi}\sqrt{\text{in}}, F_{ty} = 85 \text{ ksi}$$

$$\frac{K_{Ic}}{F_{ty}} = 0.64 > 0.33 \text{ in}^{1/2}$$

- Processes that do not have significant probability of introducing flaws will be used to fabricate the parts. **This is true.**
- At a minimum, the parts will receive an inspection for surface defects prior to assembly. Any defects that could affect part life will be cause for rejection of the low-risk classification.

The bolts are procured per the NAS1953 standard, where all bolts receive a visual inspection, and a representative sample receive inspection at 10X magnification. In addition to this, the bolts are subject to NAS4003, which requires liquid fluorescent dye-penetrant inspection on a sample from each lot. This technique is specified to be either Method B or D, and the sensitivity level is specified to be 2, 3, or 4. Metallurgical evaluation is performed for discontinuities at between 50X and 100X magnification, and for microstructure at 100X to 150X magnification on a sample of each lot. No cracks are allowed, and other discontinuities are limited to at most 0.005-inches or less.

- In addition, a maximum stress that does not exceed the endurance limit or otherwise

$$S_{max} < \frac{F_{tu}}{4\{1 - 0.5R\}}$$

where S_{max} is the local concentrated stress, F_{tu} is the ultimate tensile strength, and R is the ratio of minimum stress to maximum stress in a fatigue cycle or a damage tolerance analysis from a 0.005-in initial crack that conservatively accounts for the effects of notches and mean stress and shows a minimum of four (4) complete service lives with a factor of 1.5 on alternating stress.

The bolts have been shown by analysis to survive in excess of four service lives with a flaw of 0.005-inches.

*The electronic version is the official approved document.
Verify this is the correct version before use.*

APPROVED FOR PUBLIC RELEASE – DISTRIBUTION IS UNLIMITED

NASA-HDBK-5010, VOLUME 2, REVISION A

Space Launch System (SLS) Program/Project	
Revision: B	Document No: SLS-SPIO-PLAN-017
January 8, 2020	Page: 42 of 54
Title: SPIE MSA Fracture Control Plan	

The conclusion to be drawn from this is that the subject bolts should be considered low-risk parts.

5.4.10 Non-Fracture Critical Low-Risk Cable Attach Bracket Bolts

The cable attach bracket bolts meet the non-fracture critical low-risk fasteners and rivets classification with the following relevant characteristics.

1. The fasteners are in a local pattern of two similar fasteners.
2. Fastener and joint are within the Shuttle or International Space Station experience base.
3. Fastener are fabricated and inspected in accordance with military standard, national aircraft standard, or equivalent commercial aerospace specifications.
4. Fasteners are procured and have positive back-off prevention consistent with their criticality using NASA-STD-6008, NASA Fastener Management and Control Practices.
5. These fasteners are used in multi-cycle applications, and they are purchases with rolled threads and are fatigue rated.
6. These fasteners are fabricated from Inconel 718, nickel-base superalloy, a metal not sensitive to stress corrosion cracking as defined in NASA-STD-6016, Standard Materials and Processes Requirements for Spacecraft.
7. The fasteners are not made from a low fracture toughness alloy, e.g., Ti-6Al-4V STA titanium.
8. There is sufficient margin against gapping with specified preloads
9. No reworked or custom-made fasteners are used.

*The electronic version is the official approved document.
Verify this is the correct version before use.*

APPROVED FOR PUBLIC RELEASE – DISTRIBUTION IS UNLIMITED

NASA-HDBK-5010, VOLUME 2, REVISION A

Space Launch System (SLS) Program/Project	
Revision: B	Document No: SLS-SPIO-PLAN-017
January 8, 2020	Page: 43 of 54
Title: SPIE MSA Fracture Control Plan	

6.0 FRACTURE CONTROL RESPONSIBILITIES

The Spacecraft and Payload Integration and Evolution Office (SPIE) will be responsible for assuring compliance with the requirements of this document. Fracture criticality classifications of the MSA adapter and secondary hardware, listed in Table 5-1 and Table 5-2, will be confirmed through the MSFC Fracture Control Board and the SPIE Chief Engineer's processes. A fracture control summary report⁴ will be required to capture information regarding the efforts to establish fracture control on all components of the MSA.

6.1 Responsible Fracture Control Board

The Marshall Fracture Control Board is the Responsible Fracture Control Board that reviews and approves this Fracture Control Plan. The Fracture Control Plan covers MSA components and defines the general fracture control policies and procedures used to mitigate the risk of failure due to crack-like defects in the MSA to meet the requirements of NASA-STD-5019 and MSFC-RQMT-3479.

6.2 Fracture Control Implementation

The SPIE Chief Engineer will assure that the fracture control activity is properly implemented. Fracture control implementation will be done with the oversight, advice, and approval of the MSFC FCB.

⁴ SLS-SPIO-RPT-013, *SPIO MSA Fracture Control Report*

*The electronic version is the official approved document.
Verify this is the correct version before use.*

NASA-HDBK-5010, VOLUME 2, REVISION A

Space Launch System (SLS) Program/Project	
Revision: B	Document No: SLS-SPIO-PLAN-017
January 8, 2020	Page: 44 of 54
Title: SPIE MSA Fracture Control Plan	

APPENDIX A ACRONYMS AND ABBREVIATIONS AND GLOSSARY OF TERMS

A1.0 ACRONYMS AND ABBREVIATIONS

1U	1-Unit SPL, nanosatellites of nominal dimension of 10 x 10 x 10 cm and mass of 1.33 kg or less.
6U	6-Unit SPL, enlarging the 1U by a factor of six, e.g., 10×20×30 cm and mass of 8 kg.
12U	12-Unit SPL, enlarging the 1U by a factor of twelve, e.g., 20×20×30 cm and mass of 16 kg.
AL	Designator Indicating an Aluminum Alloy
CDR	Critical Design Review
CM Plan	Configuration Management Plan
CR	Change Request
CRES	Designator Indicating a Corrosion-Resistant (Stainless Steel) Alloy
CTE	Coefficient of Thermal Expansion
DCR	Design Certification Review
DRL	Data Requirements List
DTA	Damage Threat Assessment (Non-Metallics)
ECB	SPIO Engineering Review Board
ECF	Environmental Correction Factor
EFT-1	First Exploration Flight Test
EGS	Exploration Ground Systems
ERB	SPIO Engineering Review Board
FC	Fracture Criticality
FCB	Fracture Control Board
FCC	Fracture Control Coordinator
FCP	Fracture Control Plan
FCSR	Fracture Control Summary Report
FOD	foreign object debris
FS	Factor of Safety
FSW	friction-stir welding process or friction-stir weldment
ft	length measurement, feet
F_{tu}	Material Ultimate Strength in Tension
F_{ty}	Material Yield Strength in Tension
GFE	Government Furnished Equipment

*The electronic version is the official approved document.
Verify this is the correct version before use.*

APPROVED FOR PUBLIC RELEASE – DISTRIBUTION IS UNLIMITED

NASA-HDBK-5010, VOLUME 2, REVISION A

Space Launch System (SLS) Program/Project	
Revision: B	Document No: SLS-SPIO-PLAN-017
January 8, 2020	Page: 45 of 54
Title: SPIE MSA Fracture Control Plan	

GSE	Government Support Equipment
ICPS	Interim Cryogenic Propulsion Stage
IDPP	Impact Damage Protection Plan (Non-Metallics)
in	length measurement, inches
INVA	Nickel-Iron Alloy with low CTE
ISPE	Integrated Spacecraft and Payload Element
K_{Ic}	Plane-Strain Critical Stress Intensity Factor
KSC	Kennedy Space Center
ksi	kilo-pounds per square inch
LaRC	Langley Research Center
lbm	Mass measurement, pounds-mass
LVSA	Launch Vehicle Stage Adapter
min	As a Minimum
MPCV	Orion Multi-Purpose Crew Vehicle
MRB	Material Review Board
MSA	MPCV Stage Adapter
MSFC	Marshall Space Flight Center
NASA	National Aeronautics and Space Administration
NASGRO	NASA's preferred software for damage tolerance assessments of metallic components
NDE	Nondestructive evaluation
NFC	Non-Fracture Critical
OPR	Office of Primary Responsibility
PCH	Program-Critical Hardware
psi	Pounds per Square Inch, Stress, Young's Modulus, or Pressure
S&MA	Safety and Mission Assurance
SAR	Stress Analysis Report
sec	seconds
SLS	Space Launch System
S_{max}	Maximum Local Concentrated Stress
SPB	Secondary Payload Bracket
SPL	Secondary Payload
SPIE	Spacecraft & Payload Integration and Evolution Office (formerly SPIO)
SPIO	Spacecraft & Payload Integration Office
SS	Separation System
TBD	To be Determined

*The electronic version is the official approved document.
Verify this is the correct version before use.*

APPROVED FOR PUBLIC RELEASE – DISTRIBUTION IS UNLIMITED

NASA-HDBK-5010, VOLUME 2, REVISION A

Space Launch System (SLS) Program/Project	
Revision: B	Document No: SLS-SPIO-PLAN-017
January 8, 2020	Page: 46 of 54
Title: SPIE MSA Fracture Control Plan	

TPS Thermal Protection System
UTS Ultimate Tensile Strength

A2.0 GLOSSARY OF TERMS

Term	Description
Flight	The sequence of events that takes place between liftoff and landing of a transportation vehicle.
Impact Damage	The injury or harm inflicted by impingement of another object upon the hardware such as a dropped tool, hail, runway debris, or the bumping or striking during handling or lifting.

*The electronic version is the official approved document.
Verify this is the correct version before use.*

APPROVED FOR PUBLIC RELEASE – DISTRIBUTION IS UNLIMITED

NASA-HDBK-5010, VOLUME 2, REVISION A

Space Launch System (SLS) Program/Project	
Revision: B	Document No: SLS-SPIO-PLAN-017
January 8, 2020	Page: 47 of 54
Title: SPIE MSA Fracture Control Plan	

APPENDIX B OPEN WORK

All resolved TBDs, TBRs, and forward work items should be listed on the Change Request (CR) the next time the document is updated and submitted for formal review, and that will serve as the formal change record through the configuration management system.

B1.0 TO BE DETERMINED

Table B1-1 lists the specific To Be Determined (TBD) items in the document that are not yet known. The TBD is inserted as a placeholder wherever the required data is needed and is formatted in bold type within carets. The TBD item is sequentially numbered as applicable (i.e., <TBD-001> is the first undetermined item assigned in the document). As each TBD is resolved, the updated text is inserted in each place that the TBD appears in the document and the item is removed from this table. As new TBD items are assigned, they will be added to this list in accordance with the above described numbering scheme. Original TBDs will not be renumbered.

Table B1-1. To Be Determined Items

TBD	Section	Description
TBD-001		

B2.0 TO BE RESOLVED

Table B2-1 lists the specific To Be Resolved (TBR) issues in the document that are not yet known. The TBR is inserted as a placeholder wherever the required data is needed and is formatted in bold type within carets. The TBR issue is sequentially numbered as applicable (i.e., <TBR-001> is the first unresolved issue assigned in the document). As each TBR is resolved, the updated text is inserted in each place that the TBR appears in the document and the issue is removed from this table. As new TBR issues are assigned, they will be added to this list in accordance with the above described numbering scheme. Original TBRs will not be renumbered.

Table B2-1. To Be Resolved Issues

TBR	Section	Description
TBR-001		

*The electronic version is the official approved document.
Verify this is the correct version before use.*

NASA-HDBK-5010, VOLUME 2, REVISION A

Space Launch System (SLS) Program/Project	
Revision: B	Document No: SLS-SPIO-PLAN-017
January 8, 2020	Page: 48 of 54
Title: SPIE MSA Fracture Control Plan	

APPENDIX C MSA DIAPHRAGM DAMAGE THREAT ASSESSMENT

C1.0 INTRODUCTION

Marshall Space Flight Center (MSFC) is tasked to design, fabricate, test, and inspect a reliable and safe Orion Multipurpose Crew Vehicle (MPCV) Stage Adapter, MSA, for the SLS missions, beginning with Artemis I. The Artemis-I will not be a manned-flight, but the MSA will be under fracture control per NASA-STD-5019, Fracture Control Requirements for Spaceflight Hardware, since the same hardware is planned for manned flights after Artemis-I. The fracture control planning for the Artemis-I version of the MSA has been developed and can be found in the SLS-SPIO-PLAN-017, SPIE MSA Fracture Control Plan.

This document was adapted from the considerable work that was done on the damage threat assessment of the Constellation Program Ares I Upperstage, Ares-USO-SE-25753, Upper Stage Damage Threat Assessment for Composite and Bonded Structures. The MSA contains a volume isolator, a diaphragm which is a laminar composite layup structure. The MSA fracture control plan identifies the diaphragm as fracture critical and establishes a proof test approach for fracture critical, non-metallic components to provide fracture control for the diaphragm. This approach is discussed in MSFC-RQMT-3479, Fracture Control Requirements for Composite and Bonded Vehicle and Payload Structures, and one requirement of the approach is to perform the first of the three tasks identified for a damage threat assessment (DTA), and this document addresses that requirement.

This approach expedited development of a mature DTA, and reduced the risk of missing a threat.

C2.0 PURPOSE

The primary purpose of the DTA is to define and quantify the damage or flaws that can occur due to impact energies on composite and bonded structures. Finite-element analysis of the diaphragm has shown that the structure is relatively tolerant to a loss of structure: buckling is the design-driver for this component, and the analysis showed that the diaphragm could contain ten holes of 5-inches in diameter without buckling (beyond the two that provide passage for electrical cabling)⁵. The rejection criteria to be used for nondestructive evaluation are far smaller than this.

The manufacturing processes to be used have been carefully considered, the personnel performing the processes or otherwise occupying the vicinity of the diaphragm are conscientious and have been trained in foreign object debris (FOD) control, and the possibility of inflicting damage is low, but it is not zero. Thus, task 1 of the DTA, described in MSFC-RQMT-3479, was retained as a requirement to provide a review of the potential sources of damage that might occur.

⁵ STSB-2012-015, MPCV Diaphragm Strength and Stability Report.

*The electronic version is the official approved document.
Verify this is the correct version before use.*

NASA-HDBK-5010, VOLUME 2, REVISION A

Space Launch System (SLS) Program/Project	
Revision: B	Document No: SLS-SPIO-PLAN-017
January 8, 2020	Page: 49 of 54
Title: SPIE MSA Fracture Control Plan	

C3.0 SCOPE

This DTA assesses the diaphragm dome, the housing structures that are joined to it with fasteners.

C4.0 DAMAGE THREAT ASSESSMENT APPROACH

The DTA flow consists of three tasks as depicted below in Figure B.1. These include

- Task 1: Identify Credible Impact Damage
- Task 2: Characterize Impact Size and Energy Input
- Task 3: Establish an As-Manufactured Initial Flaw Type and Size Assessment

Only Task 1 will be performed, and the results will serve as inputs into the IDPP. The DTA will include the identification of the source and type of impact damage that poses a credible threat to the hardware, and the assessed threats will be mitigated through a combination of protective measures (covers, blankets, tethers, etc.) and surveillance.

*The electronic version is the official approved document.
Verify this is the correct version before use.*

APPROVED FOR PUBLIC RELEASE – DISTRIBUTION IS UNLIMITED

NASA-HDBK-5010, VOLUME 2, REVISION A

Space Launch System (SLS) Program/Project	
Revision: B	Document No: SLS-SPIO-PLAN-017
January 8, 2020	Page: 50 of 54
Title: SPIE MSA Fracture Control Plan	

Damage Threat Assessment

- **Primary Purpose:** Define and quantify the flaws to be addressed by fracture control
- **Consists of three tasks (DTA 1,DTA 2, and DTA 3)** as described below

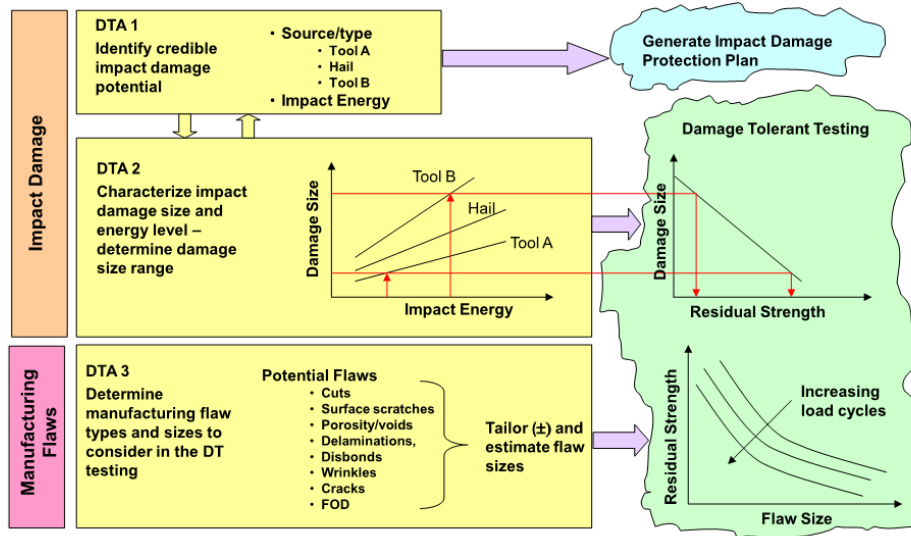


Figure C-1. Damage Threat Assessment (DTA) Tasks and Flow

C5.0 DAMAGE THREAT ASSESSMENT TASK 1: IMPACT DAMAGE SOURCE AND TYPES

The diaphragm and housings are comprised of fiber-reinforced polymer matrix composites that are attached using fasteners. No flight hazard analysis has been provided, and so the hardware is, by default, classified as fracture critical. This means that a catastrophic hazard might result if the item failed due to the presence of a flaw.

DTA Task 1 is a requirement of the proof test approach to fracture control, and this task, the identification of the damage threats, appears below.

All events and credible possibilities will be considered for the specific hardware under consideration when identifying the potential impact damage. These events would include but are not be limited to incidents such as tool drops, runway debris, hail, and bumping during handling.

*The electronic version is the official approved document.
Verify this is the correct version before use.*

NASA-HDBK-5010, VOLUME 2, REVISION A

Space Launch System (SLS) Program/Project	
Revision: B	Document No: SLS-SPIO-PLAN-017
January 8, 2020	Page: 51 of 54
Title: SPIE MSA Fracture Control Plan	

It should be noted that for relatively large structures, placement of the structure onto storage supports or cradles can result in significant impact damage.

C6.0 DIAPHRAGM ASSEMBLY DAMAGE THREAT ANALYSIS SCENARIO TABLE

The diaphragm value stream map was assessed for potential threats, and the results are shown in Table B-1, below. The damage threat assessment will begin upon the completion of post-proof NDE. Activities beyond assessment are discussed in section 5.2.2, Impact Damage Protection Plan.

Table C-1. DTA Scenario Table, MSA Diaphragm/Housing Assembly

Phase	Damage Occurring Site	Damage Scenario, Source/Type
start after proof		
NDE1 at Janicki: roll diaphragm, lower into mold, install bridge scaffolding	inside or outside surface, especially in the acreage	hit with lifting shackle or bridge scaffolding
	anywhere	hit surrounding objects or lifting device due loss of control during lifting/handling/transport
	anywhere	overstress induced by loads not encompassed by the design loads
	inside surface	drop a personal item
	anywhere	drop a tool
	anywhere	drop fasteners
	anywhere	impacts with other objects
NDE2 at Janicki	inside surface	drop a personal item
	inside surface	drop a tool
lift diaphragm, roll diaphragm, clean diaphragm, lower diaphragm into tool, remove lifting hardware, protect with foam, nylon straps over top to support wrapping sheet, install wooden T-beam on top, shrink wrap--two layers--at Janicki	inside or outside surface, especially in the acreage	hit with lifting shackle or bridge scaffolding
	anywhere	hit surrounding objects or lifting device due loss of control during lifting/handling/transport

*The electronic version is the official approved document.
Verify this is the correct version before use.*

NASA-HDBK-5010, VOLUME 2, REVISION A

Space Launch System (SLS) Program/Project	
Revision: B	Document No: SLS-SPIO-PLAN-017
January 8, 2020	Page: 52 of 54
Title: SPIE MSA Fracture Control Plan	

Phase	Damage Occurring Site	Damage Scenario, Source/Type
	flange	overstress induced by loads not encompassed by the design loads
	inside surface	drop a personal item
	inside surface	drop a tool
move wrapped part in tool to shipping trailer	anywhere	drop part and tool from forklift
	inside surface	drop something through the shrink wrap
transport part in tool to MSFC	anywhere	drop part and tool from trailer
	flange	impact part and tool with abutment, enroute
	inside surface	drop something through the shrink wrap
move to integration in 4708 area on the dolly	inside or outside surface, especially in the acreage	hit with lifting shackle
	anywhere	hit surrounding objects or lifting device due loss of control during lifting/handling/transport
	anywhere	overstress induced by loads not encompassed by the design loads
	inside surface	drop a personal item
	anywhere	drop a tool
	anywhere	drop fasteners
	anywhere	impacts with other objects
integrate diaphragm to MSA	inside or outside surface, especially in the acreage	hit with lifting shackle
	anywhere	hit surrounding objects or lifting device due loss of control during lifting/handling/transport
	anywhere	overstress induced by loads not encompassed by the design loads
	inside surface	drop a personal item
	anywhere	drop a tool
	anywhere	drop fasteners
	anywhere	impacts with other objects MSA structure, dolly
install cabling, instrumentation, and electrical interface brackets	outside surface	drop a tool
	outside surface	drop fasteners, cables clamps

*The electronic version is the official approved document.
Verify this is the correct version before use.*

APPROVED FOR PUBLIC RELEASE – DISTRIBUTION IS UNLIMITED

NASA-HDBK-5010, VOLUME 2, REVISION A

Space Launch System (SLS) Program/Project	
Revision: B	Document No: SLS-SPIO-PLAN-017
January 8, 2020	Page: 53 of 54
Title: SPIE MSA Fracture Control Plan	

Phase	Damage Occurring Site	Damage Scenario, Source/Type
	outside surface	impacts with cable connectors or cabling brackets
	outside surface	impact with fixturing--ladders, and other objects, e.g., hard hats
rotate MSA assembly into flight orientation	anywhere	hit with lifting shackle
	anywhere	hit surrounding objects or lifting device due loss of control during lifting/handling/transport
	anywhere	overstress induced by loads not encompassed by the design loads
	anywhere	drop a personal item
	anywhere	hit surrounding objects or lifting device due loss of control during lifting/handling/transport
	anywhere	overstress induced by loads not encompassed by the design loads
	anywhere	drop a tool
install into shipping container and prepare for shipping		drop GSE lifting lugs or shackles
	anywhere	hit surrounding objects or lifting device due loss of control during lifting/handling/transport
	anywhere	overstress induced by loads not encompassed by the design loads
		drop a personal item
		drop a tool
		drop fasteners
		drop cleaning or bagging materials
ship to Astrotec		transportation loads damage
storage		similar issues to those expressed above are expected
handling		
integration into the stack		
transportation to the launch pad		
launch preps		FOD
		over-pressurization above or below
launch		FOD could be vibrated against the diaphragm
		exceed design loads

*The electronic version is the official approved document.
Verify this is the correct version before use.*

APPROVED FOR PUBLIC RELEASE – DISTRIBUTION IS UNLIMITED

NASA-HDBK-5010, VOLUME 2, REVISION A

Space Launch System (SLS) Program/Project	
Revision: B	Document No: SLS-SPIO-PLAN-017
January 8, 2020	Page: 54 of 54
Title: SPIE MSA Fracture Control Plan	

Phase	Damage Occurring Site	Damage Scenario, Source/Type
		over-pressurization above or below

C7. DOCUMENTATION

All flaws detected on the flight hardware will be recorded as manufacturing anomalies and any flaws beyond the drawing limits will be worked as Material Review Board (MRB) actions.

The engineering drawings will identify fracture critical parts and bonds and specify their inspection criteria, including both visual and NDE.

*The electronic version is the official approved document.
Verify this is the correct version before use.*

NASA-HDBK-5010, VOLUME 2, REVISION A



NASA SCIENTIFIC & TECHNICAL INFORMATION PROGRAM

NF-1676 Document of Record

Document ID: 20205004146

Rights & Dissemination

NASA will distribute this STI as:	Do Not Distribute
Do Not Distribute Reason:	Other/Approval Only (please specify in Additional Information) For internal distribution on Windchill only.
Copyright Determination:	Work of the US Gov. Public Use Permitted.

Submission Details

STI Title:	SPIE Multi-Purpose Crew Vehicle Stage Adapter (MSA) FRACTURE CONTROL SUMMARY REPORT
NASA Point of Contact:	Samuel M Cordner (MSFC)
STI Type:	Other (Please specify in Additional Information)
Technical Review:	NASA Peer Committee This report has also recieved project approval for release.
Funding Number(s):	Project: Payload Adapter Fitting

Primary Distribution

Publication:	NASA Handbook 5010A
Publication Date:	October 1, 2020
Event:	
Event Date:	? - ?
Event Sponsor(s):	

Export Control

International Traffic in Arms Regulations (ITAR):	No
Export Administration Regulations (EAR):	No

Thursday, December 10, 2020 at 10:57:03 AM GMT-06:00

APPROVED FOR PUBLIC RELEASE – DISTRIBUTION IS UNLIMITED

APPENDIX B

**SPIE MULTI-PURPOSE CREW VEHICLE STAGE ADAPTER
(MSA)**

FRACTURE CONTROL SUMMARY REPORT



National Aeronautics and
Space Administration

SLS-SPIO-RPT-013

BASELINE

RELEASE DATE: 15 FEBRUARY 2018

SPIE Multi-Purpose Crew Vehicle Stage Adapter (MSA)

FRACTURE CONTROL SUMMARY REPORT

APPENDIX B-E ARE REMOVED

NASA-HDBK-5010, VOLUME 2, REVISION A

Space Launch System (SLS) Spacecraft & Payload Integration Office	
Version: baseline	Document No: SLS-SPIO-RPT-013
Release Date:	Page: 2 of 34
Title: SPIE MSA FRACTURE CONTROL SUMMARY REPORT	

VERSION AND HISTORY PAGE

Status	Version No.	Change No.	Description	Release Date
new				

APPROVED FOR PUBLIC RELEASE – DISTRIBUTION IS UNLIMITED

NASA-HDBK-5010, VOLUME 2, REVISION A

Space Launch System (SLS) Program/Project	
Revision: baseline	Document No: SLS-SPIO-RPT-013
Release Date:	Page: 3 of 34
Title: SPIE MSA FRACTURE CONTROL SUMMARY REPORT	

TABLE OF CONTENTS

VERSION AND HISTORY PAGE	2
LIST OF FIGURES	5
LIST OF TABLES	5
1.0 INTRODUCTION	6
1.1 Purpose	6
1.2 Scope	6
1.3 Change Authority/Responsibility	7
2.0 DOCUMENTS	7
2.1 Requirements	7
2.2 Fracture Control Plan	8
2.3 Drawings (Item C9)	8
2.3.1 Metallic Components	8
2.3.2 Diaphragm (see memorandum LaRC-SLS-MSA-01-032 for top-level detail of drawings)	8
2.3.3 Secondary Hardware	9
2.3.4 Wiring Harnesses and Electrical Component	9
2.3.5 Fasteners & Mounting Hardware	9
2.4 Specifications, Materials Usage Agreements	11
2.5 Certifications	11
2.6 Reports and Memoranda	11
2.7 Inspection and NDE Reports	12
2.7.1 Metallic Structure: MAPTIS Work Order NDE Reports	12
2.7.2 Metallic Structure: Vendor's Planning, Inspection, and NDE Reports	12
2.7.3 Composite Structure: MAPTIS Work Order NDE Reports	13
2.7.4 Composite Structure: Vendor Planning and Inspection Reports	13
2.8 Procedures, Lifts, and Moves	13

*The electronic version is the official approved document.
Verify this is the correct version before use.*

APPROVED FOR PUBLIC RELEASE – DISTRIBUTION IS UNLIMITED

NASA-HDBK-5010, VOLUME 2, REVISION A

Space Launch System (SLS) Program/Project	
Revision: baseline	Document No: SLS-SPIO-RPT-013
Release Date:	Page: 4 of 34
Title: SPIE MSA FRACTURE CONTROL SUMMARY REPORT	

3.0	HARDWARE OVERVIEW	13
4.0	HARDWARE OPERATION	13
5.0	SLS SPIE MSA FRACTURE CONTROL PLAN	13
6.0	FRACTURE CONTROL SUMMARY REPORT REQUIREMENTS	14
6.1	Requirements and Statements Common to All SPIE MSA Hardware	15
6.1.1	Re-Use of Hardware (Items 5 and C4).....	15
6.1.2	Life-Limited Hardware (Item 2)	15
6.1.3	Pressure Vessels and Rotating Equipment (Items 3 and C3).....	15
6.1.4	Planning and Execution (Item 6)	16
6.1.5	Verification of Materials Usage (Item 8).....	16
6.1.6	Verification of Hardware Control (Items 7 and C5).....	16
6.1.7	Configuration Management System (Item 13)	16
6.1.8	Non-Applicable Requirements (Item 12).....	16
6.2	Classifications of MSA Hardware	17
	6.3 Fracture Critical Hardware (Items 1 and C9)	17
6.4	MSA Primary Structure: Fracture Critical (Item 1)	19
6.4.1	Nondestructive Evaluation of Metallic Hardware (Item 4)	21
6.4.2	Materials Usage Agreements Verifications (Item 8)	23
6.4.3	Special Considerations (Item 11).....	23
6.5	MSA Diaphragm: Fracture Critical (Item C2)	24
6.5.1	Failure Modes	24
6.5.2	Exempt Composite Hardware (Item C1)	25
6.5.3	Non-Exempt Composite Parts (Item C2).....	25
6.5.4	Nondestructive Evaluation (NDE) of Composite Hardware (Item C2).....	26
6.5.5	Control of Composite Hardware (Item C5)	27
6.5.6	Verification of Materials Used for Fail-Safe Composite Hardware (Item C6).....	27
6.5.7	Materials Usage Agreements (Items 9 and C7)	27
6.5.8	Damage Threat Assessment	28
6.5.9	Impact Damage Protection Plan.....	28

*The electronic version is the official approved document.
Verify this is the correct version before use.*

NASA-HDBK-5010, VOLUME 2, REVISION A

Space Launch System (SLS) Program/Project	
Revision: baseline	Document No: SLS-SPIO-RPT-013
Release Date:	Page: 5 of 34
Title: SPIE MSA FRACTURE CONTROL SUMMARY REPORT	

6.5.10 Summary of Flaws Detected and Deviations (Items 9 and C8).....	28
6.6 Secondary Structure: Non-Fracture Critical.....	28
6.6.1 Low-Risk Parts (Item 1).....	28
6.6.2 Fail-Safe Parts (Item 5).....	29
6.6.3 Alternative Approaches (Item 10)	31
6.6.4 Avionics Box	33
APPENDIX A: ACRONYMS	34
APPENDIX B: TBD’S AND TBR’S.....	34
APPENDIX C, MATERIALS USAGE AGREEMENTS	Attachment 1
APPENDIX D, SPIE MSA DIAPHRAGM DRAWINGS	Attachment 2
APPENDIX E, LOW RELEASED-MASS CALCULATIONS.....	Attachment 3

LIST OF FIGURES

Figure 1: MSA Primary Structure, Identifying the Analyzed Control Points (CP).	20
--	----

LIST OF TABLES

Table 1: Location within this Document of FCSR Required Information per NASA-STD-5019 Section 4.4.3.d.....	14
Table 2: Location within this Document of FCSR Required Information per MSFC-RQMT-3479 Section 7.2	14
Table 3: Fracture Control Classifications, Group 1, Fracture Critical Parts	19
Table 4: Some Details of Analyzed Control Points on the MSA Primary Structure	21
Table 6: Low-Risk, Non-Fracture Critical Parts	29
Table 7: Fasteners—Fail-Safe and Low Released-Mass.....	30
Table 8: Fail-Safe Parts	31
Table 9: Alternative Approach Items	32

*The electronic version is the official approved document.
Verify this is the correct version before use.*

NASA-HDBK-5010, VOLUME 2, REVISION A

Space Launch System (SLS) Program/Project	
Revision: baseline	Document No: SLS-SPIO-RPT-013
Release Date:	Page: 6 of 34
Title: SPIE MSA FRACTURE CONTROL SUMMARY REPORT	

1.0 INTRODUCTION

This document is being written prior to the completion of all of the fracture control-related analyses being performed. As such, when the details are available there are a few specific “open” items that will be closed by revision to this document. Specifically, an updated analysis of the MSA volume isolator, or diaphragm, is required. This has been identified as fracture critical and all planned work has been executed. The updated analysis will appear in SLS-SPIO-RPT-038, SPIO MSA Structural Assessment Report, section 6.0 Volume Isolator and APPENDIX E – VOLUME ISOLATOR REPORT, which is planned for a revision during the summer of 2017. Also, the ADP is referenced, and this will not be produced until the flight MSA goes through hardware acceptance review.

Otherwise, this report concludes that the SLS MSA meets fracture control per NASA-STD-5019 requirements and the MSA diaphragm meets fracture control per MSFC-RQMT-3479 requirements.

1.1 Purpose

This document, the SPIE MSA Fracture Control Summary Report (FCSR) provides a brief reporting of the fracture control activities defined in the SPIE MSA Fracture Control Plan, SLS-SPIO-PLAN-017. These activities lead to the damage tolerant state of the Space Launch System (SLS) MSA.

The FCSR is identified by SPIE requirement R.ISP_MSA.022.3, NASA-STD-5019, *Fracture Control Requirements for Spaceflight Hardware*, and that requirement pertains to the MSA and the MSA diaphragm. The requirement states¹:

Qualified technical experts will provide reports with proper concurrence to assure there is sufficient evidence to verify applicable requirements of NASA-STD-5019 are satisfied. The LSE will confirm the compilation.

The MSA metallic structure fracture control requirements are identified in NASA-STD-5019. Because the MSA diaphragm is a composite structure, fracture control requirements can be found in MSFC-RQMT-3479, *Fracture Control Requirements for Composite and Bonded Vehicle and Payload Structures*, the document NASA-STD-5019 references for the requirements regarding composite and bonded structures².

1.2 Scope

Although the MSA design is expected to continue unchanged in the SLS flights, this FCSR applies specifically to the EM-1.

The required content of the FCSR for metallic components is dictated by section 4.4.3.d items (1) through (13) of NASA-STD-5019, *Fracture Control Requirements for Spaceflight Hardware*

¹ Taken from SLS-SPIO-PLAN-010-03 EM1 MSA Matrix (11-13-2014)

² See NASA-STD-5019, Sections 4.1.1.7 (Non-Fracture-Critical Composite/Bonded Structures) and 4.1.2.4 (Composite/Bonded Structures).

*The electronic version is the official approved document.
Verify this is the correct version before use.*

NASA-HDBK-5010, VOLUME 2, REVISION A

Space Launch System (SLS) Program/Project	
Revision: baseline	Document No: SLS-SPIO-RPT-013
Release Date:	Page: 7 of 34
Title: SPIE MSA FRACTURE CONTROL SUMMARY REPORT	

(5019)³, and the ordering of the information is modified to provide a clear development. The items addressed in each paragraph below are identified at the beginning of the paragraph, as follows:

(Item ##), where ## represents the numbers (1) through (13).

For the SLS MSA diaphragm, MSFC-RQMT-3479, *Fracture Control Requirements for Composite and Bonded Vehicle and Payload Structures* (3479)⁴ identifies a similar set of requirements in section 7.2 items 1 through 9. These will be addressed similarly to the metallic components, but with a “C” prefix on the number:

(Item C#), where # represents the numbers 1 through 9.

Further detail of how the hardware meets each specific requirement of 5019 and 3479 can be found in VCN-List_Frac_Control--SPIE_MSA_2017-12-27.xlsx.

For the sake of brevity, little was duplicated that appears within the SPIE MSA Fracture Control Plan (FCP). As such, using the FCP to identify background and planning and this document to provide results, discussion, and conclusions produces a reasonably complete report of fracture control activities. The data files referenced herein have not been appended to this report per 5019 recommendations.

1.3 Change Authority/Responsibility

The NASA Office of Primary Responsibility (OPR) for this document is NASA-MSFC/EM20⁵. Proposed changes to this document shall be controlled at the OPR level using procedures defined by the OPR.

2.0 DOCUMENTS

Reference documents that might prove useful in evaluating the effectiveness and completeness of the fracture control program for the SLS MSA appear below. The documents cited include drawings, specifications and procedures, inspection plans and records, certifications, and reports.

2.1 Requirements

NASA-STD-5019 *Fracture Control Requirements for Spaceflight Hardware*

MSFC-RQMT-3479 *Fracture Control Requirements for Composite and Bonded Vehicle and Payload Structures*

³ For brevity, NASA-STD-5019 will also be identified as “5019” in this document.

⁴ For brevity, MSFC-RQMT-3479 will also be identified as “3479” in this document.

⁵ A recent reorganization has caused the re-identification of the Damage Tolerance Assessment and Non-Destructive Evaluation Branch from EM20 to EM21. The requirements that identify OPR show EM20 as the OPR, and so this document is written to be consistent with that requirement.

*The electronic version is the official approved document.
Verify this is the correct version before use.*

NASA-HDBK-5010, VOLUME 2, REVISION A

Space Launch System (SLS) Program/Project	
Revision: baseline	Document No: SLS-SPIO-RPT-013
Release Date:	Page: 8 of 34
Title: SPIE MSA FRACTURE CONTROL SUMMARY REPORT	

SLS-SPIO-RQMT-013 *SPIE MPCV Stage Adapter (MSA) Technical Requirements Document*

2.2 Fracture Control Plan

SLS-SPIO-PLAN-017, Rev. A *SPIE MSA Fracture Control Plan*

2.3 Drawings (Item C9⁶)

97M62110-001 MSA Top Assembly

2.3.1 Metallic Components

97M62111-001 Access cover
97M62120-001 Machine-drilled assembly (MSA)
97M62121-001 MSA barrel panels 1, 2, and 3, respectively
97M62122-001 MSA barrel panels 1, 2, and 3, respectively
97M62123-001 MSA barrel panels 1, 2, and 3, respectively
97M62124-001 Weldment Assembly, MSA
97M62125-001 MSA forward ring
97M62127-001 MSA aft ring

2.3.2 Diaphragm (see memorandum LaRC-SLS-MSA-01-032 for top-level detail of drawings)

97M62117-001 connector plate 1
97M62118-001 connector plate 2
97M62119-001 housing layup, electrical connector
97M62140-001 MSA diaphragm
97M62141-001 diaphragm machine drill, MSA
97M62142-001 diaphragm layup, MSA
97M62143-001 Housing assembly
97M62144-001 diaphragm housing

⁶ C9: The Fracture Control Summary Report shall provide sufficient information to certify that fracture control requirements have been met. It shall include the following: 9. Drawings and sketches referenced in tabular summary.

*The electronic version is the official approved document.
Verify this is the correct version before use.*

NASA-HDBK-5010, VOLUME 2, REVISION A

Space Launch System (SLS) Program/Project	
Revision: baseline	Document No: SLS-SPIO-RPT-013
Release Date:	Page: 9 of 34
Title: SPIE MSA FRACTURE CONTROL SUMMARY REPORT	

2.3.3 Secondary Hardware

97M62115-001	electrical interface bracket 1 assembly
97M62116-001	electrical interface bracket 2 assembly
97M62171-001	MSA secondary payload brackets (SPB)

2.3.4 Wiring Harnesses and Electrical Component

39111	avionics unit
97M43341-001	MSA PF-1 WIRE HARNESS ASSEMBLIES -W341
97M43343-001	MSA PF-1 WIRE HARNESS ASSEMBLIES -W343
97M43345-001	MSA PF-1 WIRE HARNESS ASSEMBLIES-W345
97M43361-001	MSA PF-1 WIRE HARNESS ASSEMBLIES -W361
97M43362-001	MSA PF-1 WIRE HARNESS ASSEMBLIES -W362
97M43371-001	MSA PF-1 WIRE HARNESS ASSEMBLIES -W371
97M43372-001	MSA PF-1 WIRE HARNESS ASSEMBLIES -W372

2.3.5 Fasteners & Mounting Hardware

97M62145-101	bracket, connector (cable attach bracket)
97M62166-101	spacer, short (cable attach spacers)
97M62167-101	spacer, tall (cable attach spacers)
M45932/1-17DL	nut/insert, SPB assembly
MS14181-05008	bolt tension 220 ksi--SPB to MSA
MS14181-05008L	cable attach bracket bolt
MS14181-05008L	cable attach spacer bolt
MS14181-05014L	cable attach spacer bolt
MS14183L-C4	washers, SPB assembly
MS20426AD3-5A	Rivet, solid, countersunk, connector plate mount
NAS1057W4-075	spacer, wiring harness mount
NAS1057W4-150	spacer, wiring harness mount
NAS1149	washer, SPB
NAS1291C3M	housing to diaphragm nuts
NAS1291C4M	diaphragm attach barrel nuts

*The electronic version is the official approved document.
Verify this is the correct version before use.*

NASA-HDBK-5010, VOLUME 2, REVISION A

Space Launch System (SLS) Program/Project	
Revision: baseline	Document No: SLS-SPIO-RPT-013
Release Date:	Page: 10 of 34
Title: SPIE MSA FRACTURE CONTROL SUMMARY REPORT	

NAS1351C3-16	avionics mounting screw
NAS1587-4	washer, electrical interface bracket to MSA and housing to electrical plate and diaphragm to MSA
NAS1587-4C	washer, electrical interface bracket to MSA and housing to electrical plate and diaphragm to MSA
NAS1587A3C	Avionics mounting washer
NAS1587A3C	washer, countersink, housing to diaphragm
NAS1715C10KH	clamp, loop
NAS1715C11KH	clamp, loop
NAS1715C12KH	clamp, loop
NAS1715C13KH	clamp, loop
NAS1715C14KH	clamp, loop
NAS1715C6KH	clamp, loop
NAS1715C7KH	clamp, loop
NAS1715C8KH	clamp, loop
NAS1715C9KH	clamp, loop
NAS1773C4M	#10-32 self-locking nut plate, connector plate mount
NAS1805	nut/insert, SPB assembly
NAS1953C6	housing to diaphragm bolts
NAS1954	bolt, SPB assembly
NAS1954C10	diaphragm attach bolts
NAS1954C4	housing to connector plate bolt
NAS1954C5	access cover mount bolts
NAS1954C7	electrical interface bracket fasteners to MSA, bolt, hex head
NAS620C10L	washer, flat, housing to diaphragm
NAS9104	bolt, loop clamp mount
NASM14183L-C5	washer, countersunk, passivated--SPB to MSA

*The electronic version is the official approved document.
Verify this is the correct version before use.*

APPROVED FOR PUBLIC RELEASE – DISTRIBUTION IS UNLIMITED

NASA-HDBK-5010, VOLUME 2, REVISION A

Space Launch System (SLS) Program/Project	
Revision: baseline	Document No: SLS-SPIO-RPT-013
Release Date:	Page: 11 of 34
Title: SPIE MSA FRACTURE CONTROL SUMMARY REPORT	

2.4 Specifications, Materials Usage Agreements

SLS-MSA-0001	<i>No Rolled-Ring Qualification Article</i>
SLS-MSA-0002	<i>Design Properties for Multi-Purpose Crew Vehicle Stage Adapter</i>
SLS-MSA-0003	<i>No Barrel-Forming Qualification Article</i>
SLS-MSA-0004	<i>Al-Li 2195 plates were not purchased to the Ares-USO-MP-2555 specification indicated on the drawing</i>
SLS-MSA-0005	<i>MPCV Stage Adapter Diaphragm Design Properties</i>
SLS-MSA-0006	<i>Stress corrosion cracking of Al-Li 2195</i>

2.5 Certifications

NDE Certifications are recorded in CERTRAK.

2.6 Reports and Memoranda

Ares-USO-SE-25753 (draft)	<i>Upper Stage Damage Threat Assessment for Composite and Bonded Structures</i>
EM20-14-FCB-014	<i>MSFC Fracture Control Board Memo</i>
EM20-17-FCB-007	<i>MSFC Fracture Control Board Memo</i>
10000199668 ZPR 000 00	<i>Janicki Industries MSA Diaphragm Proof Load Test Report</i>
LaRC-SLS-MSA-01-024	<i>LaRC MSA Composite Material Testing Summary and Results</i>
R.ISP_MSA.022.3	<i>Requirements Verification Spreadsheet for Fracture Control of the SPIE MSA (Both NASA-STD-5019 and MSFC-RQMT-3479 are addressed in the document)</i>
SLS-SPIO-RPT-038, Rev. C	<i>SPIO MSA Structural Assessment Report</i>
STSB-2012-015	<i>MPCV Diaphragm Strength and Stability Report</i>
VCN-List_Frac_Control-SPIE_MSA_2017-12-27.xlsx	<i>Verification Spreadsheet for SPIE MSA</i>
MSA_BoltInitialVelocity_WithFractureEnergy_2017-11-13.xlsx	<i>Low Released Mass Analysis of Bolts</i>
Space Vector Document 21505-R005, Rev G	<i>NASA Secondary Payloads Avionics Box Development Structural Dynamics Analyses, Loads, and Models DR Number: 1537 DE-003</i>

*The electronic version is the official approved document.
Verify this is the correct version before use.*

APPROVED FOR PUBLIC RELEASE – DISTRIBUTION IS UNLIMITED

NASA-HDBK-5010, VOLUME 2, REVISION A

Space Launch System (SLS) Program/Project	
Revision: baseline	Document No: SLS-SPIO-RPT-013
Release Date:	Page: 12 of 34
Title: SPIE MSA FRACTURE CONTROL SUMMARY REPORT	

2.7 Inspection and NDE Reports

These are summarized in the acceptance data package (ADP). The detailed reports are below.

2.7.1 Metallic Structure: MAPTIS Work Order NDE Reports

2016-0243, Sequence 1	MSA-3 (EM-1) Cone Weld NDE (Weld A)
2016-0243, Sequence 2	Cone Weld NDE (Weld B)
2016-0243, Sequence 3	MSA-3 (EM-1) Cone Weld NDE (Weld C)
2016-0243, Sequence 4	Weld A, Weld B, Weld C (Ultrasonic Inspection Report)
2016-0435, Sequence 3	MSA-3 field RT
2016-0435, Sequence 1	MSA-3 (EM-1) Forward Circ. Weld (Ultrasonic Inspection Report)
2016-0435, Sequence 2	MSA-3 (EM-1) Aft Circ. Weld (Ultrasonic Inspection Report)
2016-0844, Sequence 1	FWD & AFT Flange Hole Eddy Current for MSA-3
2016-0870, Sequence 1	Flange Machined Surfaces (Penetrant Inspection)

2.7.2 Metallic Structure: Vendor's Planning, Inspection, and NDE Reports

The vendor NDE reports for the aft ring forging are

ATI Latish Forging Quality Department Ultrasonic Inspection Report, Ref Ladish Job J32807, see filename: P-S 68862 NM007.pdf.

Major Tool & Machine Nondestructive Test Certification for Liquid Penetrant Examination, NDT#63601, see filename: SN001_NDE.pdf.

The vendor NDE reports for the forward ring forging are:

ATI Latish Forging Quality Department Ultrasonic Inspection Report, Ref Ladish Job J32808, see filename: Inspection_P-S 68863 NM008.pdf.

Major Tool & Machine Nondestructive Test Certification for Liquid Penetrant Examination, NDT#63602, see filename: SN001_NDE.pdf.

The vendors' NDE reports for the as-fabricated and heat treated barrel panels are listed, below.

AMRO Fabricating Corporation, AFC # 551-121, Certificate of conformance, see filename: Inspection Record12.pdf

Pechiney Rolled Products Certified Test Report, Pechiney Order No. 108-100073, see filename: Raw Material.pdf.

See filename: P-25097 Ln 2 FIRST ARTICLE.pdf.

Pechiney Rolled Products Certified Test Report, Pechiney Order No. 108-100073, see filename: P-25097 Ln 2 RAW MATERIAL.pdf.

*The electronic version is the official approved document.
Verify this is the correct version before use.*

NASA-HDBK-5010, VOLUME 2, REVISION A

Space Launch System (SLS) Program/Project	
Revision: baseline	Document No: SLS-SPIO-RPT-013
Release Date:	Page: 13 of 34
Title: SPIE MSA FRACTURE CONTROL SUMMARY REPORT	

Pechiney Rolled Products Certified Test Report, Pechiney Order No. 108-100511, see filename: P-25097 Ln 3 RAW MATERIAL (160223141154).pdf.

2.7.3 Composite Structure: MPTIS Work Order NDE Reports

2016-0868, Sequence 1	Thermographic Inspection Report (Diaphragm, Reference Standard)
2016-0868, Sequence 2	Thermographic Inspection Report (Diaphragm, Post-Cure)
2016-0868, Sequence 3	Thermographic Inspection Report (Diaphragm, Post-Machining)
2016-0868, Sequence 4	Thermographic Inspection Report (Diaphragm, Post-Match Drill)
2016-0868, Sequence 5	Thermographic Inspection Report (Diaphragm, Post-Proof)

2.7.4 Composite Structure: Vendor Planning and Inspection Reports

DIR 10000151455 ZPR 000 03, J-20626	MSA Diaphragm – Manufacturing Plan, Janicki Industries
10000199668 ZPR 000 00	MSA Diaphragm Proof Load Test Report, Janicki Industries

2.8 Procedures, Lifts, and Moves

AS42-SLS-PROC-12-12-1	MPCV Stage Adapter (MSA) Cone Assembly, Removal of MSA Cone Assembly from Vertical Weld Tool (VWT) at Building 4755, and Placing Assembly onto the Floor.
AS42-SLS-PROC-1301-1	MPCV Stage Adapter (MSA) Cone Assembly, Removal of MSA Cone Assembly from Floor at Building 4755, and Placing Assembly onto the Robotic Weld Tool (RWT)
AS42-SLS-PROC-1301-2	MPCV Stage Adapter (MSA) Cone Assembly, Removal of MSA Cone Assembly from Robotic Weld Tool at Building 4755 and Placing Assembly onto the Flat Cart.

3.0 HARDWARE OVERVIEW

A detailed overview of the hardware is provided in section 3.0 of SLS-SPIO-PLAN-017, Rev. A, *SPIE MSA FRACTURE CONTROL PLAN*.

4.0 HARDWARE OPERATION

A description of hardware functions is provided in section 4.0 of SLS-SPIO-PLAN-017, Rev. A, *SPIE MSA FRACTURE CONTROL PLAN*.

5.0 SLS SPIE MSA FRACTURE CONTROL PLAN

The MSA Fracture Control Plan, SLS-SPIO-PLAN-017, Rev. A, was written to provide the planning for the EM-1 SLS MSA, with specific effectivity limited to EM-1, and it has been

*The electronic version is the official approved document.
Verify this is the correct version before use.*

NASA-HDBK-5010, VOLUME 2, REVISION A

Space Launch System (SLS) Program/Project	
Revision: baseline	Document No: SLS-SPIO-RPT-013
Release Date:	Page: 14 of 34
Title: SPIE MSA FRACTURE CONTROL SUMMARY REPORT	

reviewed by the MSFC Fracture Control Board (FCB) several times with approvals of approach identified in the following FCB memoranda: EM20-14-FCB-014, EM20-17-FCB-007.

6.0 FRACTURE CONTROL SUMMARY REPORT REQUIREMENTS

The requirements of the FCSR, appearing below, come from section 4.4.3.d items (1) through (13) in NASA-STD-5019, but with the ordering of the information modified to provide a clear development. This applies to the metallic hardware. The items addressed in each paragraph below are identified at the beginning of the paragraph, as follows:

(Item ##), where ## represents the numbers (1) through (13).

Table 1 discusses the mapping of the FCSR required information from NASA-STD-5019 to the sections within this document.

NASA-STD-5019 Section	Brief Identifier Adopted	FCSR Section
<i>4.4.3.d (1)</i>	<i>1</i>	<i>6.3, 6.4, 6.6.1</i>
<i>4.4.3.d (2)</i>	<i>2</i>	<i>6.1.2</i>
<i>4.4.3.d (3)</i>	<i>3</i>	<i>6.1.3</i>
<i>4.4.3.d (4)</i>	<i>4</i>	<i>6.4.1</i>
<i>4.4.3.d (5)</i>	<i>5</i>	<i>6.1.1, 6.6.2</i>
<i>4.4.3.d (6)</i>	<i>6</i>	<i>6.1.4</i>
<i>4.4.3.d (7)</i>	<i>7</i>	<i>6.1.6</i>
<i>4.4.3.d (8)</i>	<i>8</i>	<i>6.1.5, 6.4.2</i>
<i>4.4.3.d (9)</i>	<i>9</i>	<i>6.5.7, 6.5.10, Appendix C</i>
<i>4.4.3.d (10)</i>	<i>10</i>	<i>6.6.3</i>
<i>4.4.3.d (11)</i>	<i>11</i>	<i>6.4.3</i>
<i>4.4.3.d (12)</i>	<i>12</i>	<i>6.1.8</i>
<i>4.4.3.d (13)</i>	<i>13</i>	<i>6.1.7</i>

For the diaphragm, the contents are dictated by section 7.2 of MSFC-RQMT-3479, specifically items 1 through 9. These will be addressed similarly, but with a “C” prefix on the number:

(Item C#), where # represents the numbers 1 through 9.

Table 2 discusses the mapping of the FCSR required information from the MSFC-RQMT-3479 to the sections within this document.

MSFC-RQMT-3479 Section	Brief Identifier Adopted	Section in FCSR
<i>7.2.1</i>	<i>C1</i>	<i>6.5.2</i>
<i>7.2.2</i>	<i>C2</i>	<i>6.5, 6.5.3, 6.5.4</i>
<i>7.2.3</i>	<i>C3</i>	<i>6.1.3</i>
<i>7.2.4</i>	<i>C4</i>	<i>6.1.1</i>

*The electronic version is the official approved document.
Verify this is the correct version before use.*

NASA-HDBK-5010, VOLUME 2, REVISION A

Space Launch System (SLS) Program/Project	
Revision: baseline	Document No: SLS-SPIO-RPT-013
Release Date:	Page: 15 of 34
Title: SPIE MSA FRACTURE CONTROL SUMMARY REPORT	

Table 2: Location within this Document of FCSR Required Information per MSFC-RQMT-3479 Section 7.2

MSFC-RQMT-3479 Section	Brief Identifier Adopted	Section in FCSR
7.2.5	C5	6.1.6, 6.5.5
7.2.6	C6	6.5.6
7.2.7	C7	6.5.7
7.2.8	C8	6.5.10
7.2.9	C9	2.3, 6.3, Appendix D

6.1 Requirements and Statements Common to All SPIE MSA Hardware

Several of the requirements of NASA-STD-5019 section 4.4.3.d and of MSFC-RQMT-3479 section 7.2 are redundant and some are common to all hardware. These are referenced and discussed in the following sections.

6.1.1 Re-Use of Hardware (Items 5⁷ and C4⁸)

The SLS MSA is a single-use component, and so multiple mission requirements are not applicable.

6.1.2 Life-Limited Hardware (Item 2⁹)

All parts were evaluated, and no limited-life components were identified on the MSA assembly. Details of the design and analysis can be found in SLS-SPIO-RPT-038, *SPIO MSA Structural Assessment Report*.

6.1.3 Pressure Vessels and Rotating Equipment (Items 3¹⁰ and C3¹¹)

The MSA assembly is comprised of a metallic dry thrust structure, a laminar composite volume isolator, electrical cabling, brackets for the secondary payloads and for the electrical interfaces, an avionics box, and the fastener attachments for each. The secondary payloads are not included

⁷ d. As a minimum, the following information shall be provided in the FCSR: (5) Identification of fail-safe parts and a brief statement of the basis for classification. Re-flown fail-safe hardware shall have verification that any required "between mission" inspections have been performed.

⁸ The Fracture Control Summary Report shall provide sufficient information to certify that fracture control requirements have been met. It shall include the following: 4. Evidence for reused hardware that between-mission inspections have been done.

⁹ d. As a minimum, the following information shall be provided in the FCSR: (2) Fracture-critical parts that are limited life shall be specifically identified. A. A statement to the effect that all other parts were examined and determined to be non-fracture critical shall be included.

¹⁰ d. As a minimum, the following information shall be provided in the FCSR: (3) A statement as to whether or not the hardware contains pressure vessels or fracture-critical rotating equipment.

¹¹ The Fracture Control Summary Report shall provide sufficient information to certify that fracture control requirements have been met. It shall include the following: 3. Identification of whether or not pressure vessels, high energy rotating machinery, or high momentum rotating machinery are present.

*The electronic version is the official approved document.
Verify this is the correct version before use.*

NASA-HDBK-5010, VOLUME 2, REVISION A

Space Launch System (SLS) Program/Project	
Revision: baseline	Document No: SLS-SPIO-RPT-013
Release Date:	Page: 16 of 34
Title: SPIE MSA FRACTURE CONTROL SUMMARY REPORT	

in this accounting. The MSA assembly does not contain pressure vessels or any rotating equipment.

6.1.4 Planning and Execution (Item 6¹²)

All planned inspections and tests identified in the SLS-SPIO-PLAN-017, Rev. A and specified on the drawings have been applied. Results can be found in the ADP.

6.1.5 Verification of Materials Usage (Item 8¹³)

The materials used for the MSA primary structure and diaphragm have been verified by a METTS and NASA quality assurance review of the ADP raw material documentation tracing back to the virgin material and all associated NDE results from the mill and/or manufacturer. This data is housed in the SLS SPIE MSA ADP and was audited through the PCA process.

6.1.6 Verification of Hardware Control (Items 7¹⁴ and C5¹⁵)

The flight hardware configuration has been controlled and verified for the EM-1 SLS MSA by METTS and NASA quality assurance activities and documented in all associated manufacturing ADP's which has been provided to the program and audited through the PCA process.

6.1.7 Configuration Management System (Item 13¹⁶)

The configuration management (CM) system is defined. Proposed changes to this document will be submitted by an SPIE change request (CR) to the SPIE Engineering Review Board (ERB) for disposition. All such requests will adhere to the SLS-SPIE-PLAN-032, *SPIE Configuration Management Plan*.

6.1.8 Non-Applicable Requirements (Item 12¹⁷)

The EM-1 SLS MSA parts and procedures require the information that is identified in items (1) through (11), and, as such item (12) is not applicable.

¹² d. As a minimum, the following information shall be provided in the FCSR: (6) A statement that inspections or tests specified for fracture control were applied.

¹³ d. As a minimum, the following information shall be provided in the FCSR: (8) A statement that materials usage has been verified for fracture-critical parts.

¹⁴ d. As a minimum, the following information shall be provided in the FCSR: (7) A statement that the flight hardware configuration has been controlled and verified for all fracture-critical parts.

¹⁵ The Fracture Control Summary Report shall provide sufficient information to certify that fracture control requirements have been met. It shall include the following: 5. Evidence that hardware configuration has been controlled and verified for fail safe parts (including redundant load paths), composite containment enclosures, low risk parts, NHLBB items, and fracture critical parts.

¹⁶ d. As a minimum, the following information shall be provided in the FCSR: (13) If applicable, a summary of the configuration management (CM) system used to store records.

¹⁷ d. As a minimum, the following information shall be provided in the FCSR: (12) If during the program, no parts or procedures are identified that require information as listed above, a statement to that effect with reference to supporting documentation shall be submitted as the FCSR.

*The electronic version is the official approved document.
Verify this is the correct version before use.*

NASA-HDBK-5010, VOLUME 2, REVISION A

Space Launch System (SLS) Program/Project	
Revision: baseline	Document No: SLS-SPIO-RPT-013
Release Date:	Page: 17 of 34
Title: SPIE MSA FRACTURE CONTROL SUMMARY REPORT	

6.2 Classifications of MSA Hardware

The following is an excerpt from the fracture control plan, modified to refer to the tables of classifications shown in this document.

The ISPE consists of four components: MSA, LVSA, ICPS, and separation system, but this document will discuss fracture control of only the MSA in detail. Fracture control of the other components is covered by the respective vendors. Attachment hardware for integration of the MSA to the Multi-Purpose Crew Vehicle (MPCV) and to the Interim Cryogenic Propulsion System (ICPS) are not a part of the MSA and fracture control of those items is not discussed herein. The interface joint fasteners for the MPCV-to-MSA joint are the responsibility of the MPCV designers, and the interface joint fasteners for the MSA-to-ICPS joint are the responsibility of the ICPS designers.

Two tables of the components of the MSA appear below along with fracture control classifications: Table 3, fracture critical and Table 4, non-fracture critical (including exempt). Fracture control planning and execution for the MSA was completed for EFT-1, and most of the fracture control classifications were evaluated to the SLS loads, and so classifications should not change from EFT-1. The diaphragm is designed by MSFC, with Langley Research Center responsible for the manufacture of it. The fracture control classification for the diaphragm remains fracture critical. The fracture control summary report (FCSR) will discuss the approach relevant to each component and summarize the results, discussion, and conclusions associated with fracture control for the MSA assembly.

Secondary payload brackets (SPB) have been added to the design, and these are inserted into this document. The wiring harnesses associated with secondary payloads and avionics were also added. The secondary payload providers will be responsible for fracture control for their equipment: secondary payloads plus vibration isolators and dispensers.

6.3 Fracture Critical Hardware (Items 1¹⁸ and C9¹⁹)

Fracture critical parts have been identified as such on the engineering drawings to alert all who use the drawings as to the criticality of the part. The section below discusses additional requirements associated with fracture critical parts.

The metallic components identified as fracture critical in table 3 (all but the last of the items listed) will have requirements, as follows:

- Safe-life assessment
- NDE evaluation

¹⁸ d. As a minimum, the following information shall be provided in the FCSR: (1) Identification of fracture-critical parts and low-risk fracture parts, showing the material and heat treatment used and the basis for part acceptability (i.e., damage tolerant analysis, test, acceptable durability, insignificant fatigue loading), including the referencing of documents which contain and describe the supporting data required to demonstrate fracture control requirements of the Agency, responsible Center, and Program.

¹⁹ The Fracture Control Summary Report shall provide sufficient information to certify that fracture control requirements have been met. It shall include the following: 9. Drawings and sketches referenced in tabular summary.

*The electronic version is the official approved document.
Verify this is the correct version before use.*

NASA-HDBK-5010, VOLUME 2, REVISION A

Space Launch System (SLS) Program/Project	
Revision: baseline	Document No: SLS-SPIO-RPT-013
Release Date:	Page: 18 of 34
Title: SPIE MSA FRACTURE CONTROL SUMMARY REPORT	

- Serialization of parts
- Traceability of records of manufacture:
 - Design and Analysis
 - Hardware Configuration
 - Materials
 - Manufacturing

The parenthetic numbers in the table refer to sections in the fracture control plan where the classifications are discussed.

The last four items in table 3, are the parts and details of the MSA diaphragm and diaphragm housings, which form a composite structure that has been classified as fracture critical, and it has requirements, as follows:

- Damage Threat Assessment (DTA)
- Impact Damage Protection Plan (IDPP)

Fracture control-related processing of the MSA diaphragm appears in a section, below.

*The electronic version is the official approved document.
Verify this is the correct version before use.*

APPROVED FOR PUBLIC RELEASE – DISTRIBUTION IS UNLIMITED

NASA-HDBK-5010, VOLUME 2, REVISION A

Space Launch System (SLS) Program/Project	
Revision: baseline	Document No: SLS-SPIO-RPT-013
Release Date:	Page: 19 of 34
Title: SPIE MSA FRACTURE CONTROL SUMMARY REPORT	

Table 3: Fracture Control Classifications, Group 1, Fracture Critical Parts

Drawing Number(s)	Part Description	Material or Process	Classification (FCP Section in Parentheses)
MSA Components			
97M62121-001, 97M62122-001, 97M62123-001	MSA barrel panels 1, 2, and 3, respectively	2195-T8M4	Fracture Critical (§5.3)
97M62124-001	MSA barrel welds	conventional longitudinal FSW 2195-T8M4 plate to 2195-T8M4 plate	
97M62125-001	MSA forward ring	2219-T851 rolled ring forging	
97M62127-001	MSA aft ring	2219-T851 rolled ring forging	
97M62124-001	MSA flange to barrel welds (fore- and aft-)	self-reacting circumferential FSW 2195-T8M4 plate to 2219-T851 rolled ring forging	
97M62120-001	Machine-drilled assembly (MSA)	Weldment (2195 and 2219, per above)	Fracture Critical (§5.3)
97M62140-001	MSA diaphragm	laminare composite dome, (Newport NB32 I 3K 70P)	Fracture Critical (§§5.2 & 5.3)
97M62141-001	diaphragm machine drill, MSA	laminare composite dome, (Newport NB32 I 3K 70P)	Fracture Critical (§§5.2 & 5.3)
97M62142-001	diaphragm layup, MSA	laminare composite dome, (Newport NB32 I 3K 70P)	Fracture Critical (§§5.2 & 5.3)
97M62144-001	Diaphragm housing	laminare composite dome, (Newport NB32 I 3K 70P)	Fracture Critical (§§5.2 & 5.3)

6.4 MSA Primary Structure: Fracture Critical (Item 1²⁰)

The MSA primary structure, composed of the barrel panels, the mounting rings, and the longitudinal and circumferential welds was classified as fracture critical.

The primary structure isogrid nodes have been discussed in SLS-SPIO-PLAN-017, Rev. A, *SPIE MSA FRACTURE CONTROL PLAN*, Section 5.4.7, ft

Alternate Approach for the Threaded Nodes of the Barrel Panels”. Loads arise from the primary structural loads seen by the MSA, by the attachment of the secondary payload brackets and

²⁰ d. As a minimum, the following information shall be provided in the FCSR: (1) Identification of fracture-critical parts and low-risk fracture parts, showing the material and heat treatment used and the basis for part acceptability (i.e., damage tolerant analysis, test, acceptable durability, insignificant fatigue loading), including the referencing of documents which contain and describe the supporting data required to demonstrate fracture control requirements of the Agency, responsible Center, and Program.

*The electronic version is the official approved document.
Verify this is the correct version before use.*

NASA-HDBK-5010, VOLUME 2, REVISION A

Space Launch System (SLS) Program/Project	
Revision: baseline	Document No: SLS-SPIO-RPT-013
Release Date:	Page: 20 of 34
Title: SPIE MSA FRACTURE CONTROL SUMMARY REPORT	

electrical interface brackets to the MSA, and by the attachment of the secondary payload wiring. The nodes are failsafe relative to the attachment to the brackets, and any piece torn from the node would be contained by the bolt threaded into it. The attachment of the wiring to nodes and the primary loads are low-risk by an alternative rationale, characterized in the fracture control plan.

A safe-life assessment has been performed and the results show that the MSA primary structure meets the durability requirement with results showing more than four lives. The details of the design and analysis can be found in SLS-SPIO-RPT-038, *SPIE MSA Structural Assessment Report*. The contents discuss first the establishment of the load spectrum, leading to the local normalized stresses. The safe-life analysis was conducted by identifying 18 control points to evaluate high stress and lower strength points on the primary structure. These points were selected consistent with the “parts” in table 3, above. The circumferential weld control points 4 and 15 correspond the peak stress location along the weld, which is above or under an axial weld land. Those same points are used to evaluate the weld closeout hole, even though the holes are located in the center of a panel where the stress level is lower. Control points 17 and 18 are points on the aft ring skin that experience the highest stress during ascent and transportation respectively. The locations and significance of the control points can be seen in figure 1, below.

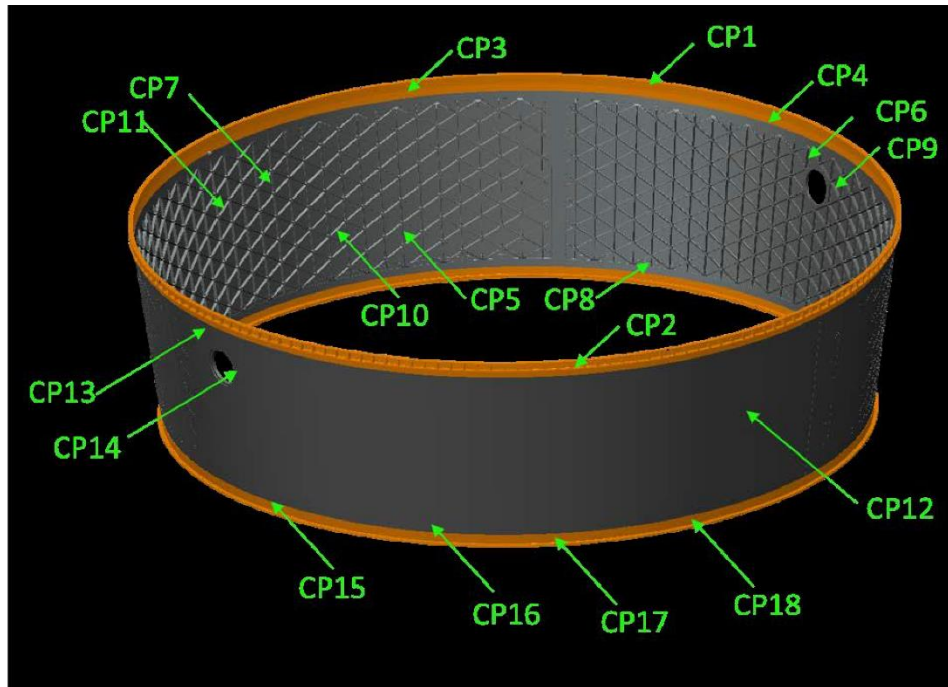


Figure 1: MSA Primary Structure, Identifying the Analyzed Control Points (CP).

*The electronic version is the official approved document.
Verify this is the correct version before use.*

NASA-HDBK-5010, VOLUME 2, REVISION A

Space Launch System (SLS) Program/Project	
Revision: baseline	Document No: SLS-SPIO-RPT-013
Release Date:	Page: 21 of 34
Title: SPIE MSA FRACTURE CONTROL SUMMARY REPORT	

The MSA panels and rings receive penetrant inspection. The axial welds receive penetrant inspection on the root side and phased array ultrasonic inspection. The circumferential welds receive a phased array ultrasonic inspection. All weld intersections and overlap regions also receive a radiographic inspection. All machined holes receive an eddy current inspection. The initial flaw size for the non-weld regions receiving penetrant inspection is based on the minimum detectable flaw size for penetrant NDE in NASA-STD-5009. The initial flaw size for the weld regions is based on twice the rejectable flaw size listed on the drawing, or a 0.250-inch-long through flaw or a 0.500 long half depth flaw. The initial flaw size for the 0.75-inch diameter weld closeout hole in the forward and aft circumferential weld is based on the minimum detectable flaw size for eddy current NDE in NASA-STD-5009 (0.075 inch by 0.075-inch corner crack).

Table 4: Some Details of Analyzed Control Points on the MSA Primary Structure

CP	Feature	Location	Material
1	Forward Ring	Back Wall	Ring
2	Forward Ring	Bottom Flange	Ring
3	Forward Ring	Aft Skin	Ring
4	Forward Ring	Circ Weld	Weld
5	Axial Rib	Acreage	Panel
6	Axial Rib	Port	Panel
7	Axial Rib	Cube Sat	Panel
8	Axial Rib	Aft Runout	Panel
9	Diagonal Rib	Port 165	Panel
10	Diagonal Rib	Acreage	Panel
11	Diagonal Rib	Cube Sat	Panel
12	Skin	Acreage	Panel
13	Skin	Fwd Transition	Panel
14	Skin	Port	Panel
15	Aft Ring	Circ Weld	Weld
16	Aft Ring	Forward Skin	Ring
17	Aft Ring	Aft Skin	Ring
18	Aft Ring	Aft Skin - Trans	Ring

A survey of compliance of the MSA primary structure with NASA-STD-5019 has been recorded in VCN-List_Frac_Control--SPIE_MSA_2017-12-27.xlsx.

6.4.1 Nondestructive Evaluation of Metallic Hardware (Item 4)

The MSA structure has been subjected to NDE, including ultrasonic inspection of the supplied raw stock, liquid fluorescent dye-penetrant inspection of the barrel panels and ring flanges, and

*The electronic version is the official approved document.
Verify this is the correct version before use.*

NASA-HDBK-5010, VOLUME 2, REVISION A

Space Launch System (SLS) Program/Project	
Revision: baseline	Document No: SLS-SPIO-RPT-013
Release Date:	Page: 22 of 34
Title: SPIE MSA FRACTURE CONTROL SUMMARY REPORT	

phased-array ultrasonic inspection of the welds. All welds, rings, and panels were found to be acceptable, and no indications were found.

The vendor NDE reports for the aft ring forging are:

ATI Latish Forging Quality Department Ultrasonic Inspection Report, Ref Ladish Job J32807, see filename: P-S 68862 NM007.pdf.

Major Tool & Machine Nondestructive Test Certification for Liquid Penetrant Examination, NDT#63601, see filename: SN001_NDE.pdf.

The vendor NDE reports for the forward ring forging are:

ATI Latish Forging Quality Department Ultrasonic Inspection Report, Ref Ladish Job J32808, see filename: Inspection_P-S 68863 NM008.pdf.

Major Tool & Machine Nondestructive Test Certification for Liquid Penetrant Examination, NDT#63602, see filename: SN001_NDE.pdf.

The vendors' NDE reports for the as-fabricated and heat treated barrel panels are listed, below.

AMRO Fabricating Corporation, AFC # 551-121, Certificate of conformance, see filename: Inspection Record12.pdf

Pechiney Rolled Products Certified Test Report, Pechiney Order No. 108-100073, see filename: Raw Material.pdf.

See filename: P-25097 Ln 2 FIRST ARTICLE.pdf.

Pechiney Rolled Products Certified Test Report, Pechiney Order No. 108-100073, see filename: P-25097 Ln 2 RAW MATERIAL.pdf.

Pechiney Rolled Products Certified Test Report, Pechiney Order No. 108-100511, see filename: P-25097 Ln 3 RAW MATERIAL (160223141154).pdf.

The MAPTIS work request system reports for all of the primary structure NDE inspections are listed, below.

2016-0243, Sequence 1, MSA-3 (EM-1) Cone Weld NDE (Weld A)

2016-0243, Sequence 2, Cone Weld NDE (Weld B)

2016-0243, Sequence 3, MSA-3 (EM-1) Cone Weld NDE (Weld C)

2016-0243, Sequence 4, Weld A, Weld B, Weld C (Ultrasonic Inspection Report)

2016-0435, Sequence 3, MSA-3 field RT

2016-0435, Sequence 1, MSA-3 (EM-1) Forward Circ. Weld (Ultrasonic Inspection Report)

2016-0435, Sequence 2, MSA-3 (EM-1) Aft Circ. Weld (Ultrasonic Inspection Report)

2016-0844, Sequence 1, FWD & AFT Flange Hole Eddy Current for MSA-3

2016-0870, Sequence 1, Flange Machined Surfaces (Penetrant Inspection)

*The electronic version is the official approved document.
Verify this is the correct version before use.*

APPROVED FOR PUBLIC RELEASE – DISTRIBUTION IS UNLIMITED

NASA-HDBK-5010, VOLUME 2, REVISION A

Space Launch System (SLS) Program/Project	
Revision: baseline	Document No: SLS-SPIO-RPT-013
Release Date:	Page: 23 of 34
Title: SPIE MSA FRACTURE CONTROL SUMMARY REPORT	

6.4.2 Materials Usage Agreements Verifications (Item 8²¹)

Approved Materials Usage Agreements (MUAs) have been developed. These MUAs cover

- SLS-MSA-0001, *No Rolled-Ring Qualification Article*
 - MUA discussing applicability of Ares I forging qualification testing to the MSA ring forging qualification article (NASA-STD-6016 section 4.2.3.1.h).
- SLS-MSA-0002, *Design Properties for Multi-Purpose Crew Vehicle Stage Adapter*
 - MUA documenting the Materials and Processes Laboratory's recommended design properties for the MSA (NASA-STD-6016 section 4.1.6).
- SLS-MSA-0003, *No Barrel-Forming Qualification Article*
 - MUA documents the rationale for proceeding without a first article cut-up for barrel forming (ARES-USO-MP-25512 section 3.5).
- SLS-MSA-0004, *Al-Li 2195 plates were not purchased to the Ares-USO-MP-2555 specification indicated on the drawing*
 - MUA discusses the fact that the Ares 2195 plate specification was not used to procure plate materials for the barrel panels.
- SLS-MSA-0006, *Stress corrosion cracking of Al-Li 2195*

All MUAs have been provided as an appendix to this report. The material usage verifications will be found in the ADP.

6.4.3 Special Considerations (Item 11²²)

The fore- and aft- mounting flanges of the MSA were manufactured by a ring forging process using 2219-T851 aluminum alloy. Data was provided using remnants from the ring forging at various locations within the cross-section near the section of the rings used to produce the mounting flanges. This has been documented using MUA SLS-SPIO-0001, *No Rolled-Ring Qualification Article*.

No data was available for the ring-to-barrel welds. This weld is a circumferential, self-reacting friction-stir weld, and the ring is a 2219-T851 forging with the barrels made from 2195-T8M4 alloy. Citing a rule of mixtures approach, the friction-stirred weld zone should have properties between welds of 2219 to 2219 and those of 2195 to 2195. To establish conservatism, 2219 to 2219 plate welds information was used. This has been documented using MUA SLS-MSA-0002, *Design Properties for Multi-Purpose Crew Vehicle Stage Adapter*.

²¹ d. As a minimum, the following information shall be provided in the FCSR: (8) A statement that materials usage has been verified for fracture-critical parts.

²² d. As a minimum, the following information shall be provided in the FCSR: (11) If applicable, identification of any special considerations involving fracture mechanics properties or data, inspections, analysis, or other parameters not covered by the requirements set here.

*The electronic version is the official approved document.
Verify this is the correct version before use.*

NASA-HDBK-5010, VOLUME 2, REVISION A

Space Launch System (SLS) Program/Project	
Revision: baseline	Document No: SLS-SPIO-RPT-013
Release Date:	Page: 24 of 34
Title: SPIE MSA FRACTURE CONTROL SUMMARY REPORT	

6.5 MSA Diaphragm: Fracture Critical (Item C2²³)

The MSA diaphragm is a laminar composite dome. Functioning as a volume isolator, the diaphragm is subjected to inertial loads, changes of temperature, and potentially a net differential pressure. This pressure differential can produce a net pressure above the diaphragm, creating a “buckling”-type loading, or below the diaphragm, creating a “burst”-type loading. Requirement MPCV 70026 I.MPCV-SLS.3162, *MSA Volume Isolator Leak Area*, defines an allowable leakage area. This suggests that some leakage of fluid would not be an issue. Because the consequences of buckling or burst failure modes are not known, the MSA diaphragm has been conservatively classified as fracture critical.

Non-metallic fracture critical components are required to be shown to be under fracture control by either a damage tolerant approach or a proof test approach, and the latter was adopted. This approach is straight forward, requiring that flight articles be proofed in excess of the anticipated flight loads (MSFC-RQMT-3479, Section 5.3.1). The part must be evaluated using nondestructive testing before and after the proof test, and this will include the areage of the dome, the flange, and the transition region where the dome curves into the flange. No indications were observed in the NDE results.

The fracture classification listed on the relevant diaphragm housing drawings is fracture critical, and the housings satisfy this criteria, as well. No failure modes different than those of the diaphragm were identified, i.e., burst or buckle. The housings were proof tested as integral parts of the diaphragm, with NDE before and after the proof test, and they satisfy the proof test approach to fracture critical composite parts. No indications were observed in the NDE results.

It should be noted that the diaphragm to housing interfaces are bolted, and these were shown to meet the requirements of the NFC fail-safe classification for the current design in SLS-SPIO-RPT-038, *SPIE MSA Structural Assessment Report*, Appendix E, Section 6.8.2.

Potential damage sources must be identified per damage threat assessment (DTA) task 1, and an impact damage protection plan (IDPP) must be put into place to ensure that any damage inflicted after the proof test is either benign or is at least known to have occurred. These two required activities are provided in SLS-SPIO-PLAN-017, Rev. A, *SPIE MSA Fracture Control Plan*.

6.5.1 Failure Modes

The fracture assessment for the MSA diaphragm indicated that two failure modes were credible: a burst mode, where the pressure below the dome was higher than above, and a buckling mode. The former mode results in a strength failure which uses a high design factor of safety of 2.0 and is pressure-relieving. The latter results in a buckling failure which uses a 1.5 factor of safety and is the failure mode of concern. Therefore, this is the failure mode considered for fracture control and the proof test.

²³ The Fracture Control Summary Report shall provide sufficient information to certify that fracture control requirements have been met. It shall include the following: 2. A tabular listing of all non-exempt composite parts (bonds), providing for each part: name, drawing number, material, NDE, fracture control classification, and reference to part sketch or drawing included in the report.

*The electronic version is the official approved document.
Verify this is the correct version before use.*

NASA-HDBK-5010, VOLUME 2, REVISION A

Space Launch System (SLS) Program/Project	
Revision: baseline	Document No: SLS-SPIO-RPT-013
Release Date:	Page: 25 of 34
Title: SPIE MSA FRACTURE CONTROL SUMMARY REPORT	

Analysis, recorded in SLS-SPIO-RPT-038, *SPIE MSA Structural Assessment Report*, Section 6.0 and Appendix E indicated that the diaphragm was quite robust. The EM-1 diaphragm was analyzed with twelve five-inch holes around the perimeter and six along a meridian through the top of the diaphragm and passing from one electrical pass-through hole to the other, and positive margins of safety resulted against buckling. The analysis was performed to SLS loads and environments, and it was found that the diaphragm was capable of sustaining damage simulated by the ten five-inch holes without buckling. A diameter of two-inches was selected for the acceptance criteria for the diaphragm in the acreage. An analysis of the flange region of the diaphragm was conducted by removing elements of the diaphragm model. This analysis indicated that a one-square-inch size did not change the margin of safety appreciably, and the resulting stress raiser was localized to within three-inches of the induced flaw. Resulting from this, an acceptance criterion of one square inch was used in the flange. This allowable flaw size was provided on the manufacturing drawings and was the basis of the NDE detection size used for evaluations of the hardware.

6.5.2 Exempt Composite Hardware (Item C1²⁴)

There is no exempt composite hardware.

6.5.3 Non-Exempt Composite Parts (Item C2²⁵)

No tabular list is provided, since there are only two non-exempt composite parts: the diaphragm and the diaphragm housings, discussed above. The diaphragm with the integrated diaphragm housings is classified fracture critical and is considered damage tolerant using the proof test approach. For the diaphragm with integrated diaphragm housings, the name, drawing number, material, fracture control classification, and damage-tolerant approach appear in section 6.5, above, and the NDE details appear in the paragraphs, below. Below is a bullet listing of the requirements of item C2:

- MSA diaphragm, 97M62140-001 and Diaphragm housing, 97M62144-001
- Fracture critical composites, damage tolerant per the proof test approach
- Material is 3K70P/NB321 Carbon Plain Weave Fabric
- NDE: thermography is used to evaluate the housing

Details of the design analysis appear in SLS-SPIO-RPT-038, *SPIE MSA Structural Assessment Report*, Section 6.0 and Appendix E, and the results of the proof test appear in document 10000199668 ZPR 000 00, *Janicki Industries MSA Diaphragm Proof Load Test Report*. All

²⁴ The Fracture Control Summary Report shall provide sufficient information to certify that fracture control requirements have been met. It shall include the following: 1. Identification of exempted hardware.

²⁵ The Fracture Control Summary Report shall provide sufficient information to certify that fracture control requirements have been met. It shall include the following: 2. A tabular listing of all non-exempt composite parts (bonds), providing for each part: name, drawing number, material, NDE, fracture control classification, and reference to part sketch or drawing included in the report.

*The electronic version is the official approved document.
Verify this is the correct version before use.*

NASA-HDBK-5010, VOLUME 2, REVISION A

Space Launch System (SLS) Program/Project	
Revision: baseline	Document No: SLS-SPIO-RPT-013
Release Date:	Page: 26 of 34
Title: SPIE MSA FRACTURE CONTROL SUMMARY REPORT	

inspections and tests specified by the Fracture Control Plan were applied, and the results appear in the ADP records, and in the EM21 inspections records on the EM20 server.

A survey of compliance of the MSA diaphragm with MSFC-RQMT-3479 has been recorded in VCN-List_Frac_Control--SPIE_MSA_2017-12-27.xlsx.

The diaphragm and diaphragm housings followed the proof test approach for fracture critical composite and bonded hardware.

- Load paths, loads, and boundary conditions are well-defined and relatively simple.
- The design of the diaphragm is driven by the potential for buckling, and this is believed to be the principal failure mode, and the proof test induced a buckling-type pressure load.
- A proof factor of 1.2 was used with an environmental correction factor of 1.14 to allow testing at room temperature. These values are recorded in document 10000199668 ZPR 000 00, *Janicki Industries MSA Diaphragm Proof Load Test Report*. This load has been shown to be below the 80% limit identified in MSFC-RQMT-3479, and details can be found in SLS-SPIO-RPT-038, *SPIO MSA Structural Assessment Report*, Section 6.0 and Appendix E.
- The effectiveness of the proof test was evaluated by the diaphragm design and analysis team, and the results appear in SLS-SPIO-RPT-038, *SPIO MSA Structural Assessment Report*, Section 6.0 and Appendix E. Included were the evaluations for the acreage of the diaphragm, as well as in the flange, and the transition from acreage to flange. Thereby, all areas of concern were properly proof tested.
- The diaphragm and housings was inspected for flaws pre- and post-proof (NDE and visual inspection), and these inspections occurred prior to shipment from the manufacturing vendor and immediately following the proof test, respectively. The inspection criteria were established by the diaphragm design and analysis team and appears in SLS-SPIO-RPT-038, *SPIE MSA Structural Assessment Report*, Section 6.0 and Appendix E, and as drawing notes (97M62140-001, *MSA Diaphragm Assembly*).

This approach was accepted by the FCB, and documented in the FCB memoranda EM20-14-FCB-014 and EM20-17-FCB-007.

6.5.4 Nondestructive Evaluation (NDE) of Composite Hardware (Item C2²⁶)

Acceptance criteria for the different regions were established (see section 6.5.1, above), and infrared thermography was set up to find flaws of half of the value of those criteria. Thermographic evaluation was performed by the vendor, and the MSA diaphragm was then evaluated using thermography after the proof test. Both evaluations showed the diaphragm to be

²⁶ The Fracture Control Summary Report shall provide sufficient information to certify that fracture control requirements have been met. It shall include the following: 2. A tabular listing of all non-exempt composite parts (bonds), providing for each part: name, drawing number, material, NDE, fracture control classification, and reference to part sketch or drawing included in the report.

*The electronic version is the official approved document.
Verify this is the correct version before use.*

NASA-HDBK-5010, VOLUME 2, REVISION A

Space Launch System (SLS) Program/Project	
Revision: baseline	Document No: SLS-SPIO-RPT-013
Release Date:	Page: 27 of 34
Title: SPIE MSA FRACTURE CONTROL SUMMARY REPORT	

free of inclusions and undamaged. NDE inspection results appear in the MAPTIS Work Request System, as identified below.

- 2016-0868, Sequence 1, Thermographic Inspection Report (Diaphragm, Reference Standard)
- 2016-0868, Sequence 2, Thermographic Inspection Report (Diaphragm, Post-Cure)
- 2016-0868, Sequence 3, Thermographic Inspection Report (Diaphragm, Post-Machining)
- 2016-0868, Sequence 4, Thermographic Inspection Report (Diaphragm, Post-Match Drill)
- 2016-0868, Sequence 5, Thermographic Inspection Report (Diaphragm, Post-Proof)

6.5.5 Control of Composite Hardware (Item C5²⁷)

Flight hardware configuration has been controlled and verified for the MSA diaphragm. This is essentially the subject of the ADP.

6.5.6 Verification of Materials Used for Fail-Safe Composite Hardware (Item C6²⁸)

There are no process certifications for composites. Instead, an equivalence testing program was conducted to certify the personnel, equipment, and facility to process the material. The equivalence reports are in LaRC-SLS-MSA-01-024, *LaRC MSA Composite Material Testing Summary and Results*. This document was generated for the EFT-1 spacecraft. This has been characterized in an MUA # SLS-MSA-0005, *MPCV Stage Adaptor Design Properties*. Verifications to these MUA's will appear in the ADP.

6.5.7 Materials Usage Agreements (Items 9²⁹ and C7³⁰)

For the diaphragm, an MUA # SLS-MSA-0005, *MPCV Stage Adaptor Design Properties* discusses the composite material used. This MUA has been provided as an appendix to this report.

²⁷ The Fracture Control Summary Report shall provide sufficient information to certify that fracture control requirements have been met. It shall include the following: 5. Evidence that hardware configuration has been controlled and verified for fail safe parts (including redundant load paths), composite containment enclosures, low risk parts, NHLBB items, and fracture critical parts.

²⁸ The Fracture Control Summary Report shall provide sufficient information to certify that fracture control requirements have been met. It shall include the following: 6. Evidence that materials usage has been verified for fail safe parts (including redundant load paths), composite containment enclosures, low risk parts, NHLBB items, and fracture critical parts.

²⁹ d. As a minimum, the following information shall be provided in the FCSR: (9) Copies of MUAs for fracture-critical or low-risk parts and a summary of the discrepancy reviews, or equivalent reviews, of anomalies that could affect the performance of fracture-critical parts.

³⁰ The Fracture Control Summary Report shall provide sufficient information to certify that fracture control requirements have been met. It shall include the following: 7. List of material usage agreements (MUAs) for fail safe parts (including redundant load paths), composite containment enclosures, low risk parts, NHLBB items, and

*The electronic version is the official approved document.
Verify this is the correct version before use.*

NASA-HDBK-5010, VOLUME 2, REVISION A

Space Launch System (SLS) Program/Project	
Revision: baseline	Document No: SLS-SPIO-RPT-013
Release Date:	Page: 28 of 34
Title: SPIE MSA FRACTURE CONTROL SUMMARY REPORT	

6.5.8 Damage Threat Assessment

Task 1 of the damage threat assessment (DTA) was tailored from the Ares-USO-SE-25753 (draft) *Upper Stage Damage Threat Assessment for Composite and Bonded Structures*. This provided a quick way to quantify the threats to the diaphragm. The DTA appears as an appendix in SLS-SPIO-PLAN-017, Rev. A, *SPIE MSA FRACTURE CONTROL PLAN*.

6.5.9 Impact Damage Protection Plan

An impact damage protection plan (IDPP) was provided in the FCP that relied on good manufacturing and handling practices, isolation of the diaphragm, and then added visual inspections at key points to identify damage. The size of damage that could be sustained without a failure was estimated to be very large, and this can be found in SLS-SPIO-RPT-038, *SPIO MSA Structural Assessment Report*, Section 6.0 and Appendix E.

6.5.10 Summary of Flaws Detected and Deviations (Items 9³¹ and C8³²)

There were no flaws detected in the MSA welded assembly.

There were no flaws detected in the MSA diaphragm. Below is a list of discrepancies reported.

- DR #8780 was written for a non-conformance (Janicki NCMR 7723) because the temperatures of diaphragm materials were not recorded in transit. This was accepted for “use as is”, after re-testing of the materials.
- DR #8823 was written for diaphragm ply angles for the +/- 45-degree plies deviating by as much as 14-degrees. This was presented to the ERB on 23 March 2017, and was accepted for “use as is”.
- DR #8862 and #8863 were written against electrical housings drilling errors (Janicki NCMRs 8105 and 8106). These were presented to the ERB on 17 January 2017 and were accepted for “use as is” after patching gouged holes.

6.6 Secondary Structure: Non-Fracture Critical

A survey of compliance of the MSA secondary structure with NASA-STD-5019 has been recorded in VCN-List_Frac_Control--SPIE_MSA_2017-12-27.xlsx.

6.6.1 Low-Risk Parts (Item 1³³)

The cable attach bracket, and associated bolts and spacers and the access cover were shown to be non-fracture critical by virtue of the low-risk classification, as shown in table 6. Details of the

fracture critical parts. Also, a summary of any discrepancies or deviations from design that could affect the structural integrity of these parts is required.

³¹ d. As a minimum, the following information shall be provided in the FCSR: (9) Copies of MUAs for fracture-critical or low-risk parts and a summary of the discrepancy reviews, or equivalent reviews, of anomalies that could affect the performance of fracture-critical parts.

³² The Fracture Control Summary Report shall provide sufficient information to certify that fracture control requirements have been met. It shall include the following: 8. A summary of flaw detections and their resolutions.

³³ d. As a minimum, the following information shall be provided in the FCSR: (1) Identification of fracture-critical parts and low-risk fracture parts, showing the material and heat treatment used and the basis for part acceptability

*The electronic version is the official approved document.
Verify this is the correct version before use.*

NASA-HDBK-5010, VOLUME 2, REVISION A

Space Launch System (SLS) Program/Project	
Revision: baseline	Document No: SLS-SPIO-RPT-013
Release Date:	Page: 29 of 34
Title: SPIE MSA FRACTURE CONTROL SUMMARY REPORT	

analysis for each can be found in SLS-SPIO-RPT-038, *SPIO MSA Structural Assessment Report*, Section 5.12.

Table 5: Low-Risk, Non-Fracture Critical Parts

Part Description	Material or Process	Classification (FCP Section in Parentheses)	Basis of Classification
access cover	2219-T876 plate	low risk (§5.4.1)	analysis
cable attach bracket	2219-T851	low risk (§5.4.1)	analysis
cable attach bracket bolt	IN718	low risk fasteners and rivets (§5.4.10)	analysis
cable attach spacers	CRES A286	low risk (§5.4.1)	analysis

6.6.2 Fail-Safe Parts (Item 5³⁴)

The parts in Tables 7 and 8 have been classified as fail-safe, non-fracture critical. The bolts and nuts and inserts used for integrating the diaphragm to the MSA, mounting and assembling the forward electrical panel to the MSA, and mounting the electrical cabling to the MSA were found to be fail-safe and low released-mass. For low-released mass, velocity $v_{bolt} \leq 35$ ft/sec, momentum $p_{bolt} \leq 8.75$ ft-lb/sec, and for low toughness materials, mass $m_{bolt} \leq 0.03$ lbm. These criteria were established for shuttle cargo bay, and they are being used as reasonable here. The analysis has been summarized in Appendix E of this report, and the detailed analysis can be found in *MSA_BoltInitialVelocity_WithFractureEnergy_2017-11-13.xlsx*. In that spreadsheet are worksheets for each of the bolt applications, and the resulting values of p_{bolt} , v_{bolt} , and m_{bolt} have been highlighted. The analyses show that for the critical flaw size identified using linear-elastic fracture mechanics, the net-section stress is reached before the crack driving force reaches the fracture toughness of the fasteners, and so the preload is released. The crack is not likely to fail, but if it were, the remaining potential energy does not produce sufficient momentum or velocity to violate the low-released mass requirements of 5019.

The wiring harness mounting brackets that affix the electrical cabling to the MSA and the secondary payload brackets are fail-safe, as well. The analysis of all of the MSA fail-safe parts is shown in SLS-SPIO-RPT-038, *SPIO MSA Structural Assessment Report*.

The forward electrical panel was classified as fail-safe. This component supports the electrical cabling that passes through the panel. All failure modes identified for the panels showed the remaining pieces of the panel would not fail.

(i.e., damage tolerant analysis, test, acceptable durability, insignificant fatigue loading), including the referencing of documents which contain and describe the supporting data required to demonstrate fracture control requirements of the Agency, responsible Center, and Program.

³⁴ d. As a minimum, the following information shall be provided in the FCSR: (5) Identification of fail-safe parts and a brief statement of the basis for classification. Re-flown fail-safe hardware shall have verification that any required "between mission" inspections have been performed.

*The electronic version is the official approved document.
Verify this is the correct version before use.*

NASA-HDBK-5010, VOLUME 2, REVISION A

Space Launch System (SLS) Program/Project	
Revision: baseline	Document No: SLS-SPIO-RPT-013
Release Date:	Page: 30 of 34
Title: SPIE MSA FRACTURE CONTROL SUMMARY REPORT	

Table 6: Fasteners—Fail-Safe and Low Released-Mass

Part Description	Material or Process	Classification (<i>FCP Section in Parentheses</i>)	Basis of Classification
diaphragm attach bolts	aerospace bolts, A286	failsafe and low released-mass (§§5.4.2 – 5.4.3)	analysis
diaphragm attach nuts	aerospace nuts 5/16-in dia., A286	failsafe and low released-mass (§§5.4.2 – 5.4.3)	analysis
electrical interface bracket mounting bolts	A286	failsafe and low released-mass (§§5.4.2 – 5.4.3)	analysis
#10-32 cap screw, electrical connector plate mount	aerospace cap screw, 18-8 stainless	failsafe and low released-mass (§§5.4.2 – 5.4.3)	analysis
Rivet, solid, countersunk, connector plate mount	AL-2117-T4	failsafe and low released-mass (§§5.4.2 – 5.4.3)	analysis
#10-32 self-locking nut plate, connector plate mount	CRES, silver plated	failsafe and low released-mass (§§5.4.2 – 5.4.3)	analysis
Secondary payload bracket assembly bolt	A286	failsafe and low released-mass (§§5.4.2 – 5.4.3)	analysis
Secondary payload bracket assembly nut(s)	A286	failsafe and low released-mass (§§5.4.2 – 5.4.3)	analysis
Secondary payload bracket mounting bolt	IN718	failsafe and low released-mass (§§5.4.2 – 5.4.3)	analysis
Avionics mounting screw	CRES steel	failsafe and low released-mass (§§5.4.2 – 5.4.3)	analysis
Avionics lid to box screw	CRES steel	failsafe and low released-mass (§§5.4.2 – 5.4.3)	analysis

*The electronic version is the official approved document.
Verify this is the correct version before use.*

NASA-HDBK-5010, VOLUME 2, REVISION A

Space Launch System (SLS) Program/Project	
Revision: baseline	Document No: SLS-SPIO-RPT-013
Release Date:	Page: 31 of 34
Title: SPIE MSA FRACTURE CONTROL SUMMARY REPORT	

Table 7: Fail-Safe Parts			
Part Description	Material or Process	Classification (<i>FCP Section in Parentheses</i>)	Basis of Classification
Electrical interface brackets	2219 aluminum alloy assembly	failsafe (§5.4.2)	analysis
Secondary payload brackets	2219	failsafe (§5.4.2)	analysis
Spacer(s), wiring harness	CRES A286	failsafe (§5.4.2)	analysis

6.6.3 Alternative Approaches (Item 10³⁵)

Table 9 has been provided below to list the parts that require an alternative approach for fracture control. The diaphragm electrical connector plates listed below are nominally 16" x 5.5" x 0.125". Numerous holes are cut into the plates to accommodate connectors. A hazard assessment has been performed and no credible catastrophic hazards resulting from failure of the part due to a flaw (see LaRC-SLS-MSA-01-030, *Multi-Purpose Crew Vehicle (MPCV) Stage Adapter (MSA) Diaphragm Flight and Ground Safety Data Package*). The acceptability of this approach can be found in memorandum of concurrence EM20-14-FCB-002.

³⁵ d. As a minimum, the following information shall be provided in the FCSR: (10) If applicable, a summary discussion of alternative approaches or specialized assessment methodology applied, but not specifically covered by guidelines.

*The electronic version is the official approved document.
Verify this is the correct version before use.*

NASA-HDBK-5010, VOLUME 2, REVISION A

Space Launch System (SLS) Program/Project	
Revision: baseline	Document No: SLS-SPIO-RPT-013
Release Date:	Page: 32 of 34
Title: SPIE MSA FRACTURE CONTROL SUMMARY REPORT	

Table 8: Alternative Approach Items			
Part Description	Material or Process	Classification <i>(FCP Section in Parentheses)</i>	Basis of Classification
diaphragm electrical connector plates A and B	Ti-6Al-4V (AMS 4911)	alternative approach: non-fracture critical documented non-hazardous failure modes (§5.4.6)	analysis
Washer, countersink, housing to diaphragm	CRES	alternative approach: non-fracture critical documented non-hazardous failure modes (see paragraph below table)	analysis
Washer, flat, housing to diaphragm	CRES	alternative approach: non-fracture critical documented non-hazardous failure modes (see paragraph below table)	analysis
Washer, EIB mounting	Corrosion resistant steel	alternative approach: non-fracture critical documented non-hazardous failure modes (see paragraph below table)	analysis
Washer, avionics mount	A286	alternative approach: non-fracture critical documented non-hazardous failure modes (see paragraph below table)	analysis
Washer, secondary payload assembly	A286	alternative approach: non-fracture critical documented non-hazardous failure modes (see paragraph below table)	analysis

*The electronic version is the official approved document.
Verify this is the correct version before use.*

NASA-HDBK-5010, VOLUME 2, REVISION A

Space Launch System (SLS) Program/Project	
Revision: baseline	Document No: SLS-SPIO-RPT-013
Release Date:	Page: 33 of 34
Title: SPIE MSA FRACTURE CONTROL SUMMARY REPORT	

Table 8: Alternative Approach Items			
Washer(s), secondary payload mounting	A286	alternative approach: non-fracture critical documented non-hazardous failure modes (see paragraph below table)	analysis
access hatch mount bolts	aerospace bolts, A286	alternate approach, fail-safe and low-risk (§5.4.8)	analysis
Cable attach spacer bolt	IN718	alternate low risk (§5.4.9)	analysis
Bolt, loop clamp cable mount	A286	alternate low risk (§5.4.9)	analysis
MSA primary structure threaded nodes	2195-T8M4	alternate approach, low-risk (§5.4.7)	analysis

A number of washers have been classified as *alternative approach: non-fracture critical documented non-hazardous failure modes*. This classification is approved in the new revision of NASA-STD-5019 (revision A), but it is offered as an alternative approach in this case, where the baseline version 5019 is the controlling document. These washers are captured between the bolts and inserts or nut and the equipment being fixed, and they are subjected to compression loads. There is no identified failure mode that could lead to a hazardous condition for these pieces.

6.6.4 Avionics Box

The avionics box and attachments were not covered well in the MSA fracture control plan, and so they are being inserted here. The avionics box is a sealed container, and parts interior to that box are contained. The lid-to-box bolts and the avionics box-to-secondary payload bracket bolts are fail-safe and low released mass, and they have been inserted into table 6, above, with the low released-mass results shown in Appendix E, and the fail-safe analysis provided in the avionics box vendor's³⁶ document 21505-R005, Rev F, *NASA Secondary Payloads Avionics Box Development, Structural Dynamics Analyses, Loads, and Models*, DR Number: 1537 DE-003.

³⁶ Space Vector Corporation

*The electronic version is the official approved document.
Verify this is the correct version before use.*

NASA-HDBK-5010, VOLUME 2, REVISION A

Space Launch System (SLS) Program/Project	
Revision: baseline	Document No: SLS-SPIO-RPT-013
Release Date:	Page: 34 of 34
Title: SPIE MSA FRACTURE CONTROL SUMMARY REPORT	

APPENDIX A: ACRONYMS

ADP	Acceptance Data Package
CM	Change Management System or Process
CR	Change Request
DCSS	Delta Cryogenic Second Stage
DTA	Damage Threat Assessment
ECB	SPIO Engineering Change Board
EFT-1	The First Exploration Flight Test
ERB	SPIO Engineering Review Board
FCB	MSFC Fracture Control Board
FCP	The EFT-1 MSA Fracture Control Plan
FCSR	The Efoot-1 MSA Fracture Control Summary Report
FSW	Friction Stir Weld
IDPP	Impact Damage Protection Plan
ITAR	International Traffic in Arms Regulations
LaRC	NASA Langley Research Center
MAPTIS	Materials and Processes Technical Information System
mbolt	mass of the released part of a failed bolt
METTS	Marshall Engineering Technicians and Trade Support Contract
MPCV	Orion Multi-Purpose Crew Vehicle
MSA	MPCV Stage Adapter
MSFC	NASA Marshall Space Flight Center
MUA	Materials Usage Agreement
NDE	Nondestructive Evaluation
NFC	Non-fracture Critical
OPR	Office of Primary Responsibility
pbolt	momentum of the released part of a failed bolt
PCA	Product Configuration Acceptance
SBU	Sensitive but Unclassified
SLS	Space Launch System
SPIE	Spacecraft and Payload Integration and Evolution Office (formerly SPIO)
SPIO	Spacecraft and Payload Integration Office
TBD	To Be Done, i.e., Something that Needs to be Completed
TBR	To Be Resolved, i.e., Something that Requires Resolution
USML	U.S. Munitions List
vbolt	velocity of the released part of a failed bolt

APPENDIX B: TBD'S AND TBR'S

There are no TBD's or TBR's.

*The electronic version is the official approved document.
Verify this is the correct version before use.*

APPROVED FOR PUBLIC RELEASE – DISTRIBUTION IS UNLIMITED

APPENDIX C

**FRACTURE CONTROL PLAN FOR THE LUNAR FLASHLIGHT
PROPULSION SYSTEM**



National Aeronautics and
Space Administration

LFPS-PLAN-111

EFFECTIVE DATE 10/20/2020

George C. Marshall Space Flight Center
Marshall Space Flight Center, Alabama 35812

Lunar Flashlight Propulsion System Fracture Control Plan

**MARSHALL SPACE FLIGHT CENTER ADVANCED EXPLORATION
SYSTEM**

NASA-HDBK-5010, VOLUME 2, REVISION A

Title: LFPS Fracture Control Plan	Document No.: LFPS-PLAN-111	Revision: B
	Effective Date: 10/20/2020	Page 2 of 28

DOCUMENT HISTORY LOG

Status (Baseline/ Revision/ Cancelled)	Document Revision	Effective Date	Page	Section	Description
Baseline		2/4/2020			
Revision	A	3/31/2020			<ul style="list-style-type: none">- Updates to include reference to approved ICD.- Revision to design loads and random vibration environments.
Revision	B	10/20/2020			<ul style="list-style-type: none">- Updated leak check scheme for tank (section 8.3)

NASA-HDBK-5010, VOLUME 2, REVISION A

Title: LFPS Fracture Control Plan	Document No.: LFPS-PLAN-111	Revision: B
	Effective Date: 10/20/2020	Page 3 of 28

APPROVALS

Prepared By:

CARLOS DIAZ Digitally signed by CARLOS DIAZ
Date: 2020.10.23
17:29:27 -05'00'

Carlos Diaz Date
ER11/LFPS Propulsion Lead

Approved By:

DANIEL CAVENDER Digitally signed by DANIEL CAVENDER
Date: 2020.10.26
08:52:27 -05'00'

Daniel Cavender Date
ST24/LFPS Project Manager

Concurrence By:

MIGNON THAMES Digitally signed by MIGNON THAMES
Date: 2020.10.26
07:54:29 -05'00'

Mignon Thames Date
EE05/LFPS Chief Engineer

JOHN PEUGEOT Digitally signed by JOHN PEUGEOT
Date: 2020.10.25
16:19:04 -05'00'

John Peugeot Date
ER11/Branch Chief

NASA-HDBK-5010, VOLUME 2, REVISION A

Title: LFPS Fracture Control Plan	Document No.: LFPS-PLAN-111	Revision: B
	Effective Date: 10/20/2020	Page 4 of 28

Contents

1.0	SCOPE.....	7
2.0	APPLICABLE DOCUMENTS.....	7
2.1	NASA Documents	7
2.2	MSFC Documents	8
3.0	PROJECT DESCRIPTION.....	9
3.1	Lunar Flashlight Propulsion System Hardware Description	9
4.0	FRACTURE CONTROL PROGRAM.....	10
4.1	NASA MSFC FCB Responsibilities.....	10
4.2	MSFC and GT Shared Responsibilities.....	10
4.3	Fracture Control Board Approval	10
4.4	Traceability and Documentation.....	11
5.0	FRACTURE CONTROL CLASSIFICATION OF COMPONENTS	12
5.1	Lunar Flashlight Propulsion System Component Classification Summary	12
5.1.1	<i>Category 1: Components Exempt from Fracture Control.....</i>	<i>12</i>
5.1.2	<i>Category 2: Non-Fracture Critical Components.....</i>	<i>13</i>
5.1.3	<i>Category 3: Fracture Critical Components.....</i>	<i>15</i>
6.0	DESIGN, ANALYSIS, TEST, AND INSPECTIONS	18
6.1	Damage Tolerance Analysis and Tests.....	18
6.2	Non-Destructive Evaluations (NDE) and Inspections	18
6.3	Design	18
6.4	Materials	19
6.5	Manufacturing	19
6.6	Quality Control.....	19
7.0	DOCUMENTATION.....	21
7.1	Fracture Control Section	21
7.2	Supporting Data.....	22
8.0	ALTERNATE APPROACHES	23
8.1	Service Valve	23
8.2	Isolation Valve	23
8.3	Propellant Tank	24
9.0	FRACTURE CONTROL PROCESS	25
10.0	APPENDIX A	26

NASA-HDBK-5010, VOLUME 2, REVISION A

Title: LFPS Fracture Control Plan	Document No.: LFPS-PLAN-111	Revision: B
	Effective Date: 10/20/2020	Page 5 of 28

NASA-HDBK-5010, VOLUME 2, REVISION A

Title: LFPS Fracture Control Plan	Document No.: LFPS-PLAN-111	Revision: B
	Effective Date: 10/20/2020	Page 6 of 28

LIST OF FIGURES

FIGURE 1 - LUNAR FLASHLIGHT PROPULSION SYSTEM (PUMP AND CONTROLLER NOT SHOWN)	10
FIGURE 2 - PROPULSION SYSTEM FRACTURE CRITICAL COMPONENTS AND WELDS	16

LIST OF TABLES

TABLE 1 - SUMMARY OF EXEMPT ELECTRICAL COMPONENTS (FULL LIST IN APPENDIX A).....	13
TABLE 2 – SUMMARY OF NON-FRACTURE CRITICAL CONTAINED PARTS (FULL LIST IN APPENDIX A).....	14
TABLE 3 - FRACTURE CRITICAL - PRESSURIZED COMPONENTS	15
TABLE 4 - FRACTURE CONTROL CLASSIFICATION FOR THE LUNAR FLASHLIGHT PROPULSION SYSTEM.....	26

NASA-HDBK-5010, VOLUME 2, REVISION A

Title: LFPS Fracture Control Plan	Document No.: LFPS-PLAN-111	Revision: B
	Effective Date: 10/20/2020	Page 7 of 28

1.0 SCOPE

This document is intended to replace a previously approved Fracture Control Plan (VACCO X16029-10-FCP1) for the Lunar Flashlight Propulsion System (LFPS). The current LFPS is a new design and therefore requires a new plan; however, the spacecraft interfaces have remained the same. This document describes the elements of the Marshall Space Flight Center (MSFC) Fracture Control Program and the responsibilities for managing these elements for the LFPS for the Lunar Flashlight CubeSat mission that will launch as a secondary payload on the Space Launch System (SLS). The purpose of this document is to establish a plan for the fracture control activities for MSFC's LFPS that will be used on the Lunar Flashlight CubeSat. This plan lists all the specific activities that will be performed to satisfy fracture control for this program. The provisions of this plan shall be met to demonstrate that the parts are in compliance with NASA's fracture control requirements for space flight hardware.

2.0 APPLICABLE DOCUMENTS

The following documents form a part of this document to the extent noted. Unless otherwise specified, the referenced documents are to be the latest issue date. In the event of a conflict between a referenced document and this document, NASA-STD-5019 will take precedence, over all documents as it is the governing fracture control document for the SLS Secondary Payloads.

2.1 NASA Documents

MSFC-STD-3029	Guidelines for the Selection of Metallic Materials for Stress Corrosion Cracking Resistance in Sodium Chloride Environments
NASA-STD-5009	Non-destructive Evaluation Requirements for Fracture Control
NASA-STD-5019	Fracture Control Requirements for Spaceflight Hardware
NASA-STD-6008	NASA Fastener Procurement, Receiving Inspection and Storage Practices for Spaceflight Hardware

NASA-HDBK-5010, VOLUME 2, REVISION A

Title: LFPS Fracture Control Plan	Document No.: LFPS-PLAN-111	Revision: B
	Effective Date: 10/20/2020	Page 8 of 28

NASA-STD-6016 Standard Materials and Processes Requirements for Spacecraft

AIAA-S-080 Space Systems – Metallic Pressure Vessels, Pressurized Structures, and Pressure Components

MIL-HDBK-6870 Inspection Program Requirements Non-Destructive for Aircraft and Missile Materials and Parts

MIL-STD-130 Identification Marking of US Military Property

2.2 MSFC Documents

LFPS-RPT-316 Fracture Control Report for Lunar Flashlight Propulsion System

LFPS-RPT-303 Structural Analysis Report for Lunar Flashlight Propulsion System

ASTM-E1417 Standard Practice for Liquid Penetrant Examination

TBD Electron Beam Weld Procedure

NASA-HDBK-5010, VOLUME 2, REVISION A

Title: LFPS Fracture Control Plan	Document No.: LFPS-PLAN-111	Revision: B
	Effective Date: 10/20/2020	Page 9 of 28

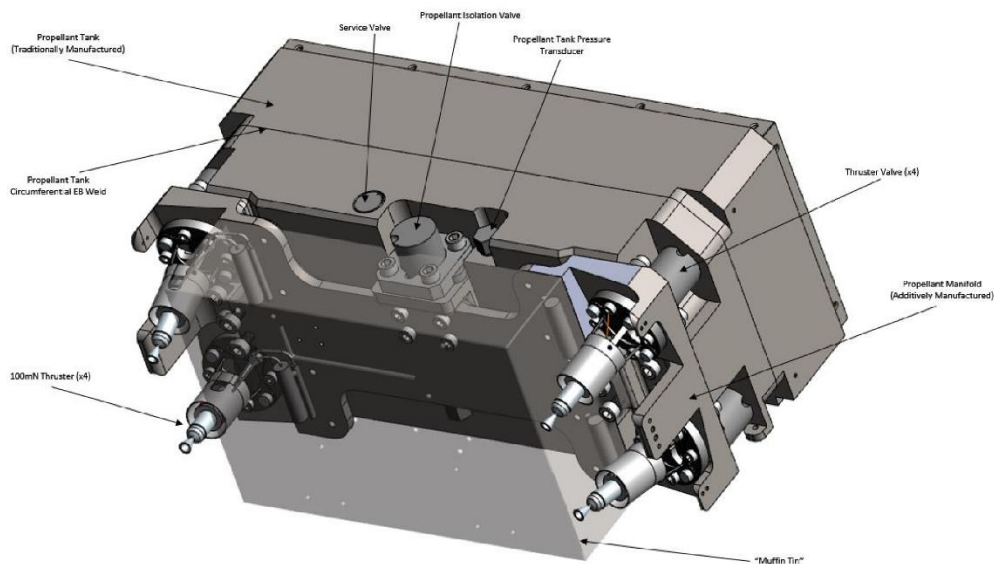
3.0 PROJECT DESCRIPTION

MSFC in conjunction with Georgia Tech Space Systems Design Laboratory (herein referred to as GT) will design the LFPS for NASA's Lunar Flashlight mission. The design will be supported by analysis, acceptance testing, and qualification testing, as necessary, to provide confidence that the hardware will meet the specified requirements.

3.1 Lunar Flashlight Propulsion System Hardware Description

The Lunar Flashlight Propulsion System is a self-contained, titanium alloy system that employs a combination of additively and traditionally manufactured parts. It has 4 canted green propellant thrusters that provide roll, pitch, yaw and ΔV . The system has a propellant storage tank that supplies propellant through a series of solenoid valves and an electrically-driven micro-pump to the four (4) thrusters.

The major external components of the Lunar Flashlight Propulsion System are identified in Figure 1.



NASA-HDBK-5010, VOLUME 2, REVISION A

Title: LFPS Fracture Control Plan	Document No.: LFPS-PLAN-111	Revision: B
	Effective Date: 10/20/2020	Page 10 of 28

Figure 1 - Lunar Flashlight Propulsion System (pump and controller not shown)

Information concerning the classification of either fracture critical or non-fracture critical components and the methodology applied on those components is shown in Appendix A.

4.0 FRACTURE CONTROL PROGRAM

4.1 NASA MSFC FCB Responsibilities

NASA MSFC FCB shall be responsible for approving the FCP, FCR, any alternative approaches, and interpreting the requirements of NASA-STD-5019.

4.2 MSFC and GT Shared Responsibilities

- Fracture classification of parts.
- Identification and specification of required Nondestructive Evaluation (NDE) Inspections or any other special requirements on fracture-critical parts. GT will follow standard NDE procedures to perform required inspection as called out on the component drawings and post weld NDE inspection on corresponding assembly drawings.
- Implementation of traceability and documentation showing adherence of hardware to approved drawings, specifications, plans, and procedures.
- Preparation of fracture mechanics and structural analyses, to include:
 - Assessment of anomalies on fracture-critical parts
 - Decisions regarding questions or issues relating to fracture control.

4.3 Fracture Control Board Approval

The NASA MSFC Fracture Control Board (FCB) must approve this fracture control plan.

NASA-HDBK-5010, VOLUME 2, REVISION A

Title: LFPS Fracture Control Plan	Document No.: LFPS-PLAN-111	Revision: B
	Effective Date: 10/20/2020	Page 11 of 28

4.4 Traceability and Documentation

Traceability will be maintained for all fracture-critical parts throughout the program.

Engineering drawings for fracture-critical parts will contain notes which:

- Identify the part as a “FRACTURE CRITICAL PART” on component drawings.
- Identify the weld as “FRACTURE CRITICAL WELD” where applicable.
- Specify the appropriate NDE technique to be used on the part. Relevant indications/discontinuities (crack size) exceeding the acceptance criteria shall be rejected and nonconformance initiated per NASA-STD-5009, Para 4.1.1.
- Specify that the part be marked with part number and serial number.

For parts that are too small to be marked on the part itself, the part will be bagged and tagged in accordance with MIL-STD-130.

All changes in design or process specifications, manufacturing discrepancies, repairs, and finished part modifications of all parts will be reviewed by NASA MSFC to ensure that fracture control requirements are still met.

NASA-HDBK-5010, VOLUME 2, REVISION A

Title: LFPS Fracture Control Plan	Document No.: LFPS-PLAN-111	Revision: B
	Effective Date: 10/20/2020	Page 12 of 28

5.0 FRACTURE CONTROL CLASSIFICATION OF COMPONENTS

Fracture control classification for all components will be determined in accordance with the requirements of NASA-STD-5019, based on failure modes, consequences of failure, applicable requirements, and experience.

5.1 Lunar Flashlight Propulsion System Component Classification Summary

5.1.1 Category 1: Components Exempt from Fracture Control

Per NASA-STD-5019 Section 4.1, exempt hardware typically includes non-structural items such as flexible insulation blankets, enclosed electrical circuit components/boards, electrical connectors (including locking devices), and wire bundles. Small mechanical parts, such as bearings and valve seats, that have been developed and qualified through strong test programs and rigorous process control to demonstrate their reliability, and whose failure does not directly lead to a catastrophic hazard may be exempt from fracture control with the approval of the RFCB.

5.1.1.1 Exempt - Non-Metallic

O-rings and seals are non-structural and exempt. They are also proof tested and checked for leakage during ATP. A listing of all o-rings and seals in the system, along with their respective fracture classifications, is provided in Appendix A.

5.1.1.2 Exempt - Electrical Components

Electrical circuit components, boards, connectors, wire bundles, and related components are non-structural and exempt per the above description. A listing of all electrical components in the system, along with their respective fracture classifications, is provided in Appendix A.

NASA-HDBK-5010, VOLUME 2, REVISION A

Title: LFPS Fracture Control Plan	Document No.: LFPS-PLAN-111	Revision: B
	Effective Date: 10/20/2020	Page 13 of 28

Table 1 - Summary of Exempt Electrical Components (full list in Appendix A)

PART NUMBER	QTY	PART DESCRIPTION
GLRG-LFPS-401	1	Main Board
GLRG-LFPS-402	1	Driver Connect Board
GLRG-LFPS-403	1	Sensor Connect Board
GLRG-LFPS-404	1	Harnessing
ThorLabs TH10K	5	Temperature Sensor
TBD	2	Propellant Tank Heater

5.1.1.3 Shims

Shims are stationary and not a primary load path during any system operating condition. Being contained, they do not contribute to any catastrophic failure scenario. Any potential shim fracture is of a fretting nature and would release only a non-hazardous small low energy mass.

5.1.1.4 External Locking Features

Lock-wire, helical inserts, and other external locking features represent secondary failure scenarios and are exempt per NASA-STD-5019 Section 4.1.1.6 and 4.1.2.3.

5.1.1.5 Non-Flight Hardware

Some packing covers, port plugs, and related hardware listed on the Bill of Material that are removed prior to mission operations are exempt from fracture control.

5.1.2 Category 2: Non-Fracture Critical Components

5.1.2.1 Non-Fracture Critical --- Contained

Per NASA-STD-5019 section 4.1.1.2, a failed part confined in a container or housing or otherwise positively restrained from free release and that does not result in a catastrophic hazard, can be classified non-fracture critical.

NASA-HDBK-5010, VOLUME 2, REVISION A

Title: LFPS Fracture Control Plan	Document No.: LFPS-PLAN-111	Revision: B
	Effective Date: 10/20/2020	Page 14 of 28

Contained hardware shall also be examined for potential damage effects of single-point mass releases inside the confinement itself. Release of masses (of any size) within a container that could credibly defeat an internal safety-critical function shall be precluded by appropriate technical measures, which can include compliance with requirements for low-risk part classification (see 4.1.1.12) or other techniques approved by the RFCB.

Release of a free mass from a fastener that is mechanically constrained (e.g., safety wired) can be assumed to be contained. All contained fasteners can be classified non-fracture critical if failure does not result in a catastrophic hazard due to loss of structural integrity of the fastener or loss of a safety-critical function.

Table 2 – Summary of Non-Fracture Critical Contained Parts (full list in Appendix A)

PART NUMBER	QTY	PART DESCRIPTION
GLRG-LFPS-902	1	Propellant Management Device Sponge
GLRG-LFPS-903	1	Propellant Management Device Vanes
GLRG-LFPS-702	1	Propellant Manifold
GLRG-LFPS-201	1	Muffin Tin Assembly
PP3490-B	4	Thruster Assembly
2212-M04X09-LF002	1	Micro-pump Assembly
IMER00761	4	Thruster Valve Assembly
TBD	1	Flow Control Device
GLRG-LFPS-803	1	Pump Recirculation Block

5.1.2.2 Low-Risk Parts

If parts have large structural margins and other considerations that make failure from a pre-existing flaw extremely unlikely, they can be classified as low-risk. For a part to be classified low-risk, it shall meet the requirements of NASA-STD-5019 section 4.1.1.12. Low-risk fasteners and shear pins shall meet only the requirements of section 4.1.1.6(b). If any fasteners are considered low-risk, low-risk fastener check sheets and evaluations will be provided in the fracture control report to demonstrate the low risk for the various fasteners. This low-risk fastener analysis calculation will be performed upon completion of the fastener analysis and will require NASA MSFC approval.

NASA-HDBK-5010, VOLUME 2, REVISION A

Title: LFPS Fracture Control Plan	Document No.: LFPS-PLAN-111	Revision: B
	Effective Date: 10/20/2020	Page 15 of 28

5.1.3 Category 3: Fracture Critical Components

Per NASA-STD-5019 section 4.1.2.1.4, lines, fittings, and other pressurized components (equipment that is part of a pressurized system) shall be considered fracture critical if they contain hazardous fluids or if loss of pressurization would result in a catastrophic hazard. All pressurized hardware within the LFPS meet the NASA-STD-5019 definition for pressurized components.

5.1.3.1 Fracture Critical --- Pressurized Components

Table 3 - Fracture Critical - Pressurized Components

PART NUMBER	QTY	PART DESCRIPTION
GLRG-LFPS-901	1	Tank Bottom Structure
GLRG-LFPS-801	1	Tank Top Structure
GLRG-LFPS-802	1	Weld Work Detail
IMER0762	1	MSFC Bulk Propellant Isolation Valve
IMER02733	1	Propellant Service Valve
TE XPS-X-150PA- /V05/L3M/Z02	1	Propellant Tank Pressure Transducer

NASA-HDBK-5010, VOLUME 2, REVISION A

Title: LFPS Fracture Control Plan	Document No.: LFPS-PLAN-111	Revision: B
	Effective Date: 10/20/2020	Page 16 of 28

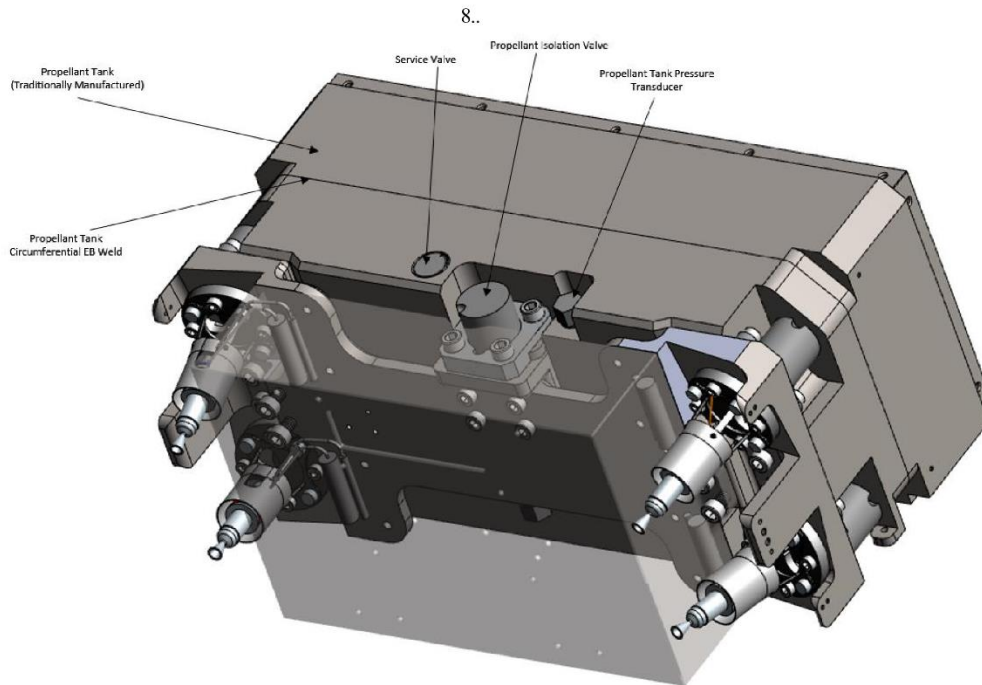


Figure 2 - Propulsion System Fracture Critical Components and Welds

Five (5) parts of the LFPS are loaded by pressure. Generally speaking, the following will be completed for these five parts (alternate approaches discussed in Section 8.0). The following components will be screened for flaws by surface NDE (penetrant inspection), and the raw material stock for the propellant tank will be screened for flaws by volumetric NDE prior to machining. Pre- and post-proof surface NDE of weld joints will also be performed. In addition, a Damage Tolerance Analysis will be prepared on the propellant tank and will be detailed in the Structural Analysis Report (LFPS-RPT-303) and Fracture Control Report (LFPS-RPT-316).

- Propellant Tank
- Propellant Tank Weldment
- Propellant Isolation Valve
- Propellant Service Valve
- Propellant Tank Pressure Transducer

NASA-HDBK-5010, VOLUME 2, REVISION A

Title: LFPS Fracture Control Plan	Document No.: LFPS-PLAN-111	Revision: B
	Effective Date: 10/20/2020	Page 17 of 28

All LFPS components will be proof tested (1.5 x MDP) during component level acceptance testing (ATP). After full system integration, system-level proof tests will be performed (1.1 x MDP of propellant tank) during the proto-flight test program (PTP) followed by leak test on all the components/weld that are loaded by pressure.

NASA-HDBK-5010, VOLUME 2, REVISION A

Title: LFPS Fracture Control Plan	Document No.: LFPS-PLAN-111	Revision: B
	Effective Date: 10/20/2020	Page 18 of 28

6.0 DESIGN, ANALYSIS, TEST, AND INSPECTIONS

6.1 Damage Tolerance Analysis and Tests

Safe-life verification, including DTA and/or tests, will be performed in accordance with NASA-STD- 5019. Any safe-life verification tests will be approved by the NASA MSFC FCB.

Where proof pressure testing is used on pressurized components, the proof test pressure shall be at least 1.5 x MDP.

Assemblies that may be candidates for proof testing to screen for flaws shall be mounted securely onto a test plate or fixture. For safety, a proof chamber or blast shield will be used during proof pressure testing. Leak tests shall be performed following proof pressure testing.

6.2 Non-Destructive Evaluations (NDE) and Inspections

All fracture critical parts will be subjected to proof testing and pre-/post-proof NDE to screen flaws. The selection of NDE methods and level of inspection will be based primarily on the safe-life acceptance requirements of the part. The NDE requirements as defined in NASA-STD-5009 will be followed, except that GT will perform NDE on fracture critical parts only. Additionally, GT will not etch sealing surfaces, other critical surfaces or highly polished surfaces, as etching will destroy those finishes. GT will not stop a surface cut operation to etch prior to cutting the final finished surface as this is not practical due to problems with setup and concentricity. Penetrant inspection will be performed per ASTM E1417, Type 1, Sensitivity Level 3. Use of initial crack sizes for geometries or NDE techniques not given in NASA-STD-5009 will require the approval of the NASA MSFC FCB.

6.3 Design

NASA-HDBK-5010, VOLUME 2, REVISION A

Title: LFPS Fracture Control Plan	Document No.: LFPS-PLAN-111	Revision: B
	Effective Date: 10/20/2020	Page 19 of 28

All parts will be designed to minimize the potential for cracks. Materials will be selected with the proper ductility and strength to withstand the specified loads and environments. Parts will have sufficient mass and material to withstand the subject loads. Edges and corners will be broken as needed to preclude stress risers and stress concentrations. A detailed stress analysis, thermal analysis, and damage tolerance analysis (if applicable) will be performed to confirm and ensure the adequacy of the design.

6.4 Materials

Materials for FC parts will be selected based on successful utilization in heritage hardware, where applicable, and to established selection criteria for new designs. NASGRO will be queried as applicable to confirm material properties as well as the crack-growth related properties. Grade "A" - Basis material will be used whenever possible. Structural properties shall be obtained from MMPDS (Metallic Materials Properties Development and Standardization, a MAPTIS replacement) when possible. A material usage agreement (MUA) will be generated and submitted to NASA MSFC that documents the criteria and rationale used for any material other than an A-Basis material.

6.5 Manufacturing

The processes used in the manufacturing of Lunar Flashlight Propulsion System will be those used for the similar or identical heritage hardware. These processes will be updated as needed to meet current requirements. Fracture critical components will be identified on the drawings and routers and will be subject to special handling, transportation and storage procedures, as applicable.

6.6 Quality Control

Quality Engineering will ensure that fracture critical components are properly identified on drawings and that these drawings contain the drawing notes and requirements applicable to fracture critical components. MSFC Quality Assurance will inspect all

NASA-HDBK-5010, VOLUME 2, REVISION A

Title: LFPS Fracture Control Plan	Document No.: LFPS-PLAN-111	Revision: B
	Effective Date: 10/20/2020	Page 20 of 28

parts received at MSFC and will ensure that all documentation required for fracture critical components has been provided.

GT Quality Assurance will inspect all parts received at GT, in accordance with the LFPS Quality Memorandum of Agreement (MOA), and will ensure that all documentation required for fracture critical components is provided to MSFC.

NASA-HDBK-5010, VOLUME 2, REVISION A

Title: LFPS Fracture Control Plan	Document No.: LFPS-PLAN-111	Revision: B
	Effective Date: 10/20/2020	Page 21 of 28

7.0 DOCUMENTATION

7.1 Fracture Control Section

To certify fracture control compliance of a product, GT/MSFC will prepare the fracture control section as part of the Stress Analysis Report for review and approval by the NASA MSFC FCB. The Section will provide evidence that the system will meet the fracture control requirements defined in NASA-STD-5019. This fracture control report will include the following items:

- A description of the usage of the hardware.
- Sufficiently detailed drawings/sketches of the system will be furnished to show the general structure and function.
- A list showing the part name, part number, idealized dimensions used for analyses or tests, material, heat-treatment used, key location references, and the fracture control disposition (safe-life, test, acceptable durability, etc.) for all components. In addition, for fracture critical components, sketches, fracture mechanics properties, locations of maximum stress, loading spectra, and types of initial flaw will be provided. Ultimate margin of safety corresponding to the max stress at the flaw location should be provided for fracture critical parts. For non-fracture critical parts, a minimum ultimate margin of safety should be provided. Fracture critical parts that are limited life must be specifically noted. May use a list of accumulated loads, flaw screening results (NDE and proof testing) as applicable, damage tolerant testing results, and flaw acceptance rationale, as reference documents.
- Analyses and/or test data supporting the fracture control disposition will be furnished.
- The NDE and/or tests applied for fracture control purposes to each fracture critical part and to each low-risk part requiring specific inspection will be identified.

NASA-HDBK-5010, VOLUME 2, REVISION A

Title: LFPS Fracture Control Plan	Document No.: LFPS-PLAN-111	Revision: B
	Effective Date: 10/20/2020	Page 22 of 28

7.2 Supporting Data

Documents supporting the Fracture Control Report will be available for review by the NASA MSFC FCB. The documents required to support the acceptability of a fracture-critical part will include the following:

- Damage tolerance analysis or test data.
- Documentation of NDE, proof-tests, and leak tests.
- A description of the loading spectrum.
- Material crack growth properties used in the DTA.

NASA-HDBK-5010, VOLUME 2, REVISION A

Title: LFPS Fracture Control Plan	Document No.: LFPS-PLAN-111	Revision: B
	Effective Date: 10/20/2020	Page 23 of 28

8.0 ALTERNATE APPROACHES

In the event a particular requirement per NASA-STD-5019 cannot be met for a specific component, but an alternative or modified fracture control approach can be utilized to preclude a catastrophic hazard to the vehicle and its crew, the alternate approach shall be approved by the NASA MSFC FCB. The following alternate approaches are planned for the LFPS.

8.1 Service Valve

Due to its size and the risk of contamination, the service valve will forego dye penetrant inspection of its single circumferential weld. In order to alleviate concerns with bypassing this inspection, the following activities will be performed during qualification and acceptance:

- Valve design employs high factors of safety on system maximum expected operating pressure (>6X MEOP).
- Qualification unit will undergo burst testing to verify maximum design pressure.
- Pre- and post-weld coupons will be cross-sectioned to verify weld process.
- Leak test performed at component level.
- Proof test performed after installation into system.
- Leak test performed after system-level proof testing.
- Service valve cap, once installed, will keep weld in compression.

8.2 Isolation Valve

Due to the isolation valve geometry, radiographic inspection of the weld joint will not be performed. In lieu of this inspection, the following activities will be performed:

- Qualification unit will undergo burst testing to verify maximum design pressure.
- Pre- and post-weld coupons will be cross-sectioned to verify weld process.
- Pre-proof pressure testing dye penetrant inspection of weld joint.
- Proof test performed at 1.5X MDP.
- Post-proof dye penetrant inspection of weld.
- Component-level leak test.

NASA-HDBK-5010, VOLUME 2, REVISION A

Title: LFPS Fracture Control Plan	Document No.: LFPS-PLAN-111	Revision: B
	Effective Date: 10/20/2020	Page 24 of 28

8.3 Propellant Tank

Due to tank weld geometry, radiographic inspection of the propellant tank weld joint will not be performed. In lieu of this inspection, the following activities will be performed:

- A damage tolerance analysis will be performed to demonstrate that the weld is capable of withstanding significant damage. This analysis will show that failure doesn't occur using a starting flaw size that exceeds 90% of the thickness.
- Qualification unit will undergo burst testing to verify maximum design pressure.
- Pre- and post-weld coupons will be cross-sectioned to verify weld process. Coupons will also be inspected via radiography and surface dye penetrant.
- Post-weld dye penetrant inspection of tank and weld.
- Proof test performed to 1.5X MDP.
- Post-proof dye penetrant inspection of tank and weld.
- Leak test at next higher assembly level.

NASA-HDBK-5010, VOLUME 2, REVISION A

Title: LFPS Fracture Control Plan	Document No.: LFPS-PLAN-111	Revision: B
	Effective Date: 10/20/2020	Page 25 of 28

9.0 FRACTURE CONTROL PROCESS

The fracture control process as detailed below will be followed:

1. **Damage Tolerance Analysis:** DTA will be performed on the propellant tank and tank weldment as defined in section 5.1.3.1.
2. **Raw Stock:** MSFC/GT will review the raw stock material certifications to check if volumetric Ultrasonic Test (UT) inspection was performed. Any relevant data will be noted in the fracture control report.
3. **EB Welding:** The weld vendor will develop the weld parameters specific the weld joint geometry and qualify the weld procedure. For the isolation valve, weld coupons will be made before and after each weld for metallographic verification of weld penetration. For the propellant tank, weld coupons will be made before and after each weld for radiographic and surface inspections, as well as metallographic verification of weld penetration.
4. **Pre-Proof Pressure Test Inspection of Welds:** Prior to proof test, a dye penetrant inspection will be performed on the isolation valve and propellant tank welds. No etching of the welds will be performed prior to inspection.
5. **Proof Pressure Test:** Proof pressure test (MDP x 1.5) will be performed on all fracture critical components and welds during hardware acceptance testing.
6. **Post-Proof Pressure Test Inspection of Welds:** Post-proof test, a dye penetrant inspection will be performed on the isolation valve and propellant tank welds. No etching of the weld will be performed prior to inspection.
7. **Burst Test:** A qualification unit for the service valve, isolation valve, and propellant tank will each be tested to burst pressure and then taken to failure to understand the failure mode of each component.

NASA-HDBK-5010, VOLUME 2, REVISION A

Title: LFPS Fracture Control Plan	Document No.: LFPS-PLAN-111	Revision: B
	Effective Date: 10/20/2020	Page 26 of 28

10.0 APPENDIX A

Table 4 - Fracture Control Classification for the Lunar Flashlight Propulsion System

<i>Part Number</i>	<i>Name</i>	<i>Qty</i>	<i>Fracture Critical</i>	<i>Fracture Criticality Rationale</i>	<i>Damage Tolerance Analysis Required?</i>	<i>NDE Method</i>
GLRG-LFPS-100	LFPS Top Assembly	1	Yes	Contains Fracture Critical Component(s)	No	N/A
GLRG-LFPS-200	LFPS Systems Assembly	1	Yes	Contains Fracture Critical Component(s)	No	N/A
GLRG-LFPS-300	LFPS System Components Assembly	1	Yes	Contains Fracture Critical Component(s)	No	N/A
GLRG-LFPS-400	LFPS Tank/Manifold Assembly	1	Yes	Contains Fracture Critical Component(s)	No	N/A
GLRG-LFPS-500	LFPS Tank Components Assembly	1	Yes	Contains Fracture Critical Component(s)	No	N/A
GLRG-LFPS-600	LFPS Tank Subassembly	1	Yes	Contains Fracture Critical Component(s)	No	N/A
GLRG-LFPS-900	Tank Bottom Subassembly	1	Yes	Contains Fracture Critical Component(s)	Yes	Dye Penetrant
GLRG-LFPS-901	Tank Bottom Structure	1	Yes	Pressurized Component	No	N/A
GLRG-LFPS-902	Propellant Management Device Sponge	1	No	Contained	No	N/A
GLRG-LFPS-903	Propellant Management Device Vanes	1	No	Contained	No	N/A
1203542-38-100-OF-B	Filter (10-micron)	1	No	Contained	No	N/A
	Fasteners	20	No	Contained	No	N/A
NASI352N04-6	PMD Sponge Fasteners	4	No	Contained	No	N/A
NASI352N02-3	PMD Vane Fasteners	6	No	Contained	No	N/A
2TLC-04C-0112	PMD Sponge Helicoils	4	No	Contained	No	N/A
2TLC-02C-0086	PMD Vane Helicoils	6	No	Contained	No	N/A
GLRG-LFPS-801	Tank Top Structure	1	Yes	Pressurized Component	No	N/A

NASA-HDBK-5010, VOLUME 2, REVISION A

Title: LFPS Fracture Control Plan	Document No.: LFPS-PLAN-111	Revision: B
	Effective Date: 10/20/2020	Page 27 of 28

GLRG-LFPS-802	Welding Work Detail	1	Yes	Pressurized Component	Yes	N/A
IMER00762	MSFC Bulk Propellant Isolation Valve	1	Yes	Pressurized Component	No	Dye Penetrant
GLRG-LFPS-701	Bulk Prop Iso Valve Bracket	1	No	Fail-safe/ Contained	No	N/A
IMER02733	Fill/Drain Valve	1	Yes	Pressurized Component	No	N/A
	Propellant Tank Heater	2	No	Exempt	No	N/A
	O-Rings	2	No	Exempt	No	N/A
OR01250396375	Iso Valve Inner O-Ring	1	No	Exempt	No	N/A
ARP-014-6375	Iso Valve Outer O-Ring	1	No	Exempt	No	N/A
	Fasteners	8	No	Contained	No	N/A
NASI352N06H6	Iso Valve Fasteners	4	No	Fail-safe/ Contained	No	N/A
MS212-9F6-20	Helicoil	4	No	Contained	No	N/A
	Sensors	4	No	Exempt	No	N/A
TE XP5-X-150PA- /V05/L3M/Z02	Propellant Tank Pressure Sensor	1	Yes	Pressurized Component	No	N/A
ThorLabs TH10K	Propellant Tank Temperature Sensor	3	No	Exempt	No	N/A
GLRG-LFPS-700	LFPS Manifold Subassembly	1	No	Contained	No	N/A
GLRG-LFPS-702	Machined Manifold Structure	1	No	Contained	No	N/A
IMER00761	Thruster Valves	4	No	Contained	No	N/A
GLRG-LFPS-800	LFPS Recirculation Block Subassembly	1	No	Contained	No	N/A
GLRG-LFPS-803	Recirculation Block (RB)	1	No	Contained	No	N/A
JETAX0550550B	Fixed Orifice	1	No	Contained	No	N/A
	O-Rings	10	No	Exempt	No	N/A
OR01250396375	Thruster Valve Inner O-Ring	4	No	Contained	No	N/A
ARP-014-6375	Thruster Valve Outer O-Ring	4	No	Contained	No	N/A
AS-568A-K-011	Recirculation Block Inlet O-Ring	1	No	Contained	No	N/A
AS-568A-K-008	Recirculation Block Outlet O-Ring	1	No	Contained	No	N/A
	Fasteners	15	No	Contained	No	N/A
NASI352N06H6	Thruster Valve Fasteners	8	No	Contained	No	N/A
NASI352N04H6	Recirculation Block Fasteners	4	No	Contained	No	N/A
	Sensors	2	No	Exempt	No	N/A
TE XP5-X-150PA- /V05/L3M/Z02	Manifold Pressure Sensor	1	No	Contained	No	N/A
ThorLabs TH10K	Manifold Temperature Sensor	1	No	Exempt	No	N/A
	O-Rings	2	No	Exempt	No	N/A
OR01250396375	Pass-through Inner O-Ring	1	No	Exempt	No	N/A
ARP-014-6375	Pass-through Outer O-Ring	1	No	Exempt	No	N/A

27

APPROVED FOR PUBLIC RELEASE – DISTRIBUTION IS UNLIMITED

NASA-HDBK-5010, VOLUME 2, REVISION A

Title: LFPS Fracture Control Plan	Document No.: LFPS-PLAN-111	Revision: B
	Effective Date: 10/20/2020	Page 28 of 28

	Fasteners	8	No	Contained	No	N/A
NAS1352N06H6	Pass-through Fasteners	4	No	Contained	No	N/A
NAS1352N08H6	Structural Fasteners	4	No	Contained	No	N/A
2212-M04X09-LF002	Pump	1	No	Contained	No	N/A
	Fasteners	6	No	Contained	No	N/A
NAS1352N04H6	Pump Fasteners	6	No	Contained	No	N/A
	Sensors	1	No	Contained	No	N/A
ThorLabs TH10K	Pump Temperature Sensor	1	No	Exempt	No	N/A
	Boards	3	No	Contained	No	N/A
GLRG-LFPS-401	Main Board	1	No	Contained	No	N/A
GLRG-LFPS-402	Sensor Connect Board	1	No	Contained	No	N/A
GLRG-LFPS-403	Driver Connect Board	1	No	Contained	No	N/A
GLRG-LFPS-404	Harnessing	1	No	Exempt	No	N/A
	Fasteners	30	No	Contained	No	N/A
93655A093	Connect Board Standoffs (6mm M3)	8	No	Contained	No	N/A
93655A222	Main Board Standoffs (22mm M3)	10	No	Contained	No	N/A
91828A211	M3 Nuts	2	No	Contained	No	N/A
91292A109	4mm M3 Screws	10	No	Contained	No	N/A
PP3490-B	Thrusters	4	No	Contained	No	N/A
GLRG-LFPS-201	Muffin Tin Structure	1	No	Contained	No	N/A
GLRG-LFPS-202	Thruster Covers	2	No	Non-flight	No	N/A
	Fasteners	20	No	Contained	No	N/A
NAS1352N04H4	Thruster Screws	16	No	Contained	No	N/A
NAS1352N08H10	Muffin Tin Screws	4	No	Contained	No	N/A

Note that all assemblies/sub-assemblies that contain fracture critical components are considered fracture critical. Since NDE is performed at component level, fracture critical assemblies/sub-assemblies show an NDE Method of "NA" or not applicable.

APPENDIX D

**FRACTURE CONTROL REPORT – LUNAR FLASHLIGHT
PROPULSION SYSTEM**



National Aeronautics and
Space Administration

LFPS-RPT-316
EFFECTIVE DATE 3/22/2021

George C. Marshall Space Flight Center
Marshall Space Flight Center, Alabama 35812

Lunar Flashlight Propulsion System
Fracture Control Report
Revision B

MARSHALL SPACE FLIGHT CENTER ADVANCED EXPLORATION SYSTEM

APPROVED FOR PUBLIC RELEASE – DISTRIBUTION IS UNLIMITED

NASA-HDBK-5010, VOLUME 2, REVISION A

Contents

Revision B	1
1.0 SCOPE	1
1.1 Revision Log.....	1
1.1.1 Revision A.....	1
1.1.2 Revision B.....	1
2.0 APPLICABLE DOCUMENTS	2
2.1 NASA Documents	2
2.2 MSFC Documents	3
3.0 Introduction	4
3.1 Hardware Description.....	4
3.1.1 Tank	5
3.1.2 Manifold	6
3.1.3 Muffin Tin	7
3.1.4 Isolation Valve	7
3.1.5 Isolation Valve Mounting Plate	9
3.1.6 Service Valve	9
3.1.7 Pressure Transducer	10
3.1.8 Other Components.....	11
3.2 Fracture Disposition and Summary	12
3.3 Geometry	13
3.3.1 Tank Top/Bottom.....	13
3.3.2 Weld Dimensions	15
3.3.3 NDE Inspection Methods	17
3.3.4 Isolation Valve Mounting Plate	18
3.3.5 Isolation Valve Mounting Plate Fasteners.....	18
3.4 Factors of Safety	19
4.0 Material Properties	20
4.1 Ti-6Al-4V Bar (AMS 4928).....	20
4.2 Ti-6Al-4V Weld.....	21
4.3 AM Ti-6Al-4V	22
4.4 Aluminum 7075-T7351	23
4.5 A286 Bolts:.....	23
4.6 CRES 304L	24
4.7 430 CRES (ASTM A276).....	25
4.8 CRES 304L to ASTM A276 Weld.....	26

NASA-HDBK-5010, VOLUME 2, REVISION A

4.9	15-5 PH Service Valve	26
5.0	Loads and Environments	27
5.1	Mission Profile.....	27
5.2	Pressure.....	28
5.3	Thermal.....	28
5.4	Inertial.....	29
5.4.1	<i>RV Cycle Spectra Creation</i>	30
6.0	Component Details.....	35
6.1	Tank Top, Tank Bottom, and Tank Weld.....	35
6.1.1	<i>Stress Analysis Results</i>	35
6.1.2	<i>Stress Assumptions</i>	44
6.1.3	<i>Load Combinations</i>	45
6.1.4	<i>Tank Top/Bottom Safe-Life / Damage Tolerance Analysis</i>	48
6.1.5	<i>Tank Weld Alternative Approach / Safe-Life / Damage Tolerance Analysis</i>	48
6.2	Isolation Valve.....	51
6.3	Isolation Valve Mounting Plate.....	52
6.3.1	<i>Finite Element Model</i>	52
6.3.2	<i>Static Strength Assessment</i>	53
6.3.3	<i>Fastener Check</i>	53
6.3.4	<i>Fatigue Check</i>	53
6.3.5	<i>Seal Check</i>	54
6.4	Isolation Valve Mounting Plate Fasteners.....	55
6.4.1	<i>Finite Element Model</i>	55
6.4.2	<i>Static Strength Assessment</i>	56
6.4.3	<i>Fastener Check</i>	56
6.4.4	<i>Fatigue Check</i>	56
6.4.5	<i>Seal Check</i>	57
6.5	Service Valve.....	58
6.6	Pressure Transducer.....	59
6.7	NFC – Contained Components.....	60
6.8	Exempt Components.....	60
7.0	ACRONYMS AND ABBREVIATIONS	61

NASA-HDBK-5010, VOLUME 2, REVISION A

LIST OF FIGURES

FIGURE 1 LFPS PRIMARY STRUCTURAL COMPONENTS	4
FIGURE 2 TANK TOP	5
FIGURE 3 TANK BOTTOM	5
FIGURE 4 MANIFOLD (11/29/2019 DESIGN)	6
FIGURE 5 MUFFIN TIN (11/29/2019 DESIGN)	7
FIGURE 6 ISOLATION VALVE LOCATION	7
FIGURE 7 ISOLATION VALVE CROSS SECTION	8
FIGURE 8 ISOLATION VALVE SUBCOMPONENTS (INCLUDING THE MOUNTING PLATE)	8
FIGURE 9 ISOLATION VALVE MOUNTING PLATE	9
FIGURE 10 SERVICE VALVE CROSS SECTION	9
FIGURE 11 SERVICE VALVE LOCATION	10
FIGURE 12 PRESSURE TRANSDUCER LOCATION	10
FIGURE 13 TANK TOP CRITICAL DIMENSION LOCATIONS	13
FIGURE 14 TANK TOP CRITICAL DIMENSION LOCATIONS	14
FIGURE 15 NASGRO TANK TOP/BOTTOM DIMENSIONS	15
FIGURE 16 WORST CASE WELD GEOMETRY – TANK TOP	16
FIGURE 17 WORST CASE WELD GEOMETRY – TANK BOTTOM	16
FIGURE 18 NASGRO WELD DIMENSIONS	17
FIGURE 19 SLS DISPENSER LOCAL COORDINATE SYSTEM	29
FIGURE 20 LOAD COMBINATION SPREADSHEET RESULTS	30
FIGURE 21 LOAD COMBINATION SPREADSHEET CALCULATIONS	30
FIGURE 22 PRIMARY TANK Y MODE SHAPE (MODE 58, 1429HZ)	31
FIGURE 23 PRIMARY TANK Y MODE SHAPE (MODE 22, 909HZ)	31
FIGURE 24 PRIMARY TANK Z MODE SHAPE (MODE 41, 1034HZ)	31
FIGURE 25 RAYLEIGH DISTRIBUTION DISCRETIZATION	34
FIGURE 26 MAX PRINCIPLE STRESS LOCATION DUE TO MDP IN TANK TOP/BOTTOM	38
FIGURE 27 MAX PRINCIPLE STRESS LOCATION DUE TO MDP IN TANK TOP/BOTTOM – SUBMODEL	38
FIGURE 28 MAX PRINCIPLE STRESS LOCATION DUE TO INERTIA (FULL TANK) IN TANK TOP/BOTTOM (56.5 G LOAD FACTOR, CORRECTION FACTOR: 32.6/56.5)	39
FIGURE 29 MAX PRINCIPLE STRESS LOCATION DUE TO INERTIA (FULL TANK) IN TANK TOP/BOTTOM – SUBMODEL (56.5 G LOAD FACTOR, CORRECTION FACTOR: 32.6/56.5)	39
FIGURE 30 MAX PRINCIPLE STRESS LOCATION DUE TO INERTIA (EMPTY TANK) IN TANK TOP/BOTTOM (32.6 G LOAD FACTOR)	40
FIGURE 31 MAXIMUM SHEAR STRESS DUE TO INERTIA (FULL TANK) IN WELD (56.5 G LOAD FACTOR, CORRECTION FACTOR: 32.6/56.5)	40
FIGURE 32 MAXIMUM TENSILE STRESS DUE TO INERTIA (FULL TANK) IN WELD (56.5 G LOAD FACTOR, CORRECTION FACTOR: 32.6/56.5)	41

NASA-HDBK-5010, VOLUME 2, REVISION A

FIGURE 33 MAXIMUM SHEAR STRESS DUE TO INERTIA (EMPTY TANK) IN WELD (32.6 G LOAD FACTOR)	41
FIGURE 34 MAXIMUM TENSILE STRESS DUE TO INERTIA (EMPTY TANK) IN WELD (32.6 G LOAD FACTOR)	42
FIGURE 35 WELD SUBMODEL LOCATIONS	42
FIGURE 36 MAXIMUM PRINCIPLE STRESS DUE TO MDP AT WELD LOCATION A (-Y)	43
FIGURE 37 MAXIMUM PRINCIPLE STRESS DUE TO MDP AT WELD LOCATION B (+Y)	43
FIGURE 38 MAXIMUM PRINCIPLE STRESS DUE TO MDP AT WELD LOCATION C (\pm X)	44
FIGURE 39 NASGRO SC30 FORMULATION	48
FIGURE 40 NASGRO SC30 FORMULATION	50
FIGURE 41 ISOLATION VALVE MOUNTING PLATE FAILSAFE PLATE CONDITION	52
FIGURE 42 ISOLATION VALVE SEAL PERFORMANCE FOLLOWING MOUNTING PLATE FAILURE	54
FIGURE 43 ISOLATION VALVE MOUNTING PLATE FAILSAFE BOLT CONDITION	55
FIGURE 44 ISOLATION VALVE SEAL PERFORMANCE FOLLOWING BOLT FAILURE	57

LIST OF TABLES

TABLE 1 FRACTURE SUMMARY	12
TABLE 2 FACTORS OF SAFETY	19
TABLE 3 MISSION PROFILE	27
TABLE 4 LFPS LOAD FACTORS.....	29
TABLE 5 MODAL ANALYSIS: MASS PARTICIPATION RESULTS	32
TABLE 6 RAYLEIGH DISTRIBUTION DISCRETIZATION	33
TABLE 7 RV SPECTRA APPROXIMATION	34
TABLE 8 LIMIT STRESS RESULTS – TANK FLUID INCLUDED	37
TABLE 9 LIMIT STRESS RESULTS – TANK FLUID EXCLUDED.....	37
TABLE 10 TANK TOP/BOTTOM STRESS RESULTS	44
TABLE 11 TANK WELD STRESS RESULTS	45
TABLE 12 NASGRO LONGBLOCK DATA – TANK TOP/BOTTOM INTERIOR/EXTERIOR FLAW	46
TABLE 13 NASGRO LONGBLOCK DATA – TANK WELD – LOCATION A (-Y) INTERIOR/EXTERIOR FLAW	46
TABLE 14 NASGRO LONGBLOCK DATA – TANK WELD – LOCATION B (+Y) INTERIOR/EXTERIOR FLAW	47
TABLE 15 NASGRO LONGBLOCK DATA – TANK WELD – LOCATION C (\pm X) INTERIOR/EXTERIOR FLAW	47
TABLE 16 NASGRO RESULTS – TANK TOP/BOTTOM.....	48
TABLE 17 NASGRO RESULTS – TANK WELD LIFE.....	50

NASA-HDBK-5010, VOLUME 2, REVISION A

1.0 SCOPE

This document describes how the Lunar Flashlight Propulsion System (LFPS) meets the requirements listed in the LFPS Fracture Control Plan (FCP) (LFPS-PLAN-111). This document lists all the specific analyses and justifications to show that fracture control is satisfied for this program. The provisions of this plan shall be met to demonstrate that the parts are in compliance with NASA's fracture control requirements for space flight hardware.

1.1 Revision Log

1.1.1 Revision A

This document is released as part of memorandum ER41 (20-027). The changes to this document are listed below:

- The pre and post proof tank leak checks have been removed from the weld alternate approach rationale to align with the new procedure. A leak check is still performed at the assembly level.
- The alternate approaches in sections 6.1.5, 6.2, and 6.5 have been rewritten to match those in the Fracture Control Plan.

1.1.2 Revision B

This document is released as part of memorandum ER41 (20-027). The changes to this document are listed below:

- Added the Material Usage Agreement (MUA), Additive Manufacturing Control Plan (AMCP), and Certificates of Conformance (CoC) to the applicable documents (section 2.2).

NASA-HDBK-5010, VOLUME 2, REVISION A

2.0 APPLICABLE DOCUMENTS

The following documents form a part of this document to the extent noted. Unless otherwise specified, the referenced documents are to be the latest issue date. In the event of a conflict between a referenced document and this document, NASA-STD-5019 will take precedence, over all documents as it is the governing fracture control document for the SLS Secondary Payloads.

2.1 NASA Documents

MMPDS-13	Metallic Material Properties Development and Standardization Handbook
NASA-STD-5001	Structural Design and Test Factors of Safety for Spaceflight Hardware
NASA-STD-5009	Non-destructive Evaluation Requirements for Fracture Control
NASA-STD-5019	Fracture Control Requirements for Spaceflight Hardware
NASA-STD-5020	Requirements for Threaded Fastening Systems in Spaceflight Hardware
AIAA-S-080	Space Systems – Metallic Pressure Vessels, Pressurized Structures, and Pressure Components

NASA-HDBK-5010, VOLUME 2, REVISION A

2.2 MSFC Documents

5074913 (XP5-X-150PA)	Purchase Order - Certificate of Conformance, Measurement Specialties Inc.
5074913 (XP5-X-750PA)	Purchase Order - Certificate of Conformance, Measurement Specialties Inc.
AMS 2680C	Electron Beam Weld Procedure
C-LFPS-001	Lunar Flashlight Certification Material Usage Agreement (MUA)
D-98572	LFPS Safety Data Package (10/10/2019 version)
LFPS-PLAN-111	Fracture Control Plan for Lunar Flashlight Propulsion System
LFPS-PLAN-112	LFPS Additive Manufacturing Control Plan
LFPS-RPT-303	Structural Analysis Report for Lunar Flashlight Propulsion System Also part of Memorandum ER41 (20-027)
Memorandum ER41 (18-028)	Structural Analysis of the Cubesat Fill Valve Assembly
Memorandum ER41 (20-009)	Lunar Flashlight Propulsion System Critical Design Review Detailed Structural Assessments - Draft, For Record
SPIE-SP-LFPS-0001	MUA - AF-M315E Fluid Compatibility
SPIE-SP-LFPS-0002	MUA - Stress Corrosion Cracking

3.0 INTRODUCTION

3.1 Hardware Description

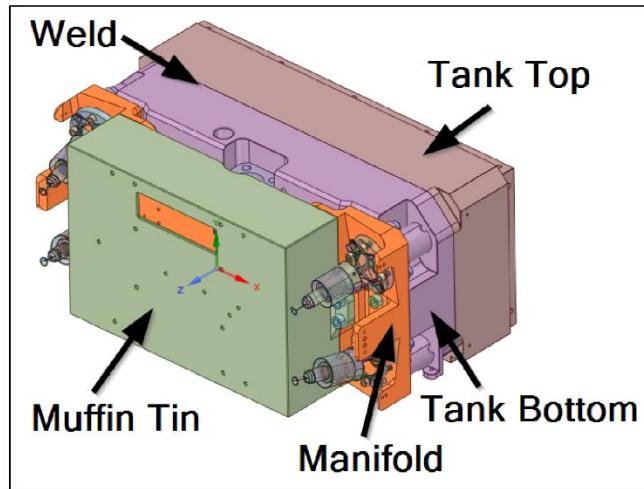


Figure 1 LFPS Primary Structural Components

The LFPS is comprised of four primary structural components (tank top, tank bottom, manifold, and muffin tin). These components support other smaller components within LFPS and are fastened to the rest of the Lunar Flashlight CubeSat.

3.1.1 Tank

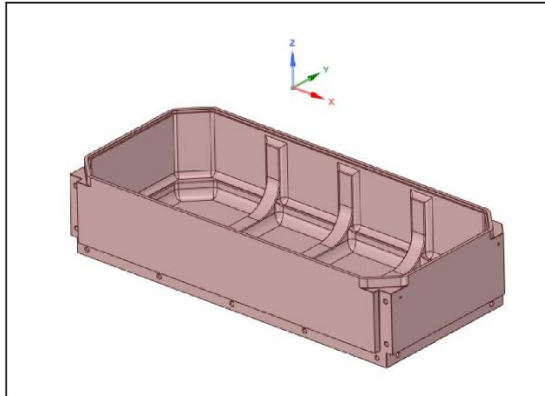


Figure 2 Tank Top

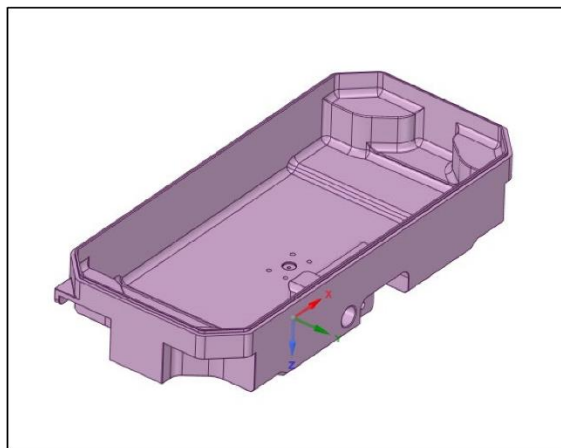


Figure 3 Tank Bottom

The tank top and bottom are traditionally manufactured and are EB welded together circumferentially. The tank is filled and pressurized prior to launch with AF-M315E propellant. The tank is fracture critical and contains the Propellant Management Device (PMD). Everything downstream of the tank is only pressurized with propellant following separation from SLS. There are three devices leading from the pressurized volume:

1. Pressure Transducer
2. Service Valve

NASA-HDBK-5010, VOLUME 2, REVISION A

3. Isolation Valve

Note that there is a tube within the tank bottom that is downstream of the isolation valve, this does not contain any hazardous fluid while fracture control is enforced.

3.1.2 Manifold

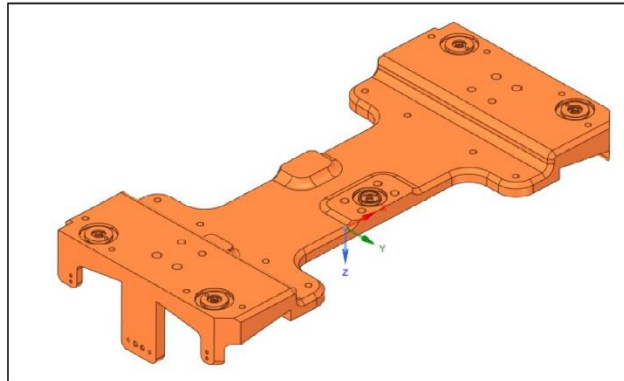


Figure 4 Manifold (11/29/2019 Design)

The Manifold is an additively manufactured part. It is not filled with a hazardous fluid while fracture control is enforced. The primary purpose of the Manifold is to support parts and route fluids using embedded channels. The fluid is routed through the pump, recirculation block, pressure transducer, valves, and thrusters. This component also supports the thrusters, valves (excluding the isolation and service valves), electronics, muffin tin, pump, and solar panels for the experiment.

3.1.3 Muffin Tin

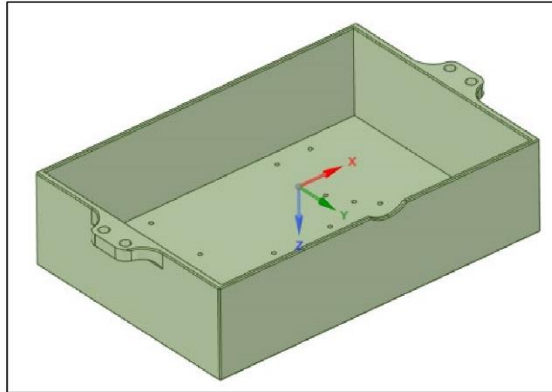


Figure 5 Muffin Tin (11/29/2019 Design)

The muffin tin shrouds some of the smaller components (electronics and pump) of the LFPS from direct sunlight and the thrusters. It also supports various experiment components (not a part of LFPS).

3.1.4 Isolation Valve

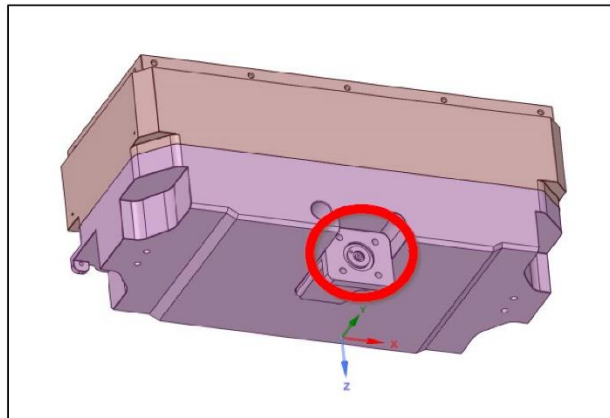


Figure 6 Isolation Valve Location

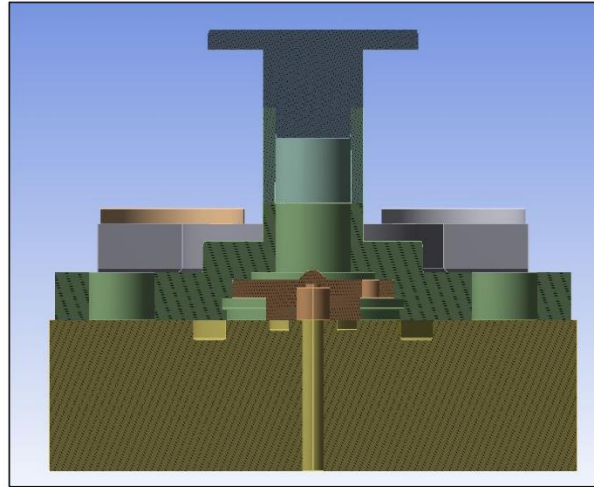


Figure 7 Isolation Valve Cross Section

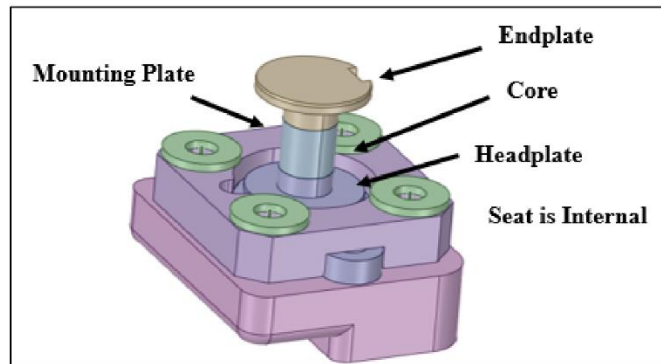


Figure 8 Isolation Valve Subcomponents (Including the Mounting Plate)

The isolation valve is mounted on the tank and isolates the hazardous fluid within the tank from the rest of the LFPS while on board SLS. After Lunar Flashlight is launched from SLS, the valve is commanded open for the duration of the mission. The micro-valve part used on the tank is the same as the four used on the manifold for thruster control.

3.1.5 Isolation Valve Mounting Plate

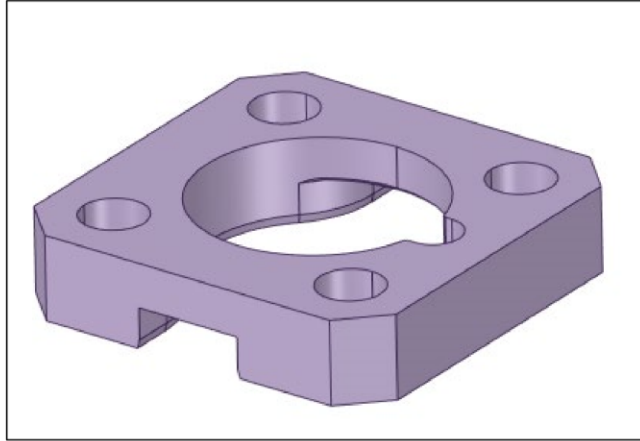


Figure 9 Isolation Valve Mounting Plate

The isolation valve is clamped to the tank underneath the isolation valve mounting plate. The two bolt fastener pattern of the micro-valve prevents the bolts from being designated as fail safe. The mounting plate allows for more fasteners and is used to prevent the bolts from being deemed fracture critical. The mounting plate does not see significant loads following installation.

3.1.6 Service Valve

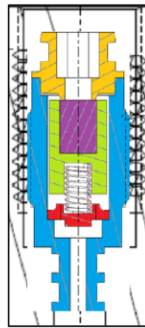


Figure 10 Service Valve Cross Section

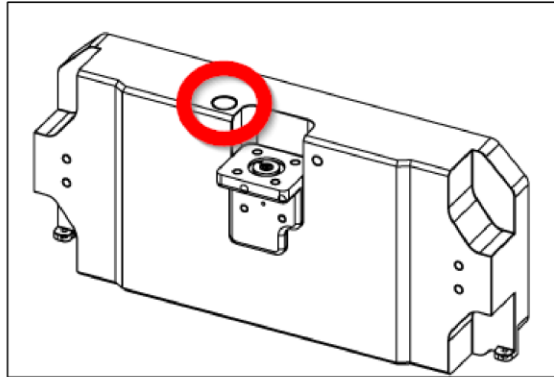


Figure 11 Service Valve Location

The service valve is used to fill, drain, and pressurize the tank. The service valve is a previously qualified part that was assessed to higher pressures for another program. This component is in a different configuration on the ground compared to flight. The ground support half is removed and the opening is plugged prior to launch. See memo ER41 (18-028) for structural analysis.

3.1.7 Pressure Transducer

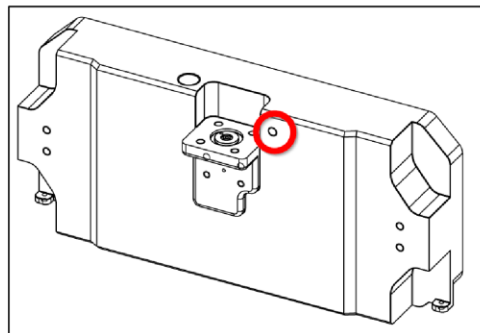


Figure 12 Pressure Transducer Location

The pressure transducer is a commercial off the shelf component that is installed into the tank bottom. It is qualified to a much higher pressure than that of the tank. The stress analysis for this part is discussed in the LFPS Structural Analysis Report.

NASA-HDBK-5010, VOLUME 2, REVISION A

3.1.8 Other Components

The other components are of less importance for the fracture analysis, as these components are to be designated as NFC-Contained or Exempt. None of these components are used to contain the hazardous fluid during launch. These components include:

1. Controller
2. Pump
3. Recirculation block
4. Propellant management device (PMD)
5. Thrusters
6. Thruster valves
7. Seals
8. All fasteners other than those on the isolation valve

NASA-HDBK-5010, VOLUME 2, REVISION A

3.2 Fracture Disposition and Summary

Table 1 Fracture Summary

Part Name	Part Numbers	Materials	Heat Treatment	Fracture Disposition	Ult. MS
Tank Top	GT-PN 1111-001 B	Ti 6Al-4V	AMS 4928	FC – Pressurized Vessel – Safe-Life Analysis	+0.06
Tank Bottom	GT-PN 1111-001 E	Ti 6Al-4V	AMS 4928		
Tank Weld	N/A	Ti 6Al-4V	Stress Relieved		+0.77
Manifold	GT-PN 1210-001 C	DMLS Ti 6Al-4V	AMS 2801B	NFC – Contained	+1.92
Muffin Tin	GT-PN 1261-001 C	Ti 6Al-4V	AMS 4967	NFC – Contained	+9.17
Isolation Micro-Valve	GT-PN 1121-001 A	CRES 304L CRES 430	Annealed	FC – Pressurized Component	+0.09
Isolation Valve Mounting Plate	GT-PN 1122-001 A	CRES 304L	Annealed	NFC – Failsafe	+0.23
Isolation Valve Fasteners	NAS1352N08L8	A286	N/A	NFC – Failsafe	+0.00
Service Valve	GT-PN 1134-001 A	15-5PH	H900	FC – Pressurized Component	N/A
Pressure Transducer	GT-PN 1131-001 A TE XP5-X-150PA- /V05/L3M/Z02	COTS – N/A	N/A	FC – Pressurized Component	N/A
Pump	GT-PN 1241/4-001 A	Various	N/A	NFC – Contained	N/A
Recirculation Block	GT-PN 1234-001 C	DMLS Ti 6Al-4V	AMS 2801B	NFC – Contained	+0.67
PMD Vanes	GLRG-LFPS-903	Ti 6Al-4V	ASTM B265 Grade 5	NFC-Contained	+8.37
PMD Sponge	GLRG-LFPS-902	DMLS Ti 6Al-4V	AMS 2801B	NFC-Contained	+0.62
Thrusters	GT-PN 1221/4-001 A	Various	N/A	NFC – Contained	N/A
Thruster Micro-Valve	GT-PN 1241/4-001 A	CRES 304L CRES 430	Annealed	NFC – Contained	+0.09
All fasteners except those on isolation valve	NAS1352	A286	N/A	NFC – Contained	+0.00
Controller	GT-PN 1250-001 C	N/A	N/A	Exempt	N/A

NASA-HDBK-5010, VOLUME 2, REVISION A

3.3 Geometry

3.3.1 Tank Top/Bottom

The tank geometry used in the finite element model (FEM) accounts for worst case GD&T on the wall thicknesses. The tolerances and nominal CAD model are based on the 11/22/2019 design freeze. The geometry provided was held to a general tolerance of $\pm 0.014''$, so the wall thicknesses were reduced by $0.028''$ everywhere but at the weld. Fillet radii, bolt hole locations, and feature locations were not geometrically changed in the model to account for tolerances. These features should not impact the stress results significantly. The tank geometry was reviewed on 4/1/2020 and was determined that the final tolerances are better than those used in the 11/22/2019 FEM, therefore a rerun is not necessary.

The damage tolerance analysis assumes a minimum thickness based on the worst location in the entire tank. The ER41 Design assisted and interrogated the 4/1/2020 model to check 6 locations for minimum thicknesses. Tolerance stackups were developed at these locations to find the minimum dimension between the pressurized space and the exterior of the tank. Each location of interest is described here:

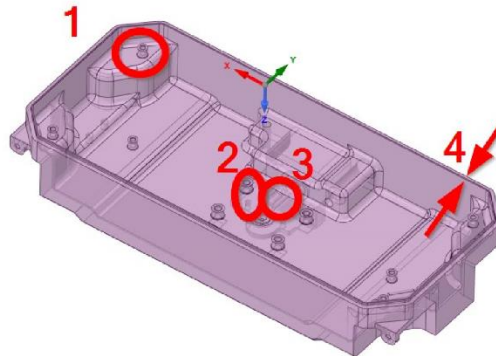


Figure 13 Tank Top Critical Dimension Locations

1. The minimum thickness locations are in the tank bottom, located at the outermost standoffs for the PMD Vanes. The worst case distance between the bottom of the bolt holes and the tank exterior is $0.087''$.
2. Bolt holes are close to each other in the bottom of the tank. On one side are the PMD standoffs and the other is the manifold connection. The minimum distance between these holes is $0.123''$.

NASA-HDBK-5010, VOLUME 2, REVISION A

3. The two fluid lines drilled into the bottom of the tank are 0.113" apart worst case. One tube is under pressure during launch, while the other is unpressurized, realistically, a flaw that propagates here would not necessarily result in a catastrophic hazard, but it is assumed that this is the case. This location will be inspected with eddy current, as dye penetrant inspection is impossible in this enclosed space.
4. The tank walls are 0.118" thick nominally, with a minimum thickness of 0.108". These tank walls will only be inspected with dye penetrant NDE.

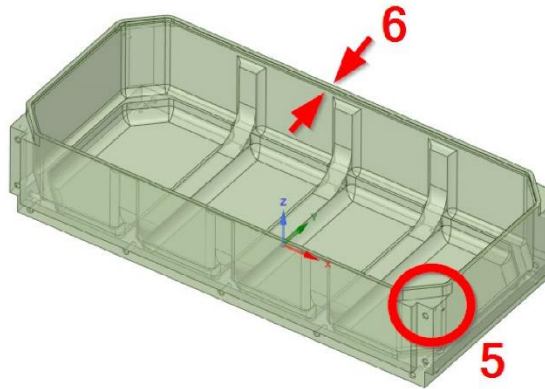


Figure 14 Tank Top Critical Dimension Locations

5. Holes are drilled into the tank exterior for connecting LFPS to the remainder of the Lunar Flashlight. The minimum dimension between these holes and the tank interior is 0.108".
 6. The tank walls are 0.118" thick nominally, with a minimum thickness of 0.108". These tank walls will only be inspected with dye penetrant NDE.
- Note that the isolation valve interface has seal grooves that are thinner (0.050") than the flaws that eddy current can inspect for (0.1"). Flaws at this location are screened using leak checks during testing. Additionally, this location is not expected to see significant stresses during flight (<2 ksi during MDP pressures) so flaws are not expected to grow.

NASA-HDBK-5010, VOLUME 2, REVISION A

The above geometry is used in the finite element analysis and the NASGRO analysis. The specific dimensions used in the NASGRO analysis are shown in the figure below:

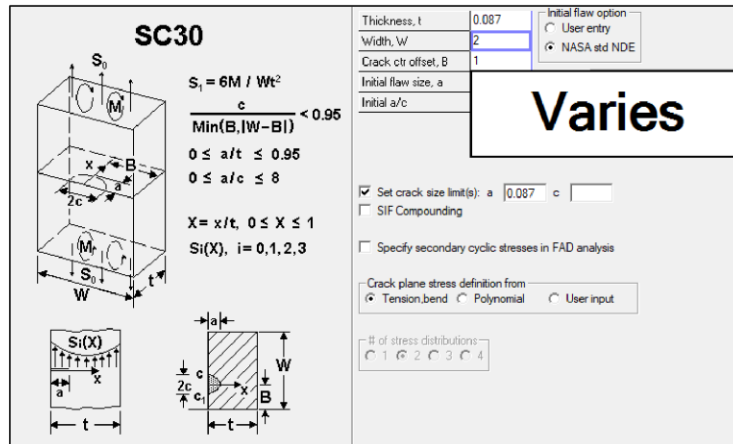


Figure 15 NASGRO Tank Top/Bottom Dimensions

3.3.2 Weld Dimensions

The weld dimensions used in the analysis are from the 11/22/2019 geometry design freeze, but align with tolerances from the 4/1/2020 design. The weld is held to AMS 2680C, which allows a 10% reduction in depth; this is not accounted for in the FEM analysis, but is accounted for in the damage tolerance analysis. The worst case weld depth is 0.067", accounting for AMS 2680C. The worst case geometry used in the FEM can be seen in the following figures:

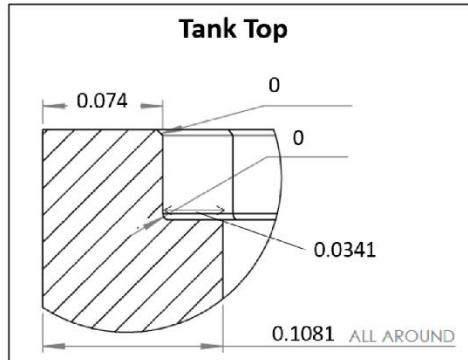


Figure 16 Worst case Weld Geometry – Tank Top

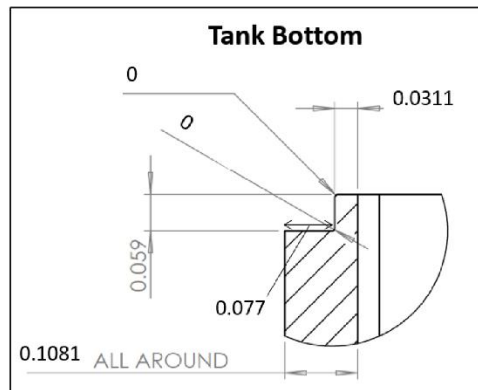


Figure 17 Worst Case Weld Geometry – Tank Bottom

NASA-HDBK-5010, VOLUME 2, REVISION A

The above geometry is used in the finite element analysis and the NASGRO analysis. The specific dimensions used in the NASGRO analysis are shown in the figure below:

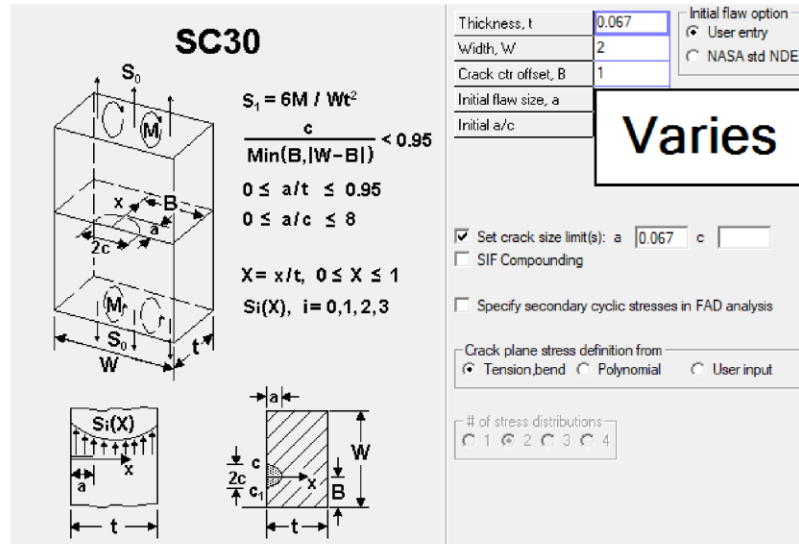


Figure 18 NASGRO Weld Dimensions

3.3.3 NDE Inspection Methods

Various NDE methods are used on lunar flashlight:

- Tank Top and Bottom pre-machining – Ultrasonic inspection of the raw stock per NASA-STD-5009B.
- Tank Top and Bottom post-machining – dye penetrant inspection where possible, eddy current inspection everywhere else. Flaw detection criteria & dimensions are per NASA-STD-5009B. The damage tolerance analysis conservatively uses dye penetrant flaw sizes in all locations.
- Tank Weld – Dye penetrant inspection, before and after tank proof test. Flaw size used will be 90% of the thickness, as noted in the alternative approaches section of the Fracture Control Plan.
- Isolation Valve – the valve will be inspected on the exterior using dye penetrant per NASA-STD-5009B. 2

NASA-HDBK-5010, VOLUME 2, REVISION A

3.3.4 Isolation Valve Mounting Plate

The isolation mounting plate model is run with nominal dimensions. The part has sufficient margin that this is not a concern.

3.3.5 Isolation Valve Mounting Plate Fasteners

The fastener information is listed below:

- Bolt: NAS1352N08L6
- 0.164-32 Threads
- 15 in*lbf max locking torque
- 8-10 in*lbf installation torque (above running torque)
- 0.97 Thermal knockdown (140°F, MMPDS13, see LFPS Structural Analysis Report)
- Plate 2: Mounting Plate & Valve (0.25" thick)
- Plate 3: Tank (0.125" thread engagement)

NASA-HDBK-5010, VOLUME 2, REVISION A

3.4 Factors of Safety

Factors of Safety are referenced per LFPS-SPEC-201, Safety document “LF-04 Pressure System Rupture 20191010”, AIAA S-080-1998, NASA-STD-5019, and NASA-STD-5001.

Table 2 Factors of Safety

Load Case		Proof / Yield Factor of Safety	Burst / Ultimate Factor of Safety
Ground / Launch / On-Orbit / Proof / Burst / Buckling	Inertia	1.25 ³	1.4 ³
	Pressure	1.5 ²	2.5 ¹

Notes:

1. Burst/ultimate pressure test includes safety factor (2.5) (per LFPS-SPEC-201 & AIAA S-080-1998), and an ECF of 1.06 (required by NASA-STD-5019). This aligns/exceeds the factors listed in “LF-04 Pressure System Rupture 20191010.doc §1.1.
2. Proof/yield pressure test includes a 1.5x safety factor (LFPS-SPEC-201) and an ECF of 1.06 (required by NASA-STD-5019). This aligns with “LF-04 Pressure System Rupture 20191010.doc §1.1.
3. From NASA-STD-5001 Table 1

NASA-HDBK-5010, VOLUME 2, REVISION A

4.0 MATERIAL PROPERTIES

Material properties are used in a variety of analyses and descriptions will be sorted by material type. This data includes material properties used in all analyses, as some non-fracture critical parts are included in analysis of fracture critical components. Additionally, some of these properties are only used in the LFPS Structural Analysis Report.

4.1 Ti-6Al-4V Bar (AMS 4928)

Used on:

- Tank top
- Tank bottom
- Muffin tin

Material Stock Information:

- Formerly AMS 4967
- Condition: Annealed, stress relieved after weld (tank only)
- Form: Bar
- Stock: 6-10" T (conservative)

Static MS Calculations:

- These properties are used to determine static margins of safety for the parts, fastener static analyses, fastener thermal analysis, factor of safety for proof testing, and fatigue analyses
- $F_{tu}=130$ ksi (MMPDS13)
- $F_{ty} = 119$ ksi (MMPDS13)
- $E=16.9 \times 10^6$ psi (MMPDS13)
- $\alpha_{300^{\circ}\text{F}}= 5.1 \times 10^{-6}$ in/in/ $^{\circ}\text{F}$ (MMPDS13 F5.4.1.0(a2))
- $ECF_{\text{NonOp}} = 0.94$ (F_{tu} & F_{ty} - 140 $^{\circ}\text{F}$ - MMPDS13 F5.4.1.2.1)

NASGRO Properties:

- These properties are used exclusively in the NASGRO/NASFLA analyses. The material is based on the data in the NASGRO material library with some modifications.
- Material ID: P3EA13AB1
- Material description: Ti-6Al-4V; MA(1450F/788C/0.5hr/AC) 0.25in Plt; L-T; Lab Air
- Modifications:
 - BK=0 – This change is required by NASA-STD-5019

Material properties: ID P3EA13AB1, Ti-6Al-4V, MA(1450F/788C/0.5hr/AC) 0.25in Plt; L-T; Lab Air									
UTS	Yield	K1e	K1c	Ak	Bk	a0[eg.0.0015]	Kth(e)/Kth(l) [eg.0.2]		
146	138	65	50	1	0	0.0015	0.2		
Crack growth parameters: equation constants									
C	n	p	q	DK1	Cth	Cth-	Alpha	Smax/Flow	
2.5E-9	3.0	0.5	0.75	2.1	0.0	0.1	2.5	0.3	
Threshold fanning exponent									
<input checked="" type="radio"/> Cth					<input type="radio"/> Pth				
Cth value used in analysis									
<input type="radio"/> 0 initially					<input checked="" type="radio"/> 0 throughout				
<input type="radio"/> input cell value throughout					<input type="checkbox"/> Suppress closure				

FEM Properties:

- ER41 Material Library – 1.37
- Ti-6Al-4V STA, Bar, AMS 4967, 3" > t > 4", 4" > W > 8" (Acceptable because model is within elastic range)

Fatigue properties:

- S-N curve from MMPDS13, Figure 5.4.1.1.8(a)
- S-N curve is read at 10⁷ cycles, unnotched, R=-1: S_{eq}=45 ksi

NASA-HDBK-5010, VOLUME 2, REVISION A

4.2 Ti-6Al-4V Weld

Used on:

- Tank weld

Material information:

- Same material as tank, but EB welded and heat treated

Static MS Calculations:

- These properties are used to determine static margins of safety for the parts and fatigue analyses
- Based on fatigue data from the “Atlas of Fatigue Curves,” the yield and ultimate stress allowables can be assumed to be greater than 100 ksi
- ECF_{NonOp} , ECF_{Op} are assumed to be the same as the tank

NASGRO Properties:

- These properties are used exclusively in the NASGRO/NASFLA analyses. The material is based on the data in the NASGRO material library with some modifications.
- Properties have been coordinated with EM21 (Doug Wells)
- Material ID: P3EMD2LA4
- Material Description: Ti-6Al-4V (ELI); RA(1700F/927C/4h); EB – Electron Beam weld/parallel/stress relieved; LG; -320F/-196C Liq. N2
- Modifications per EM21/ Doug Wells: UTS=120, YS=110, K1c=55.0, K1c=45.0, DK1=1.0, BK=0

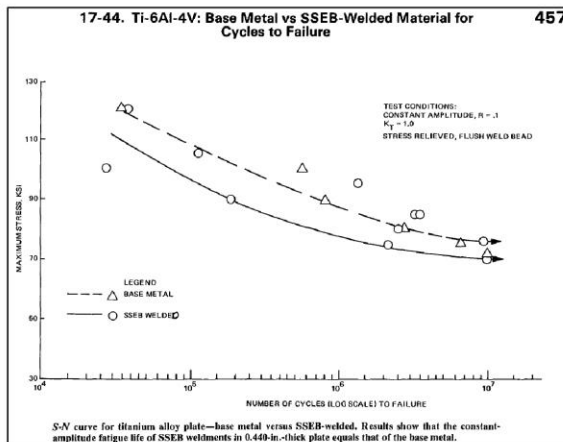
Material properties: ID P3EMD2LA4, Ti-6Al-4V (ELI); RA(1700F/927C/4h) Forg; EB-welded-SR; welding: -320F/-1...									
UTS	Yield	K1e	K1c	Ak	Bk	a0[eg:0.0015]	Kth(s)/Kth(l)	[eg:0.2]	
120	110	55	45	0.4	0	0.0015	0.2		
Crack growth parameters: equation constants									
C	n	p	q	DK1	Cth	Cth-	Alpha	Smax/Flow	
7e-10	3.2	0.5	0.5	1	0.1	0.1	2.5	0.3	

FEM Properties:

- ER41 Material Library – 1.37
- Ti-6Al-4V STA, Bar, AMS 4967, 3”>t>4”, 4”>W>8”

Fatigue properties:

- S-N curve from Atlas of Fatigue Curves, ASM International (1986), Page 457
- S-N curve is read at 10^7 cycles, unnotched, and $R=0.1$: $S_{eq}=70$ ksi



NASA-HDBK-5010, VOLUME 2, REVISION A

4.3 AM Ti-6Al-4V

Used On:

- Manifold
- Pump Block
- PMD Sponge

Material Information

- Additively Manufactured DMLS Titanium

Static MS Calculations:

- These properties are used to determine static margins of safety for the parts, fastener static analyses, fastener thermal analysis, factor of safety for proof testing, and fatigue analyses
- Source: "Metal Additive Manufacturing. A Review of Mechanical Properties" – Lewandowski Seifi – 2016 – Provided by Omar Rodriguez / EM31
- $F_{ty} = 111.4$ ksi
- $F_{tu} = 117.6$ ksi
- ECF_{NonOp} , ECF_{Op} are assumed to be similar to the tank

NASGRO Properties:

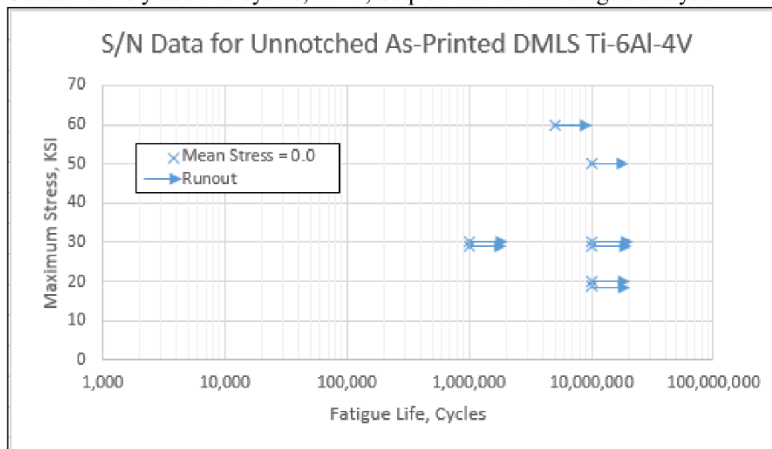
- N/A (no damage tolerance analysis performed)

FEM Properties:

- ER41 Material Library – 1.37
- Ti-6Al-4V STA, Bar, AMS 4967, 3" > t > 4", 4" > W > 8"

Fatigue Properties

- All 8 tests ran out at different stresses and cycles
- Data shown in the figure on the right
- Samples are from the same print as the flight manifold
- Conservatively use 106 cycles, $R=-1$, $Seq=30$ ksi for the fatigue analysis



NASA-HDBK-5010, VOLUME 2, REVISION A

4.4 Aluminum 7075-T7351

Used On:

- Lunar Flashlight Spaceframe

Material Information:

- Aluminum 7075-T7351

FEM Properties:

- ER41 Material Library – 9.17
- Al 7075-T7351, Plate, AMS 4078, 0.5” > t > 1.0”

NASGRO Properties:

- N/A (no damage tolerance analysis performed)

4.5 A286 Bolts:

Used on:

- All Fasteners

Material Information

- A286 Per FF-S-86E

Static MS Calculations:

- These properties are used to determine fastener static analyses, fastener thermal analysis, factor of safety for proof testing, and fatigue analyses
- $F_{tu} = 160$ ksi per FF-S-86E
- $F_{ty} = 120$ ksi per FF-S-86E
- $E = 29.1 \times 10^6$ psi (MMPDS13)
- $\alpha_{300^\circ F} = 9.3 \times 10^{-6}$ in/in/°F (MMPDS13 F6.2.1.0(b))
- $ECF_{NonOp} = 0.97$ (F_{tu} & F_{ty} - 140°F - MMPDS13 F6.2.1.1.1)

FEM Properties:

- ER41 Material Library – 10.1
- A286 STA, sheet/strip/plate, AMS 5525
- Plastic properties used only in the isolation valve FEM:

Properties of Outline Row 7: A286 per FF-S-86 (140F only)

	A	B	C
1	Property	Value	Unit
2	Material Field Variables	Table	
3	Isotropic Elasticity		
4	Derive from	Young's Modulus...	
5	Young's Modulus	2.91E+07	psi
6	Poisson's Ratio	0.31	
7	Bulk Modulus	2.5526E+07	psi
8	Shear Modulus	1.1107E+07	psi
9	Bilinear Kinematic Hardening		
10	Yield Strength	1.16E+05	psi
11	Tangent Modulus	3.2333E+05	psi

NASGRO Properties:

- N/A (no damage tolerance analysis performed)

Fatigue Properties:

- Heritage shuttle data used
- S-N curve is read at 106 cycles, unnotched, and R=-1: Seq=50 ksi

NASA-HDBK-5010, VOLUME 2, REVISION A

4.6 CRES 304L

Used On:

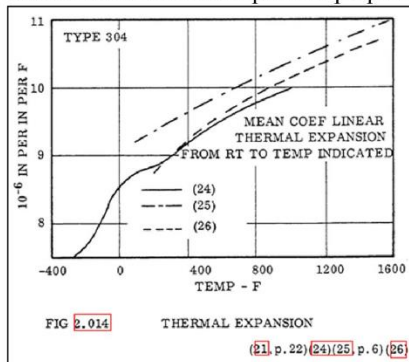
- Isolation Valve Core and Mounting Plate
- Thruster Valve Core

Material Information:

- CRES 304L

Static MS Calculations:

- These properties are used to determine static margins of safety for the parts, fastener static analyses, fastener thermal analysis, and fatigue analyses
- $F_{tu} = 70$ ksi per ASTM A276
- $F_{ty} = 25$ ksi per ASTM A276
- $ECF_{NonOp} = 0.94$ (F_{tu} & $F_{ty} - 140^{\circ}F$ - MMPDS13 F2.7.1.1(a)&(b))
- $E = 29 \times 10^6$ psi per MMPDS13
- $e = 0.30$ in/in (MMPDS-13 T2.7.1.0(b3)) (Used in point strain calculations)
- Coefficient of thermal expansion properties are from ASMH Figure 2.014



FEM Properties:

- ER41 Material Library – 8.1
- AISI 304 Stainless Steel – Solution Treated – AMS 5513

NASGRO Properties:

- N/A (no damage tolerance analysis performed)

Fatigue Properties:

- Sourced from heritage shuttle data
- S-N curve is read at 10^6 cycles, unnotched, and $R = -1$: $S_{eq} = 24$ ksi

NASA-HDBK-5010, VOLUME 2, REVISION A

4.7 430 CRES (ASTM A276)

Used On:

- Isolation Valve Headplate and Endplate
- Thruster Valve Headplate and Endplate

Material Information:

- 430 CRES per ASTM A276

Static MS Calculations:

- These properties are used to determine static margins of safety for the parts, fastener static analyses, fastener thermal analysis, and fatigue analyses
- $F_{tu} = 60$ ksi per ASTM A276
- $F_{ty} = 30$ ksi per ASTM A276
- Modulus of elasticity and coefficient of thermal expansion provided by EM31
- Assume ECF is the same as CRES 304L
- $e=0.20$ in/in (MMPDS-13 T2.7.1.0(b3)) (Used in point strain calculations)
- $E=29000$ ksi (Assume same as 304L) (Used in point strain calculations)

FEM Properties:

- ER41 Material Library – 16.1
- AISI 430 – Annealed – ASTM A276

NASGRO Properties:

- N/A (no damage tolerance analysis performed)

Fatigue Properties:

- Sourced from heritage shuttle data
- S-N curve is read at 10^6 cycles, unnotched, and $R=-1$: $S_{eq}=42$ ksi

NASA-HDBK-5010, VOLUME 2, REVISION A

4.8 CRES 304L to ASTM A276 Weld

Used on:

- Welds for the isolation and thruster valves. Specifically between the core and the adjacent components.

Static Properties:

- Based on historical ER41 documentation and processes for EB weld knockdown factors (60%) and the worst properties of the two welded materials
- $F_{tu} = 36$ ksi
- $F_{ty} = 15$ ksi
- Assume ECF is the same as CRES 304L

Fatigue Properties:

- Sourced from heritage shuttle data
- S-N curve is read at 10^6 cycles, unnotched, and $R=-1$: $Seq=21$ ksi

NASGRO Properties:

- N/A (no damage tolerance analysis performed)

4.9 15-5 PH Service Valve

Used On:

- Service Valve

Fatigue Properties:

- $F_{tu} = 185.9$ ksi (Memo ER41(18-028))
- S-N curve from MMPDS13 Fig. 2.6.7.2.8(b)
- S-N curve is read at 10^6 cycles, unnotched, and $R=0.1$: $Seq=166$ ksi

NASGRO Properties:

- N/A (no damage tolerance analysis performed)

NASA-HDBK-5010, VOLUME 2, REVISION A

5.0 LOADS AND ENVIRONMENTS

5.1 Mission Profile

The Lunar Flashlight undergoes a single mission launched from SLS during Artemis-1. Following testing and launch, it is jettisoned from SLS at “Bus Stop 1” and will make passes around the moon using LFPS multiple times to change its orbit. Some components see testing prior to system integration.

Table 3 Mission Profile

Event	Cycles	Operational Load
Micro Valve Proof 1	1 cycle ³ (valves only)	600 psi ³
Micro Valve Proof 2	1 cycle ³ (valves only)	1307 psi ³
Tank Fill Events	10 cycles ⁴ (tank & valves)	-1 atmosphere to 1x MDP ¹⁴
Pressure Tests	50 cycles ⁴ (tank, lines, & valves)	1x MDP ¹
Tank Proof Test	1 cycle ⁴ (tank & valves)	159 psi ¹²
System Proof Test	1 cycle ⁴ (tank, lines, & valves)	1.1x MDP ⁴
System Proto-Qual RV Test	3 events	Unpressurized Various Inertia Loads
Launch	1 event	1x MDP Various Inertia Loads
Mission Pressure	<200 events ⁵ (lines and valves)	1x MDP

References

1. LFPS-SPEC-201
2. Tank proof test has been increased 6% (NASA-STD-5019 required environmental correction factor, with MMPDS-13 data)
3. Brad Addona / ER14
4. Carlos Diaz & Hunter Williams / ER11
5. The pump output pressures will vary insignificantly during each thruster event.

Notes

- Tank fill and pressure cycles are increased as the test plan isn’t finalized
- Inertial cycles have been derived from available data and are discussed later
- LFPS-SPEC-205 §3.2.7.3 requires 50,000 operation cycles of the micro-valve

NASA-HDBK-5010, VOLUME 2, REVISION A

- Thermal cycles are assumed to be insignificant due to low cycle counts and a benign thermal environment. The total number of thermal cycles is estimated as the number of days LFPS sits in SLS (365 days per LFPS-SPEC-201) plus the number of firing events (<200 per ER12 on 7/21/2020).

5.2 Pressure

The tank is designed such that the pressure will not exceed MDP of 100 psi. The lines downstream of the pump have an MDP of 500 psi. The analysis assumes that MDP is achieved in all pressurized events (assembly, test, launch, and operation). Additionally, 1 atmosphere crush pressure is assumed for tank fill events as a vacuum is pulled prior to fluid loading. It is worth noting that the service, isolation, and thruster valves are tested to a proof pressure greater than what is necessary on LFPS. The MDP pressures, burst factors, and proof factors are derived from requirements in LFPS-SPEC-201, specifically LFPS-REQ-011, LFPS-REQ-012, and LFPS-REQ-013.

5.3 Thermal

The thermal environment is benign. The analysis assumes non-operational temperatures will occur at the same time as worst case loads. Material thermal degradation factors are used on all static margins. Thermal expansion is ignored for all analyses except for fasteners. The below temperatures were obtained from LFPS-SPEC-201 requirement LFPS-REQ-061 (converted from Celsius):

1. Non-operational: 5°-140°F
2. Operational: 41°-104°F

NASA-HDBK-5010, VOLUME 2, REVISION A

5.4 Inertial

The LFPS undergoes five inertial events: handling, ground transportation, system level RV testing, launch, and thruster firings. Handling, ground transportation and thruster firings are ignored. Thruster firings generate 0.0034 g's (per ER11), which is negligible.

The load factors on the LFPS are sourced from LFPS-SPEC-201 requirements LFPS-REQ-059 and LFPS-REQ-060. The low frequency and RV load factors are combined in the below table and are listed in the SLS dispenser local coordinate system.

Table 4 LFPS Load Factors

	Axial		Lateral		Radial	
LC1	31.02	-32.64	3.00	-3.00	4.58	-2.18
LC2	2.82	-4.44	18.60	-18.60	4.58	-2.18
LC3	2.82	-4.44	3.00	-3.00	22.58	-20.18

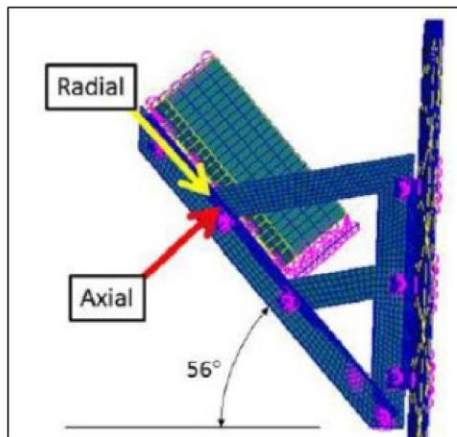


Figure 19 SLS Dispenser Local Coordinate System

NASA-HDBK-5010, VOLUME 2, REVISION A

	A	B	C	D	E	F	G	H	I	J	
1											
2											
3		Rotation			deg	rad					
4					-56	-0.97738					
5											
6		Rand Vibe Loads *			LFPS REQ Table 4						
7		In LF Frame			Axial	Lateral	Radial				
8					28.20	-28.20	15.60	-15.60	18.00	-18.00	
9											
10		Low Freq loads (S*)			LFPS REQ Table 5						
11		In SLS Frame			Vertical	Lateral	Radial				
12					0.6	-3.5	3	-3	3	-3	
13											
14		Low Freq Loads (S)			Table 5 converted to LF coordinates						
15		In LF Frame			Axial	Lateral	Radial				
16					2.82	-4.44	3.00	-3.00	4.58	-2.18	
17											
18		Combined loads			Combined loads from STD-3676						
19					Axial	Lateral	Radial				
20					LC1	31.02	-32.64	3.00	-3.00	4.58	-2.18
21					LC2	2.82	-4.44	18.60	-18.60	4.58	-2.18
22					LC3	2.82	-4.44	3.00	-3.00	22.58	-20.18
23											

Figure 20 Load Combination Spreadsheet Results

	A	B	C	D	E	F	G	H	I	J	
1											
2											
3		Rotation			deg	rad					
4					=E4*PI()/180						
5											
6		Rand Vibe Loads *			LFPS REQ Table 4						
7		In LF Frame			Axial	Lateral	Radial				
8					28.2	-28.2	15.6	-15.6	18	-18	
9											
10		Low Freq loads (S*)			LFPS REQ Table 5						
11		In SLS Frame			Vertical	Lateral	Radial				
12					0.6	-3.5	3	-3	3	-3	
13											
14		Low Freq Loads (S)			Table 5 converted to LF coordinates						
15		In LF Frame			Axial	Lateral	Radial				
16					=E12*COS(SF4)-J12*SIN(SF4)	=F12*COS(SF4)-J12*SIN(SF4)	3	-3	=COS(SF54)*I12+SIN(SF54)*F12	=COS(SF54)*J12+SIN(SF54)*E12	
17											
18		Combined loads			Combined loads from STD-3676						
19					Axial	Lateral	Radial				
20					LC1	=E16+E8	=F16+F8	=G16	=H16	=I16	=J16
21					LC2	=E16	=F16	=G16+G8	=H16+H8	=I16	=J16
22					LC3	=E16	=F16	=G16	=H16	=I16+I8	=J16+J8
23											

Figure 21 Load Combination Spreadsheet Calculations

5.4.1 RV Cycle Spectra Creation

The RV spectra isn't defined in the parent specifications for the LFPS. A conservative spectra has been generated using information from test plans, SLS, and the structural analysis FEM.

A conservative modal analysis was run to determine the fundamental frequencies of the LFPS. The structural analysis FEM was used (see LFPS Structural Analysis Report for more details on the model). The boundary conditions in the structural FEM should be much stiffer than those of the launch environment, which is conservative. Mass participations were extracted to help identify which modes

excited the tank. Note that the modes that excited other components (e.g. the muffin tin) are ignored. The fluid, thruster, valve, PMD, pump, and controller masses are conservatively ignored. The mass participation results and the three fundamental modal shapes can be seen below.

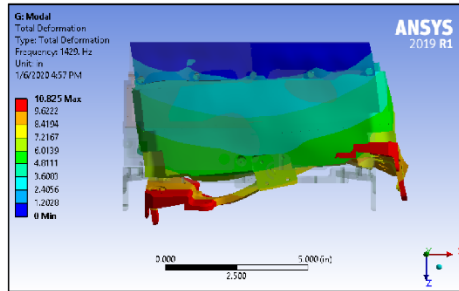


Figure 22 Primary Tank Y Mode Shape (Mode 58, 1429Hz)

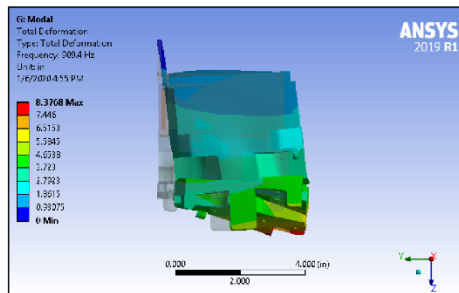


Figure 23 Primary Tank Y Mode Shape (Mode 22, 909Hz)

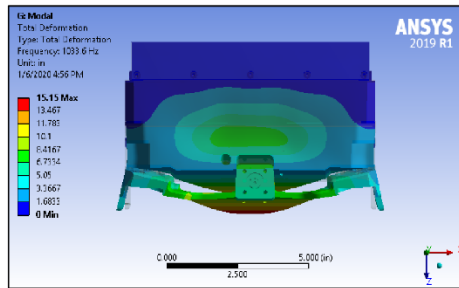


Figure 24 Primary Tank Z Mode Shape (Mode 41, 1034Hz)

NASA-HDBK-5010, VOLUME 2, REVISION A

Table 5 Modal Analysis: Mass Participation Results

Mode	Freq. (Hz)	Mass Participation Percentage			Mode	Freq. (Hz)	Mass Participation Percentage		
		X%	Y%	Z%			X%	Y%	Z%
1	234	0%	1%	0%	33	939	0%	0%	0%
2	495	0%	0%	0%	34	940	0%	0%	0%
3	581	0%	25%	0%	35	940	0%	0%	0%
4	588	0%	0%	0%	36	940	0%	0%	0%
5	590	0%	0%	0%	37	941	0%	0%	0%
6	590	0%	0%	0%	38	942	0%	0%	0%
7	590	0%	0%	0%	39	966	0%	32%	1%
8	659	1%	0%	0%	40	1026	1%	0%	0%
9	670	0%	0%	0%	41	1034	0%	1%	13%
10	674	0%	0%	0%	42	1043	0%	0%	0%
11	693	18%	0%	0%	43	1054	0%	1%	1%
12	702	0%	0%	0%	44	1059	0%	0%	0%
13	703	1%	0%	0%	45	1065	0%	0%	0%
14	791	0%	0%	6%	46	1065	0%	0%	0%
15	796	0%	0%	0%	47	1079	0%	8%	8%
16	800	1%	0%	0%	48	1179	0%	0%	0%
17	818	0%	0%	0%	49	1180	0%	0%	0%
18	818	0%	0%	0%	50	1181	0%	0%	0%
19	865	0%	0%	0%	51	1181	0%	0%	0%
20	874	0%	0%	0%	52	1194	0%	0%	3%
21	906	0%	0%	0%	53	1302	0%	0%	0%
22	909	0%	10%	2%	54	1349	0%	0%	0%
23	929	0%	0%	0%	55	1351	0%	0%	0%
24	933	0%	0%	0%	56	1405	0%	0%	0%
25	934	0%	0%	0%	57	1405	0%	0%	0%
26	934	0%	0%	0%	58	1429	28%	0%	0%
27	934	0%	0%	0%	59	1446	1%	0%	0%
28	937	0%	0%	0%	60	1515	0%	0%	0%
29	938	0%	0%	0%	61	1521	0%	0%	0%
30	938	0%	1%	0%	62	1551	1%	0%	0%
31	939	0%	0%	0%	63	1649	6%	0%	13%
32	939	0%	0%	0%	64	1660	12%	0%	8%

NASA-HDBK-5010, VOLUME 2, REVISION A

It is assumed that the random vibration events will occur at these fundamental frequencies. The random vibration tests are performed once in each direction, each directional test will excite the corresponding mode shape. It is conservatively assumed that the launch event will excite the direction with the highest frequency.

The RV test durations are listed in LFPS-SPEC-201 requirement LFPS-REQ-059 to be 60 seconds in each direction. The effective RV duration for the CubeSat on SLS launch was determined to be 13 seconds (Lowery Duvall/ER41). Both of these factors are conservatively multiplied by a 4.0 scatter factor. This results in 240 seconds of RV in each direction during test and 52 seconds during launch. Assuming that each event occurs at the fundamental frequencies determined in the modal analysis: $240 * (1429 + 909 + 1034) = 809,280$ cycles are expected during RV testing and $52 * 1429 = 74,308$ cycles are expected during launch.

These cycles are spread across a Rayleigh distribution based on methods from NASA-TM-X-64669. An upward bound of 3σ is used to align with the assumptions made to develop the RV load factors. The curve is approximated using discretization at midpoints with a 10% interval, as seen in the below figure and table.

Table 6 Rayleigh Distribution Discretization

Rayleigh Approximation		
Max	Min	Cycles
10%	-10%	4.48%
20%	-20%	12.29%
30%	-30%	17.10%
40%	-40%	18.28%
50%	-50%	16.40%
60%	-60%	12.78%
70%	-70%	8.80%
80%	-80%	5.41%
90%	-90%	2.98%
100%	-100%	1.48%

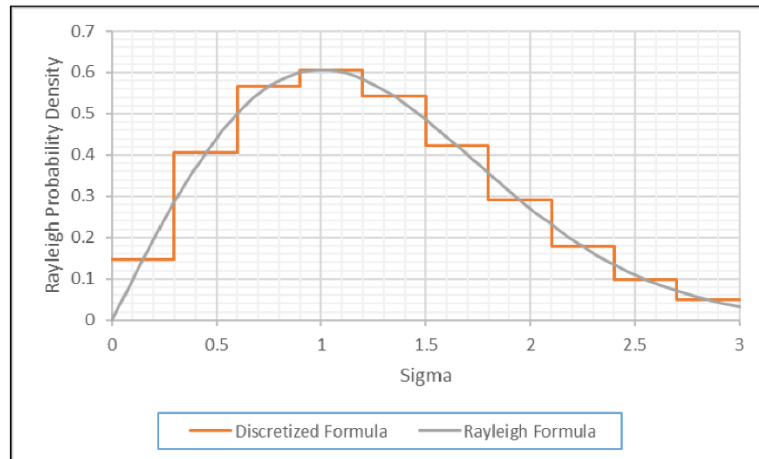


Figure 25 Rayleigh Distribution Discretization

The cycle counts are spread across this distribution for the flight and RV test cycles. The resulting spectra can be seen in the table below.

Table 7 RV Spectra Approximation

Max	Min	Test Cycles	Flight Cycles
10%	-10%	36,256	3,329
20%	-20%	99,461	9,132
30%	-30%	138,387	12,707
40%	-40%	147,936	13,584
50%	-50%	132,722	12,187
60%	-60%	103,426	9,497
70%	-70%	71,217	6,539
80%	-80%	43,782	4,020
90%	-90%	24,117	2,214
100%	-100%	11,977	1,100

6.0 COMPONENT DETAILS

6.1 Tank Top, Tank Bottom, and Tank Weld

The tank is classified as a fracture critical pressure vessel as it contains a hazardous fluid. The tank meets NASA-STD-5019 and AIAA-S-080-1998 requirements by verifying the safe life analysis and testing requirements are met.

6.1.1 Stress Analysis Results

A FEM was used to find the data needed to develop the stress spectra for the NASGRO damage tolerance analysis. The stress model and results are described in detail within the LFPS Structural Analysis Report. The models used are listed below:

1. Inertial model with 1.0x load factor and fluid modeled in the tank. 9 directions are checked to ensure the worst case load direction is assessed.
 - Submodels are used to obtain values at stress concentrations in the tank top/bottom
2. Inertial model with 1.0x load factor and no fluid modeled in the tank. Submodels are not used as the stress concentrations are in artificial sharp corner locations on the tank top/bottom.
3. Pressure model with 1.0x load factor on MDP
 - Submodels are used to obtain values at stress concentrations on the tank top/bottom
 - Submodels are used at three critical locations along the weld. The weld submodel stress results are recorded at the interior and exterior of the weld surface. These locations have been selected to envelope the worst cases. Locations A and B were chosen because they have the highest stresses. Location C was selected because the weld stress field had bending stress acting in the opposite direction from A and B.

Max principle stresses are used in the tank top/bottom and in the weld (pressure model only). Inertial weld stresses are taken at the weld surface by combining the peak tension and shear stresses together using the Von Mises equivalent stress equation:

$$\sigma_{Eq} = \sqrt{\sigma_T^2 + 3 * \tau^2}$$

Stresses in the weld are recorded at the interior and exterior of the weld surface for the pressure load case. Note that some inertial cases used magnitudes that were greater than the expected environments,

NASA-HDBK-5010, VOLUME 2, REVISION A

so these results are scaled down. The stress results shown with load magnitudes of 56.5 g's are scaled down linearly to 32.6 g's. Results and critical stress contours are shown below.

NASA-HDBK-5010, VOLUME 2, REVISION A

Table 8 Limit Stress Results – Tank Fluid Included

#	Load Case	Load Magnitude (g)	Weld Stress (ksi) (tension, shear, combined)	Tank Stress (ksi)	Weld Stress (adjusted) (ksi)	Tank Stress (adjusted) (ksi)
N/A	Pressure Only	N/A	N/A	51.6	N/A	51.6
1	Inertia +/-/+	56.5	3.5, 1.6, 4.5	10.0	2.6	5.8
2	Inertia +/+/+	56.5	2.7, 1.1, 3.3	11.8	1.9	6.8
3	Inertia +/-/-	56.5	3.1, 1.4, 3.9	8.8	2.3	5.1
4	Inertia +/+/-	56.5	2.4, 0.8, 2.8	10.8	1.6	6.2
5	Inertia +/ /	32.6	1.7, 0.8, 2.2	6.0	2.2	6.0
6	Inertia /+/	32.6	0.9, 0.3, 1.0	4.1	1.0	4.1
7	Inertia / /+	32.6	0.8, 0.3, 1.0	5.4	1.0	5.4
8	Inertia /- /	32.6	1.4, 0.6, 1.7	3.4	1.7	3.4
9	Inertia / /-	32.6	0.4, 0.2, 0.5	6.5	0.5	6.5
N/A	Inertia -/any/any	Assumed to be enveloped by the other inertial cases				

Table 9 Limit Stress Results – Tank Fluid Excluded

#	Load Case	Load Magnitude (g)	Weld Stress (psi) (tension, shear, combined)	Tank Stress (psi)	Weld Stress (adjusted) (psi)	Tank Stress (adjusted) (psi)
1	Inertia +/-/+	56.5	570, 727, 1382	1197	798	691
2	Inertia +/+/+	56.5	608, 754, 1441	1341	831	773
3	Inertia +/-/-	56.5	901, 787, 1634	1824	943	1052
4	Inertia +/+/-	56.5	1034, 780, 1701	1897	982	1094
5	Inertia +/ /	32.6	212, 237, 462	681	462	681
6	Inertia /+/	32.6	667, 576, 1200	1464	1200	1464
7	Inertia / /+	32.6	108, 188, 343	677	343	677
8	Inertia /- /	32.6	534, 576, 1132	1260	1132	1260
9	Inertia / /-	32.6	363, 188, 488	774	488	774
N/A	Inertia -/any/any	Assumed to be enveloped by the other inertial cases				

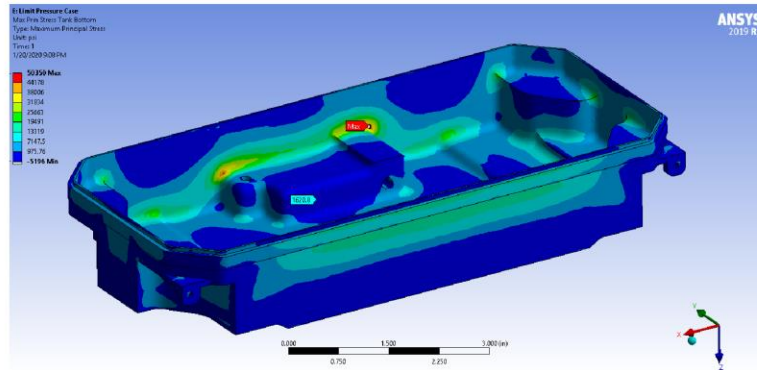


Figure 26 Max Principle Stress Location Due to MDP in Tank Top/Bottom

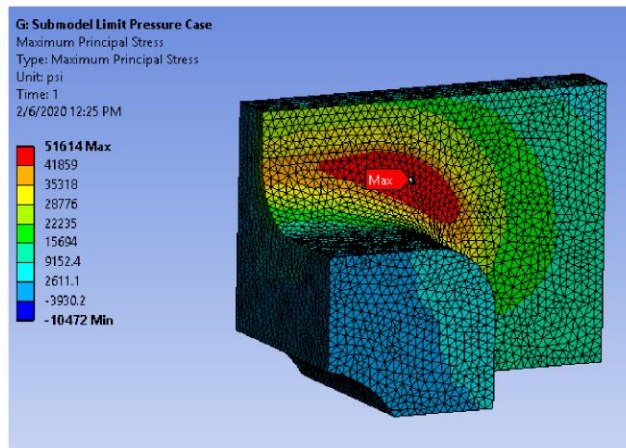


Figure 27 Max Principle Stress Location Due to MDP in Tank Top/Bottom – Submodel

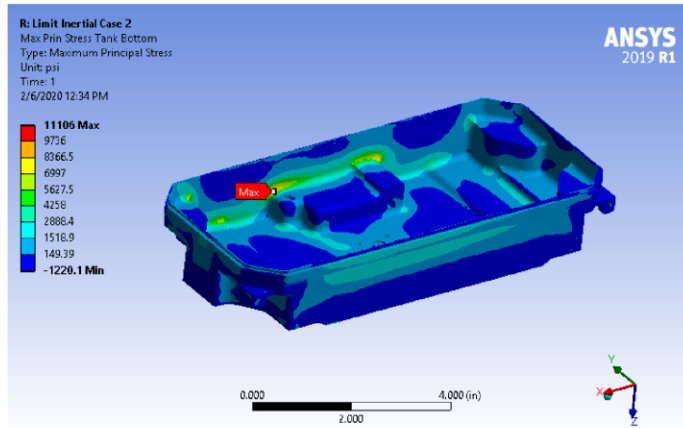


Figure 28 Max Principle Stress Location Due to Inertia (Full Tank) in Tank Top/Bottom (56.5 g Load Factor, Correction Factor: 32.6/56.5)

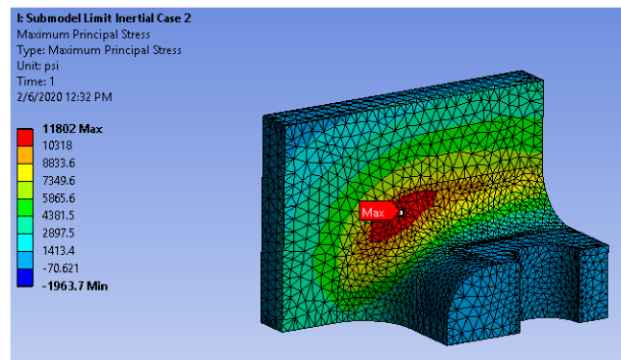


Figure 29 Max Principle Stress Location Due to Inertia (Full Tank) in Tank Top/Bottom – Submodel (56.5 g Load Factor, Correction Factor: 32.6/56.5)

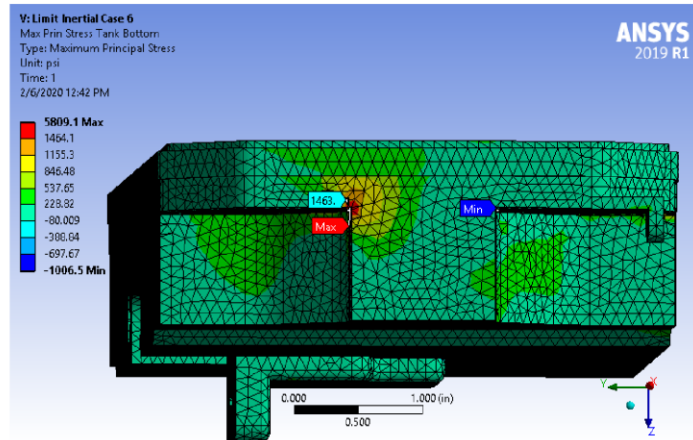


Figure 30 Max Principle Stress Location Due to Inertia (Empty Tank) in Tank Top/Bottom (32.6 g Load Factor)

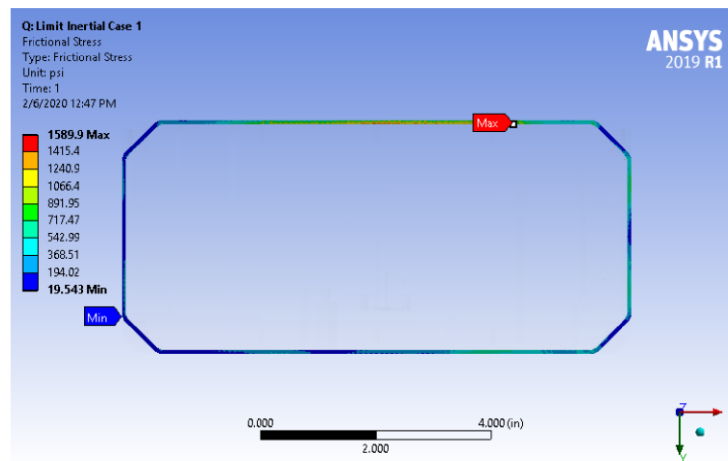


Figure 31 Maximum Shear Stress Due to Inertia (Full Tank) in Weld (56.5 g Load Factor, Correction Factor: 32.6/56.5)

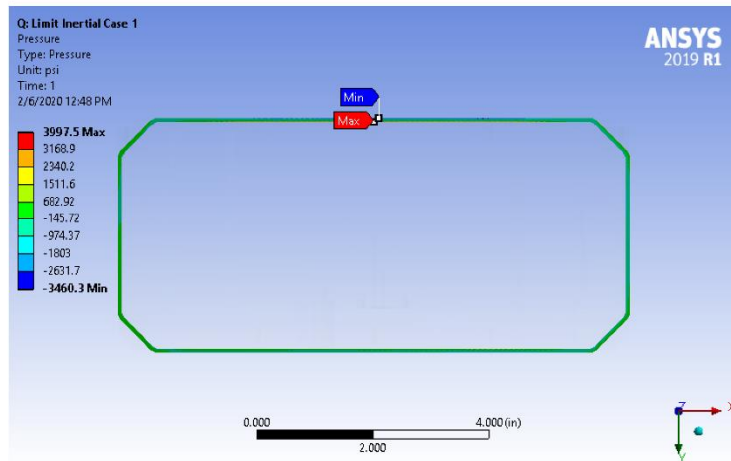


Figure 32 Maximum Tensile Stress Due to Inertia (Full Tank) in Weld (56.5 g Load Factor, Correction Factor: 32.6/56.5)

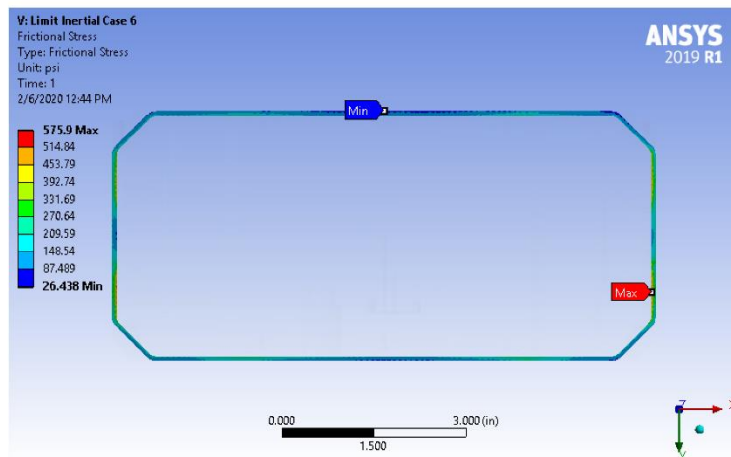


Figure 33 Maximum Shear Stress Due to Inertia (Empty Tank) in Weld (32.6 g Load Factor)

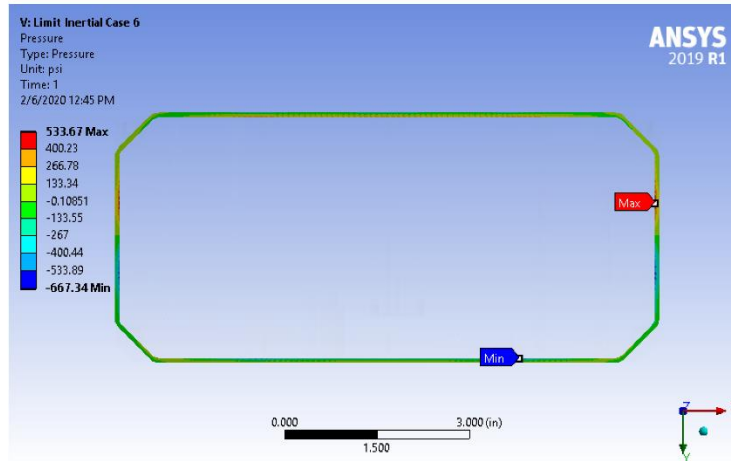


Figure 34 Maximum Tensile Stress Due to Inertia (Empty Tank) in Weld (32.6 g Load Factor)

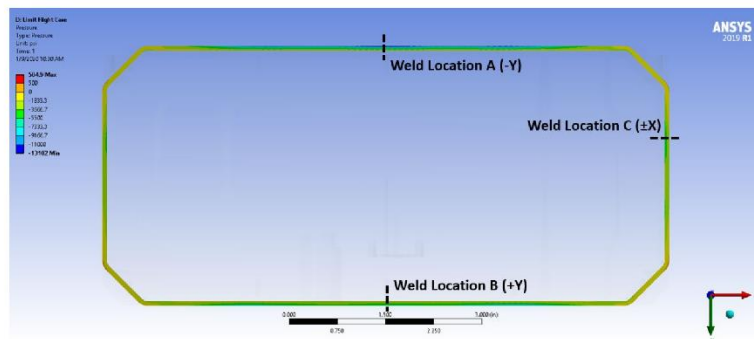


Figure 35 Weld Submodel Locations

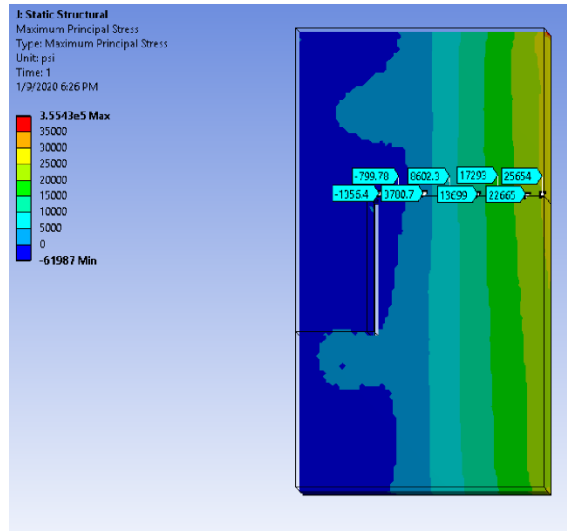


Figure 36 Maximum Principle Stress Due to MDP at Weld Location A (-Y)

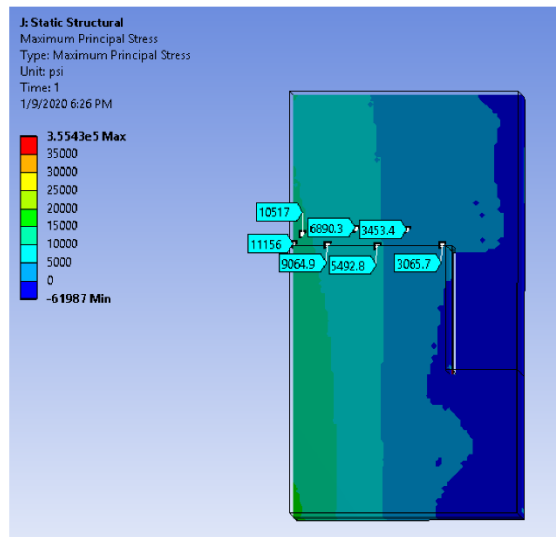


Figure 37 Maximum Principle Stress Due to MDP at Weld Location B (+Y)

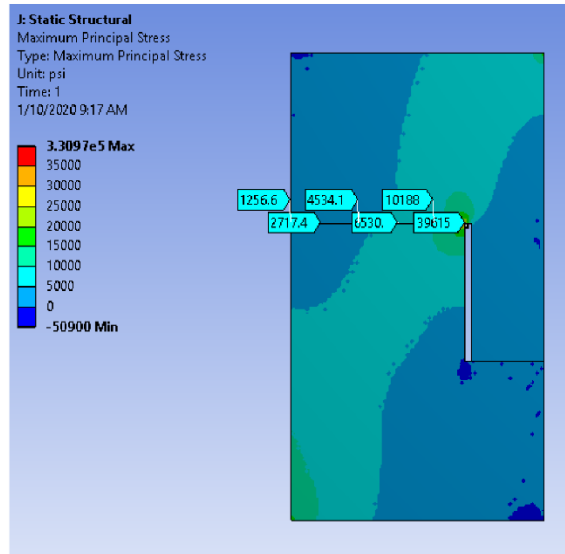


Figure 38 Maximum Principle Stress Due to MDP at Weld Location C ($\pm X$)

6.1.2 Stress Assumptions

The tank top/bottom stresses are combined within NASGRO SC30 analyses assuming they are split evenly between S0 and S1. This is reasonable as all peak stress locations on the interior of the tank have compressive max principle stresses on the exterior. The assumed stress fields from interior to exterior (or vice versa) are conservative as the peak stresses are nonlinear concentrations but are assumed to be linear. The idealized stresses are listed in the table below, showing the split between S0 (tension in NASGRO) and S1 (bending in NASGRO).

Table 10 Tank Top/Bottom Stress Results

Inertia Stress (Empty Tank)		Inertia Stress (Full Tank)		MDP Stress	
S0 (ksi)	S1 (ksi)	S0 (ksi)	S1 (ksi)	S0 (ksi)	S1 (ksi)
0.7	0.7	3.4	3.4	25.8	25.8

The tank weld stresses are modeled differently. Inertial stresses are assumed to be pure tension using peak values across the entire weld. The stresses due to pressure are modeled at three locations, with a linear distribution from interior to exterior. The idealized stresses are listed in the table below, showing the split between S0 (tension in NASGRO) and S1 (bending in NASGRO).

NASA-HDBK-5010, VOLUME 2, REVISION A

Table 11 Tank Weld Stress Results

Location	Inertia Stress (Empty Tank)		Inertia Stress (Full Tank)		MDP Stress	
	S0 (ksi)	S1 (ksi)	S0 (ksi)	S1 (ksi)	S0 (ksi)	S1 (ksi)
Weld A	1.2	0	2.6	0	12.2	13.6
Weld B	1.2	0	2.6	0	7.2	4.1
Weld C	1.2	0	2.6	0	5.7	-4.4

6.1.3 Load Combinations

RV test cycles have a mean stress of 0 because they are unpressurized. Flight RV cycles use MDP results as the mean stress. Pressure events (proof tests, pressure tests, and pressurization cycles) are assumed to occur without inertial loads. It's important to note that the pressurization cycles have a vacuum pulled on the tank prior to propellant loading, seen in the following tables as a non-zero initial state. The proof pressure test includes factors on top of MDP: 1.5x according to system requirements (LFPS-SPEC-201), 1.06 environmental correction factor (corresponding to the tank Ft_u ECF) as required by NASA-STD-5019, and an inadvertent 1.05 factor (conservative). Note that cases are run for flaws on the both the interior and exterior of the tank. This is done by reversing the bending stresses (S1 in NASGRO).

The combined stresses, cycles, and events can be seen in the following tables. These are used as direct inputs into NASGRO using longblock files.

NASA-HDBK-5010, VOLUME 2, REVISION A

Table 12 NASGRO Longblock Data – Tank Top/Bottom Interior/Exterior Flaw

	Cycle	Interior Flaw				Exterior Flaw			
		SOT1	SOT2	SIT1	SIT2	SOT1	SOT2	SIT1	SIT2
Operational Pressure Tests	50	0	25.8	0	25.8	0	25.8	0	-25.8
Tank Proof Test	1	0	43.2	0	43.2	0	43.2	0	-43.2
System Proof Test	1	0	28.4	0	28.4	0	28.4	0	-28.4
Pressurization Cycles	10	-3.8	25.8	-3.8	25.8	-3.8	25.8	3.8	-25.8
	3336	25.5	26.1	25.5	26.1	25.5	26.1	-25.5	-26.1
	9152	25.1	26.5	25.1	26.5	25.1	26.5	-25.1	-26.5
	12733	24.8	26.8	24.8	26.8	24.8	26.8	-24.8	-26.8
	13612	24.4	27.2	24.4	27.2	24.4	27.2	-24.4	-27.2
	12212	24.1	27.5	24.1	27.5	24.1	27.5	-24.1	-27.5
Flight RV Cycles (Full Tank)	9516	23.8	27.8	23.8	27.8	23.8	27.8	-23.8	-27.8
	6553	23.4	28.2	23.4	28.2	23.4	28.2	-23.4	-28.2
	4029	23.1	28.5	23.1	28.5	23.1	28.5	-23.1	-28.5
	2219	22.7	28.9	22.7	28.9	22.7	28.9	-22.7	-28.9
	1102	22.4	29.2	22.4	29.2	22.4	29.2	-22.4	-29.2
	36439	-0.1	0.1	-0.1	0.1	-0.1	0.1	-0.1	0.1
	99962	-0.1	0.1	-0.1	0.1	-0.1	0.1	-0.1	0.1
	139085	-0.2	0.2	-0.2	0.2	-0.2	0.2	-0.2	0.2
	148682	-0.3	0.3	-0.3	0.3	-0.3	0.3	-0.3	0.3
	133391	-0.4	0.4	-0.4	0.4	-0.4	0.4	-0.4	0.4
Test RV Cycles (Empty Tank)	103947	-0.4	0.4	-0.4	0.4	-0.4	0.4	-0.4	0.4
	71576	-0.5	0.5	-0.5	0.5	-0.5	0.5	-0.5	0.5
	44003	-0.6	0.6	-0.6	0.6	-0.6	0.6	-0.6	0.6
	24238	-0.7	0.7	-0.7	0.7	-0.7	0.7	-0.7	0.7
	12038	-0.7	0.7	-0.7	0.7	-0.7	0.7	-0.7	0.7

Table 13 NASGRO Longblock Data – Tank Weld – Location A (-Y) Interior/Exterior Flaw

	Cycle	Interior Flaw				Exterior Flaw			
		SOT1	SOT2	SIT1	SIT2	SOT1	SOT2	SIT1	SIT2
Operational Pressure Tests	50	0	12.2	0	13.6	0	12.2	0	-13.6
Tank Proof Test	1	0	20.4	0	22.7	0	20.4	0	-22.7
System Proof Test	1	0	13.4	0	14.9	0	13.4	0	-14.9
Pressurization Cycles	10	-1.8	12.2	-2	13.6	-1.8	12.2	2	-13.6
	3336	11.9	12.4	13.6	13.6	11.9	12.4	-13.6	-13.6
	9152	11.6	12.7	13.6	13.6	11.6	12.7	-13.6	-13.6
	12733	11.4	12.9	13.6	13.6	11.4	12.9	-13.6	-13.6
	13612	11.1	13.2	13.6	13.6	11.1	13.2	-13.6	-13.6
Flight RV Cycles (Full Tank)	12212	10.9	13.5	13.6	13.6	10.9	13.5	-13.6	-13.6
	9516	10.6	13.7	13.6	13.6	10.6	13.7	-13.6	-13.6
	6553	10.3	14	13.6	13.6	10.3	14	-13.6	-13.6
	4029	10.1	14.2	13.6	13.6	10.1	14.2	-13.6	-13.6
	2219	9.8	14.5	13.6	13.6	9.8	14.5	-13.6	-13.6
	1102	9.6	14.8	13.6	13.6	9.6	14.8	-13.6	-13.6
	36439	-0.1	0.1	0	0	-0.1	0.1	0	0
	99962	-0.2	0.2	0	0	-0.2	0.2	0	0
	139085	-0.4	0.4	0	0	-0.4	0.4	0	0
	148682	-0.5	0.5	0	0	-0.5	0.5	0	0
	133391	-0.6	0.6	0	0	-0.6	0.6	0	0
Test RV Cycles (Empty Tank)	103947	-0.7	0.7	0	0	-0.7	0.7	0	0
	71576	-0.8	0.8	0	0	-0.8	0.8	0	0
	44003	-1	1	0	0	-1	1	0	0
	24238	-1.1	1.1	0	0	-1.1	1.1	0	0
	12038	-1.2	1.2	0	0	-1.2	1.2	0	0

NASA-HDBK-5010, VOLUME 2, REVISION A

Table 14 NASGRO Longblock Data – Tank Weld – Location B (+Y) Interior/Exterior Flaw

	Cycle	Interior Flaw				Exterior Flaw			
		SOT1	SOT2	S1T1	S1T2	SOT1	SOT2	S1T1	S1T2
Operational Pressure Tests	50	0	7.2	0	4.1	0	7.2	0	-4.1
Tank Proof Test	1	0	12	0	6.8	0	12	0	-6.8
System Proof Test	1	0	7.9	0	4.5	0	7.9	0	-4.5
Pressurization Cycles	10	-1.1	7.2	-0.6	4.1	-1.1	7.2	0.6	-4.1
	3336	6.9	7.4	4.1	4.1	6.9	7.4	-4.1	-4.1
	9152	6.6	7.7	4.1	4.1	6.6	7.7	-4.1	-4.1
	12733	6.4	7.9	4.1	4.1	6.4	7.9	-4.1	-4.1
	13612	6.1	8.2	4.1	4.1	6.1	8.2	-4.1	-4.1
Flight RV Cycles (Full Tank)	12212	5.9	8.5	4.1	4.1	5.9	8.5	-4.1	-4.1
	9516	5.6	8.7	4.1	4.1	5.6	8.7	-4.1	-4.1
	6553	5.3	9	4.1	4.1	5.3	9	-4.1	-4.1
	4029	5.1	9.2	4.1	4.1	5.1	9.2	-4.1	-4.1
	2219	4.8	9.5	4.1	4.1	4.8	9.5	-4.1	-4.1
	1102	4.6	9.8	4.1	4.1	4.6	9.8	-4.1	-4.1
	36439	-0.1	0.1	0	0	-0.1	0.1	0	0
	99962	-0.2	0.2	0	0	-0.2	0.2	0	0
	139085	-0.4	0.4	0	0	-0.4	0.4	0	0
	148682	-0.5	0.5	0	0	-0.5	0.5	0	0
Test RV Cycles (Empty Tank)	133391	-0.6	0.6	0	0	-0.6	0.6	0	0
	103947	-0.7	0.7	0	0	-0.7	0.7	0	0
	71576	-0.8	0.8	0	0	-0.8	0.8	0	0
	44003	-1	1	0	0	-1	1	0	0
	24238	-1.1	1.1	0	0	-1.1	1.1	0	0
	12038	-1.2	1.2	0	0	-1.2	1.2	0	0

Table 15 NASGRO Longblock Data – Tank Weld – Location C (±X) Interior/Exterior Flaw

	Cycle	Interior Flaw				Exterior Flaw			
		SOT1	SOT2	S1T1	S1T2	SOT1	SOT2	S1T1	S1T2
Operational Pressure Tests	50	0	5.7	0	-4.4	0	5.7	0	4.4
Tank Proof Test	1	0	9.5	0	-7.3	0	9.5	0	7.3
System Proof Test	1	0	6.2	0	-4.8	0	6.2	0	4.8
Pressurization Cycles	10	-0.8	5.7	0.6	-4.4	-0.8	5.7	-0.6	4.4
	3336	5.4	5.9	-4.4	-4.4	5.4	5.9	4.4	4.4
	9152	5.1	6.2	-4.4	-4.4	5.1	6.2	4.4	4.4
	12733	4.9	6.4	-4.4	-4.4	4.9	6.4	4.4	4.4
	13612	4.6	6.7	-4.4	-4.4	4.6	6.7	4.4	4.4
Flight RV Cycles (Full Tank)	12212	4.4	7	-4.4	-4.4	4.4	7	4.4	4.4
	9516	4.1	7.2	-4.4	-4.4	4.1	7.2	4.4	4.4
	6553	3.8	7.5	-4.4	-4.4	3.8	7.5	4.4	4.4
	4029	3.6	7.7	-4.4	-4.4	3.6	7.7	4.4	4.4
	2219	3.3	8	-4.4	-4.4	3.3	8	4.4	4.4
	1102	3.1	8.3	-4.4	-4.4	3.1	8.3	4.4	4.4
	36439	-0.1	0.1	0	0	-0.1	0.1	0	0
	99962	-0.2	0.2	0	0	-0.2	0.2	0	0
	139085	-0.4	0.4	0	0	-0.4	0.4	0	0
	148682	-0.5	0.5	0	0	-0.5	0.5	0	0
Test RV Cycles (Empty Tank)	133391	-0.6	0.6	0	0	-0.6	0.6	0	0
	103947	-0.7	0.7	0	0	-0.7	0.7	0	0
	71576	-0.8	0.8	0	0	-0.8	0.8	0	0
	44003	-1	1	0	0	-1	1	0	0
	24238	-1.1	1.1	0	0	-1.1	1.1	0	0
	12038	-1.2	1.2	0	0	-1.2	1.2	0	0

NASA-HDBK-5010, VOLUME 2, REVISION A

6.1.4 Tank Top/Bottom Safe-Life / Damage Tolerance Analysis

A safe life analysis was carried out in NASGRO to check that sufficient life exists with worst case loads, flaw, materials, dimensions, and environments. The material properties used in this analysis can be seen in §4.1. The mission and associated spectra used in the DT analysis are described in §5.0 and are combined with stresses in §6.1.3. The flaw sizes and cross sections used in the NASGRO analyses are described in §3.3.1 and §3.3.3. The flaws are assumed to be surface cracks using NASGRO SC30 formulation.

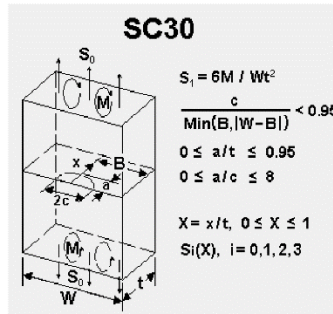


Figure 39 NASGRO SC30 Formulation

Failure criteria include unstable crack growth, net section failure, and surface cracks transitioning to through cracks (fluid leakage is unacceptable). Four lives are required by NASA-STD-5019 and AIAA S-080-1998. The tank top and bottom have sufficient life, with a minimum prediction of 20 lives before failure. The NASGRO analyses are summarized in the table below.

Table 16 NASGRO Results – Tank Top/Bottom

	Initiated on Interior	Initiated on Exterior
Deep Flaw a=0.075” a/c=1	23 lives completed	20 lives completed
Shallow Flaw a=0.025” a/c=0.2	>100 lives completed	36 lives completed

6.1.5 Tank Weld Alternative Approach / Safe-Life / Damage Tolerance Analysis

The tank weld is classified as a fracture critical as it contains a hazardous fluid. The weld meets NASA-STD-5019 and AIAA-S-080-1998 requirements through an alternative approach.

NASA-HDBK-5010, VOLUME 2, REVISION A

Alternative Approach Justification:

- Due to tank weld geometry, radiographic inspection of the propellant tank weld joint will not be performed. In lieu of this inspection, the following activities will be performed:
 - A damage tolerance analysis will be performed to demonstrate that the weld is capable of withstanding significant damage. This analysis will show that failure doesn't occur using a starting flaw size that exceeds 90% of the thickness.
 - Qualification unit will undergo burst testing to verify maximum design pressure.
 - Pre- and post-weld coupons will be cross-sectioned to verify weld process. Coupons will also be inspected via radiography and surface dye penetrant.
 - Post-weld dye penetrant inspection of tank and weld.
 - Proof test performed to 1.5X MDP.
 - Post-proof dye penetrant inspection of tank and weld.
 - Leak test at next higher assembly level

A safe-life analysis was carried out in NASGRO to check that the weld is capable of withstanding significant damage. The analysis assumes worst case loads, flaw, materials, dimensions, and environments. The material properties used in this analysis can be seen in §4.1. The mission and associated spectra used in the DT analysis are described in §5.0 and are combined with stresses in §6.1.3. The flaw sizes and cross sections used in the NASGRO analyses are described in §3.3.2 and §3.3.3. The flaws are assumed to be surface cracks with 90% depth using NASGRO SC30 formulation.

NASA-HDBK-5010, VOLUME 2, REVISION A

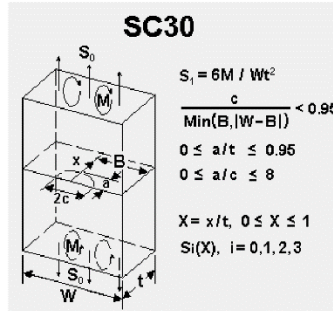


Figure 40 NASGRO SC30 Formulation

Failure criteria include unstable crack growth, net section failure, and surface cracks transitioning to through cracks (fluid leakage is unacceptable). Four lives are required by NASA-STD-5019 and AIAA S-080-1998. The critical flaw size hasn't been reached after 4 lives for those originating on the weld exterior and interior, so there is sufficient life. The NASGRO analyses are summarized in the table below.

Table 17 NASGRO Results – Tank Weld Life

Flaw Shape	Flaw Location	Weld Location A	Weld Location B	Weld Location C
Deep Flaw a=0.0603" a/c=1	Interior Flaw	>100 lives completed	>100 lives completed	>100 lives completed
	Exterior Flaw	>100 lives completed	>100 lives completed	>100 lives completed
Wide Flaw a=0.0603" a/c=0.2	Interior Flaw	5 lives completed	6 lives completed	7 lives completed
	Exterior Flaw	5 lives completed	6 lives completed	7 lives completed

NASA-HDBK-5010, VOLUME 2, REVISION A

6.2 Isolation Valve

The isolation valve is classified as a fracture critical pressurized component as it contains a hazardous fluid. The valve meets NASA-STD-5019 and AIAA-S-080-1998 requirements through an alternative approach.

Alternative Approach Justification:

- Due to the isolation valve geometry, radiographic inspection of the weld joint will not be performed. In lieu of this inspection, the following activities will be performed:
 - Qualification unit will undergo burst testing to verify maximum design pressure.
 - Pre- and post-weld coupons will be cross-sectioned to verify weld process.
 - Pre-proof pressure testing dye penetrant inspection of weld joint.
 - Proof test performed at 1.5x MDP
 - Post-proof dye penetrant inspection of weld.
 - Component-level leak test.

NASA-HDBK-5010, VOLUME 2, REVISION A

6.3 Isolation Valve Mounting Plate

The isolation valve mounting plate is classified as “NFC-Fail Safe” as it contains a hazardous fluid, but can withstand a single failure without creating a hazard. The plate meets NASA-STD-5019 and AIAA-S-080-1998 requirements by verifying the remaining damaged system meets strength, life, and functional (leak) requirements.

6.3.1 Finite Element Model

The finite element model used and described in the memo ER41 (20-005) was used to develop the failsafe case. Two changes were made to the model:

- The mounting plate is assumed to fail along the section shown in the figure below. This simulates a failure along the highest stressed/loaded section, which meets NASA-STD-5019 requirements for fail safety.
- The bolts are preloaded differently from the nominal model to account for the new geometry and are preloaded by adjusting length instead of by prescribing a load. The original model (described in the LFPS Structural Analysis Report Rev. A) was interrogated and the average bolt lengths at the end of the preload step were used in this analysis. The overall effect should be acceptable and will properly imitate a preload prior to failing the mounting plate.

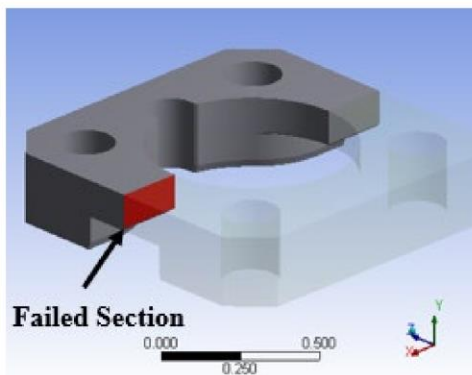


Figure 41 Isolation Valve Mounting Plate Failsafe Plate Condition

NASA-HDBK-5010, VOLUME 2, REVISION A

6.3.2 Static Strength Assessment

The static strength assessment of the damaged mounting plate is discussed in the ER41 Structural Analysis Report Rev. A. The critical strength margin is +0.23 for the failsafe condition.

6.3.3 Fastener Check

The fasteners are assessed for strength and life in the failsafe condition in the ER41 Structural Analysis Report Rev. A. The minimum margin of safety is +0.00 due to fastener yield failure.

6.3.4 Fatigue Check

The fatigue checks performed as part of the LFPS Structural Analysis Report Rev. A account for the failsafe load case described in this analysis. The fatigue analysis described in that memo confirms that the fasteners and the plate have sufficient life (>4 lives).

NASA-HDBK-5010, VOLUME 2, REVISION A

6.3.5 Seal Check

The resulting seal gap underneath the isolation valve is 4.7×10^{-5} inches and can be seen in the figure below. There is no hard allowable associated with this valve design, but this value was determined to be acceptable per ER14 on 1/27/2020, see §6.3.5.1.

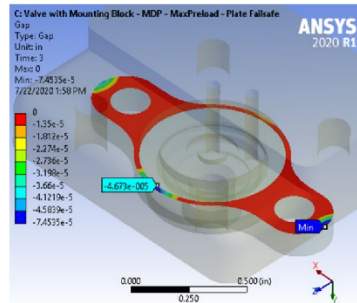


Figure 42 Isolation Valve Seal Performance Following Mounting Plate Failure

6.3.5.1 Seal Performance Email from MSFC ER14

From: Addona, Brad M. (MSFC-ER14) <brad.m.addona@nasa.gov>
Sent: Monday, January 27, 2020 1:21 PM
To: Dymont, Samuel R. (MSFC-ER41) <samuel.r.dymont@nasa.gov>
Subject: RE: Micro Valve Allowable Gap

There isn't a hard limit. That number is very small and seems just fine.

Brad

From: Dymont, Samuel R. (MSFC-ER41) <samuel.r.dymont@nasa.gov>
Sent: Saturday, January 25, 2020 2:37 PM
To: Addona, Brad M. (MSFC-ER14) <brad.m.addona@nasa.gov>
Subject: Micro Valve Allowable Gap

Hey Brad,

What's the acceptable gap for the isolation valve? I'm seeing 1.3×10^{-4} inches as a maximum during a failsafe condition and am wondering if that's acceptable.

Thanks,

*Sam Dymont
ER41
Work: 256-544-6462*

6.4 Isolation Valve Mounting Plate Fasteners

The isolation valve mounting plate fasteners are classified as “NFC-Fail Safe” as they contain a hazardous fluid, but can withstand a single failure without creating a hazard. The fasteners meet NASA-STD-5019 and AIAA-S-080-1998 requirements by verifying the remaining damaged system meets strength, life, and functional (leak) requirements.

6.4.1 Finite Element Model

The finite element model used and described in the ER41 Structural Analysis Report Rev. A was used to develop the failsafe case. The nominal model was only changed to remove the highest loaded bolt, which is shown in the figure below:

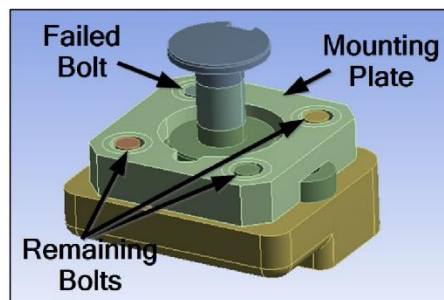


Figure 43 Isolation Valve Mounting Plate Failsafe Bolt Condition

NASA-HDBK-5010, VOLUME 2, REVISION A

6.4.2 Static Strength Assessment

The static strength assessment of the damaged mounting plate is discussed in the ER41 Structural Analysis Report Rev. A. The critical strength margin is +0.23 for the failsafe condition.

6.4.3 Fastener Check

The fasteners are assessed for strength and life in the failsafe condition in the ER41 Structural Analysis Report Rev. A.. The minimum margin of safety is +0.00 due to fastener yield failure.

6.4.4 Fatigue Check

The fatigue checks performed as part of the LFPS Structural Analysis Report account for the failsafe load case described in this analysis. The fatigue analysis described in that memo confirms that the fasteners and the plate have sufficient life (>4 lives).

6.4.5 Seal Check

The resulting seal gap underneath the isolation valve is 8.4×10^{-5} inches and can be seen in the figure below. There is no hard allowable associated with this valve design, but this value was determined to be acceptable per ER14 on 1/27/2020, see §6.3.5.1.

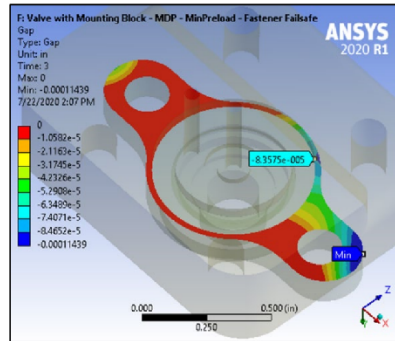


Figure 44 Isolation Valve Seal Performance Following Bolt Failure

NASA-HDBK-5010, VOLUME 2, REVISION A

6.5 Service Valve

The service valve is classified as a fracture critical pressurized component as it contains a hazardous fluid. The valve meets NASA-STD-5019 and AIAA-S-080-1998 requirements through an alternative approach.

Alternative Approach Justification:

- Due to its size and the risk of contamination, the service valve will forego dye penetrant inspection of its single circumferential weld. In order to alleviate concerns with bypassing this inspection, the following activities will be performed during qualification and acceptance:
 - Valve design employs high factors of safety on system maximum expected operating pressure (>6X MEOP, see ER41 Memorandum (18-028)).
 - Qualification unit will undergo burst testing to verify maximum design pressure.
 - Pre- and post-weld coupons will be cross-sectioned to verify weld process.
 - Leak test performed at component level.
 - Proof test performed after installation into system.
 - Leak test performed after system-level proof testing.
 - Service valve cap, once installed, will keep weld in compression.

NASA-HDBK-5010, VOLUME 2, REVISION A

6.6 Pressure Transducer

The pressure transducer is classified as a fracture critical pressurized component as it contains a hazardous fluid. The transducer meets NASA-STD-5019 and AIAA-S-080-1998 requirements through an alternative approach.

Alternative Approach Justification:

- Due to its size and the risk of contamination, the transducer will forgo flaw inspection and analysis. In order to alleviate concerns with bypassing this inspection, the following activities will be performed during qualification and acceptance:
 - Transducer design employs high factors of safety on system maximum design pressure (components are rated to 3X LFPS MDP for proof and 7.5x LFPS MDP for burst (TE Connectivity part number is TE XP5-X-150PA-/V05/L3M/Z02)).
 - 1.1X LFPS MDP Proof test performed after installation into system.
 - Leak check performed after system-level proof testing.

NASA-HDBK-5010, VOLUME 2, REVISION A

6.7 NFC – Contained Components

All other LFPS components that are not explicitly described above or as “Exempt” are considered “NFC-Contained”. These components do not pose a hazard to SLS because they are isolated from the hazardous fluid and are contained by the CubeSat launcher. These components are listed below:

- Manifold
- Muffin tin
- Controller
- Pump
- Pump interface block
- Propellant management device (PMD)
- Thrusters
- Thruster valves
- Seals
- All fasteners other than those on the isolation valve

6.8 Exempt Components

The controller and all cables on the LFPS are considered exempt.

NASA-HDBK-5010, VOLUME 2, REVISION A

7.0 ACRONYMS AND ABBREVIATIONS

Acronym / Abbreviation	Definition
α	Coefficient of thermal expansion
§	Section
a	Surface crack depth
AIAA	American Institute of Aeronautics and Astronautics
AM	Additively manufactured
AMS	Aerospace material specification
ANSYS	Engineering simulation and 3D design software
AMCP	Additive Manufacturing Control Plan
ASMH	Aerospace Structural Metals Handbook
c	Surface half crack width
CAD	Computer aided design
COTS	Commercial off the shelf
CRES	Corrosion resistant steel
DMLS	Direct metal laser sintering
DT	Damage tolerance
E	Young's Modulus
EB	Electron Beam
ECF	Environmental Correction Factor
ER11	MSFC Spacecraft and Vehicle Propulsion Branch
ER14	MSFC Valves, Actuators, Ducts Design & Development Branch
ER41	MSFC Propulsion Structures and Design Branch
F	Fahrenheit
FC	Fracture Critical
FCB	Fracture Control Board
FCP	Fracture Control Plan
FEM	Finite element model
FSU	Ultimate factor of safety
FSY	Yield factor of safety
F_u	Tensile ultimate stress
F_y	Tensile yield stress
GD&T	Geometric dimensioning and tolerancing
GT	Georgia Institute of Technology
HDBK	Handbook
in	Inches

NASA-HDBK-5010, VOLUME 2, REVISION A

Acronym / Abbreviation	Definition
ksi	Thousand pounds-force per square inch
lbf	Pounds-force
LC	Load case
LFPS	Lunar Flashlight Propulsion System
MDP	Maximum Design Pressure
Memo	Memorandum
MEOP	Maximum expected operating pressure
MMPDS	Metallic Materials Properties Development and Standardization
MS	Margin of safety
MSFC	Marshall Space Flight Center
MUA	Material Usage Agreement
NASA	National Aeronautics and Space Administration
NASGRO	NASA Crack Growth Computer Program
NDE	Non-destructive evaluation
NDY	Non-detrimental yielding
NFC	Non-fracture critical
PMD	Propellant management device
psi	Pounds-force per square inch
Rev.	Revision
RV	Random vibration
S-N	Stress-life curve
S ₀	Tensile stress in NASGRO SC30
S ₁	Bending stress in NASGRO SC30
S _{Alt}	Alternating stress
SC30	Surface crack formulation in NASGRO
SLS	Space Launch System
STA	Solution Treated and Aged
Ult.	Ultimate
Yld.	Yield

APPROVED FOR PUBLIC RELEASE – DISTRIBUTION IS UNLIMITED

APPENDIX E

FRACTURE CONTROL BOARD EXAMPLE

E.1 Fracture Control Board

The Fracture Control Plan for the *Example Project* will be implemented through the activities of the Contractor FCB, defined in Contractor FCB Charter. The structure of the board is shown in Figure E.1-1, Fracture Control Board Structure. Technical specialists may be used to review technical issues that lie outside the expertise of the other members of the board.

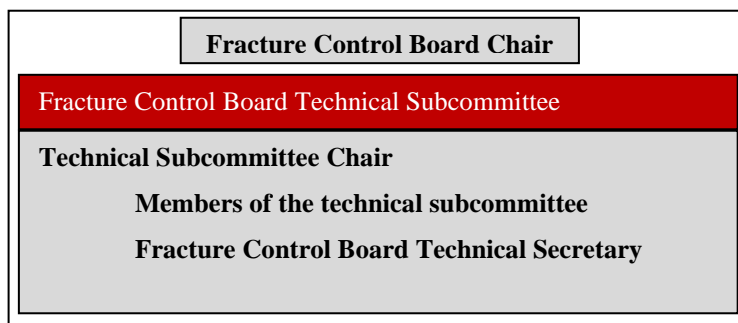


Figure E.1-1—Fracture Control Board Structure

The focus of the FCB is to facilitate the use of sound engineering practices in the design, selection of materials, analysis, inspection, fabrication, maintenance and operation of structures to reduce the risk of catastrophic failure from either a material defect or damage.

In general, the FCB is responsible to verify adequate systems are in place to ensure:

- Implementation of traceability and documentation showing adherence of hardware to approved drawings, specifications, plans, and procedures
- Compilation and configuration control of the fracture control and related structural documentation for the lifetime of the hardware
- Establishment of management procedures/policies for implementing Fracture Control Plans to define fracture-related activities and practices for fracture-sensitive hardware.

Members of the FCB Technical Subcommittee have specific responsibility to:

- Create and/or review and approve fracture control documents that include fracture control plans, fracture control analysis reports (FCARs), etc. (these documents are also reviewed and approved by the chief engineer and program management)
 - Establish fracture classification of parts
 - Perform fracture mechanics and damage tolerance analyses
- Identify required NDE or other requirements for fracture critical parts

NASA-HDBK-5010, VOLUME 2, REVISION A

- Assess anomalies related to fracture-critical parts
- Provide direction for questions or issues relating to fracture control
- Review drawing and document changes to assess potential fracture impact
- Develop fracture control test plans
 - Review and approve all fracture control test data
- Work as technical resource to *Contractor* engineering and program management
 - Be a resource for MRB related to potential fracture issues
- Serve as technical resource in failure investigations
- Communicate fracture concerns to program office
- Serve as technical resources for issues with tooling, facilities, etc.

Formal reviews by the Contractor FCB are required for the following:

- Approval of fracture approaches or proposals that will be presented to a MSFC FCB
- Approval of part fracture classifications and fracture control approaches for major subsystems
- Approval of the fracture control approach, technical rationale, and recommendations used to address a significant fracture control issue

E.2 Contractor FCB Interaction with the MSFC FCB

Figure E.2-1, Interaction of the Contractor FCB and MSFC FC Team, provides a schematic representation showing how the Contractor FCB or FCB member typically interacts with the MSFC FCB or FCB member. The interaction may be driven by MRB issues, product or process changes, by direct request of the Contractor Program Office or by the personal initiative of an Contractor FCB member to discuss or coordinate a fracture-related technical issue with a MSFC FCB member.

NASA-HDBK-5010, VOLUME 2, REVISION A

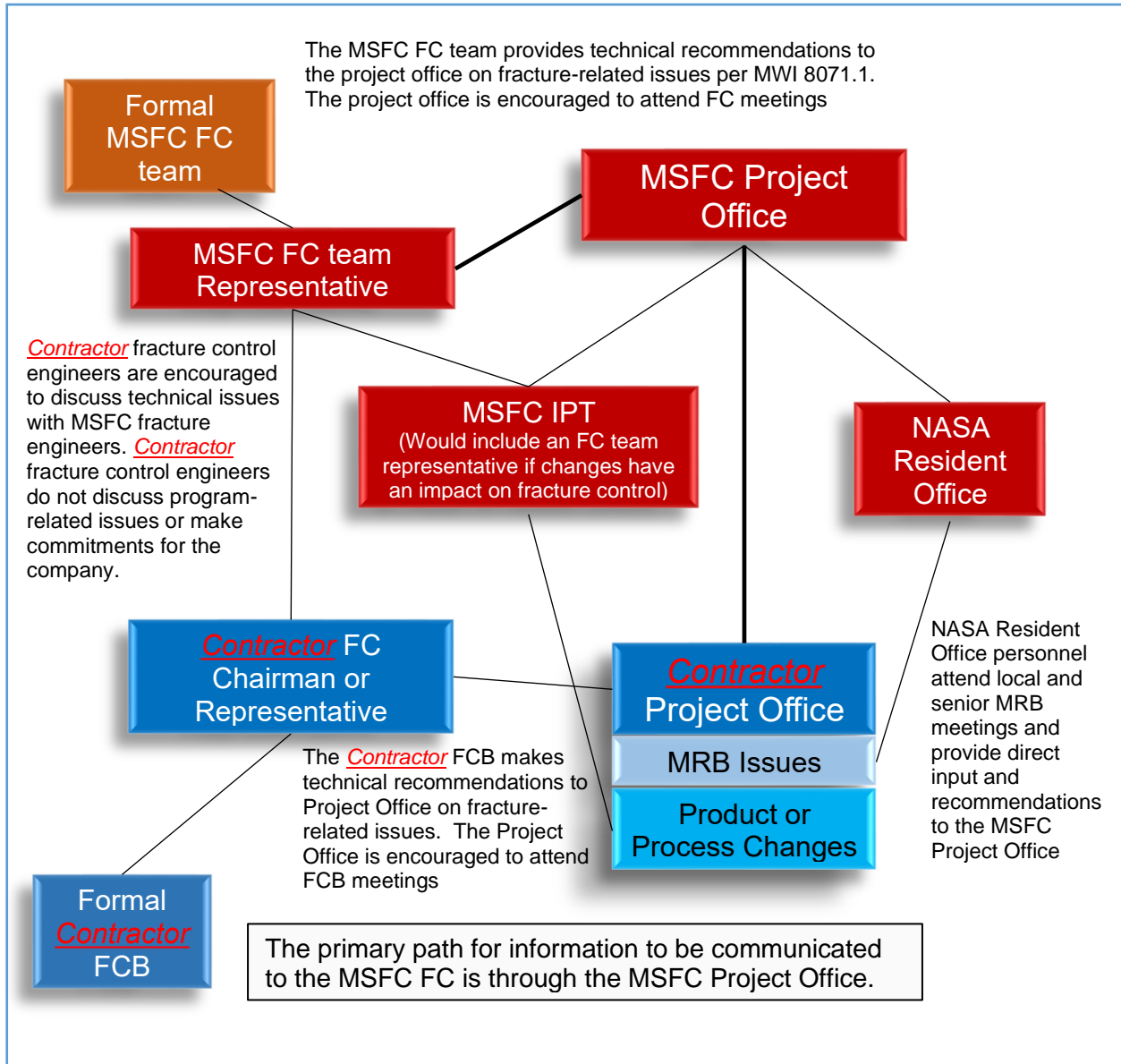


Figure E.2-1—Interaction of the Contractor FCB and MSFC FC Team

E.3 Material Review Board Activities and Fracture Control

All Material Review Board (MRB) activity related to fracture critical parts will be coordinated with a Contractor FCB Technical Subcommittee member. Issues that are deemed a Fracture Control Board Concern by the Technical Subcommittee member will require the fracture mechanics aspect of the discrepancy to be addressed in the MRB disposition and will require concurrence of the subcommittee member.

The following are examples of Fracture Control Board Concerns:

- Any issues that relate to proof testing

APPROVED FOR PUBLIC RELEASE – DISTRIBUTION IS UNLIMITED

NASA-HDBK-5010, VOLUME 2, REVISION A

- Rework or repairs after proof testing
- NDE inspection for flaws (including visual inspection), such as NDE indications, and any condition that prevents adequate NDE inspection for flaws
- Fracture toughness, K1c, J1c or KJ1c
- Any damage that may alter material properties or induce residual stress
- Any damage that may cause cracks
- Material interactions that may cause hydrogen embrittlement or stress corrosion cracking, such as metal surface exposure to foreign substances, or non-qualified materials

The Contractor FCB Subcommittee member may identify other issues as Fracture Control Board Concerns if, in their judgment, they may represent a fracture concern for the hardware.

Include a reference to the Contractor Safety and Mission Assurance Plan (if appropriate) for the Material Review Board process.

E.4 Product or Process Changes and Fracture Control

For changes that may impact the fracture control of a part or a fracture critical process, Project Engineers coordinate design or process changes with member of the Contractor fracture control board who has signature authority for fracture control. The Project Engineer develops a formal Change Request that is reviewed by a NASA Integrated Product Team (IPT). For changes that affect a fracture-controlled part or critical process (NDE, proof test, fabrication controls, etc.) a member of the MSFC FCB is generally invited to participate in the discussion of the change at the IPT meeting.

Following review by the IPT, the Change Request is reviewed by the Contractor Configuration Control Board (CCB). After the CCB has reviewed and approved the change, fracture-related changes are reviewed by the MSFC Engineering Review Board (ERB). MSFC FCB representatives are generally requested to review proposed changes that may impact fracture critical processes or parts.

The description provided above is a simplified version of how critical hardware or process changes are made.

NASA-HDBK-5010, VOLUME 2, REVISION A

APPENDIX F

ACKNOWLEDGEMENTS

NASA-HDBK-5010, Volume 2, Revision A, was developed by NASA in collaboration with The Aerospace Corporation. The development of this volume was under the leadership of Kauser Intiaz, Gilda Battista, and Kenneth Hamm. The key contributors to Volume 2 were Gilda Battista (NASA) and the following individuals from The Aerospace Corporation: Vinay Goyal, Jacob Rome, Christopher Sagrillo, Pavel Babuska, and Zachary Fox. The following additional members provided weekly inputs that improved the product: James Smith (NASA), Greg Swanson (NASA), and Wayne Gregg (NASA).